Targeting von Wirkstoffen gegen Krebszellen

Dissertation

zur Erlangung des Doktorgrades der Naturwissenschaften

(Dr. rer. nat.)

der

Naturwissenschaftlichen Fakultät II

Chemie, Physik, Mathematik

der Martin-Luther-Universität

Halle-Wittenberg

vorgelegt von

Herrn Paul Jänicke

geb. am 25.12.1991 in Merseburg

Die vorliegende Arbeit wurde im Zeitraum vom Juli 2016 bis zum Oktober 2020 am Leibniz-Institut für Pflanzenbiochemie in Halle (Saale) in der Abteilung Natur- und Wirkstoffchemie unter der Betreuung von Prof. Dr. Ludger A. Wessjohann und Mitbetreuung von Prof. Dr. Goran Kaluđerović angefertigt.

Die Anfertigung dieser Dissertation wurde von der Konrad-Adenauer-Stiftung gefördert.

Tag der Verteidigung: 17.11.2021

Gutachter:

1. Prof. Dr. Ludger A. Wessjohann
2. Prof. Dr. Norbert Sewald

Das Schönste, was wir erleben können, ist das Geheimnisvolle.

Albert Einstein

To my family for all the love and help!

Acknowledgement

This dissertation has been finished after a long way of passion and efforts, but wouldn't have been achieved without the support of many people. That is the point to thank all of them.

First of all, I'd like to thank a lot my supervisor Prof. Dr. Ludger A. Wessjohann for the opportunity to do my PhD in his group at the Leibniz Institute of Plant Biochemistry and to take part in many conferences and also to travel a lot! Thus, I gathered in the last years in his group more than pure scientific experience!

Secondly, I want to thank my co-supervisor and former project group leader Prof. Dr. Goran Kaluđerović for his scienfitic and personal support. Thanks to him I got many opportunities to work on interesting projects in Halle, Belgrade and Dortmund. I have appreciated his advices as mentor and friend!

I also thank Dr. Robert Rennert for being my project group leader and adviser in many scientific questions. I have appreciated very much his knowledge and experience in the field of cell culture.

Beside my supervisors and my mentors I thank Prof. Dr. Bernhard Westermann for synthetic input and helpful discussions about chemistry.

While I synthesized the compounds and performed the biological assays, I got much support from Katharina Wolf in the synthesis of building blocks of tubugi, from Gudrun Hahn and Dr. Andrea Porzel measuring NMR, from Anja Ehrlich performing many HPLC and from Mandy Dorn, Andrej Frolov and Elana Kysil measuring HRMS. Additionally, I thank Martina Lerbs, Mohamad Saoud and Ibrahim Morgan for versatile help in the cell lab and Dr. Manuel Garcia Ricardo as well as Dr. Aldrin Vasco Vidal for introducing me to SPPS. Thanks a lot!

But what would be a PhD project without pleasant atmosphere and social life? I have received much mental support and had a nice time thanks to following people.

The lab R203 with Angela Schaks, Thomas Eichhorn, Dr. Yanira Mendez Gomez, Dr. Aldrin Vaco Vidal, David Edeler, Javiel Fernández Marrero and Ana Rodriguez Humpierre contributed to a very pleasant, friendly, interesting working atmosphere. Especially the group around Angela Schaks, Thomas Eichhorn, Goran & Milena Kaluđerović gave me a lot of motivation! ☺

There were many nice opportunities and events comprising pleasant talks with Nicole Hünecke, Martina Brode, Martina Lerbs and Katharina Wolf as well as with Annegret Laub & Dr. Micjel Chavez Morejon, Leo Gonzalez Ceballos, Dr. Manuel García Ricardo & Dayma Llanes Martinez, Dr. Tuvshin Budragchaa, Dr. Haider Sultani and Dr. Martin Nin Brauer. Moreover, I also thank Ines Stein for nice talks and her help regarding organisation of

business trips, contracts and many things more! At this point I don't want to forget colleagues in Belgrade and particularly in Cuba for spending a instructive, enjoyable time there!

I also like to thank the Konrad-Adenauer-Stiftung for funding my PhD and for offering really nice as well as interesting seminars.

Beyond the lab I got a lot of warm advices and diversion by my friends and my family. Especially my parents who made it possible that I could got this way, supporting me in manifold manner and had patience for less time in the last months! Thanks a lot!

I hope, I haven't forgotten somebody. If I have, I'd like to thank them too!

Abstract

Targeting strategies exhibit a high importance to fight against malignant diseases like cancer. Drug conjugates based on antibodies as actively targeting moieties have succeeded and are already in clinical use and many other candidates still need to pass pre-clinical trials. Within the pool of selective addressing strategies the application of peptides as active drug carriers represent another very hopeful way due to their beneficial properties. Their biocompatiblity, easy and low-cost production and broad chemical variability make them a powerful tool. However, the selectivity to cancer cells alone does not guarantee success of treatment. The highly potent tubugis, a class of tubulysin derivatives, increase the impact to the cancer cells and by this, drug resistance can be overcome. The strongly bioactive compound is conjugated via a cleavable linker system which is mainly responsible for release of the active drug from the peptide-drug conjugate.

The present thesis focuses on the synthesis of peptide-drug conjugates comprising tubugi 1 and tubugi 4 as toxins. To make those very cytotoxic tubugi derivatives attractive for medical applications, a multiple cleavable linker-spacer system was developed which can be attached to various peptides.

In chapter 1 an overview is given over cancer drug targeting and which challenges need to be considered in order to develop new strategies in this field.

In chapter 2 the synthetic approach towards peptide-drug conjugates based on the well-known octreotide and the peptide sequence CNGRC is reported. In addition, optimization of the synthesis of tubugi 1 and tubugi 4 was displayed. Considering many requirements, the design and synthesis of a linker-spacer system that can be cleaved off at multiple trigger points under physiological conditions inside the cancer cells is presented. Fluorescence measurements for studies on the receptor-mediated internalization of fluorescent conjugates as well as investigations on the cell viability treating cancer cell lines expressing distinguishable levels of the respective targets of conjugates based on cyclic peptides are presented.

In chapter 3 the synthesis of bombesin-tubugi conjugates is described. Beside the insertion of the multiple cleavable linker-spacer system, the introduction of simplified linker-spacer system based on hydrophobic side-chains is shown. In contrast to previously discussed cyclized conjugates, bombesin exhibits binding affinity in its linear form. Fluorescence measurements exploiting flow cytometry and fluorescence microscopy are displayed. Moreover, the biological evaluation concerning investigations on correlation between expression level of the receptor and the efficacy of the conjugates is illustrated.

Chapter 4 is oriented to the synthesis of peptide-drug conjugates using the novel peptide WSC02 for targeted delivery to cancer tissue. WSC02 has not been reported yet in combination with a drug to treat tumor cells. WSC02 is proven to effeciently bind to its receptor in its linear form. Internalization studies as well as bioassays for studies on expression level-depending activity are also shown and discussed.

Zusammenfassung

Zielgerichtete Strategien haben eine große Bedeutung für den Kampf gegen Tumorerkrankungen. Auf Antikörper beruhende Wirkstoffkonjugate haben als aktiv zielende Substanzen Erfolg gezeigt und werden bereits klinisch verwendet. Viele andere Kandidaten müssen noch vorklinische Untersuchungen durchlaufen. Innerhalb der zielgerichteten Stratgien stellt die Verwendung von Peptiden aufgrund deren vorteilhaften Eigenschaften einen weiteren vielversprechenden Weg für den aktiven Wirkstofftransport dar. Ihre Bioverträglichkeit, einfache und kostengünstige Produktion und die große chemische Vielfalt machen sie zu einem nützlichen Werkzeug. Jedoch die Selektivität zu den Krebszellen alleine garantiert nicht den Erfolg der Behandlung. Die hoch wirksamen Tubugis, einer Klasse von Tubulysinderivaten, steigern die Wirksamkeit gegen die Krebszellen und tragen außerdem zur Überwindung einer Wirkstoffresistenz bei. Die sehr bioaktiven Wirkstoffe sind mittels eines spaltbaren Linkersystems, das hauptsächlich für die Freisetzung des aktiven Wirkstoffs aus dem Peptid-Wirkstoff-Konjugat verantwortlich ist, mit dem Peptid verbunden. Die vorliegende Dissertation befasst sich hauptsächlich mit der Herstellung von Peptid-Wirkstoff-Konjugaten, die Tubugi 1 und Tubugi 4 als Wirkstoffe beinhalten. Um diese hoch aktiven Wirkstoffe für medizinsche Zwecke nutzbar zu machen, wurde ein mehrfach spaltbares Linker-Spacer-System entwickelt, das an verschiedene Peptide gebunden werden kann.

Im Kapitel 1 wird ein allgemeiner Überblick über Stratgien des gezielten Wirkstofftransports hin zu den Krebszellen sowie über die Herausforderungen, die es bei der Entwicklung neuer Stratgien zu beachten gilt, gegeben.

Im Kapitel 2 wird die Synthese von Peptid-Wirkstoff-Konjugaten basierend auf dem gut erforschten Oktreotid und der Peptidsequenz CNGRC dargestellt. Weiterhin wird die Verbesserung der Synthese der Wirkstoffe Tubugi 1 und Tubugi 4 präsentiert. Die Entwicklung und die Synthese des Linker-Spacer-Systems, das unter den physiologischen Gegebenheiten in den Krebszellen an mehreren Sollbruchstellen gespalten werden kann, wird unter Betrachtung verschiedener Faktoren aufgeführt. Überdies werden Fluoreszenzmessungen zur Untersuchung der rezeptorvermittelten Aufnahme fluoreszierender Konjugate und Zellviabilitätsmessungen an Zellen mit unterschiedlicher Expression der jeweiligen Rezeptoren gezeigt.

In Kapitel 3 wird die Herstellung von Bombesin-Tubugi-Konjugaten beschrieben. Die Verwendung eines vereinfachten Linker-Spacer-Systems mit unpolaren Seitenketten wird neben der Verwendung des merhfach spaltbaren Linker-Spacer-System dargestellt. Im Gegensatz zu den zuvor diskutierten zyklischen Konjugaten bindet das Peptid Bombesin in seiner linearen Form an den entsprechenden Rezeptor. Die Ergebnisse der Flusszytometrie und Fluoreszenzmikroskopie werden aufgeführt. Überdies wird die biologische Evaluierung zur Untersuchung der Beziehung zwischen dem Rezeptorexpressionslevel und der Wirksamkeit der Konjugate illustriert.

Das Kapitel 4 fokussiert die Herstellung von Peptid-Wirkstoff-Konjugaten, die das neue Peptid WSC02 für den gezielten Transport der Konjugate hin zum Krebsgewebe beinhalten. Über das Peptid WSC02 ist bisher noch nicht im Zusammenhang mit einem zielgerichten Wirkstofftransport hin zu Krebszellen publiziert worden. WSC02 bindet nachweislich effizient in seiner linearen Form an die entsprechenden Rezeptoren. Die Fluoreszenzaufnahmen sowie die Zelltests werden ebenfalls diskutiert, um die Aufnahme fluoreszierender WSC02-Konjugate und die Wirksamkeit der WSC02-Tubugi-Konjugate in Abhängigkeit des Reptorexpressionslevels zu untersuchen.

Table of contents

Zusammenfassung VIII
List of abbreviations XI
1. Introduction 1
1.1. General about cancer 1
1.2. Targeted drug delivery in cancer therapy 2
1.3. Tubulysins and their derivatives tubugis 5
1.4. Crucial role of linker system 8
1.5. Aim of the study 11
1.6. References 12
2. Peptide-drug conjugates based on SSTR2- and CD13-targeting peptides 18
2.1. Introduction 18
2.1.1. Octreotide as targeting peptide 18
2.1.2. NGR sequence as targeting moiety 19
2.2. Synthetic strategy 21
2.2.1. Synthesis of tubugis 21
2.2.2. Synthesis of linker-spacer system 25
2.2.3. Synthesis of cyclic peptide-drug conjugates 27
2.2.4. Synthesis of fluorescently labeled peptide conjugates 28
2.3. Biological evaluation 30
2.3.1. Studies on cellular internalization of fluorescently labeled peptide conjugates 30
2.3.2. Evaluation of the cytotoxic activity of the peptide-drug conjugates based on SSTR2- and CD13-targeting peptides 33
2.4. Experimental part 37
2.4.1. Materials 37
2.4.2. Analytical Methods 38
2.4.3. Glutathione test 40
2.4.4. Biological Assays 40
2.4.5. General synthetic procedures 43
2.4.6. Syntheses of tubugi 1 and tubugi 4 44
2.4.7. Syntheses of linker and spacer compounds 63
2.4.8. Syntheses of peptides and conjugates 66
2.4.9. Syntheses of fluorophore conjugates 72
2.5. Conclusion 74
2.6. References 75

3. Peptide-drug conjugates based on a GRPR-targeting peptide 80
3.1. Introduction 80
3.2. Synthetic strategy 81
3.2.1. Synthesis of multiple cleavable peptide-drug conjugates 81
3.2.2. Synthesis of lipid peptide-drug conjugates 83
3.2.3. Synthesis of fluorescently labeled peptide conjugates 84
3.3. Biological evaluation 88
3.3.1. Studies on cellular internalization of fluorescently labeled peptide conjugates 88
3.3.2. Evaluation of the cytotoxic activity of the bombesin-drug conjugates 90
3.4. Experimental part 93
3.4.1. Syntheses of linker and spacer compounds 93
3.4.2. Syntheses of peptides and conjugates 96
3.4.3. Syntheses of fluorophore conjugates 104
3.5. Conclusion 110
3.6. References 111
4. Peptide-drug conjugates based on a CXCR4-targeting peptide 114
4.1. Introduction 114
4.2. Synthetic strategy 115
4.2.1. Synthesis of multiple cleavable peptide-drug conjugates 115
4.2.2. Synthesis of fluorescently-labeled peptide conjugates 116
4.3. Biological evaluation 118
4.3.1. Studies on cellular internalization of fluorescent peptide conjugates 118
4.3.2. Evaluation of the cytotoxic activity of the WSC02 peptide-drug conjugates 121
4.4. Experimental part 123
4.4.1. Syntheses of peptides and conjugates 123
4.4.2. Syntheses of fluorophore conjugates 126
4.5. Conclusion 127
4.6. References 128
Appendix I: Register of internal IPB codes of compounds XV
Appendix II: NMR spectra XVII
Appendix III: Fluorescence spectra LXXXIII
Appendix IV: Graphs and tables of IC_{50} values LXXXV

List of abbreviations

ACN	acetonitrile
ADC	antibody-drug conjugate
AMP	antimicrobial peptides
a.u.	arbitrary unit
cCNGRC	cyclo(-cysteine-asparagine-glycine-arginine-cysteine-)
CNGRC	cysteine-asparagine-glycine-arginine-cysteine
CD13	aminopeptidase N
cDNA	complementary deoxyribonucleic acid
CXCL12	C-X-C motif chemokine 12
CXCR4	C-X-C chemokine receptor type 4
DAPI	4',6-diamidino-2-phenylindole
DCC	*N*,*N'*-dicyclohexylcarbodiimide
DCM	dichloromethane
DIC	*N*,*N'*-diisopropylcarbodiimide
DIPEA	*N*,*N*-diisopropylethylamine
DMAP	*N*,*N*-dimethyl-4-aminopyridine
DMEM	Dulbecco's modified eagle medium
DMF	*N*,*N*-dimethylformamide
DMP	Dess-Martin periodinane
DMSO	dimethyl sulfoxide
DNA	deoxyribonucleic acid
DNase	deoxyribonuclease
DPBS	Dulbecco's phosphate-buffered saline
EDC	1-ethyl-3-(3-dimethylaminopropyl)carbodiimide
EDT	1,2-ethanedithiol
EDTA	ethylenediamine-*N*,*N*,*N'*,*N'*-tetraacetic acid
ELISA	enzyme-linked immunosorbent assay

EPI-X4	endogenous peptide inhibitor of CXCR4
EPR	enhanced permeability and retention (effect)
ESI MS	electrospray ionization mass spectrometry
Et_3N	triethylamine
EtOAc	ethyl acetate
EtOH	ethanol
Et_2O	diethyl ether
FACS	fluorescence activated cell sorting
FCS	fetal calf serum
FITC	fluorescein isothiocyanate
FRET	Förster resonance energy transfer
GPCR	G protein-coupled receptor
GRP	gastrin-releasing peptide
GRPR	gastrin-releasing peptide receptor
GSH	reduced glutathione
GVHD	Graft-versus-host disease
HATU	hexafluorophosphate azabenzotriazole tetramethyl uronium
HOBt	1-hydroxybenzotriazole
HPLC	high performance liquid chromatography
HRMS	high resolution mass spectrometry
HT-29	human colon cancer cell line
hTNF	human tumor necrosis factor α
IC_{50}	concentration of half maximal inhibition
Ile	L-isoleucine
MDA-MB-231	human breast cancer cell line
MDA-MB-468	human breast cancer cell line
MDR	multidrug resistance
Mep	D-*N*-methyl pipecolic acid

MeOH	methanol
MIA	*N*-methyl isatoic anhydride
MIC	microwave
mRNA	messenger ribonucleic acid
NADH	reduced nicotinamide adenine dinucleotide
NADPH	reduced nicotinamide adenine dinucleotide phosphate
NGR	asparagine-glycine-arginine
NMM	*N*-methylmorpholine
NMP	*N*-methyl-2-pyrrolidone
NMR	nuclear magnetic resonance
NPY	neuropeptide Y
PC3	human prostate cancer cell line
PDC	peptide-drug conjugate
PFA	paraformaldehyde
P-gp	P-glycoprotein
pH	potential of hydrogen
ppm	parts per million
PyBOP	benzotriazol-1-yl-oxytripyrrolidinophosphonium hexafluorophosphate
RFU	relative fluorescence unit
RGD	arginine -glycine-aspartic acid
RNA	ribonucleic acid
RNase	ribonuclease
R-PE	R-phycoerythrin
RPMI-1640	Roswell Park Memorial Institute (medium used in cell culture)
rt	room temperature
RT-qPCR	real-time quantitative polymerase chain reaction after reverse transcription
SK-N-MC	Ewing’s sarcoma cancer cell line
SPPS	solid phase peptide synthesis

SRL	somatostatin receptor ligands
SST	somatostatin
SSTR	somatostatin receptor
SSTR2	somatostatin receptor subtype 2
T-47D	human breast cancer cell line
TBDMSCl	*tert*-butyl dimethylsilylchloride
TCEP	tris(2-carboxyethyl)phosphine
TEMPO	(2,2,6,6-tetramethylpiperidin-1-yl)oxyl
TFA	trifluoroacetic acid
THF	tetrahydrofuran
TIS	triisopropyl silane
TLC	thin layer chromatography
TNF	tumor necrosis factor α
t_R	retention time
Tup	tubuphenylalanine
Tut	tubutyrosine
Tuv	tubuvalin
w/o	without
WSC02	derivative of EPI-X4

1. Introduction

1.1. General about cancer

Accompanied by the growth and aging of the global population in the last decades, the number of people suffering from cancer has increased rapidly.[1] Even in 2018, 17 millon new cases of cancer were diagnosed.[2] Roughly 9.6 million deaths globally and per year are attributed to cancer. Thus, that malignant neoplasmic disease is the second leading cause of death.[3]

The research on therapies and drugs to treat and cure cancer has got a lot of attention in last decades due to its high importance.[4-6]

Cancer describes in general a disease of rapid and uncontrolled cell growth leading to the formation of tumor tissue, angiogenesis and metastasis, including lymphomas and leukemias.[7] There are various types of cancer, e.g. lung, breast, colorectal, prostate, skin and stomach cancer. In 2018 the most cases of cancer death worldwide were attributed to lung, colorectal, stomach, liver and breast cancer. The abnormal cell proliferation progresses from genetic mutations which are partly caused intrinsically and partly by external factors: physical carcinogens (e.g. ionizing radiation), chemical carcinogens (e.g. tobacco) and biological carcinogens (e.g. viruses).[3, 8, 9] Those genetic mutations are mainly reflected in two types of genes: proto-oncogenes and tumor suppressor genes. Proto-oncogenes are normally regulated genes in healthy cells which instigate cell division and which can mutate to oncogenes being responsible for uncontrolled cell growth of cancer cells. Tumor suppressor genes represent the counterpart to oncogenes and inhibit cell division. This antiproliferative function is deactivated during tumor transformation. The fast tumor cell growth is accompanied by an altered metabolism. Thus, cancer cells cover their energy consumption to a far higher extent by anaerobic glycolysis, called Warburg effect, whereas healthy cells produce energy by mitochondrial oxidative phosphorylation. The changed metabolism leads to an acidic pH inside the tumor cells (in endosomes pH 5.0 to 6.5, in lysosomes 4.5 to 5.0) compared to normal cells which raised interest for the design of cleavable linker structures.[8, 10-15] It has also been revealed that proteases play a significant role in growth, vascularization and metastases of tumors. The tumor cells are able to invade into the surrounding tissue by local proteolysis induced by proteases. Thus, overexpression of specific enzymes, for instance the well-studied cathepsin B, is observed in cancer cells.[13, 16] Furthermore, an elevated interstitial pressure exists inside the cancer cells that correlates with the occurrence of angiogenesis, the growth of new blood vessels.[17-19]

Several different treatment techniques are in use or under development today which can generally be grouped in five categories: surgery, radiation, chemotherapy, targeted therapies, and immunotherapy.

In the past, many therapies and drugs have been developed to fight against that highly life-threatening disease. In ancient times, malignant neoplasms were surgically removed and treated with medicinal herbs. The first effective chemotherapy against cancer (in this case leukemia) was performed in 1865 by Lissauer.[20] The first clinical trial was carried out in 1942 by Goodman and Gilman using β-chlorethyl amine as cytostatic drug. In the first half of the 20th century the radiation therapy could be established as another, partly more effective technique.[21] In the last

century, manifold therapies, for instance chemotherapy,[9] immunotherapy,[22, 23] oncolytic viral therapy,[24, 25] targeted therapies,[26] have been developed and improved in order to increase the efficacy of the treatment and the survivability of the patients.[27, 28]

However, also currently used chemotherapeutics like 5-fluorouracil,[29] chlorambucil[30] or cisplatin[9] lack a specificity to tumor cells and hamper the cure of patients (Figure 1.1).

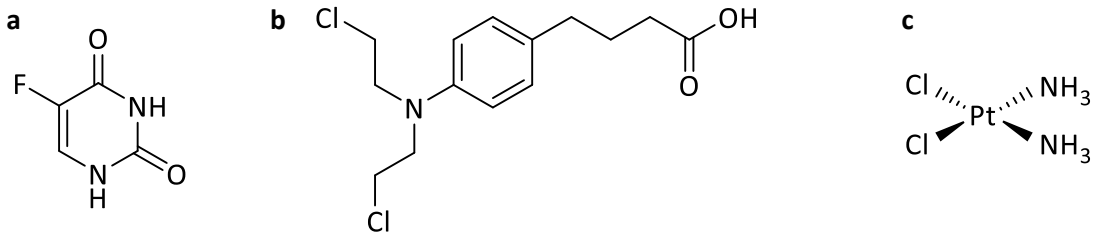

Figure 1.1 Examples of clinically applied chemotherapeutics: a) 5-fluorouracil, b) chlorambucil and c) cisplatin.

Therapeutically used drugs are usually administered intravenously and circulate through the body via the bloodstream, whereby they reach and attack rapidly dividing cells which can include, however, also some healthy cells. Moreover, those unspecific drugs hardly reach the tumor cells in high concentrations because of low vascularization of the malignant tissue. The conflict between side effect-causing toxicity from which patients suffer and noncellular resistance affords a narrow therapeutic window and reduces the efficacy of the chemotherapy.[8, 9, 29, 31-33] Another severe limitation emerges due to the multidrug resistance (MDR) of cancer cells. The P-glycoprotein (P-gp) expressed and located in the cell membrane acts as a transmembrane pump repelling xenobiotics from the cell. Some tumor cells overexpress those proteins and are capable of pumping drugs out the cell before the drug takes its effect. Especially passively penetrating drugs are easily eliminated.[8, 34, 35] Furthermore, some conventional cytostatic drugs lack bioavailability and metabolic stability. Though, the therapeutic success of antitumor drugs can be enhanced by optimized delivery and biodistribution to the diseased tissue.[11, 36-38] Therefore, the interest in drug targeting has increased tremendously in recent years. Promising carrier systems are, for example, mesoporous silica nanoparticles,[39-41] antibody-drug conjugates[42] and peptide-drug conjugates.[11]

1.2. Targeted drug delivery in cancer therapy

Nanoparticles of suitable size (Figure 1.2a), in general, passively accumulate in the malignant tissue due to the EPR (enhanced permeability and retention) effect exploiting leaky vasculature caused by fast cell growth and angiogenesis. Hence, nanoparticles open a tempting way as drug delivery systems. Nanomaterials comprise carbon dots, nanoshells, meosporous silica, metal particles in nanoscale up to lower microscale. Bioactive compounds either are bound to the nanomaterial's surface or are loaded into porous or mesoporous nanomaterials. The first clinically applied anticancer drug based on liposomal nanoparticles containing the drug doxorubicin was doxil in 1995 used to treat Kaposi's sarcoma.[41, 45-49]

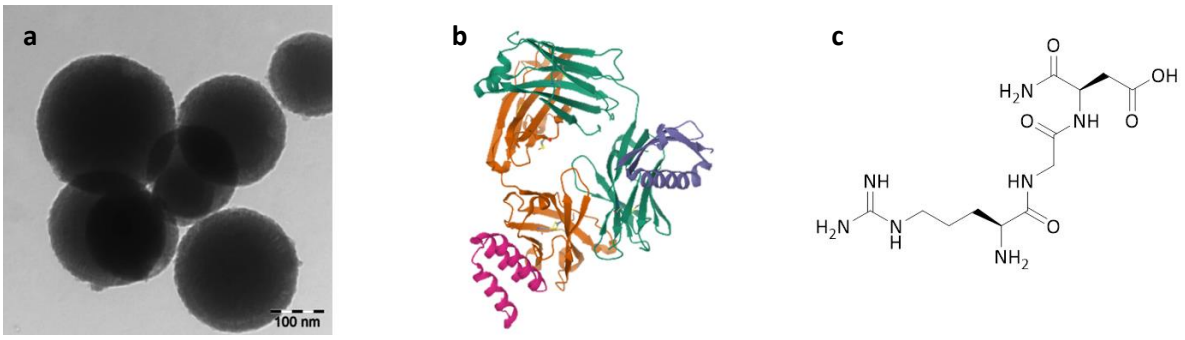

Figure 1.2 Examples of carrier systems: a) silica nanoparticles (SNM),[41] b) antibodies (trastuzumab)[43] and c) peptides (RGD).[44]

Beside passively targeting strategy, active targeting utilizes differences between cells of interest and nontargeted cells. Properties discriminating cells are the expression level of certain receptors on the cell membrane, location of the cells, metabolic as well as structural characteristics. The affinity to receptors that allows to discriminate diseased cells from heathly cells by the presence or absence of receptors on the cell membrane has become an attractive mechanism to transport highly toxic payloads to malignant cells. Antibodies (Figure 1.2b) and peptides (Figure 1.2c) are capable to work as a delivery system for active targeting of toxic compounds to overexpressed receptors appearing on the surface of cancer cells (Figure 1.3). The interaction between a carrier and its proper receptor not only forwards the efficacy by localization, but also directly affects cellular processes, interupts pathways or triggers internalization of the conjugates across the cell membrane, called receptor-mediated endocytosis, followed by quick intracellular release of the cytotoxic payload (Figure 1.4). Thus, the administration of even low doses leads to sufficient concentration in cancer cells in order to kill them on the one hand and in order to circumvent resistance on the other hand.[6, 8, 50-55]

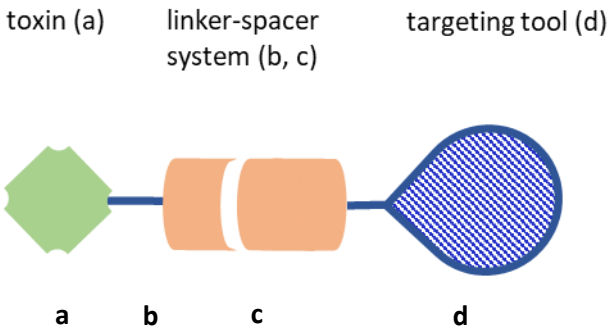

Figure 1.3 Scheme of actively targeting carrier system comprising a) the toxic compound, b) a self-immolative spacer for release of the drug, c) a cleavable linker as trigger point for release and linkage to d) the targeting tool, i.e. antibodies, peptides, vitamins *etc*.

Antibodies are large protein molecules which are involved in the immune system and disarray pathogens by recognition as well as binding to specific surface areas of pathogens, the antigens. In medicine, antibodies are used, for instance, to induce immune response. Rituximab was applied as the first therapeutic antibody for the treatment of cancer in 1997.[55] Beside their therapeutic properties, the interest in the use of antibodies for targeted delivery has increased in the last decades, because the specifity of humanized monoclonal antibodies to cells overexpressing

suitable antigens could be shown. Even in case of antibodies without therapeutic efficacy their selectivity towards tumor-specific antigens can be exploited and strengthened by conjugation to potent toxins. In addition to the selectivity, targeted delivery systems have to fulfill some prerequisites to be successful. Despite the attached payload, the selectivity of the antibody to the proper receptor has to be maintained. The targeting moiety itself as well as the ADC (antibody-drug conjugate) have to show a metabolic stability in the bloodstream. The receptor-mediated endocytosis facilitates the internalization into the targeted cell, where the ADC unrolls its impact by release of the bioactive payload.[4, 14, 56]

In 2011 brentuximab vedotin was approved as the first ADC and registered for clinical application against anaplastic large-cell lymphoma and Hodgkin's disease. The pioneer of clinically successfully tested ADC targets the receptor CD30 and contains the drug monomethyl auristatin E connected to the antibody via a protease-cleavable linker. The second ADC registered in USA and Europe is ado-trastuzumab emtansine which was approved in 2013 in order to treat breast cancer. That ADC contains a maytansine derivative which is linked to HER2 targeting trastuzumab via a protease-cleavable linker. Many other ADC are still optimized and in pre-clincal trial. Currently, about 25 ADCs for tumor treatment undergo different clinical phases, for example IMMU-130 against colorectal cancer and IMGN242 against pancreatic cancer.[36, 57]

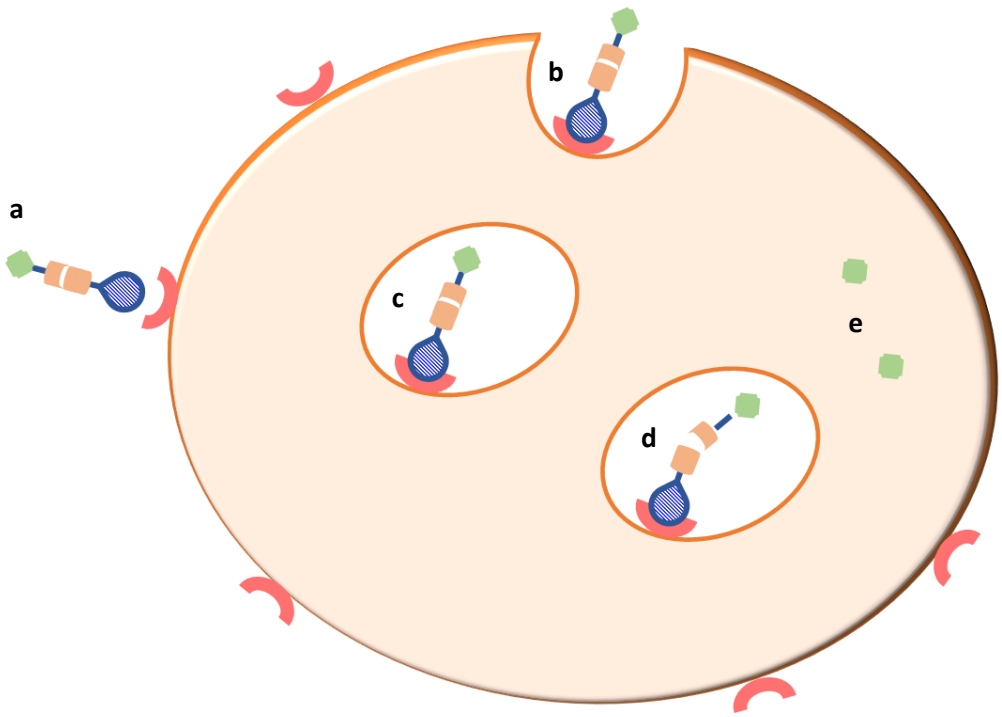

Figure 1.4 Mechanism of receptor targeting: a) recognition of specific receptor, b) receptor-mediated internalization, c) endosome, d) endosomal cleavage and e) intracellular toxin liberation.

Beside antibodies, peptides are also capable to bind selectively to receptors overexpressed in various tumors and offer further versatile possiblities in pharmaceutical research. Thus, peptides are biocompatible and can be synthesized easily as well as cost-saving in large amounts, providing

wide-ranging chemical variety. The molecular weight and the regioselectivity can be governed. Moreover, the immunogenity of peptides is lower compared to antibodies. Depending on application and kind of peptide, they can be internalized by receptor-mediated endocytosis (Figure 1.4), by passing ion channels or in case of cell penetrating cation-rich peptides due to the proton sponge effect. The challenging metabolic stability of many peptides can be circumvented by cyclization or capping which in the first case may lead to better or worse selectivity because of the constrained conformation. Since small molecules weighing up to 40 kDa are rather quickly excreted from the blood into the urine by the kidneys (renal excretion), the risk is diminished that remaining PDCs (peptide-drug conjugates) not being rapidly bound to overexpressed targets on the membrane are internalized by cells exhibiting lower expression of the respective receptors.[6, 50, 58-63]

Currently, just one PDC, ^{177}Lu-dotatat, is approved in the USA and a few other PDCs against malignant diseases passed different phases of clinical trials at the moment. ^{177}Lu-dotatat is a radiotherapeutic agent based on the peptide somatostatin and applied against gastroenteropancreatic neuroendocrine tumors. TH1902 and TH1904 are highly promising candidates in clinical trials combating breast and ovarian cancer.[36, 64]

1.3. Tubulysins and their derivatives tubugis

To increase the efficiency of drugs in general and drug conjugates particularly, it is important to link highly potent toxins to such a specific targeting tool. In nature, strongly effective compounds can be found in large numbers. Plants as well as other natural products have already been applied to cure diseases since ancient times. Considering their bioactivity and taking into account that natural products and their derivatives show higher patient acceptance than synthetic drugs, the extraction of natural products and the scientific research on their use in cancer treatment began in the 1950s. The first representative of naturally occurring compounds in clinical application displays the vinca alkaloid vinblastin, showing effective bioactivity against lymphoma and leukemia. More examples for natural chemotherapeutics are camptothecin derivatives and paclitaxel.[5, 9, 65-68]

Further natural compounds possessing exceptionally high cytotoxicity in nanomolar and even in picomolar range are tubulysins (Table 1).[69] Sasse *et al.* first isolated as well as described them as new class of cytotoxins in 2000.[70] They are found in strains of the myxobacteria *Archangium gephyra* and *Angiococcus disciformis*. Interestingly, each strain of the myxobacteria produces distinguishable tubulysin analogues. For instance, *Archangium gephyra* preferentially produces the analogues tubulyisin A, B, C, G and I. All tubulysins are tetrapeptides consisting of the peptides *N*-methyl pipecolic acid (Mep), L-isoleucine (Ile) and also two uncommon amino acids, tubuvaline (Tuv) and, depending on the analogue, tubutyrosine (Tut, R^3 = OH) or tubuphenylalanine (Tup, R^3 = H) (Figure 1.5). A further characteristic feature of this compound class represents the labile *N*,*O*-acetal close to the Tuv part prolonged by *O*-acylated fatty acids.[71, 72] Tubulysins were shown to possess antimitotic, proapoptotic, antiproliferative, antiangiogenic capability and to be able to overcome MDR.[35, 69] Elucidating their bioactivity it was found that tubulysins act like vinca alkaloids, but exceeding their impact 20 to 1000 fold. That means, they strongly bind to the so

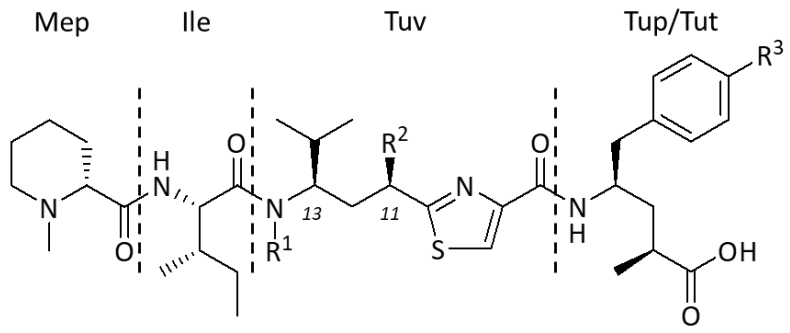

Figure 1.5 General structure of selection of tubulysin derivatives.[76, 82]

Table 1 Natural and artificial tubulysin derivatives and their bioactivities against several human cancer cell lines.[76, 78, 79, 82]

Tubulysin	R^1	R^2	R^3	IC_{50} [nM]
A	$CH_2OC(O)CH_2CH(CH_3)_2$	OAc	OH	0.08–1.16
B	$CH_2OC(O)CH_2CH_2CH_3$	OAc	OH	0.11–2.77
C	$CH_2OC(O)CH_2CH_3$	OAc	OH	0.37–4.90
D	$CH_2OC(O)CH_2CH(CH_3)_2$	OAc	H	0.01–0.30
E	$CH_2OC(O)CH_2CH_2CH_3$	OAc	H	0.02–0.31
F	$CH_2OC(O)CH_2CH_3$	OAc	H	0.02–0.44
G	$CH_2OC(O)CH{=}C(CH_3)_2$	OAc	OH	0.11–3.44
H	$CH_2OC(O)CH_3$	OAc	H	0.04–1.65
I	$CH_2OC(O)CH_3$	OAc	OH	0.85–8.48
U	H	OAc	H	1.96
V	H	H	H	1086.47
W	$CH_2OC(O)CH_2CH_2CH_3$	OAc	OH	-
X	H	OAc	OH	-
Z	H	H	OH	-

called vinca domain which is the α/β contact surface of the tubulin heterodimer. Tubulin is composed of the two subunits α- and β-tubulin which polymerize to the noncovalent heterodimer tubulin. Due to that binding to the vinca domain, the polymerization of the tubulin is interrupted, while depolymerization of microtubules is induced at the same time. The continous alternation of polymerization and depolymerization results in high dynamics. These tubulin heterodimers build up microtubules which are dynamic as well as tubular biopolymers. Beside actin filaments and

intermediate filaments, microtubules shape the cytoskeleton of eukaryotic cells. Microtubules are involved in cell mitosis, because they support the formation of the mitotic spindle apparatus which is responsible for the transport of the replicated chromosomes to the daugther cells. Thus, microtubules play a crucial role in the proliferation as well as migration of cancer cells and are revealed to be a proper target for therapeutic treatment of cancer. Beside tubulysins, paclitaxel and vinblastin represent anticancer drugs that target and affect microtubules by stabilization or destabilzation.[35, 69, 71-75]

An other reason for the tremendous antiproliferative efficacy of tubulysins compared to other bioactive compounds is their capability to overcome MDR. Tubulysins are shown to be no substrate for up-regulated membrane P-gp pumps and remain inside the cells after uptake.[35]

Investigations on tubulysins for the development of highly promising anticancer agents were limited by low availability from the slow growing strains of myxobacteria.[76] For that reason, many groups have searched for synthetic approaches to obtain naturally occurring tubulysin analogues or synthesize novel derivatives.[76-81]

The antiproliferative effectivity differs within the palette of tubulysin analogues which is attributed to different structural features. Considering of lipophilicity in relation to cytotoxicity and also the replacement of structural moieties eludicated which moieties strengthened the bioactivity of tubulysins.[71, 82] The tertiary amine as well as the *R*-configuration of the Mep group was shown to be necessary for the bioiactivity.[83] The impact to inhibit the polymerization of the tubulin can be attributed to the lipophilic side chain at the Tuv group. The derivative tubulysin D shows the strongest lipophilicity and also the lowest IC_{50} value compared to the other derivatives.[71] The isopropyl group at C13 of Tuv seems to be very important for the bioactivity (see in Figure 1.5). In contrast to that, the acetyl group at C11 can be replaced by certain other moieties, but deacetylation leads to significant loss of cytotoxic potency (see in Figure 1.5). Moreover, the natural configuration at both positions (11*R*,13*S*) need to be maintained for bioactivity.[77, 84] Comparing the natural variations containing Tut or Tup, the tubulysin analogues with Tup exhibit a stronger activity than those with Tut.[71] Esterification of *C*-terminus drops the activity which might be interesting for the development of less active prodrugs.[82, 85] The C11-acetoxy moiety in the Tuv component is responsible for binding to the tubulin. The loss of the acetate group leads to > 100-fold less potency of the tubulysin which might be a risk considering the circulation of drugs *in vivo* for many days as well as the esterase-mediated deacetylation. The oxygene of the acetate group does not interact with tubulin, but the methyl group of the acetate goes suitably into the hydrophobic pocket. Thus, the stabilzation of the tubuylsin by introduction of ether at position C11 results in comparable bioactivity *in vitro* and was shown to improve the efficacy *in vivo*.[53, 73, 86-88]

Pando *et al.* from the Wessjohann research group published the synthesis of tubugis, a novel class of highly potent tubulysin analogues, via UGI multicomponent reaction in 2009. Tubugis embrace beneficial structural elements of the most active tubulysin derivative, tubulysin D, and replacement of the labile as well as synthetically challenging *N*,*O*-acetal-ester motive (orange group in Figure 1.6a) by an *N*-alkyl amide moiety (green group in Figure 1.6b). The improvement of stability against basic and acidic as well as enzymatic conditions supports the toxicity to cells considering lower pH value inside the cells, particularly in the endosomes. Tubugi 1 (Figure 1.6b) shows the highest activity against cancer cells *in vitro* in picomolar range and was shown to induce uncommon apoptosis comprising fragmentation of DNA and the formation of apoptotic bodies. In

general, apoptosis represents a form of controlled cell death resulting in efferocytosis by which death cells are removed quickly. A recently published study elucidated that tubugi 1 induces an irregular apoptosis independent from phosphatidylserine that signals to macrophages and triggers efferocytosis.[71, 80, 89, 90]

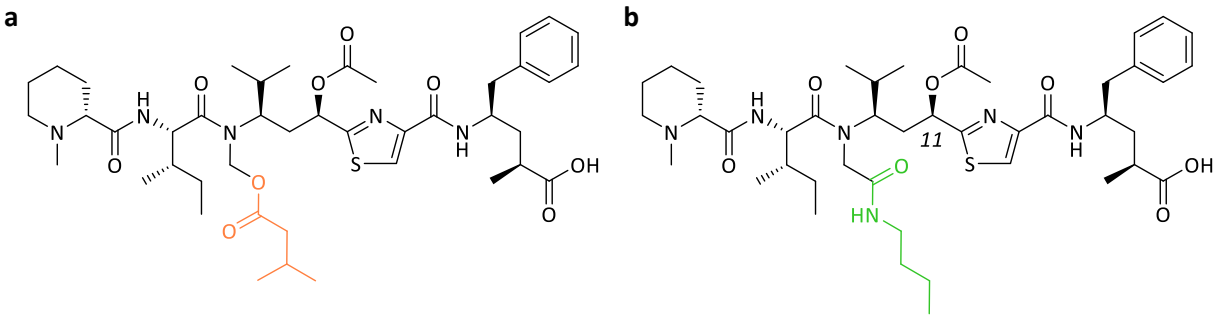

Figure 1.6 Comparison of structural features of a) tubulysin D and b) tubugi 1.

Due to the high toxicity, tubulysin analogues and derivatives have been exploited for the synthesis of targeting conjugates. Beside the increased impact by drug targeting, the tubulysins and particularly the tubugis are masked during the circulation in the blood stream.[82] The first tubulysin conjugate was reported in 2008 by Vlahov *et al.* presenting conjugates which contain tubulysin A and B as drug and folate as a targeting tool.[51] Preclinical trials on this conjugate, named EC1456, against folate receptor positive tumors point to clinical trials in future. Another folate based tubulysin conjugate, called EC0531, was tested in a phase I/II clinical trial in dogs. Because of promising results, it has been suggested that further studies could be performed in human.[91, 92] Beside the folate motive, further strategies have been developed to target cancer cells specifically. Thus, tubulysins have been linked to a linear, h-cyclodextrin-based polymer, dendrimers and several antibodies. Recently, first studies on a tubugi-NPY (neuropeptide Y) conjugate were published pointing to a synthetic approach for this work.[86, 87, 93-98]

1.4. Crucial role of linker system

Although the targeting tool and the toxic payload exhibit high importance for the success of selective treatment of cancer cells, a key role devolves to the linker system which facilitates the release of the potent drug from toxin-masking conjugates. The idea behind masking the toxins is to protect healthy cells from the high bioactivity of drugs during their blood circulation.[98]

In general, drug conjugates consist of the toxic compound, the targeting moiety and the tethering linker system. The design of the linker system requires to consider extra- and intracellular conditions for selective cleavage inside the cancer cells. Moreover, the influence of the linker system to binding affinity of the targeting tool as well as to the activity of the drug needs to be limited. In general, receptor-mediated internalization of drug conjugates supports several cleavage meachnisms shown below (Scheme 1.1).[8, 50, 63]

Many linker compounds have been studied concerning their stability in intracellular environment. As already mentioned, the pH value in tumor cells ranges from 4.0 to 6.5, whereas pH value in blood and healthy cells is between 7.3 and 7.5. This difference between pH values of tumor and

normal tissue suffices to keep or to cleave an acid-sensitive compound. Consequently, linkers containing acetals, esters (Scheme 1.1a) or hydrazones (Scheme 1.1b) offer sufficient stability under physiological conditions in the blood circulation, but are degraded at acidic pH.[14, 63, 86, 99-101]

It was revealed that the redox potential across the plasma membrane of most eukaryotic cells differs significantly. An excess of natural antioxidants like reduced glutathione (GSH), thioredoxin and nicotinamide adenine dinucleotides (NADH and NADPH) cause reducing properties of cells. As a consequence, reduction sensitive moieties that remain thermodynamically stable in plasma, for instance disulfides (Scheme 1.1c) and azo compounds (Scheme 1.1d), have been widely used. The main focus points to glutathione, since it exists in mM-range in cells, typically in cancer cells, compared to concentrations at µM-level in blood plasma. Indeed, disulfide bridges are susceptible to thiol–disulfide exchange which can be problematic in extracellular space of tumor tissue. However, the risk of reduction in extracellular space can be overcome by sterical hinderance by introducing substituents close to the sulfhydryl group.[36, 100, 102-108]

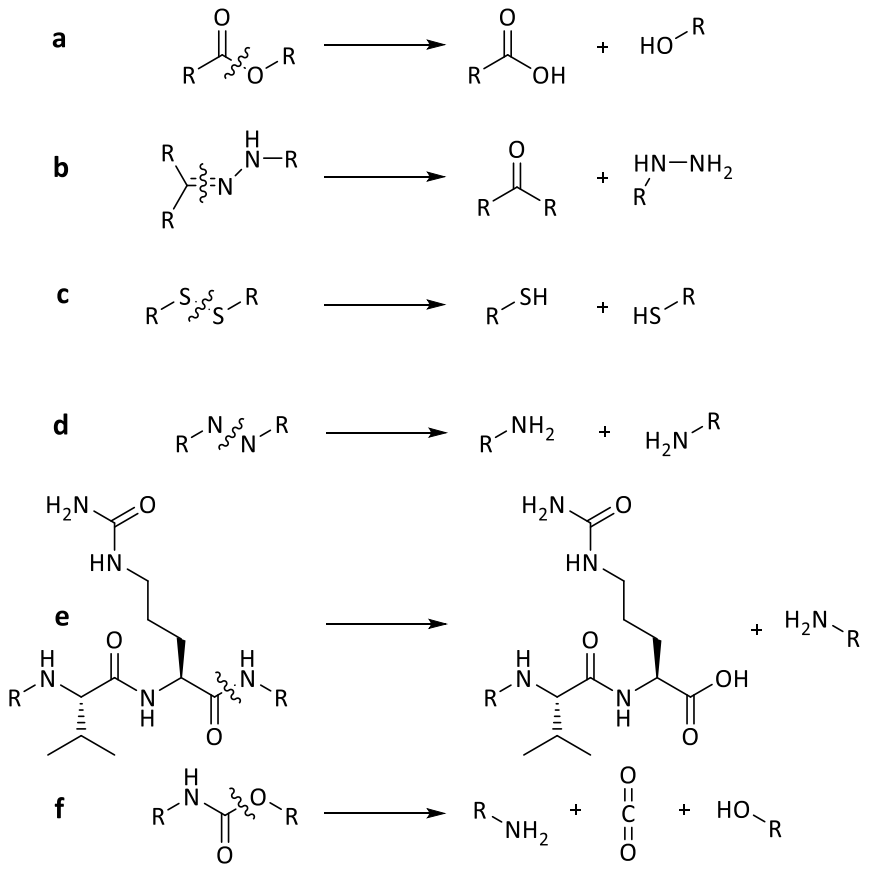

Scheme 1.1 Examples of linker technologies - acid-labile linkers: a) ester, b) hydrazone, reduction-sensitive linkers: c) disulfide, d) azo, enzymatically cleavable linkers: e) Val-Cit, f) carbamate.[100]

Furthermore, the prescence of enzymes specifically occurring in cancer cells has been shown to be helpful for cleavage of chemical entities like amides (Scheme 1.1e) and ester bonds or carbamates (Scheme 1.1f). Esterases are able to crack esters and cytochrome P450 selectively fissures carbamates, but both, esters and carbamates, leak sufficient stability in the blood. In contrast, amides exhibit higher stability in blood plasma, because the activity of the respective hydrolases is suppressed by inhibitors in the blood plasma.[100] Moreover, some proteases involved in cancer development and growth, like cathepsin B, are overexpressed in prostate, breast, colon, lung and

gastric tumors. Well known and frequently applied peptide sequences, e.g. Phe-Lys, Gly-Phe-Leu-Gly and Val-Cit (Scheme 1.1e), are preferentially degraded by lyosomal cathepsin B.[16, 36, 63, 100, 109] Many studies have been done on their stability *in vivo* and their selective scission properties under specific enzymatic conditions.[110, 111]

All linker compounds attached to the bioactive component drop the efficacy of the drug and might lead to complications in pharmacokinetics. However, this drawback can be circumvented by choice of molecules that release the drug traceless after cleavage or that can be released by a self-immolvative mechanism. Mostly self-immolative spacers are introduced in order to liberate the active form of the drug. They are divided by the reaction mechanism into elimination-based (Scheme 1.2a) and cyclization-based spacers (Scheme 1.2b–d). The widely used para-aminobenzyl (PAB) spacer is tracelessly degraded via an 1,6-elimination initiated by the scission of the linker at the anilin moiety (Scheme 1.2a). The self-immolation process based on cyclization is often associated with disulfide bridges (Scheme 1.2d). In combination with an ester bond close to the disulfide, the free thiol nucleophile arising by reduction of the disulfide bridge attackes the ester bond followed by an intramolecular cyclization.[36, 63, 100, 110-114]

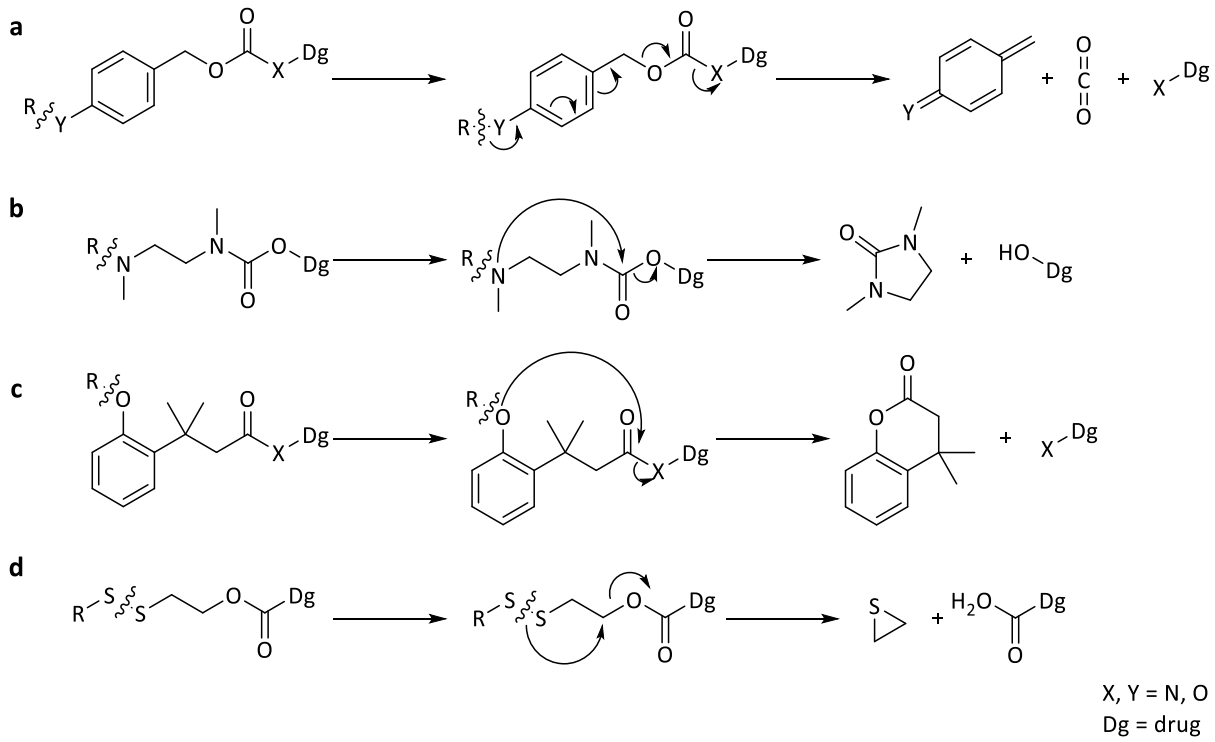

Scheme 1.2 Cleavage mechanism of self-immolative spacers: a) 1,6-benzyl elimination, b) cyclization, c) cyclization (lactonization), d) thio-assisted cyclization.[99, 100]

1.5. Aim of the study

There is an enormous importance and interest on targeting of anticancer drugs to tumor tissue as elucidated in chapter 1.2. Thus, the herein presented PhD project is focused on the synthesis of peptide-drug conjugates including tubugis as toxin and on the biological evaluation of the peptide-drug conjugates.

In order to gain the overall aim following objectives need to be fulfilled:

- the synthesis of a novel linker-spacer system respecting metabolic stability on the one hand and selective cleavage inside the cancer cells;

- the synthesis of peptide-drug conjugates involving established as well as promising peptides as targeting tool and tubugi derivatives as toxic agents;

- the synthesis of fluorescently labeled conjugates in order to gain deeper understanding of internalization by bioimaging;

- the investigation of efficacy of the conjugates depending on the expression level of respective targets.

1.6. References

1. American Cancer Society, Global Cancer Facts & Figures, https://www.cancer.org/research/cancer-facts-statistics/global.html. (accessed 08.04.2020).
2. Cancer Research UK, https://www.cancerresearchuk.org/health-professional/cancer-statistics/worldwide-cancer. (accessed 18.03.2020).
3. World Health Organization, Cancer - Key facts, https://www.who.int/news-room/fact-sheets/detail/cancer. (accessed 18.03.2020).
4. Johnson, J. R.; Ford, C. H.; Newman, C. E.; Woodhouse, C. S.; Rowland, G. F.; Simmonds, R. G., A vindesine-anti-CEA conjugate cytotoxic for human cancer cells in vitro. *Br J Cancer* **1981,** *44* (3), 472-5.
5. Liebmann, J. E.; Cook, J. A.; Lipschultz, C.; Teague, D.; Fisher, J.; Mitchell, J. B., Cytotoxic studies of paclitaxel (Taxol) in human tumour cell lines. *Br J Cancer* **1993,** *68* (6), 1104-9.
6. Lu, R. M.; Chen, M. S.; Chang, D. K.; Chiu, C. Y.; Lin, W. C.; Yan, S. L.; Wang, Y. P.; Kuo, Y. S.; Yeh, C. Y.; Lo, A.; Wu, H. C., Targeted drug delivery systems mediated by a novel Peptide in breast cancer therapy and imaging. *PLoS One* **2013,** *8* (6), e66128.
7. Zentrum für Krebsregisterdaten, Krebsarten, https://www.krebsdaten.de/Krebs/DE/Content/Krebsarten/Krebs_gesamt/krebs_gesamt_node.html. (accessed 13.01.2021).
8. Kakde, D.; Jain, D.; Shrivastava, V.; Kakde, R.; Patil, A. T., Cancer Therapeutics-Opportunities, Challenges and Advances in Drug Delivery. *J Appl Pharm Sci* **2011,** *1* (9), 1-10.
9. Corrie, P. G., Cytotoxic chemotherapy: clinical aspects. *Medicine* **2011,** *39* (12), 717-722.
10. Swietach, P.; Vaughan-Jones, R. D.; Harris, A. L.; Hulikova, A., The chemistry, physiology and pathology of pH in cancer. *Philos Trans R Soc Lond B Biol Sci* **2014,** *369* (1638), 20130099.
11. Vrettos, E. I.; Mezo, G.; Tzakos, A. G., On the design principles of peptide-drug conjugates for targeted drug delivery to the malignant tumor site. *Beilstein J Org Chem* **2018,** *14*, 930-954.
12. Galluzzi, L.; Kepp, O.; Vander Heiden, M. G.; Kroemer, G., Metabolic targets for cancer therapy. *Nat Rev Drug Discov* **2013,** *12* (11), 829-46.
13. DeBerardinis, R. J.; Chandel, N. S., Fundamentals of cancer metabolism. *Sci Adv* **2016,** *2* (5), e1600200.
14. Ducry, L.; Stump, B., Antibody-drug conjugates: linking cytotoxic payloads to monoclonal antibodies. *Bioconjug Chem* **2010,** *21* (1), 5-13.
15. Kato, Y.; Ozawa, S.; Miyamoto, C.; Maehata, Y.; Suzuki, A.; Maeda, T.; Baba, Y., Acidic extracellular microenvironment and cancer. *Cancer Cell Int* **2013,** *13* (1), 89.
16. Koblinski, J. E.; Ahram, M.; Sloane, B. F., Unraveling the role of proteases in cancer. *Clin Chim Acta* **2000,** *291*, 113–135.
17. Risau, W., Mechanisms of angiogenesis. *Nature* **1997,** *386* (6626), 671-4.
18. Zetter, B. R., Angiogenesis and tumor metastasis. *Annu Rev Med* **1998,** *49*, 407-24.
19. Nathan, S. S.; Huvos, A. G.; Casas-Ganem, J. E.; Yang, R.; Linkov, I.; Sowers, R.; DiResta, G. R.; Gorlick, R.; Healey, J. H., Tumor interstitial fluid pressure may regulate angiogenic factors in osteosarcoma. *J Orthop Res* **2008,** *26* (11), 1520-5.
20. Lissauer, A., Zwei Fälle von Leucaemie. *Berl Klin Wochenschr* **1865,** *2*, 403–404.
21. Kaplan, H. S., Historic milestones in radiobiology and radiation therapy. *Semin Oncol* **1979,** *6* (4), 479-89.
22. Subudhi, S. K.; Vence, L.; Zhao, H.; Blando, J.; Yadav, S. S.; Xiong, Q.; Reuben, A.; Aparicio, A.; Corn, P. G.; Chapin, B. F.; Pisters, L. L.; Troncoso, P.; Tidwell, R. S.; Thall, P.; Wu, C. J.; Zhang, J.; Logothetis, C. L.; Futreal, A.; Allison, J. P.; Sharma, P., Neoantigen

responses, immune correlates, and favorable outcomes after ipilimumab treatment of patients with prostate cancer. *Sci Transl Med* **2020,** *12* (537).
23. Yang, Y., Cancer immunotherapy: harnessing the immune system to battle cancer. *J Clin Invest* **2015,** *125* (9), 3335-7.
24. Smith, T. T.; Roth, J. C.; Friedman, G. K.; Gillespie, G. Y., Oncolytic viral therapy: targeting cancer stem cells. *Oncolytic Virother* **2014,** *2014* (3), 21-33.
25. Meerani, S.; Yao, Y., Oncolytic Viruses in Cancer Therapy. *EJSR* **2010,** *40* (1), 156 -171.
26. Gerber, D. E., Targeted Therapies: A New Generation of Cancer Treatments. *AFP* **2008,** *77* (3), 311-319.
27. Feng, S.-S.; Chien, S., Chemotherapeutic engineering: Application and further development of chemical engineering principles for chemotherapy of cancer and other diseases. *Chem Eng Sci* **1997,** *58* (18), 4087-4114.
28. Papac, R. J., Origins of cancer therapy. *Yale J Biol Med* **2001,** *74* (6), 391-8.
29. Focaccetti, C.; Bruno, A.; Magnani, E.; Bartolini, D.; Principi, E.; Dallaglio, K.; Bucci, E. O.; Finzi, G.; Sessa, F.; Noonan, D. M.; Albini, A., Effects of 5-fluorouracil on morphology, cell cycle, proliferation, apoptosis, autophagy and ROS production in endothelial cells and cardiomyocytes. *PLoS One* **2015,** *10* (2), e0115686.
30. Nussbaumer, S.; Bonnabry, P.; Veuthey, J. L.; Fleury-Souverain, S., Analysis of anticancer drugs: a review. *Talanta* **2011,** *85* (5), 2265-89.
31. Schally, A. V.; Nagy, A., Cancer chemotherapy based on targeting of cytotoxic peptide conjugates to their receptors on tumors. *Eur J Endocrinol* **1999,** *141* (1), 1-14.
32. Okarvi, S. M., Peptide-based radiopharmaceuticals and cytotoxic conjugates: potential tools against cancer. *Cancer Treat Rev* **2008,** *34* (1), 13-26.
33. Links, M.; Brown, R., Clinical relevance of the molecular mechanisms of resistance to anti-cancer drugs. *Expert Rev Mol Med* **1999,** *1999*, 1-21.
34. Ling, V., Multidrug resistance: molecular mechanisms and clinical relevance. *Cancer Chemother Pharmacol* **1997,** *40 Suppl*, S3-8.
35. Kaur, G.; Hollingshead, M.; Holbeck, S.; Schauer-Vukasinović, V.; Camalier, R. F.; Dömling, A.; Agarwal, S., Biological evaluation of tubulysin A: a potential anticancer and antiangiogenic natural product. *Biochem J* **2006,** *396* (2), 235-42.
36. Vhora, I.; Patil, S.; Bhatt, P.; Misra, A., Protein- and Peptide-drug conjugates: an emerging drug delivery technology. *Adv Protein Chem Struct Biol* **2015,** *98*, 1-55.
37. Stuurman, F. E.; Nuijen, B.; Beijnen, J. H.; Schellens, J. H., Oral anticancer drugs: mechanisms of low bioavailability and strategies for improvement. *Clin Pharmacokinet* **2013,** *52* (6), 399-414.
38. Maiti, S.; Sen, K. K., *Bio-targets and drug delivery approaches*. **2017**.
39. Perez-Quintanilla, D.; Gomez-Ruiz, S.; Zizak, Z.; Sierra, I.; Prashar, S.; del Hierro, I.; Fajardo, M.; Juranić, Z. D.; Kaluđerović, G. N., A new generation of anticancer drugs: mesoporous materials modified with titanocene complexes. *Chemistry* **2009,** *15* (22), 5588-97.
40. Bulatović, M. Z.; Maksimović-Ivanić, D.; Bensing, C.; Gomez-Ruiz, S.; Steinborn, D.; Schmidt, H.; Mojić, M.; Korac, A.; Golić, I.; Perez-Quintanilla, D.; Momcilović, M.; Mijatović, S.; Kaluđerović, G. N., Organotin(IV)-loaded mesoporous silica as a biocompatible strategy in cancer treatment. *Angew Chem Int Ed Engl* **2014,** *53* (23), 5982-7.
41. Jänicke, P.; Lennicke, C.; Meister, A.; Seliger, B.; Wessjohann, L. A.; Kaluđerović, G. N., Fluorescent spherical mesoporous silica nanoparticles loaded with emodin: Synthesis, cellular uptake and anticancer activity. *Mater Sci Eng C* **2021,** *119*.
42. Tsuchikama, K.; An, Z., Antibody-drug conjugates: recent advances in conjugation and linker chemistries. *Protein Cell* **2018,** *9* (1), 33-46.
43. King, J. D.; Ma, Y.; Kuo, Y. C.; Bzymek, K. P.; Goodstein, L. H.; Meyer, K.; Moore, R. E.; Crow, D.; Colcher, D. M.; Singh, G.; Horne, D. A.; Williams, J. C., Template-Catalyzed,

Disulfide Conjugation of Monoclonal Antibodies Using a Natural Amino Acid Tag. *Bioconjug Chem* **2018,** *29* (6), 2074-2081.

44. Arap, W.; Pasqualini, R.; Ruoslahti, E., Cancer treatment by targeted drug delivery to tumor vasculature in a mouse model. *Science* **1998,** *279* (5349), 377-80.
45. Fu, B.; Dang, M.; Tao, J.; Li, Y.; Tang, Y., Mesoporous platinum nanoparticle-based nanoplatforms for combined chemo-photothermal breast cancer therapy. *J Colloid Interface Sci* **2020,** *570*, 197-204.
46. Cordani, M.; Somoza, A., Targeting autophagy using metallic nanoparticles: a promising strategy for cancer treatment. *Cell Mol Life Sci* **2019,** *76* (7), 1215-1242.
47. Davis, M. E.; Chen, Z. G.; Shin, D. M., Nanoparticle therapeutics: an emerging treatment modality for cancer. *Nat Rev Drug Discov* **2008,** *7* (9), 771-82.
48. Wolfram, J.; Ferrari, M., Clinical Cancer Nanomedicine. *Nano Today* **2019,** *25*, 85-98.
49. Bayda, S.; Adeel, M.; Tuccinardi, T.; Cordani, M.; Rizzolio, F., The History of Nanoscience and Nanotechnology: From Chemical-Physical Applications to Nanomedicine. *Molecules* **2019,** *25* (1).
50. Majumdar, S.; Siahaan, T. J., Peptide-mediated targeted drug delivery. *Med Res Rev* **2012,** *32* (3), 637-58.
51. Vlahov, I. R.; Wang, Y.; Kleindl, P. J.; Leamon, C. P., Design and regioselective synthesis of a new generation of targeted chemotherapeutics. Part II: Folic acid conjugates of tubulysins and their hydrazides. *Bioorg Med Chem Lett* **2008,** *18* (16), 4558-61.
52. Vlahov, I. R.; Santhapuram, H. K.; Kleindl, P. J.; Howard, S. J.; Stanford, K. M.; Leamon, C. P., Design and regioselective synthesis of a new generation of targeted chemotherapeutics. Part 1: EC145, a folic acid conjugate of desacetylvinblastine monohydrazide. *Bioorg Med Chem Lett* **2006,** *16* (19), 5093-6.
53. Leverett, C. A.; Sukuru, S. C.; Vetelino, B. C.; Musto, S.; Parris, K.; Pandit, J.; Loganzo, F.; Varghese, A. H.; Bai, G.; Liu, B.; Liu, D.; Hudson, S.; Doppalapudi, V. R.; Stock, J.; O'Donnell, C. J.; Subramanyam, C., Design, Synthesis, and Cytotoxic Evaluation of Novel Tubulysin Analogues as ADC Payloads. *ACS Med Chem Lett* **2016,** *7* (11), 999-1004.
54. Burke, P. J.; Hamilton, J. Z.; Pires, T. A.; Setter, J. R.; Hunter, J. H.; Cochran, J. H.; Waight, A. B.; Gordon, K. A.; Toki, B. E.; Emmerton, K. K.; Zeng, W.; Stone, I. J.; Senter, P. D.; Lyon, R. P.; Jeffrey, S. C., Development of Novel Quaternary Ammonium Linkers for Antibody-Drug Conjugates. *Mol Cancer Ther* **2016,** *15* (5), 938-45.
55. Schrama, D.; Reisfeld, R. A.; Becker, J. C., Antibody targeted drugs as cancer therapeutics. *Nat Rev Drug Discov* **2006,** *5* (2), 147-59.
56. Jain, N.; Smith, S. W.; Ghone, S.; Tomczuk, B., Current ADC Linker Chemistry. *Pharm Res* **2015,** *32* (11), 3526-40.
57. Thomas, A.; Teicher, B. A.; Hassan, R., Antibody-drug conjugates for cancer therapy. *Lancet Oncol* **2016,** *17* (6), e254-e262.
58. Peraro, L.; Kritzer, J. A., Emerging Methods and Design Principles for Cell-Penetrant Peptides. *Angew Chem Int Ed Engl* **2018,** *57* (37), 11868-11881.
59. Zhang, X. X.; Eden, H. S.; Chen, X., Peptides in cancer nanomedicine: drug carriers, targeting ligands and protease substrates. *J Control Release* **2012,** *159* (1), 2-13.
60. Choi, H.; Jeena, M. T.; Palanikumar, L.; Jeong, Y.; Park, S.; Lee, E.; Ryu, J. H., The HA-incorporated nanostructure of a peptide-drug amphiphile for targeted anticancer drug delivery. *Chem Commun (Camb)* **2016,** *52* (32), 5637-40.
61. Fosgerau, K.; Hoffmann, T., Peptide therapeutics: current status and future directions. *Drug Discov Today* **2015,** *20* (1), 122-8.
62. Vives, E.; Schmidt, J.; Pelegrin, A., Cell-penetrating and cell-targeting peptides in drug delivery. *Biochim Biophys Acta* **2008,** *1786* (2), 126-38.
63. Srinivasarao, M.; Galliford, C. V.; Low, P. S., Principles in the design of ligand-targeted cancer therapeutics and imaging agents. *Nat Rev Drug Discov* **2015,** *14* (3), 203-19.

64. Cooper, B. M.; Iegre, J.; DH, O. D.; Olwegard Halvarsson, M.; Spring, D. R., Peptides as a platform for targeted therapeutics for cancer: peptide-drug conjugates (PDCs). *Chem Soc Rev* **2020**.
65. Prakash, O.; Kumar, A.; Kumar, P.; Ajeet, A., Anticancer Potential of Plants and Natural Products: A Review. *Am J Pharmacol Sci* **2013,** *1* (6), 104-115.
66. Jänicke, P.; ad. Wessjohann, L. A. Mesoporous silica nanoparticles grafted with plant natural products and extracts. Master thesis, Martin Luther University of Halle-Wittenberg, **2016**.
67. Cragg, G. M.; Newman, D. J., Plants as a source of anti-cancer agents. *J Ethnopharmacol* **2005,** *100* (1-2), 72-9.
68. Hamilton, G.; Olszewski, U.; Klameth, L.; Ulsperger, E.; Geissler, K., Synergistic Anticancer Activity of Topotecan— Cyclin-Dependent Kinase Inhibitor Combinations against Drug-Resistant Small Cell Lung Cancer (SCLC) Cell Lines. *J Cancer Ther* **2013,** *4*, 47-53.
69. Khalil, M. W.; Sasse, F.; Lunsdorf, H.; Elnakady, Y. A.; Reichenbach, H., Mechanism of action of tubulysin, an antimitotic peptide from myxobacteria. *Chembiochem* **2006,** *7* (4), 678-83.
70. Sasse, F.; Steinmetz, H.; Heil, J.; Höfle, G.; Reichenbach, H., Tubulysins, new cytostatic peptides from myxobacteria acting on microtubuli. Production, isolation, physico-chemical and biological properties. *J Antibiot (Tokyo)* **2000,** *53* (9), 879-85.
71. Steinmetz, H.; Glaser, N.; Herdtweck, E.; Sasse, F.; Reichenbach, H.; Höfle, G., Isolation, crystal and solution structure determination, and biosynthesis of tubulysins--powerful inhibitors of tubulin polymerization from myxobacteria. *Angew Chem Int Ed Engl* **2004,** *43* (37), 4888-92.
72. Höfle, G.; Glaser, N.; Leibold, T.; Karama, U.; Sasse, F.; Steinmetz, H., Semisynthesis and degradation of the tubulin inhibitors epothilone and tubulysin. *Pure Appl Chem* **2003,** *75* (2-3), 167–178.
73. Wang, Y.; Benz, F. W.; Wu, Y.; Wang, Q.; Chen, Y.; Chen, X.; Li, H.; Zhang, Y.; Zhang, R.; Yang, J., Structural Insights into the Pharmacophore of Vinca Domain Inhibitors of Microtubules. *Mol Pharmacol* **2016,** *89* (2), 233-42.
74. Jordan, M. A., Mechanism of Action of Antitumor Drugs that Interact with Microtubules and Tubulin. *Curr Med Chem* **2002,** *2*, 1-17.
75. Zhou, J.; Giannakakou, P., Targeting microtubules for cancer chemotherapy. *Curr Med Chem Anticancer Agents* **2005,** *5* (1), 65-71.
76. Dömling, A.; Beck, B.; Eichelberger, U.; Sakamuri, S.; Menon, S.; Chen, Q. Z.; Lu, Y.; Wessjohann, L. A., Total synthesis of tubulysin U and V. *Angew Chem Int Ed Engl* **2006,** *45* (43), 7235-9.
77. Shibue, T.; Hirai, T.; Okamoto, I.; Morita, N.; Masu, H.; Azumaya, I.; Tamura, O., Total syntheses of tubulysins. *Chemistry* **2010,** *16* (38), 11678-88.
78. Peltier, H. M.; McMahon, J. P.; Patterson, A. W.; Ellman, J. A., The total synthesis of tubulysin D. *J Am Chem Soc* **2006,** *128* (50), 16018-9.
79. Pando, O.; Dörner, S.; Preusentanz, R.; Denkert, A.; Porzel, A.; Richter, W.; Wessjohann, L., First total synthesis of tubulysin B. *Org Lett* **2009,** *11* (24), 5567-9.
80. Pando, O.; Stark, S.; Denkert, A.; Porzel, A.; Preusentanz, R.; Wessjohann, L. A., The multiple multicomponent approach to natural product mimics: tubugis, N-substituted anticancer peptides with picomolar activity. *J Am Chem Soc* **2011,** *133* (20), 7692-5.
81. Barreto, A. F. S.; Andrade, C. K. Z., Synthesis of (macro)heterocycles by consecutive/repetitive isocyanide-based multicomponent reactions. *Beilstein J Org Chem* **2019,** *15*, 906-930.
82. Colombo, R.; Wang, Z.; Han, J.; Balachandran, R.; Daghestani, H. N.; Camarco, D. P.; Vogt, A.; Day, B. W.; Mendel, D.; Wipf, P., Total Synthesis and Biological Evaluation of Tubulysin Analogues. *J Org Chem* **2016,** *81* (21), 10302-10320.

83. Shankar, P. S.; Bigotti, S.; Lazzari, P.; Manca, I.; Spiga, M.; Sani, M.; Zanda, M., Synthesis and cytotoxicity evaluation of diastereoisomers and N-terminal analogues of tubulysin-U. *Tetrahedron Lett* **2013,** *54*, 6137–6141.
84. Shankar, S. P.; Jagodzinska, M.; Malpezzi, L.; Lazzari, P.; Manca, I.; Greig, I. R.; Sani, M.; Zanda, M., Synthesis and structure-activity relationship studies of novel tubulysin U analogues--effect on cytotoxicity of structural variations in the tubuvaline fragment. *Org Biomol Chem* **2013,** *11* (14), 2273-87.
85. Hoffmann, J.; Gorges, J.; Junk, L.; Kazmaier, U., Synthesis of pretubulysin-derivatives via the TubUgi-approach. *Org Biomol Chem* **2015,** *13* (21), 6010-20.
86. Tumey, L. N.; Rago, B.; Han, X., In vivo biotransformations of antibody-drug conjugates. *Bioanalysis* **2015,** *7* (13), 1649-64.
87. Tumey, L. N.; Leverett, C. A.; Vetelino, B.; Li, F.; Rago, B.; Han, X.; Loganzo, F.; Musto, S.; Bai, G.; Sukuru, S. C.; Graziani, E. I.; Puthenveetil, S.; Casavant, J.; Ratnayake, A.; Marquette, K.; Hudson, S.; Doppalapudi, V. R.; Stock, J.; Tchistiakova, L.; Bessire, A. J.; Clark, T.; Lucas, J.; Hosselet, C.; O'Donnell, C. J.; Subramanyam, C., Optimization of Tubulysin Antibody-Drug Conjugates: A Case Study in Addressing ADC Metabolism. *ACS Med Chem Lett* **2016,** *7* (11), 977-982.
88. Burke, P. J.; Hamilton, J. Z.; Pires, T. A.; Lai, H. W. H.; Leiske, C. I.; Emmerton, K. K.; Waight, A. B.; Senter, P. D.; Lyon, R. P.; Jeffrey, S. C., Glucuronide-Linked Antibody-Tubulysin Conjugates Display Activity in MDR(+) and Heterogeneous Tumor Models. *Mol Cancer Ther* **2018,** *17* (8), 1752-1760.
89. Pearce, T. R.; Shroff, K.; Kokkoli, E., Peptide targeted lipid nanoparticles for anticancer drug delivery. *Adv Mater* **2012,** *24* (28), 3803-22, 3710.
90. Draca, D.; Mijatović, S.; Krajnović, T.; Pristov, J. B.; Dukić, T.; Kaluđerović, G. N.; Wessjohann, L. A.; Maksimović-Ivanić, D., The synthetic tubulysin derivative, tubugi-1, improves the innate immune response by macrophage polarization in addition to its direct cytotoxic effects in a murine melanoma model. *Exp Cell Res* **2019,** *380* (2), 159-170.
91. Reddy, J. A.; Dorton, R.; Bloomfield, A.; Nelson, M.; Dircksen, C.; Vetzel, M.; Kleindl, P.; Santhapuram, H.; Vlahov, I. R.; Leamon, C. P., Pre-clinical evaluation of EC1456, a folate-tubulysin anti-cancer therapeutic. *Sci Rep* **2018,** *8* (1), 8943.
92. Szigetvari, N. M.; Dhawan, D.; Ramos-Vara, J. A.; Leamon, C. P.; Klein, P. J.; Ruple, A. A.; Heng, H. G.; Pugh, M. R.; Rao, S.; Vlahov, I. R.; Deshuillers, P. L.; Low, P. S.; Fourez, L. M.; Cournoyer, A. M.; Knapp, D. W., Phase I/II clinical trial of the targeted chemotherapeutic drug, folate-tubulysin, in dogs with naturally-occurring invasive urothelial carcinoma. *Oncotarget* **2018,** *9* (97), 37042-37053.
93. Schluep, T.; Gunawan, P.; Ma, L.; Jensen, G. S.; Duringer, J.; Hinton, S.; Richter, W.; Hwang, J., Polymeric tubulysin-peptide nanoparticles with potent antitumor activity. *Clin Cancer Res* **2009,** *15* (1), 181-9.
94. Floyd, W. C., 3rd; Datta, G. K.; Imamura, S.; Kieler-Ferguson, H. M.; Jerger, K.; Patterson, A. W.; Fox, M. E.; Szoka, F. C.; Frechet, J. M.; Ellman, J. A., Chemotherapeutic evaluation of a synthetic tubulysin analogue-dendrimer conjugate in c26 tumor bearing mice. *ChemMedChem* **2011,** *6* (1), 49-53.
95. Cheng, H.; Cong, Q.; Dervin, D.; Stevens, A.; Vemuri, K.; Huber, M.; Juliano, J.; Cuison, S.; Sung, J.; Passmore, D.; Chong, C.; Greenbaum, M.; Kwok, E.; Jiang, J.; Pan, C.; Rao-Naik, C.; Rangan, V.; Kempe, T.; Tatum, A.; Deshpande, S.; Cardarelli, P.; Vite, G.; Gangwar, S., Synthesis and Biological Evaluation of a Carbamate-Containing Tubulysin Antibody-Drug Conjugate. *Bioconjug Chem* **2020,** *31* (10), 2350-2361.
96. Faria, M.; Peay, M.; Lam, B.; Ma, E.; Yuan, M.; Waldron, M.; Mylott, W. R., Jr.; Liang, M.; Rosenbaum, A. I., Multiplex LC-MS/MS Assays for Clinical Bioanalysis of MEDI4276, an Antibody-Drug Conjugate of Tubulysin Analogue Attached via Cleavable Linker to a Biparatopic Humanized Antibody against HER-2. *Antibodies (Basel)* **2019,** *8* (1).

97. Cohen, R.; Vugts, D. J.; Visser, G. W.; Stigter-van Walsum, M.; Bolijn, M.; Spiga, M.; Lazzari, P.; Shankar, S.; Sani, M.; Zanda, M.; van Dongen, G. A., Development of novel ADCs: conjugation of tubulysin analogues to trastuzumab monitored by dual radiolabeling. *Cancer Res* **2014,** *74* (20), 5700-10.
98. Kufka, R.; Rennert, R.; Kaluđerović, G. N.; Weber, L.; Richter, W.; Wessjohann, L. A., Synthesis of a tubugi-1-toxin conjugate by a modulizable disulfide linker system with a neuropeptide Y analogue showing selectivity for hY1R-overexpressing tumor cells. *Beilstein J Org Chem* **2019,** *15*, 96-105.
99. Kratz, F.; Müller, I. A.; Ryppa, C.; Warnecke, A., Prodrug strategies in anticancer chemotherapy. *ChemMedChem* **2008,** *3* (1), 20-53.
100. Böhme, D.; Beck-Sickinger, A. G., Drug delivery and release systems for targeted tumor therapy. *J Pept Sci* **2015,** *21* (3), 186-200.
101. Yang, J.; Chen, H.; Vlahov, I. R.; Cheng, J. X.; Low, P. S., Characterization of the pH of folate receptor-containing endosomes and the rate of hydrolysis of internalized acid-labile folate-drug conjugates. *J Pharmacol Exp Ther* **2007,** *321* (2), 462-8.
102. Yang, J.; Chen, H.; Vlahov, I. R.; Cheng, J. X.; Low, P. S., Evaluation of disulfide reduction during receptor-mediated endocytosis by using FRET imaging. *Proc Natl Acad Sci U S A* **2006,** *103* (37), 13872-7.
103. Meister, A.; Anderson, M. E., Glutathione. *Annu Rev Biochem* **1983,** *52*, 711-60.
104. Leriche, G.; Chisholm, L.; Wagner, A., Cleavable linkers in chemical biology. *Bioorg Med Chem* **2012,** *20* (2), 571-82.
105. Low, P. S.; Henne, W. A.; Doorneweerd, D. D., Discovery and development of folic-acid-based receptor targeting for imaging and therapy of cancer and inflammatory diseases. *Acc Chem Res* **2008,** *41* (1), 120-9.
106. Lee, M. H.; Sessler, J. L.; Kim, J. S., Disulfide-based multifunctional conjugates for targeted theranostic drug delivery. *Acc Chem Res* **2015,** *48* (11), 2935-46.
107. Lee, M. H.; Yang, Z.; Lim, C. W.; Lee, Y. H.; Dongbang, S.; Kang, C.; Kim, J. S., Disulfide-cleavage-triggered chemosensors and their biological applications. *Chem Rev* **2013,** *113* (7), 5071-109.
108. Jones, L. R.; Goun, E. A.; Shinde, R.; Rothbard, J. B.; Contag, C. H.; Wender, P. A., Releasable luciferin-transporter conjugates: tools for the real-time analysis of cellular uptake and release. *J Am Chem Soc* **2006,** *128* (20), 6526-7.
109. Dubowchik, G. M.; Firestone, R. A., Cathepsin B-sensitive dipeptide prodrugs. 1. A model study of structural requirements for efficient release of doxorubicin. *Bioorg Med Chem Lett* **1998,** *8* (23), 3341-6.
110. Dal Corso, A.; Pignataro, L.; Belvisi, L.; Gennari, C., alphavbeta3 Integrin-Targeted Peptide/Peptidomimetic-Drug Conjugates: In-Depth Analysis of the Linker Technology. *Curr Top Med Chem* **2016,** *16* (3), 314-29.
111. Dal Corso, A.; Pignataro, L.; Belvisi, L.; Gennari, C., Innovative Linker Strategies for Tumor-Targeted Drug Conjugates. *Chemistry* **2019,** *25* (65), 14740-14757.
112. DeWit, M. A.; Gillies, E. R., Design, synthesis, and cyclization of 4-aminobutyric acid derivatives: potential candidates as self-immolative spacers. *Org Biomol Chem* **2011,** *9* (6), 1846-54.
113. Gauthier, F.; Bertrand, J. R.; Vasseur, J. J.; Dupouy, C.; Debart, F., Conjugation of Doxorubicin to siRNA Through Disulfide-based Self-immolative Linkers. *Molecules* **2020,** *25* (11).
114. Vlahov, I. R.; Leamon, C. P., Engineering folate-drug conjugates to target cancer: from chemistry to clinic. *Bioconjug Chem* **2012,** *23* (7), 1357-69.

2. Peptide-drug conjugates based on SSTR2- and CD13-targeting peptides

2.1. Introduction

Cyclic peptides possess versatile beneficial properties which are useful for pharmaceutical applications. For that reason, they have been studied intensively for the past 20 years. Compared to linear peptides, the cyclization increases the conformational stability which promotes resistance in the metabolism against proteases as well as the binding affinity to the targets, i.e. receptors, if the correct conformation is fixed.[1] Especially cyclic peptides containing up to ten amino acids are rather stable.[2, 3]

2.1.1. Octreotide as targeting peptide

The natural polypeptide somatostatin (SST) represents such a cyclic peptide which is used as a therapeutic agent. Due to its targeting properties and additional direct inhibiting effect against growth hormones, particularly the growth hormone somatotropin, it was given the name somatostatin ("somatotropin inhibitor").[4, 5] It has been revealed that somatostatin shows antimitotic and antiproliferative effects against pancreatic, prostatic and breast tumors by inducing cell arrest as well as apoptosis. It also inhibits angiogenesis. Somatostatin was first isolated from ovine hypothalamic extracts in 1973 and is produced, for instance, in the central nervous system, in pancreas and kidneys.[4] There are two biologically active forms, the SST14 containing 14 amino acids and the SST28 containing 28 amino acids (Figure 2.1a and b), which form an extended antiparallel β-pleated sheet and incorporate a cysteine-cysteine bridge. It has been shown that the four amino acids Phe_7-Trp-Lys-Thr_{10} play a crucial role for the bioactivity of somatostatin.[6-10]

The somatostatin forms bind to the five subtypes of somatostatin receptors (SSTR1 to SSTR5) which appertain to the 7-transmembrane domain family of G protein-coupled receptors (GPCRs). Those subtypes of SSTRs are highly expressed in many human tumors, for instance in neuroendocrine and breast tumor. But SSTR are also found in normal cells. Though, the expression level of SSTR, especially SSTR2, in neuroendocrine, metastatic, breast, lung, lymphoma, meningeoma and prostate carcinomas excel the expression level in normal cells.[10-16]

The binding of SST to SSTRs triggers different signal pathways leading, among others, to inhibition of secretion of growth hormones.[17]

The stability of natural somatostatin in blood plasma is limited by its half-life which is three minutes. Therefore, more stable, but also growth hormone inhibiting derivatives, called somatostatin receptor ligands (SRL), were developed. In 1982 Bauer *et al.* synthesized an octapeptide, called octreotide, comprising the essential amino acids Phe_7-Trp-Lys-Thr_{10} and replaced the L-Trp by the D-form in order to stabilize the β-conformation (Figure 2.1c).[7, 9] Moreover, the half-life in plasma was prolongated up to two hours and selectiviy to the respective SSTRs was increased. Octreotide binds with high affinity to SSTR2 and with a weaker affinity to SSTR3 and SSTR5. The most prevalent SSTR2 is particularly overexpressed in neuroblastomas, lymphomas, renal cells and breast tumors, whereas the other subtyes of SSTR are less or not expressed in those carcinomas.[12, 17-20] In the 1980s octreotide became the first clinically applied SRL in order to inhibit the release of insulin, to treat various hormone producing tumors and to carry radionuclides for

visualization and treatmennt of tumor tissues. As in case of somatostatin, the antiproliferative effect of octreotide is attributed to the activitation of protein tyrosine phosphatases which control the cell cycle. Moreover, it is assumed that another mechanism, the telomerase signaling, is important for the antimalignant activity. It was revealed by radiolabeling that cells internalize octreotide rapidly by receptor-mediated endocytosis through SSTR2.[11, 13, 17, 21-24]

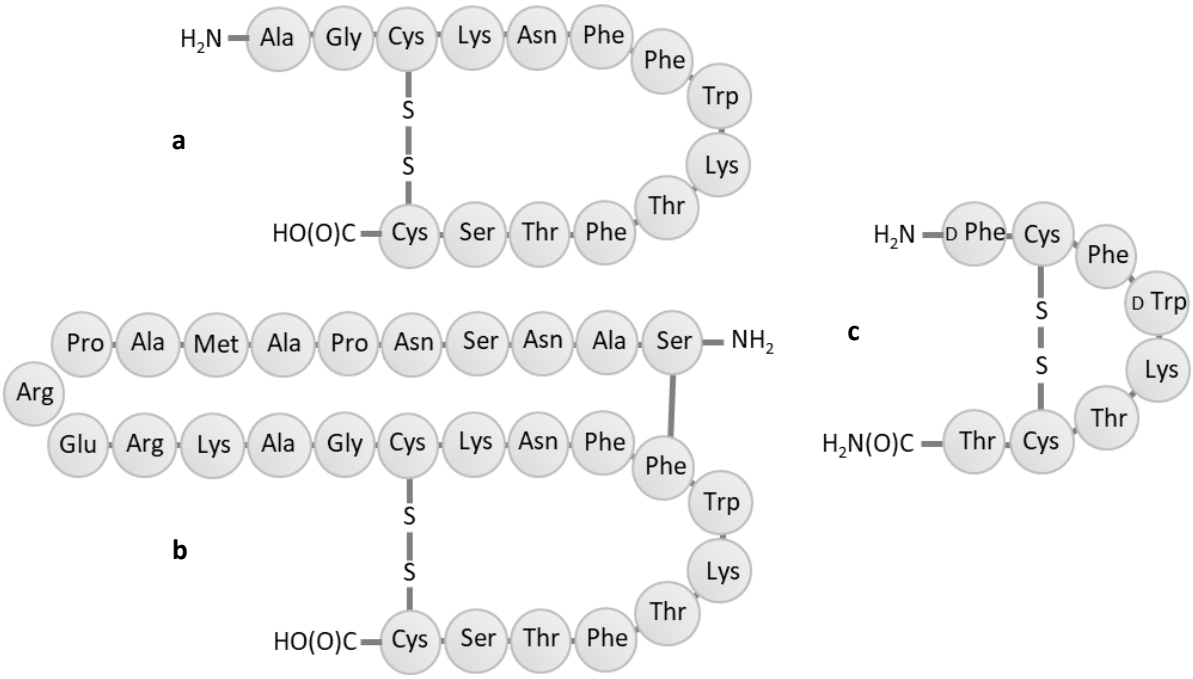

Figure 2.1 Amino acid sequences of a) SST14, b) SST28 and c) octreotide.

In addition to radiopharmaceuticals involving octreotide, conjugates containing octreotide as targeting agent have been successfully investigated. Thus, paclitaxel was conjugated to octreotide in order to circumvent multidrug resistance and to diminish the toxicitiy to normal cells by selective delivery of the cytotoxin. Furthermore, the apoptotic effect of paclitaxel was strengthened owing to the conjugation to octreotide. Also the expression-depending impact of octreotide conjugates were studied. Conjugates of octreotide and periplocymarin, a cardiac glycoside, were applied to cancer cell lines expressing different levels of receptors. It was proven that the viability of cells overexpressing regarding receptors was much lower than in case of weakly receptor expression. The conjugation to the peptide had been carried out via the *N*-terminus giving a stable amide bond.[14, 24-28] Lelle *et al.* presented a cleavable, but in blood serum stable linkage between the octreotide and doxorubicin by inserting an intercalating crosslinker.[29] This disulfide-intercalating crosslinker inserted between the cysteines of the octreotide can be cleaved by reductive conditions inside cancer cells.

2.1.2. NGR sequence as targeting moiety

The Asn-Gly-Arg motif (NGR) was found as a result of phage display for integrin homing peptides in the peptide Cys-Asn-Gly-Arg-Cys-Val-Ser-Gly-Cys-Ala-Gly-Arg-Cys and was identified as receptor homing part of the peptide. Integrins are transmembrane receptors for proteins of the extracellular matrix like fibronectin (binds to $\alpha_5\beta_1$ integrin) and vitronectin (binds to $\alpha_v\beta_3$ $\alpha_v\beta_5$ integrins) which contain the Arg-Gly-Asp (RGD) motif.[30-32] Moreover, a integrin-mediated internalization of the

peptide was proven.[33] The *in vivo* screening elucidated that the NGR sequence embedded in various peptides also homes integrins, whereas cyclic NGR-comprising peptides – even the small peptide cyclo(-Cys-Asn-Gly-Arg-Cys-) (cCNGRC) (Figure 2.2) – compete with linear peptides in receptor selectivity due to the constrained conformation. The cyclization is formed by flanking cysteines via a disulfide bridge. Although the NGR motif shows good activities, it possesses a lower affinity to integrins than the RGD motif.[32] Further investigations revealed that the NGR motif targets another enzyme, the membrane protein aminopeptidase N. Aminopeptidase N, also called CD13, is found in many cells and particularly expressed in endothelial cells, e.g. of renal proximal tubule, prostate, bile duct canaliculi and small intenstine, but also in angiogenesis inducing tissues like corpus luteum. It was proven that different isoforms of CD13 reside in blood vessels of tumor and normal tissue, whereas the NGR motif targets selectively a CD13 isoform overexpressed in endothelial cells of tumor tissue and shows low or no affinity to isoforms in normal epithelial and myeloid cells.[34-37] The capability of the NGR motif to selectively bind to two targets, the integrins and CD13, is attributed to non-enzymatic deamidation comprising a succinimide ring formation and following hydrolysis. Thus, derivatives of aspartic (DGR) and isoaspartic acid (isoDGR), which binds to the integrin, are formed.[38, 39]

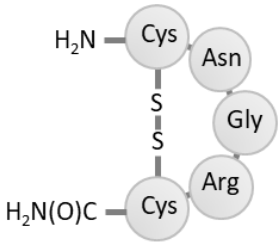

Figure 2.2 Amino acid sequence of cyclic CNGRC.

A library of various analogues was screened and it was figured out that cyclic and shorter peptides possess the best affinity to CD13. Especially the short, cyclic peptide cCNGRC was identified to selectively target $\alpha_v\beta_3$ integrin as well as CD13.[32, 40]

The protein CD13 is involved in chemokine processing and plays a role in metastasis and angiogenesis like integrins $\alpha_v\beta_3$ and $\alpha_v\beta_5$. Thus, antagonists of CD13 evoke an antiangiogenic effect. In addition, CD13 might be engaged with the decay of regulatory peptides and is incorporated into the immune system.[34, 36, 41] The selectivity and tumor homing capability of this peptide pattern have been exploited to attach the sequence to chemotherapeutic drugs (doxorubicin, platinum complex), to antimicrobial peptides (AMPs), proapoptotic peptides and to the protein coagulase. One NGR-conjugate, NGR-hTNF, possesses tremendous antitumor activity and has already passed a randomised, double-blind, placebo-controlled phase III trial. The conjugate NGR-hTNF was synthesized by attachment of the tumor necrosis factor α (TNF) to cCNGRC.[32, 42-49] The first synthesized NGR-conjugate containing doxorubicin as drug had been demonstrated to possess an antiproliferative effect against tumor *in vitro* as well as *in vivo*, but a selective distinction between CD13-expressing and non-expressing cells was missing. This problem was attributed to the relatively labile disulfide bridge responsible for the advantageous cyclization between the cysteines.[32, 38, 39, 42]

2.2. Synthetic strategy

In previous approaches,[50, 51] conjugates of tubulysins or tubugi have already been investigated. The cyclic targeting peptides octreotide and CNGRC were chosen for success in cancer therapy and to target a broader range of tumor types. Thereby, the most challenging part of peptide drug-conjugates is the linker system which provides the stability under physiological conditions, but also the cleavage within the malignant cells. The linker components need to be incorporated during the synthesis of the conjugates. Hence, too labile or too stable linker molecules cannot be used and at the same time, syntheses have to be carried out under mild conditions.[52] Although cancer cells slightly differ in their properties, the linker-spacer system should be compatible with most of them. Therefore, the presented linker-spacer system was designed to be cleavable under various tumor-specific conditions: reduction by glutathione (Figure 2.3a), enzymatic degradation by cathepsin B (Figure 2.3b) and hydrolysis under acid conditions (Figure 2.3c). Moreover, an improved synthesis of the novel tubugi derivative tubugi 4 is presented. As result the metabolic stability of tubugis was increased, opening the path for *in vivo* experiments of tubugi-containing conjugates.

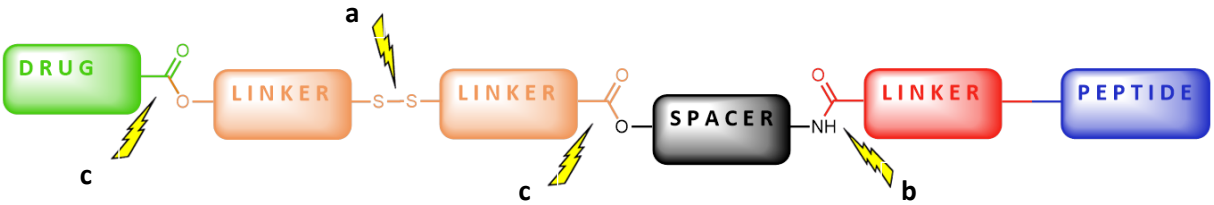

Figure 2.3 Layout of linker-spacer system containing multiple trigger points cleaved a) by reduction, b) by enzymatic degradation or c) under acid conditions.

In addition to PDCs, fluorescently labeled peptide conjugates based on octreotide and CNGRC were synthesized to analyze the internalization of the peptide conjugates by the respective receptors.

2.2.1. Synthesis of tubugis

The synthesis of the highly potent tubugi 1 was developed and described before by Pando *et al.* and Kufka *et al.*[51, 53] In general, tubugi 1 was synthesized according to the procedures of these former group members. Thus, the building block Mep-Ile was produced, starting from commercially available D-pipecolic acid to which L-Ile-OMe was coupled after Cbz-protection of the secondary amine of Mep. Finally, compound **4** was prepared by Cbz-deprotection followed by methylation and hydrolysis (Scheme 2.1).

For the synthesis of the Tuv component, H_2S and then ethyl bromopyruvate were added to pyruvonitrile. Furthermore, *iso*-butanal was attached via an aldol reaction and *tert*-butylcarbamat was attached via aza-MICHAEL addition yielding compound **8**. The ethyl ester of Tuv (**11**) was obtained after reduction of the ketone via CBS-oxazaborolidine, TBDMS-protecting and following Boc-deprotection (Scheme 2.2).[54]

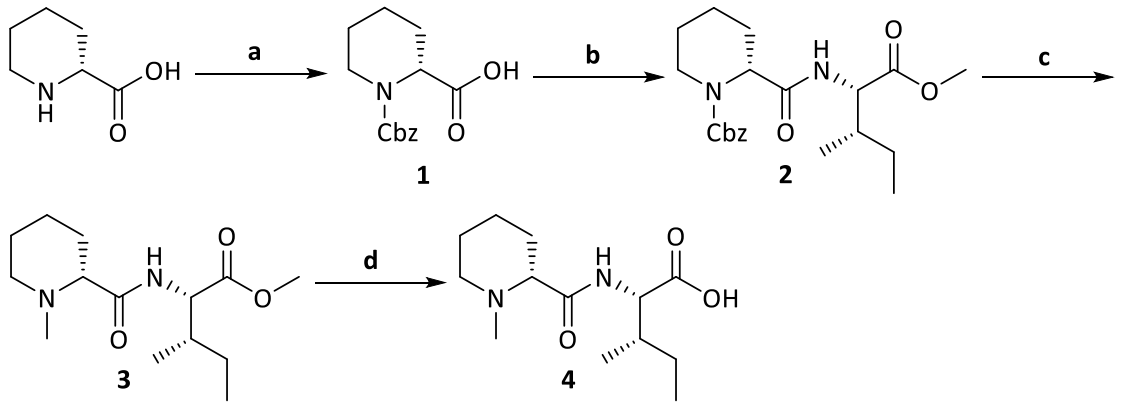

Scheme 2.1 a) in 2 M NaOH at 0 °C, CbzCl, rt, overnight, 98 %; b) L-Ile-OMe, EDC × HCl, HOBt, 2,5-lutidine, in DMF, rt, overnight, 94 %; c) PFA, $Pd(OH)_2/C$, H_2, in MeOH, rt, overnight, 40 %; d) in THF/H_2O, pH = 1, reflux, 7 d, quant. yield.

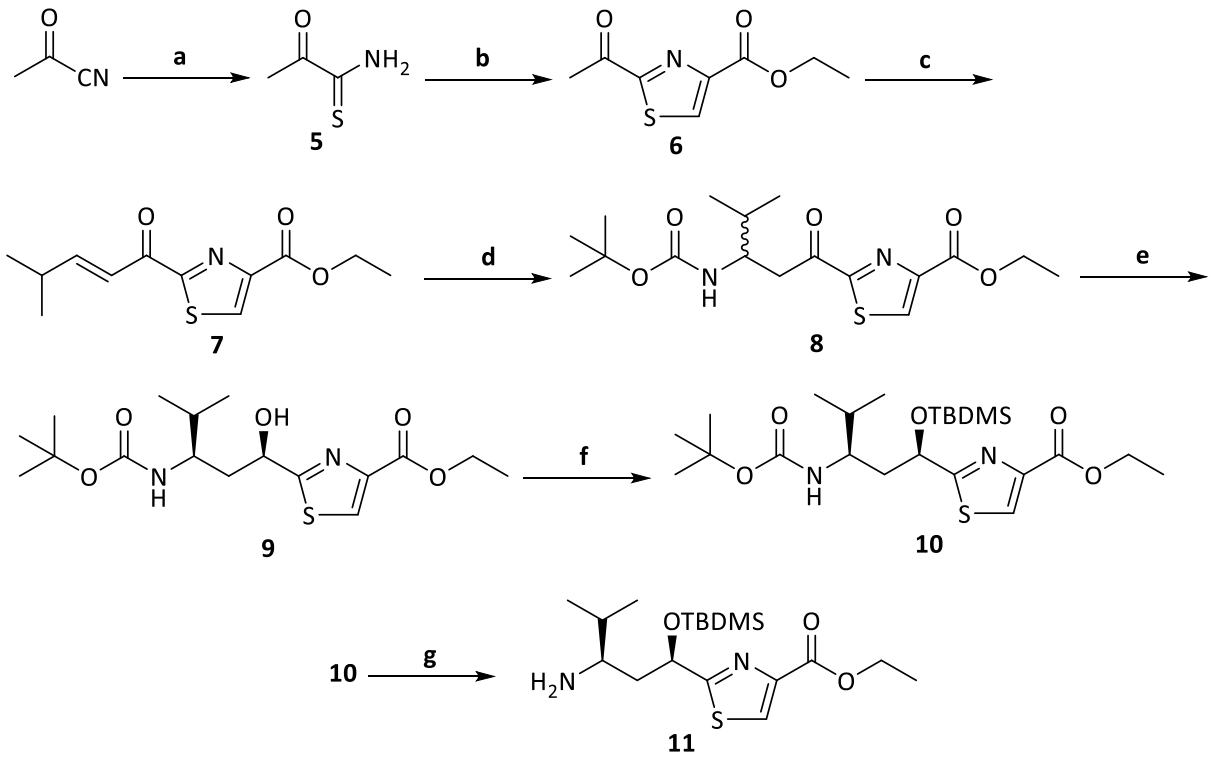

Scheme 2.2 a) H_2S, 30 min, Et_3N, rt, overnight, in Et_2O, 30 min, 88 %; b) ethyl bromopyruvate, in EtOH, reflux, 1 h, 23 %; c) $TiCl_4$ at 0 °C for 40 min, Et_3N and *iso*-butanal at −78 °C for 1 h, in THF, 59 %; d) $Sn(OTf)_2$ *tert*-butylcarbamat, rt, 3 h, in ACN, 63 %; e) $BH_3 \times Me_2S$, CBS catalyst, 0 °C -> rt, 3 h, in THF, 40 %; f) TBDMSCl, imidazole, rt, overnight, in DMF, 98 %; g) TFA, 0 °C, 6 h, in DCM, 86 %.

In an alternative synthetic approach the Tuv building block was obtained more easily starting from purchased *N*-Boc-*O*-acetyl-tubuvalin ethyl ester (**12**). A transesterification was carried out using sodium methoxide and then the former synthetic route was continued by protecting the hydroxyl group with TBDMSCl and removing the Boc group with TFA in order to gain compound **15** (Scheme 2.3).

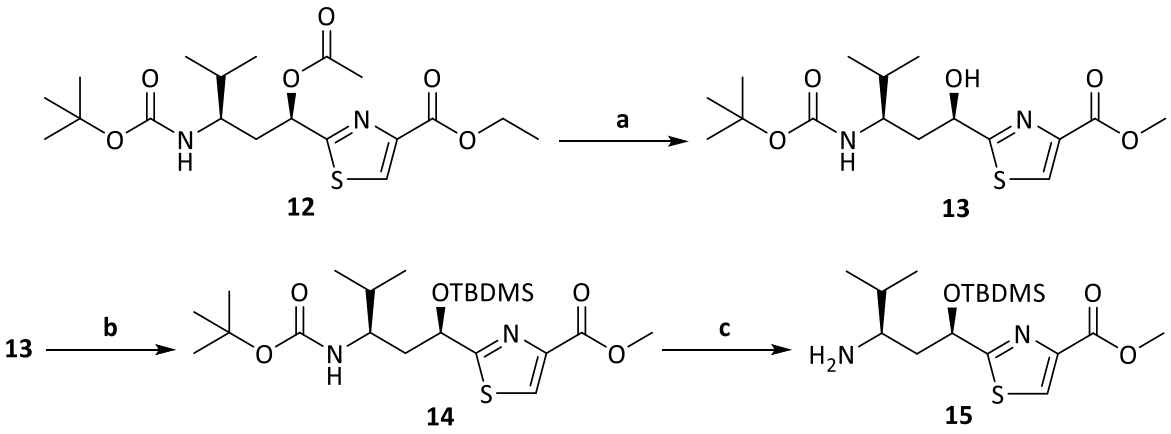

Scheme 2.3 a) NaOMe, rt, 4 h, in MeOH, 72 %; b) TBDMSCl, imidazole, rt, overnight, in DMF, 85 %; c) TFA, 0 °C, 6 h, in DCM, quant. yield.

Since the discovery that the acetate ester at C11 position as a crucial binding moiety is cleaved off within 74 h in mouse plasma resulting in a strong decrease of efficacy of tubugi 1 (**33**) *in vivo*,[55] the acetate at C11 was replaced by a much more stable propyl ether leading to the novel tubugi derivative tubugi 4 (**34**). The substitution of acetate ester by an ethyl ether leads to a comparable cytotoxicity and offers improved metabolic stability as well as facilitated synthetic access.[56] Assuming that a propyl ether resembles an acetate ester more than an ethyl ether, *N*-Boc-*O*-propyl-tubuvalin ethyl ester (**16**) was used for further synthesis after Boc-deprotection (Scheme 2.4).

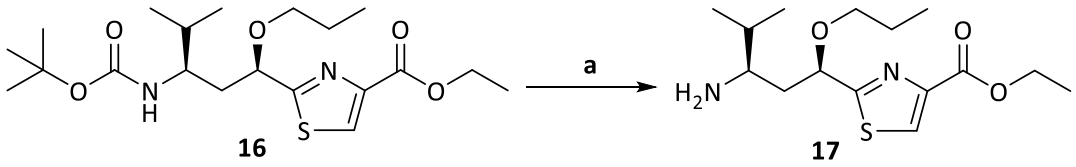

Scheme 2.5 a) TFA, rt, 4 h, in DCM, quant. yield.

In the first step, of the synthesis of the *C*-terminal building block (Tup), *N*-Boc-L-phenylalaninol was oxidized followed by WITTIG reaction, hydrogenation, hydrolysis and a stereoselective esterification. The subsequent hydrolysis was performed to remove the Boc-group and the menthyl group. In a final step, compound **23** was methylated yielding compound **24** (Scheme 2.6).

The successive UGI reaction was facilitated by performing the reaction in the microwave (MIC) affording also good yields about 50 % and accelerating the reaction time (2 h instead of 24 h, Scheme 2.7).

After removal of protection groups (Scheme 2.7a, b), the Tup component was attached to Mep-Ile-Tuv (**28**, **29**) exploiting HATU-mediated amide coupling. Afterwards, tubugi 1 (**33**) was afforded by hydrolysis and acetylation at C11 and tubugi 4 (**34**) was obtained by hydrolysis (Scheme 2.8).

In a final step, the tubugis (**33**, **34**) were modified by the disulfide bridge containing compound **35** in order to gain the activated toxin-precursors (**36**, **37**) for the attachment to the linker-spacer system and also to introduce the self-immolative spacer.

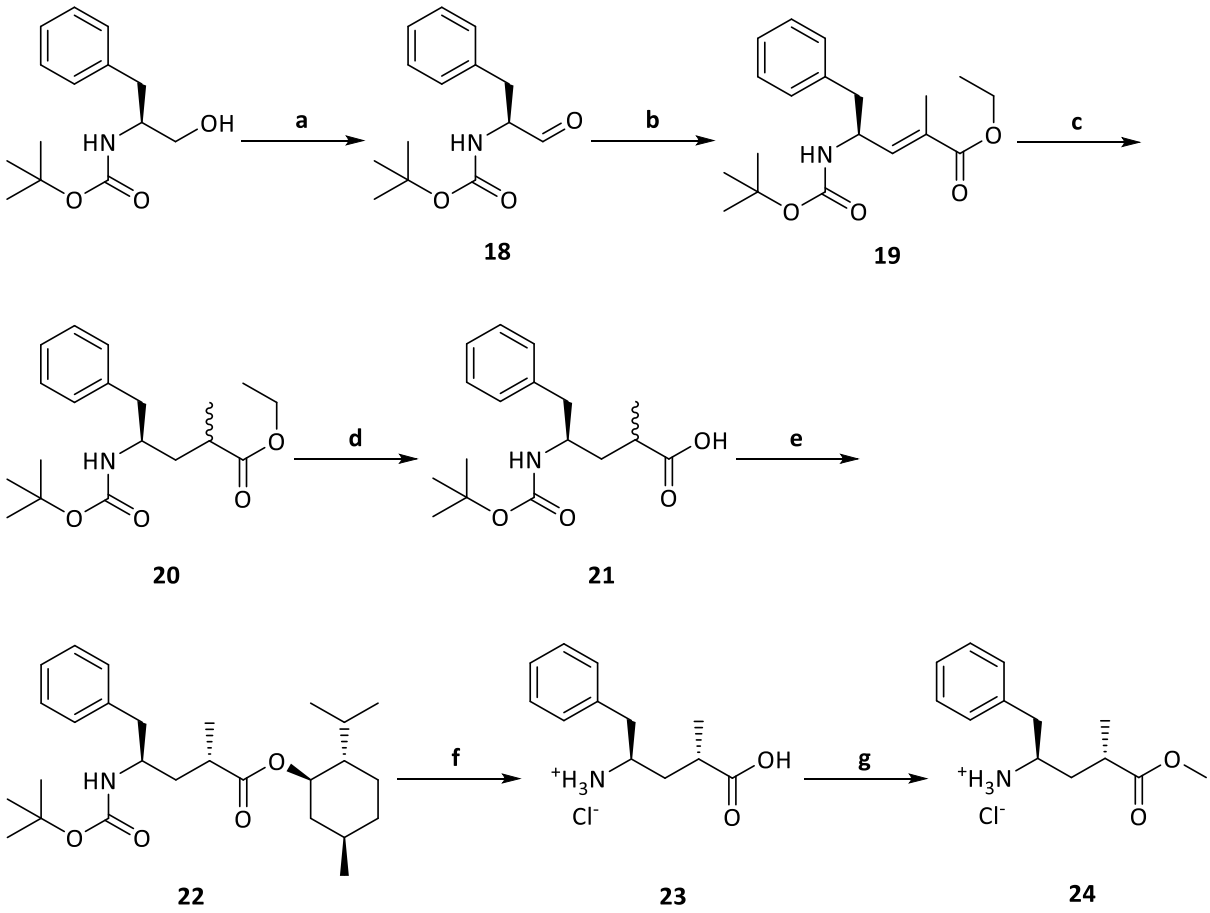

Scheme 2.6 a) NaBr, TEMPO, NaOCl at 0 °C, rt, 4 h, in H_2O/EtOAc/toluene, 95 %; b) $Ph_3P{=}C(CH_3)CO_2Et$ at 0 °C, rt, 16 h, in DCM, 39 %; c) $Pd(OH)_2/C$, H_2, rt, overnight, in MeOH, 93 %; d) KOH, rt, overnight, in THF/H_2O, 80 %; e) (−)-menthol, DCC, DMAP, rt, overnight, in DCM, 55 %; f) 6 M HCl, reflux, 5 h, quant. yield; g) $HCl_{conc.}$, 50 °C, 27 h, in MeOH, quant. yield.

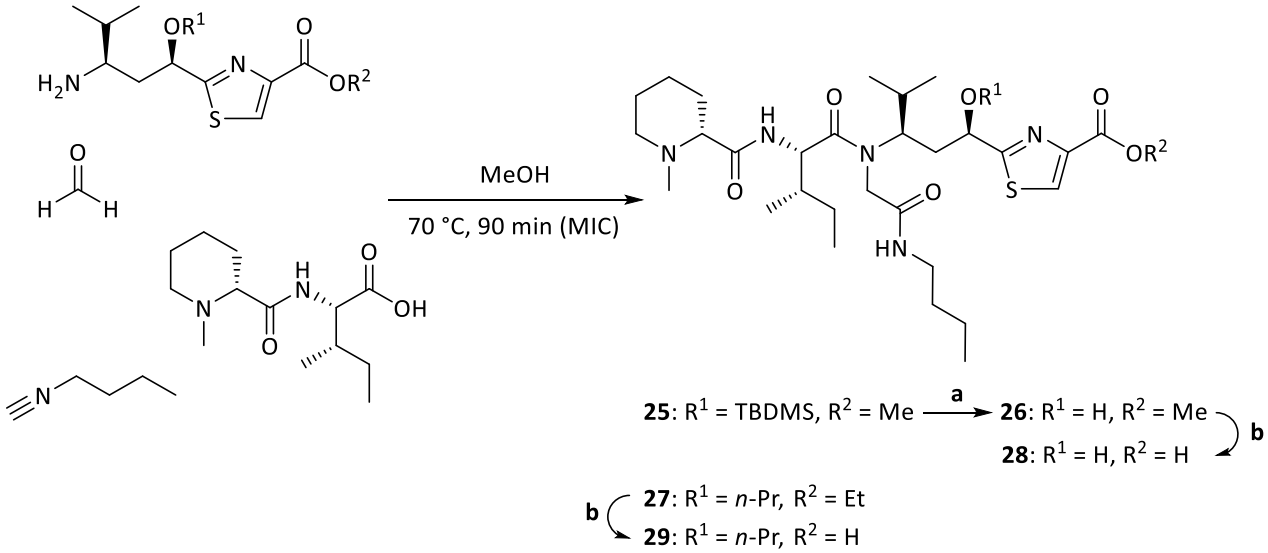

Scheme 2.7 UGI reaction for synthesis of tubugis under microwave heating (MIC), 42 % (**25**)/ 78 % (**27**); a) TFA/THF/H_2O, rt, 20 h, quant. yield; b) LiOH × H_2O, in THF/H_2O, rt, 8 h, quant. yield.

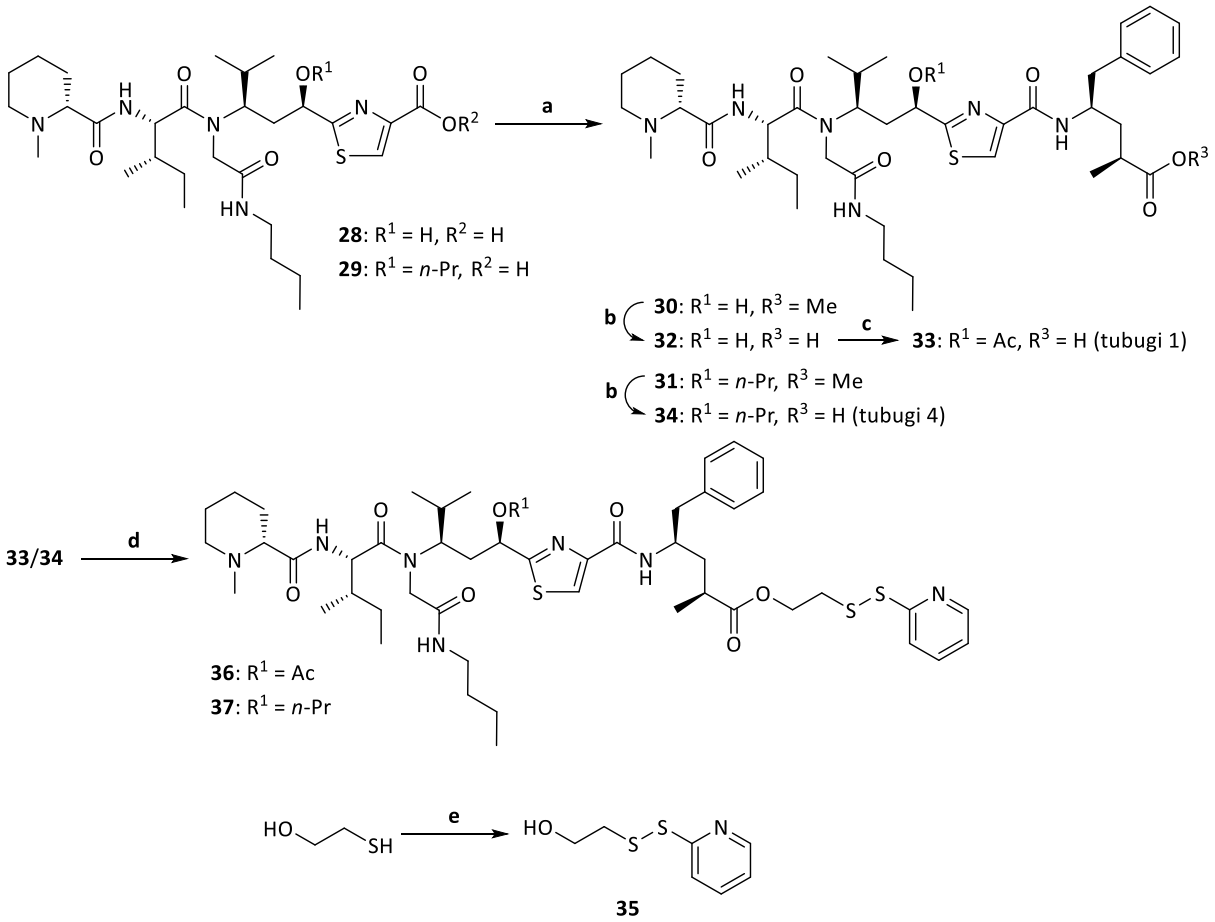

Scheme 2.8 a) HATU, DIPEA, 24, rt, 3 d, quant. yield (**30**)/overnight, 69 % (**31**), in DMF; b) LiOH × H_2O rt, 3 d (**32**)/24 h (**34**), in THF/H_2O, quant. yield; c) Ac_2O at 0 °C, rt, 3 d, in pyridine, 92 %; d) EDC × HCl, **35**, DMAP, rt, overnight, in DCM, 71 % (**36**)/63 % (**37**); e) 2,2'-dipyridyl disulfide, rt, 4 h, in MeOH, 60 %.

2.2.2. Synthesis of linker-spacer system

The skeleton of a linker system based on the well-known and *in vivo* proven PAB-Cit-Val sequence is recognized and split enzymatically by cathepsin B at the *C*-terminus of Cit.[57, 58] This commercially available linker component was elongated by compound **38**, providing a sterically hindered thiol for a disulfide bridge and forming an acid-sensitive ester towards PAB moiety via STEGLICH esterification (Scheme 2.9a). Two geminal methyl groups in alpha position to the disulfide bridge were verified to double the half-life of the disulfide bridge.[59, 60] The disulfide precursor **38** was obtained by the protection of the thiol group of 4-mercapto-4-methylpentanoic acid in a reversible way by introduction of a pyridin-2-yldisulfanyl group using 2,2'-dipyridyl disulfide (Scheme 2.9b).[61-63] Thus, side-reactions were avoided in further syntheses of the building block. At the same time, the sulfhydryl group is activated by this step for the formation of a disulfide bridge by nucleophilic attack of a free sulfhydryl group.[64]

After removing the *N*-terminal Boc-protecting group, the dibromomaleimide containing building block **42** was attached to **40** by STEGLICH coupling, generating linker-spacer system **43** (Scheme 2.10a). The dibromomaleimde component was found to be an efficient tool for bridging two

cysteines in antibodies[65-67] and for cyclization of peptides connecting two cysteines.[68, 69] The dibromomaleimide **42** was synthesized from maleic anhydride by bromination (Scheme 2.10b) using aluminum chloride as a catalyst and a subsequently performed functionalization by 4-aminopentanoic acid under reflux (Scheme 2.10c).[70]

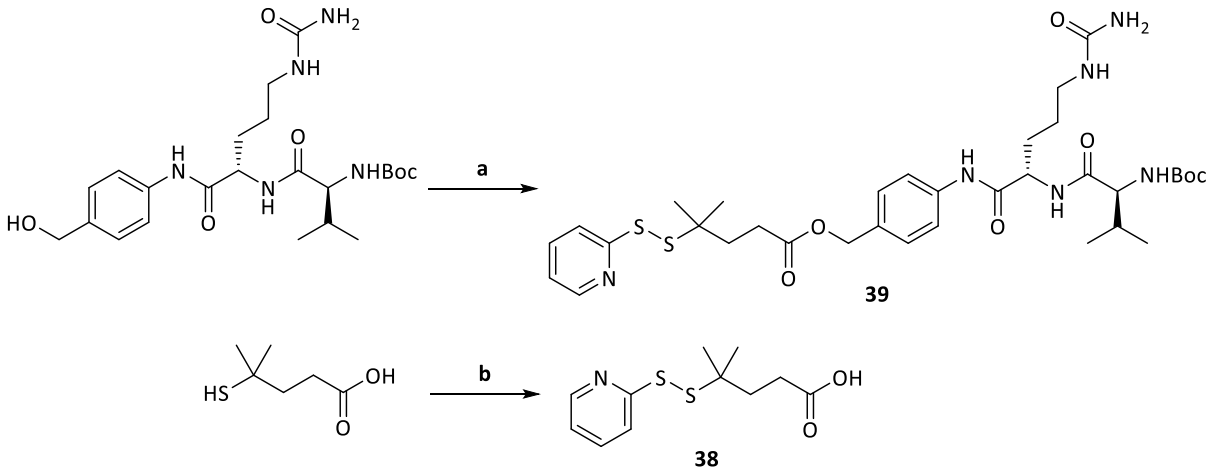

Scheme 2.9 a) **38**, DIC, DMAP, rt, 22 h, in DCM, 87 %; b) 2,2'-dipyridyl disulfide, rt, 6 h, in MeOH, 46 %.

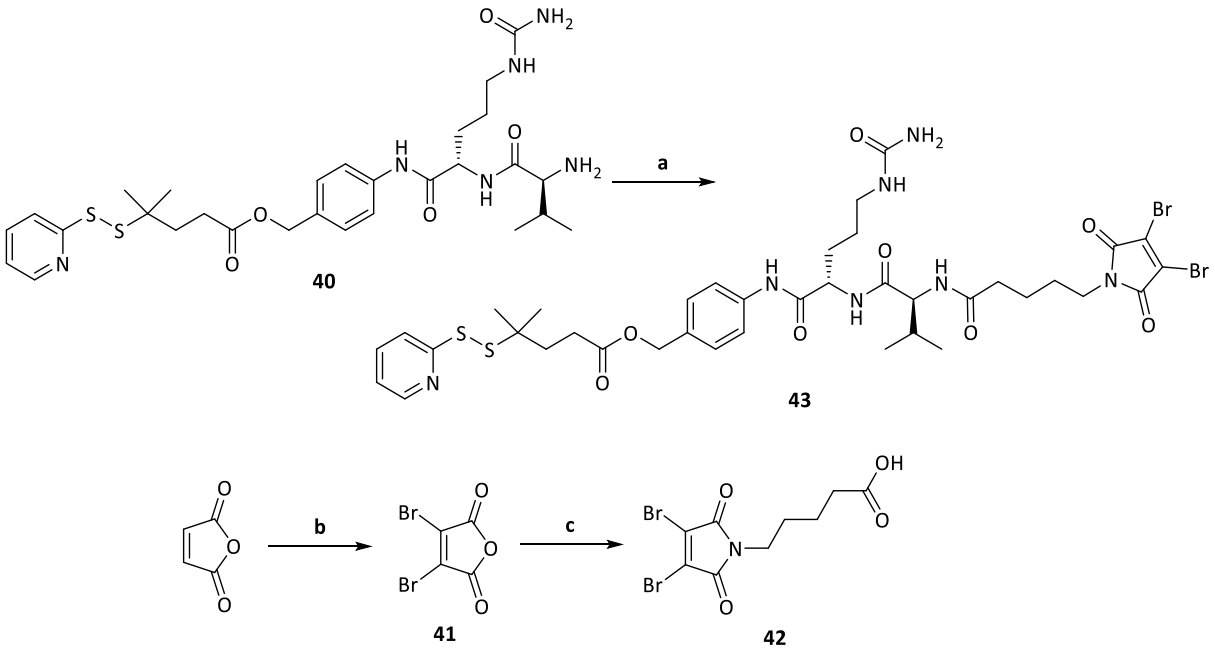

Scheme 2.10 a) **42**, DIC, DMAP, rt, 4 h, in DCM, 60 %; b) Br_2, $AlCl_3$, 80 °C, 16 h, 74 %; c) 4-amino-pentanoic acid, reflux, 4 h, in AcOH, 96 %.

2.2.3. Synthesis of cyclic peptide-drug conjugates

In the next step, the peptides were attached to the linker-spacer system. The peptides octreotide (**44** in Figure 2.4) and CNGRC (**46** in Figure 2.5) were produced on solid phase and obtained as linear peptides after cleavage. The active form of both peptides was achieved by cyclization by the previously described linker-spacer system (**43**) in 5 mM solution of the peptide. The bridging of two cysteines in each peptide was enabled by the dibromomaleimide moiety in the linker-spacer system forming each two thioether bonds (Scheme 2.10a & 2.11a). In parallel, both peptides were cyclized by DMSO oxidation in buffer solution to obtain **45** and **47** as reference compounds for cell viability assays. The cyclization of octreotide took significantly longer (6 d) than the cyclization of the shorter CNGRC (1 d). This observation can be attributed to the chain length or prefolding of the peptides, but also to number of bulky amino acids in the sequence of octreotide (Lys, D-Phe).[71]

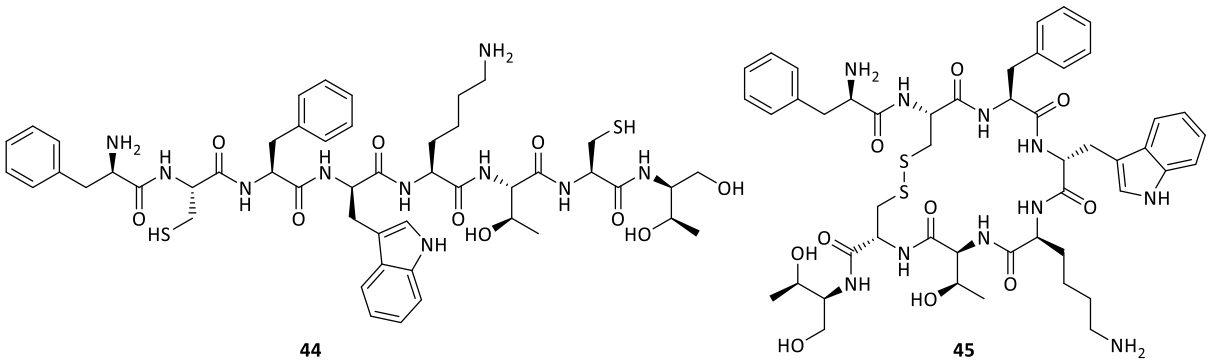

Figure 2.4 Linear octreotide **44** and cyclized form **45**.

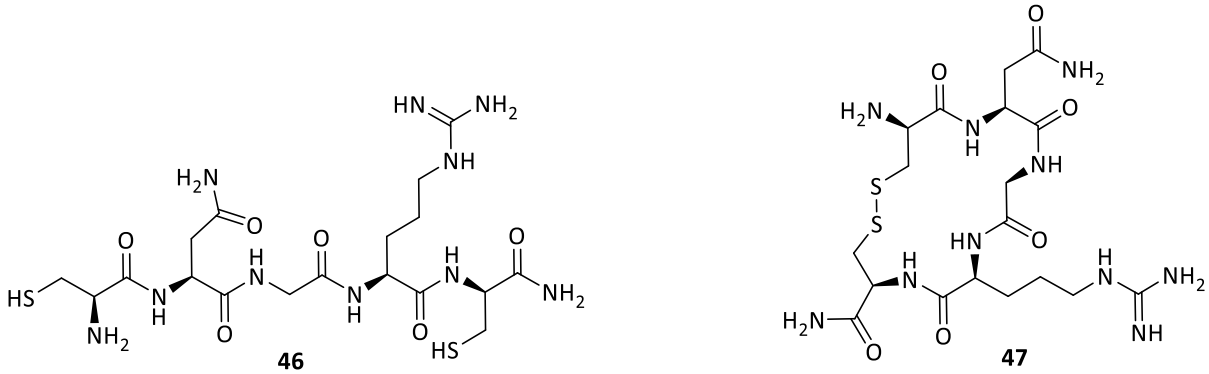

Figure 2.5 Linear CNGRC **46** and cyclized form **47**.

The cyclization process of the dibromomaleimide containing linker-spacer system (**43**) was followed by reduction of the blocked thiol moiety using the mild reducing agent TCEP (Scheme 2.10a & 2.11a). Thus, a free sulfhydryl group was provided for thiol–disulfide exchange to connect to the modified toxin.

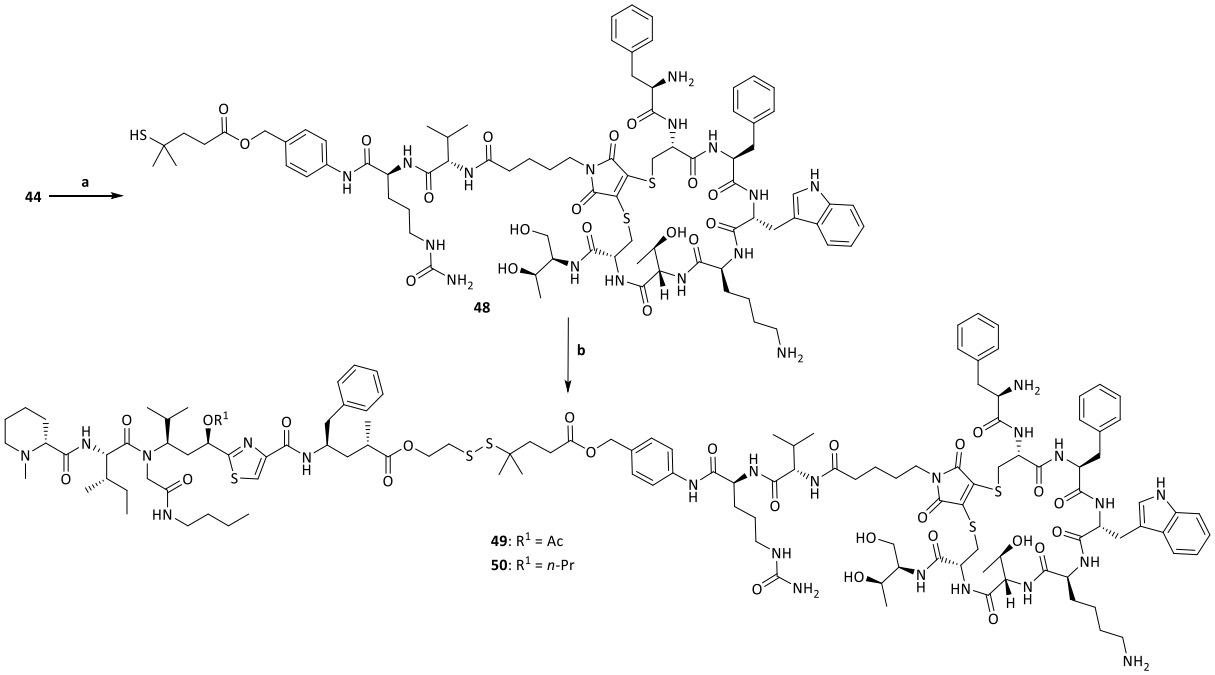

Scheme 2.11 a) 1. **43**, rt, 5 d, in H_2O/DMF, 2. TCEP, rt, 14 d; b) **36**, rt, 46 h, 20 % (**49**)/**37**, rt, 5 d, 24 % (**50**), in DMF.

In a final step, the activated tubugi precursors (**36**, **37**) were attached to the respective building blocks forming a disulfide bridge (Scheme 2.10b & 2.11b).[50]

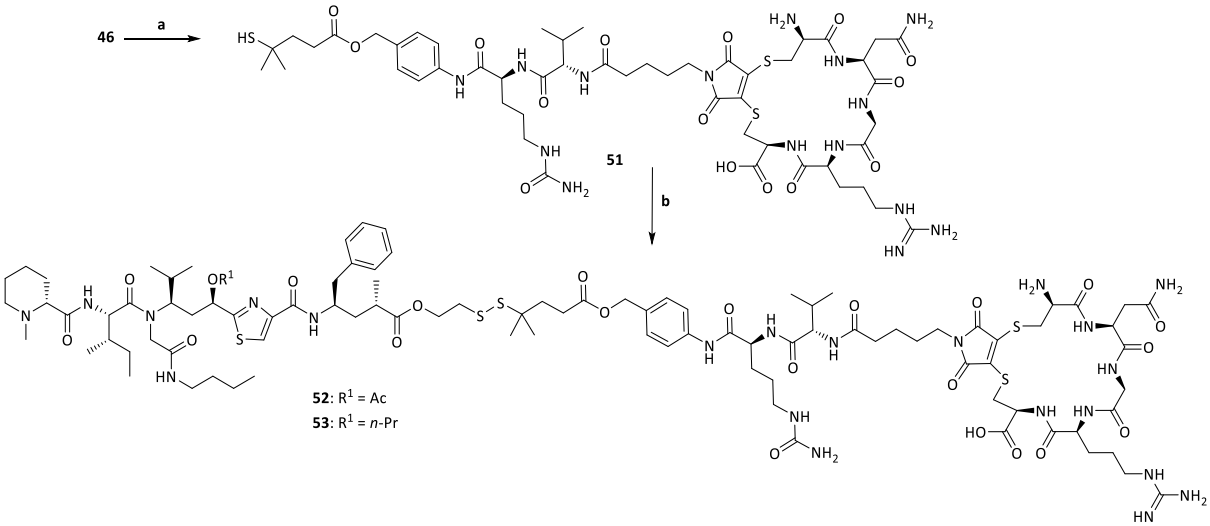

Scheme 2.12 a) 1. **43**, rt, overnight, in H_2O/DMF, 2. TCEP, rt, overnight; b) **36**, rt, 46 h, 32 % (**52**)/**37**, rt, 5 d, 28 % (**53**), in DMF.

2.2.4. Synthesis of fluorescently labeled peptide conjugates

The synthesis and application of toxin-free, fluorescently labeled conjugates containing octreotide or CNGRC as targeting moiety were conducted in order to visualize and semi-quantify the target-mediated internalization of the conjugates into the tumor cells. Rhodamine B was chosen as

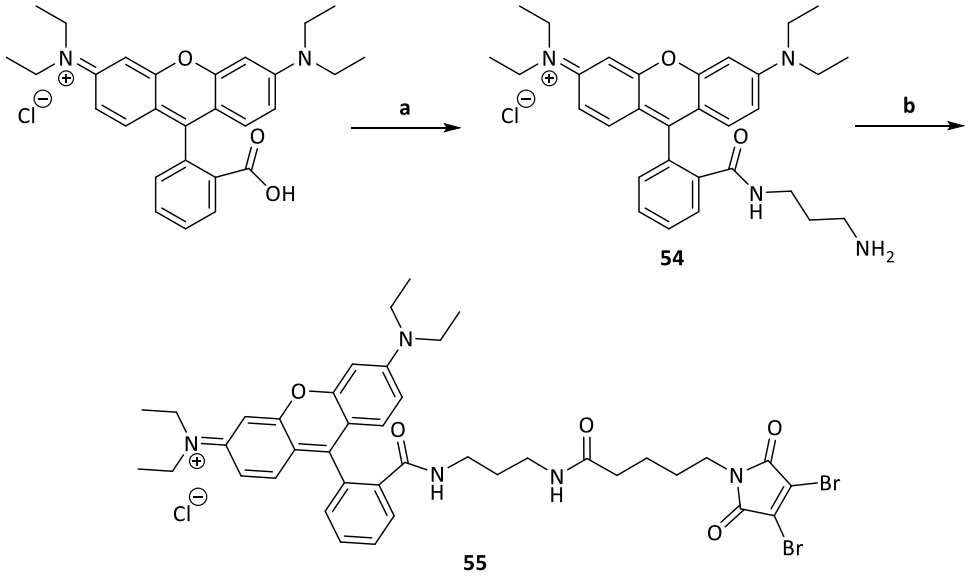

Scheme 2.13 a) 1,3-Diaminopropane, rhodamine B, EDC × HCl, rt, 22 h, in DCM, 45 %; b) **42**, EDC × HCl, rt, overnight, in DCM, 89 %.

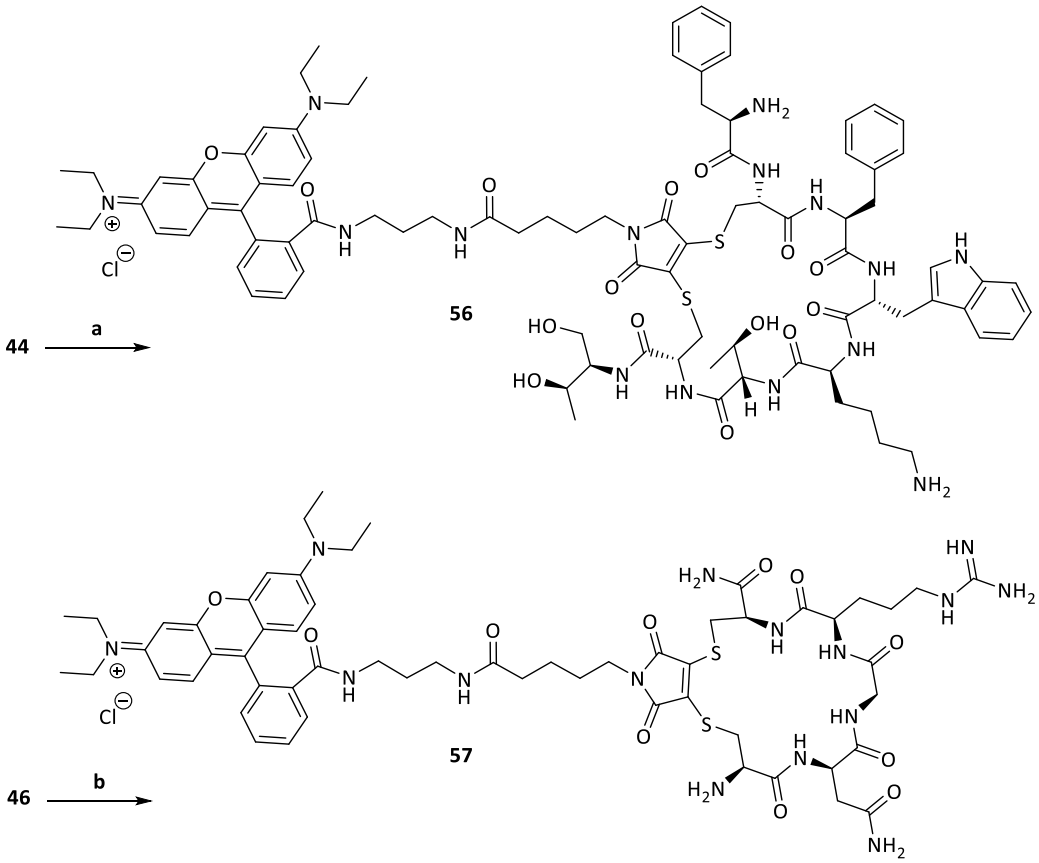

Scheme 2.14 a) **55**, rt, 3 d, in DMF, 16 %; b) **55**, rt, 17 h, in DMF, 46 %.

fluorophore attached to the peptides.[72, 73] In a first step, rhodamine B was modified by 1,3-diaminopropane providing a uncleavable linker system via STEGLICH coupling (Scheme 2.13a).

Afterwards, the dibromomaleimide linker (**42**) was introduced also via STEGLICH coupling preparing the attachment to octreotide (**44**) and CNGRC (**46**) (Scheme 2.13b).

A nucleophilic substitution linked **55** to the peptides **44** and **46**, respectively, forming a thioether bond to the free thiols of the cysteines, resulting in cyclization of the peptides (Scheme 2.14).

2.3. Biological evaluation

Fluorescence microscopic measurements and flow cytometric analyses were conducted to evaluate the receptor-mediated internalization of the fluorophore conjugates based on octreotide and CNGRC. Subsequently, the cell viability was determined in order to study the correlation between the different expression levels (high, moderate, low) of the respective receptors and the efficacy of the conjugates to the cancer cells. Moreover, the influence of the duration time of treatment for the efficacy was evaluated.

2.3.1. Studies on cellular internalization of fluorescently labeled peptide conjugates

The selectivity of the peptides **45** and **47** depends on the density of the targets SSTR2 and CD13, respectively, on the cell membrane. Thus, the rate and dimension of internalization of peptide conjugates were investigated by fluorescence measurements applying fluorescently labeled conjugates **56** and **57** to tumor cell lines expressing distinguishable levels of relative receptors (high, medium, low). RT-qPCR analyses were performed in triplicate to determine the expression of studied receptors in the studied cancer cell lines. The determined expression levels in case of the SSTR2 corresponded to the ratio reported in the literature (Figure 2.6a).[74] In case of CD13 the available PC3 cancer cell line expressed less mRNA of CD13 than MDA-MB-468 (Figure 2.6b). The determined expression level of CD13 in PC3 cancer cell line was less than expected according to literature.[74] That observation might be attributed to mutations of the available PC3 cancer cell line. As stated in the literature, such expression levels indicated by RT-qPCR analyses also correlate with membrane-specific ELISA tests elucidating receptor protein levels at the cell surfaces.[75, 76] Though, such independent ELISA tests could not be performed within this work.

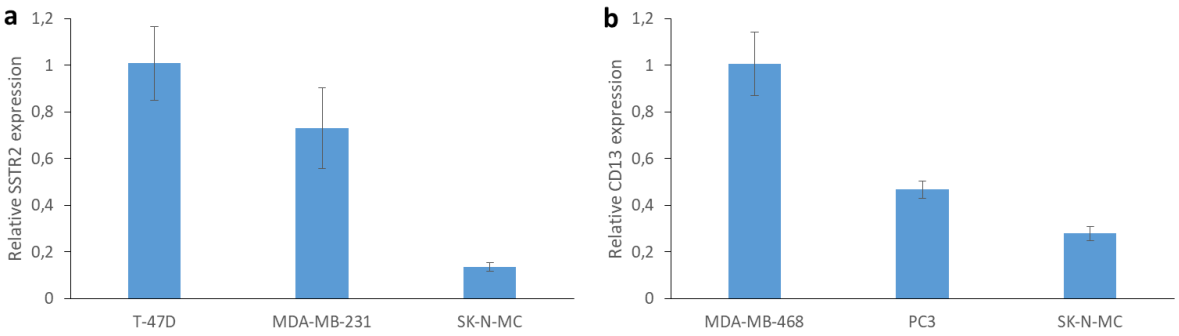

Figure 2.6 a) Expression levels of SSTR2 in T-47D breast cancer cells, MDA-MB-231 breast cancer cells and SK-N-MC Ewing's sarcoma cells, b) expression levels of CD13 in MDA-MB-468, PC3 and SK-N-MC.

The fluorescent conjugates were designed to be non-toxic, because the application of cytotoxic compounds to the cells would have limited the time frame of observation (see Appendix IV,

Figure A 137). Moreover, the syntheses of the fluorescent conjugates were simplified, since the fluorescence measurement focused on the peptide-target interaction resulting in the internalization of the conjugates. Thus, the fluorescent compounds consisted of the fluorophore rhodamine B connected to the targeting peptide via an uncleavable linker to ensure the visualization of the entire conjugate. The cancer cell lines possessing the highest target level were treated with the fluorescent conjugates for different initial incubation times. Thus, the octreotide-rhodamine B conjugate (**56**) was applied to T-47D cells and MDA-MB-468 cells were exposed to the CNGRC-rhodamine B conjugate (**57**). For comparison, the fluorescent conjugates were also applied to SK-N-MC cancer cell line showing lower expression level of the mRNA of both targets.

In advance, fluorescence spectra were recorded to determine excitation and emission wavelengths of the pure fluorophore rhodamine B (λ_{ex} = 545 nm, λ_{em} = 576 nm) and of the fluorescent linker **54** (λ_{ex} = 553 nm, λ_{em} = 581 nm) (see in Appendix III, Figure A 133 & 134). Photographs by fluorescence microscope were taken in order to visualize the internalization of fluorescent conjugates as red-fluorescent spots. Both fluorescent conjugates (**56**, **57**) entered the cells within 30 min (Figure 2.7) and were not detected in surrounding medium after the incubation time. In case of conjugate **56**, most of fluorescent spots were located inside the cells close to the cell membrane and might point to endosomes because of the endocytotic internalization of **56** (Figure 2.7c). Conjugate **57** was more widespread distributed inside the cell (Figure 2.7f) which might be attributed to its release from the endosomal vesicle. But fluorescent spots were also seen which might indicate that some conjugate **57** remains in endosomal vesicles too.

Flow cytometric analyses were performed in order to confirm and semi-quantify the internalization of the fluorescent conjugates. SSTR2-overexpressing cancer cells (T-47D) were treated with fluorescent conjugate **56** and CD13-overexpressing cancer cells (MDA-MB-468) were exposed to fluorescent conjugate **57** for 1 min, 1 h and 6 h. As reference, both conjugates were applied to SK-N-MC cancer cells for 6 h, since SK-N-MC cancer cells show lower expression levels for both targets. After finalized incubation, the cancer cells were washed using culture medium and trypsinized. Trypsinized cells were washed using tryptophan (100 mM in water/acetonitrile 2:1) to quench fluorophores that might remain unspecifically bound to the outer membrane (see Appendix III, Figure A 135).[77] The octreotide-based conjugate **56** was already internalized by T-47D cells after 1 min – virtually representing a “no internalization” control even though cells were exposed to conjugate – 1.21-fold over untreated T-47D cells (Table 2.1 and Figure 2.8a). After 1 h the maximal internalization was almost reached (2.36-fold over untreated T-47D cells). Comparing the behavior of T-47D cells to SK-N-MC cells possessing lower secretion level of SSTR2, the recognition of the target and the following receptor-mediated internalization occurred in a significant manner (Figure 2.8b). Thus, SK-N-MC cancer cells internalized less fluorescent conjugates after 6 h than T-47D cancer cells after 1 min.

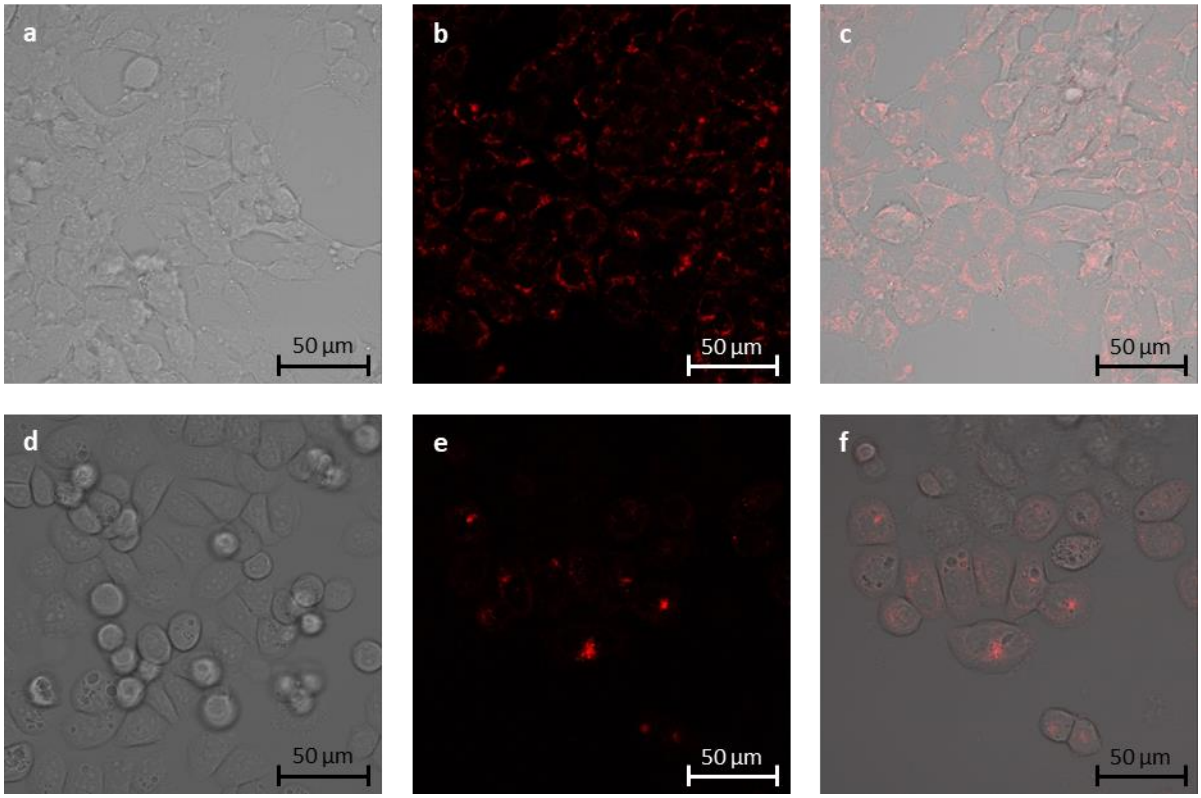

Figure 2.7 Fluorescence microphotographs of untreated a) T-47D and d) MDA-MB-468 cells, b) T-47D cells treated with red-fluorescent **56** after 30 min of incubation, c) merged image of T-47D cells and red-fluorescent **56** inside (30 min), e) MDA-MB-468 cells treated with red-fluorescent **57** after 30 min of incubation, f) merged image of MDA-MB-468 cells with internalized red-fluorescent **57** (after 30 min treatment).

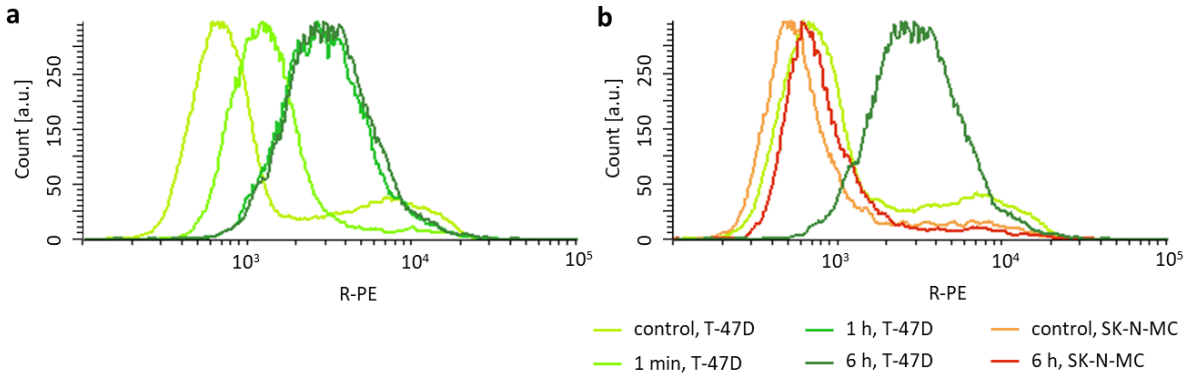

Figure 2.8 Flow cytometric analyses of **56** a) at different incubation times on T-47D cancer cell line, b) comparison between internalization into SSTR2 higher expressing cancer cell line (T-47D, green) and SSTR2 lower expressing cancer cell line (SK-N-MC, red) after 6 h.

The fluorescent conjugate **57** was internalized 1.26-fold over untreated MDA-MB-468 cells after 1 min (Table 2.1). Within 30 min the uptake of conjugate **57** by MDA-MB-468 doubled. The internalization still increased until 6 h incubation, but slowed down (Figure 2.9a). SK-N-MC cancer cells internalized conjugate **57** in the same rate as MDA-MB-468 cancer cells, although RT-qPCR analyses indicated less mRNA expression of CD13 in SK-N-MC cells than in MDA-MB-468 cells. Since the NGR sequence of the targeting peptide homes integrins as well, conjugate **57** might be

internalized not only via CD13. However, the expression of integrins in the used cancer cell lines was not investigated by RT-qPCR analyses. Moreover, SK-N-MC Ewing's sarcoma cells are known to rapidly recycle receptors leading to compensation of weaker internalization of conjugate **57** by CD13-mediated endocytosis.[78]

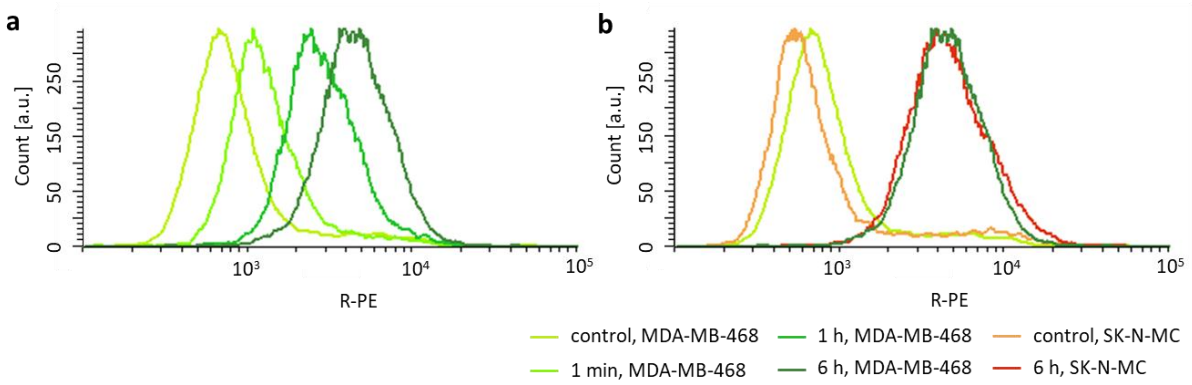

Figure 2.9 Flow cytometric analyses of **57** a) at different incubation times on MDA-MB-468 cancer cell line, b) comparison between internalization into CD13 higher expressing cancer cell line (MDA-MB-468, green) and CD13 lower expressing cancer cell line (SK-N-MC, red) after 6 h.

Table 2.1 Relative quantification of the cellular internalization of fluorescent conjugates **56** in T-47D cancer cells and **57** in MDA-MB-468 cancer cells in relation to untreated T-47D cells and MDA-MB-468 cancer cells, respectively, and SK-N-MC cancer cells expressing both targets less.

	56		**57**	
	RFU[1]	x-fold over untreated	RFU	x-fold over untreated
1 min	20.18	1.21	17.84	1.26
30 min	32.19	1.94	28.38	2.00
1 h	39.31	2.36	35.97	2.54
6 h	41.59	2.50	55.86	3.94
6 h, SK-N-MC	14.92	1.04	59.64	4.15

2.3.2. Evaluation of the cytotoxic activity of the peptide-drug conjugates based on SSTR2- and CD13-targeting peptides

Based on the results of the fluorescent experiments, the correlation between the expression levels of SSTR2 and CD13 and the uptake of the PDCs as well as their efficacy was studied. Thus, the synthesized peptide-drug conjugates based on octreotide (**49**, **50**) and CNGRC (**52**, **53**) as well as pure tubugi 1 (**33**), the spacer containing tubugi 1 (**36**), tubugi 4 (**34**), the spacer containing

[1] relative fluorescence unit

tubugi 4 (**37**), cyclized octreotide (**45**) and cyclized CNGRC (**47**) as reference compounds were tested on cancer cell lines expressing distinguishable levels of relative receptors (high, medium, low).

All bioassays on the cancer cells were performed in biological and technical triplicates and analyzed by resazurin-based fluorometric assay. Based on the IC_{50} values presented in former works,[56] concentrations for dilution series of testing compounds were chosen. Beside the dependence of the activity on the expression level of the receptors, the importance of the incubation time was also investigated. Thus, the cancer cells were exposed to the conjugates as well as the reference compounds for 6, 24 and 72 h. Irrespective of the initial incubation time, the cells were allowed to grow for 72 h after treatment initialization until cell viability was determined. In case of initial compound incubation shorter than these 72 h – i.e. 6 h and 24 h incubation, respectively – incubation solutions were discarded, cells were washed and allowed to grow up in fresh culture medium until measurement after 72 h.

The cell viability test showed that the octreotide-tubugi 1 conjugate (**49**) had a stronger impact on SSTR2-expressing cancer cells (T-47D – high level, MDA-MB-231 – medium level, SK-N-MC – low level) than the octreotide-tubugi 4 conjugate (**50**). This observation might be attributed to the more lipophilic, but more stable moiety at position C11 of the toxin **34**. An interaction between the more lipophilic moiety of **34** and the receptor might lead to decelerated internalization of conjugate **50**. Therefore, conjugate **50** might unfold its activity more slowly. Looking at the graphs (Figure 2.10), the correlation between the expression levels of the receptor SSTR2 to the efficacy of both octreotide-containing conjugates was not as significant as assumed by RT-qPCR (Figure 2.6a) and by FACS (flow cytometry) measurements (Figure 2.8b). However, the dependence of the toxic impact to the cells from the expression level of the respective receptor was clarified by the values (see Appendix IV, Tables A 5 & 6). In general, the efficacy of the conjugates **49** and **50** increased by longer exposure (Figure 2.10a, c, e as well as Figure 2.10b, d, f) and by higher expression level of SSTR2. But the activity of **49** to MDA-MB-231 cell line drifted significantly after 6 h and 72 h from the main tendency. This observation could be attributed to the standard deviation seen in the RT-qPCR evaluation (Figure 2.6a). The reasons for missing outstanding selectivity might be weak internalization of the conjugates or extracellular decomposition of the peptide-drug conjugates. Since octreotide-drug conjugates having a linker system inserted into the peptide cycle have been successfully studied,[29] the change of the conformation of the octreotide might not be the reason. The octreotide-tubugi conjugates were proven to be stable in a 10 mM glutathione solution at 37 °C for more than 6 h. The cleavage product was detected after 24 h by means of ESI MS. An extracellular reduction at the cell membrane might be a cause for the difference between the antitumor activity after 6 h and after 24 h, whereas the activity did not increase that strong between 24 h and 72 h. On the other hand, it is widely known that the receptor-mediated internalization occurs rather fast. Therefore, small amounts of conjugates cleaved inside the cancer cells might cause a sufficiently strong impact to the cells. The bioassays on the reference compounds elucidated that cyclized octreotide (**45**) did not possess any activity against all tumor cell lines at the tested concentrations (lower than 10 µM, see in Appendix IV, Figure A 139), but tubugi 1 (**33**) as well as tubugi 4 (**34**) displayed similar IC_{50} values in lower nanomolar and picomolar range (see Appendix IV, Figures A 143 & 144, Tables 1 & 2). The tubugis elongated with a self-immolative spacer (**36**, **37**) were found to be less effective (see Appendix IV, Figures A 145 & 146, Tables 3 & 4). In case of **36** the efficacy dropped 3- to 4-fold compared to **33**, whereas in case of **37** a decrease about 10- to 20-fold was observed compared to **34** (see Appendix IV, Tables A 1–4).

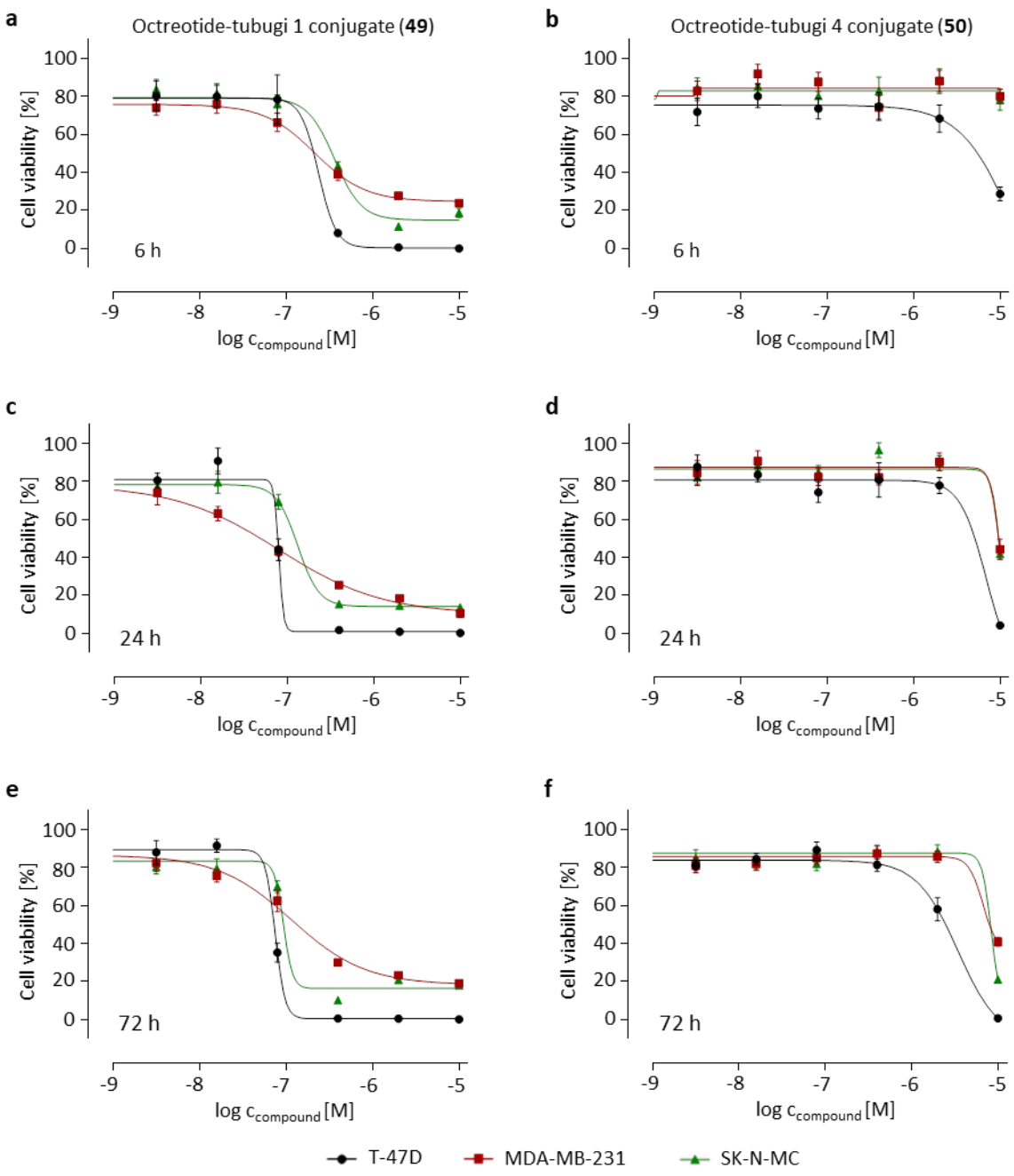

Figure 2.10 *In vitro* antitumor activity of **49** after a) 6, c) 24, e) 72 h initial treatment and of **50** after b) 6, d) 24 and f) 72 h initial treatment in T-47D breast cancer cells (high SSTR2), MDA-MB-231 breast cancer cells (medium SSTR2) and SK-N-MC Ewing's sarcoma cells (low SSTR2) (for SSTR2 expression see Figure 2.6a).[2]

The *in vitro* assays on CD13-expressing cancer cell lines (MDA-MB-468 – high level, PC3 – medium level, SK-N-MC – low level) elucidated that the CNGRC-tubugi 1 conjugate (**52**) exhibited more bioactive effect to the tumor cells than the conjugate containing tubugi 4 (**53**), as it was observed in case of the octreotide-tubugi conjugates (Figure 2.11). The lower activity of **53** might be explained by the more lipophilic moiety at position C11 of the toxin **34** as well. In case of cells treated with **52**,

[2] This extract zooms in on the inflection points representing the IC_{50} values. The full size graphs are seen in Appendix IV, Figure A 159.

the cell viability of cells expressing a high level of CD13 was significantly lower than the cell viability of low expressing cells (see Appendix IV, Table A 7), but expectedly the difference of the IC_{50} values decreased with a longer duration of treatment. As shown by flow cytometry, a significant correlation between the impact of **52** and the expression level of CD13 and also of the time was not

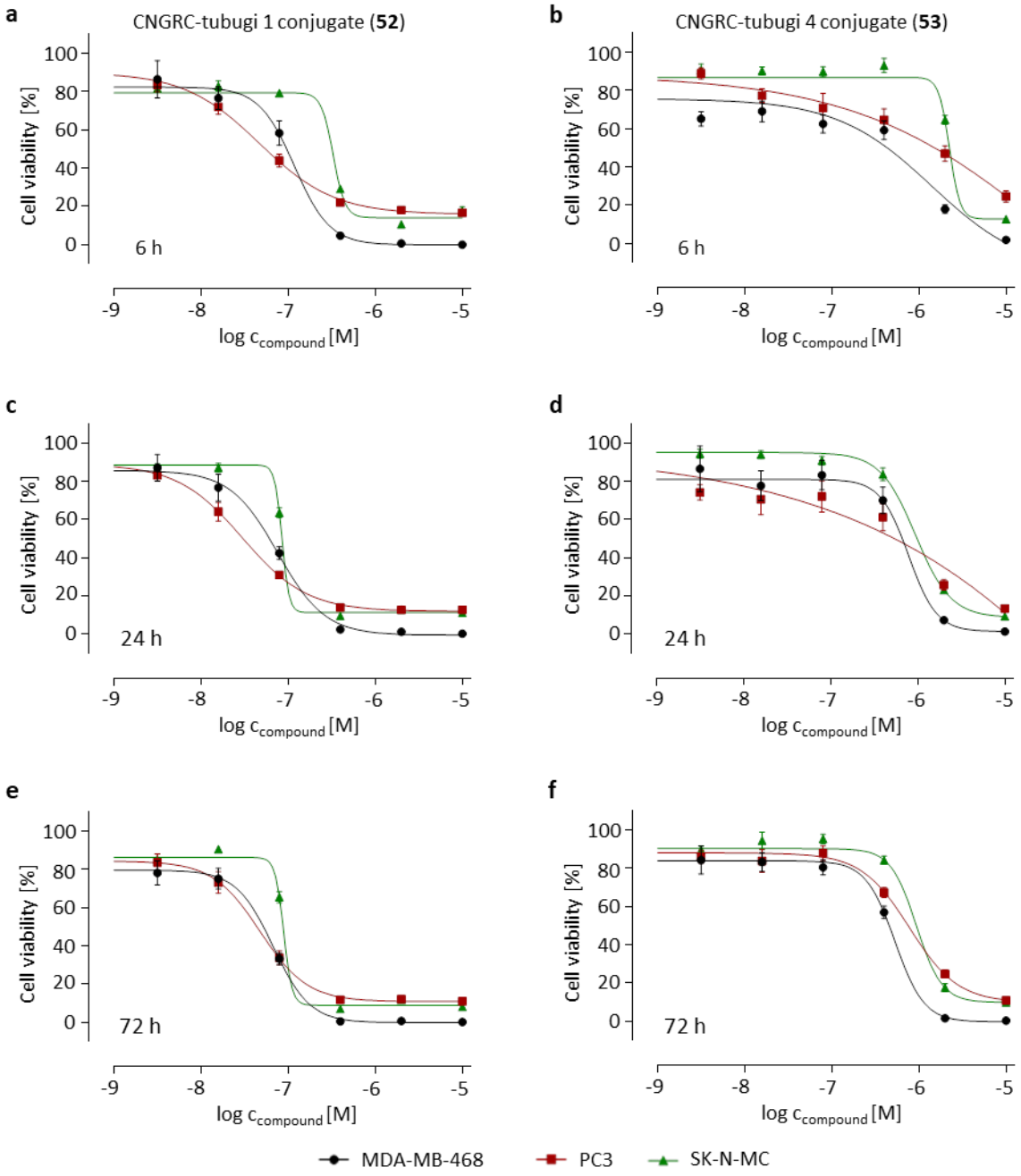

Figure 2.11 *In vitro* antitumor activity of **52** after a) 6, c) 24, e) 72 h initial treatment and of **53** after b) 6, d) 24 and f) 72 h initial treatment in MDA-MB-468 breast cancer cells (high CD13), PC3 prostate cancer cells (medium CD13) and SK-N-MC Ewing's sarcoma cells (low CD13) (for CD13 expression see Figure 2.6b).[3]

[3] This extract zooms in on the inflection points representing the IC_{50} values. The full size graphs are seen in Appendix IV, Figure A 160.

proven. The lowest IC_{50} was determined after 24 h. The correlation between the effect on the cells and the expression level as well as the incubation time was more clearly seen in case of **53** (Figure 2.11b, d, f). The efficacy of **53** rose during longer exposure (see Appendix IV, Table A 8) and by higher expression level of CD13. Only the early 6 h value of treatment on PC3 cancer cells deviated from this tendency. The cytotoxic effect of compounds **33**, **34**, **36** and **37** on the cancer cell lines expressing different levels of CD13 led to the same observation as in case of the SSTR2-expressing cell lines. Thus, the tubugis (**33**, **34**) showed comparable IC_{50} values in lower nanomolar and picomolar range (see Appendix IV, Figures A 147 & 148, Tables A 1–2) and the tubugis containing the spacer compound (**36**, **37**) unfolded a weaker impact than the respective tubugis (see Appendix IV, Figures A 149 & 150, Tables 3 & 4). In contrast, the cyclized CNGRC (**47**) did not show a cytotoxic activity against tested cancer cell lines (see Appendix IV, Figure A 140). The reason for weak selectivity of PDCs based on NGR targeting might be an internalization of the PDCs through another pathway or an extracellular decomposition of the peptide-drug conjugates. The NGR-tubugi conjugates were shown to be stable at 37 °C and in a 10 mM glutathione solution for more than 6 h. The cleavage product was detected after 24 h. As a consequence, an extracellular reduction at the cell membrane likely is not the cause of the degradation of the PDCs.

2.4. Experimental part

2.4.1. Materials

Preparative technique

The syntheses, except for those involving peptides, were carried out in dry solvents. Dry solvents were stored over molecular sieves.

All peptides were automatically synthesized using an Intavis ResPep SL automated peptide synthesizer.

Purchased materials and starting materials

All chemicals and solvents were purchased from abcr (Karlsruhe, Germany), Alfa Aesar (Heysham, United Kingdom), Carbolution (St. Ingbert, Germany), Carl Roth (Karlsruhe, Germany), Iris Biotech (Marktredwitz, Germany), Merck (Darmstadt, Germany), TCI (Tokyo, Japan) and TUBE Pharmaceuticals (Wien, Austria). The silica gel 60 (0.040–0.063 mm) from Merck was used for performing column chromatography.

In vitro cytotoxicity studies − reagents and cells

FCS (fetal calf serum), RPMI-A (RPMI 1640 with L-glutamine), RPMI-XRXA (RPMI 1640, w/o L-glutamine, w/o phenol red), DMEM-HA (DMEM high glucose (4.5 g/L), with L-glutamine), trypsin-EDTA (0.05 %) in DPBS (1x), DPBS (1x, w/o Ca & Mg, w/o phenol red), penicillin/streptomycin (100x) were purchased from Capricorn Scientific (Ebsdorfergrund, Germany), L-tryptophan from Fluka (Charlotte, United States), DMSO from Duchefa Biochemie (Haarlem, Netherlands), insulin (10 mg/mL) from PAN-Biotech (Aidenbach, Germany) and digitonin from Riedel-de Haën (Seelze, Germany). Resazurin sodium salt and trypan blue were ordered from Merck (Darmstadt, Germany), agarose from Carl Roth (Karlsruhe, Germany) and ethidium bromide solution (1 %) from PanReac

AppliChem (Barcelona, Spain; Darmstadt, Germany). MDA-MB-231 breast cancer cells, MDA-MB-468 breast cancer cells, T-47D breast cancer cells, SK-N-MC Ewing's sarcoma cells, HT-29 colon cancer cells and PC3 prostate cancer cells were purchased from ATCC (Manassas, United States). The kit Quick-RNA™ Miniprep was purchased from Zymo research (Freiburg, Germany), the kit for reverse transcription from Thermo Fisher Scientific (Waltmore, United States) and the qPCR GreenMaster lowROX from Jena Bioscience (Jena, Germany).

The cells were routinely cultivated in cell line-specific culture medium (Table 2.2) containing 10 % FCS and 1 % penicillin/streptomycin at 37 °C in a humidified atmosphere with 5 % CO_2.

Table 2.2 Used cancer cell lines and corresponding cultivation medium.

Cell line	Medium
T-47D	RPMI-A + 420 µL insulin per 500 mL
HT-29	RPMI-XRXA
PC3	RPMI-XRXA
MDA-MB-468	DMEM-HA
MDA-MB-231	RPMI-XRXA
SK-N-MC	DMEM-HA

2.4.2. Analytical Methods

Thin layer chromatography (TLC)

The thin layer chromatography was performed on silica coated aluminum plates (silica 60 F_{254}, aluminum sheets Merck, Darmstadt, Germany). The spots of the compounds were detected by UV light (254 or 366 nm) Camag UV cabinet or visualized by the following stain:

Ninhydrin stain: ninhydrin (1.5 g) in *n*-butanol (100 mL) and acetic acid (3 mL).

ESI mass spectrometry

Mass spectra were obtained from API3200 (Co.: AB Sciex) equipped with a Triple Quadrupole MS. The sample solutions were introduced continuously via syringe pump with a flow rate of 250 µL · min^{-1}. Methanol was used as solvent.

High resolution mass spectrometry (HR-MS)

High resolution ESI mass spectra were recorded on Orbitrap Elite mass spectrometer (Co.: Thermofisher Scientific) equipped with an HESI electrospray ion source (spray voltage 4.0 kV, capillary temperature 275 °C, source heater temperature 40 °C; FTMS resolution 60.000). Nitrogen was used as sheath gas. The sample solutions were introduced continuously via a 500 µL Hamilton syringe pump with a flow rate of 5 µL · min^{-1}. The instrument was externally calibrated by the Pierce® LTQ Velos ESI positive ion calibration solution (product number 88323) and Pierce® ESI

negative ion calibration solution (product number 88324) from Thermofisher Scientific. The data were evaluated by the Xcalibur software 2.7 SP1.

HPLC

In general, a mixture of methanol/water was used as eluent for the high pressure liquid chromatography starting with 30 % of methanol and increasing by isocratic gradient up to 100 % methanol in 15 min. The used column (125×4 mm) was filled with LiChrospher® with particle size of 5 µm and a pore size of 100 Å. The signals were recorded by an UV-detector. The measurements were performed at 20 °C with a flow rate of 1 mL · min^{-1} on 1260 infinity system (Co.: Agilent Technologies).

NMR spectroscopy

All samples were measured in 5 mm NMR tubes at 298 K. 1D (^{1}H, ^{13}C) and 2D (HSQC, HMBC, COSY, TOCSY) spectra were recorded on Agilent DD2 400 MHz and on Bruker AVANCE NEO 500 MHz NMR spectrometer. The chemical shifts of the ^{1}H NMR spectra are referenced to the internal standard TMS (δ = 0.000 ppm) and the ^{13}C NMR spectra are referenced to the solvent signals of the deuterated organic solvents. As deuterated solvents CD_3OD (^{1}H δ = 3.31, ^{13}C δ = 49.0), $CDCl_3$ (^{1}H δ = 7.26, ^{13}C δ = 77.2) and DMSO-d6 (^{1}H δ = 2.50, ^{13}C δ = 39.5) were used.

FACS analysis

FACSAria III (Co.: BD Biosciences) was used for flow cytometry experiments.

Cell counter

Number of cells was determined on Countess II FL (Co.: Life Technologies).

Plate reader

The optical analyses of resazurin-based fluorometric assay (λ_{ex} = 540 nm, λ_{em} = 590 nm) and the record of absorbance as well as fluorescence spectra were recorded on SpectraMax M5 (Co.: Molecular Devices).

Microvolume Spectrometer

The concentration of the regarding RNA and the A260/280 were determined by Colibri (Co.: Titertek Berthold).

Real-Time PCR Detection

The RT-qPCR measurements were analyzed by CFX96™ real-time system and C1000™ thermal cycler (Co.: Bio Rad).

Electrophoresis

Electrophoresis was carried out by means of Biometra P25 and Biometra PS 300 (Co.: Analytik Jena).

Fluorescence microscope

Fluorescence microscopic measurements were performed on Zeiss LSM780 laser scanning confocal microscope (Co.: Carl Zeiss).

2.4.3. Glutathione test

The release of the tubugis from the peptide-drug conjugates was determined *in vitro* under reductive conditions imitating conditions inside tumor cells. Thus, all bioactive compounds (c = 0.05 mM) were exposed to 10 mM glutathione (reduced form) solution at 37 °C. ESI MS measurements were performed after different time points: 1, 30 min, 1, 2, 6, 24, 48 and 72 h. The time points were chosen to screen the cleavage process at the beginning of treatment and then after the incubation times.

2.4.4. Biological Assays

In vitro investigations of cell viability by resazurin-based fluorometric assay

The viability of treated tumor cells was determined by resazurin-based fluorometric assay. The stock solutions were dissolved in DMSO and diluted by RPMI medium to applied working concentrations which were used immediately. The cells were removed from the cultivation bottle by standard trypsinization and counted in the cell counter. 100 µL of cell suspension were seeded in each well of a 96-well plate at densities specific for each cancer cell line (Table 2.3). After incubation overnight, the old medium was discarded and 80 µL of fresh cell line-specific medium were added. Afterwards, prepared 5-fold working solutions of the test compounds were added resulting in serial dilution: 25.6, 128, 640 pM, 3.2, 16, 80, 400 nM, 2, 10 µM. The peptide-drug conjugates and precursors were applied to cancer cell lines expressing high, moderate and low levels of receptors to which the regarding peptide binds. Furthermore, cells were exposed to the conjugates for different initial incubation times (6, 24, 72 h). Thus, after these initial incubation times the incubation media were discarded, each well was washed with 100 µL RPMI medium (1 ×), 100 µL of cell line-specific medium was added and the cells were allowed to grow for 72 h (after 6, 24 h) in the incubator. After total incubation ad 72 h, medium was discarded and each well was washed with 100 µL RPMI medium. Subsequently, 80 µL of resazurin solution (50 µM in RPMI medium w/o phenol red) were added. After incubation at 37 °C for 2 h the optical density of each well was read using the plate reader (λ_{ex} = 540 nm, λ_{em} = 590 nm, auto Cutoff). Results were normalized referring to negative (1 % DMSO) and positive (100 µM digitonin) control and arbitrarily set to 100 %. All experiments were carried out in biological and technical triplicates. IC_{50} values, defined as the concentrations of the compound at which 50 % of cell inhibition occur (±SD), were calculated using four-parameter logistic function and presented as mean from three independent experiments.

Table 2.3 Amount of seeded cells per cancer cell line and plate size.

Cell line	8-chamber slide	24-well plate	96-well plate
T-47D	70,000	90,000	5,000
HT-29	70,000	90,000	4,000
PC3	–	–	2,000
MDA-MB-468	70,000	60,000	5,000
MDA-MB-231	–	–	4,000
SK-N-MC	–	70,000	12,000

Fluorescence microscopy investigations

The cells were removed from the cultivation bottle by standard trypsinization and counted in the cell counter. 200 µL of cell suspension were seeded in each well of an 8-chamber slide at densities specific for each cancer cell line (Table 2.3). After incubation for 48 h and obtaining a confluency about 80 %, the old medium was discarded. The cells were washed with RPMI medium (200 µL, w/o FCS, w/o phenol red) and RPMI medium (w/o FCS, w/o phenol red) was to wells of untreated control (200 µL) and to them of compounds (199.9 µL). The fluorescent compounds (0.1 µL, 20 mM) were added in order to obtain a 10 µM final concentration in the regarding wells. Fluorescence microscopic measurements were performed after 30 min of incubation.

Flow cytometric analyses

The cells were removed from the cultivation bottle by standard trypsinization and counted in the cell counter. 400 µL of cell suspension were seeded in each well of a 24-well plate at densities specific for each cancer cell line (Table 2.3). After incubation for 48 h and obtaining a confluency about 70 %, the old medium was discarded. The cells were washed with RPMI medium (500 µL, w/o FCS, w/o phenol red) and then fresh RPMI medium (w/o FCS, w/o phenol red) was added to all wells of untreated control (400 µL) and to wells of compounds (399.5 µL). The fluorescent compounds (0.5 µL, 20 mM) were added to defined wells at respective time points (1 min, 30 min, 1 h, 6 h) in order to obtain 5 µM in concentration. The treated cells were left to incubate at 37 °C for resepctive duration. Afterwards, the incubation medium was discarded and the cells were washed with RPMI medium (500 µL, w/o FCS, w/o phenol red). Trypsin/EDTA (150 µL) was added to each well and left to incubate at 37 °C for 3 min. Trypsinization was stopped by ice-cold RPMI medium (500 µL, with FCS) and cells were transferred to culture tubes. Tryptophan was added in order to quench extracellular fluorophore (100 µL, 100 mM in water/acetonitrile 2:1). The mixture was centrifuged, the supernatant was discarded, DPBS (500 µL) was added for washing, centrifuged and the supernatant was discarded. DPBS (800 µL) was added. Immediately before performing FACS measurements (channel: PE 582/15), each sample was vortexed.

Real-time quantitative polymerase chain reaction (RT-qPCR)

In a first step, the RNA was isolated applying the kit Quick-RNA™ Miniprep. The cells were removed from the cultivation bottle by standard trypsinization and counted in the cell counter. 4×10^6 cells

were tranferred to a Eppendorf tube, centrifuged and the supernatant was discarded. Lysis buffer (300 µL) was added and it was vortexed until the cell suspension got homogenous. Then the suspension was centrifuged at 16000 g for 1 min. The emulsion (300 µL) was given to the yellow column and centrifuged at 16000 ×g for 1 min. Ethanol (300 µL, 96 %) was added to the filtrate, vortexed and transferred to the green column, which was centrifuged at 16000 ×g for 1 min. The flow through was discarded and RNA wash buffer (400 µL) was added to the green column followed by centrifuging at 16000 ×g for 1 min and discarding the flow through. The DNase-1 working solution was prepared in a separate Eppendorf tube to which DNase-1 (5 µL) and DNA digestion buffer (75 µL) were added. This DNase-1 working solution was transferred to the green column (80 µL) and left to incubate for 15 min at rt. RNA prep buffer (400 µL) was added to the green column followed by centrifuging at 16000 ×g for 1 min and discarding the flow through. RNA wash buffer (700 µL) was added to the green column followed by centrifuging at 16000 ×g for 1 min and discarding the flow through. Further RNA wash buffer (400 µL) was added to the green column followed by centrifuging at 16000 ×g for 2 min and discarding the flow through. DNase/RNase free water (100 µL) was added to the green column and left to centrifuge for 1 min.

In a second step, the properties of the isolated RNA were determined. Firstly, the absorbance of the previously isolated RNA solution (1 µL) was measured in order to obtain the concentration and the A260/280 value (ideally 1.5-2). In an other experiment, agarose gel electrophoresis was performed. Thus, agarose (0.5 g) was suspended in TAE buffer (50 mL) and heated in the microwave for 1 min in order to afford a clear solution. Ethidium bromide (2.5 µL) was added to the mixture which was then poured in the gel holder. A comb was put in the cast to keep wells for addition of the samples and then the gel was left to solidify for 30 min. Meanwhile the isolated RNA solution (9 µL) was transferred to an Eppendorf tube and treated with 10× DNA loading buffer (1 µL). In the first well of solid gel 1 kb DNA ladder (9 µL + 1 µL 10× DNA loading buffer → 8 µL for injection) was injected and in the following wells the prepared RNA samples (8 µL) were injected. After running the gel for 60 min at 100 V and maximal ampere, the gel was observed in the UV cabinet.

The third step embraces the reverse transcription of the DNA using the kit for reverse transcription. A mixture of the isolated RNA (500 ng), Oligo (dT) 18 Primer (1 µL) and PCR water (filling volume up to 12.5 µL) was prepared in a sterile Eppendorf PCR tube. The mixture was vortexed, centrifuged and left to incubate at 65 °C for 5 min. Subsequently, the mixture was cooled down in ice and supplemented by 5× Reaction Buffer (4 µL), RiboLock RNase Inhibitor (40 U · μL^{-1}, 0.5 µL), dNTP Mix (10 mM ea, 2 µL) and RevertAid Reverse Transcriptase (200 U · μL^{-1}, 1 µL). The mixture was gently vortexed, centrifuged and left to incubate at 42 °C for 60 min. The reaction was terminated by heating at 70 °C for 10 min. At the end the obtained cDNA was diluted using PCR water (180 µL).

In the final step, the RT-qPCR analyses were carried out by using the qPCR GreenMaster lowROX. The qPCR master mix was prepared in a Eppendorf tube. For each sample n n+2 qPCR master mixes were prepared. Thus, the qPCR GreenMaster with lowROX (10 µL), primer forward (10 µM, 0.6 µL), the primer reverse (10 µM, 0.6 µL) and PCR water (3.8 µL) were added to the tube followed by vortexing. The qPCR master mix (15 µL) and afterwards the cDNA sample (5 µL) were added to wells of the PCR plate. The plate was covered with an adhesive foil and centrifuged (1000 rpm, 3 min). The cycling conditions to quantify the amplified DNA are presented in Table 2.4.

Table 2.4 Cyclic conditions for amplification of DNA.

Step	Temperature [°C]	Duration [min]	Iteration
Initial denaturation and polymerase activation	95	2	1 ×
Denaturation	95	0.25	35–45 ×
Annealing and elongation[4]	60–65	1	35–45 ×

2.4.5. General synthetic procedures

Solid phase peptide synthesis (SPPS) **G1**[79-82]

The coupling reactions for the syntheses of peptides were automatically and stepwise performed on an Intavis ResPep SL automated peptide synthesizer according to the widely used Fmoc/tBu strategy comprising a 5-fold excess of Fmoc-protected amino acids as well as PyBop and a 10-fold excess of NMM at rt for 15 min in 100 µmol scale regarding the used resin. The resin was left to swell twice 1 min in dichloromethane before starting automated synthesis. The automated syntheses were completed by the removal of the Fmoc group using 10 % piperidine in DMF followed by manually washing using DMF (3 × 1 min) and dichloromethane (3 × 1 min). A minicleavage was performed to check, if the reaction succeeded. Afterwards, the peptide was cleaved from the resin using a cleavage solution (TFA/TIS/EDT/H_2O 91:3:3:3) followed by precipitation from ice-cold diethyl ether, centrifugation and washing in ice-cold diethyl ether (2 ×). The crude peptide was dissolved in a mixture of water/acetonitrile (2:1), frozen in liquid nitrogen and lyophilized.

Kaiser test **G2**

The Kaiser test was performed to monitor the progress of SPPS and to detect free amino groups. A small amount of the resin (a few resin beads) were transferred to a small test tube and washed (addition of methanol, vortex, keep steady, remove supernatant, repeat once). After that, a few drops of potassium cyanide, ninhydrin solution and phenol were added. The mixture was heated at 100 °C for 5 min. A blue coloring indicates the presence of free amino groups, i.e. not completed reaction, whereas a yellow solution indicates the completed conversion.

Minicleavage **G3**

A small amount of the resin (a few resin beads) were transferred to an Eppendorf tube and cleavage mixture (TFA/TIS/H_2O 94:3:3, 320 µL) were added. The suspension was left to shake for 2 h followed by removal of the solvents under nitrogen flow. Ice-cold diethyl ether (500 µL) was added to precipitate the cleaved peptide. Then, the suspension was centrifuged for 3 min and subsequently,

[4] The annealing temperature depends on the melting temperature of the primers and DNA probe used and the elongation time depends on the length of the amplicon. A time of 1 min for a fragment of up to 500 bp is recommended.

the precipitated peptide was dissolved in water/acetonitrile (2:1) in order to check the mass by ESI MS.

2.4.6. Syntheses of tubugi 1 and tubugi 4

D-*N*-Benzyloxycarbonyl pipecolic acid (**1**)

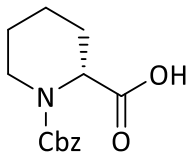

D-pipecolic acid (5.00 g, 37.94 mmol) was dissolved in 2 M NaOH (18 mL) and cooled to 0 °C. Benzyl chloroformate (6.04 mL, 40.21 mmol) was dissolved in 2 M NaOH (18 mL) and dropped slowly to the solution of D-pipecolic acid. The mixture was left to stir at rt overnight. Then the crude product was extracted with diethyl ether (3 × 50 mL). The remaining aqueous layer was set to pH = 2 by citric acid and then extracted with ethyl acetate (4 × 60 mL). The organic layers were combined, dried over Na_2SO_4, filtered and the solvent was removed under reduced pressure to obtain **1** (9.75 g, 98 %) as a colorless solid.

^{1}H NMR (400 MHz, CD_3OD): δ = 1.28−1.35 (m, 1H), 1.39−1.49 (m, 1H), 1.63−1.74 (m, 3H), 2.20−2.22 (t, 1H), 2.96−3.13 (m, 1H), 4.02 (s, 1H), 4.81−4.82 (dd, 1H), 5.08−5.16 (m, 2H), 7.28−7.36 (m, 5H) ppm.

^{13}C NMR (101 MHz, CD_3OD): δ = 20.2, 24.3, 26.4, 41.5, 54.2, 54.5, 67.0, 127.2, 127.3, 127.6, 136.6, 173.2 ppm.

HRMS calculated for $C_{14}H_{18}NO_4$ $[M+H]^+$: m/z = 264.1236, found: m/z = 264.1219.

calculated for $C_{14}H_{16}NO_4$ $[M-H]^-$: m/z = 262.1079, found: m/z = 262.1079.

(D-*N*-Benzyloxycarbonyl piperidine-2-carbonyl)-L-isoleucin methyl ester (**2**)

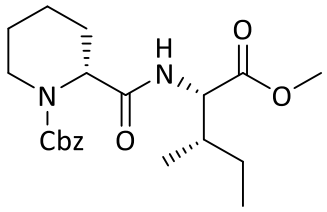

1 (9.75 g, 36.29 mmol) was dissolved in DMF (130 mL) under nitrogen atmosphere and to that solution L-Ile-OMe (6.80 g, 36.29 mmol), EDC × HCl (7.19 mL, 39.92 mmol), HOBt (5.56 g, 39.92 mmol) and 2,6-lutidine (4.74 mL, 39.92 mmol) were added. The mixture was left to stir at rt overnight. The crude was diluted with water (100 mL) and extracted with diethyl ether (3 × 100 mL). The organic layers were combined and washed with sat. $NaHCO_3$ solution (1 × 50 mL) and brine (2 × 50 mL), dried over Na_2SO_4, filtered and concentrated under reduced pressure to afford **2** (13.31 g, 94 %) as a bright yelllow oil.

^{1}H NMR (400 MHz, $CDCl_3$): δ = 0.86−0.89 (m, 6H), 1.33−1.67 (m, 6H), 1.88 (s, 1H), 2.30−2.36 (m, 1H), 2.88−3.01 (m, 2H), 3.72 (s, 3H), 4.09−4.15 (dd, 1H), 4.56−4.59 (dd, 1H), 5.20 (s, 2H), 7.29−7.35 (m, 5H) ppm.

^{13}C NMR (101 MHz, $CDCl_3$): δ = 11.5, 14.2, 15.6, 20.4, 21.0, 24.9, 36.4, 37.5, 42.2, 52.0, 54.6, 56.4, 60.3, 67.6, 120.1, 127.8, 128.5, 136.5, 157.6, 170.6, 172.3 ppm.

HRMS calculated for $C_{21}H_{31}N_2O_5$ $[M+H]^+$: m/z = 391.2235, found: m/z = 391.2211.

(D-*N*-Methyl piperidine-2-carbonyl)-L-isoleucin methyl ester (**3**)

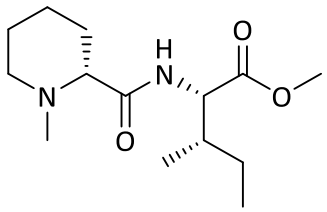

2 (12.99 g, 32.60 mmol) was dissolved in methanol (150 mL), then paraformaldehyde (1.24 g, 39.12 mmol) and $Pd(OH)_2$ (20 % on carbon, 1.60 g) were added. The mixture was left to stir at rt overnight under hydrogen atmosphere. The crude product was filtered through celite and then washed with methanol. The solvent was removed under reduced pressure to obtain **3** (3.49 g, 40 %) as colorless oil.

R_f = 0.2 (ethyl acetate)

^{1}H NMR (400 MHz, $CDCl_3$): δ = 0.91−0.96 (m, 6H), 1.16−1.27 (m, 2H), 1.42−1.66 (m, 4H), 1.71−1.76 (m, 1H), 1.89−2.07 (m, 3H), 2.24 (s, 3H), 2.49−2.52 (dd, 1H), 2.91−2.94 (dd, 1H), 3.73 (s, 3H), 4.56−4.60 (dd, 1H), 7.04−7.07 (d, 1H) ppm.

^{13}C NMR (101 MHz, $CDCl_3$): δ = 11.5, 15.8, 23.2, 25.1, 25.2, 30.6, 37.6, 44.9, 51.9, 55.4, 55.8, 69.6, 172.4, 174.4 ppm.

HRMS calculated for $C_{14}H_{27}N_2O_3$ $[M+H]^+$: m/z = 271.2023, found: m/z = 271.2016.

(D-*N*-Methyl piperidine-2-carbonyl)-L-isoleucin (**4**)

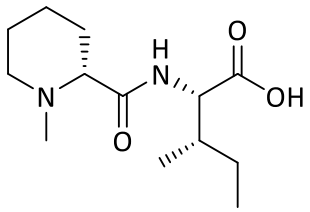

3 (0.98 g, 3.44 mmol) was dissolved in THF/H_2O (2:1, 60 mL) and acidified with concentrated HCl to pH = 1. The mixture was left to stir under reflux for 7 d. The solvents were removed under reduced pressure to obtain **4** in quantitative yield (0.96 g) as a yellowish oil.

R_f = 0.15 (ethyl acetate/methanol/formic acid 5:4:1)

^{1}H NMR (400 MHz, $CDCl_3$): δ = 0.86−1.01 (m, 6H), 1.27−1.34 (m, 1H), 1.48−1.54 (m, 1H), 1.59−1.71 (m, 1H), 1.80−2.15 (m, 6H), 2.71 (s, 3H), 3.47−3.78 (m, 2H), 4.39 (s, 1H), 8.40−8.61 (d, 1H) ppm.

^{13}C NMR (101 MHz, $CDCl_3$): δ = 11.9, 15.5, 22.9, 25.9, 28.4, 30.0, 38.1, 41.3, 59.1, 62.5, 70.9, 167.4, 174.5 ppm.

HRMS calculated for $C_{13}H_{25}N_2O_3$ $[M+H]^+$: m/z = 257.1867, found: m/z = 257.1882.

calculated for $C_{13}H_{23}N_2O_3$ $[M-H]^-$: m/z = 255.1707, found: m/z = 255.1719.

Oxopropane thioamide (**5**)

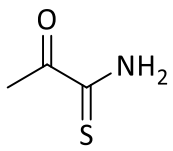

Pyruvonitrile (24.94 g, 325.00 mmol) was dissolved in dry diethyl ether (250 mL) and cooled to 0 °C. H_2S was bubbled through the solution over a period of 30 min. Subsequently, Et_3N (1.05 mL, 7.50 mmol) was added (the solution turned wine-red) and the resulting mixture was left to stir at rt overnight. The crude product was washed with brine (2 × 50 mL). The organic phase was separated, dried over anhydrous Na_2SO_4, filtered and the solvent was removed under reduced pressure to afford **5** (29.43 g, 88 %) as dark red solid.

^{1}H NMR (400 MHz, $CDCl_3$): δ = 2.66 (s, 3H) ppm.

^{13}C NMR (101 MHz, $CDCl_3$): δ = 25.1, 190.9, 192.6 ppm.

HRMS calculated for C_3H_6NOS $[M+H]^+$: m/z = 104.0172, found: m/z = 104.0156.

2-Acetyl 4-ethyl carboxylthiazole (**6**)

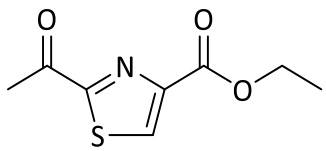

Compound **5** (23.15 g, 202.00 mmol) was dissolved in ethanol (40 mL). Ethyl bromopyruvate (30.98 g, 222.20 mmol) was added and the mixture was left to reflux for 1 h. After that, the solvent was removed under reduced pressure and the crude product was purified by silica column chromatography to afford **6** (9.19 g, 23 %) as a yellow solid.

R_f = 0.31 (*n*-hexane/ethyl acetate)

^{1}H NMR (400 MHz, $CDCl_3$): δ = 1.42−1.45 (t, 3H), 2.79 (s, 3H), 4.43−4.49 (dd, 2H), 8.43 (s, 1H) ppm.

^{13}C NMR (101 MHz, $CDCl_3$): δ = 14.3, 26.1, 61.8, 133.3, 148.7, 160.8, 167.4, 191.6 ppm.

2-(4-Methylpent-2-enoyl)-4-ethyl carboxylthiazole (**7**)

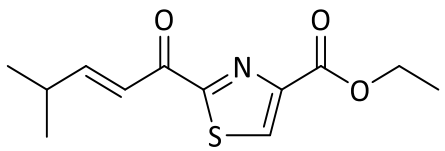

Compound **6** (9.51 g, 40.58 mmol) was dissolved in THF (180 mL) under nitrogen atmosphere and cooled to 0 °C. Titaniumtetrachloride (1 M in toluene, 89.28 mL, 89.28 mmol) was added under nitrogen atmosphere. The mixture was left to stir at 0 °C for 40 min and then cooled down to −78 °C. Et_3N was added and *iso*-butanal (9.88 mL, 107.14 mmol) was added dropwise after further 10 min at −78 °C. The mixture was left to stir at −78 °C for 1 h. After removing the cooling bath, the mixture was allowed to reach rt within 1 h. The reaction was quenched by addition of sat. NH_4Cl solution (100 mL). The aqueous phase was extracted with ethyl acetate (3 ×). The organic layers were combined, dried over Na_2SO_4, filtered, the solvent was removed under reduced pressure and the crude product was purified by silica column chromatography to afford **7** (6.02 g, 59 %) as a colorless oil.

R_f = 0.27 (*n*-hexane/ethyl acetate 5:1)

^{1}H NMR (400 MHz, $CDCl_3$): δ = 1.15−1.16 (d, 6H), 1.42−1.46 (dd, 3H), 2.58−2.70 (m, 1H), 4.44−4.49 (dd, 2H), 7.32−7.33 (m, 2H), 8.43 (s, 1H) ppm.

^{13}C NMR (101 MHz, $CDCl_3$): δ = 14.3, 21.2, 31.8, 61.8, 121.3, 133.1, 148.6, 158.7, 160.9, 168.8, 181.7 ppm.

HRMS calculated for $C_{12}H_{16}NO_3S$ $[M+H]^+$: m/z = 254.0853, found: m/z = 254.0837.

2-[3-(*tert*-Butyloxycarbonyl)amino-4-methylpentanoyl]-4-ethyl carboxylthiazole (**8**)

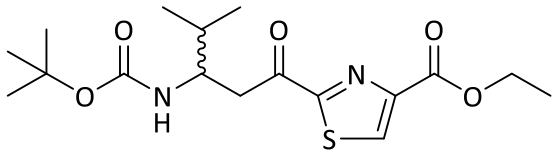

Compound **7** (7.73 g, 30.19 mmol) was dissolved in acetonitrile (121 mL) under nitrogen atmosphere. $Sn(OTf)_2$ (2.57 g, 6.04 mmol) and *tert*-butylcarbamat (4.33 g, 36.23 mmol) were added to that solution. The resulting mixture was stirred at rt for 3 h. The solvent was removed under reduced pressure and the crude product was purified by silica column chromatography to obtain **8** (7.06 g, 63 %) as a colorless solid.

R_f = 0.44 (*n*-hexane/ethyl acetate 7:5)

^{1}H NMR (400 MHz, $CDCl_3$): δ = 0.96−0.98 (dd, 6H), 1.38 (s, 9H), 1.41−1.45 (dd, 3H), 1.88−1.94 (m, 1H), 3.28−3.40 (m, 2H), 3.99−4.06 (m, 1H), 4.42−4.48 (dd, 2H), 4.82−4.85 (d, 1H), 8.44 (s, 1H) ppm.

^{13}C NMR (101 MHz, $CDCl_3$): δ = 14.2, 18.2, 19.2, 28.2, 32.1, 41.3, 52.9, 61.7, 79.0, 133.2, 148.5, 155.4, 160.7, 167.3, 192.3 ppm.

HRMS calculated for $C_{17}H_{27}N_2O_5S$ $[M+H]^+$: m/z = 371.1642, found: m/z = 371.1615.

2-[(1*R*,3*R*) 3-(*tert*-Butyloxycarbonyl)amino-1-hydroxy-4-methylpentyl]-4-ethyl carboxylthiazole or *N*-Boc-tubuvalin ethyl ester (**9**)

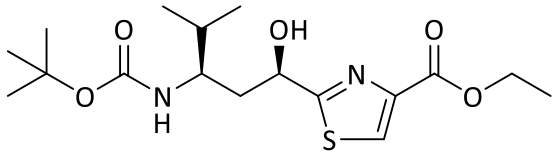

Borane dimethyl sulfide complex (0.73 mL, 7.50 mmol) and (*S*)-2-methyl-CBS-oxazaborolidine (1 M in THF, 1.25 mL, 1.25 mmol) were dissolved in THF (19 mL) at 0 °C under nitrogen atmosphere. The solution was stirred at 0 °C for 10 min and then a solution of **8** (2.34 g, 6.25 mmol) in dry THF (8 mL) was added. After further 10 min, the cooling bath was removed and the mixture was left to stir at rt for 3 h. The reaction was quenched with methanol (20 mL) and the solvent was removed under reduced pressure. The crude product was purified by silica column chromatography to yield the (1*R*,3*R*) diastereomer **9** (0.92 g, 40 %) as a colorless solid.

R_f = 0.35 (*n*-hexane/ethyl acetate 3:2)

^{1}H NMR (400 MHz, $CDCl_3$): δ = 0.94−0.97 (dd, 6H), 1.38−1.42 (dd, 3H), 1.45 (s, 9H), 1.74−1.81 (m, 2H), 2.05−2.12 (m, 1H), 3.69−3.77 (m, 1H), 4.39−4.44 (dd, 2H), 4.55−4.57 (d, 1H), 5.00−5.03 (d, 1H), 5.19 (s, 1H), 8.12 (s, 1H) ppm.

^{13}C NMR (101 MHz, $CDCl_3$): δ = 14.4, 18.3, 19.4, 28.3, 32.1, 41.9, 52.3, 61.3, 69.1, 80.4, 127.2, 146.8, 158.0, 161.5, 176.5 ppm.

N-Boc-*O*-TBDMS-tubuvalin ethyl ester (**10**)

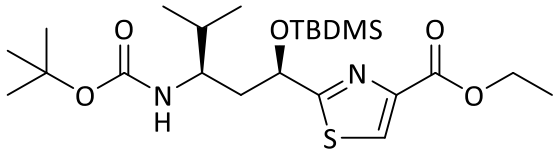

Compound **9** (2.48 g, 6.59 mmol) was dissolved in DMF (25 mL) under nitrogen atmosphere and cooled to 0 °C. Then TBDMSCl (2.46 g, 15.81 mmol) and imidazole (1.13 g, 16.47 mmol) were added to that solution. The reaction mixture was allowed to reach rt within 1 h, left to stir overnight and diluted with diethyl ether (60 mL). The mixture was washed with sat. $NaHCO_3$ solution (2 ×) and brine (1 ×). The layers were separated and the organic portion was dried over Na_2SO_4, filtered and the solvent was removed under reduced pressure. The crude product was purified by silica column chromatography to afford **10** (3.15 g, 98 %) as a yellow oil.

R_f = 0.63 (*n*-hexane/ethyl acetate 3:2)

^{1}H NMR (400 MHz, $CDCl_3$): δ = 0.08−0.14 (m, 9H), 0.82−0.85 (m, 12H), 0.93 (s, 9H), 1.37−1.41 (dd, 3H), 1.42 (s, 9H), 1.64−1.70 (m, 1H), 1.79−1.85 (m, 2H), 3.62−3.67 (m, 1H), 4.38−4.44 (dd, 2H), 4.63−4.65 (d, 1H), 5.17−5.19 (dd, 1H), 8.08 (s, 1H) ppm.

^{13}C NMR (101 MHz, $CDCl_3$): δ = −5.3, −4.7, −3.6, −3.0, 14.4, 18.1, 25.7, 28.4, 32.5, 41.4, 51.9, 61.4, 70.3, 78.8, 127.1, 146.6, 155.3, 161.4, 178.3 ppm.

HRMS calculated for $C_{23}H_{43}N_2O_5SSi$ $[M+H]^+$: m/z = 487.2664, found: m/z = 487.2665.

O-TBDMS-tubuvalin ethyl ester (**11**)

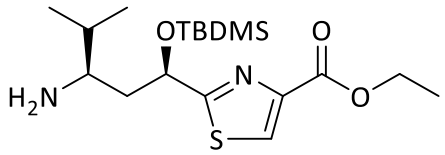

Compound **10** (1.34 g, 2.47 mmol) was dissolved in dichloromethane (10 mL) under nitrogen atmosphere and cooled to 0 °C. Then TFA (2.5 mL) was added and the mixture was left to stir at 0 °C for 6 h. The solvent was removed under reduced pressure. The resulting oil was taken up in dichloromethane and extracted with sat. $NaHCO_3$ solution (2 ×) and brine (1 ×). The combined organic layers were dried over Na_2SO_4, filtered, reduced and finally purified by silica column chromatography to yield **11** (0.82 g, 86 %) as a yellow oil.

R_f = 0.24 (dichloromethane/methanol/Et_3N 30:1:0.2 %)

^{1}H NMR (400 MHz, $CDCl_3$): δ = 0.15 (s, 6H), 0.83−0.87 (m, 6H), 0.95 (s, 9H), 1.38−1.42 (dd, 3H), 1.53−1.60 (m, 2H), 1.70−1.76 (m, 1H), 1.85−1.91 (m, 1H), 2.69−2.73 (m, 1H), 4.39−4.44 (dd, 2H), 5.38−5.41 (dd, 1H), 8.09 (s, 1H) ppm.

^{13}C NMR (101 MHz, $CDCl_3$): δ = −4.9, 14.4, 17.4, 18.0, 18.7, 25.8, 34.3, 44.3, 52.7, 61.3, 71.4, 126.9, 146.8, 161.6, 178.8 ppm.

HRMS calculated for $C_{18}H_{35}N_2O_3SSi$ $[M+H]^+$: m/z = 387.2139, found: m/z = 387.2164.

N-Boc-tubuvalin methyl ester (**13**)

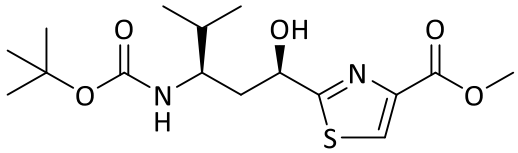

N-Boc-*O*-acetyl-tubuvalin ethyl ester (**12**) (1.20 g, 2.29 mmol) was dissolved in methanol (50 mL) and sodium methoxide (0.33 g, 5.04 mmol) was added. The mixture was left to stir at rt for 4 h. The crude product was taken up in dichloromethane (100 mL) and washed with HCl (0.07 M). After that, the organic layer was neutralized using $NaHCO_3$ (1 ×). The organic phase was separated, dried over anhydrous Na_2SO_4, filtered and the solvent was removed under reduced pressure to otbain **13** (0.71 g, 72 %) as colorless solid.

R_f = 0.63 (dichloromethane/methanol 30:1)

^{1}H NMR (400 MHz, $CDCl_3$): δ = 0.94−0.97 (dd, 6H), 1.44 (s, 9H), 1.73−1.80 (dd, 2H), 2.03−2.10 (dd, 1H), 3.94 (s, 3H), 4.54−4.56 (d, 1H), 4.99−5.03 (dd, 1H), 5.20−5.25 (m, 1H), 8.14 (s, 1H) ppm.

^{13}C NMR (101 MHz, $CDCl_3$): δ = 14.2, 18.4, 19.4, 21.0, 28.3, 29.7, 32.1, 42.0, 52.4, 60.4, 69.1, 80.4, 127.5, 146.4, 158.0, 162.0, 176.6 ppm.

HRMS calculated for $C_{16}H_{27}N_2O_5S$ $[M+H]^+$: m/z = 359.1642, found: m/z = 359.1647.

N-Boc-*O*-TBDMS-tubuvalin methyl ester (**14**)

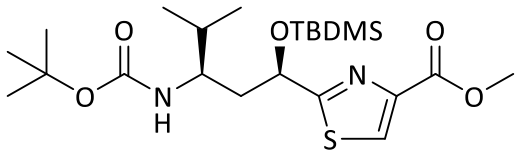

Compound **13** (0.71 g, 1.78 mmol) was dissolved in DMF (10 mL) under nitrogen atmosphere and cooled to 0 °C. Then TBDMSCl (1.10 g, 7.11 mmol) and imidazole (0.49 g, 7.11 mmol) were added to that solution. The reaction mixture was allowed to reach rt within 1 h, left to stir overnight and diluted with diethyl ether (30 mL). The mixture was washed with sat. $NaHCO_3$ solution (2 ×) and brine (1 ×). The layers were separated and the organic portion was dried over Na_2SO_4, filtered and the solvent was removed under reduced pressure. The crude product was purified by silica column chromatography to afford **14** (0.71 g, 85 %) as a yellow oil.

R_f = 0.59 (*n*-hexane/ethyl acetate 3:2)

^{1}H NMR (400 MHz, $CDCl_3$): δ = 0.05 (m, 6H), 0.14 (s, 3H), 0.83 (s, 2H), 0.84 (s, 4H), 0.86 (d, 6H), 0.91 (s, 3H), 0.93 (s, 9H), 1.43 (s, 9H), 1.61−1.70 (m, 2H), 1.84 (m, 2H), 3.48 (s, 1H), 3.66 (m, 1H), 3.95 (s, 3H), 4.62 (d, 1H), 5.18 (dd, 1H), 8.12 (s, 1H) ppm.

^{13}C NMR (101 MHz, $CDCl_3$): δ = −5.3, −4.7, −3.6, −3.0, 17.7, 17.9, 18.1, 25.7, 28.4, 32.5, 41.5, 51.8, 52.4, 70.3, 78.8, 127.5, 146.2, 155.3, 161.9, 178.5 ppm.

HRMS calculated for $C_{22}H_{41}N_2O_5SSi$ $[M+H]^+$: m/z = 473.2507, found: m/z = 473.2491.

O-TBDMS-tubuvalin methyl ester (**15**)

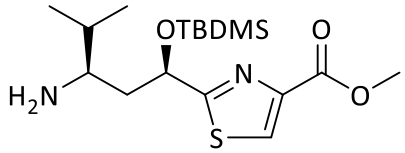

Compound **14** (0.70 g, 1.40 mmol) was dissolved in dichloromethane (20 mL) under nitrogen atmosphere and cooled to 0 °C. Then TFA (3.3 mL) was added and the mixture was left to stir at 0 °C for 6 h. The solvent was removed under reduced pressure. The resulting oil was redissolved in dichloromethane and then evaporated (repeated several times) to yield **15** in quantitative yield (0.50 g) as a yellow oil.

^{1}H NMR (400 MHz, $CDCl_3$): δ = 0.01−0.09 (m, 6H), 0.86−0.90 (m, 9H), 0.97−1.00 (dd, 6H), 1.99−2.04 (dd, 1H), 2.10−2.33 (m, 2H), 3.34 (s, 1H), 3.89 (s, 3H), 5.41−5.43 (d, 1H), 8.04 (s, 2H), 8.10 (s, 1H) ppm.

^{13}C NMR (101 MHz, $CDCl_3$): δ = −3.6, −3.0, 17.5, 18.4, 25.6, 25.7, 30.8, 36.4, 52.5, 54.3, 67.9, 128.1, 146.1, 162.2, 177.0 ppm.

HRMS calculated for $C_{17}H_{33}N_2O_3SSi$ $[M+H]^+$: m/z = 373.1983, found: m/z = 373.1999.

O-Propyl-tubuvalin ethyl ester (**17**)

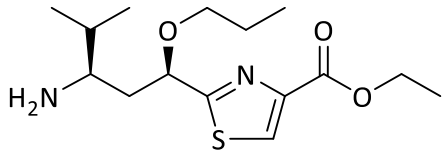

N-Boc-*O*-propyl-tubuvalin ethyl ester (**16**) (0.12 g, 0.27 mmol) was dissolved in dichloromethane (5 mL) and cooled to 0 °C. TFA (1 mL) was added and the mixture was left to stir at rt for 4 h. The mixture was concentrated under reduced pressure. The resulting oil was redissolved in dichloromethane and then evaporated (repeated several times). The crude was purified by silica column chromatography to obtain **17** in quantitative yield (0.12 g) as a yellow oil.

R_f = 0.14 (dichloromethane/methanol/Et_3N 30:1:0.2 %)

^{1}H NMR (400 MHz, $CDCl_3$): δ = 0.87−0.92 (dd, 6H), 0.92−0.96 (t, 3H), 1.39−1.42 (t, 3H), 1.60−1.68 (m, 2H), 1.77−1.93 (m, 2H), 2.43 (s, 2H), 2.87−2.92 (m, 1H), 3.49−3.55 (m, 2H), 4.39−4.45 (m, 2H), 5.00−5.04 (m, 1H), 8.14 (s, 1H) ppm.

^{13}C NMR (101 MHz, $CDCl_3$): δ = 10.5, 14.3, 17.2, 18.7, 23.0, 33.7, 41.9, 52.9, 61.3, 72.5, 77.5, 127.4, 146.9, 161.4, 176.8 ppm.

HRMS calculated for $C_{15}H_{27}N_2O_3S$ $[M+H]^+$: m/z = 315.1744, found: m/z = 315.1743.

N-Boc-L-phenylalaninal (**18**)

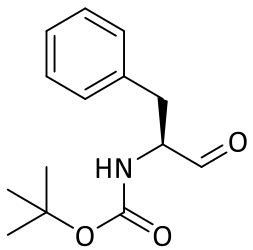

N-Boc-L-phenylalaninol (10.13 g, 39.90 mmol) was dissolved in a mixture of water, ethyl acetate and toluene (20 / 110 / 110 mL) and cooled to 0 °C. NaBr (4.15 g, 39.90 mmol) and TEMPO (0.32 g, 2.00 mmol) were added at 0 °C. NaOCl (20.70 mL, 39.90 mmol) was added dropwise and slowly to the mixture at 0 °C. After that, the mixture was allowed to reach rt and left to stir for 4 h. The phases were separated and the aqueous layer was washed with ethyl acetate (3×). The combined organic layers were washed with KI (600 mg per 40 mL) in sat. $NaHSO_4$ solution, then with sat. $Na_2S_2O_5$ solution and brine. The organic layer was dried over Na_2SO_4, filtered and the solvent was removed under reduced pressure to afford crude **18** (9.43 g, 95 %) as a colorless solid.

R_f = 0.31 (*n*-hexane/ethyl acetate 4:1)

^{1}H NMR (400 MHz, $CDCl_3$): δ = 1.41 (s, 14H), 1.43 (s, 9H), 2.83−2.85 (d, 4H), 3.11−3.13 (d, 2H), 3.53−3.69 (m, 4H), 3.87 (s, 1H), 4.75−4.77 (d, 2H), 7.16−7.25 (m, 9H), 7.29−7.30 (m, 3H), 9.63 (s, 1H) ppm.

^{13}C NMR (101 MHz, $CDCl_3$): δ = 27.4, 28.3, 35.5, 37.4, 126.5, 128.7, 129.3, 137.7, 156.1, 199.4 ppm.

HRMS calculated for $C_{14}H_{20}NO_3$ $[M+H]^+$: m/z = 250.1445, found: m/z = 250.1419.

(4*R*)-4-(*tert*-Butyloxycarbonyl)amino-2-methyl-5-phenyl pent-2-enoic acid ethyl ester (**19**)

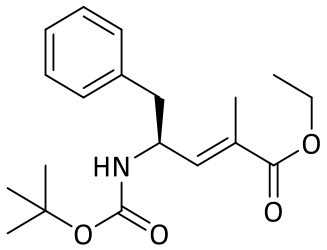

Compound **18** (9.27 g, 36.80 mmol) was dissolved in dry dichloromethane (400 mL) under nitrogen atmosphere and cooled to 0°C. After addition of (1-ethoxycarbonylethylidene) triphenylphosphorane (16.50 g, 44.16 mmol), the mixture was allowed to reach rt and left to stir for 16 h. The solvent was removed under reduced pressure and the crude product was purified by silica column chromatography to yield **19** (4.74 g, 39 %) as a colorless solid.

R_f = 0.55 (*n*-hexane/ethyl acetate 4:1)

^{1}H NMR (400 MHz, $CDCl_3$): δ = 1.26−1.30 (t, 3H), 1.40 (s, 9H), 1.70 (s, 3H), 2.75−2.81 (m, 1H), 2.91 (m, 1H), 4.09−4.15 (dd, 1H), 4.15−4.20 (dd, 2H), 4.62 (s, 1H), 6.51−6.53 (d, 1H), 7.16−7.30 (m, 5H) ppm.

^{13}C NMR (101 MHz, $CDCl_3$): δ = 12.6, 14.2, 21.0, 27.7, 28.3, 41.2, 60.3, 60.7, 126.6, 128.4, 129.3, 129.5, 136.7, 154.9, 167.7 ppm.

HRMS calculated for $C_{19}H_{28}NO_4$ $[M+H]^+$: m/z = 334.2020, found: m/z = 334.2019.

(4*R*)-4-(*tert*-Butyloxycarbonyl)amino-2-methyl-5-phenyl pentanoic acid ethyl ester (**20**)

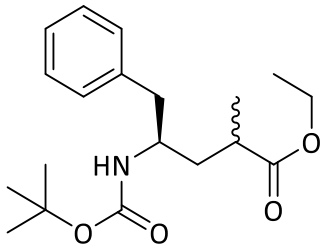

Compound **19** (4.74 g, 14.08 mmol) was dissolved in methanol (100 mL) and then 10 w% $Pd(OH)_2$ (20 % on carbon, 0.47 g) was added. The mixture was left to stir under hydrogen atmosphere. The crude product was filtered through celite and then washed with methanol. The solvent was removed under reduced pressure to obtain **20** (4.40 g, 93 %) as a colorless oil.

R_f = 0.37 (*n*-hexane/ethyl acetate 4:1)

^{1}H NMR (400 MHz, CD_3OD): δ = 1.08−1.16 (m, 3H), 1.18−1.26 (m, 5H), 1.35−1.46 (m, 9H), 1.78−1.85 (m, 1H), 2.65−2.74 (m, 2H), 3.70−3.74 (m, 1H), 4.05−4.10 (dd, 2H), 7.14−7.26 (m, 5H) ppm.

^{13}C NMR (101 MHz, CD_3OD): δ = 14.5, 18.4, 28.8, 37.8, 39.3, 43.2, 51.5, 61.5, 79.7, 127.2, 129.2, 130.5, 139.9, 157.8, 178.0 ppm.

HRMS calculated for $C_{19}H_{29}NO_4$ $[M+H]^+$: m/z = 336.2177, found: m/z = 336.2175.

(4*R*)-4-(*tert*-Butyloxycarbonyl)amino-2-methyl-5-phenyl pentanoic acid (**21**)

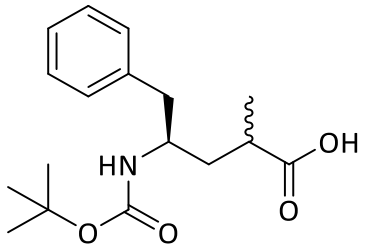

Compound **20** (4.74 g, 14.00 mmol) was dissolved in THF/H_2O (2:1, 140 mL) and cooled to 0 °C. Then KOH (6.28 g, 112.00 mmol) was added. The mixture was left to stir at rt overnight. THF was removed under reduced pressure and the aqueous phase was set to pH = 1 by 6 M HCl. Subsequently, the aqueous phase was extracted with ethyl acetate (3 ×). The organic layers were combined, dried over Na_2SO_4, filtered and the solvent was removed under reduced pressure to obtain **21** (3.46 g, 80 %) as colorless solid.

R_f = 0.03 (*n*-hexane/ethyl acetate 4:1)

^{1}H NMR (400 MHz, CD_3OD): δ = 1.09−1.18 (m, 3H), 1.23−1.36 (m, 9H), 1.81−1.88 (m, 1H), 2.51−2.58 (m, 1H), 2.70−2.71 (m, 2H), 3.78−3.81 (m, 1H), 7.15−7.26 (m, 5H) ppm.

^{13}C NMR (101 MHz, CD_3OD): δ = 18.6, 28.8, 37.8, 39.5, 42.9, 51.7, 79.7, 127.1, 129.2, 130.4, 139.9, 157.9, 180.2 ppm.

HRMS calculated for $C_{16}H_{24}NO_4$ $[M-H]^+$: m/z = 306.1704, found: m/z = 306.1721.

(2*S*,4*R*)-4-(*tert*-Butyloxycarbonyl)amino-2-methyl-5-phenyl pentanoic acid (−)-menthyl ester (**22**)

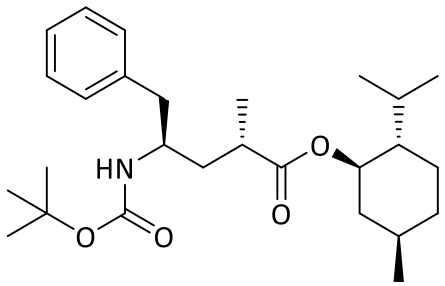

Compound **21** (0.50 g, 1.59 mmol) was dissolved in dichloromethane (15 mL) under nitrogen atmosphere and cooled to 0 °C. (−)-Menthol (0.63 g, 3.99 mmol), DCC (1.25 g, 5.98 mmol) and DMAP (19.90 mg, 0.16 mmol) were added. The suspension was left to stir at rt overnight. Then the mixture was diluted with diethyl ether (9 mL), filtered and quenched with methanol (10 mL). The solvent was removed under reduced pressure. The crude product was purified by silica column chromatography to give **22** (0.39 g, 55 %) as a colorless solid.

R_f = 0.39 (*n*-hexane/ethyl acetate 5:1)

^{1}H NMR (400 MHz, CD_3OD): δ = 0.73−0.81 (m, 4H), 0.89−0.98 (m, 9H), 1.10−1.12 (d, 3H), 1.38 (s, 9H), 1.68−1.97 (m, 6H), 2.52−2.58 (m, 1H), 2.62−2.75 (m, 2H), 3.75−3.80 (m, 1H), 4.59−4.66 (m, 1H), 7.17−7.27 (m, 5H) ppm.

^{13}C NMR (101 MHz, CD_3OD): δ = 16.5, 18.6, 21.2, 22.5, 24.4, 27.4, 28.9, 32.7, 35.5, 38.0, 39.3, 42.0, 43.2, 51.5, 75.4, 79.7, 127.2, 129.2, 130.5, 139.9, 157.7, 177.7 ppm.

HRMS calculated for $C_{27}H_{44}NO_4$ $[M+H]^+$: m/z = 446.3272, found: m/z = 446.3265.

(2*S*,4*R*)-Tubuphenylalanine hydrochloride (**23**)

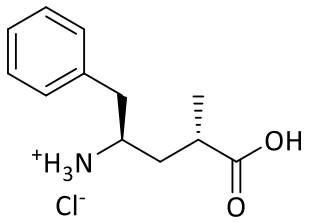

Compound **22** (1.12 g, 2.01 mmol) was dissolved in 6 M HCl (35 mL) and left to stir under reflux for 5 h until the starting material was consumed. After cooling to rt, ethyl acetate (30 mL) was added and the layers were separated. Following the extraction, the aqueous phase was concentrated under reduced pressure to afford **23** in quantitative yield (1.01 g) as a colorless solid.

^{1}H NMR (400 MHz, CD_3OD): δ = 1.17−1.19 (d, 3H), 1.61−1.68 (m, 1H), 1.96−2.03 (m, 1H), 2.60−2.69 (m, 1H), 2.89−2.99 (m, 2H), 3.53−3.60 (m, 1H), 7.26−7.38 (m, 5H) ppm.

^{13}C NMR (101 MHz, CD_3OD): δ = 17.9, 36.9, 37.2, 40.3, 52.5, 128.5, 130.1, 130.4, 136.8, 178.9 ppm.

HRMS calculated for $C_{12}H_{18}NO_2$ $[M+H]^+$: m/z = 208.1339, found: m/z = 208.1325.

calculated for $C_{12}H_{16}NO_2$ $[M-H]^+$: m/z = 206.1179, found: m/z = 206.1175.

(2*S*,4*R*)-Tubuphenylalanine methyl ester hydrochloride (**24**)

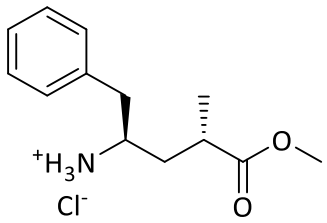

Compound **23** (0.14 g, 0.45 mmol) was dissolved in methanol (5 mL). HCl (37 %, 2.8 µL, 0.09 mmol) was added and the solution was left to stir at 50 °C for 27 h. The solvent was removed under reduced pressure to yield **24** in quantitative yield (0.13 g) as a yellowish solid.

^{1}H NMR (400 MHz, CD_3OD): δ = 1.16−1.17 (d, 3H), 1.61−1.68 (m, 1H), 1.97−2.04 (m, 1H), 2.65−2.74 (m, 1H), 2.87−3.01 (m, 2H), 3.50−3.56 (m, 1H), 3.64 (s, 3H), 7.26−7.38 (m, 5H) ppm.

^{13}C NMR (101 MHz, CD_3OD): δ = 17.9, 36.9, 37.1, 40.2, 52.4, 52.5, 128.5, 130.0, 130.4, 136.8, 177.2 ppm.

HRMS calculated for $C_{13}H_{20}NO_2$ $[M+H]^+$: m/z = 222.1496, found: m/z = 222.1473.

D-Mep-L-Ile-*O*-TBDMS-Tuv-OMe (**25**)

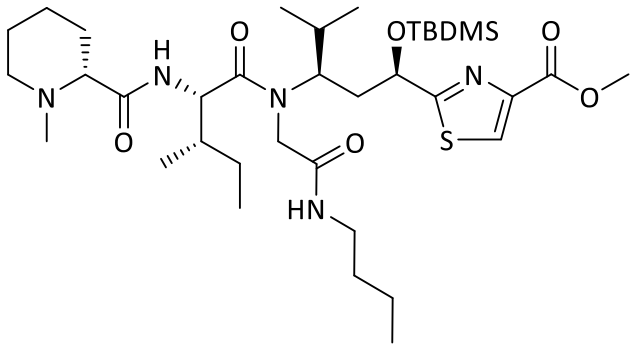

Compound **15** (200 mg, 0.43 mmol) was dissolved in methanol (15 mL). Then PFA (18 mg, 0.56 mmol) was added and the mixture was left to stir in the microwave at 70 °C for 30 min. **4** (207 mg, 0.69 mmol) and *n*-butyl isocyanide (0.05 mL, 0.47 mmol) were dissolved in methanol (5 mL) and added. The mixture was left to stir in the microwave at 70 °C for 90 min. The solvent was removed under reduced pressure and the crude product was purified by silica column chromatography to afford **25** (121 mg, 42 %) as a yellowish oil.

R_f = 0.07 (dichloromethane/methanol/Et_3N 30:1:0.1 %)

^{1}H NMR (400 MHz, CD_3OD): δ = 0.83−1.29 (m, 20H), 1.31−1.40 (m, 6H), 1.42−1.62 (m, 5H), 1.72−1.84 (m, 2H), 1.89−2.02 (m, 5H), 2.06−2.35 (m, 3H), 2.75−2.77 (d, 3H), 2.97−3.03 (t, 1H), 3.12−3.28 (m, 3H), 3.43−3.46 (d, 1H), 3.64−4.06 (m, 4H), 4.34−4.39 (dd, 3H), 4.50−4.56 (m, 1H), 4.98−5.33 (m, 2H), 8.23−8.30 (2s, 4H) ppm.

^{13}C NMR (101 MHz, CD_3OD): δ = 11.1, 12.0, 14.1, 14.6, 16.1, 20.6, 21.1, 22.5, 24.2, 25.4, 30.4, 31.8, 32.4, 37.8, 38.3, 38.7, 40.5, 43.2, 43.4, 46.5, 56.2, 56.7, 62.3, 68.6, 69.9, 129.1, 147.7, 166.4, 169.4, 170.8, 173.7, 179.4 ppm.

HRMS calculated for $C_{36}H_{66}N_5O_6SSi$ $[M+H]^+$: m/z = 724.4505, found: m/z = 724.4532.

D-Mep-L-Ile-Tuv-OMe (**26**)

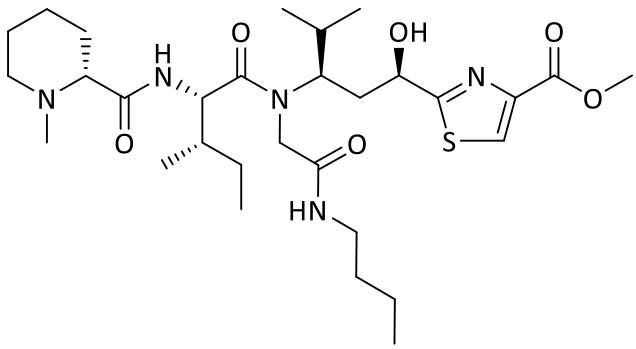

Compound **25** (63 mg, 0.08 mmol) was dissolved in TFA/THF/H_2O (2:2:1, 7.5 mL) and was left to stir at rt for 20 h. The mixture was concentrated under reduced pressure and the resulting oil was dissolved in dichloromethane to remove TFA (repeat several times). Crude **26** was obtained in quantitative yield (56 mg) as a yellow oil.

^{1}H NMR (400 MHz, $CDCl_3$): δ = 0.78−1.09 (m, 21H), 1.18−1.43 (m, 8H), 1.89−2.14 (m, 10H), 2.26−2.53 (m, 2H), 2.76−2.88 (m, 3H), 3.44−3.47 (m, 1H), 3.64−3.96 (m, 9H), 4.35−4.43 (m, 2H), 5.18−5.44 (m, 2H), 7.97 (s, 1H), 8.14 (s, 1H) ppm.

^{13}C NMR (101 MHz, $CDCl_3$): δ = 11.2, 13.5, 15.4, 17.3, 18.4, 19.9, 21.0, 22.1, 22.7, 25.0, 25.5, 30.7, 36.5, 42.2, 52.0, 52.4, 54.5, 57.9, 68.1, 68.7, 114.3, 117.1, 128.0, 146.4, 160.8, 161.2, 161.9, 171.2, 176.8 ppm.

HRMS calculated for $C_{30}H_{52}N_5O_6S$ $[M+H]^+$: m/z = 610.3640, found: m/z = 610.3636.

D-Mep-L-Ile-*O*-propyl-Tuv-OEt (**27**)

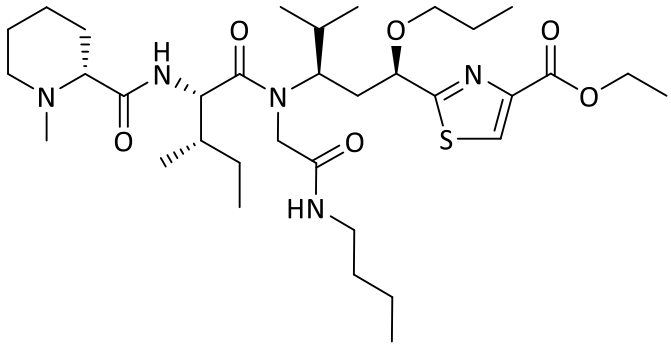

Compound **17** (150 mg, 0.38 mmol) was dissolved in methanol (15 mL). Then PFA (16 mg, 0.50 mmol) was added and the mixture was left to stir in the microwave at 70 °C for 30 min. **4** (184 mg, 0.61 mmol) and *n*-butyl isocyanide (0.05 mL, 0.42 mmol) were dissolved in methanol (5 mL) and added. The mixture was left to stir in the microwave at 70 °C for 90 min. The solvent was removed under reduced pressure and the crude product was purified by silica column chromatography to afford **27** (197 mg, 78 %) as a yellow oil.

R_f = 0.23 (dichloromethane/methanol/Et_3N 30:1:0.1 %)

^{1}H NMR (400 MHz, CD_3OD): δ = 0.78−0.80 (d, 3H), 0.86−0.90 (t, 9H), 0.92−0.94 (m, 5H), 0.99−1.05 (m, 8H), 1.35−1.39 (m, 7H), 1.61−1.64 (m, 4H), 1.87−1.93 (m, 2H), 2.01−2.07 (m, 2H), 2.17 (s, 3H), 2.21−2.22 (m, 1H), 2.54−2.58 (m, 1H), 2.90−2.93 (m, 2H), 3.22−3.27 (m, 2H), 3.39 (s, 1H), 3.48−3.53 (m, 3H), 3.77−3.81 (d, 1H), 4.35−4.37 (m, 2H), 4.56−4.59 (d, 1H), 4.74−4.81 (m, 2H), 8.30 (s, 1H) ppm.

^{13}C NMR (101 MHz, CD_3OD): δ = 11.0, 14.1, 14.6, 16.5, 20.2, 20.7, 21.1, 24.3, 24.4, 25.6, 26.2, 31.7, 31.9, 32.5, 37.9, 40.2, 40.5, 44.8, 55.0, 56.6, 62.2, 65.4, 67.0, 70.5, 73.8, 77.3, 129.1, 148.1, 162.7, 170.8, 174.5, 175.3, 175.6, 176.5 ppm.

HRMS calculated for $C_{34}H_{60}N_5O_6S$ $[M+H]^+$: m/z = 666.4266, found: m/z = 666.4286.

D-Mep-L-Ile-Tuv-OH (**28**)

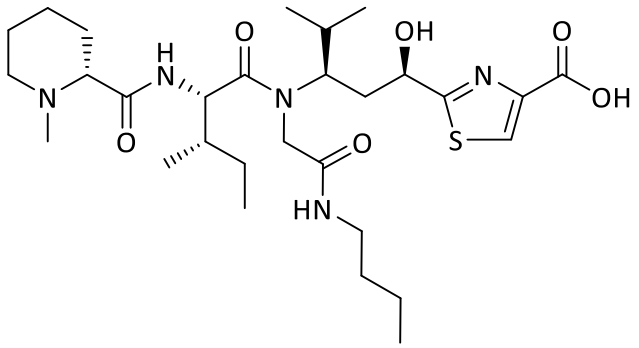

Compound **26** (47 mg, 0.07 mmol) was dissolved in THF/H_2O (2:1, 4.5 mL) and LiOH × H_2O (0.1 M, 18 mg) was added at 0 °C. The mixture was allowed to reach rt and left to stir for 8 h. The pH was set to 4 by addition of 10 % $NaHSO_4$ and the solvents were removed under reduced pressure to afford **28** in quantitative yield (42 mg) as a yellow oil.

^{1}H NMR (400 MHz, CD_3OD): δ = 0.82−1.06 (m, 16H), 1.21−1.39 (m, 4H), 1.43−1.53 (m, 2H), 1.58−1.67 (m, 2H), 1.71−1.84 (m, 2H), 1.86−.05 (m, 5H), 2.12−2.22 (m, 2H), 2.78−2.82 (m, 3H), 3.07−3.25 (m, 3H), 3.45−3.59 (m, 2H), 3.70−4.05 (m, 2H), 4.35−4.55 (m, 1H), 5.14−5.19 (m, 1H), 8.27−8.33 (s, 1H) ppm.

^{13}C NMR (101 MHz, CD_3OD): δ = 11.1, 11.9, 14.1, 16.1, 17.8, 18.6, 21.1, 22.3, 24.0, 26.2, 30.1, 32.0, 37.6, 38.0, 40.5, 42.9, 55.4, 56.3, 58.5, 68.2, 69.8, 129.3, 148.4, 164.0, 168.9, 169.7, 174.0, 178.9, 179.2 ppm.

HRMS calculated for $C_{29}H_{48}N_5O_6S$ $[M-H]^+$: m/z = 594.3324, found: m/z = 594.3341.

D-Mep-L-Ile-*O*-propyl-Tuv-OH (**29**)

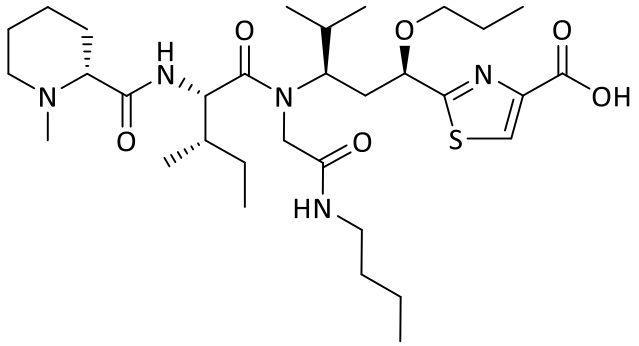

Compound **27** (348 mg, 0.50 mmol) was dissolved in THF/H_2O (2:1, 24 mL) and cooled to 0 °C. LiOH × H_2O (100 mg, 0.1 M) was added to the mixture which was allowed to reach rt and left to stir for 8 h. The reaction was quenched by addition of 10 % $NaHSO_4$ (pH = 4). The solvents were removed under reduced pressure to obtain **29** in quantitative yield (322 mg) as a yellow oil.

R_f = 0.04 (dichloromethane/methanol/Et_3N 30:1:0.3 %)

^{1}H NMR (400 MHz, CD_3OD): δ = = 0.81−0.83 (d, 3H), 0.89−0.93 (m, 9H), 0.95−1.02 (m, 13H), 1.16−1.19 (m, 3H), 1.28−1.40 (m, 6H), 1.46−1.53 (m, 4H), 1.78−1.83 (m, 4H), 1.92−1.95 (m, 4H),

2.02−2.08 (m, 3H), 2.84 (s, 3H), 3.17−3.24 (m, 2H), 3.51−3.53 (m, 3H), 3.60−3.62 (m, 1H), 3.83−3.87 (m, 1H), 4.50−4.52 (m, 1H), 4.63−4.67 (d, 1H), 4.88−4.91 (d, 1H), 8.44 (s, 1H) ppm.

^{13}C NMR (101 MHz, CD_3OD): δ = 9.5, 9.7, 12.7, 15.0, 17.0, 19.0, 19.3, 19.7, 20.9, 22.6, 22.8, 23.9, 28.9, 30.3, 31.0, 36.5, 37.0, 39.1, 41.7, 54.5, 54.8, 56.9, 66.7, 72.4, 76.1, 128.3, 145.1, 161.1, 167.7, 169.3, 173.5, 176.6 ppm.

HRMS calculated for $C_{32}H_{56}N_5O_6S$ $[M+H]^+$: m/z = 638.3953, found: m/z = 638.3955.

D-Mep-L-Ile-Tuv-Tup-OMe (**30**)

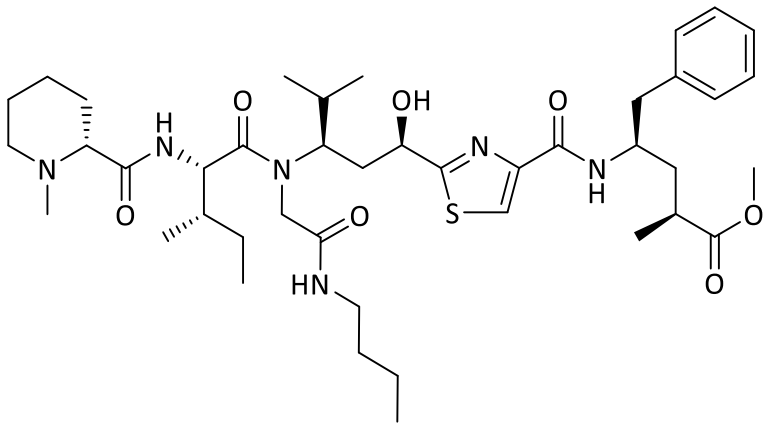

Compound **28** (137 mg, 0.22 mmol), HATU (100 mg, 0.26 mmol) and DIPEA (140 µL, 0.79 mmol) were dissolved in dry DMF (10 mL). **24** (55 mg, 0.20mmol) was added to previous mixture and the mixture was left to stir at rt for 3 d. The mixture was neutralized with sat. $NaHSO_4$ solution. The crude product was purified by silica column chromatography to afford **30** in quantitative yield (102 mg) as a yellow oil.

R_f = 0.05 (dichloromethane/methanol 30:1)

^{1}H NMR (400 MHz, $CDCl_3$): δ = 0.84−0.99 (m, 10H), 1.06−1.08 (d, 5H), 1.13−1.19 (m, 4H), 1.26−1.41 (m, 5H), 1.46−1.56 (m, 3H), 1.61−1.78 (m, 6H), 1.92−2.25 (m, 10H), 2.53−2.63 (m, 3H), 2.80−2.98 (m, 4H), 3.04−3.27 (m, 3H), 3.50−3.76 (m, 4H), 3.81−4.40 (m, 3H), 4.69−4.72 (m, 1H), 5.10−5.12 (m, 1H), 7.16−7.25 (m, 4H), 7.29−7.37 (m, 1H), 8.02−8.08 (m, 1H) ppm.

^{13}C NMR (101 MHz, $CDCl_3$): δ = 11.7, 13.7, 16.2, 16.3, 17.7, 20.1, 20.2, 20.7, 22.6, 31.2, 31.4, 36.7, 37.9, 38.6, 39.3, 41.5, 42.8, 47.1, 51.8, 67.2, 77.2, 123.1, 126.6, 128.4, 128.8, 129.1, 129.4, 129.5, 137.7, 169.4, 176.6, 180.8 ppm.

HRMS calculated for $C_{42}H_{67}N_6O_7S$ $[M+H]^+$: m/z = 799.4794, found: m/z = 799.4798.

D-Mep-L-Ile-*O*-propyl-Tuv-Tup-OMe (**31**)

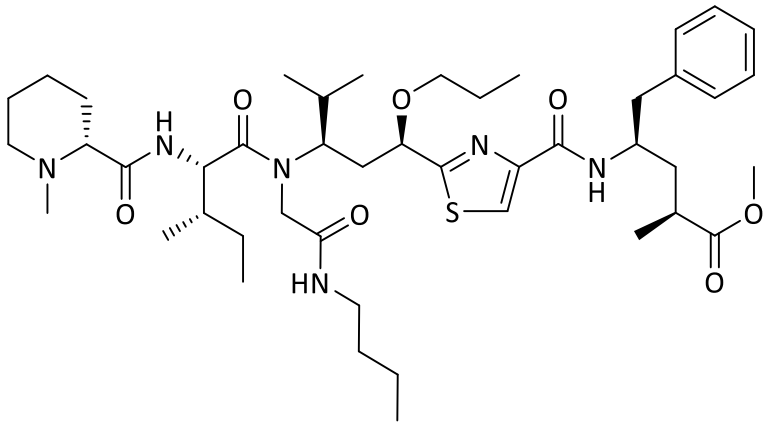

Compound **29** (250 mg, 0.35 mmol), HATU (150 mg, 0.39 mmol) and DIPEA (0.23 mL, 1.28 mmol) were dissolved in DMF (3.5 mL). **24** (92 mg, 0.32 mmol) was added to that mixture and the mixture was left to stir at rt overnight. The mixture was neutralized by $NaHSO_4$ and subsequently purified by silica column chromatography to yield **31** (186 mg, 69 %) as yellow oil.

R_f = 0.42 (dichloromethane/methanol 10:1)

^{1}H NMR (400 MHz, $CDCl_3$): δ = 0.72−0.74 (d, 1H), 0.80−0.96 (m, 11H), 1.04−1.16 (m, 6H), 1.24−1.31 (m, 2H), 1.40−1.46 (m, 2H), 1.54−1.62 (m, 4H), 1.93−2.04 (m, 3H), 2.12−2.19 (m, 3H), 2.42−2.45 (m, 1H), 2.75−2.90 (m, 8H), 3.34−3.52 (m, 2H), 3.58−3.60 (m, 3H), 4.07−4.50 (m, 3H), 4.82−4.99 (m, 1H), 7.12−7.22 (m, 6H), 7.93−7.95 (m, 1H) ppm.

^{13}C NMR (101 MHz, $CDCl_3$): δ = 10.4, 10.9, 11.6, 13.6, 15.9, 16.4, 17.7, 19.6, 19.9, 20.3, 23.1, 24.4, 24.9, 30.6, 31.3, 36.3, 38.4, 39.4, 44.8, 48.3, 51.5, 55.2, 60.0, 69.3, 71.1, 72.7, 75.3, 76.1, 122.8, 126.2, 128.2, 128.6, 129.2, 129.4, 137.6, 149.8, 160.8, 162.4, 168.7, 170.6, 172.6, 173.5, 174.1, 174.7, 176.4 ppm.

HRMS calculated for $C_{45}H_{73}N_6O_7S$ $[M+H]^+$: m/z = 841.5263, found: m/z = 841.5235.

Tubugi 1 (**33**)

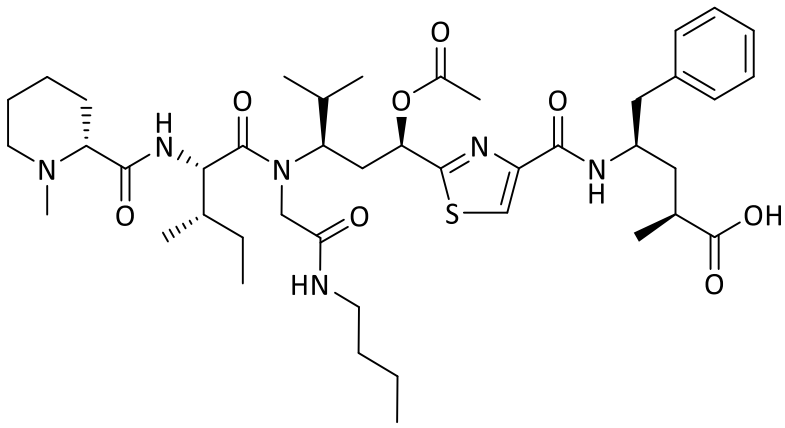

Compound **30** (47 mg, 0.05 mmol) was dissolved in THF/H_2O (2:1, 1.8 mL) and LiOH×H_2O (0.06 M, 5 mg) was added at 0 °C. The mixture was allowed to reach rt and left to stir for 3 d. The mixture

was acidified with aqueous 10 % $NaHSO_4$ solution to pH = 4 and then concentrated under reduced pressure obtaining **32**.

HRMS calculated for $C_{41}H_{65}N_6O_7S$ $[M+H]^+$: m/z = 785.4637, found: m/z = 785.4630.

calculated for $C_{41}H_{63}N_6O_7S$ $[M-H]^+$: m/z = 783.4477, found: m/z = 783.4548.

The residue was taken up in pyridine (1 mL) and cooled to 0 °C. Acetic anhydride (3.7 µL, 0.04 mmol) was added and the mixture was allowed to reach rt and left to stir for 3 d. Then the mixture was cooled to 0 °C and water (1 mL) was added. After further stirring for 30 min, solvents were removed under reduced pressure. The purification was performed by HPLC to yield **33** (38 mg, 92 %).

^{1}H NMR (400 MHz, CD_3OD): Tup δ = 1.15−1.17 (d, 3H), 1.64−1.68 (m, 1H), 1.96−1.98 (m, 1H), 2.50−2.57 (m, 1H), 2.76−2.82 (dd, 2H), 4.33−4.40 (m, 1H), 7.13−7.18 (m, 1H), 7.22−7.23 (m, 4H) ppm. Tuv δ = 0.78−0.79 (d, 3H), 0.84−0.88 (t, 3H), 1.06−1.08 (d, 6H), 1.29−1.33 (m, 2H), 1.40−1.45 (m, 2H), 1.80 (m, 1H), 1.93 (m, 1H), 2.15 (s, 3H), 2.29−2.36 (m, 1H), 3.07−3.14 (m, 1H), 3.21−3.26 (m, 1H), 3.78−3.83 (m, 1H), 4.56 (s, 1H), 4.70−4.75 (m, 1H), 6.29−6.32 (dd, 1H), 8.05 (s, 1H) ppm. L-Ile δ = 0.87−0.91 (t, 3H), 0.98−1.00 (d, 3H), 1.10−1.13 (m, 1H), 1.54−1.57 (m, 1H), 1.99−2.03 (m, 1H), 4.43−4.45 (m, 1H) ppm. D-Mep δ = 1.35−1.39 (m, 1H), 1.61−1.63 (m, 1H), 1.75−1.82 (m, 3H), 2.44 (s, 3H), 2.76−2.77 (d, 1H), 3.84−3.90 (m, 2H) ppm.

^{13}C NMR (101 MHz, CD_3OD): Tup δ = 18.6, 38.1, 39.2, 42.8, 50.8, 127.2, 129.3, 130.4, 138.9, 178.9 ppm. Tuv δ = 14.1, 20.2, 20.9, 21.1, 31.2, 32.5, 36.4, 40.5, 46.3, 57.3, 71.6, 125.2, 150.8, 163.0, 171.2, 171.7, 172.4 ppm. L-Ile δ = 10.8, 16.4, 25.2, 37.5, 55.4, 175.5 ppm. D-Mep δ = 25.1, 25.5, 31.2, 43.9, 54.8, 70.4, 173.9 ppm.

t_R = 6.9 min (10 % ACN (2min)>15 min>95 %>5 min>100 % (10 min))

HRMS calculated for $C_{43}H_{67}N_6O_8S$ $[M+H]^+$: m/z = 827.4743, found: m/z = 827.4761.

calculated for $C_{43}H_{65}N_6O_8S$ $[M-H]^+$: m/z = 825.4583, found: m/z = 825.4627.

<u>Tubugi 4 (**34**)</u>

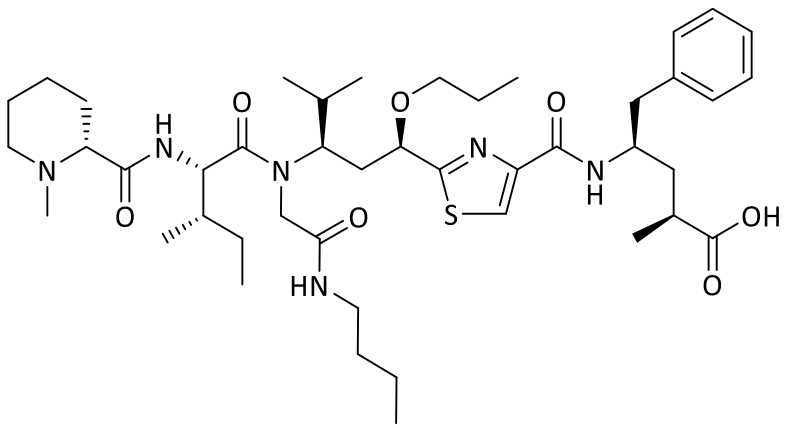

Compound **31** (186 mg, 0.21 mmol) was dissolved in THF/H_2O (2:1, 15 mL) and LiOH×H_2O (0.1 M, 63 mg) was added at 0 °C. The mixture was allowed to reach rt and left to stir for 24 h. The mixture

was acidified with aqueous 10 % $NaHSO_4$ solution to pH = 4 and then concentrated under reduced pressure to obtain the crude **34** in quantitative yield (169 mg) as yellowish solid.

^{1}H NMR (400 MHz, CD_3OD): δ = 0.74–1.16 (m, 12H), 1.16 (4H), 1.20–1.46 (m, 8H), 1.53–1.83 (m, 4H), 1.86 (s, 4H), 1.92–2.30 (m, 3H), 2.65 (s, 4H), 2.65–2.99 (m, 4H), 3.10 (tt, 1H), 3.31–3.54 (m, 2H), 3.70–3.91 (m, 2H), 4.72 (d, 8H), 7.10–7.25 (m, 6H), 7.23–7.34 (m, 3H), 8.31 (s, 1H) ppm.

^{13}C NMR (101 MHz, CD_3OD): δ = 11.0, 14.1, 16.4, 18.7, 20.1, 20.8, 21.1, 22.7, 24.2, 25.4, 30.6, 31.5, 32.5, 36.4, 37.7, 39.0, 40.5, 42.5, 42.8, 43.3, 50.8, 54.8, 55.6, 56.2, 68.4, 73.4, 77.5, 125.0, 127.4, 127.6, 129.3, 129.5, 130.4, 130.5, 138.9, 139.6, 150.7, 163.2, 170.4, 170.9, 175.1, 176.2, 179.9, 183.0 ppm.

t_R = 6.6 min (10 % ACN (2min)>15 min>95 %>5 min>100 % (10 min))

HRMS calculated for $C_{44}H_{71}N_6O_7S$ $[M+H]^+$: m/z = 825.4947, found: m/z = 825.4923.

2-(Pyridine-2-yl-disulfanyl) ethanol (**35**)

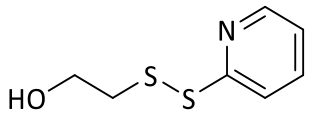

2,2'-Dipyridyl disulfide (3.13 g, 13.94 mmol) was dissolved in methanol (30 mL) under nitrogen atmosphere. Then 2-mercaptoethanol (0.90 mL, 12.67 mmol) was added and the mixture was left to stir for 4 h. The crude product was suspended in ethyl acetate and filtered off. The filtrate was concentrated and then purified by silica column chromatography to obtain **35** (1.42 g, 60 %) as a colorless oil.

R_f = 0.2 (ethyl acetate/*n*-hexane 7:4)

^{1}H NMR (400 MHz, $CDCl_3$): δ = 2.94−2.97 (dd, 2H), 3.79−3.82 (dd, 2H), 5.64 (s br, 1H), 7.13−7.17 (m, 1H), 7.41−7.43 (m, 1H), 7.57−7.61 (m, 1H), 8.49−8.51 (m, 1H) ppm.

^{13}C NMR (101 MHz, $CDCl_3$): δ = 42.6, 58.2, 121.4, 121.8, 136.8, 149.7, 159.0 ppm.

HRMS calculated for $C_7H_{10}NOS_2$ $[M+H]^+$: m/z = 188.0206, found: m/z = 188.0191.

2-(Pyridine-2-yl-disulfanyl) ethyl ester of tubugi 1 (**36**)

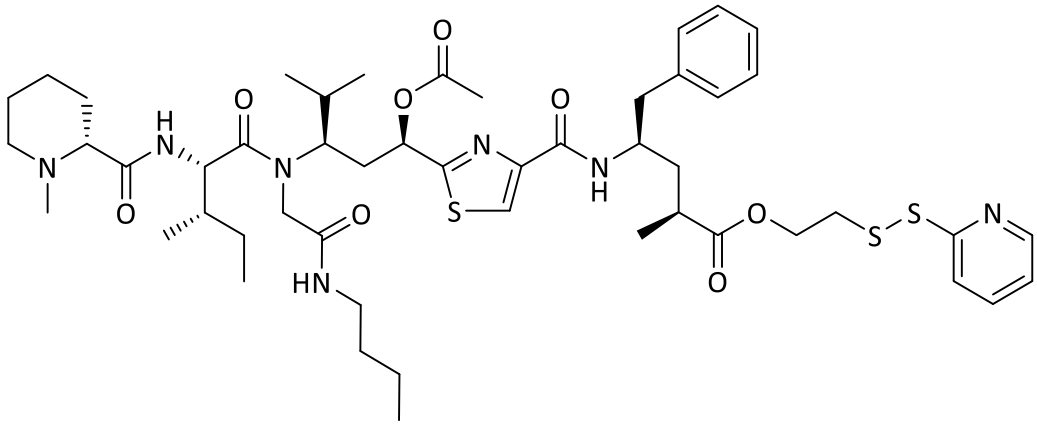

Compound **33** (52 mg, 0.06 mmol) was dissolved in dichloromethane (10 mL) and cooled down to 0 °C. EDC × HCl (15 mg, 0.08 mmol), **35** (15 mg, 0.08 mmol) and DMAP (0.7 mg, 0.01 mmol) were sequentially added to that solution. After 5 minutes, the mixture was allowed to reach rt and left to stir overnight. The crude product was purified by silica column chromatography to afford **36** (42 mg, 71 %) as a colorless oil.

R_f = 0.12 (dichloromethane/methanol 20:1)

^{1}H NMR (400 MHz, CD_3OD): δ = 0.76−0.78 (d, 3H), 0.83−0.90 (m, 8H), 0.98−1.00 (d, 3H), 1.05−1.08 (m, 5H), 1.12−1.14 (d, 5H), 1.28−1.35 (m, 4H), 1.37−1.46 (m, 3H), 1.54−1.63 (m, 3H), 1.71−1.78 (m, 3H), 1.86−1.93 (m, 2H), 2.14 (s, 3H), 2.34 (s, 3H), 2.53−2.59 (m, 1H), 2.72−2.84 (m, 2H), 2.88−2.94 (m, 2H), 3.00−3.04 (m, 2H), 3.22−3.27 (m, 1H), 3.76−3.80 (m, 1H), 4.21−4.25 (m, 2H), 4.31−4.37 (m, 1H), 4.42−4.44 (d, 1H), 4.56−4.62 (t, 1H), 4.72−4.77 (m, 1H), 6.31−6.33 (dd, 1H), 7.20−7.23 (m, 7H), 7.79−7.83 (m, 2H), 8.05 (s, 1H) ppm.

^{13}C NMR (101 MHz, CD_3OD): δ = 10.8, 14.1, 16.5, 18.2, 20.1, 20.9, 20.9, 21.1, 23.8, 25.5, 25.6, 31.2, 31.3, 32.6, 36.4, 36.6, 37.5, 37.8, 38.6, 38.8, 40.5, 42.6, 42.8, 44.2, 46.5, 50.3, 54.8, 55.2, 56.5, 57.6, 63.3, 69.8, 71.2, 71.5, 121.2, 122.4, 125.4, 127.4, 129.4, 130.4, 139.1, 139.5, 150.4, 171.0, 171.8, 175.6, 177.3 ppm.

t_R = 10.5 min (10 % ACN (2min)>15 min>95 %>5 min>100 % (10 min))

HRMS calculated for $C_{50}H_{74}N_7O_8S_3$ $[M+H]^+$: m/z = 996.4763, found: m/z = 996.4763.

<u>2-(Pyridine-2-yl-disulfanyl) ethyl ester of tubugi 4 (**37**)</u>

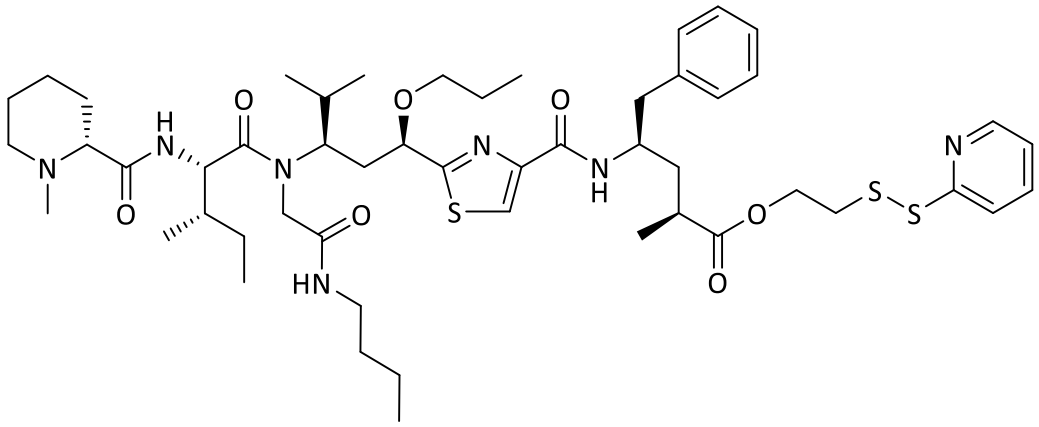

Compound **34** (244 mg, 0.27 mmol) was dissolved in dichloromethane (15 mL) and cooled down to 0 °C. EDC × HCl (68 mg, 0.35 mmol), **35** (71 mg, 0.37 mmol) and DMAP (3.3 mg, 0.03 mmol) were sequentially added to that solution. After 5 minutes, the mixture was allowed to reach rt and left to stir overnight. The crude product was purified by silica column chromatography to afford **37** (168 mg, 63 %) as a yellow oil.

R_f = 0.14 (dichloromethane/methanol 20:1)

^{1}H NMR (400 MHz, CD_3OD): δ = 0.74–1.27 (m, 10H), 1.23–1.48 (m, 1H), 1.64 (ddd, 6H), 1.67 (s, 4H), 1.89–2.12 (m, 1H), 2.40–2.67 (m, 2H), 2.74–3.02 (m, 1H), 2.98–3.31 (m, 2H), 3.31–3.55 (m, 1H), 3.79 (t, 6H), 4.12–4.30 (m, 1H), 4.44–4.69 (m, 1H), 4.70–4.83 (m, 1H), 7.09–7.33 (m, 3H), 7.68–7.85 (m, 1H), 8.37 (tt, 2H) ppm.

^{13}C NMR (101 MHz, CD_3OD): δ = 11.0, 14.1, 15.4, 16.5, 16.7, 18.3, 20.1, 20.7, 20.8, 21.1, 23.5, 24.2, 25.3, 25.5, 31.1, 31.5, 31.8, 32.2, 32.5, 37.7, 37.9, 38.6, 39.1, 39.6, 40.5, 42.9, 44.0, 50.3, 55.3, 56.4, 58.0, 63.1, 66.6, 69.4, 73.3, 77.5, 121.2, 122.3, 122.4, 125.2, 127.4, 127.8, 129.4, 129.6, 130.4, 130.7, 138.7, 139.1, 139.3, 139.6, 150.2, 150.4, 150.5, 150.7, 161.2, 161.3, 171.0, 175.3, 176.2, 177.2, 179.3 ppm.

t_R = 8.2 min (10 % ACN (2min)>15 min>95 %>5 min>100 % (10 min))

HRMS calculated for $C_{51}H_{78}N_7O_7S_3$ $[M+H]^+$: m/z = 996.5127, found: m/z = 996.5163.

2.4.7. Syntheses of linker and spacer compounds

4-Methyl-4-(pyridin-2-yldisulfanyl)pentanoic acid (**38**)

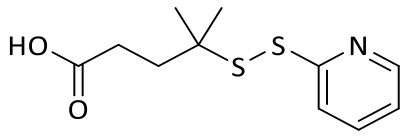

2,2'-Dipyridyl disulfide (3.01 g, 13.39 mmol) was dissolved in methanol (100 mL). To that mixture 4-mercapto-4-methyl-pentane acid (1.62 g, 12.18 mmol) was added. The mixture was left to stir for 6 h. The solvent was removed under reduced pressure and the crude was purified by silica column chromatography to obtain **38** (1.24 g, 46 %) as a colorless solid.

R_f = 0.20 (*n*-hexane/ethyl acetate 5:3)

^{1}H NMR (400 MHz, CD_3OD): δ = 1.29 (s, 6H), 1.85–1.94 (m, 2H), 2.36–2.45 (m, 2H), 7.20 (ddd, 1H), 7.77 (ddd, 1H), 7.86 (dt, 1H), 8.36 (ddd, 1H) ppm.

^{13}C NMR (101 MHz, CD_3OD): δ = 27.6, 30.7, 36.9, 52.9, 121.9, 122.4, 139.0, 150.3, 162.1, 176.8 ppm.

HRMS calculated for $C_{11}H_{16}NO_2S_2$ $[M+H]^+$: m/z = 258.0624, found: m/z = 258.0618.

calculated for $C_{11}H_{14}NO_2S_2$ $[M-H]^-$: m/z = 256.0464, found: m/z = 256.0469.

4-Methyl-4-(pyridin-2-yldisulfanyl)pentanoic ester of PAB-Cit-Val(Boc) (**39**)

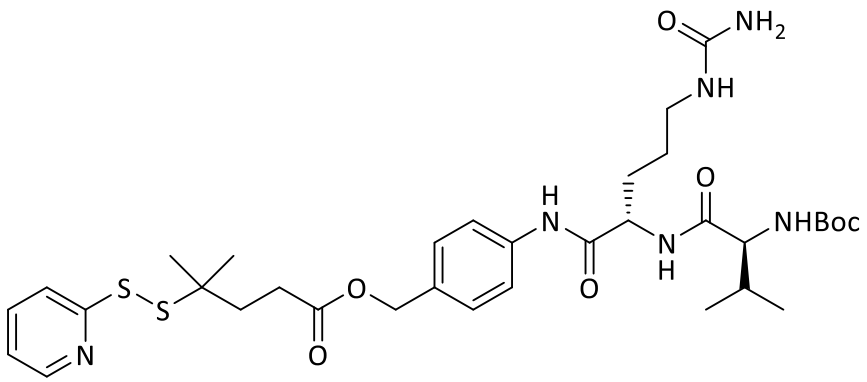

PAB-Cit-Val(Boc) (0.20 g, 0.40 mmol) was dissolved in dichloromethane (5 mL) and cooled to 0 °C. DMF (1 mL) was added to get a better solubility. DIC (0.07 mL, 0.52 mmol), **38** (0.13 g, 0.48 mmol) and DMAP (0.01 g, 0.04 mmol) were added. After 5 min the mixture was allowed to reach rt and left

to stir for 22 h. The crude was purified by silica column chromatography (dichloromethane/ethanol 5:1) to yield **39** (0.25 g, 87 %) as a colorless, viscous oil.

R_f = 0.66 (dichloromethane/ethanol 5:1)

^{1}H NMR (400 MHz, CD_3OD): δ = 0.95 (dd, 8H), 1.10 (d, 14H), 1.27 (s, 6H), 1.44 (s, 11H), 1.53–1.66 (m, 1H), 1.84–1.93 (m, 2H), 1.98–2.12 (m, 2H), 2.41–2.50 (m, 2H), 3.15 (ddt, 3H), 3.78 (p, 2H), 3.91 (d, 1H), 4.53 (dd, 1H), 4.85 (s, 8H), 5.02 (s, 2H), 7.14 (ddd, 1H), 7.29 (t, 2H), 7.58 (dd, 2H), 7.69 (ddd, 1H), 7.80 (dt, 1H), 8.30 (d, 1H) ppm.

^{13}C NMR (101 MHz, CD_3OD: δ = 18.6, 19.8, 22.5, 27.6, 28.7, 30.5, 31.0, 31.9, 36.8, 42.7, 52.8, 54.9, 61.7, 67.0, 80.7, 121.2, 122.0, 122.4, 130.1, 133.4, 138.9, 139.6, 150.1, 161.9, 162.3, 172.3, 174.5 ppm.

HRMS calculated for $C_{34}H_{51}N_6O_7S_2$ $[M+H]^+$: m/z = 719.3262, found: m/z = 719.3291.

<u>4-Methyl-4-(pyridin-2-yldisulfanyl)pentanoic ester of PAB-Cit-Val (**40**)</u>

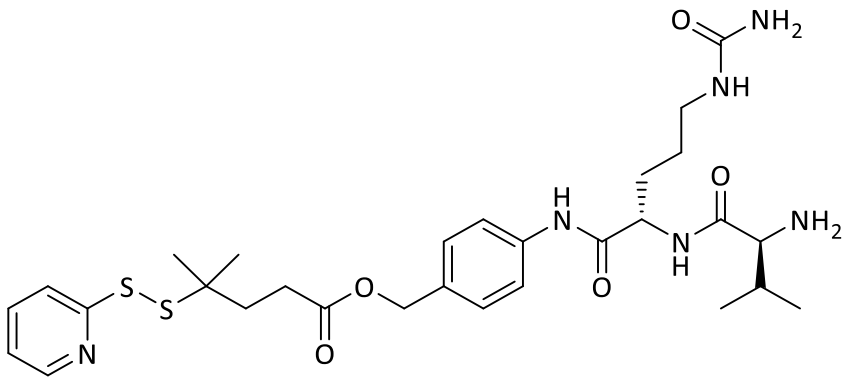

Compound **39** (0.28 g, 0.32 mmol) was dissolved in dichloromethane (8.5 mL) and cooled to 0 °C. TFA (1.5 mL) was added and the mixture was left to stir at 0 °C for 4 h. The mixture was concentrated under reduced pressure. The resulting oil was redissolved in dichloromethane and then evaporated. That was repeated a few times. The crude was purified by silica column chromatography to afford **40** in quantitative yield (0.22 g) as a colorless solid.

R_f = 0.10 (dichloromethane/ethanol 4:1)

^{1}H NMR (400 MHz, CD_3OD): δ = 0.84–1.08 (m, 8H), 1.24 (t, 4H), 1.27 (s, 6H), 1.51–1.66 (m, 2H), 1.84–1.96 (m, 3H), 2.01 (s, 3H), 2.02–2.15 (m, 2H), 2.39–2.50 (m, 2H), 3.07–3.27 (m, 2H), 3.40 (d, 1H), 4.10 (q, 2H), 4.57 (dd, 1H), 5.04 (d, 2H), 7.15 (ddd, 1H), 7.30 (dd, 2H), 7.49–7.61 (m, 2H), 7.69 (td, 1H), 7.81 (dd, 1H), 8.28–8.34 (m, 1H) ppm.

^{13}C NMR (101 MHz, CD_3OD): δ = 14.5, 17.8, 19.5, 19.7, 20.9, 27.6, 30.5, 31.0, 32.8, 36.8, 52.8, 54.9, 60.8, 61.5, 67.0, 121.1, 122.0, 122.4, 130.1, 133.4, 139.0, 139.6, 150.0, 161.9, 172.3, 174.5 ppm.

HRMS calculated for $C_{29}H_{43}N_6O_5S_2$ $[M+H]^+$: m/z = 619.2738, found: m/z = 619.2723.

3,4-Dibromomaleic anhydride (**41**)

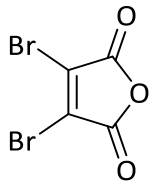

Maleic anhydride (1.50 g, 15.14 mmol), bromine (1.57 g, 30.29 mmol) and aluminum chloride (0.03 g, 0.23 mmol) were added into a sealed microwave tube under nitrogen atmosphere and heated at 80 °C for 16 h. The tube was cooled to rt and the mixture was taken up in ethyl acetate, followed by filtration. The filtrate was concentrated under reduced pressure to give **41** as a yellowish solid (2.87 g, 74 %).

^{13}C NMR (101 MHz, $CDCl_3$): δ = 131.3, 158.5 ppm.

Melting point: θ = 104–113 °C

Proof by silver nitrate: 10 mg dissolved in absolute ethanol (0.5 mL) and $AgNO_3$ solution (2 % in absolute ethanol, 0.5 mL) and seen after 5 min as a colorless precipitate

5-(3,4-Dibromo-2,5-dioxo-2,5-dihydro-1*H*-pyrrol-1-yl)pentanoic acid (**42**)

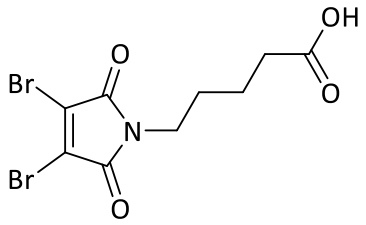

Compound **41** (0.55 g, 1.61 mmol) was dissolved in acetic acid (5.64 mL). 4-Aminopentanoic acid (0.21 g, 1.77 mmol) was added to that mixture and the mixture was left to stir under reflux for 4 h. The solvent was removed under reduced pressure and the crude was purified by silica column chromatography (ethyl acetate/*n*-hexane/formic acid 7:3:0.1 %) to afford **42** (0.55 g, 96 %) as a colorless solid.

R_f = 0.60 (ethyl acetate/*n*-hexane/formic acid 4:1:0.1 %)

^{1}H NMR (400 MHz, $CDCl_3$): δ = 1.67 (dtdt, 4H), 2.40 (t, 2H), 3.64 (t, 2H) ppm.

^{13}C NMR (101 MHz, $CDCl_3$): δ = 21.6, 27.7, 33.1, 39.2, 129.4, 163.9, 178.5 ppm.

HRMS calculated for $C_9H_{10}NO_4Br_2$ $[M+H]^+$: m/z = 353.8978, found: m/z = 353.8953.

4-Methyl-4-(pyridin-2-yldisulfanyl)pentanoic ester of PAB-Cit-Val to dibromomaleimide (**43**)

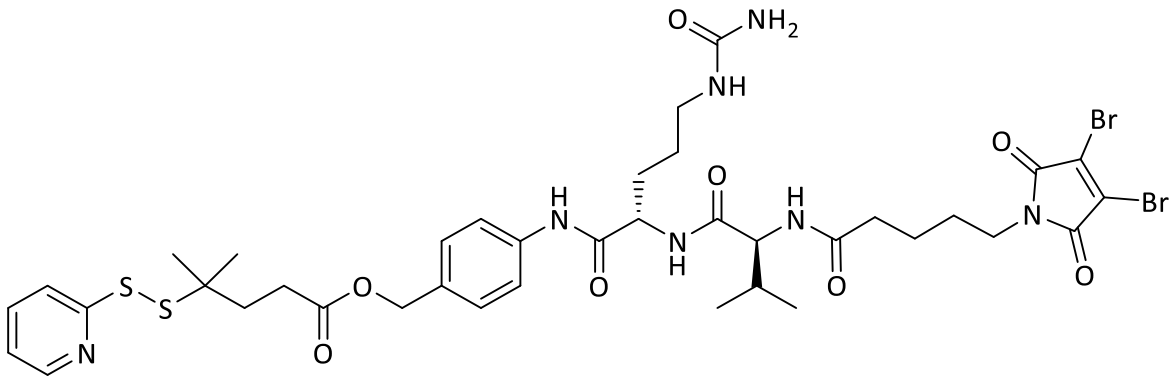

Compound **42** (20.0 mg, 0.05 mmol) was dissolved in dichloromethane (1.5 mL) under nitrogen atmosphere and cooled to 0 °C. DIC (10 µL, 0.07 mmol), **40** (40.6 mg, 0.06 mmol) dissolved in dichloromethane (0.5 mL) and DMAP (0.6 mg, 0.01 mmol) were added. After 5 min the mixture was allowed to reach rt and left to stir for 4 h. The crude was purified by silica column chromatography to afford **43** (29 mg, 60 %) as a colorless solid.

R_f = 0.69 (dichloromethane/ethanol 4:1)

^{1}H NMR (400 MHz, CD_3OD): δ = 0.84–0.92 (m, 1H), 0.93–1.03 (m, 4H), 1.10 (d, 25H), 1.19–1.35 (m, 7H), 1.52–1.66 (m, 4H), 1.86–1.92 (m, 2H), 1.99–2.12 (m, 1H), 2.31 (s, 1H), 2.43–2.49 (m, 2H), 3.56–3.62 (m, 1H), 3.78 (hept, 4H), 5.02 (s, 1H), 7.26–7.31 (m, 1H), 7.53–7.61 (m, 1H) ppm.

^{13}C NMR (101 MHz, CD_3OD): δ = 18.9, 19.8, 23.5, 24.0, 27.6, 28.9, 31.0, 35.9, 36.8, 40.1, 42.7, 52.9, 55.0, 60.6, 67.0, 121.1, 122.0, 122.5, 130.1, 130.3, 133.3, 139.0, 139.6, 150.1, 159.9, 161.9, 162.3,165.5, 172.3, 174.0, 174.6, 176.0 ppm.

HRMS calculated for $C_{38}H_{50}N_7O_8S_2Br_2$ $[M+H]^+$: m/z = 954.1531, found: m/z = 954.1540.

2.4.8. Syntheses of peptides and conjugates

Octreotide (**44**)

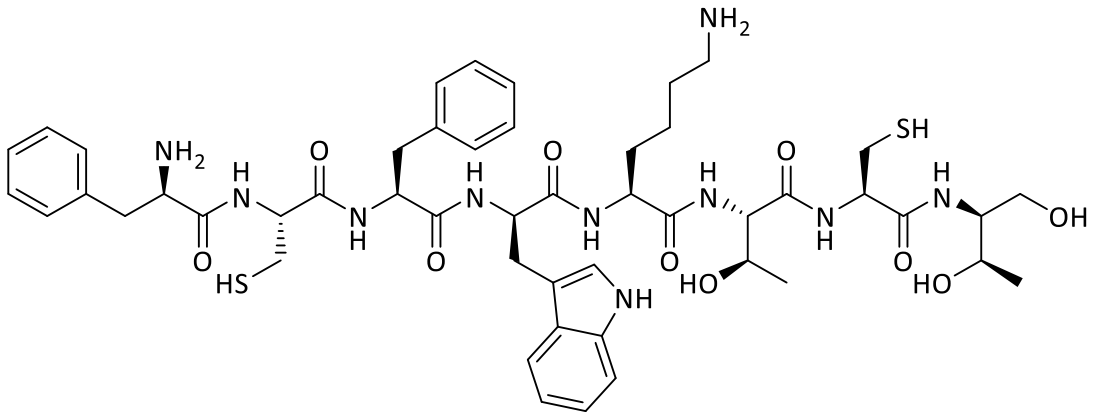

Compound **44** was synthesized according to the general procedure **G1** in 100 µmol scale on H-L-Thr(tBu)-ol-2CT resin (139 mg, loading: 0.72 mmol/g). The cleavage was performed as described in

G1 (> 95 % purity). The peptide was employed in the following reaction steps without further purification.

^{1}H NMR (400 MHz, DMSO-d6): δ = 0.96–1.20 (m, 9H), 1.19–1.30 (m, 1H), 1.46 (q, 4H), 1.59–1.67 (m, 1H), 2.02 (t, 1H), 2.51–2.58 (m, 2H), 2.67–2.86 (m, 5H), 2.83–3.04 (m, 2H), 3.04–3.20 (m, 2H), 3.32 (dd, 1H), 3.41–3.54 (m, 1H), 3.65 (s, 1H), 3.87 (m, 1H), 4.00 (m, 1H), 4.16 (s, 1H), 4.30–4.59 (m, 3H), 4.66 (m, 1H), 5.03 (s, 1H), 6.94–7.15 (m, 7H), 7.13–7.27 (m, 2H), 7.24–7.38 (m, 6H), 7.54 (dd, 1H), 7.69 (dd, 1H), 7.79 (s, 4H), 7.88–8.06 (m, 2H), 8.13 (s, 1H), 8.20 (d, 3H), 8.30 (dd, 1H), 8.68 (d, 1H), 10.81–10.86 (m, 1H) ppm.

^{13}C NMR (101 MHz, DMSO-d6): δ = 19.6, 20.1, 22.0, 26.4, 26.6, 31.3, 37.2, 38.7, 52.1, 53.2, 54.1, 54.9, 55.9, 58.4, 60.5, 64.2, 66.4, 109.8, 111.2, 115.7, 118.1, 118.6, 120.8, 124.0, 126.2, 127.2, 127.9, 128.5, 129.2, 129.6, 131.3, 134.8, 136.1, 137.6, 157.8, 158.1, 158.4, 168.1, 168.9, 169.5, 169.8, 170.4, 171.3, 171.7 ppm.

t_R = 9.7 min (10 % ACN (2min)>15 min>95 %>5 min>100 % (10 min))

HRMS calculated for $C_{49}H_{69}N_{10}O_{10}S_2$ $[M+H]^+$: m/z = 1021.4641, found: m/z = 1021.4634.

<u>Cyclized octreotide (**45**)</u>

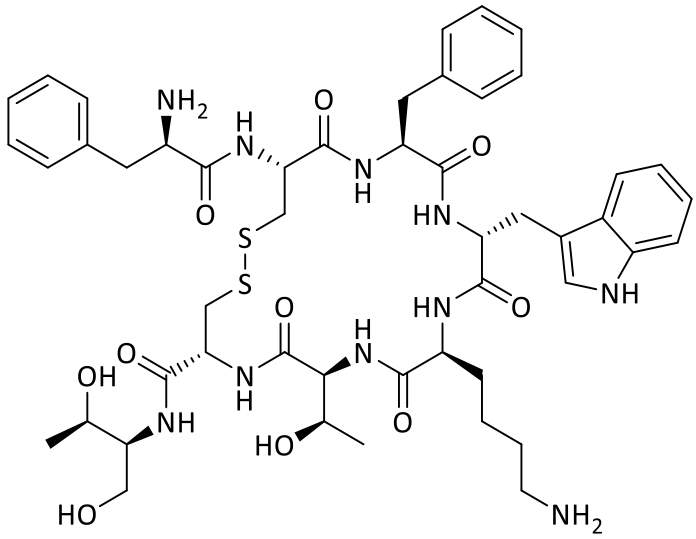

Compound **44** (119.0 mg, 0.11 mmol, 0.2 mM) was dissolved in water (577.30 mL) with acetic acid (30.40 mL, 5 %). The pH was adjusted to 6 by addition of ammonia solution (30.50 mL). DMSO (159.50 mL, 20 %) was added and the mixture was left to stir at rt until **44** disappeared. The crude was purified by HPLC to yield **45** (80 mg, 71 %) as a colorless solid.

^{1}H NMR (400 MHz, DMSO-d6): δ = 0.85 (m, 2H), 0.95–1.27 (m, 10H), 1.30–1.43 (m, 5H), 1.67–1.78 (m, 2H), 2.62 (d, 3H), 2.68–2.91 (m, 6H), 2.90–3.09 (m, 2H), 3.06–3.29 (m, 2H), 3.30–3.55 (m, 3H), 3.67 (ddt, 2H), 3.89–4.10 (m, 3H), 4.13–4.34 (m, 1H), 4.50 (ddd, 2H), 4.95–5.12 (m, 2H), 6.95–7.40 (m, 18H), 7.41–7.77 (m, 4H), 8.15–8.27 (m, 1H), 8.34–8.53 (m, 3H), 8.71 (dd, 1H), 10.84 (s, 1H) ppm.

t_R = 5.5 min (10 % ACN (2min)>15 min>95 %>5 min>100 % (10 min))

HRMS calculated for $C_{49}H_{67}N_{10}O_{10}S_2$ $[M+H]^+$: m/z = 1019.4485, found: m/z = 1019.4663.

Peptide CNGRC (**46**)

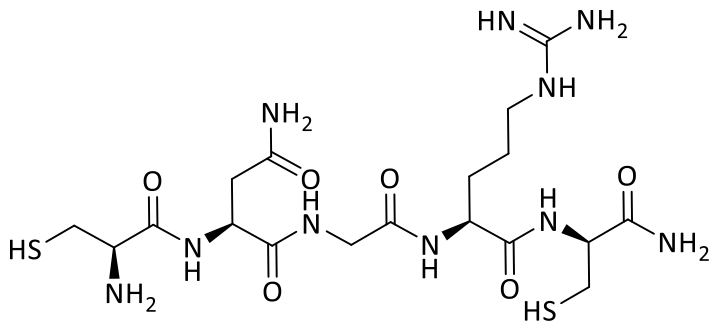

Compound **46** was synthesized according to the general procedure **G1** in 100 µmol scale on Fmoc-Rink-Amid-MBHA resin (149.3 mg, loading: 0.67 mmol/g). The cleavage was performed as described in **G1** (> 95 % purity). The peptide was used in following reactions without further purification.

^{1}H NMR (400 MHz, D_2O): δ = 1.57–1.75 (m, 4H), 1.87 (m, 3H), 2.73–2.86 (m, 1H), 2.83–3.08 (6H), 3.05–3.15 (m, 2H), 3.21–3.24 (t, 3H), 3.58–3.67 (m, 2H), 3.71 (m, 10H), 3.99 (s, 3H), 4.26–4.29 (t, 1H), 4.38–4.41 (t, 1H), 4.48–4.51 (dd, 1H), 4.81 (s, 1H) ppm.

^{3}C NMR (101 MHz, D_2O): δ = 25.4, 26.0, 26.3, 29.1, 37.0, 41.5, 43.6, 51.7, 54.5, 55.3, 56.5, 70.6, 116.0, 118.9, 121.8, 157.8, 169.2, 172.3, 173.6, 174.7, 175.1 ppm.

t_R = 1.7 min (10 % ACN (2min)>15 min>95 %>5 min>100 % (10 min))

HRMS calculated for $C_{18}H_{35}N_{10}O_6S_2$ $[M+H]^+$: m/z = 551.2184, found: m/z = 551.2214.

Cyclized peptide CNGRC (**47**)

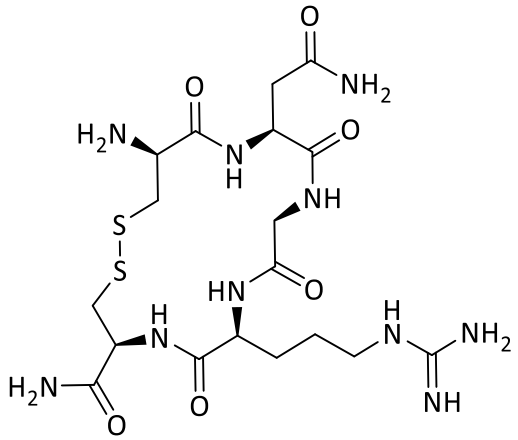

Compound **46** (69.0 mg, 0.11 mmol, 0.2 mM) was dissolved in water (180.50 mL) with acetic acid (9.50 mL, 5 %). The pH was adjusted to 6 by addition of ammonia solution (17.70 mL). DMSO (51.90 mL, 20 %) was added and the mixture was left to stir at rt until **46** disappeared. The crude was purified by HPLC to yield **47** (48 mg, 78 %) as a colorless solid.

^{1}H NMR (400 MHz, DMSO-d6): δ = 1.51 (m, 2H), 1.76 (m, 1H), 1.86–1.89 (dd, 2H), 2.55 (m, 12H), 2.71 (m, 1H), 3.00 (s, 1H), 3.19 (m, 2H), 3.55 (m, 1H), 3.73 m, 2H), 4.12–4.50 (m, 5H), 7.23 (m, 3H) ppm.

t_R = 1.5 min 10 % ACN (2min)>15 min>95 %>5 min>100 % (10 min)

HRMS calculated for $C_{18}H_{33}N_{10}O_6S_2$ $[M+H]^+$: m/z = 549.2028, found: m/z = 549.2011.

Cyclized octreotide containing linker system (**48**)

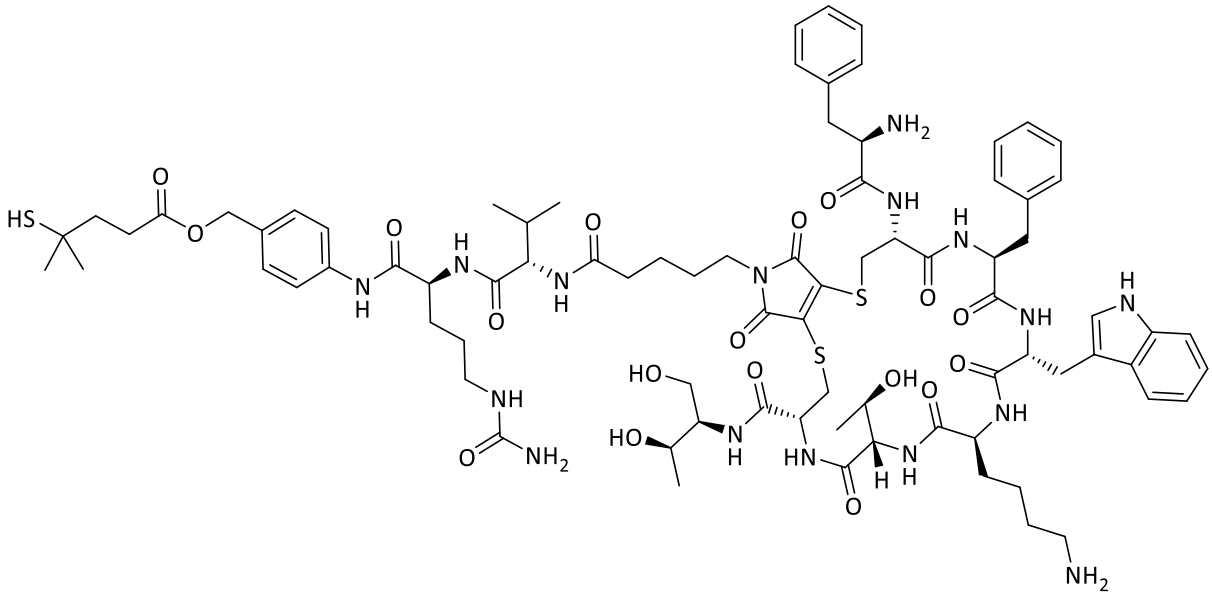

Compound **44** (80.0 mg, 0.07 mmol, 5 mM) was dissolved in water (7.44 mL) and then **43** dissolved in DMF (7.44 mL) was added dropwise. The mixture was left to stir at rt for 5 d.

HRMS calculated for $C_{87}H_{116}N_{17}O_{18}S_4$ $[M+H]^+$: m/z = 1814.7569, found: m/z = 1814.7725.

TCEP (26.1 mg, 0.09 mmol) was added and the mixture was left to stir at rt for 14 d. The solvent were removed under reduced pressure to afford crude **48** as a yellow solid.

^{1}H NMR (400 MHz, D_2O): δ = 0.93 (s, 3H), 1.17 (s, 4H), 1.27 (d, 1H), 1.41 (d, 12H), 1.62–1.70 (m, 4H), 1.77 (s, 2H), 2.19 (s, 2H), 2.42 (s, 1H), 3.21 (s, 1H), 3.35 (d, 1H), 3.61–3.81 (m, 3H), 4.71 (t, 1H), 7.15–7.37 (m, 10H), 8.46 (s, 2H) ppm.

HRMS calculated for $C_{82}H_{113}N_{16}O_{18}S_3$ $[M+H]^+$: m/z = 1705.7583, found: m/z = 1705.7653.

Conjugate containing octreotide and tubugi 1 (**49**)

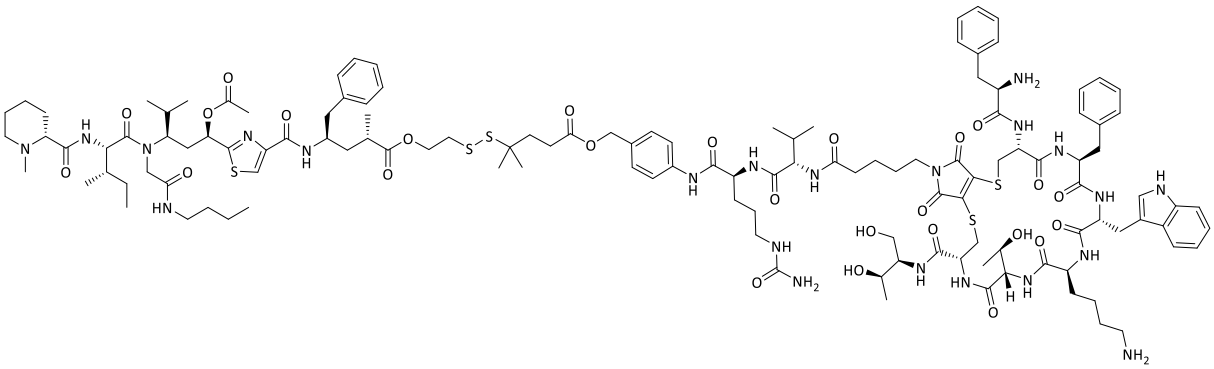

Compound **48** (15.0 mg, 0.01 mmol, 5 mM) was dissolved in dry DMF (0.80 mL). To that solution **36** (8.3 mg, 0.01 mmol) dissolved in dry DMF (0.08 mL) was added. The mixture was left to stir at rt for 46 h. The crude product was purified by an RP C18 column (water/methanol) followed by HPLC to obtain **49** (4 mg, 20 %) as a yellowish solid.

t_R = 17.3 min (10 % ACN (2min)>15 min>95 %>5 min>100 % (10 min))

HRMS calculated for $C_{127}H_{183}N_{22}O_{26}S_5$ $[M+H]^{3+}$: m/z = 864.0761, found: m/z = 864.0745.

Conjugate containing octreotide and tubugi 4 (**50**)

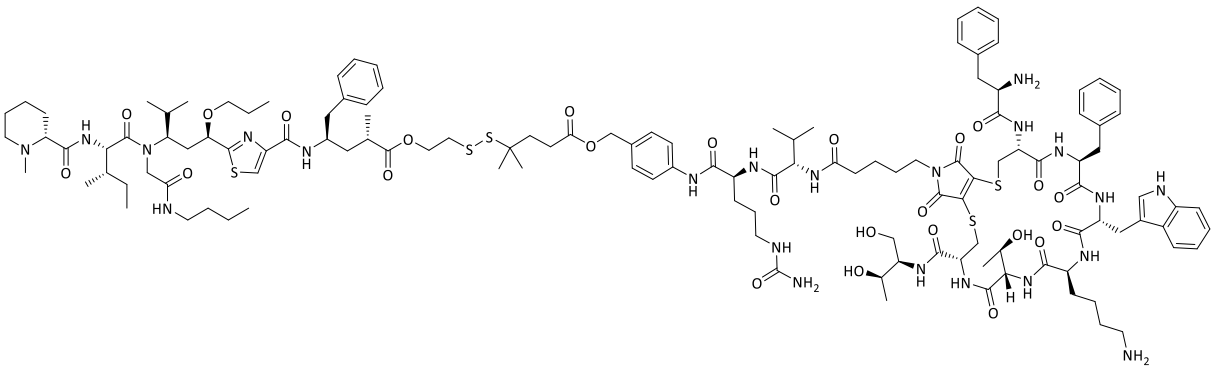

Compound **48** (15.0 mg, 0.01 mmol, 5 mM) was dissolved in dry DMF (0.80 mL). To that solution **37** (8.3 mg, 0.01 mmol) dissolved in dry DMF (0.80 mL) was added. The mixture was left to stir at rt for 5 d. The crude product was purified by an RP C18 column (water/methanol) followed by HPLC to obtain **50** (5 mg, 24 %) as a yellowish solid.

t_R = 17.5 min (10 % ACN (2min)>15 min>95 %>5 min>100 % (10 min))

HRMS calculated for $C_{128}H_{187}N_{22}O_{25}S_5$ $[M+H]^{3+}$: m/z = 864.0882, found: m/z = 864.0861.

Cyclized CNGRC containing linker system (**51**)

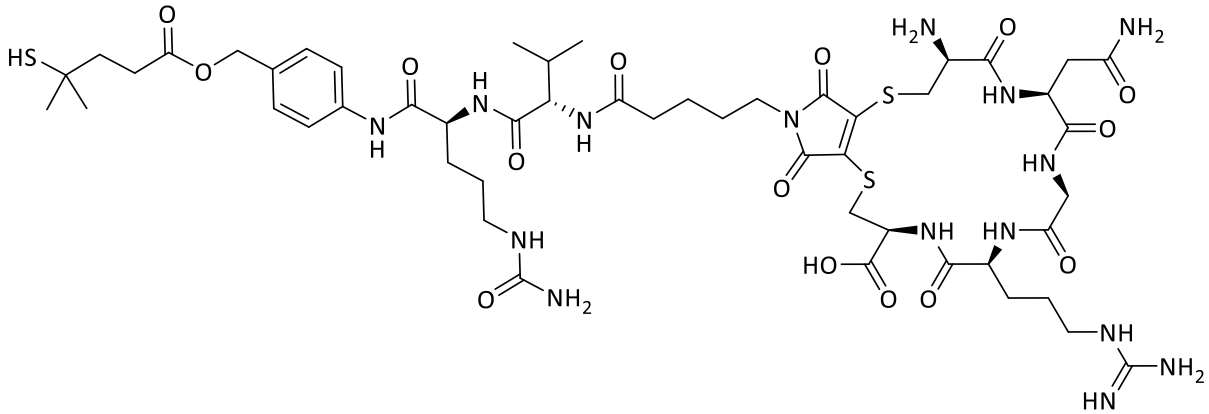

Compound **46** (30.0 mg, 0.05 mol, 5 mM) was dissolved in water (5.18 mL) and then **43** dissolved in DMF (5.18 mL) was added dropwise. The mixture was left to stir at rt overnight.

HRMS calculated for $C_{56}H_{83}N_{17}O_{14}S_4$ $[M+H]^{+}$: m/z = 1344.5112, found: m/z = 1344.5133.

TCEP (16.7 mg, 0.06 mmol) was added and the mixture was left to stir at rt overnight. The solvent were removed under reduced pressure to afford crude **51** as a yellow solid.

^{1}H NMR (400 MHz, DMSO-d6): δ = 0.85 (m, 2H), 1.02 (s, 24H), 1.10–1.34 (m, 2H), 1.45 (s, 6H), 1.66–1.88 (m, 2H), 1.95 (m, 2H), 2.08–2.41 (m, 2H), 2.57–2.71 (m, 1H), 2.84–3.17 (m, 2H), 3.64 (ddt, 8H), 3.99–4.61 (m, 4H), 5.01 (d, 2H), 5.49 (d, 8H), 6.91–7.63 (m, 2H), 7.67–7.87 (m, 2H) ppm.

HRMS calculated for $C_{51}H_{79}N_{16}O_{14}S_3$ $[M+H]^+$: m/z = 1235.5126, found: m/z = 1235.5153.

Conjugate containing CNGRC and tubugi 1 (**52**)

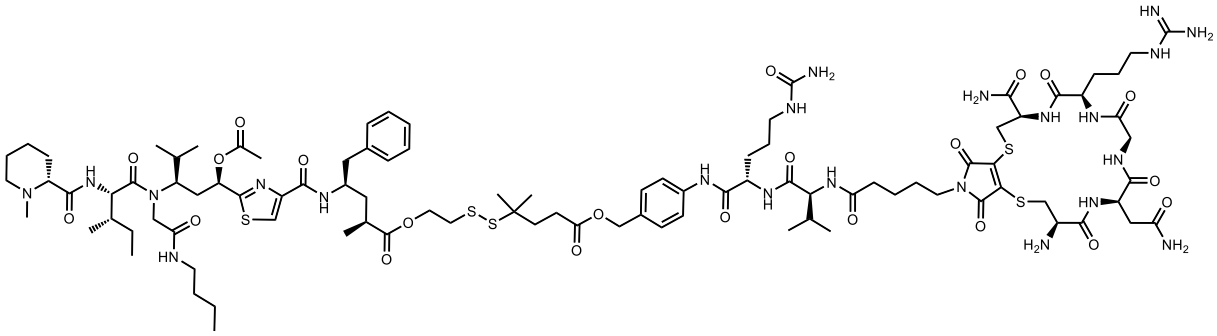

Compound **46** (16.0 mg, 0.01 mmol, 5 mM) was dissolved in dry DMF (1.17 mL). To that solution **36** (12.2 mg, 0.01 mmol) dissolved in dry DMF (1.17 mL) was added. The mixture was left to stir at rt for 46 h. The crude product was purified by an RP C18 column (water/methanol) to obtain **52** (8 mg, 32 %) as a yellowish solid.

t_R = 8.7 min (10 % ACN (2min)>15 min>95 %>5 min>100 % (10 min))

HRMS calculated for $C_{96}H_{149}N_{22}O_{22}S_5$ $[M+H]^{3+}$: m/z = 707.3275, found: m/z = 707.3314.

Conjugate containing CNGRC and tubugi 4 (**53**)

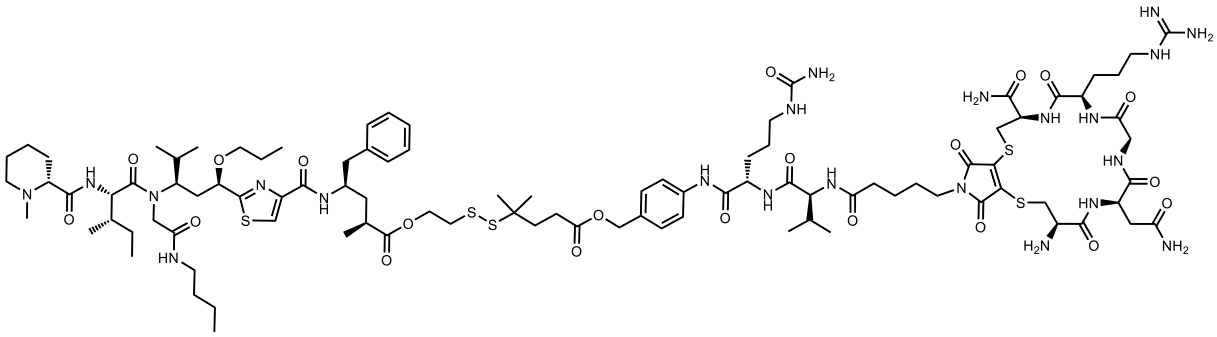

Compound **46** (16.0 mg, 0.01 mmol, 5 mM) was dissolved in dry DMF (1.17 mL). To that solution **37** (12.2 mg, 0.01 mmol) dissolved in dry DMF (1.17 mL) was added. The mixture was left to stir at rt for 5 d. The crude product was purified by an RP C18 column (water/methanol) to obtain **53** (7 mg, 28 %) as a yellowish solid.

t_R = 8.7 min (10 % ACN (2min)>15 min>95 %>5 min>100 % (10 min))

HRMS calculated for $C_{97}H_{153}N_{22}O_{21}S_5$ $[M+H]^{3+}$: m/z = 707.3396, found: m/z = 707.3377.

2.4.9. Syntheses of fluorophore conjugates

Rhodamine B modified with 1,3-diaminopropane (**54**)

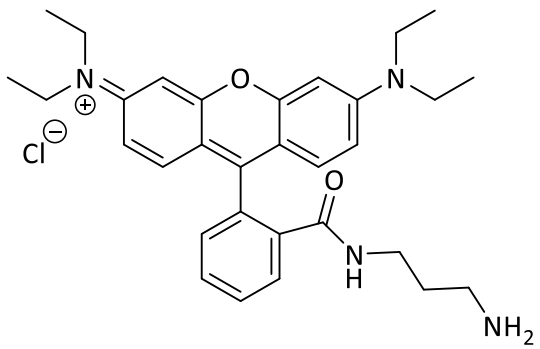

1,3-Diaminopropane (0.84 mL, 9.92 mmol) was dissolved in dichloromethane (20 mL) and cooled to 0 °C. Rhodamine B (1.00 g, 1.98 mmol) and EDC × HCl (0.50 g, 2.58 mmol) were dissolved in dichloromethane (30 mL), cooled to 0 °C and dropped to previous solution. After 5 min, the mixture was allowed to reach rt and left to stir at rt for 22 h. The crude was purified by silica column chromatography to afford **54** (0.48 g, 45 %) as a red oil.

R_f = 0.35 (dichloromethane/ethanol 4: 1)

^{1}H NMR (500 MHz, CD_3OD): δ = 1.20 (t, 12H), 1.29 (m, 1H), 1.51 (m, 2H), 2.84 (t, 2H), 3.29–3.38 (m, 2H), 3.62–3.74 (m, 8H), 6.99 (dd, 2H), 7.11–7.19 (m, 1H), 7.28 (m, 2H), 7.59–7.69 (m, 4H), 7.98 (m, 1H) ppm.

^{13}C NMR (126 MHz, CD_3OD): δ = 11.0, 12.8, 27.8, 38.2, 38.3, 38.4, 46.8, 53.6, 65.7, 118.5, 124.5, 124.9, 130.9, 131.5, 135.2, 153.6, 153.9, 171.2 ppm.

HRMS calculated for $C_{31}H_{41}N_4O_2$ $[M+H]^{2+}$: m/z = 250.1574, found: m/z = 250.6600.

Dibromomaleimide-linked rhodamine B (**55**)

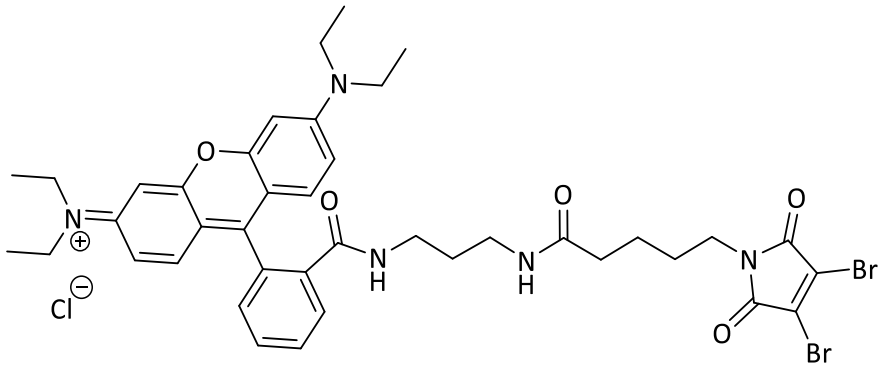

Compound **42** (90.0 mg, 0.24 mmol) was dissolved in dichloromethane (20 mL) and cooled to 0 °C. EDC × HCl (61.3 mg, 0.31 mmol) and **54** (122.1 mg, 0.22 mmol) were added and mixture was allowed to reach rt and left to stir overnight. The crude was purified by silica column chromatography to yield **55** (186 mg, 89 %) as a pink solid.

R_f = 0.67 (dichloromethane/methanol 10: 1)

^{1}H NMR (500 MHz, CD_3OD): δ = 1.18 (t, 12H), 1.23–1.35 (m, 1H), 1.50–1.65 (m, 4H), 2.14 (t, 2H), 2.86 (s, 5H), 2.93 (t, 2H), 2.99 (d, 2H), 3.09–3.20 (m, 2H), 3.51–3.63 (m, 9H), 6.70 (s, 2H), 7.06–7.15 (m, 1H), 7.59 (m, 2H), 7.98 (s, 2H) ppm.

^{13}C NMR (126 MHz, CD_3OD): δ = 11.8, 12.9, 23.9, 28.9, 29.4, 31.7, 36.3, 37.0, 37.7, 39.2, 40.0, 46.8, 66.0, 97.2, 114.8, 124.0, 125.0, 130.3, 131.8, 134.1, 134.6, 138.8, 154.1, 164.8, 170.0, 175.1 ppm.

HRMS calculated for $C_{40}H_{47}N_5O_5Br_2$ $[M+H]^+$: m/z = 835.1940, found: m/z = 835.1914.

Rhodamine B labeled octreotide (**56**)

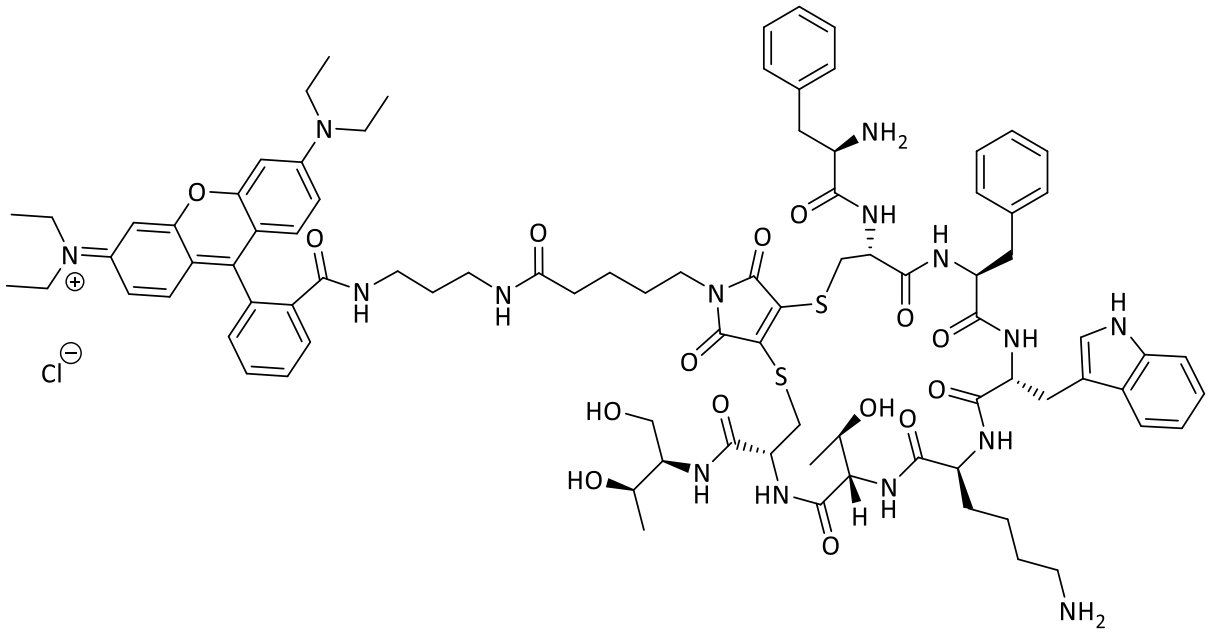

Compound **44** (40.0 mg, 0.04 mmol, 5 mM) was dissolved in dry DMF (3.72 mL). To that solution **55** (30.7 mg, 0.03 mmol) dissolved in dry DMF (3.72 mL) was added dropwise. The mixture was left to stir at rt for 3 d. The crude product was purified by an RP C18 column (water/methanol) to obtain **56** (9 mg, 16 %) as a pink solid.

t_R = 12.6 min (10 % ACN (2min)>15 min>95 %>5 min>100 % (10 min))

HRMS calculated for $C_{89}H_{115}N_{15}O_{15}S_2$ $[M+H]^{3+}$: m/z = 565.9379, found: m/z = 565.9385.

Rhodamine B labeled CNGRC (**57**)

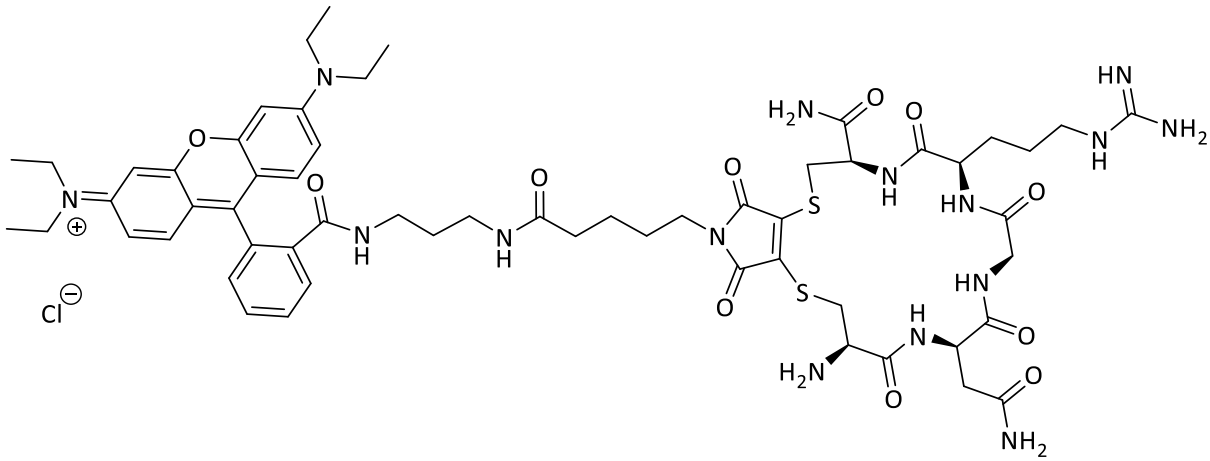

Compound **46** (40.0 mg, 0.07 mmol, 5 mM) was dissolved in dry DMF (6.90 mL). To that solution **55** (57.0 mg, 0.06 mmol) dissolved in dry DMF (6.90 mL) was added dropwise. The mixture was left to stir at rt for 17 h. The crude product was purified by an RP C18 column (water/methanol) to obtain **57** (36 mg, 46 %) as a pink solid.

t_R = 6.4 min (10 % ACN (2min)>15 min>95 %>5 min>100 % (10 min))

HRMS calculated for $C_{58}H_{81}N_{15}O_{11}S_2$ $[M+H]^{3+}$: m/z = 409.1894, found: m/z = 409.1892.

2.5. Conclusion

The synthesis of a novel linker-spacer system based on a combination of already known components is presented. This linker system was successfully built into peptide-drug conjugates by cyclization of the peptides octreotide (**49**, **50**) and CNGRC (**52**, **53**). The cyclization of the targeting peptides was performed by dibromomaleimide in the linker system. The drugs tubugi 1 and tubugi 4 were attached to the linker-spacer system through the formation of a disulfide bridge towards a self-immolative spacer. The cleavage of these PDCs triggered by reduction of the disulfide bridge was proven to occur within 24 h. Fast and quantitative internalization of fluorescent conjugates based on the peptides octreotide (**56**) and CNGRC (**57**) was observed by fluorescence measurements with a confocal microscope and flow cytometer. A good selectivity resulting in receptor-mediated internalization was confirmed in case of the octreotide-containing conjugate (**56**). In contrast, a selectivity of CNGRC-containing conjugate (**57**) and a correlation to the expression level of CD13 was not shown, but a more efficient uptake by the cells. This observation might be attributed to a rapid receptor recycling by SK-N-MC Ewing's sarcoma cells and to the occurrence of other receptors at the cell surface through which endocytosis can be triggered by binding to the NGR sequence. Particularly, the affinity of CNGRC to further targets might also explain the good activities of CNGRC-tubugi conjugates (**52**, **53**). The performed cell viability assays revealed that CNGRC-tubugi conjugates (**52**, **53**) were more effective against cancer cells than octreotide-tubugi conjugates (**49**, **50**). The lowest IC_{50} values after 72 h in case of the CNGRC containing conjugates were 47.6 ± 2.0 nM (**52**) as well as 531.0 ± 4.3 nM (**53**) and in case of octreotide containing conjugates the IC_{50} were 75.0 ± 2.3 nM (**49**) as well as 3431.0 ± 36.3 nM (**50**).

Considering the IC_{50} values with respect to incubation times as well as the expression levels of the respective targets, an increased efficacy of the PDCs correlated with a higher expression level as well as longer exposure to the cancer cell were proven. Although the observed correlations were more clearly seen in case of octreotide-based conjugates (**49**, **50**), in both cases the selectivity was not as significant as expected. The octreotide-tubugi 4 conjugate (**50**) was found to be the most promising candidate considering selectivity and rate of internalization.

2.6. References

1. Wessjohann, L. A.; Rivera, D. G.; Vercillo, O. E., Multiple Multicomponent Macrocyclizations (MiBs): A Strategic DevelopmentToward Macrocycle Diversity. *Chem Rev* **2009,** *109*, 796–814.
2. Dougherty, P. G.; Sahni, A.; Pei, D., Understanding Cell Penetration of Cyclic Peptides. *Chem Rev* **2019,** *119* (17), 10241-10287.
3. Gentilucci, L.; De Marco, R.; Cerisoli, L., Chemical modifications designed to improve peptide stability: incorporation of non-natural amino acids, pseudo-peptide bonds, and cyclization. *Curr Pharm Des* **2010,** *16* (28), 3185-203.
4. Brazeau, P.; Vale, W.; Burgus, R.; Ling, N.; Butcher, M.; Rivier, J.; Guillemin, R., Hypothalamic polypeptide that inhibits the secretion of immunoreactive pituitary growth hormone. *Science* **1973,** *179* (4068), 77-9.
5. Frühwald, M. C.; Rickert, C. H.; O'Dorisio, M. S.; Madsen, M.; Warmuth-Metz, M.; Khanna, G.; Paulus, W.; Kühl, J.; Jürgens, H.; Schneider, P.; Müller, H. L., Somatostatin receptor subtype 2 is expressed by supratentorial primitive neuroectodermal tumors of childhood and can be targeted for somatostatin receptor imaging. *Clin Cancer Res* **2004,** *10* (9), 2997-3006.
6. Lamberts, S. W.; Krenning, E. P.; Reubi, J. C., The role of somatostatin and its analogs in the diagnosis and treatment of tumors. *Endocr Rev* **1991,** *12* (4), 450-82.
7. Bauer, W.; Briner, U.; Doepfner, W.; Haller, R.; Huguenin, R.; Marbach, P.; Petcher, T. J.; Pless, SMS 201-995: a very potent and selective octapeptide analogue of somatostatin with prolonged action. *Life Sci* **1982,** *31* (11), 1133-40.
8. Melacini, G.; Zhu, Q.; Goodman, M., Multiconformational NMR analysis of sandostatin (octreotide): equilibrium between beta-sheet and partially helical structures. *Biochemistry* **1997,** *36* (6), 1233-41.
9. Veber, D. F.; Holly, F. W.; Nutt, R. F.; Bergstrand, S. J.; Brady, S. F.; Hirschmann, R.; Glitzer, M. S.; Saperstein, R., Highly active cyclic and bicyclic somatostatin analogues of reduced ring size. *Nature* **1979,** *280* (5722), 512-4.
10. Cuevas-Ramos, D.; Fleseriu, M., Somatostatin receptor ligands and resistance to treatment in pituitary adenomas. *J Mol Endocrinol* **2014,** *52* (3), R223-40.
11. Xu, C.; Zhang, H., Somatostatin receptor based imaging and radionuclide therapy. *Biomed Res Int* **2015,** *2015*, 917968.
12. Reubi, J. C.; Waser, B.; Schaer, J. C.; Laissue, J. A., Somatostatin receptor sst1-sst5 expression in normal and neoplastic human tissues using receptor autoradiography with subtype-selective ligands. *Eur J Nucl Med* **2001,** *28* (7), 836-46.
13. Waser, B.; Cescato, R.; Liu, Q.; Kao, Y. J.; Körner, M.; Christ, E.; Schonbrunn, A.; Reubi, J. C., Phosphorylation of sst2 receptors in neuroendocrine tumors after octreotide treatment of patients. *Am J Pathol* **2012,** *180* (5), 1942-9.
14. Zhang, H. Y.; Xu, W. Q.; Zheng, Y. Y.; Omari-Siaw, E.; Zhu, Y.; Cao, X.; Tong, S. S.; Yu, J. N.; Xu, X. M., Octreotide-periplocymarin conjugate prodrug for improving targetability and anti-tumor efficiency: synthesis, in vitro and in vivo evaluation. *Oncotarget* **2016,** *7* (52), 86326-86338.

15. Arnold, R.; Wied, M.; Behr, T. H., Somatostatin analogues in the treatment of endocrine tumors of the gastrointestinal tract. *Expert Opin Pharmacother* **2002,** *3* (6), 643-56.
16. de Herder, W. W.; Lamberts, S. W., Somatostatin and somatostatin analogues: diagnostic and therapeutic uses. *Curr Opin Oncol* **2002,** *14* (1), 53-7.
17. Patel, Y. C., Somatostatin and its receptor family. *Front Neuroendocrinol* **1999,** *20* (3), 157-98.
18. Ben-Shlomo, A.; Melmed, S., Somatostatin agonists for treatment of acromegaly. *Mol Cell Endocrinol* **2008,** *286* (1-2), 192-8.
19. Patel, Y. C.; Greenwood, M. T.; Panetta, R.; Demchyshyn, L.; Niznik, H.; Srikant, C. B., The somatostatin receptor family. *Life Sci* **1995,** *57* (13), 1249-65.
20. Song, S. H.; Leng, X. S.; Li, T.; Qin, Z. Z.; Peng, J. R.; Zhao, L.; Wei, Y. H.; Yu, X., Expression of subtypes of somatostatin receptors in hepatic stellate cells. *World J Gastroenterol* **2004,** *10* (11), 1663-5.
21. Lamberts, S. W.; van der Lely, A. J.; de Herder, W. W.; Hofland, L. J., Octreotide. *N Engl J Med* **1996,** *334* (4), 246-54.
22. Ayiomamitis, G. D.; Notas, G.; Zaravinos, A.; Drygiannakis, I.; Georgiadou, M.; Sfakianaki, O.; Mastrodimou, N.; Thermos, K.; Kouroumalis, E., Effects of octreotide and insulin on colon cancer cellular proliferation and correlation with hTERT activity. *Oncoscience* **2014,** *1* (6), 457-67.
23. Hofland, L. J.; Lamberts, S. W., The pathophysiological consequences of somatostatin receptor internalization and resistance. *Endocr Rev* **2003,** *24* (1), 28-47.
24. Hofman, M. S.; Lau, W. F.; Hicks, R. J., Somatostatin receptor imaging with 68Ga DOTATATE PET/CT: clinical utility, normal patterns, pearls, and pitfalls in interpretation. *Radiographics* **2015,** *35* (2), 500-16.
25. Okarvi, S. M., Peptide-based radiopharmaceuticals and cytotoxic conjugates: potential tools against cancer. *Cancer Treat Rev* **2008,** *34* (1), 13-26.
26. Sun, M. L.; Wei, J. M.; Wang, X. W.; Li, L.; Wang, P.; Li, M.; Yi, C. H., Paclitaxel-octreotide conjugates inhibit growth of human non-small cell lung cancer cells in vitro. *Exp Oncol* **2007,** *29* (3), 186-91.
27. Shen, Y.; Zhang, X. Y.; Chen, X.; Fan, L. L.; Ren, M. L.; Wu, Y. P.; Chanda, K.; Jiang, S. W., Synthetic paclitaxel-octreotide conjugate reverses the resistance of paclitaxel in A2780/Taxol ovarian cancer cell line. *Oncol Rep* **2017,** *37* (1), 219-226.
28. Nagy, A.; Schally, A. V.; Halmos, G.; Armatis, P.; Cai, R. Z.; Csernus, V.; Kovacs, M.; Koppan, M.; Szepeshazi, K.; Kahan, Z., Synthesis and biological evaluation of cytotoxic analogs of somatostatin containing doxorubicin or its intensely potent derivative, 2-pyrrolinodoxorubicin. *Proc Natl Acad Sci U S A* **1998,** *95* (4), 1794-9.
29. Lelle, M.; Kaloyanova, S.; Freidel, C.; Theodoropoulou, M.; Musheev, M.; Niehrs, C.; Stalla, G.; Peneva, K., Octreotide-Mediated Tumor-Targeted Drug Delivery via a Cleavable Doxorubicin-Peptide Conjugate. *Mol Pharm* **2015,** *12* (12), 4290-300.
30. Koivunen, E.; Wang, B.; Ruoslahti, E., Phage libraries displaying cyclic peptides with different ring sizes: ligand specificities of the RGD-directed integrins. *Biotechnology (N Y)* **1995,** *13* (3), 265-70.
31. Koivunen, E.; Wang, B.; Ruoslahti, E., Isolation of a highly specific ligand for the alpha 5 beta 1 integrin from a phage display library. *J Cell Biol* **1994,** *124* (3), 373-80.
32. Arap, W.; Pasqualini, R.; Ruoslahti, E., Cancer treatment by targeted drug delivery to tumor vasculature in a mouse model. *Science* **1998,** *279* (5349), 377-80.
33. Hart, S. L.; Knight, A. M.; Harbottle, R. P.; Mistry, A.; Hunger, H. D.; Cutler, D. F.; Williamson, R.; Coutelle, C., Cell binding and internalization by filamentous phage displaying a cyclic Arg-Gly-Asp-containing peptide. *J Biol Chem* **1994,** *269* (17), 12468-74.
34. Pasqualini, R.; Koivunen, E.; Kain, R.; Lahdenranta, J.; Sakamoto, M.; Stryhn, A.; Ashmun, R. A.; Shapiro, L. H.; Arap, W.; Ruoslahti, E., Aminopeptidase N is a receptor for tumor-homing peptides and a target for inhibiting angiogenesis. *Cancer Res* **2000,** *60* (3), 722-7.

35. Curnis, F.; Arrigoni, G.; Sacchi, A.; Fischetti, L.; Arap, W.; Pasqualini, R.; Corti, A., Differential binding of drugs containing the NGR motif to CD13 isoforms in tumor vessels, epithelia, and myeloid cells. *Cancer Res* **2002,** *62* (3), 867-74.
36. Olsen, J.; Kokholm, K.; Norén, O.; Sjöström, H., Structure and expression of aminopeptidase N. *Adv Exp Med Biol* **1997,** *421*, 47-57.
37. Thundimadathil, J., Cancer treatment using peptides: current therapies and future prospects. *J Amino Acids* **2012,** *2012*, 967347.
38. Enyedi, K. N.; Czajlik, A.; Knapp, K.; Lang, A.; Majer, Z.; Lajko, E.; Kohidai, L.; Perczel, A.; Mezo, G., Development of cyclic NGR peptides with thioether linkage: structure and dynamics determining deamidation and bioactivity. *J Med Chem* **2015,** *58* (4), 1806-17.
39. Enyedi, K. N.; Toth, S.; Szakacs, G.; Mezo, G., NGR-peptide-drug conjugates with dual targeting properties. *PLoS One* **2017,** *12* (6), e0178632.
40. Soudy, R.; Ahmed, S.; Kaur, K., NGR peptide ligands for targeting CD13/APN identified through peptide array screening resemble fibronectin sequences. *ACS Comb Sci* **2012,** *14* (11), 590-9.
41. Corti, A.; Curnis, F.; Arap, W.; Pasqualini, R., The neovasculature homing motif NGR: more than meets the eye. *Blood* **2008,** *112* (7), 2628-35.
42. van Hensbergen, Y.; Broxterman, H. J.; Elderkamp, Y. W.; Lankelma, J.; Beers, J. C.; Heijn, M.; Boven, E.; Hoekman, K.; Pinedo, H. M., A doxorubicin-CNGRC-peptide conjugate with prodrug properties. *Biochem Pharmacol* **2002,** *63* (5), 897-908.
43. Ndinguri, M. W.; Solipuram, R.; Gambrell, R. P.; Aggarwal, S.; Hammer, R. P., Peptide targeting of platinum anti-cancer drugs. *Bioconjug Chem* **2009,** *20* (10), 1869-78.
44. Zhang, Z.; Hou, L.; Feng, L.; Huang, S.; Luo, M.; Shao, S.; Zhang, X.; Gu, S.; Zhao, X., An antimicrobial peptide containing NGR motif has potent antitumor activity against CD13+ and CD13- tumor cells. *Tumour Biol* **2015,** *36* (10), 8167-75.
45. Ellerby, H. M.; Arap, W.; Ellerby, L. M.; Kain, R.; Andrusiak, R.; Rio, G. D.; Krajewski, S.; Lombardo, C. R.; Rao, R.; Ruoslahti, E.; Bredesen, D. E.; Pasqualini, R., Anti-cancer activity of targeted pro-apoptotic peptides. *Nat Med* **1999,** *5* (9), 1032-8.
46. Seidi, K.; Jahanban-Esfahlan, R.; Monhemi, H.; Zare, P.; Minofar, B.; Daei Farshchi Adli, A.; Farajzadeh, D.; Behzadi, R.; Mesgari Abbasi, M.; Neubauer, H. A.; Moriggl, R.; Zarghami, N.; Javaheri, T., NGR (Asn-Gly-Arg)-targeted delivery of coagulase to tumor vasculature arrests cancer cell growth. *Oncogene* **2018,** *37* (29), 3967-3980.
47. Gregorc, V.; Cavina, R.; Novello, S.; Grossi, F.; Lazzari, C.; Capelletto, E.; Genova, C.; Salini, G.; Lambiase, A.; Santoro, A., NGR-hTNF and Doxorubicin as Second-Line Treatment of Patients with Small Cell Lung Cancer. *Oncologist* **2018,** *23* (10), 1133-e112.
48. Gregorc, V.; Gaafar, R. M.; Favaretto, A.; Grossi, F.; Jassem, J.; Polychronis, A.; Bidoli, P.; Tiseo, M.; Shah, R.; Taylor, P.; Novello, S.; Muzio, A.; Bearz, A.; Greillier, L.; Fontana, F.; Salini, G.; Lambiase, A.; O'Brien, M., NGR-hTNF in combination with best investigator choice in previously treated malignant pleural mesothelioma (NGR015): a randomised, double-blind, placebo-controlled phase 3 trial. *Lancet Oncol* **2018,** *19* (6), 799-811.
49. Santoro, A.; Pressiani, T.; Citterio, G.; Rossoni, G.; Donadoni, G.; Pozzi, F.; Rimassa, L.; Personeni, N.; Bozzarelli, S.; Rossoni, G.; Colombi, S.; De Braud, F. G.; Caligaris-Cappio, F.; Lambiase, A.; Bordignon, C., Activity and safety of NGR-hTNF, a selective vascular-targeting agent, in previously treated patients with advanced hepatocellular carcinoma. *Br J Cancer* **2010,** *103* (6), 837-44.
50. Vlahov, I. R.; Wang, Y.; Kleindl, P. J.; Leamon, C. P., Design and regioselective synthesis of a new generation of targeted chemotherapeutics. Part II: Folic acid conjugates of tubulysins and their hydrazides. *Bioorg Med Chem Lett* **2008,** *18* (16), 4558-61.
51. Kufka, R.; Rennert, R.; Kaluđerović, G. N.; Weber, L.; Richter, W.; Wessjohann, L. A., Synthesis of a tubugi-1-toxin conjugate by a modulizable disulfide linker system with a neuropeptide Y analogue showing selectivity for hY1R-overexpressing tumor cells. *Beilstein J Org Chem* **2019,** *15*, 96-105.

52. Böhme, D.; Beck-Sickinger, A. G., Drug delivery and release systems for targeted tumor therapy. *J Pept Sci* **2015,** *21* (3), 186-200.
53. Pando, O.; Stark, S.; Denkert, A.; Porzel, A.; Preusentanz, R.; Wessjohann, L. A., The multiple multicomponent approach to natural product mimics: tubugis, N-substituted anticancer peptides with picomolar activity. *J Am Chem Soc* **2011,** *133* (20), 7692-5.
54. Pando, O.; ad. Wessjohann, L. A. Total Synthesis of Tubulysins and Derivatives by Multicomponent Reactions. Dissertation, Martin Luther Universität Halle-Wittenberg, 2011.
55. Tumey, L. N.; Leverett, C. A.; Vetelino, B.; Li, F.; Rago, B.; Han, X.; Loganzo, F.; Musto, S.; Bai, G.; Sukuru, S. C.; Graziani, E. I.; Puthenveetil, S.; Casavant, J.; Ratnayake, A.; Marquette, K.; Hudson, S.; Doppalapudi, V. R.; Stock, J.; Tchistiakova, L.; Bessire, A. J.; Clark, T.; Lucas, J.; Hosselet, C.; O'Donnell, C. J.; Subramanyam, C., Optimization of Tubulysin Antibody-Drug Conjugates: A Case Study in Addressing ADC Metabolism. *ACS Med Chem Lett* **2016,** *7* (11), 977-982.
56. Preusentanz, R.; ad. Wessjohann, L. A. Synthese von Tubulysin-Derivaten, -Chimären und -Konjugaten mit Targeting-Komponenten. Dissertation, Martin Luther University Halle-Wittenberg, 2016.
57. Dal Corso, A.; Pignataro, L.; Belvisi, L.; Gennari, C., Innovative Linker Strategies for Tumor-Targeted Drug Conjugates. *Chemistry* **2019,** *25* (65), 14740-14757.
58. Dal Corso, A.; Pignataro, L.; Belvisi, L.; Gennari, C., alphavbeta3 Integrin-Targeted Peptide/Peptidomimetic-Drug Conjugates: In-Depth Analysis of the Linker Technology. *Curr Top Med Chem* **2016,** *16* (3), 314-29.
59. Flygare, J. A.; Pillow, T. H.; Aristoff, P., Antibody-drug conjugates for the treatment of cancer. *Chem Biol Drug Des* **2013,** *81* (1), 113-21.
60. Kellogg, B. A.; Garrett, L.; Kovtun, Y.; Lai, K. C.; Leece, B.; Miller, M.; Payne, G.; Steeves, R.; Whiteman, K. R.; Widdison, W.; Xie, H.; Singh, R.; Chari, R. V.; Lambert, J. M.; Lutz, R. J., Disulfide-linked antibody-maytansinoid conjugates: optimization of in vivo activity by varying the steric hindrance at carbon atoms adjacent to the disulfide linkage. *Bioconjug Chem* **2011,** *22* (4), 717-27.
61. Jones, L. R.; Goun, E. A.; Shinde, R.; Rothbard, J. B.; Contag, C. H.; Wender, P. A., Releasable luciferin-transporter conjugates: tools for the real-time analysis of cellular uptake and release. *J Am Chem Soc* **2006,** *128* (20), 6526-7.
62. Henne, W. A.; Doorneweerd, D. D.; Hilgenbrink, A. R.; Kularatne, S. A.; Low, P. S., Synthesis and activity of a folate peptide camptothecin prodrug. *Bioorg Med Chem Lett* **2006,** *16* (20), 5350-5.
63. Henne, W. A.; Kularatne, S. A.; Ayala-Lopez, W.; Doorneweerd, D. D.; Stinnette, T. W.; Lu, Y.; Low, P. S., Synthesis and activity of folate conjugated didemnin B for potential treatment of inflammatory diseases. *Bioorg Med Chem Lett* **2012,** *22* (1), 709-12.
64. Brocklehurst, K.; Carlsson, J.; Kierstan, M. P.; Crook, E. M., Covalent chromatography by thiol-disulfide interchange. *Methods Enzymol* **1974,** *34*, 531-44.
65. Nunes, J. P.; Morais, M.; Vassileva, V.; Robinson, E.; Rajkumar, V. S.; Smith, M. E.; Pedley, R. B.; Caddick, S.; Baker, J. R.; Chudasama, V., Functional native disulfide bridging enables delivery of a potent, stable and targeted antibody-drug conjugate (ADC). *Chem Commun (Camb)* **2015,** *51* (53), 10624-7.
66. Schumacher, F. F.; Nunes, J. P.; Maruani, A.; Chudasama, V.; Smith, M. E.; Chester, K. A.; Baker, J. R.; Caddick, S., Next generation maleimides enable the controlled assembly of antibody-drug conjugates via native disulfide bond bridging. *Org Biomol Chem* **2014,** *12* (37), 7261-9.
67. Jones, M. W.; Strickland, R. A.; Schumacher, F. F.; Caddick, S.; Baker, J. R.; Gibson, M. I.; Haddleton, D. M., Polymeric dibromomaleimides as extremely efficient disulfide bridging bioconjugation and pegylation agents. *J Am Chem Soc* **2012,** *134* (3), 1847-52.

68. Schumacher, F. F.; Nobles, M.; Ryan, C. P.; Smith, M. E.; Tinker, A.; Caddick, S.; Baker, J. R., In situ maleimide bridging of disulfides and a new approach to protein PEGylation. *Bioconjug Chem* **2011,** *22* (2), 132-6.
69. Smith, M. E.; Schumacher, F. F.; Ryan, C. P.; Tedaldi, L. M.; Papaioannou, D.; Waksman, G.; Caddick, S.; Baker, J. R., Protein modification, bioconjugation, and disulfide bridging using bromomaleimides. *J Am Chem Soc* **2010,** *132* (6), 1960-5.
70. Dubernet, M.; Caubert, V.; Guillard, J.; Viaud-Massuard, M.-C., Synthesis of substituted bis(heteroaryl)maleimides. *Tetrahedron* **2005,** *61*, 4585–4593.
71. Thakkar, A.; Trinh, T. B.; Pei, D., Global analysis of peptide cyclization efficiency. *ACS Comb Sci* **2013,** *15* (2), 120-9.
72. Beija, M.; Afonso, C. A.; Martinho, J. M., Synthesis and applications of Rhodamine derivatives as fluorescent probes. *Chem Soc Rev* **2009,** *38* (8), 2410-33.
73. Alford, R.; Simpson, H. M.; Duberman, J.; Hill, G. C.; Ogawa, M.; Regino, C.; Kobayashi, H.; Choyke, P. L., Toxicity of Organic Fluorophores Used in Molecular Imaging: Literature Review. *Mol Imaging* **2009,** *8* (6), 341–354.
74. The Broad Institute of MIT & Harvard, Cancer Cell Line Encyclopedia, https://portals.broadinstitute.org/ccle/. (accessed 17.06.2020).
75. Singh, S. P.; Han, L.; Murali, R.; Solis, L.; Roth, J.; Ji, L.; Wistuba, I.; Kundra, V., SSTR2-Based Reporters for Assessing Gene Transfer into Non–Small Cell Lung Cancer: Evaluation Using an Intrathoracic Mouse Model. *Hum Gene Ther* **2011,** *22*, 55–64.
76. Iaffaldano, L.; Nardelli, C.; Raia, M.; Mariotti, E.; Ferrigno, M.; Quaglia, F.; Labruna, G.; Capobianco, V.; Capone, A.; Maruotti, G. M.; Pastore, L.; Di Noto, R.; Martinelli, P.; Sacchetti, L.; Del Vecchio, L., High Aminopeptidase N/CD13 Levels Characterize Human Amniotic Mesenchymal Stem Cells and Drive Their Increased Adipogenic Potential in Obese Women. *Stem Cells Dev* **2013,** *22* (16).
77. Doose, S.; Neuweiler, H.; Sauer, M., A close look at fluorescence quenching of organic dyes by tryptophan. *Chemphyschem* **2005,** *6* (11), 2277-85.
78. Gicquiaux, H.; Lecat, S.; Gaire, M.; Dieterlen, A.; Mely, Y.; Takeda, K.; Bucher, B.; Galzi, J. L., Rapid internalization and recycling of the human neuropeptide Y Y(1) receptor. *J Biol Chem* **2002,** *277* (8), 6645-55.
79. Coin, I.; Beyermann, M.; Bienert, M., Solid-phase peptide synthesis: from standard procedures to the synthesis of difficult sequences. *Nat Protoc* **2007,** *2* (12), 3247-56.
80. Barany, G.; Albericio, F., A Three-Dimensional Orthogonal Protection Scheme for Solid-Phase Peptide Synthesis under Mild Conditions. *J Am Chem Soc* **1985,** *107*, 4936-4942.
81. Musaimi, O. A.; de la Torre, B. G.; Albericio, F., Greening Fmoc/tBu solid-phase peptide synthesis. *Green Chem* **2020,** *22*, 996.
82. Valeur, E.; Bradley, M., Amide bond formation: beyond the myth of coupling reagents. *Chem Soc Rev* **2009,** *38* (2), 606-31.

3. Peptide-drug conjugates based on a GRPR-targeting peptide

3.1. Introduction

The naturally occurring tetradecapeptide bombesin (Figure 3.2a) shows versatile pharmacological activities. This neuropeptide was first discovered in the skin of two European frogs, Bombina bombina and Bombina variegata variegata, in 1971.[1]

Shortly after that, the gastrin-releasing peptide (GRP) was isolated from the porcine gastric tissue and was identified as the mammalian counterpart of the amphibian bombesin. Compared to bombesin, GRP consists of 27 amino acids (Figure 3.1).[1-3] Bombesin and GRP differ just a bit in their structure resulting in similar properties, like strong and selective affinity to the bombesin receptor type 2, also called gastrin-releasing peptide receptor (GRPR).[4, 5] Bombesin is involved in smooth muscle contraction, in mitogenesis as well as proliferation of cells, including cancer cells, and in many hormone secretion processes, comprising gastrin and growth hormones, in which bombesin performs as a neuroregulatory hormone and growth factor. Interestingly, an autocrine effect of these bombesin-like peptides was detected in human small cell lung tumor. The proliferative effect of bombesin has already been investigated in lung, pancreatic, breast and colon cancer.[2, 5-12] It was discovered that primary human cancer cells can synthesize bombesin and beside that, the regarding receptor is overexpressed on many cancer types. The gastrin-releasing peptide receptor belonging to the 7-transmembrane domain family of G protein-coupled receptors (GPCRs) is also connected to the development of cancer, whereas the bombesin as an agonist activates these processes. Hence, this receptor was found to be overexpressed on prostate, breast, renal cell tumors and other cells in the central nervous system.[2, 5, 6, 13]

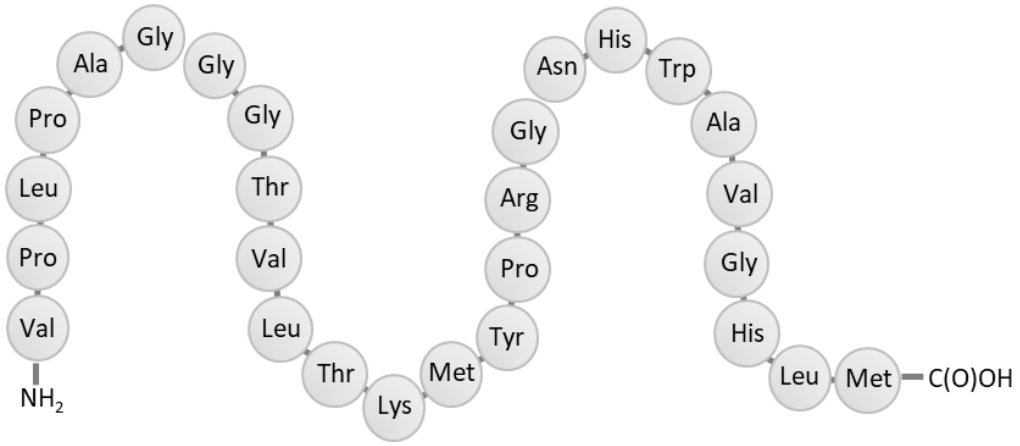

Figure 3.1 Amino acid sequences of native gastrin-releasing peptide.

The high binding affinity of bombesin to cancer-specific receptors awakens interest for medical applications. Thus, ^{99m}Tc-RP527, radiolabeled bombesin, is used for visualization of tumors, such as breast and prostate cancer. Especially in case of prostate cancer, radiography displays an useful diagnostic method, since GRP receptors are strongly overexpressed on neoplastic prostate tissues, compared to the low expression level on normal prostate tissue. Further investigations about

bioimaging have been performed on fluorescent bombesin conjugates as another diagnostic utensil.[14-18]

An antagonist of the GRPR, RC-3095, has already passed the phase I clinical trial and shows enduring inhibiting efficacy against tumor tissue *in vitro* and *in vivo*.[19, 20] This bombesin-based drug contains a shortened sequence of the native bombesin in order to increase the metabolic stability. Studies on the stability of native bombesin elucidated a quick degradation in serum with a half-life of 60 min, whereas shorter derivatives of bombesin were proven to be more stable.[20-23] However, it was revealed that the *C*-terminal sequence mainly causes the capability for binding to the GRP receptor. Screening bombesin fragments differing in length of the *C*-terminal sequence, it was found that the undecapeptide and nonapeptide possess comparable binding properties as native bombesin, but the heptapeptide and pentapeptide did not show an effect.[6, 7] Such truncated derivatives of the bombesin have been used for the synthesis of peptide-drug conjugates in combination with doxorubicin and have been tested *in vitro* and *in vivo* with promising results.[6, 24, 25]

The nonapeptide bombesin(6-14) (Figure 3.2b) was chosen for the synthesis of peptide-drug conjugates because of the good binding affinity to GRP receptor as well as an increased metabolic stability compared to native bombesin.

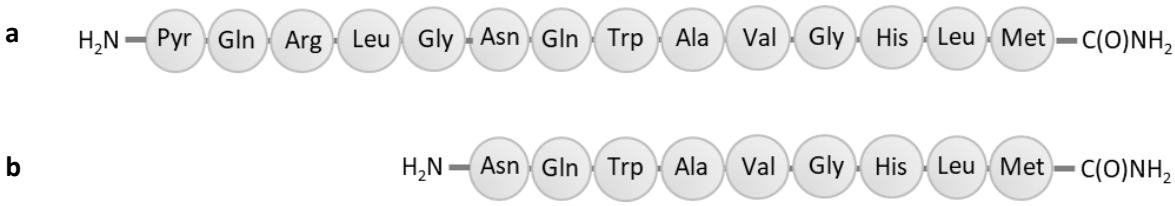

Figure 3.2 Amino acid sequences of a) native bombesin and b) truncated bombesin(6-14).

3.2. Synthetic strategy

Bombesin and its derivatives have shown good targeting properties towards GRPR-overexpressing tumor cells. Nevertheless, extensive studies on the usage of bombesin for the synthesis of peptide-drug conjugates have not performed yet. Bombesin(6-14) was attached to two types of linker-spacer systems to investigate the efficacy of the targeting depending on the linker-spacer system. On the one hand, a multiple cleavable linker-spacer system was used. On the other hand, a less complex linker-spacer system that can be split just in a reductive environment was synthesized. For good comparison to the peptide-drug conjugates presented in chapter 2, the multiple cleavable linker-spacer system was attached to tubugi 1 and tubugi 4. Considering that tubugi 4 remains stable under physiological conditions, the simplified linker-spacer systems were anchored to tubugi 4. Beside bioactive PDCs, fluorescently tagged bombesin conjugates were synthesized in order to perform fluorescence measurements.

3.2.1. Synthesis of multiple cleavable peptide-drug conjugates

The high nucleophilic property of the sulfhydryl group of cysteine was exploited for the formation of a thioether using a maleimide.[26] Maleimides are established entities for the linkage to cysteines as well as to free thiol groups in general in antibodies and peptides.[27, 28] The basic structure of the maleimide including linker system was adopted from the linker-spacer system presented in

chapter 2.2.2. The maleimide **58** was produced from maleic anhydride that was elongated by 4-aminopentanoic acid under reflux (Scheme 3.1a). Afterwards, the maleimide **58** was coupled to building block **40** by means of STEGLICH coupling (Scheme 3.1b).

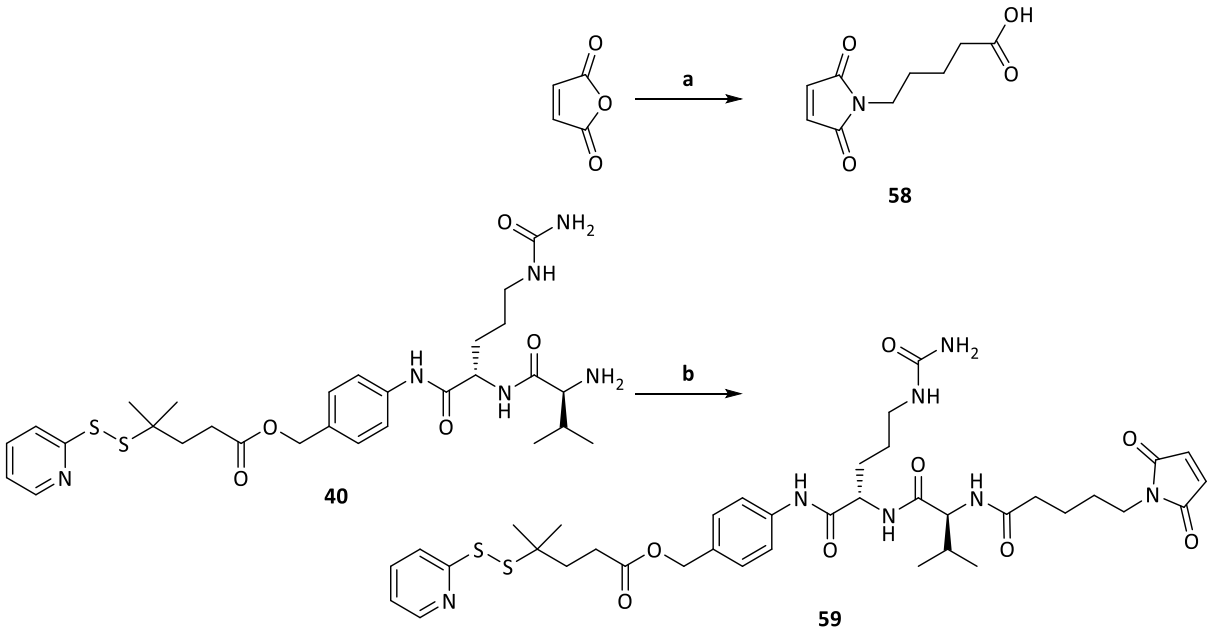

Scheme 3.1 a) 4-aminopentanoic acid, reflux, 7 h, in AcOH, 56 %; b) **58**, DIC, DMAP, rt, 48 h, in DCM, 34 %.

The linear bombesin was not used in its native form, because it was revealed that sequence from amino acids 6 to 14 show the same high affinity to the GRP receptor and the production of the peptide as well as the linkage to it can be facilitated. Lysine was introduced to *N*-terminus to afford a convenient moiety for functionalization.[24] (Pyridin-2-yldisulfanyl)propanoic acid (**60**) was attached to the free amine of lysine of the peptide **63** via an amide coupling in solid phase avoiding competition between free amines in case of release from resin. Afterwards, the disulfide bridge was reduced by TCEP in order to obtain free thiol of the peptide **64** (Scheme 3.2a). Thus, bombesin(6-14) was prepared for the attachment of the linker building block **59** forming a thioether via MICHAEL-type addition (Scheme 3.2b). Subsequently, the protected sulfhydryl moiety in the linker part was reduced by TCEP. A disulfide bridge to the tubugis was formed via thiol–disulfide exchange resulting in bombesin-tubugi 1 conjugate (**69**) and bombesin-tubugi 4 conjugate (**70**) (Scheme 3.2c).

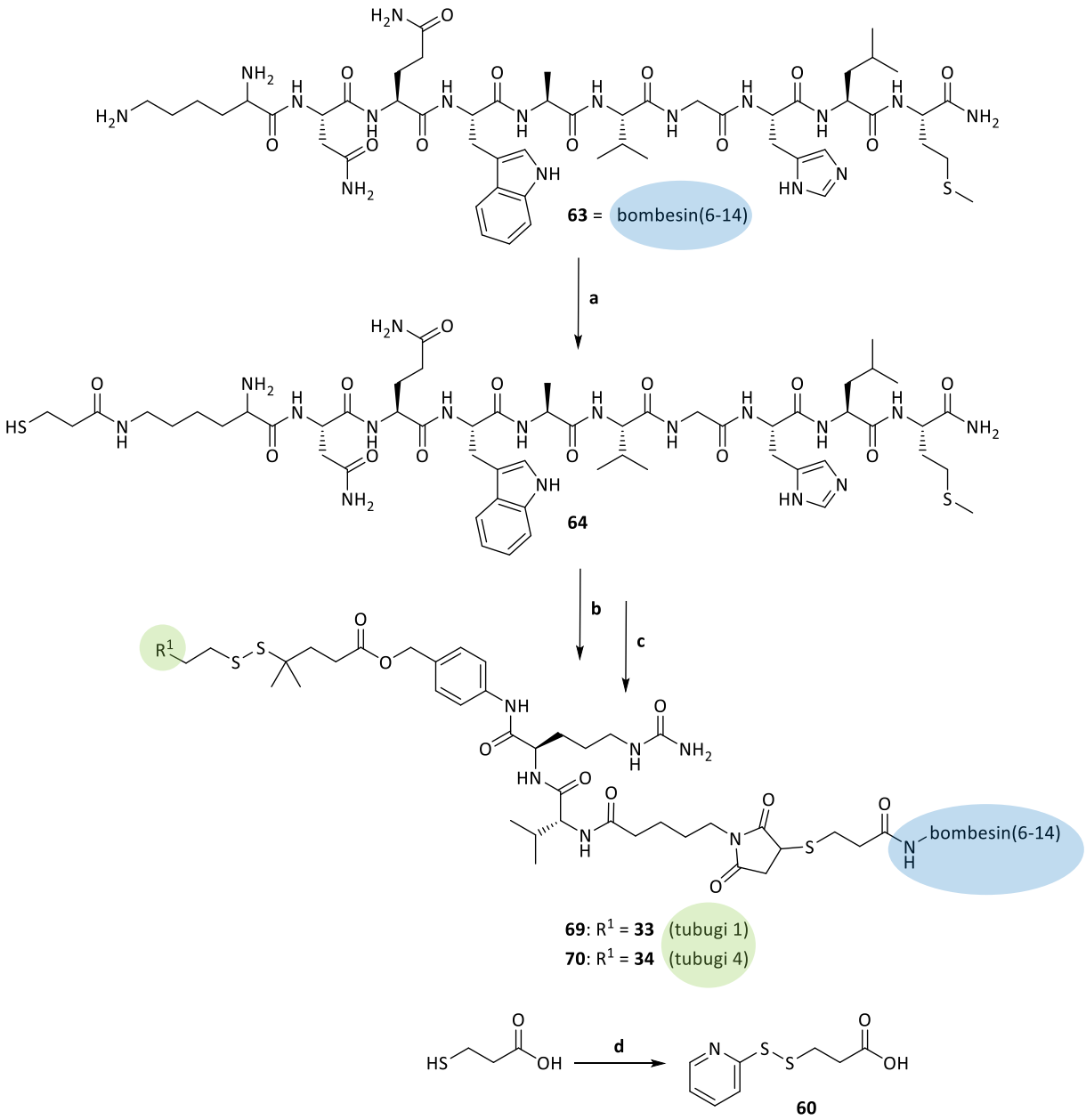

Scheme 3.2 a) 1. **60**, DIC, rt, overnight, in DCM, 2. TCEP, rt, 3 h, in H_2O/DMF, 34 %; b) **59**, TCEP, rt, overnight, in DPBS; c) **36**/**37**, rt, 3 d, in DMF, 31 % (**69**)/27 % (**70**); d) 2,2'-dipyridyl disulfide, rt, overnight, in MeOH, 41 %.

3.2.2. Synthesis of lipid peptide-drug conjugates

The simplified linker-spacer systems were synthesized on solid phase in conjugation with the targeting peptide synthesis. A thiol component was inserted offering the formation of the disulfide bridge to the self-immolative spacer of the toxin building block. In addition, hydrophobic alkyl chains alternating in length (n = 4, 12, 18) were integrated to the linker-spacer system, because lipid chains are able to enhance the binding to the cell membrane supporting the receptor binding.[29, 30] Moreover, a too fast reduction of the disulfide bridge is slowed by increasing length of the lipid moiety. Thus, different alkyl moieties allow more insight into the role of hydrophobicity on stability as well as efficacy of the conjugates. Employing HOFMANN isocyanide synthesis *n*-dodecyl (**62**) and *n*-

octadecyl isocyanide (**61**) were produced in moderate yields. An UGI four-component reaction was carried out on solid phase to combine bombesin(6-14) as amine component, the alkyl isocyanides, (pyridin-2-yldisulfanyl)propanoic acid and PFA.[31] The subsequent reduction was accomplished with excess of TCEP in solid phase allowing to use TCEP in excess enabling a short reaction time compared to carful addition of TCEP to reaction in liquid phase. After cleavage of the modified peptide from the resin, disulfide bridges between tubugi 4 and each peptide were built.

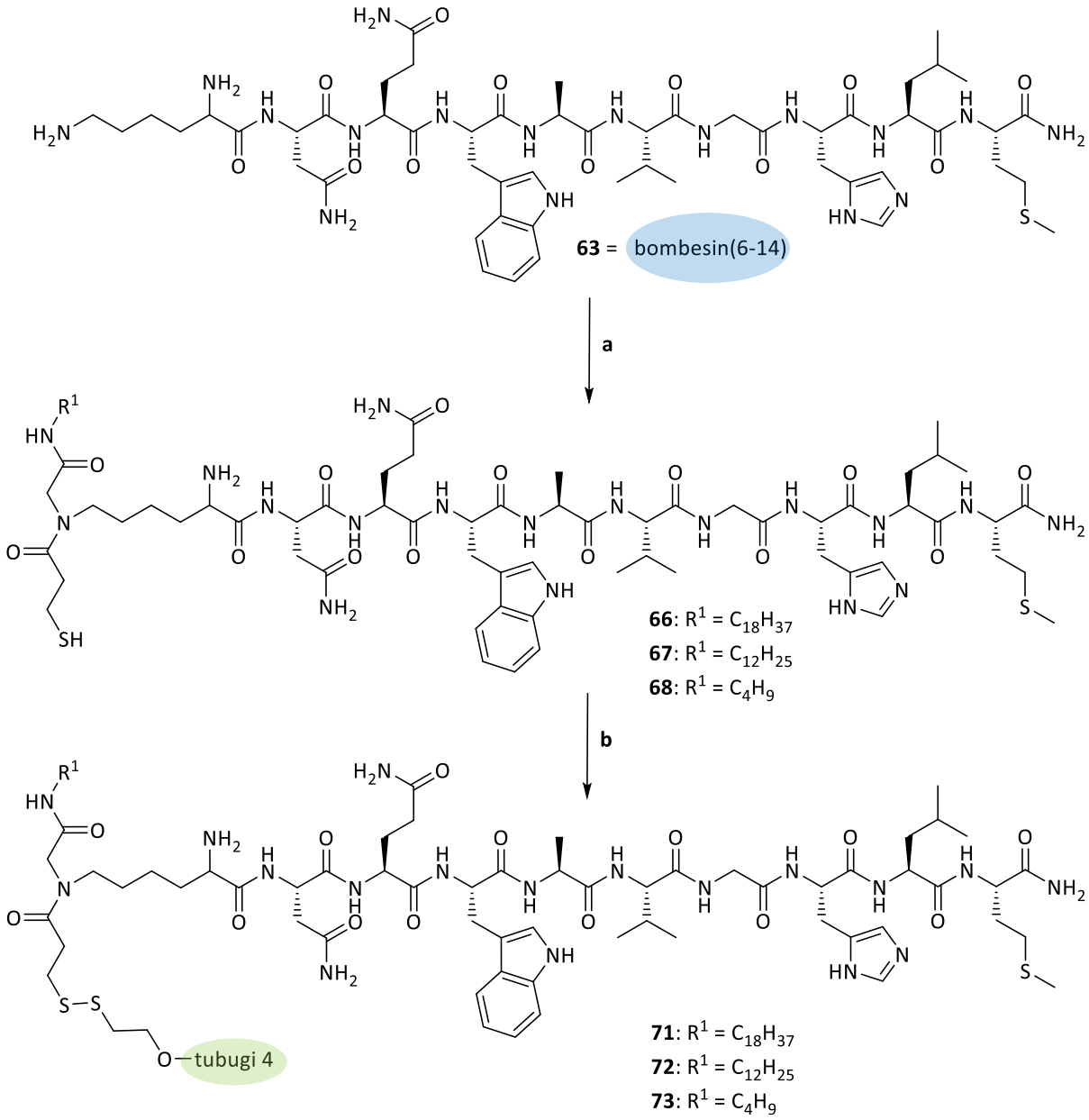

Scheme 3.3 a) PFA, pyrrolidine, **60**, *n*-octadecyl or *n*-dodecyl or *n*-butyl isocyanide, rt, 24 (**66**)/ 45 (**67**)/45 h (**68**), TCEP, in MeOH/THF, 78 % (**66**)/40 % (**67**)/57 % (**68**); b) **37**, rt, 18 h, in DMF, 24 % (**71**)/16 % (**72**)/12 % (**73**).

3.2.3. Synthesis of fluorescently labeled peptide conjugates

Fluorescently labeled conjugates without cytotoxic impact were synthesized in order to visualize and to investigate the internalization and degradation inside the cancer cells over time.

An uncleavable bombesin conjugate exploiting rhodamine B as fluorophore was synthesized to visualize the receptor-mediated internalization by fluorescence microscopy and to semi-quantify this process by flow cytometry.[32] As presented in chapter 2.2.4, 1,3-diaminopropane was linked to rhodamine B using STEGLICH coupling (Scheme 3.4a). Then, the maleimide component **58** was attached to the modified rhodamine B (**54**) using STEGLICH coupling yielding compound **74** (Scheme 3.4b). The attachment of fluorescent linker compound **74** to the modified bombesin(6-14) (**64**) was performed by forming a thioether bound towards the free thiol of **64** obtaining the red-fluorescently labeled, uncleavable bombesin conjugate **75** (Scheme 3.4c).

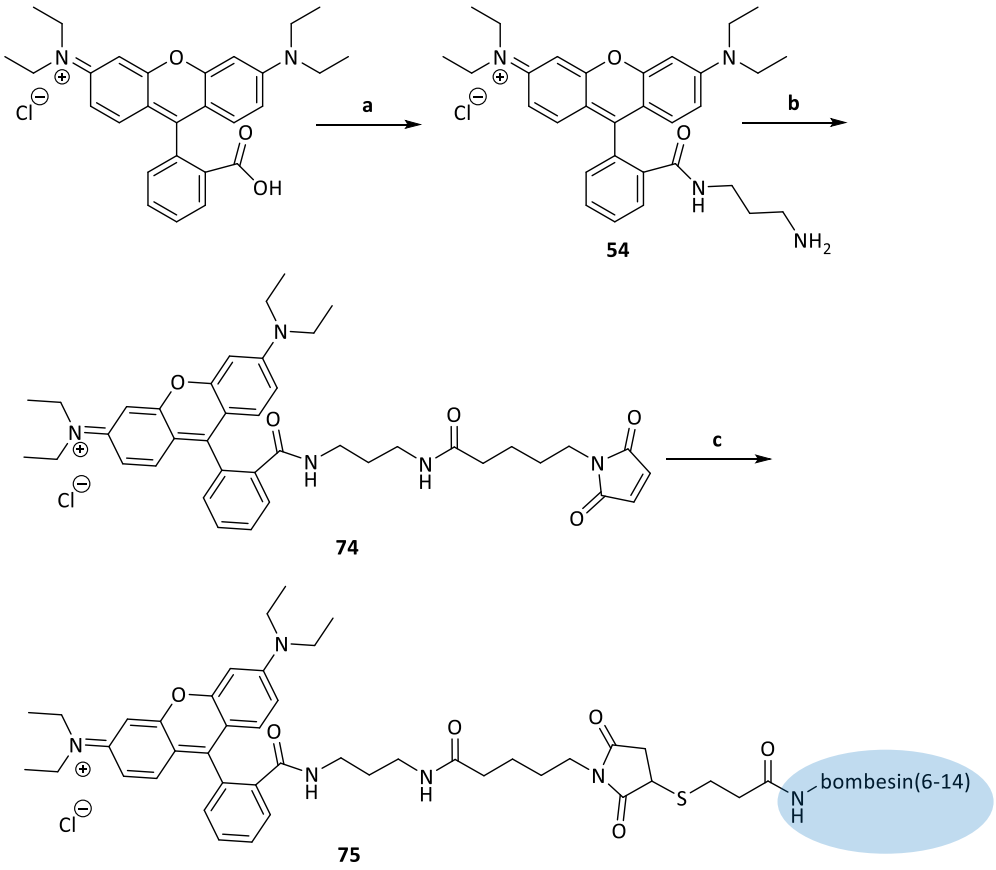

Scheme 3.4 a) 1,3-Diaminopropane, EDC × HCl, rt, 22 h, in DCM, 45 %; b) **58**, EDC × HCl, rt, overnight, in DCM, 86 %; c) **64**, rt, 3 d, in DMF, 52 %.

A cleavable bombesin conjugate was synthesized to evaluate the conjugate's decomposition after internalization mainly for studying the stability of the disulfide bridge *in vitro*. Thus, the conjugate was designed to consist of the fluorescently tagged peptide and a second fluorophore that can be released from the peptide. Both components were connected via a cleavable linker-spacer system similar to that of bioactive conjugates. In advance, the fluorophores were chosen not to be too bulky in order to avoid several side effects. Furthermore, the fluorophores were chosen to be excitable separately and not to interfere in absorbance as well as emission wavelengths. The building block including the peptide was labeled by the blue-fluorescent *N*-methyl isatoic anhydride (MIA) and at the drug position the red-fluorescent rhodamine B was placed.[33, 34]

It was considered to create a simplified linker-spacer system, but comparable to the linker-spacer system of the toxic conjugates. Thus, MIA was coupled to lysine under reflux mimicing the citrulline

(Scheme 3.5a), whereas rhodamine B was modified by thiol-protected 2-mercapto ethanol (**35**) by means of STEGLICH esterification mimicing the tetrapeptide tubugi (Scheme 3.5c).

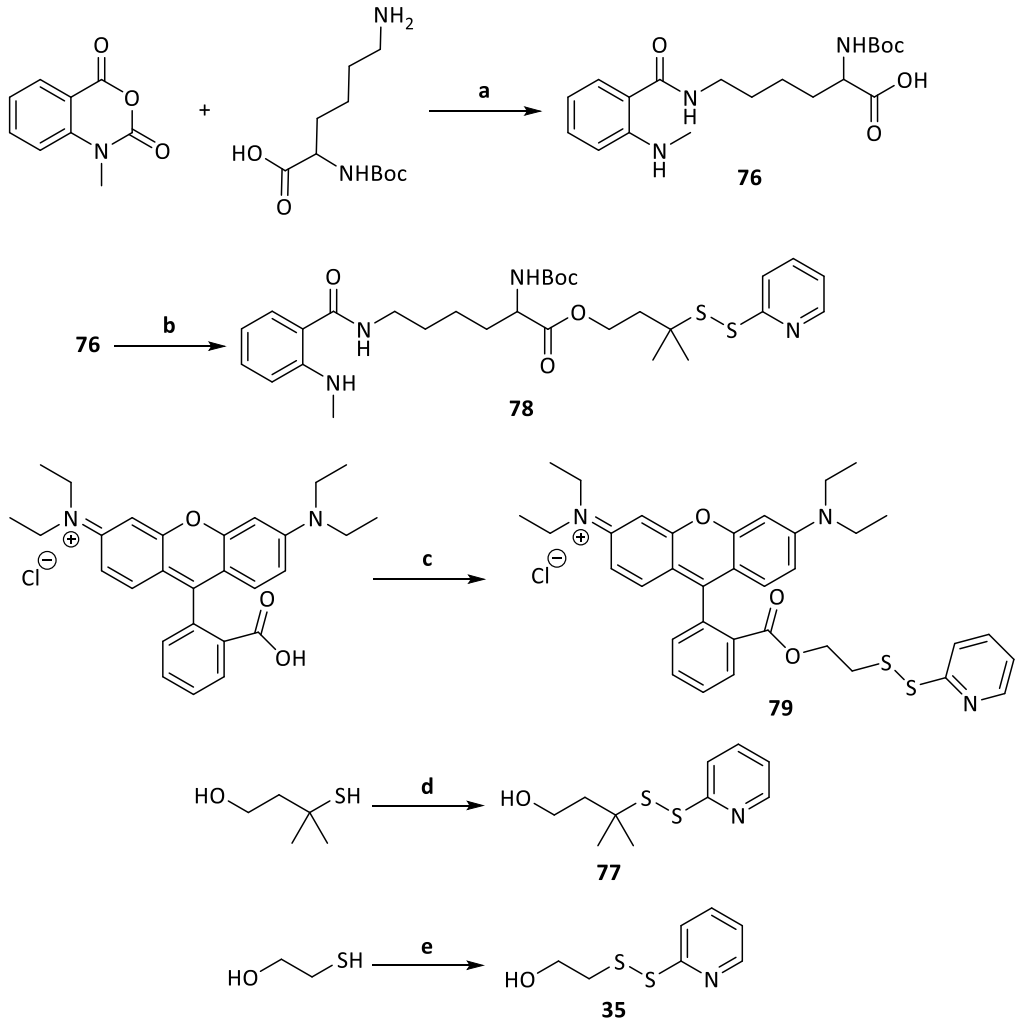

Scheme 3.5 a) reflux, overnight, in toluene, 91 %; b) EDC × HCl, **77**, DMAP, rt, overnight, in DCM, 83 %; c) DIC; **35**, DMAP, rt, overnight, in DCM, 71 %; d) 2,2'-dipyridyl disulfide, rt, 5 h, in MeOH, 98 %; e) 2,2'-dipyridyl disulfide, rt, 4 h, in MeOH, 60 %.

Another STEGLICH esterification was applied to couple the fluorescent lysine (**76**) to sterically hindered as well as thiol-protected 3-mercapto-3-methyl-butan-1-ol (**77**) (Scheme 3.5b). Thereby, the build up of the disulfide bridge was prepared. After reducing **78** by TCEP (Scheme 3.6a), the blue-fluorescent, reduced building block **78** was conjugated to the red-fluorescent building block **79** forming a disulfide bridge (Scheme 3.6b).

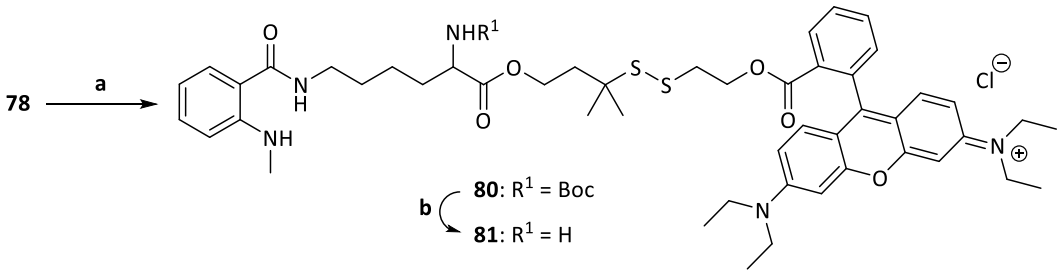

Scheme 3.6 a) TCEP, **79**, rt, 8 h, H_2O/DMF, 77 %; b) TFA/DCM, 0 °C, 4 h, 65 %.

A STEGLICH coupling was performed in order to supplement the double-dye building block **81** by maleimide **58** (Scheme 3.7a). In the last step, linker system containing MIA and rhodamine B (**82**) was tethered to the modified peptide **64** via MICHAEL-type addition resulting in the cleavable, double-labeled bombesin conjugate **83** (Scheme 3.7b).

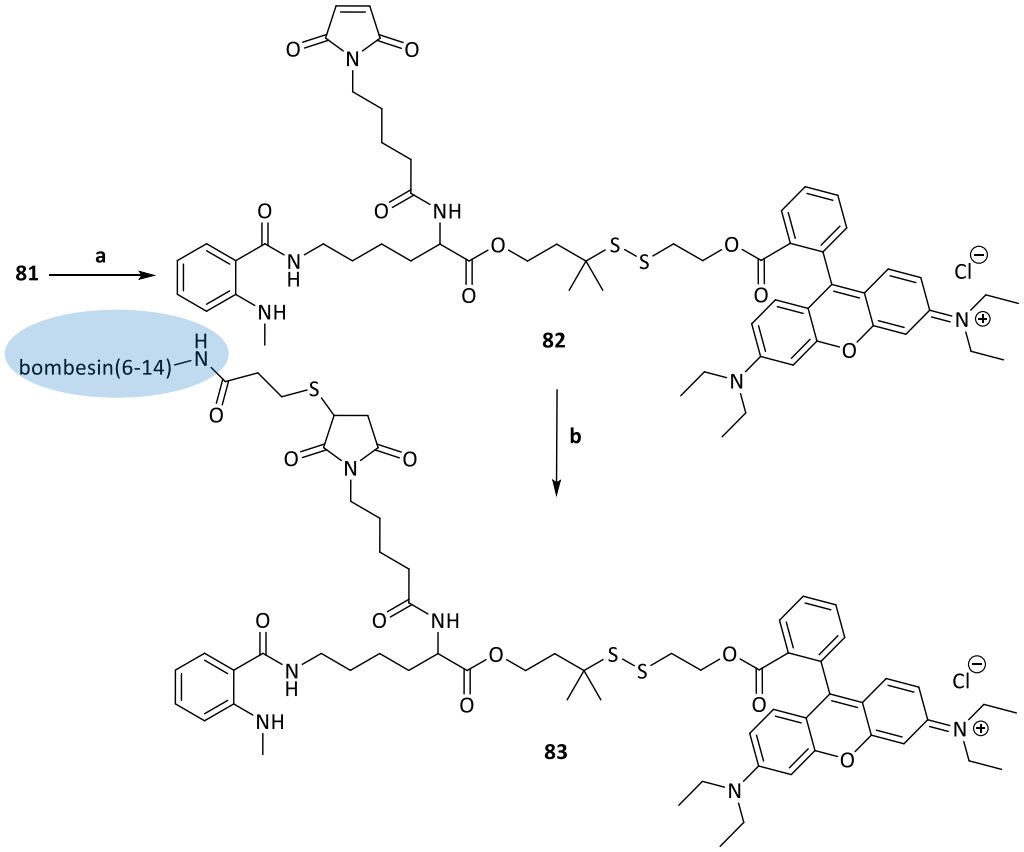

Scheme 3.7 a) DIC; **58**, DMAP, rt, overnight, in DCM, 71 %; b) **64**, rt, 6 d, in DMF, 54 %.

3.3. Biological evaluation

The GRPR-mediated internalization of fluorescently labeled bombesin conjugates and their cleavage inside the cells were studied applying fluorescence microscopy and flow cytometry. Additionally, bioassays were performed to reveal the dependence of the efficacy of the PDCs on distinguishable expression levels (high, medium, low) of GRPR and the incubation time.

3.3.1. Studies on cellular internalization of fluorescently labeled peptide conjugates

Fluorescence measurements were performed in order to study the selectivity of the bombesin-tubugi conjugates applying fluorescently labeled conjugates to cancer cell lines expressing high, moderate and low level of GRP receptor for different initial incubation times. Based on literature,[35] RT-qPCR analyses were carried out in triplicate to evaluate the expression of gastrin-releasing peptide receptor. Although the PC3 prostate cancer cell line is known to express relatively high level of GRPR[25] like T-47D, the determined expression level in PC3 drifted from published data base values,[35] whereas the other cell lines expressed mRNA to the expected extent (Figure 3.3). As already mentioned in chapter 2, the available PC3 cancer cell line appears to have mutated, because expression levels of both CD13 (see chapter 2.3.1) and also of GRPR were lower than found in literature.[35] Published studies documented a good correlation between RT-qPCR tests and ELISA assays of studied cancer cell lines.[36] Independent ELISA assays were not conducted within this work.

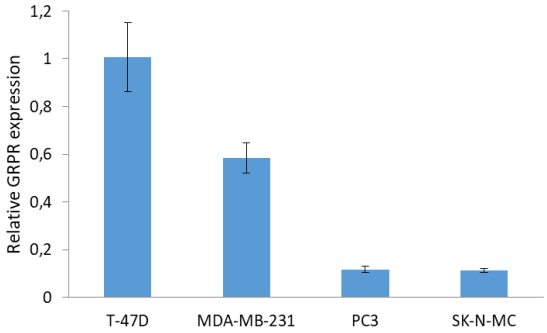

Figure 3.3 Expression levels of GRPR in T-47D breast cancer cells, MDA-MB-231 breast cancer cells, PC3 prostate cancer cells and SK-N-MC Ewing's sarcoma cells.

Although the fluorescent conjugates were designed to be non-toxic, the bioassays elucidated bioactivity after 72 h. In case of **75**, an IC_{50} value about 8 µM was determined on T-47D breast cancer cell line. The conjugate **83** was found to have an IC_{50} values about 9 µM on T-47D breast cancer cell line. However, the cells were exposed to the fluorescent conjugates at concentrations about 5 µM for 6 h only. Based on measured excitation and emission wavelengths of the pure fluorophore rhodamine B (λ_{ex} = 545 nm, λ_{em} = 576 nm) and of the fluorescent linker **54** (λ_{ex} = 553 nm, λ_{em} = 581 nm) (see in Appendix III, Figure A 133 & 134), fluorescence microphotographs were recorded in order to visualize internalized uncleavable fluorescent bombesin conjugate **75** as red-fluorescent spots (Figure 3.4b, c). It was found that most of conjugate **75** were internalized within 30 min and the spotted localization of rhodamine B bound to bombesin might indicate that the conjugate remained in endosomes at high concentrations (Figure 3.4c). Fluorescent spots were detected at much lower concentration in surrounding culture medium (Figure 3.4c).

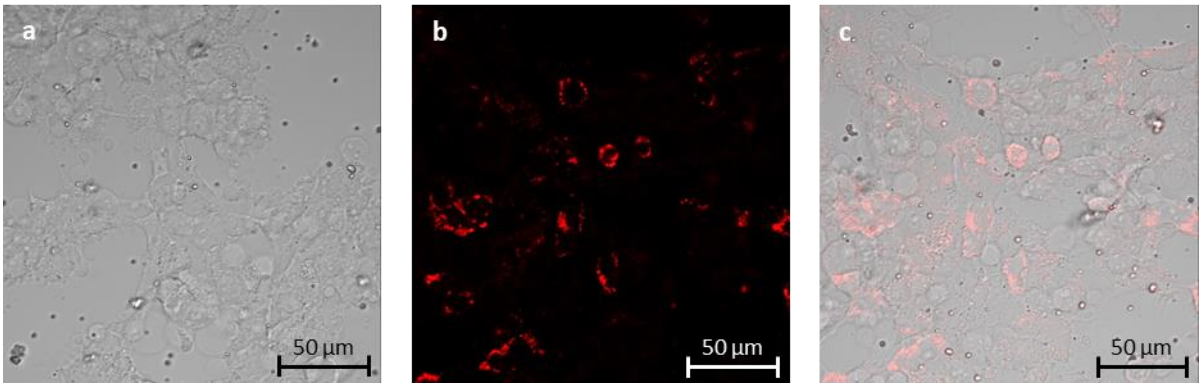

Figure 3.4 Fluorescence microphotographs of a) untreated T-47D cells, b) T-47D cells treated with red-fluorescent **75** after 30 min of incubation and c) merged image of T-47D cells with internalized red-fluorescent **75** (after 30 min treatment).

Rate and dimension of the internalization were evaluated using the uncleavable conjugate **75** in flow cytometric study. GRPR-overexpressing T-47D cancer cells were exposed to **75** for 1 min, 1 h and 6 h and GRPR lower expressing SK-N-MC cancer cells were treated with **75** for 6 h. After respective incubation times, trypsinized cells were washed using tryptophan (100 mM in water/acetonitrile 2:1) to quench fluorophores which had not entered the cells and might still be bound unspecifically to the outer cell surface (see Appendix III, Figure A 135).[37] Already after 1 min – virtually representing a "no internalization" control despite treatment of the cells with conjugate – a clear receptor-mediated uptake by T-47D cells was observed (4.5-fold over untreated T-47D cells) and doubled within 30 min to 10.97-fold over untreated T-47D cells (Figure 3.5a, Table 3.1). The maximal internalization was achieved after 1 h when the internalization rate increased 13.37-fold over untreated T-47D cells (Figure 3.5a). In comparison to GRPR lower expressing cancer cell line (SK-N-MC, Figure 3.5b), around 35 % more fluorescent conjugates were internalized by T-47D cells (Table 3.1).

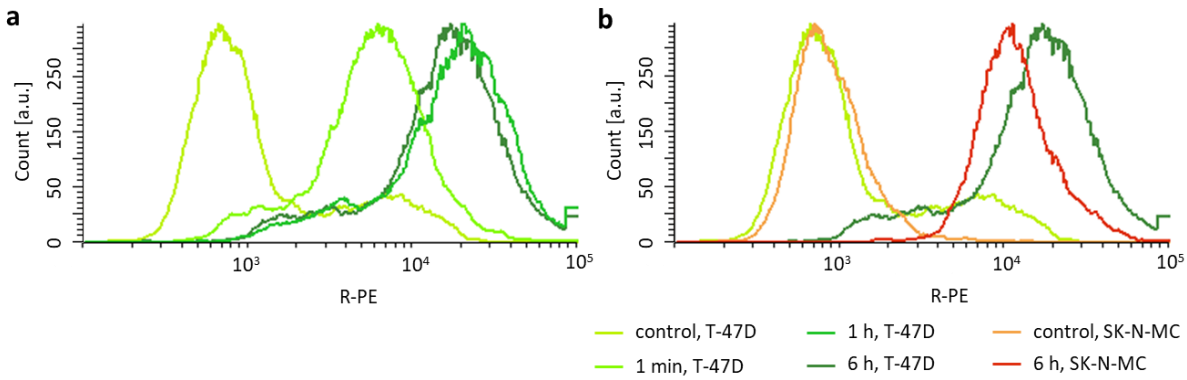

Figure 3.5 Flow cytometric analyses of **75** a) at different incubation times on T-47D cancer cell line, b) comparison between internalization into GRPR higher expressing cancer cell line (T-47D, green) and GRPR lower expressing cancer cell line (SK-N-MC, red) after 6 h.

Table 3.1 Relative quantification of the cellular internalization of fluorescent conjugates **75** in T-47D cancer cells in relation to untreated cells and SK-N-MC cancer cells expressing GRPR less.

	75	
	RFU[5]	x-fold over untreated
1 min, T-47D	81.61	4.52
30 min, T-47D	198.05	10.97
1 h, T-47D	241.52	13.37
6 h, T-47D	227.39	12.59
6 h, SK-N-MC	139.53	9.72

The cleavage process inside the cancer cells was studied using the cleavable conjugate **83**. The idea was to investigate the cleavage of the disulfide bridge leading to a separation of the red-fluorescent payload part and the blue-fluorescent peptide part by fluorescence microscopy. Fluorescence spectra were recorded to determine excitation and emission wavelengths of both fluorophores and to ensure that MIA (λ_{ex} = 222 nm, λ_{em} = 428 nm) and rhodamine B (λ_{ex} = 545 nm, λ_{em} = 576 nm) do not interfere (see in Appendix III, Figure A 133 & 136). The conjugate **83** was applied to T-47D cells and observed by laser scanning confocal microscope. Because of technical reasons – limited resolution of the microscope – the cleavage process could not be detected. Considering the technical conditions, the usability of the concept to visualize the cleavage *in vitro* by separate excitation of two fluorophores appears limited.

3.3.2. Evaluation of the cytotoxic activity of the bombesin-drug conjugates

The synthesized bombesin-drug conjugates (**69**–**73**) as well as pure tubugi 1 (**33**), the spacer containing tubugi 1 (**36**), tubugi 4 (**34**), the spacer containing tubugi 4 (**37**) and truncated bombesin(6-14) (**63**) as reference compounds were tested on cancer cell lines expressing certain levels of respective receptors (high, medium, low) to investigate the role of the expression level on the efficacy of the conjugates.

All cell viability tests on selected tumor cell lines were carried out in biological and technical triplicates and analyzed by resazurin-based fluorometric assay. The concentrations for dilution series of testing compounds were selected according to the literature.[38] Beside the relationship between the activity and the expression level of the receptors, the dependence on the incubation time was also investigated. Thus, the cancer cells were exposed to the conjugates as well as the reference compounds for 6, 24 and 72 h. All cells were allowed to grow for 72 h after initial treatment until cell viability was measured. In case of initial incubation shorter than these 72 h – i.e. 6 h and 24 h incubation, respectively – solutions containing tested compounds were discarded, cells were washed and allowed to grow up in fresh culture medium until measurement after 72 h.

[5] relative fluorescence unit

The bioassays revealed the cytotoxic activity of all bombesin-tubugi 4 conjugates (**70**, **71**, **72**, **73**) against tumor cells (Figure 3.6 & Figure 3.7). In contrast, the bombesin-tubugi 1 comprising the multiple cleavable linker-spacer system (**69**) did not possess any cytotoxicity below 10 µM (see Appendix IV, Figure A 161). In previous studies, it was proven that he acetyl group at C11 can be

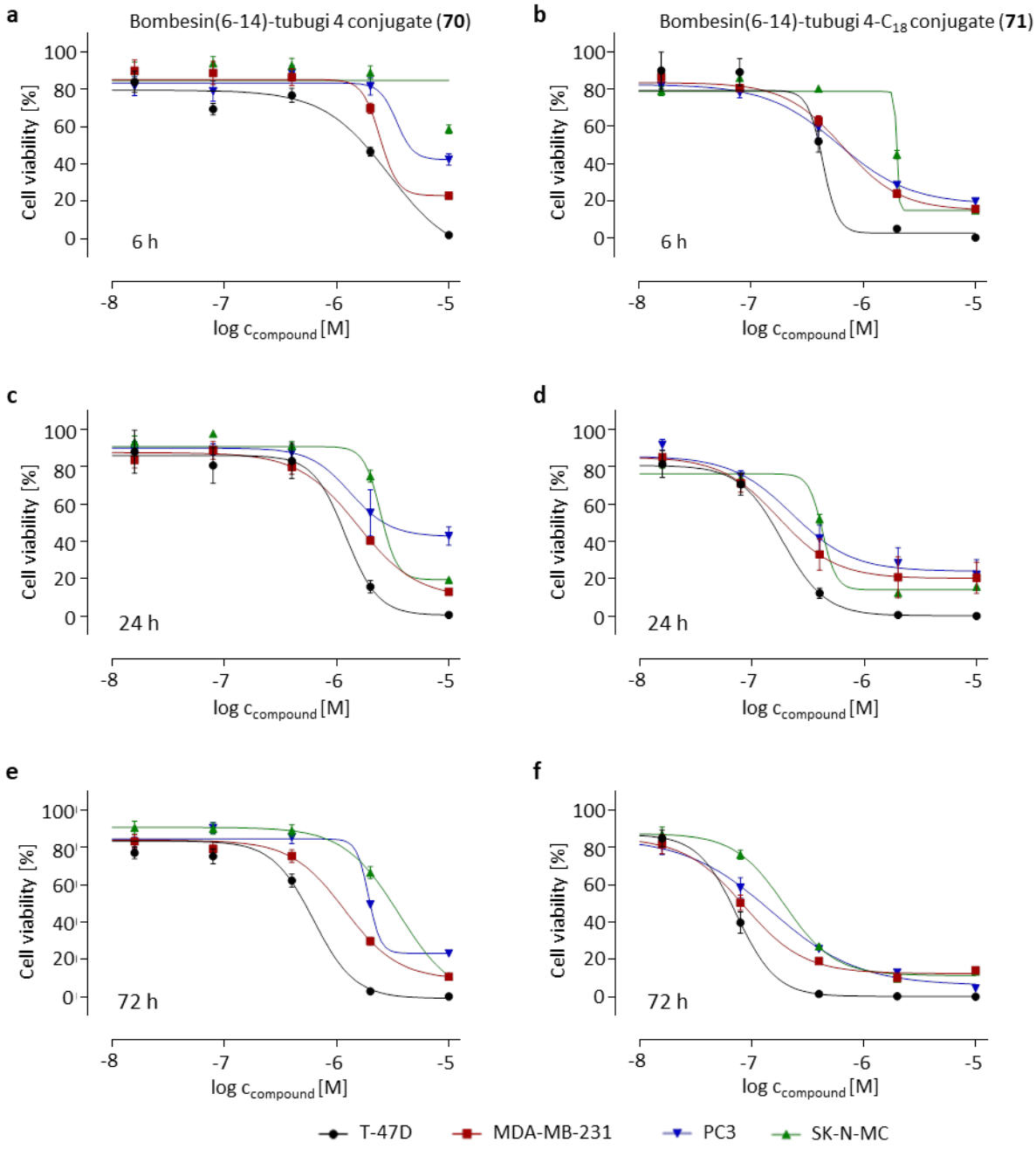

Figure 3.6 *In vitro* antitumor activity of **70** after a) 6, c) 24, e) 72 h initial treatment and of **71** after b) 6, d) 24 and f) 72 h initial treatment in T-47D breast cancer cells (high GRPR), MDA-MB-231 breast cancer cells (medium GRPR), PC3 prostate cancer cells and SK-N-MC Ewing's sarcoma cells (low GRPR) (for GRPR expression see Figure 3.3).[6]

[6] This extract zooms in on the inflection points representing the IC_{50} values. The full size graphs are seen in Appendix IV, Figure A 162.

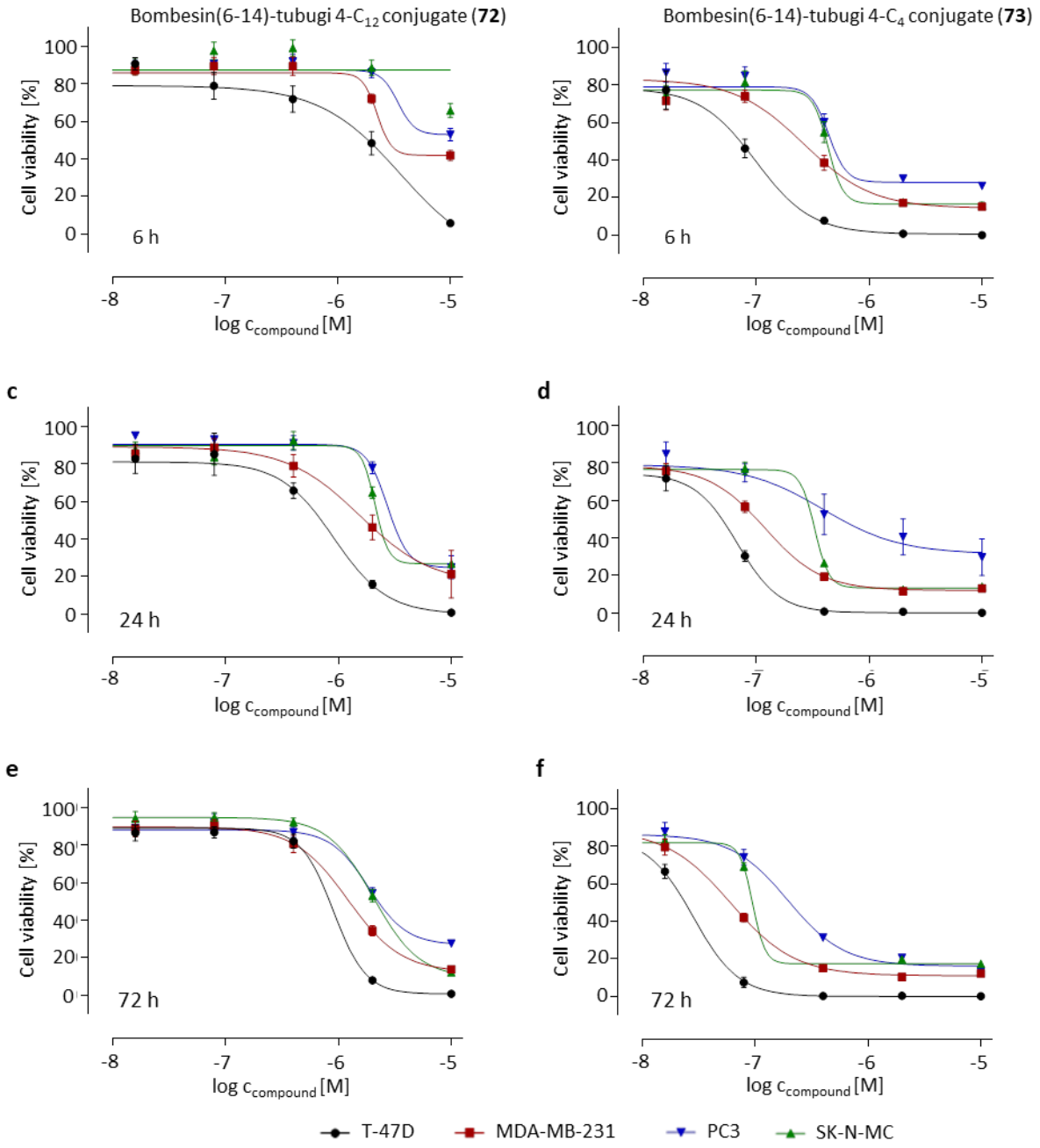

Figure 3.7 *In vitro* antitumor activity of **72** after a) 6, c) 24, e) 72 h initial treatment and of **73** after b) 6, d) 24 and f) 72 h initial treatment in T-47D breast cancer cells (high GRPR), MDA-MB-231 breast cancer cells (medium GRPR), PC3 prostate cancer cells and SK-N-MC Ewing's sarcoma cells (low GRPR) (for GRPR expression see Figure 3.3).[7]

metabolically cleaved.[39] Hence, the loss of that crucial moiety might cause the weak bioactivity of conjugate **69**. Comparing the sigmoidal curves of all bombesin-tubugi 4 conjugates (Figure 3.6 &Figure 3.7), selective distinction between different expression levels of the receptor and the efficacy was observed. The IC_{50} values showed that the longer the cancer cells were exposed to the compounds as well as the higher the expression level of the receptor was, the higher the efficacy (see Appendix IV, Tables A 10–13). Conjugate **70** containing the linker system **59** and conjugate **72**

[7] This extract zooms in on the inflection points representing the IC_{50} values. The full size graphs are seen in Appendix IV, Figure A 163.

containing the simplified linker system showed a similar effect on the cells (see Appendix IV, Tables A 10 & 13), whereas simplified conjugates **71** and **73** were about 10 times more active (see Appendix IV, Tables A 11 & 12). Conjugate **73** comprising the simplified, hydrophobic linker system with the C_4 alkyl chain exhibited the strongest and also most selective efficacy against the cancer cells (see Appendix IV, Table A 13) assuming that the shorter side chain did not disturb the binding of bombesin(6-14) to GRPR leading to efficient GRPR-mediated internalization. In case of conjugate **72**, the longer C_{12} alkyl chain might sterically hinder the binding of bombesin(6-14) to GRPR. Interestingly, conjugate **71** showed stronger efficacy to the cells than **72**. The reason behind that observation might be the structure of cell membranes, since the thickness of monolayers correspond roughly the length of C_{18} alkyl chain. Thus, the C_{18} alkyl chain of **71** might support the internalization of the conjugate by anchoring to the cell surface.[40] The bombesin-tubugi conjugates based on the linker system **59** (**69**, **70**) were found to be stable in a 10 mM glutathione solution at 37 °C for at least 6 h and to be cleaved within 24 h using ESI MS. The stability of the simplified bombesin-tubugi 4 conjugates comprising just a lipid side chain (**71**, **72**, **73**) was shown to be lower than 6 h. The cleavage product was detected after 2 h in case of **71**, whereas the decomposition of the disulfide bridge was observed after 6 h in case of **72** and **73**. This observation indicated that a shorter alkyl side chain might be more capable to protect the disulfide bridge from reduction resulting in raised stability of the PDC. In contrast, a longer side chain might be involved in anchoring to the cell membrane or might move very dynamically leaving the disulfide bridge unprotected. Thus, another explanation of good activities of **71** might be the more rapid release of tubugi 4 while the conjugate was bound to the receptor at the cell surface. Furthermore, **63** was found to possess no efficacy against all tumor cell lines at tested concentrations (lower than 10 µM). Tubugi 1 (**33**) and tubugi 4 (**34**) were effective against cancer cells in nano- and picomolar range (see Appendix IV, Tables A 1 & 3). As expected, the attached self-immolative spacer compound (**36**, **37**) diminished the efficacy of the free tubugis 3- to 4-fold in case of **36** (see Appendix IV, Table A 2) and 10- to 20-fold in case of **37** (see Appendix IV, Table A 4), respectively.

3.4. Experimental part

The used materials, applied analytical methods as well as the protocols of biological assays are described in detail in chapter 2.4. The syntheses of several compounds and building blocks mentioned in this chapter are already described in chapter 2.4 as well.

3.4.1. Syntheses of linker and spacer compounds

5-(2,5-Dioxo-2,5-dihydro-1*H*-pyrrol-1-yl)pentanoic acid (**58**)

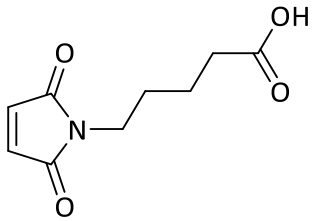

Maleic anhydride (0.50 g, 5.05 mmol) was dissolved in acetic acid (17.67 mL). 4-Aminopentanoic acid (0.66 g, 5.55 mmol) was added to that mixture and the mixture was left to stir under reflux for 7 h. The solvent was removed under reduced pressure and the crude was purified by silica column chromatography to obtain **58** (0.56 g, 56 %) as a colorless solid.

R_f = 0.46 (ethyl acetate/*n*-hexane/formic acid 7:3:0.1 %)

^{1}H NMR (400 MHz, $CDCl_3$): δ = 1.64 (tdt, 4H), 2.39 (t, 2H), 3.55 (t, 2H), 6.70 (s, 2H) ppm.

^{13}C NMR (101 MHz, $CDCl_3$): δ = 21.7, 27.8, 33.2, 37.3, 134.1, 170.8, 179.0 ppm.

HRMS calculated for $C_9H_{12}NO_4$ $[M+H]^+$: m/z = 196.0608, found: m/z = 196.0618.

4-Methyl-4-(pyridin-2-yldisulfanyl)pentanoic ester of PAB-Cit-Val to maleimide (**59**)

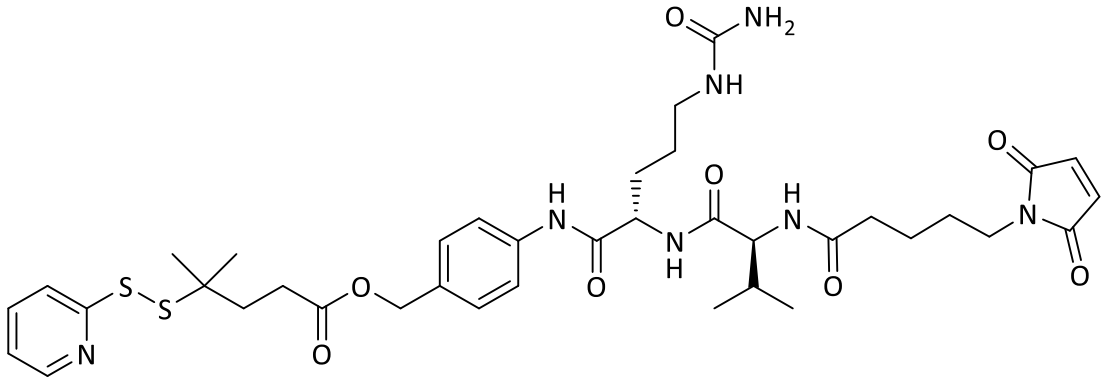

Compound **58** (0.13 mg, 0.59 mmol) was dissolved in dichloromethane (8 mL) under nitrogen atmosphere and cooled to 0 °C. DIC (121 µL, 0.77 mmol), **40** (0.45 mg, 0.65 mmol) dissolved in dichloromethane (7 mL) and DMAP (7.4 mg, 0.06 mmol) were added. After 5 min the mixture was allowed to reach rt and left to stir for 48 h. The crude was purified by silica column chromatography to yield **59** (0.16 g, 34 %) as a colorless solid.

R_f = 0.47 (dichloromethane/ethanol 4:1)

^{1}H NMR (400 MHz, CD_3OD): δ = 0.95 (dd, 4H), 1.26 (s, 5H), 1.57 (m, 12H), 1.83–1.90 (m, 2H), 2.29 (t, 6H), 2.40–2.49 (m, 2H), 2.85 (d, 6H), 2.98 (d, 5H), 3.50 (t, 6H), 4.17 (d, 1H), 4.51 (dt, 1H), 5.01 (s, 2H), 6.79 (s, 4H), 7.10–7.20 (m, 1H), 7.23–7.31 (m, 2H), 7.57 (td, 2H), 7.68 (td, 1H), 7.73–7.83 (m, 1H), 7.97 (s, 2H), 8.30 (ddd, 1H) ppm.

^{13}C NMR (101 MHz, CD_3OD): δ = 18.9, 19.8, 23.1, 24.1, 27.6, 28.9, 31.0, 31.7, 34.2, 36.0, 36.8, 37.0, 38.1, 52.8, 54.9, 60.5, 67.0, 121.1, 121.9, 122.4, 130.1, 133.3, 135.3, 138.9, 139.6, 150.0, 161.9, 164.8, 172.5, 173.9, 174.5, 176.0, 177.1 ppm.

HRMS calculated for $C_{38}H_{52}N_7O_8S_2$ $[M+H]^+$: m/z = 798.3321, found: m/z = 798.3297.

3-(Pyridin-2-yldisulfanyl)propanoic acid (**60**)

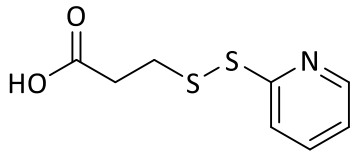

2,2'-Dipyridyl disulfide (1.97 g, 8.75 mmol) was dissolved in methanol (15 mL). To that mixture, 3-mercaptopropionic acid (0.70 mL, 7.96 mmol) was added. The mixture was left to stir overnight. The solvent was removed under reduced pressure. The crude was suspended in ethyl acetate and

filtered off. The filtrate was concentrated and purified by silica column chromatography to afford **60** (0.7 g, 41 %) as a colorless solid.

R_f = 0.05 (*n*-hexane/ethyl acetate 7:3)

^{1}H NMR (400 MHz, $CDCl_3$): δ = 2.81 (t, 2H), 3.07 (t, 2H), 7.09–7.20 (m, 1H), 7.57–7.72 (m, 2H), 8.48 (ddd, 1H) ppm.

^{13}C NMR (101 MHz, $CDCl_3$): δ = 34.8, 119.8, 120.7, 121.3, 137.4, 149.4, 159.2, 175.4 ppm.

HRMS calculated for $C_8H_{10}NO_2S_2$ $[M+H]^+$: m/z = 216.0155, found: m/z = 216.0140.

<u>*n*-Octadecyl isocyanide (**61**)</u>

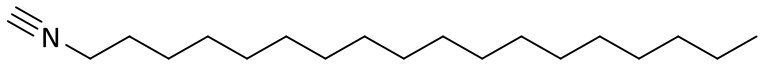

Water (2.97 mL) was cooled to 0 °C and sodium hydroxide (2.97 g, 14.70 mmol) was added in portions to maintain efficient stirring. A mixture of benzyltriethylammonium chloride (0.04 g, 0.04 mmol) and chloroform (2.21 mL, 5.51 mmol) dissolved in dichloromethane (2.97 mL) was added to previous solution followed by *n*-octadecylamine (5.00 g, 3.68 mmol). The mixture was left to stir at 50 °C for 24 h. Ice-cold water (20 mL) was added and organic layer was separated. The aqueous layer was washed with dichloromethane (3 ×) and then the combined organic fractions were washed with water (2 ×), brine (1 ×) and dried over Na_2SO_4. The crude was purified by silica column chromatography (frit) to obtain **61** (0.66 g, 13 %) as a colorless solid.

R_f = 0.65 (*n*-hexane/ethyl acetate 10:1)[8]

^{1}H NMR (400 MHz, $CDCl_3$): δ = 0.88 (t, 6H), 1.29 (d, 19H), 1.39–1.45 (m, 5H), 1.65–1.72 (ddt, 4H), 3.35–3.40 (tt, 4H) ppm.

^{13}C NMR (101 MHz, $CDCl_3$): δ = 14.1, 22.7, 26.3, 28.7, 29.1, 29.4, 29.5, 29.6, 29.6, 29.6, 29.7, 29.7, 31.9, 41.5, 41.6, 41.6, 155.5 ppm.

<u>*n*-Dodecyl isocyanide (**62**)</u>

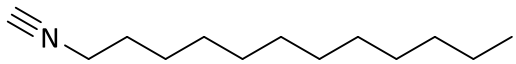

Water (8.08 mL) was cooled to 0 °C and sodium hydroxide (8.08 g, 200.00 mmol) was added in portions to maintain efficient stirring. A mixture of *n*-dodecylamine (9.46 g, 50.00 mmol), benzyltriethylammonium chloride (0.10 g, 0.10 mmol) and chloroform (6.01 mL, 75.00 mmol) dissolved in dichloromethane (8.08 mL) was added to previous solution. The mixture was left to stir at 45 °C for 5 h. Ice-cold water (20 mL) was added and organic layer was separated. The aqueous layer was washed with dichloromethane (2 ×) and then the combined organic fractions were washed with water (2 ×), brine (1 ×) and dried over Na_2SO_4. The crude was purified by silica column chromatography (frit) to obtain **62** (3.63 g, 37 %) as a yellowish oil.

R_f = 0.57 (*n*-hexane/ethyl acetate 10:1)[9]

[8] TLC plate was stained with ninhydrin staining solution.

^{1}H NMR (400 MHz, $CDCl_3$): δ = 0.88 (t, 3H), 1.28 (d, 16H), 1.39–1.47 (p, 2H), 1.63–1.71 (dddd, 2H), 3.35–3.39 (tt, 2H) ppm.

^{13}C NMR (101 MHz, $CDCl_3$): δ = 14.0, 22.6, 26.2, 28.6, 29.0, 29.2, 29.4, 29.5, 31.8, 41.4, 41.4, 41.5, 155.6 ppm.

3.4.2. Syntheses of peptides and conjugates

Truncated bombesin(6-14) (**63**)

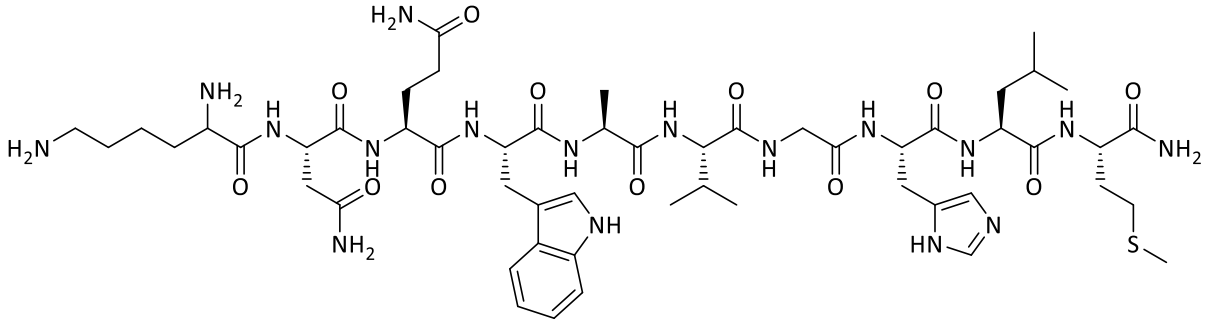

Compound **63** was synthesized according to the general procedure **G1** in 100 µmol scale on Fmoc-Rink-Amid-MBHA resin (140.8 mg, loading: 0.71 mmol/g). The peptide of one batch remained on the resin for further synthesis of peptide **64**. In an other batch the cleavage and subsequent HPLC were performed as described in **G1** in order to obtain pure **63** as reference compound for biological evaluation.

^{1}H NMR (400 MHz, D_2O): δ = 0.72–0.99 (m, 14H), 1.31 (d, 3H), 1.32–1.46 (m, 2H), 1.48–1.74 (m, 5H), 1.74–1.95 (m, 4H), 1.92–2.18 (m, 4H), 2.08 (s, 4H), 2.43–2.71 (m, 4H), 2.92–3.02 (m, 2H), 3.03–3.37 (m, 4H), 3.83–4.04 (m, 5H), 4.17–4.36 (m, 3H), 4.59–4.72 (m, 3H), 7.07–7.26 (m, 5H), 7.45 (d, 1H), 7.58 (d, 1H) ppm.

^{13}C NMR (101 MHz, D_2O): δ = 15.1, 17.6, 19.0, 19.3, 21.7, 22.2, 23.1, 25.3, 27.3, 28.0, 30.4, 30.9, 31.1, 31.4, 31.7, 36.9, 40.0, 40.5, 43.4, 50.6, 51.4, 53.3, 53.6, 53.8, 54.5, 55.3, 61.0, 109.9, 112.9, 113.0, 118.2, 119.2, 120.4, 123.0, 125.4, 127.8, 129.4, 134.5, 137.1, 163.8, 164.1, 170.5, 172.2, 172.4, 173.1, 173.7, 174.1, 174.9, 175.0, 175.4, 175.6, 177.0, 178.6 ppm.

t_R = 8.8 min (10 % ACN (2min)>15 min 95 %>5 min 100 %>100 % (5 min))

HRMS calculated for $C_{53}H_{84}N_{17}O_{12}S$ $[M+H]^+$: m/z = 1182.6208, found: m/z = 1182.6243.

[9] TLC plate was stained with ninhydrin staining solution.

N-terminal modification of bombesin(6-14) (**64**)

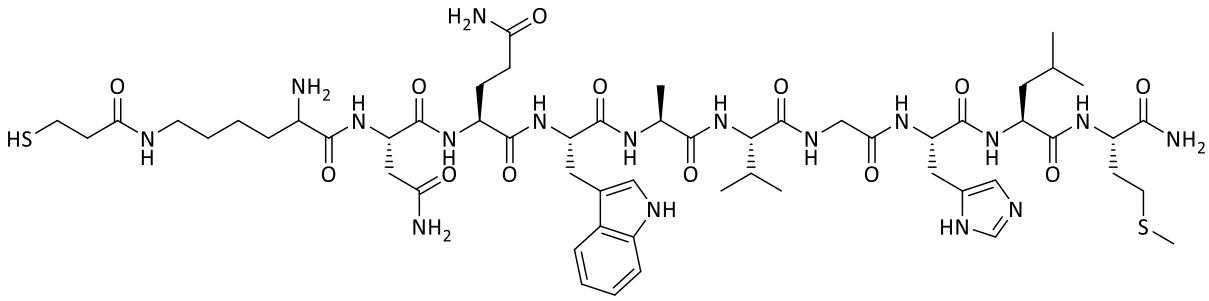

Compound **64** was synthesized on solid phase. The protected **63** (0.10 mmol) on resin was left to swell by dichloromethane. **60** (95.7 mg, 0.40 mmol) was dissolved in dichloromethane and then added to reaction tube followed by addition of DIC (63 µL, 0.40 mmol). The mixture was left to shake overnight and monitored by Kaiser test (**G2**). After complete conversion, the resin was washed with DMF (2 × 1 min) and dichloromethane (2 × 1 min).

HRMS calculated for $C_{61}H_{92}N_{18}O_{13}S_3$ $[M+H]^{2+}$: m/z = 690.3129, found: m/z = 690.3122.

The resin was left to swell with dichloromethane. TCEP (35.1 mg, 0.12 mmol) was dissolved in DMF/water and added to the reaction tube. The mixture was left to stir for 3 h at rt. After completion of the reaction, the resin was washed with DMF (2 × 1 min) and dichloromethane (2 × 1 min) followed by cleavage from the resin (see in **G1**) in order to afford **64** (43 mg, 34 %) as a colorless solid.

^{1}H NMR (400 MHz, DMSO-d6): δ = 0.71–0.90 (m, 12H), 1.23 (d, 3H), 1.30 (d, 1H), 1.37 (t, 1H), 1.47–1.53 (m, 3H), 1.84 (ddt, 1H), 2.01 (m, 2H), 2.01 (s, 3H), 2.32–2.50 (m, 2H), 2.53–2.69 (m, 2H), 2.88 (m, 2H), 3.01 (dt, 3H), 3.13–3.23 (m, 1H), 3.36 (s, 2H), 3.74 (d, 2H), 4.10 (m, 1H), 4.11–4.59 (m, 5H), 6.79 (s, 1H), 6.93–7.20 (m, 6H), 7.32 (d, 1H), 7.53 (s, 2H), 7.57 (d, 1H), 7.90 (dt, 2H), 8.02–8.14 (m, 2H), 8.24 (m, 2H), 8.41 (d, 1H) ppm.

^{13}C NMR (101 MHz, DMSO-d6): δ = 14.6, 17.5, 17.9, 19.2, 20.0, 21.3, 22.2, 23.1, 24.0, 27.3 28.9, 29.8, 30.4, 31.2, 31.3, 33.9, 37.0, 38.3, 40.2, 42.3, 48.3, 49.5, 51.7, 53.0, 53.5, 57.8, 110.1, 111.3, 118.2, 118.3, 120.8, 123.5, 127.2, 134.8, 136.0, 168.7, 169.8, 170.0, 171.2, 171.2, 171.3, 171.5, 171.9, 172.1, 172.2, 173.3, 173.9 ppm.

HRMS calculated for $C_{56}H_{89}N_{17}O_{13}S_2$ $[M+H]^{2+}$: m/z = 635.8136, found: m/z = 635.8114.

Bombesin(6-14) containing linker system (**65**)

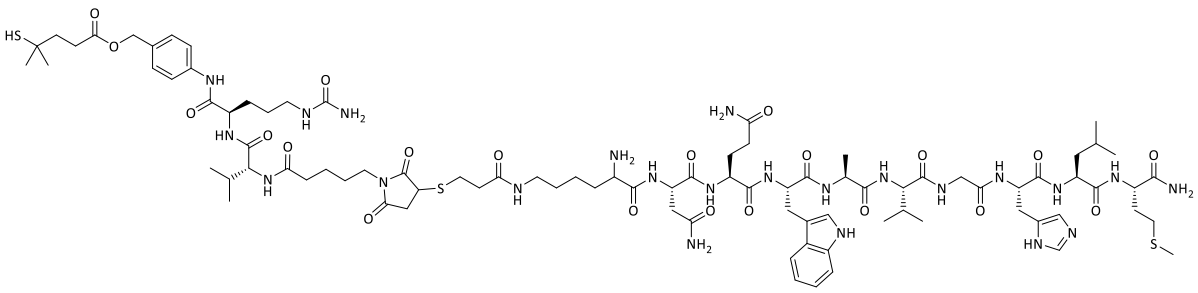

Compound **64** (40.0 mg, 0.03 mmol) was dissolved in DPBS (2.83 mL) and then **59** (21.4 mg, 0.03 mmol) dissolved in DMF (2.83 mL) was added dropwise. The mixture was left to stir overnight.

^{1}H NMR (400 MHz, DMSO-d6): δ = 0.74–0.89 (m, 14H), 1.20–1.32 (m, 8H), 1.36–1.56 (m, 15H), 1.71 (s, 2H), 1.78–1.87 (m, 2H), 2.02 (d, 3H), 2.21 (t, 5H), 2.37–2.50 (m, 2H), 2.73 (s, 13H), 2.89 (s, 14H), 2.99 (dd, 3H), 3.38 (dt, 4H), 3.66–3.79 (m, 2H), 4.98 (s, 1H), 5.45 (s, 1H), 6.15 (s, 1H), 6.78–7.01 (m, 4H), 6.92–7.16 (m, 4H), 7.29 (dd, 2H), 7.60 (dd, 2H), 7.71–7.79 (m, 2H), 7.95–8.16 (m, 6H), 8.22–8.31 (m, 1H), 8.38 (dt, 1H), 10.13 (d, 1H), 10.86 (s, 1H) ppm.

^{13}C NMR (101 MHz, DMSO-d6): δ = 14.6, 17.5, 17.9, 18.2, 19.2, 21.3, 21.6, 21.7, 22.6, 23.0, 26.5, 26.8, 26.8, 27.4, 28.5, 29.4, 29.7, 30.3, 30.7, 33.0, 34.6, 35.3, 35.8, 36.7, 36.9, 38.2, 38.8, 39.1, 39.3, 39.5, 39.6, 39.7, 39.8, 39.9, 40.0, 40.1, 40.2, 51.8, 65.3, 110.0, 119.0, 119.6, 121.2, 127.2, 128.8, 134.4, 134.4, 136.0, 137.5, 138.8, 149.2, 158.9, 159.5, 162.3, 168.7, 171.0, 171.0, 172.0, 172.3, 173.2, 173.9, 174.1 ppm.

HRMS calculated for $C_{94}H_{141}N_{24}O_{21}S_4$ $[M+H]^{3+}$: m/z = 689.9864, found: m/z = 689.9842.

TCEP (10.8 mg, 0.04 mmol) was added and the mixture was left to stir overnight. The solvent was removed under reduced pressure to afford crude **65** as a yellowish solid.

^{1}H NMR (400 MHz, DMSO-d6): δ = 0.84 (tt, 10H), 1.19–1.28 (m, 6H), 1.38–1.52 (m, 14H), 1.70 (d, 2H), 1.77–2.05 (m, 9H), 2.17–2.27 (m, 4H), 2.38–2.50 (m, 8H), 2.57–2.67 (m, 4H), 2.67 (s, 4H), 2.73 (s, 12H), 2.89 (m, 16H), 3.00 (dd, 1H), 3.18 (t, 2H), 4.98 (m, 1H), 5.45 (m, 1H), 6.89–7.01 (m, 1H), 7.00–7.11 (m, 1H), 7.13–7.23 (m, 2H), 7.30 (dd, 2H), 7.54–7.66 (m, 2H), 7.69–7.81 (m, 2H), 7.95 (m, 7H), 8.25 (m, 1H), 8.38 (dt, 1H) ppm.

HRMS calculated for $C_{89}H_{135}N_{23}O_{21}S_3$ $[M+H]^{2+}$: m/z = 978.9685, found: m/z = 978.9768.

<u>*N*-terminal modification of bombesin(6-14) by UGI reaction (**66**)</u>

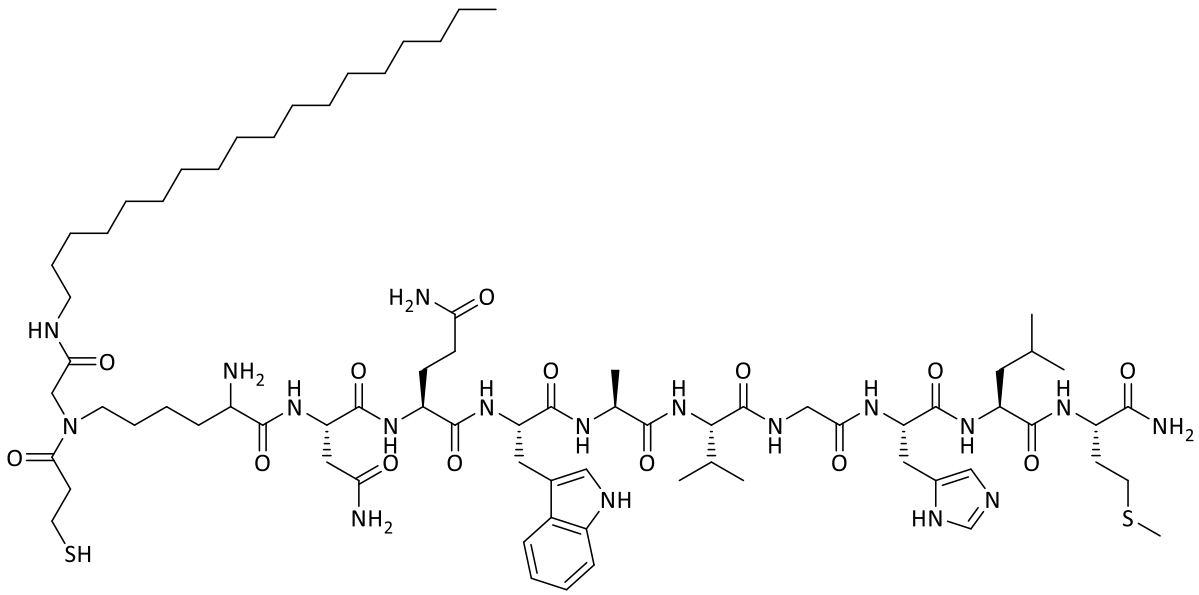

Compound **66** was synthesized on solid phase. **63** (0.10 mmol) on resin was left to swell by dichloromethane and washed with methanol/THF (1:1). PFA (12.6 mg, 0.40 mmol) and pyrrolidine

(33.8 µL, 0.40 mmol) were dissolved in methanol/THF (2 mL, 1:1) and left to shake for 10 min. That mixture was added to reaction tube containing **63** on the resin and left to shake for 40 min. The resin was washed with methanol/THF (1:1, 2 × 1 min). **60** (95.7 mg, 0.40 mmol) dissolved in methanol/THF (1:1, 1 mL) was added. After a few minutes, **61** (176.5 mg, 0.60 mmol) was dissolved in methanol/THF (1:1, 1 mL) and added. The mixture was left to shake for 24 h. After complete conversion, the resin was washed with DMF (2 × 1 min) and dichloromethane (2 × 1 min).

HRMS calculated for $C_{81}H_{131}N_{19}O_{14}S_3$ $[M+H]^{2+}$: m/z = 844.9645, found: m/z = 844.9648.

The resin was left to swell with dichloromethane. TCEP (35.1 mg, 0.12 mmol) was dissolved in DMF/water and added to the reaction tube. The mixture was left to stir at rt for 6 h. After completion of the reaction, the resin was washed with DMF (2 × 1 min) and dichloromethane (2 × 1 min) followed by cleavage from the resin (see in **G1**) in order to afford **66** (124 mg, 78 %) as a colorless solid. The peptide was purified by HPLC.

^{1}H NMR (400 MHz, DMSO-d6): δ = 0.77–0.90 (m, 15H), 1.24 (s, 36H), 1.35–1.41 (m, 5H), 1.50 (d, 3H), 1.83 (m, 1H), 1.96–2.07 (m, 4H), 2.35–2.44 (m, 1H), 2.54–2.68 (m, 2H), 2.85–3.01 (m, 4H), 3.06 (dt, 1H), 3.51 (s, 3H), 3.73 (d, 2H), 3.87 (d, 1H), 4.09 (d, 1H), 4.13–4.40 (m, 3H), 4.40–4.58 (m, 2H), 6.81 (d, 2H), 6.92–7.14 (m, 4H), 7.12–7.19 (m, 2H), 7.32 (d, 1H), 7.49–7.60 (m, 3H), 7.63–7.74 (m, 1H), 7.95 (s, 1H), 8.02–8.14 (m, 3H), 8.21 (m, 3H), 10.78 (s, 1H) ppm.

^{13}C NMR (101 MHz, DMSO-d6): δ = 13.9, 14.6, 17.5, 17.8, 19.2, 19.8, 21.3, 22.1, 23.1, 24.0, 26.4, 28.7, 29.0, 29.0, 29.8, 30.4, 31.3, 38.9, 39.1, 39.3, 39.5, 39.56, 39.7, 39.8, 39.9, 40.0, 40.1, 40.2, 48.3, 51.7, 53.0, 69.8, 110.2, 111.2, 118.3, 120.8, 123.5, 127.2, 136.0, 158.3, 163.6, 168.7, 171.2, 171.5, 172.0, 172.1, 173.3, 173.9 ppm.

t_R = 14.8 min (10 % ACN (2min)>15 min 95 %>5 min 100 %>100 % (5 min))

HRMS calculated for $C_{76}H_{128}N_{18}O_{14}S_2$ $[M+H]^{2+}$: m/z = 790.4651, found: m/z = 790.4636.

<u>*N*-terminal modification of bombesin(6-14) by UGI reaction (**67**)</u>

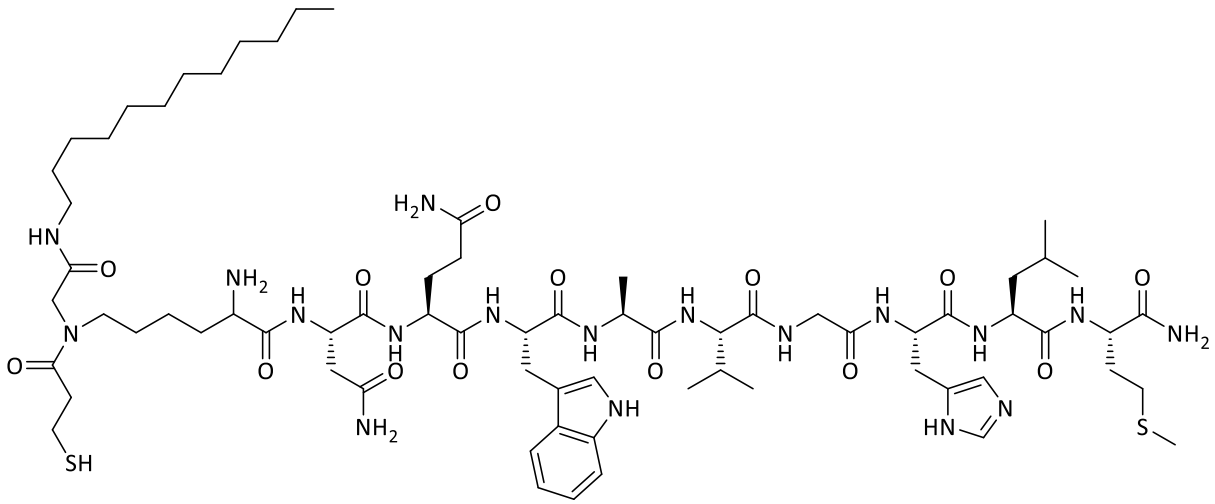

Compound **67** was synthesized on solid phase. **63** (0.10 mmol) on resin was left to swell by dichloromethane and washed with methanol/THF (1:1). PFA (12.6 mg, 0.40 mmol) and pyrrolidine

(33.8 µL, 0.40 mmol) were dissolved in methanol/THF (2 mL, 1:1) and left to shake for 10 min. That mixture was added to reaction tube containing **63** on the resin and left to shake for 40 min. The resin was washed with methanol/THF (1:1, 2 × 1 min). **60** (95.7 mg, 0.40 mmol) dissolved in methanol/THF (1:1, 1 mL) was added. After a few minutes, **62** (123.4 mg, 0.60 mmol) was dissolved in methanol/THF (1:1, 1 mL) and added. The mixture was left to shake for 45 h. After complete conversion, the resin was washed with DMF (2 × 1 min) and dichloromethane (2 × 1 min).

HRMS calculated for $C_{75}H_{119}N_{19}O_{14}S_3$ $[M+H]^{2+}$: m/z = 802.9175, found: m/z = 802.9224.

The resin was left to swell with dichloromethane. TCEP (35.1 mg, 0.12 mmol) was dissolved in DMF/water and added to the reaction tube. The mixture was left to stir at rt for 6 h. After completion of the reaction, the resin was washed with DMF (2 × 1 min) and dichloromethane (2 × 1 min) followed by cleavage from the resin (see in **G1**) in order to yield **67** (60 mg, 40 %) as a colorless solid. The peptide was purified by HPLC.

^{1}H NMR (400 MHz, DMSO-d6): δ = 0.81–0.93 (m, 15H), 1.22 (s, 1H), 1.24 (s, 12H), 1.27 (d, 1H), 1.36–1.41 (m, 3H), 1.50 (t, 2H), 1.66–1.71 (m, 2H), 1.79–1.89 (m, 2H), 1.91–2.09 (m, 3H), 2.45 (d, 3H), 2.51–2.68 (m, 2H), 2.95–3.12 (m, 2H), 3.14–3.21 (m, 4H), 3.75 (s, 3H), 3.88 (d, 1H), 4.11–4.16 (m, 2H), 4.26 (dd, 2H), 4.31–4.38 (m, 1H), 4.47–4.52 (m, 1H), 4.57–4.63 (m, 3H), 6.76–6.81 (m, 1H), 6.95–7.10 (m, 4H), 7.13–7.19 (m, 2H), 7.24–7.36 (m, 3H), 7.52–7.61 (m, 2H), 7.94–7.99 (m, 1H), 8.09–8.14 (m, 4H), 8.11–8.20 (m, 1H), 8.19–8.27 (m, 4H), 8.70–8.86 (m, 3H), 10.80 (s, 1H) ppm.

^{13}C NMR (101 MHz, DMSO-d6): δ = 13.9, 14.6, 17.5, 18.0, 19.1, 19.6, 19.8, 20.0, 21.4, 22.1, 22.5, 23.0, 23.1, 24.1, 26.4, 27.2, 28.7, 28.8, 29.0, 29.0, 29.5, 30.4, 31.3, 31.4, 31.7, 36.7, 38.9, 39.1, 39.3, 39.5, 39.6, 39.7, 39.8, 39.9, 40.0, 40.1, 40.2, 48.3, 51.6, 51.8, 57.8, 110.0, 111.3, 115.8, 116.9, 118.2, 118.3, 118.8, 120.8, 123.6, 127.2, 133.7, 136.0, 157.8, 158.1, 158.4, 168.0, 168.5, 168.8, 169.9, 170.2, 171.3, 171.5, 172.1, 172.9, 173.8 ppm.

t_R = 12.7 min (10 % ACN (2min)>15 min 95 %>5 min 100 %>100 % (5 min))

HRMS calculated for $C_{70}H_{116}N_{18}O_{14}S_2$ $[M+H]^{2+}$: m/z = 748.4182, found: m/z = 748.4128.

<u>*N*-terminal modification of bombesin(6-14) by UGI reaction (**68**)</u>

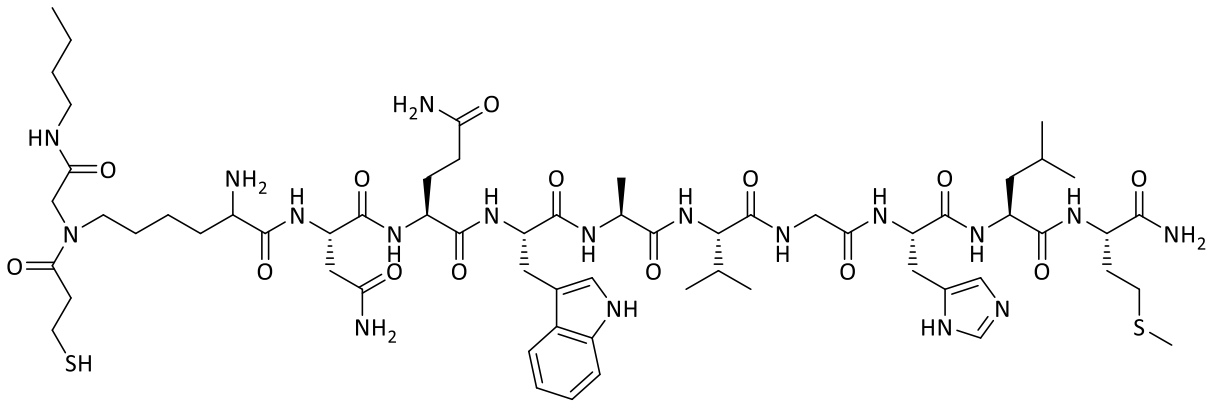

Compound **68** was synthesized on solid phase. **63** (0.10 mmol) on resin was left to swell by dichloromethane and washed with methanol/THF (1:1). PFA (12.6 mg, 0.40 mmol) and pyrrolidine (33.8 µL, 0.40 mmol) were dissolved in methanol/THF (2 mL, 1:1) and left to shake for 10 min. That

mixture was added to reaction tube containing **63** on the resin and left to shake for 40 min. The resin was washed with methanol/THF (1:1, 2 × 1 min). **60** (95.7 mg, 0.40 mmol) dissolved in methanol/THF (1:1, 1 mL) was added. After a few minutes, *n*-butyl isocyanide (64.3 µL, 0.60 mmol) was dissolved in methanol/THF (1:1, 1 mL) and added. The mixture was left to shake for 45 h. After complete conversion, the resin was washed with DMF (2 × 1 min) and dichloromethane (2 × 1 min).

HRMS calculated for $C_{67}H_{103}N_{19}O_{14}S_3$ $[M+H]^{2+}$: m/z = 746.8549, found: m/z = 746.8526.

The resin was left to swell with dichloromethane. TCEP (35.1 mg, 0.12 mmol) was dissolved in DMF/water and added to the reaction tube. The mixture was left to stir at rt for 6 h. After completion of the reaction, the resin was washed with DMF (2 × 1 min) and dichloromethane (2 × 1 min) followed by cleavage from the resin (see **G1**) in order to yield **68** (79 mg, 57 %) as a colorless solid. The peptide was purified by HPLC.

^{1}H NMR (400 MHz, D_2O): δ = 0.86 (dt, 6H), 0.88–1.00 (m, 13H), 1.22–1.39 (m, 7H), 1.44 (dd, 1H), 1.48–1.66 (m, 8H), 1.86 (d, 5H), 1.96–2.15 (m, 9H), 2.44–2.64 (m, 3H), 2.63–2.76 (m, 4H), 3.07–3.39 (m, 3H), 3.84–4.10 (m, 4H), 4.20 (s, 1H), 4.27–4.36 (m, 3H), 4.41–4.46 (m, 1H), 4.62–4.72 (m, 4H), 7.08–7.26 (m, 5H), 7.46 (d, 1H), 7.59 (d, 1H), 8.49–8.54 (m, 1H) ppm.

^{13}C NMR (101 MHz, D_2O): δ = 14.0, 14.0, 15.1, 17.7, 19.0, 19.4, 20.4, 20.4, 20.5, 20.5, 21.0, 21.6, 21.8, 22.4, 23.1, 25.3, 27.2, 27.5, 28.5, 28.9, 30.4, 30.9, 31.1, 31.5, 31.5, 31.8, 37.0, 37.1, 37.6, 39.8, 40.1, 40.3, 40.4, 40.5, 43.4, 48.1, 50.4, 50.7, 50.8, 51.4, 53.3, 53.5, 53.6, 53.9, 54.6, 55.4, 61.1, 109.8, 112.9, 115.9, 118.2, 118.8, 119.2, 120.4, 123.0, 125.4, 127.9, 129.2, 134.4, 137.1, 163.8, 164.1, 170.5, 170.6, 171.2, 171.6, 172.2, 172.3, 173.0, 173.7, 173.8, 174.2, 174.9, 175.1, 175.3, 175.4, 175.6, 177.0, 178.5 ppm.

t_R = 10.3 min (10 % ACN (2min)>15 min 95 %>5 min 100 %>100 % (5 min))

HRMS calculated for $C_{62}H_{100}N_{18}O_{14}S_2$ $[M+H]^{2+}$: m/z = 692.3556, found: m/z = 692.3538.

<u>Conjugate containing **65** and tubugi 1 (**69**)</u>

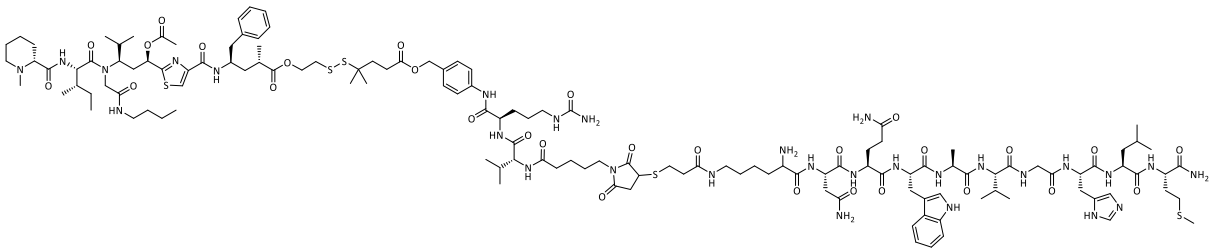

Compound **65** (20.0 mg, 0.01 mmol, 5 mM) was dissolved in dry DMF (0.92 mL). To that solution **36** (9.6 mg, 0.01 mmol) dissolved in dry DMF (0.92 mL) was added. The mixture was left to stir at rt for 3 d. The crude product was purified by an RP C18 column (water/methanol) to obtain **69** (8 mg, 31 %) as a colorless solid.

t_R = 9.8 min (10 % ACN (2min)>15 min 95 %>5 min 100 %>100 % (5 min))

HRMS calculated for $C_{134}H_{208}N_{29}O_{29}S_5$ $[M+H]^{5+}$: m/z = 569.4861, found: m/z = 569.4916.

Conjugate containing **65** and tubugi 4 (**70**)

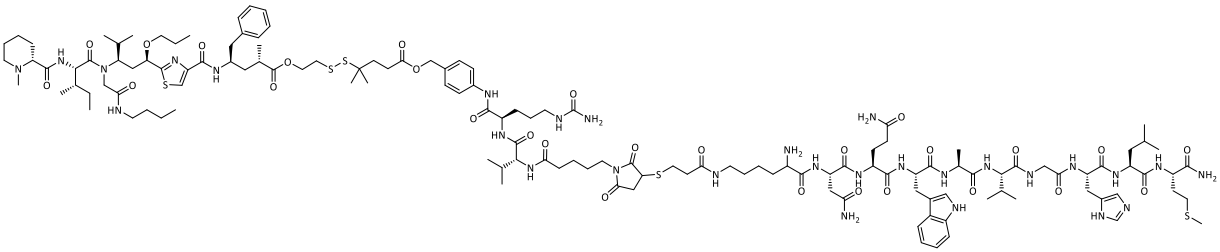

Compound **65** (20.0 mg, 0.01 mmol, 5 mM) was dissolved in dry DMF (0.92 mL). To that solution **37** (9.6 mg, 0.01 mmol) dissolved in dry DMF (0.92 mL) was added. The mixture was left to stir at rt for 3 d. The crude product was purified by an RP C18 column (water/methanol) to obtain **70** (7 mg, 27 %) as a yellowish solid.

t_R = 9.8 min (10 % ACN (2min)>15 min 95 %>5 min 100 %>100 % (5 min))

HRMS calculated for $C_{135}H_{211}N_{29}O_{28}S_5$ $[M+H]^{4+}$: m/z = 711.6147, found: m/z = 711.6094.

Conjugate containing **66** and tubugi 4 (**71**)

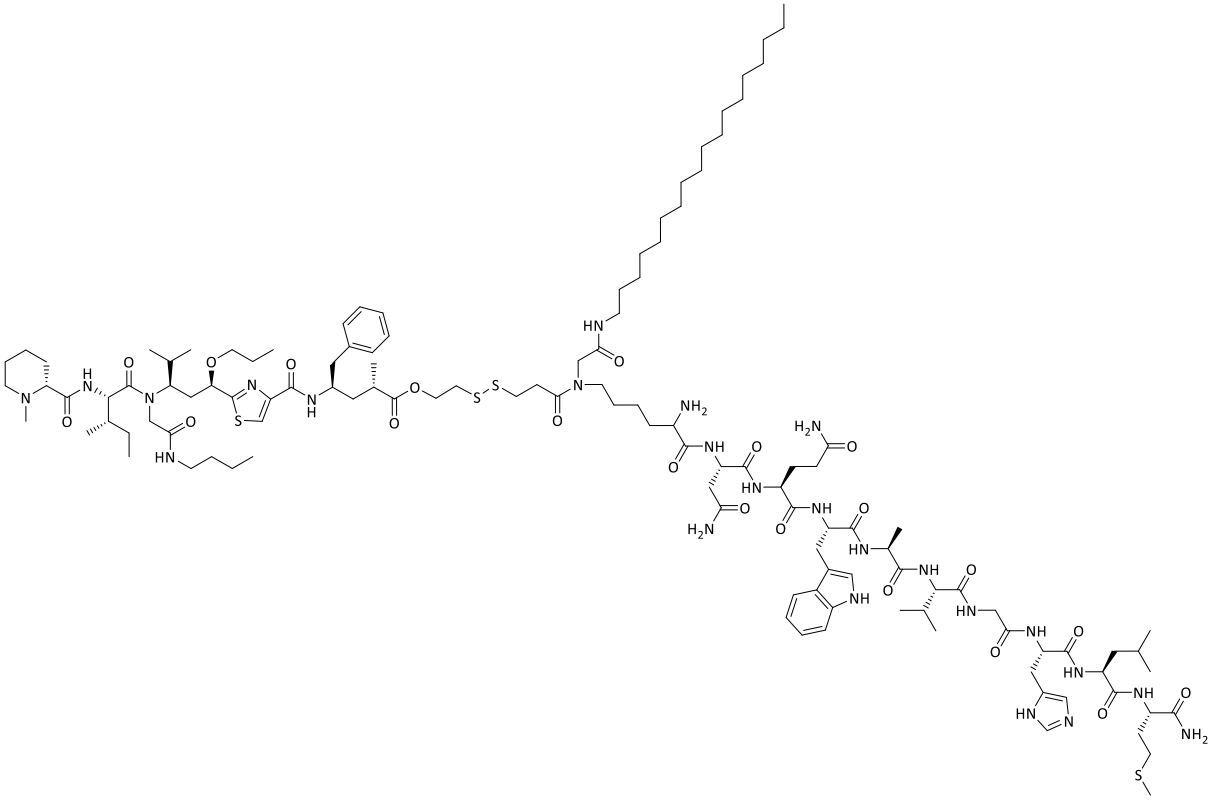

Compound **66** (25.0 mg, 0.02 mmol, 5 mM) was dissolved in dry DMF (1.51 mL). To that solution **37** (15.8 mg, 0.02 mmol) dissolved in dry DMF (1.51 mL) was added. The mixture was left to stir at rt for 18 h. The crude product was purified by an RP C18 column (water/methanol) to obtain **71** (9 mg, 24 %) as a colorless solid.

t_R = 14.4 min (10 % ACN (2min)>15 min 95 %>5 min 100 %>100 % (5 min))

HRMS calculated for $C_{122}H_{201}N_{24}O_{21}S_4$ $[M+H]^{3+}$: m/z = 822.1429, found: m/z = 822.1424.

Conjugate containing **67** and tubugi 4 (**72**)

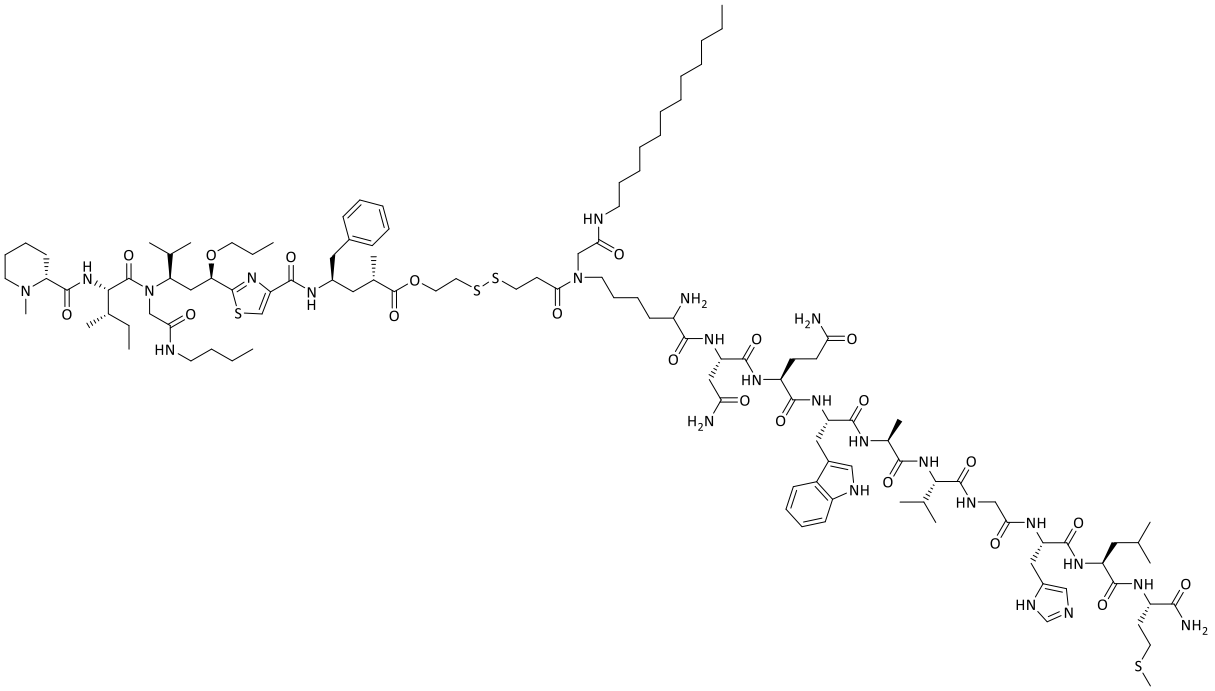

Compound **67** (25.0 mg, 0.02 mmol, 5 mM) was dissolved in dry DMF (1.59 mL). To that solution **37** (16.7 mg, 0.02 mmol) dissolved in dry DMF (1.59 mL) was added. The mixture was left to stir at rt for 18 h. The crude product was purified by an RP C18 column (water/methanol) to obtain **72** (6 mg, 16 %) as a colorless solid.

t_R = 13.2 min (10 % ACN (2min)>15 min 95 %>5 min 100 %>100 % (5 min))

HRMS calculated for $C_{116}H_{188}N_{24}O_{21}S_4$ $[M+H]^{2+}$: m/z = 1190.6634, found: m/z = 1190.6632.

Conjugate containing **68** and tubugi 4 (**73**)

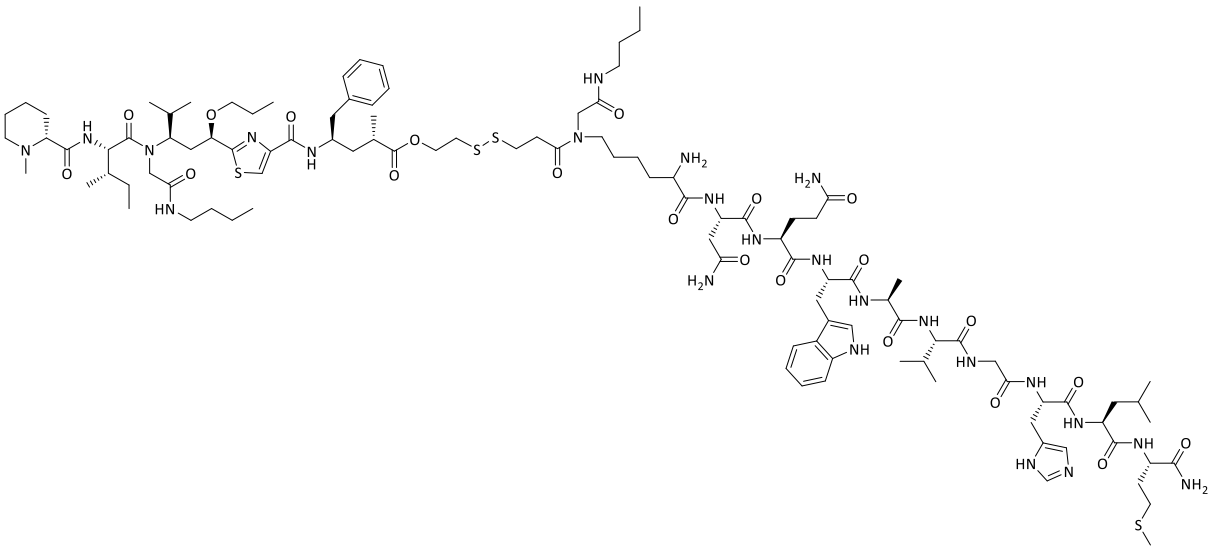

Compound **68** (21.0 mg, 0.01 mmol, 5 mM) was dissolved in dry DMF (1.44 mL). To that solution **37** (15.1 mg, 0.01 mmol) dissolved in dry DMF (1.44 mL) was added. The mixture was left to stir at rt for 18 h. The crude product was purified by an RP C18 column (water/methanol) to obtain **73** (4 mg, 12 %) as a colorless solid.

t_R = 11.7 min (10 % ACN (2min)>15 min 95 %>5 min 100 %>100 % (5 min))

HRMS calculated for $C_{108}H_{172}N_{24}O_{21}S_4$ $[M+H]^{2+}$: m/z = 1134.6008, found: m/z = 1134.6010.

3.4.3. Syntheses of fluorophore conjugates

Maleimide-linked rhodamine B (**74**)

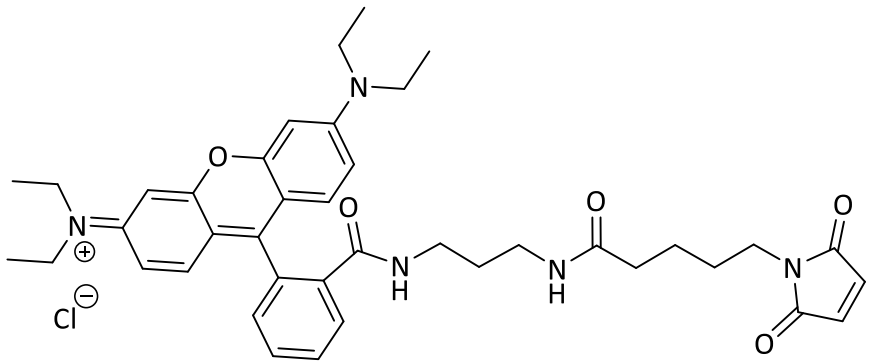

Compound **58** (40.0 mg, 0.19 mmol) was dissolved in dichloromethane (20 mL) and cooled to 0 °C. EDC × HCl (49.0 mg, 0.25 mmol) and **54** (119.4 mg, 0.21 mmol) were added and mixture was allowed to reach rt and left to stir overnight. The crude was purified by silica column chromatography to yield **74** (118 mg, 86 %) as a pink solid.

R_f = 0.64 (dichloromethane/methanol 10: 1)

^{1}H NMR (400 MHz, CD_3OD): δ = 1.19 (dt, 12H), 1.29 (dt, 2H), 1.46–1.61 (m, 4H), 2.12 (t, 2H), 2.93 (t, 2H), 3.21 (t, 2H), 3.55 (dt, 4H), 3.71 (m, 8H), 6.81 (s, 2H), 7.01 (d, 2H), 7.30–7.38 (m, 2H), 7.59–7.70 (m, 2H), 7.73–7.78 (m, 2H), 7.96–7.99 (m, 2H) ppm.

^{13}C NMR (101 MHz, CD_3OD): δ = 10.9, 18.4, 24.1, 29.1, 29.6, 36.4, 37.9, 38.2, 39.6, 54.5, 65.3, 113.0, 119.4, 124.4, 125.0, 131.0, 131.4, 132.2, 135.0, 135.4, 140.7, 153.4, 153.5, 170.1, 172.6, 175.3 ppm.

HRMS calculated for $C_{40}H_{49}N_5O_5$ $[M+H]^+$: m/z = 679.3730, found: m/z = 679.3696.

Rhodamine B labeled bombesin(6-14) (**75**)

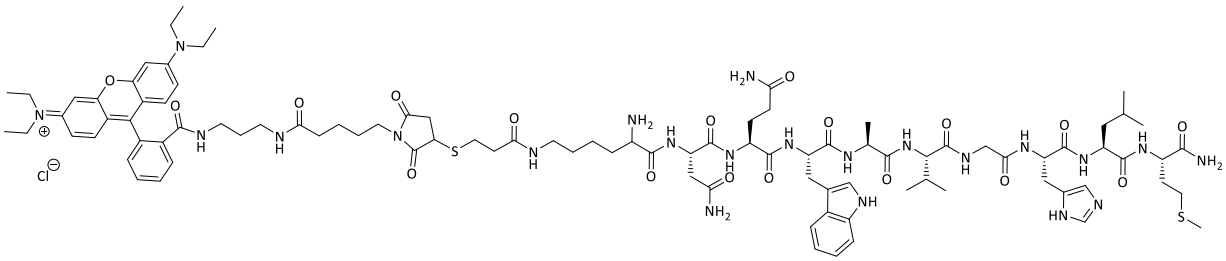

Compound **64** (50.0 mg, 0.04 mmol, 5 mM) was dissolved in dry DMF (3.54 mL). To that solution **74** (24.0 mg, 0.03 mmol) dissolved in dry DMF (3.54 mL) was added dropwise. The mixture was left to stir at rt for 3 d. The crude product was purified by an RP C18 column (water/methanol) to afford **75** (33 mg, 52 %) as a pink solid.

t_R = 12.3 min (10 % ACN (2min)>15 min>95 %>5 min>100 % (10 min))

HRMS calculated for $C_{96}H_{138}N_{22}O_{18}S_2$ $[M+H]^{3+}$: m/z = 650.3334, found: m/z = 650.3311.

<u>*N*-alpha-(*tert*-Butyloxycarbonyl)-*N*6-(2-(methylamino)benzoyl)lysine (**76**)</u>

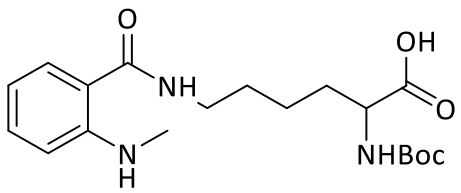

N-methyl isatoic anhydride (0.20 g, 1.02 mmol) was dissolved in toluene (25 mL) and *N*-alpha-(*tert*-butyloxycarbonyl)-L-lysine (0.26 g, 1.02 mmol) was added. The mixture was left to reflux overnight. The crude was purified by silica column chromatography to yield **76** (0.35 g, 91 %) as a yellowish oil.

R_f = 0.23 (ethyl acetate/*n*-hexane/formic acid 7:1:0.1%)

^{1}H NMR (400 MHz, CD_3OD): δ = 1.42 (s, 9H), 1.44–1.51 (m, 3H), 1.58–1.73 (m, 3H), 1.81–1.84 (m, 1H), 2.83 (s, 3H), 3.32–3.34 (d, 2H), 4.06–4.10 (m, 1H), 6.57–6.61 (dd, 1H), 6.68 (d, 1H), 7.27–7.31 (dd, 1H), 7.42–7.44 (dd, 1H) ppm.

^{13}C NMR (101 MHz, CD_3OD): δ = 24.4, 28.7, 29.9, 30.1, 32.5, 40.2, 54.8, 80.4, 111.9, 115.9, 117.6, 124.9, 129.1, 133.5, 138.4, 151.3, 158.2, 172.3, 176.3 ppm.

HRMS calculated for $C_{19}H_{30}N_3O_5$ $[M+H]^+$: m/z = 380.2187, found: m/z = 380.2187.

calculated for $C_{19}H_{28}N_3O_5$ $[M-H]^-$: m/z = 378.2027, found: m/z = 378.2034.

<u>3-Methyl-3-(pyridin-2-yldisulfanyl)butan-1-ol (**77**)</u>

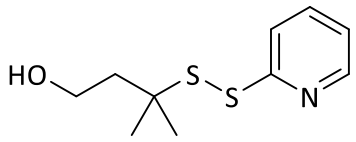

2,2'-Dipyridyl disulfide (0.50 g, 2.22 mmol) was dissolved in methanol (10 mL). To that mixture 3-mercapto-3-methyl-butan-1-ol (0.25 g, 2.02 mmol) was added. The mixture was left to stir for 5 h. The solvent was removed under reduced pressure and the crude was suspended in ethyl acetate and filtered off. The filtrate was concentrated under reduced pressure and then purification by silica column chromatography was performed to obtain **77** (0.45 g, 98 %) as a colorless oil.

R_f = 0.31 (ethyl acetate/*n*-hexane 3:1)

^{1}H NMR (400 MHz, CD_3OD): δ = 1.32 (s, 6H), 1.87 (t, 2H), 3.69 (t, 2H), 7.20 (ddd, 1H), 7.77 (ddd, 1H), 7.88 (dt, 1H), 8.36 (ddd, 1H) ppm.

^{13}C NMR (101 MHz, CD_3OD): δ = 28.1, 44.5, 52.2, 59.6, 121.6, 122.3, 138.9, 149.9, 162.4 ppm.

HRMS calculated for $C_{10}H_{16}NOS_2$ $[M+H]^+$: m/z = 230.0675, found: m/z = 230.0659.

3-Methyl-3-(pyridin-2-yldisulfanyl)butyl *N*-alpha-(*tert*-butyloxycarbonyl)-*N*6-(2-(methylamino) benzoyl)lysinate (**78**)

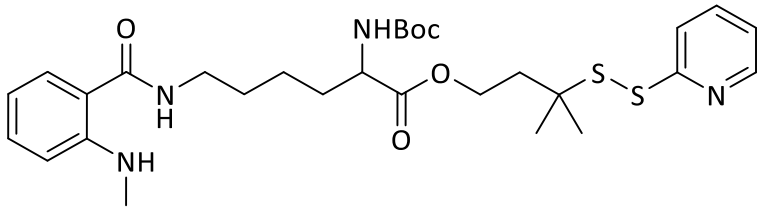

Compound **76** (180 mg, 0.45 mmol) was dissolved in dichloromethane (10 mL) and cooled down to 0 °C. EDC × HCl (115 mg, 0.59 mmol), **77** (120 mg, 0.50 mmol) and DMAP (5.6 mg, 0.05 mmol) were sequentially added to that solution. After 5 minutes, the mixture was allowed to reach rt and left to stir for 23 h. The crude product was purified by silica column chromatography to afford **78** (221 mg, 83 %) as a colorless oil.

R_f = 0.65 (ethyl acetate/*n*-hexane 8:1)

^{1}H NMR (400 MHz, $CDCl_3$): δ = 1.25 (td, 2H), 1.32 (d, 4H), 1.42 (d, 9H), 1.63 (dtt, 4H), 1.76–1.86 (m, 1H), 1.96 (t, 1H), 2.84 (d, 3H), 3.37 (m, 2H), 4.11 (m, 1H), 4.15–4.27 (m, 3H), 6.55 (td, 1H), 6.64 (d, 1H), 7.02–7.09 (m, 1H), 7.29 (ddt, 1H), 7.31–7.34 (m, 1H), 7.61 (td, 1H), 7.72 (d, 1H), 8.38–8.43 (m, 1H) ppm.

^{13}C NMR (101 MHz, $CDCl_3$): δ = 14.4, 21.2, 23.0, 27.9, 28.5, 29.4, 29.9, 39.4, 51.0, 53.5, 60.6, 61.5, 62.5, 80.0, 111.2, 114.6, 120.3, 120.9, 127.4, 132.9, 137.1, 149.5, 150.6, 155.7, 161.0, 170.2, 173.0 ppm.

HRMS calculated for $C_{29}H_{43}N_4O_5S_2$ $[M+H]^+$: m/z = 591.2677, found: m/z = 591.2651.

(Pyridin-2-yldisulfanyl)ethyl ester of rhodamine B (**79**)

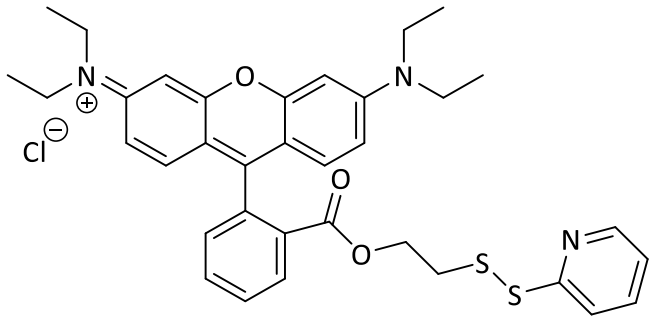

Rhodamine B (0.15 g, 0.30 mmol) was dissolved in dichloromethane (10 mL) and cooled down to 0 °C. DIC (60.9 µL, 0.39 mmol), **35** (0.08 g, 0.42 mmol) and DMAP (3.7 mg, 0.03 mmol) were sequentially added to that solution. After 5 minutes, the mixture was allowed to reach rt and left to stir overnight. The crude product was purified by silica column chromatography to afford **79** (42 mg, 71 %) as a pink solid.

R_f = 0.11 (dichloromethane/methanol 10:1)

^{1}H NMR (400 MHz, CD_3OD): δ = 1.29 (t, 12H), 2.76 (t, 2H), 3.58–3.74 (m, 8H), 4.15–4.28 (m, 2H), 6.93–7.08 (m, 4H), 7.07–7.23 (m, 3H), 7.45 (dt, 1H), 7.59 (dt, 1H), 7.69 (ddd, 1H), 7.76–7.95 (m, 2H), 8.26–8.39 (m, 2H) ppm.

^{13}C NMR (101 MHz, CD_3OD): δ = 12.8, 14.0, 38.4, 39.6, 46.9, 49.8, 62.5, 64.1, 66.6, 97.2, 97.4, 114.9, 115.6, 121.0, 122.4, 131.5, 131.7, 132.5, 134.2, 134.8, 139.0, 139.3, 150.2, 150.5, 157.2, 159.4, 159.8, 160.8, 166.5 ppm.

HRMS calculated for $C_{35}H_{39}N_3O_3S_2$ $[M+H]^+$: m/z = 613.2429, found: m/z = 613.2426.

Disulfide bridging of (3-methyl-3-sulfanyl)butyl *N*-alpha-(tert-butyloxycarbonyl)-*N*6-(2-(methyl amino) benzoyl)lysinate to rhodamine B ester (**80**)

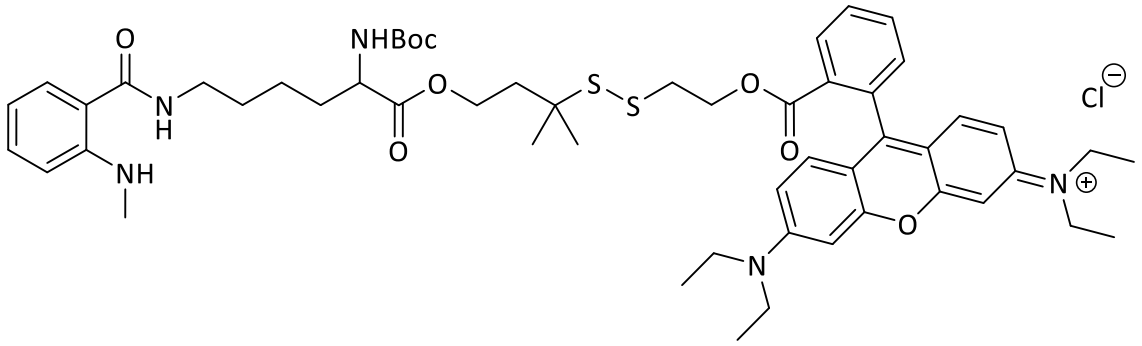

Compound **78** (78 mg, 0.13 mmol) was dissolved in water/DMF (1:1, 12.6 mL) and TCEP (40 mg, 0.14 mmol) was added. After stirring for 4 h, **79** (94 mg, 0.14 mmol) was added and the mixture was left to stir for further 4 h. The crude product was purified by silica column chromatography to afford **80** (99 mg, 77 %) as a pink solid.

R_f = 0.19 (dichloromethane/methanol 10:1)

^{1}H NMR (400 MHz, CD_3OD): δ = 0.84 (d, 2H), 0.85–0.98 (m, 7H), 1.04 (d, 9H), 1.17–1.35 (m, 2H), 1.45 (dt, 1H), 2.22 (dt, 1H), 2.40–2.55 (m, 3H), 2.53–2.64 (m, 1H), 2.89–3.00 (m, 4H), 3.29 (d, 2H), 3.65–3.92 (m, 3H), 4.21 (s, 7H), 4.37 (s, 1H), 6.14–6.34 (m, 2H), 6.51–6.71 (m, 2H), 6.75 (dd, 1H), 6.86–6.98 (m, 1H), 7.01–7.14 (m, 1H), 7.37–7.53 (m, 1H) ppm.

^{13}C NMR (101 MHz, CD_3OD): δ = 12.9, 14.5, 24.3, 28.3, 28.7, 29.9, 32.2, 32.3, 37.0, 38.0, 39.0, 40.1, 40.3, 46.9, 50.4, 55.1, 62.2, 63.2, 64.2, 64.3, 66.8, 67.3, 80.6, 97.4, 111.9, 114.9, 115.6, 115.9, 129.1, 131.5, 132.3, 132.5, 133.6, 134.1, 134.6, 151.4, 157.1, 159.4, 166.8, 172.3 ppm.

HRMS calculated for $C_{54}H_{73}N_5O_8S_2$ $[M+H]^+$: m/z = 983.4897, found: m/z = 983.4966.

Disulfide bridged double-dye compound of (3-methyl-3-sulfanyl)butyl *N*6-(2-(methylamino) benzoyl)lysinate and rhodamine B ester (**81**)

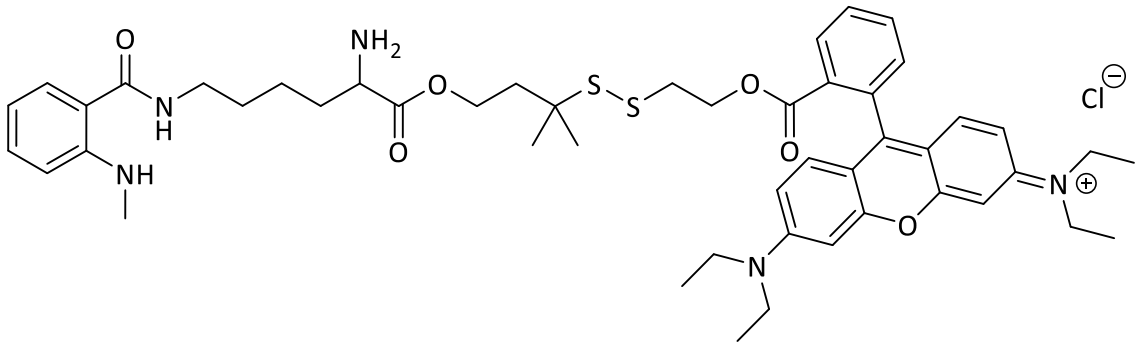

Compound **80** (60 g, 0.05 mmol) was dissolved in dichloromethane (5.0 mL) and cooled to 0 °C. TFA (1.0 mL) was added and the mixture was left to stir at 0 °C for 75 min. The mixture was concentrated under reduced pressure. The resulting oil was redissolved in dichloromethane and then evaporated. That was repeated a few times. The crude was purified by silica column chromatography to afford **81** (28 mg, 65 %) as a pink solid.

R_f = 0.09 (dichloromethane/methanol 10:1)

^{1}H NMR (400 MHz, CD_3OD): δ = 1.21 (s, 5H), 1.26–1.37 (m, 15H), 1.62 (m, 1H), 1.67–1.85 (m, 1H), 1.87 (t, 3H), 2.58 (t, 1H), 2.74–2.86 (m, 2H), 3.56–3.74 (m, 10H), 4.10–4.28 (m, 4H), 6.57 (t, 1H), 6.66 (d, 1H), 6.91–7.09 (m, 4H), 7.05–7.34 (m, 4H), 7.38–7.47 (m, 2H), 7.67 (d, 1H), 7.71–7.96 (m, 3H), 8.27–8.45 (m, 2H) ppm.

^{13}C NMR (101 MHz, CD_3OD): δ = 12.9, 14.4, 23.3, 28.2, 29.9, 31.1, 31.2, 38.4, 39.0, 40.1, 46.9, 50.3, 53.9, 62.5, 63.6, 64.1, 64.3, 64.5, 66.5, 67.3, 97.2, 97.3, 114.9, 115.5, 129.4, 131.5, 131.7, 132.4, 134.2, 134.7, 139.5, 157.1, 159.4, 159.8, 166.6, 170.6 ppm.

HRMS calculated for $C_{49}H_{65}N_5O_6S_2$ $[M+H]^+$: m/z = 883.4373, found: m/z = 883.4298.

Maleimide linker to disulfide bridged double-dye compound of (3-methyl-3-sulfanyl)butyl *N*6-(2-(methylamino) benzoyl)lysinate and rhodamine B ester (**82**)

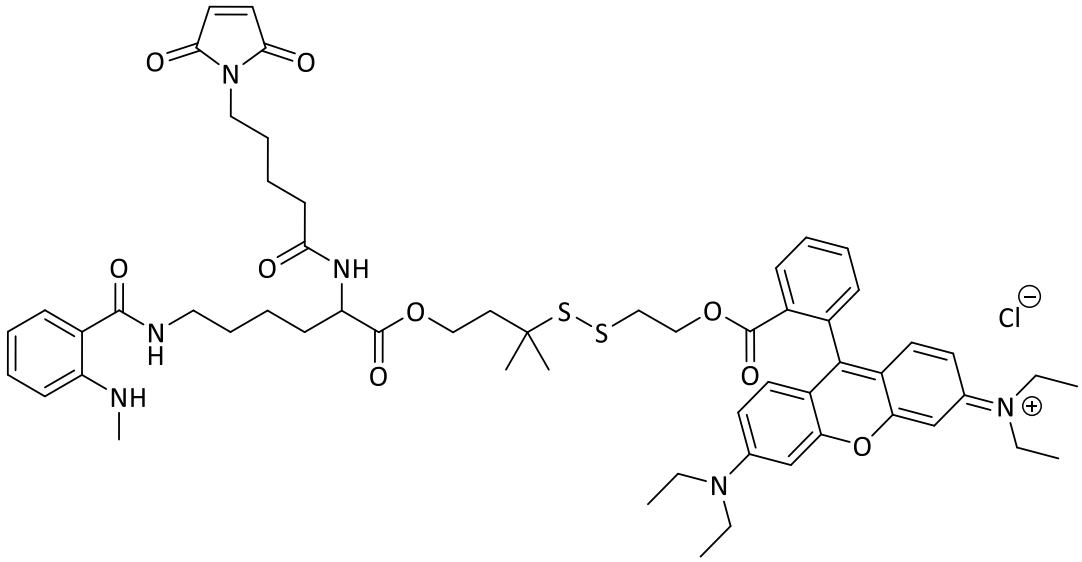

Compound **81** (0.15 g, 0.30 mmol) was dissolved in dichloromethane (10 mL) and cooled down to 0 °C. DIC (60.9 µL, 0.39 mmol), **58** (0.08 g, 0.42 mmol) and DMAP (3.7 mg, 0.03 mmol) were sequentially added to that solution. After 5 minutes, the mixture was allowed to reach rt and left to stir overnight. The crude product was purified by silica column chromatography to afford **82** (42 mg, 71 %) as a pink solid.

R_f = 0.10 (dichloromethane/methanol 10:1)

^{1}H NMR (400 MHz, CD_3OD): δ = 0.84–1.01 (m, 1H), 1.22 (dd, 5H), 1.25–1.35 (m, 17H), 1.40–1.50 (m, 1H), 1.52–1.66 (m, 6H), 1.85 (td, 2H), 2.23 (t, 1H), 2.51–2.60 (m, 2H), 2.81 (s, 2H), 3.41–3.55 (m, 3H), 3.60–3.74 (m, 9H), 4.10–4.28 (m, 4H), 4.36 (ddd, 1H), 6.57 (t, 1H), 6.66 (d, 1H), 6.73–6.82 (m, 2H), 6.94–7.08 (m, 4H), 7.09–7.21 (m, 2H), 7.28 (tt, 1H), 7.37–7.55 (m, 2H), 7.84 (dddd, 2H), 8.26–8.36 (m, 1H) ppm.

HRMS calculated for $C_{58}H_{74}N_6O_9S_2$ $[M+H]^+$: m/z = 1062.4955, found: m/z = 1062.4865.

<u>Cleavable and fluorescently labeled bombesin(6-14) conjugate (**83**)</u>

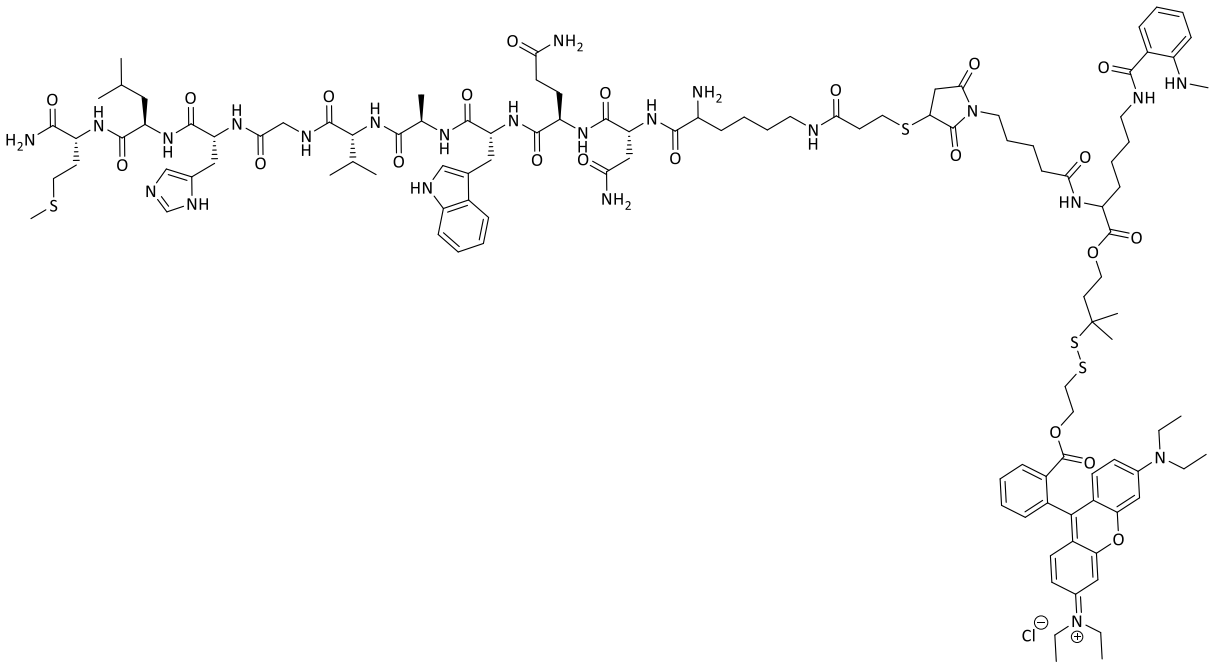

Compound **64** (6.5 mg, 0.01 mmol, 2 mM) was dissolved in dry DMF (1.15 mL). To that solution **82** (4.8 mg, 0.01 mmol) dissolved in dry DMF (1.15 mL) was added. The mixture was left to stir at rt for 6 d. The crude product was purified by an RP C18 column (water/methanol) to obtain **83** (5.3 mg, 54 %) as a pink solid.

t_R = 12.7 min (10 % ACN (2min)>15 min>95 %>5 min>100 % (10 min))

HRMS calculated for $C_{114}H_{163}N_{23}O_{22}S_4$ $[M+H]^{3+}$: m/z = 778.0409, found: m/z = 778.0419.

3.5. Conclusion

The selective targeting of bombesin conjugates towards GRPR-expressing cancer cells was presented. Quick and selective GRPR-mediated internalization of uncleavable, fluorescently labeled conjugate (**75**) by cancer cells was illustrated by fluorescence microscopy and flow cytometry. Fluorometric investigations about the cleavage of the cleavable conjugate **83** inside the cancer cells did not succeed due to technical reasons. In future work, the visualization might be enabled exploiting Förster resonance energy transfer (FRET). Thus, a donor fluorophore excites an acceptor fluorophore in the same linker system and the acceptor fluorophore might be detected. The energy transfer might be disrupted by the cleavage inside the cancer cells and just the donor fluorophore might be detected. Bombesin-toxin conjugates contained the linker system shown in chapter 2 that was modified substituting the dibromomaleimide by a maleimide, because the linker was designed to attach to a single thiol moiety in bombesin. The bombesin was used in its truncated form bombesin(6-14) to facilitate successful tethering to the linker system. Thus, multiple cleavable bombesin conjugates comprising tubugi 1 (**69**) and tubugi 4 (**70**), respectively, were successfully synthesized. Furthermore, three simplified bombesin-tubugi 4 conjugates (**71**, **72**, **73**) were synthesized possessing different alkyl chains in the linker system in order to anchor to the lipid cell membrane as well as to protect the disulfide bridge from reduction. The reduction of the disulfide bridge occurred under physiological conditions within 24 h in case of the conjugates based on the complex linker system (**69**, **70**). In case of the conjugates containing an alkyl-linker (**71**, **72**, **73**), the release of the drug occurred after 2 h (C_{18} alkyl chain, **71**) and 6 h (C_{12} and C_4 alkyl chain, **72** as well as **73**). Interestingly, a longer alkyl side chain did not protect the disulfide bridge from reduction hypothesizing that the C_{18} alkyl chain might anchor to the cell membrane or might move very dynamically leading to inefficient protection of the disulfide bridge. The cytotoxic studies elucidated that the bombesin-tubugi 1 conjugate (**69**) did not show an impact in concentrations below 10 µM, whereas the other four conjugates containing tubugi 4 (**70**, **71**, **72**, **73**) showed good activities and also good selectivity relative to the expression levels of gastrin-releasing peptide receptor. It was supposed that the relatively low activity of conjugate **69** might be explained by the loss of crucial acetyl group at C11 of the toxin. The most promising candidate, the simplified bombesin-tubugi 4-C_4 conjugate **73**, exhibited an IC_{50} value about 28.3 ± 2.0 nM and remained stable at least 6 h under physiological conditions inside the cancer cells. Comparing to conjugate **71** (C_{18} alkyl chain) and **72** (C_{12} alkyl chain), longer aliphatic side chains might lead to hindered receptor-mediated internalization as in case of conjugate **72** and to less stability of the disulfide bridge as in case of conjugate **71**. However, conjugate **71** showed rather good antitumor activity assuming beneficial effect of chain length on anchoring to cell membrane. Moreover, unspecific release of the toxin due to lower stability of the conjugate might lead to less selectivity regarding the GRPR expression level after longer incubation.

3.6. References

1. Anastasi, A.; Erspamer, V.; Bucci, M., Isolation and structure of bombesin and alytesin, 2 analogous active peptides from the skin of the European amphibians Bombina and Alytes. *Experientia* **1971,** *27* (2), 166-7.
2. Fleischmann, A.; Waser, B.; Gebbers, J. O.; Reubi, J. C., Gastrin-releasing peptide receptors in normal and neoplastic human uterus: involvement of multiple tissue compartments. *J Clin Endocrinol Metab* **2005,** *90* (8), 4722-9.
3. McDonald, T. J.; Nilsson, G.; Vagne, M.; Ghatei, M.; Bloom, S. R.; Mutt, V., A gastrin releasing peptide from the porcine nonantral gastric tissue. *Gut* **1978,** *19* (9), 767-74.
4. Kiaris, H.; Schally, A. V.; Nagy, A.; Sun, B.; Armatis, P.; Szepeshazi, K., Targeted cytotoxic analogue of bombesin/gastrin-releasing peptide inhibits the growth of H-69 human small-cell lung carcinoma in nude mice. *Br J Cancer* **1999,** *81* (6), 966-71.
5. Reubi, J. C., Peptide receptors as molecular targets for cancer diagnosis and therapy. *Endocr Rev* **2003,** *24* (4), 389-427.
6. Nagy, A.; Armatis, P.; Cai, R. Z.; Szepeshazi, K.; Halmos, G.; Schally, A. V., Design, synthesis, and in vitro evaluation of cytotoxic analogs of bombesin-like peptides containing doxorubicin or its intensely potent derivative, 2-pyrrolinodoxorubicin. *Proc Natl Acad Sci U S A* **1997,** *94* (2), 652-6.
7. Gargosky, S. E.; Wallace, J. C.; Upton, F. M.; Ballard, F. J., C-terminal bombesin sequence requirements for binding and effects on protein synthesis in Swiss 3T3 cells. *Biochem J* **1987,** *247* (2), 427-32.
8. Carney, D. N.; Cuttitta, F.; Moody, T. W.; Minna, J. D., Selective stimulation of small cell lung cancer clonal growth by bombesin and gastrin-releasing peptide. *Cancer Res* **1987,** *47* (3), 821-5.
9. Cuttitta, F.; Carney, D. N.; Mulshine, J.; Moody, T. W.; Fedorko, J.; Fischler, A.; Minna, J. D., Bombesin-like peptides can function as autocrine growth factors in human small-cell lung cancer. *Nature* **1985,** *316* (6031), 823-6.
10. Cassano, G.; Resta, N.; Gasparre, G.; Lippe, C.; Guanti, G., The proliferative response of HT-29 human colon adenocarcinoma cells to bombesin-like peptides. *Cancer Lett* **2001,** *172* (2), 151-7.
11. Nelson, J.; Donnelly, M.; Walker, B.; Gray, J.; Shaw, C.; Murphy, R. F., Bombesin stimulates proliferation of human breast cancer cells in culture. *Br J Cancer* **1991,** *63* (6), 933-6.
12. Wang, Q. J.; Knezetic, J. A.; Schally, A. V.; Pour, P. M.; Adrian, T. E., Bombesin may stimulate proliferation of human pancreatic cancer cells through an autocrine pathway. *Int J Cancer* **1996,** *68* (4), 528-34.
13. Reubi, J. C., Somatostatin and other Peptide receptors as tools for tumor diagnosis and treatment. *Neuroendocrinology* **2004,** *80 Suppl 1*, 51-6.
14. Van de Wiele, C.; Dumont, F.; Vanden Broecke, R.; Oosterlinck, W.; Cocquyt, V.; Serreyn, R.; Peers, S.; Thornback, J.; Slegers, G.; Dierckx, R. A., Technetium-99m RP527, a GRP analogue for visualisation of GRP receptor-expressing malignancies: a feasibility study. *Eur J Nucl Med* **2000,** *27* (11), 1694-9.
15. Scopinaro, F.; De Vincentis, G.; Varvarigou, A. D.; Laurenti, C.; Iori, F.; Remediani, S.; Chiarini, S.; Stella, S., 99mTc-bombesin detects prostate cancer and invasion of pelvic lymph nodes. *Eur J Nucl Med Mol Imaging* **2003,** *30* (10), 1378-82.
16. Okarvi, S. M., Peptide-based radiopharmaceuticals and cytotoxic conjugates: potential tools against cancer. *Cancer Treat Rev* **2008,** *34* (1), 13-26.
17. Markwalder, R.; Reubi, J. C., Gastrin-releasing peptide receptors in the human prostate: relation to neoplastic transformation. *Cancer Res* **1999,** *59* (5), 1152-9.
18. Sturzu, A.; Sheikh, S.; Echner, H.; Nagele, T.; Deeg, M.; Amin, B.; Schwentner, C.; Horger, M.; Ernemann, U.; Heckl, S., Rhodamine-marked bombesin: a novel means for prostate cancer fluorescence imaging. *Invest New Drugs* **2014,** *32* (1), 37-46.

19. Schwartsmann, G.; DiLeone, L. P.; Horowitz, M.; Schunemann, D.; Cancella, A.; Pereira, A. S.; Richter, M.; Souza, F.; da Rocha, A. B.; Souza, F. H.; Pohlmann, P.; De Nucci, G., A phase I trial of the bombesin/gastrin-releasing peptide (BN/GRP) antagonist RC3095 in patients with advanced solid malignancies. *Invest New Drugs* **2006,** *24* (5), 403-12.
20. Radulović, S.; Miller, G.; Schally, A. V., Inhibition of growth of HT-29 human colon cancer xenografts in nude mice by treatment with bombesin/gastrin releasing peptide antagonist (RC-3095). *Cancer Res* **1991,** *51* (21), 6006-9.
21. Schally, A. V.; Nagy, A., Cancer chemotherapy based on targeting of cytotoxic peptide conjugates to their receptors on tumors. *Eur J Endocrinol* **1999,** *141* (1), 1-14.
22. Tateishi, K.; Klee, G. G.; Cunningham, J. M.; Lennon, V. A., Stability of bombesin in serum, plasma, urine, and culture media. *Clin Chem* **1985,** *31* (2), 276-8.
23. Accardo, A.; Galli, F.; Mansi, R.; Del Pozzo, L.; Aurilio, M.; Morisco, A.; Ringhieri, P.; Signore, A.; Morelli, G.; Aloj, L., Pre-clinical evaluation of eight DOTA coupled gastrin-releasing peptide receptor (GRP-R) ligands for in vivo targeting of receptor-expressing tumors. *EJNMMI Res* **2016,** *6* (1), 17.
24. Begum, A. A.; Moyle, P. M.; Toth, I., Investigation of bombesin peptide as a targeting ligand for the gastrin releasing peptide (GRP) receptor. *Bioorg Med Chem* **2016,** *24* (22), 5834-5841.
25. Plonowski, A.; Nagy, A.; Schally, A. V.; Sun, B.; Groot, K.; Halmos, G., In vivo inhibition of PC-3 human androgen-independent prostate cancer by a targeted cytotoxic bombesin analogue, AN-215. *Int J Cancer* **2000,** *88* (4), 652-7.
26. Hermanson, G. T., *Bioconjugate Techniques*. San Diego, California, USA, 1996.
27. Ducry, L.; Stump, B., Antibody-drug conjugates: linking cytotoxic payloads to monoclonal antibodies. *Bioconjug Chem* **2010,** *21* (1), 5-13.
28. Langer, M.; Kratz, F.; Rothen-Rutishauser, B.; Wunderli-Allenspach, H.; Beck-Sickinger, A. G., Novel peptide conjugates for tumor-specific chemotherapy. *J Med Chem* **2001,** *44* (9), 1341-8.
29. Menger, F. M.; Guo, Y.; Lee, A. S., Synthesis of a lipid/peptide/drug conjugate: N4-(acylpeptidyl)-ara-C. *Bioconjug Chem* **1994,** *5* (2), 162-6.
30. Banerjee, S.; Kundu, A., Lipid-drug conjugates: a potential nanocarrier system for oral drug delivery applications. *Daru* **2018,** *26* (1), 65-75.
31. Morales, F. E.; Garay, H. E.; Munoz, D. F.; Augusto, Y. E.; Otero-Gonzalez, A. J.; Reyes Acosta, O.; Rivera, D. G., Aminocatalysis-Mediated on-Resin Ugi Reactions: Application in the Solid-Phase Synthesis of N-Substituted and Tetrazolo Lipopeptides and Peptidosteroids. *Org Lett* **2015,** *17* (11), 2728-31.
32. Beija, M.; Afonso, C. A.; Martinho, J. M., Synthesis and applications of Rhodamine derivatives as fluorescent probes. *Chem Soc Rev* **2009,** *38* (8), 2410-33.
33. Terai, T.; Nagano, T., Small-molecule fluorophores and fluorescent probes for bioimaging. *Pflugers Arch* **2013,** *465* (3), 347-59.
34. DeAngelis, P. L., Polysaccharide labeling with N-methylisatoic anhydride: generation of ultraviolet chromophores and blue fluorophores. *Anal Biochem* **2000,** *284* (1), 167-9.
35. The Broad Institute of MIT & Harvard, Cancer Cell Line Encyclopedia, https://portals.broadinstitute.org/ccle/. (accessed 17.06.2020).
36. Pu, F.; Qiao, J.; Xue, S.; Yang, H.; Patel, A.; Wei, L.; Hekmatyar, K.; Salarian, M.; Grossniklaus, H. E.; Liu, Z.-R.; Yang, J. J., GRPR-targeted Protein Contrast Agents for Molecular Imaging of Receptor Expression in Cancers by MRI. *Sci Rep* **2015,** *5* (16214).
37. Doose, S.; Neuweiler, H.; Sauer, M., A close look at fluorescence quenching of organic dyes by tryptophan. *Chemphyschem* **2005,** *6* (11), 2277-85.
38. Preusentanz, R.; ad. Wessjohann, L. A. Synthese von Tubulysin-Derivaten, -Chimären und -Konjugaten mit Targeting-Komponenten. Dissertation, Martin Luther University Halle-Wittenberg, 2016.

39. Tumey, L. N.; Leverett, C. A.; Vetelino, B.; Li, F.; Rago, B.; Han, X.; Loganzo, F.; Musto, S.; Bai, G.; Sukuru, S. C.; Graziani, E. I.; Puthenveetil, S.; Casavant, J.; Ratnayake, A.; Marquette, K.; Hudson, S.; Doppalapudi, V. R.; Stock, J.; Tchistiakova, L.; Bessire, A. J.; Clark, T.; Lucas, J.; Hosselet, C.; O'Donnell, C. J.; Subramanyam, C., Optimization of Tubulysin Antibody-Drug Conjugates: A Case Study in Addressing ADC Metabolism. *ACS Med Chem Lett* **2016,** *7* (11), 977-982.
40. Gleue, L.; Schupp, J.; Zimmer, N.; Becker, E.; Frey, H.; Tuettenberg, A.; Helm, M., Stability of Alkyl Chain-Mediated Lipid Anchoring in Liposomal Membranes. *Cells* **2020,** *9* (10).

4. Peptide-drug conjugates based on a CXCR4-targeting peptide

4.1. Introduction

The naturally occurring peptide EPI-X4 (endogenous peptide inhibitor of CXCR4) comprising 16 amino acids was identified by screening of peptide libraries of human hemofiltrate that remained after dialysis of patients with renal disease in order to find bioactive peptides against HIV-1 infection. This novel peptide suppressing the internalization of HIV-1 is produced from the albumin precursor by proteases under acidic conditions. Since local acidification is referred to inflammatory processes and cancer, the correlation between several diseases and EPI-X4 has been investigated (Figure 4.1a).[1-4] Associated with Graft-versus-host disease (GVHD) which often follows hematopoietic cell transplantation, this blood-derived peptide was spotted in urine up to 15 days before the development of GVHD. Thus, EPI-X4 indicates renal inflammation, because it is produced to act against inflammatory processes. Exploiting this evidence, EPI-X4 might be applied as an urinary peptide biomarker in order to detect late acute GVHD.[5] Beside its antiinflammatory effect, interesting relationships to proliferative processes of malignant cells allow the development of strategies to treat cancer.[1, 2, 4-7] This novel peptide binds highly selectively as an antagonist to the G protein-coupled receptor CXCR4 and competes for binding with CXCL12, the endogenous ligand of the CXCR4 receptor. As consequence of the specific binding, the EPI-X4 suppresses the receptor signaling of CXCR4 induced by CXCL12.[1, 2] Inhibition of the CXCR4-CXCL12 signaling pathway is supposed to affect cancer-related processes, for example migration and invasion of tumor cells, suggesting an antimetastatic effect of EPI-X4. Moreover, the CXCR4-CXCL12 axis has been demonstrated to support the drug-resistance of proliferative cells.[1, 4, 8]

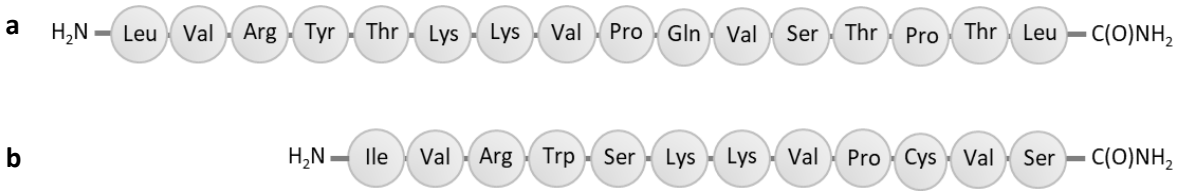

Figure 4.1 Amino acid sequences of a) EPI-X4 and b) WSC02.

The CXC-motif-chemokine receptor 4 (CXCR4) belongs to the 7-transmembrane domain family of G protein-coupled receptors (GPCRs) and is endogenously activated by the chemokine CXCL12. This well studied interaction plays a crucial role in many physiological processes, e.g. trafficking and homeostasis of immune cells as well as cell activation, proliferation and chemotaxis causing organogenesis and hematopoiesis.[1, 3, 6, 8-10] CXCR4 is expressed in many cells, especially in proliferating cells, and an up-regulated expression causes many diseases. Thus, CXCR4 occurs with high expression levels in numerous tumors, for instance colon cancer, breast cancer, prostate and kidney cancer as well as cancer stem cells.[4, 6, 7, 11-14] It is important to consider that CXCR4 is also involved in embryogenesis, limiting the range of its application as a tool against cancer.[6, 10] Due to the correlation of CXCR4 to many diseases, various antagonists have been developed. The synthetic T140 has been already tested in preclinical trials and used for radiolabel-based visualization. Further examples display the humanized antibody MDX1338 and so called nanobodies. The so far most prominent and already clinically applied CXCR4 antagonist is the bicyclam analogue AMD3100

(Figure 4.2) which was initially discovered in 1990s as an agent against HIV, but was also proven to be effective against cancer.[2, 7, 13, 15]

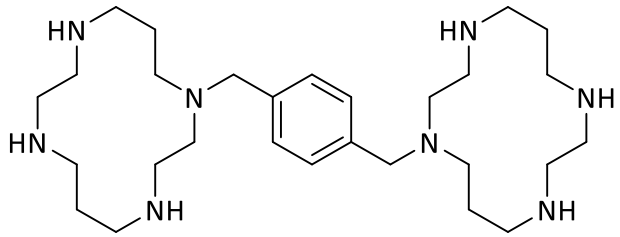

Figure 4.2 Structure of the clinically applied CXCR4 antagonist AMD3100.

Since CXCR4 is involved in the growth of many tumors and EPI-X4 has been shown to be a highly promising antagonist blocking CXCR4, this correlation can be exploited for drug-targeting. By using a computational modeling approach, the structure of EPI-X4 was optimized in order to circumvent the problem regarding the short half-life of around 17 min in human plasma. It was elucidated that the monomeric derivative WSC02 (Figure 4.1b) shows high stability in human plasma and represents a proper candidate.[1, 4, 9, 14, 16]

4.2. Synthetic strategy

The novel WSC02 peptide was found to possess promising targeting properties towards CXCR4-overexpressing cancer cells. In order to investigate the potential of its usability in applied drug targeting tubugi 1 and tubugi 4 toxins were linked to the WSC02 monomer peptide. The conjugation of the peptide to toxins was performed via the multiple cleavable linker-spacer system that was already presented in chapter 3.2.1. The linker-spacer system was designed to remain intact under physiological conditions, while it is supposedly cleaved off within various types of tumor cells. Thus, different trigger points were built in to spark decomposition under reductive conditions or by certain enzymes, e.g. cathepsin B, or in acidic environment. Moreover, fluorescently labeled WSC02 conjugates were synthesized to conduct fluorometric cell viability assays.

4.2.1. Synthesis of multiple cleavable peptide-drug conjugates

The sequence of WSC02 (**84**) contains one cysteine which can directly be exploited for attachment to the maleimide containing linker-spacer system (**59**). The linker **59** presented in chapter 3.2.1 was attached to the cysteine of WSC02 by forming a thioether via MICHAEL-type addition. Afterwards, the protected sulfhydryl moiety in the linker part was reduced by TCEP yielding peptide **85** (Scheme 4.1a). The addition of tubugis activated by the introduction of pyridin-2-yldisulfanyl group (**36**, **37**) led to the formation of disulfide bridges to the thiol of peptide **85** via thiol–disulfide exchange resulting in **86** and **87** (Scheme 4.1b).

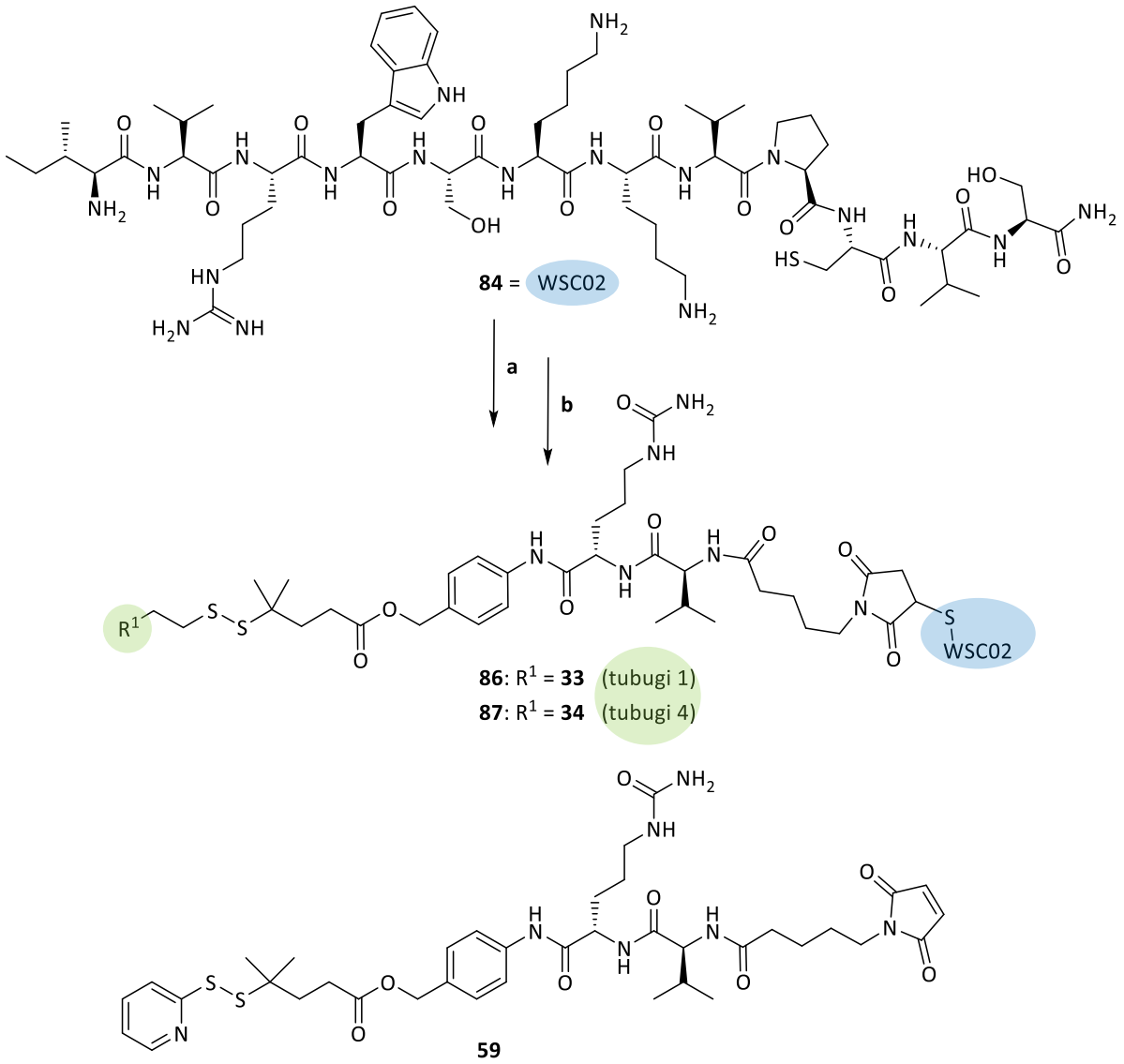

Scheme 4.1 a) **59**, TCEP, rt, 4 d, in DPBS; b) **36**/**37**, rt, 7 d, in DMF, 42 % (**86**)/37 % (**87**).

4.2.2. Synthesis of fluorescently-labeled peptide conjugates

Non-toxic fluorescently-labeled WSC02 conjugates were synthesized in order to semi-quantify and to visualize the CXCR4-mediated internalization of the peptide-toxin conjugates and the cleavage behavior inside the cancer cells over time.

An uncleavable WSC02-rhodamine B conjugate was synthesized to semi-quantify and to evaluate the receptor-mediated internalization by flow cytometry.[17] Rhodamine B was linked to maleimide via an amide linker as presented in chapter 3.2.3. This modified rhodamine B (**74**) was attached to peptide **84** via MICHAEL-type addition towards the free thiol of WSC02 obtaining the red-fluorescent, uncleavable WSC02 conjugate **88** (Scheme 4.2).

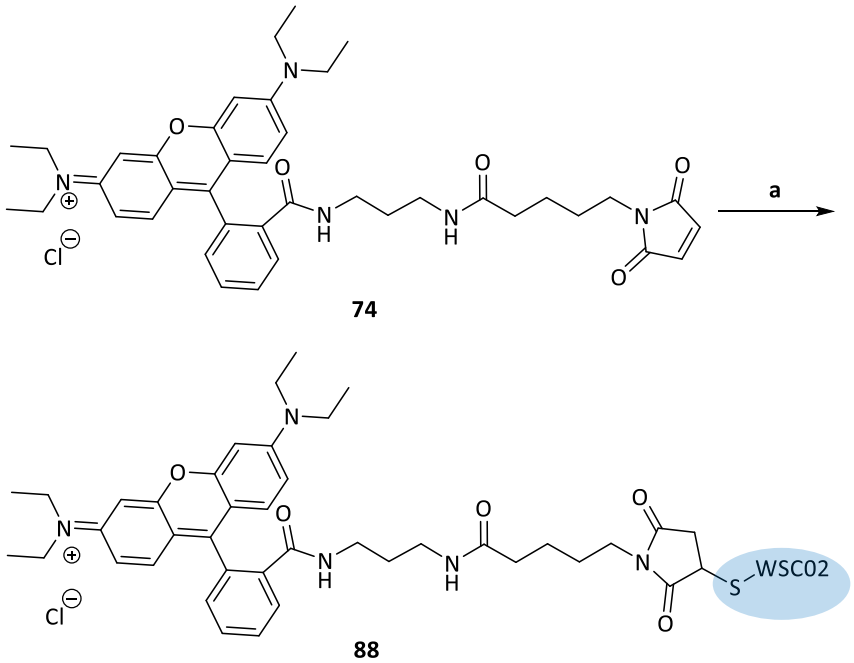

Scheme 4.2 a) **84**, rt, 2 d, in DMF, 47 %.

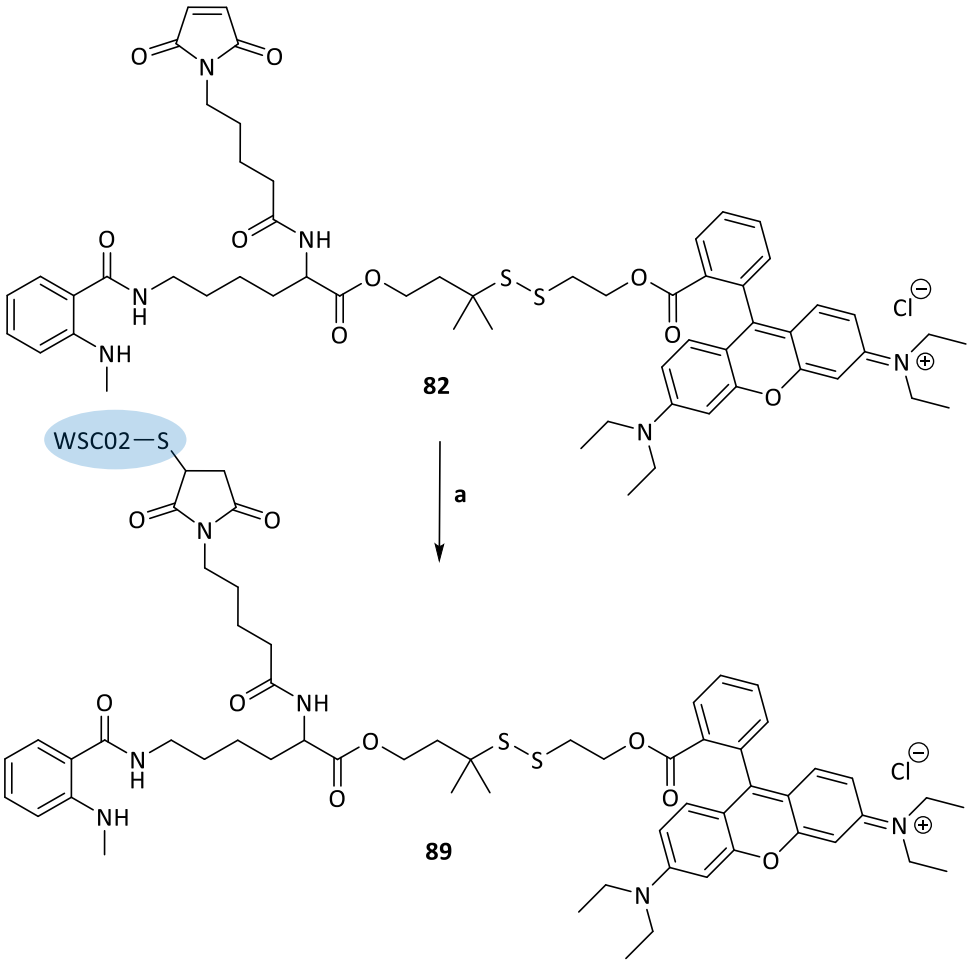

Scheme 4.3 a) **84**, rt, 3 d, in DMF, 74 %.

A cleavable fluorescently-labeled WSC02 conjugate was synthesized to study the cleavage of the disulfide bridge inside the cancer cells after internalization. As presented in chapter 3.2.3, the conjugate was designed to consist of two fluorophores connected via a cleavable linker-spacer system mimicking that of the bioactive conjugates. The peptide part of the conjugate was blue dye-tagged using *N*-methyl isatoic anhydride (MIA) and the drug position was red dye-labeled using rhodamine B.[18, 19] Thus, the building block **82** comprising MIA as well as rhodamine B was conjugated to peptide **84** via MICHAEL-type addition forming the double-labeled WSC02 conjugate **89** (Scheme 4.3).

4.3. Biological evaluation

The internalization of fluorescently labeled WSC02 conjugates and the cleavage of the linker-spacer system inside the cancer cells were investigated by fluorescence microscopy and flow cytometry. Cell viability assays were conducted to investigate the conjugates' antiproliferative efficacy against CXCR4-expressing tumor cells and to correlate those results with the different CXCR4 expression levels (high, moderate, low) of the cells. The treatment time dependency of the antitumor effect was evaluated as well.

4.3.1. Studies on cellular internalization of fluorescent peptide conjugates

The correlation between receptor-mediated internalization of fluorescently labeled WSC-based conjugates and the incubation time as well as the expression levels of the CXCR4 receptor in cancer cells was studied by fluorescence measurements. RT-qPCR analyses were carried out in triplicate to evaluate the expression of CXCR4 in the investigated tumor cell lines. Indeed, the relative expression levels throughout the cell lines, as shown in Figure 4.3, corresponded to published data base values.[20] Moreover, according to published data the expression levels determined by RT-qPCR were in good agreement to membrane-specific ELISA tests reflecting receptor protein levels at the cell surfaces of the tumor cell lines.[21] However, independent ELISA assays were not conducted within this work.

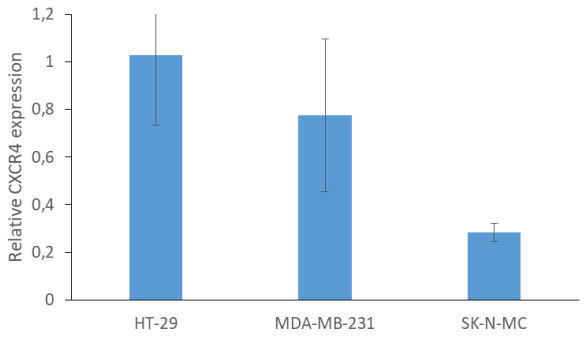

Figure 4.3 Expression levels of CXCR4 in HT-29 colon cancer cells, MDA-MB-231 breast cancer cells and SK-N-MC Ewing's sarcoma cells.

The non-toxic fluorescent conjugates containing different linker systems were synthesized and used to visualize their receptor-mediated internalization into viable tumor cells over 6 h. Fluorescence microphotographs were taken and showed internalized uncleavable fluorescent WSC02 conjugate (**88**) as red-fluorescent spots inside the cells (Figure 4.4). The conjugate **88** entered the cells within

30 min and the spotted localization of rhodamine B bound to WSC02 inside the cells might display that the conjugate remained after endocytosis in endosomal vesicles at higher concentrations. In surrounding culture medium fluorescent **88** was not detected due to rapid and efficient internalization.

Flow cytometric analyses were performed to semi-quantify the conjugate internalization. For that purpose, the CXCR4-overexpressing HT-29 cancer cells were treated with conjugate **88** for 1 min, 1 h and 6 h. As reference, CXCR4 lower expressing SK-N-MC cancer cells were treated with conjugate **88** for 6 h. After finalized incubation, the fluorescent compound was removed, the cells were washed and trypsinized. After that, cells were rinsed with tryptophan (100 mM in water/acetonitrile 2:1) to quench exposed rhodamine fluorescence to ensure visualization of only

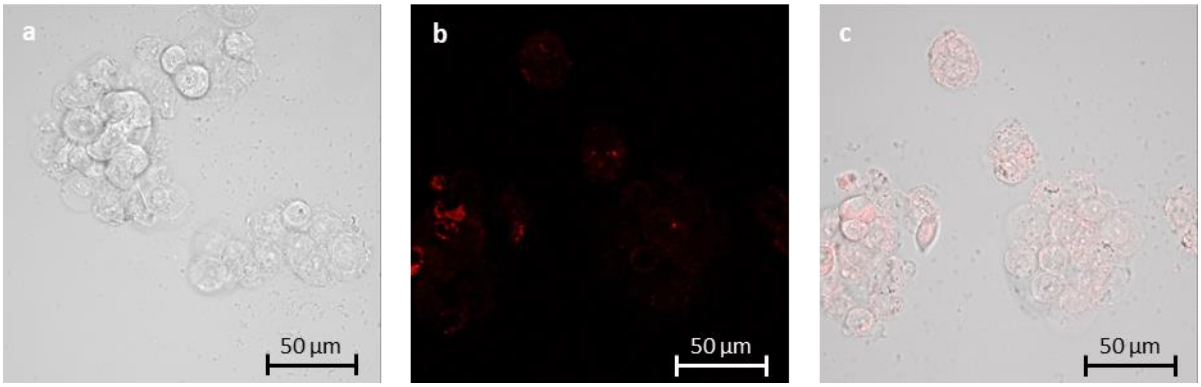

Figure 4.4 Fluorescence microphotographs of a) untreated HT-29 cells, b) HT-29 cells treated with red-fluorescent **88** after 30 min of incubation and c) merged image of HT-29 cells with internalized red-fluorescent **88** (after 30 min treatment).

such fluorophores which are internalized (see Appendix III, Figure A 135), not fluorophores that might still be bound unspecifically to the outer cell surface.[22] After 1 min incubation – virtually representing a "no internalization" control albeit comprising exposure of the cells with conjugate – 1.1-fold increased internalization by HT-29 cells over untreated HT-29 cells was observed (Table 4.1). A strong jump of internalization occurred between 1 min and 1 h (Figure 4.5a). Interestingly, the fluorescent conjugate **88** was taken up by the CXCR4 higher expressing cells (HT-29) and the CXCR4 lower expressing cells (SK-N-MC) to approximately the same extent (Figure 4.5b), although RT-qPCR analyses revealed distinguishable expressions levels of CXCR4 in tested cancer cells (Figure 4.3). A reason for that observation might be the antagonistic behavior of WSC02 to CXCR4 receptor leading to weak receptor-mediated internalization despite higher expression levels of CXCR4 in HT-29 cells.

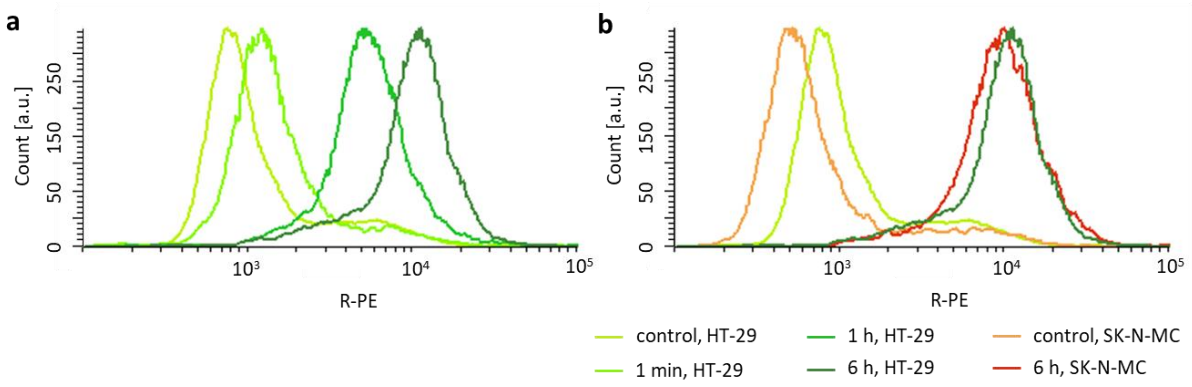

Figure 4.5 Flow cytometric analyses of **88** a) at different incubation times on HT-29 cancer cell line, b) comparison between internalization into CXCR4 higher expressing cancer cell line (HT-29, green) and CXCR4 lower expressing cancer cell line (SK-N-MC, red) after 6 h.

However, it has not been clarified yet for this ligand-CXCR4 correlation – in case of other GPCR as well –, whether only agonistic binding to CXCR4 will trigger an internalization.[23, 24] Presumed an efficient binding of the ligand WSC02 to CXCR4, but weak influence on the internalization, the strong internalization of conjugate **88** by SK-N-MC might be attributed to another mechanism inducing endocytosis. Because SK-M-MC Ewing's sarcoma cells are known to internalize receptors efficiently compared to other cancer cells, the conjugate **88** bound to CXCR4 might be passively internalized.[25]

Table 4.1 Relative quantification of the cellular internalization of fluorescent conjugate **88** in HT-29 cancer cells in relation to untreated cells and SK-N-MC tumor cells expressing CXCR4 less.

	88	
	RFU[10]	x-fold over untreated
1 min, HT-29	22.64	1.09
30 min, HT-29	45.36	2.18
1 h, HT-29	70.72	3.40
6 h, HT-29	121.60	5.84
6 h, SK-N-MC	120.71	8.41

The cleavable WSC02 conjugate **89** was applied to HT-29 cells expressing high level of CXCR4 in order to observe the cleavage under physiological conditions inside the cancer cells. The idea was to visualize the decomposition of the conjugate due to the separation of the conjugate into a blue-labeled peptide part and a red-labeled payload part by reduction of the disulfide bridge. Fluorescence spectra were recorded to determine excitation and emission wavelengths of both fluorophores and to ensure that MIA (λ_{ex} = 222 nm, λ_{em} = 428 nm) and rhodamine B (λ_{ex} = 545 nm,

[10] relative fluorescent unit

λ_{em} = 576 nm) do not interfere (see in Appendix III, Figure A 133 & 136). HT-29 cells were exposed to conjugate **89** and were observed by laser scanning confocal microscope. A distinguishable detection of both fluorescent fragments after cleavage could not be achieved due to limited resolution of the microscope. Considering the available technical conditions, the usability of the concept to visualize the cleavage *in vitro* by separate excitation of two fluorophores appears limited.

4.3.2. Evaluation of the cytotoxic activity of the WSC02 peptide-drug conjugates

Investigations regarding the efficacy of the synthesized WSC02-tubugi conjugates (**86**, **87**) as well as pure tubugi 1 (**33**), the spacer containing tubugi 1 (**36**), tubugi 4 (**34**), the spacer containing tubugi 4 (**37**) and WSC02 peptide (**84**) as reference compounds were performed. Thus, those compounds were applied to cancer cell lines expressing various densities of CXCR4 receptor (high, medium, low) on their cell membrane to check for correlation between expression levels of CXCR4 and the efficacy of the conjugates.

All cell viability tests on selected tumor cell lines were carried out in biological and technical triplicates and analyzed by resazurin-based fluorometric assay. The concentrations for dilution series of testing compounds were chosen in range of the IC_{50} values of the tubugi derivatives.[26] Moreover, the cells were treated with the compounds for different initial incubation times (6, 24, 72 h) to get insights in the progress of impact to the cells. Irrespective of the initial incubation time, the cells were allowed to grow for 72 h post treatment initialization until cell viability was measured. In case of initial compound incubation shorter than these 72 h – i.e. 6 h and 24 h incubation, respectively – incubation solutions were discarded, cells were washed and allowed to grow in fresh, test compound-free culture medium until measurement after 72 h. The conjugate containing tubugi 1 (**86**) had a much stronger impact to the cancer cells than the conjugates containing tubugi 4 (**87**) (Figure 4.6). This observation might be attributed to the more lipophilic moiety at position C11 of the toxin **34**. An interaction between the more lipophilic moiety of **34** and the receptor might lead to decelerated internalization of conjugate **87**. Hence, conjugate **87** might unfold its activity more slowly. Although a selectivity regarding the expression level of CXCR4 could not be elucidated by flow cytometry applying a fluorescent WSC02 conjugate, a distinguishable efficacy in dependence on the expression level of CXCR4 was more obvious after 6 h than after 24 h and 72 h. After longer incubation times the IC_{50} values after 24 h and 72 h assimilated in case of **86** and **87** (Figure 4.6c, e and d, f, see Appendix IV, Tables A 14 & 15) as in case of the conjugates based on octreotide and CNGRC (chapter 2.3.2), because unspecific release of toxins from the PDCs might affect cancer cells during longer incubation in spite of distinguishable target expression levels. Thereby, IC_{50} values equaled after longer incubation. Moreover, endocytosis active cells like SK-N-MC cancer cells might internalize intact PDCs rapidly leading to higher IC_{50} value after longer incubation. All synthesized conjugates were found to be stable in a 10 mM glutathione solution at 37 °C for more than 6 h. The cleavage product was detected after 24 h using ESI MS assuming that unspecific release of the toxin outside the cancer cells might not be explained by the reduction of the disulfide bridge. The effect of **86** as well as **87** to MDA-MB-231 breast cancer cell line remained after 24 h and 72 h on similar level. Thus, the correlation between expression level of CXCR4 and WSC02-drug conjugates was not as evident as after 6 h (see in Appendix IV, Table A 14 & 15). Moreover, the sigmoidal curves of MDA-MB-231 breast cancer cell line indicated that a plateau at 20–40 % cell viability was reached assuming that the conjugates did not lead to a cytotoxic, but just to a cytostatic effect. In that context, the 20–40 % cell viability correlates to the initial MDA-MB-231

cell confluency at the point when the treatment was started (time point 0). Even the biological evaluation of pure tubugis revealed that tubugis caused a cytostatic effect to MDA-MB-231 cancer cells (see in Appendix IV, Figure A 155 & 156).

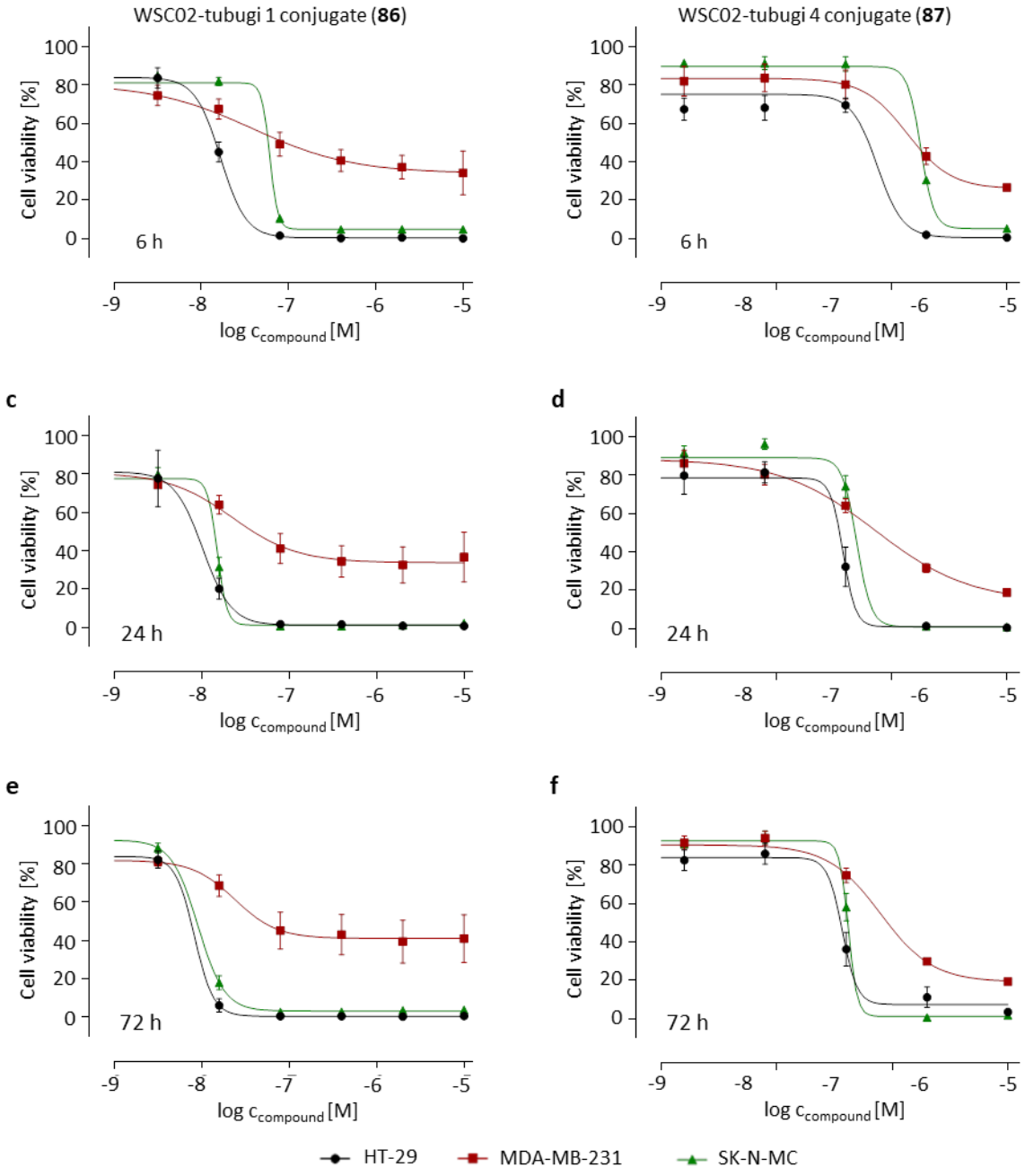

Figure 4.6 *In vitro* antitumor activity of **86** after a) 6, c) 24, e) 72 h initial treatment and of **87** after b) 6, d) 24 and f) 72 h initial treatment in HT-29 colon cancer cells (high CXCR4), MDA-MB-231 breast cancer cells (medium CXCR4) and SK-N-MC Ewing's sarcoma cells (low CXCR4) (for CXCR4 expression see Figure 4.3).[11]

The peptide itself (**84**) did not show any effect to the cells. The tubugis **33** and **34** were effective against cancer cells in nano- and picomolar range (see Appendix IV, Table A 1 & 3). Not surprisingly,

[11] This extract zooms in on the inflection points representing the IC_{50} values. The full size graphs are seen in Appendix IV, Figure A 164.

the attached self-immolative spacer compound (**36**, **37**) decreased the activity of the free tubugis 3- to 4-fold in case of **36** (see Appendix IV, Table A 2) and 10- to 20-fold in case of **37** (see Appendix IV, Table A 4), respectively.

4.4. Experimental part

The used materials, applied analytical methods as well as the protocols of biological assays are described in detail in chapter 2.4. The syntheses of several compounds and building blocks mentioned in this chapter are already described in chapter 2.4 as well.

4.4.1. Syntheses of peptides and conjugates

Peptide WSC02 (**84**)

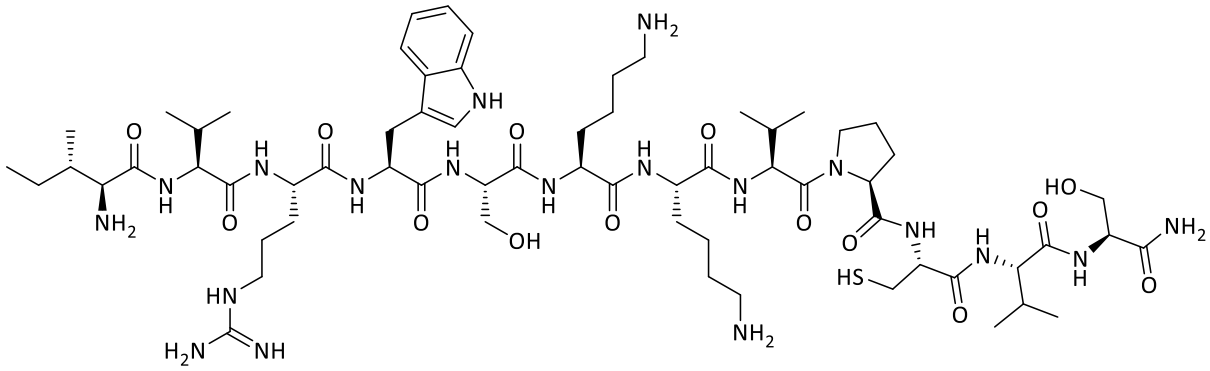

Compound **84** was synthesized according to the general procedure **G1** in 100 µmol scale on Fmoc-Rink-Amid-MBHA resin (149.3 mg, loading: 0.67 mmol/g). The cleavage was performed as described in **G1** (> 95 % purity). The peptide was used in following syntehsis without further purification.

^{1}H NMR (500 MHz, DMSO-d6): δ = 0.76–0.95 (m, 22H), 1.09 (ddt, 1H), 1.21–1.38 (m, 3H), 1.43–1.58 (m, 2H), 1.62 (m, 1H), 1.67–2.09 (m, 5H), 2.37 (dd, 1H), 2.67–2.83 (m, 2H), 2.95 (dd, 1H), 3.01–3.16 (m, 3H), 3.47–3.64 (m, 4H), 3.65–3.78 (m, 2H), 4.14–4.41 (m, 6H), 4.46 (m, 1H), 4.64 (m, 1H), 6.95 (t, 1H), 7.01–7.10 (m, 2H), 7.11–7.27 (m, 2H), 7.32 (d, 1H), 7.56 (d, 1H), 7.75 (t, 1H), 7.81 (s, 5H), 7.79–7.97 (m, 5H), 8.11 (ddt, 7H), 8.35 (d, 1H), 10.79 (d, 1H) ppm.

^{13}C NMR (126 MHz, DMSO-d6): δ = 11.0, 14.4, 17.8, 18.0, 18.3, 19.1, 19.1, 19.2, 22.1, 22.3, 22.6, 23.9, 24.5, 25.0, 26.0, 26.6, 26.7, 27.8, 29.1, 30.1, 30.5, 30.6, 31.2, 36.3, 38.4, 38.7, 39.6, 39.8, 39.9, 40.4, 52.2, 52.4, 53.0, 54.9, 55.6, 56.1, 57.8, 59.3, 61.6, 61.9, 109.7, 111.2, 115.8, 118.1, 118.4, 120.8, 123.5, 124.2, 127.4, 136.0, 156.9, 158.4, 158.7, 167.8, 169.3, 169.8, 170.0, 170.4, 171.0, 171.2, 171.6, 171.7, 171.9 ppm.

t_R = 8.0 min (10 % ACN (2min)>15 min 95 %>5 min 100 %>100 % (5 min))

HRMS calculated for $C_{64}H_{110}N_{19}O_{14}S$ $[M+H]^{2+}$: m/z = 700.9141, found: m/z = 700.9163.

WSC02 containing linker system (**85**)

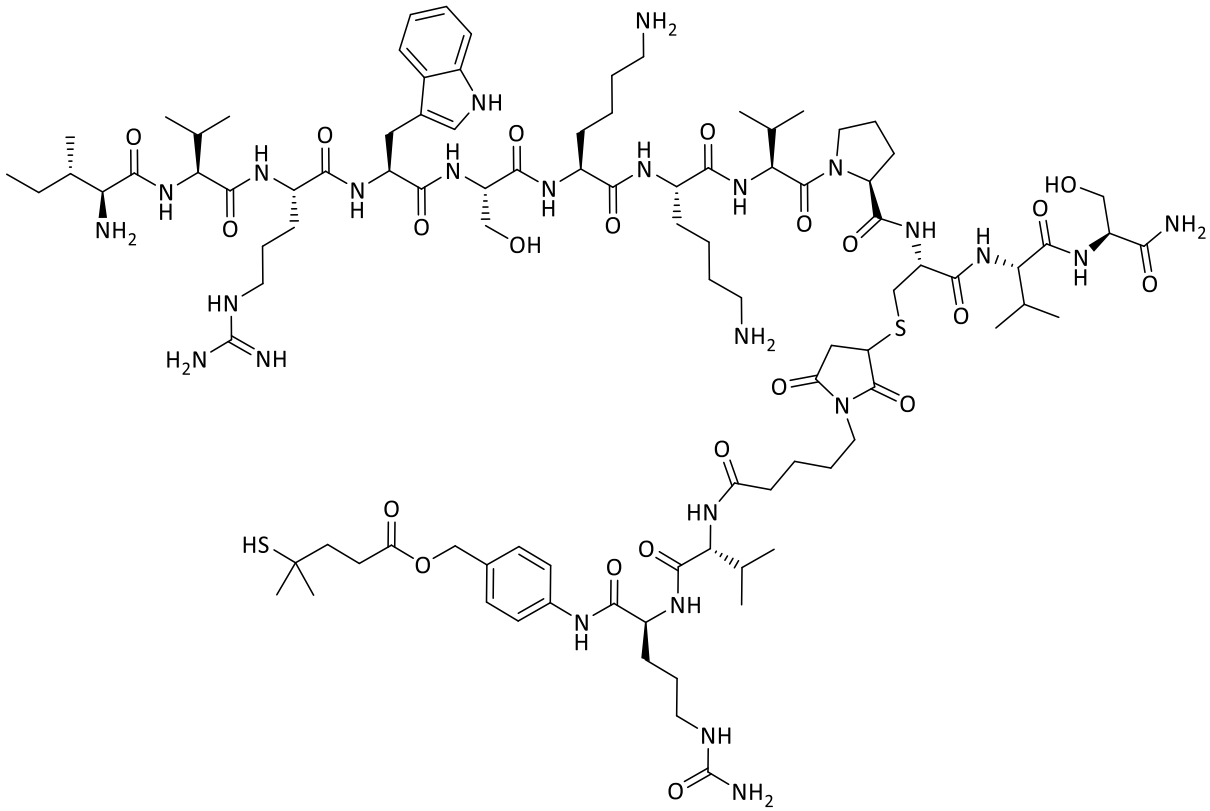

Compound **84** (40.0 mg, 0.03 mmol) was dissolved in DPBS (1.28 mL) and then **59** (21.4 mg, 0.03 mmol) dissolved in DMF (2.83 mL) was added dropwise. The mixture was left to stir for 4 d.

HRMS calculated for $C_{102}H_{164}N_{26}O_{22}S_3$ $[M+H]^{4+}$: m/z = 550.2921, found: m/z = 550.2937.

TCEP (8.8 mg, 0.03 mmol) was added and the mixture was left to stir for 24 h. The solvent were removed under reduced pressure to afford crude **85** as a colorless solid.

^{1}H NMR (400 MHz, DMSO-d6): δ = 0.77–0.95 (m, 12H), 0.98–1.16 (m, 1H), 1.27 (d, 6H), 1.47 (d, 4H), 1.81 (d, 2H), 1.85–2.01 (m, 4H), 2.22 (t, 3H), 2.38–2.51 (m, 5H), 2.54 (s, 6H), 2.59–2.68 (m, 2H), 2.73 (d, 32H), 2.89 (m, 25H), 3.06 (m, 1H), 3.15–3.24 (m, 2H), 3.50–3.80 (m, 2H), 4.22 (s, 2H), 4.28 (m, 1H), 4.62 (d, 1H), 5.01 (d, 1H), 5.44 (d, 1H), 6.95 (t, 1H), 7.05 (dd, 2H), 7.16–7.23 (m, 1H), 7.30 (dd, 2H), 7.53–7.66 (m, 2H), 7.69–7.80 (m, 1H), 7.95 (s, 8H), 8.32–8.42 (m, 1H), 10.81 (s, 1H) ppm.

HRMS calculated for $C_{97}H_{160}N_{25}O_{22}S_2$ $[M+H]^{3+}$: m/z = 697.0539, found: m/z = 697.0560.

Conjugate containing **85** and tubugi 1 (**86**)

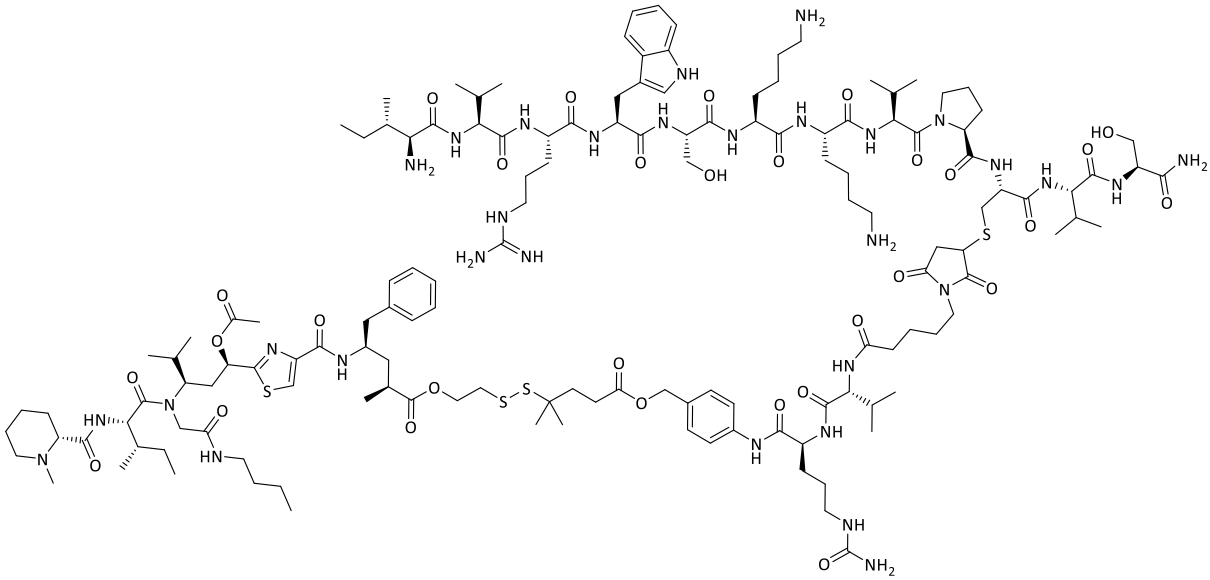

Compound **85** (15.0 mg, 0.01 mmol, 5 mM) was dissolved in dry DMF (0.65 mL). Then solution **36** (6.8 mg, 0.01 mmol) dissolved in dry DMF (0.65 mL) was added. The mixture was left to stir at rt for 7 d. The crude product was purified by an RP C18 column (water/methanol) to obtain **86** (8 mg, 42 %) as a colorless solid.

t_R = 9.0 min (10 % ACN (2min)>15 min 95 %>5 min 100 %>100 % (5 min))

HRMS calculated for $C_{142}H_{229}N_{31}O_{30}S_4$ $[M+H]^{4+}$: m/z = 744.1559, found: m/z = 744.1564.

Conjugate containing **85** and tubugi 4 (**87**)

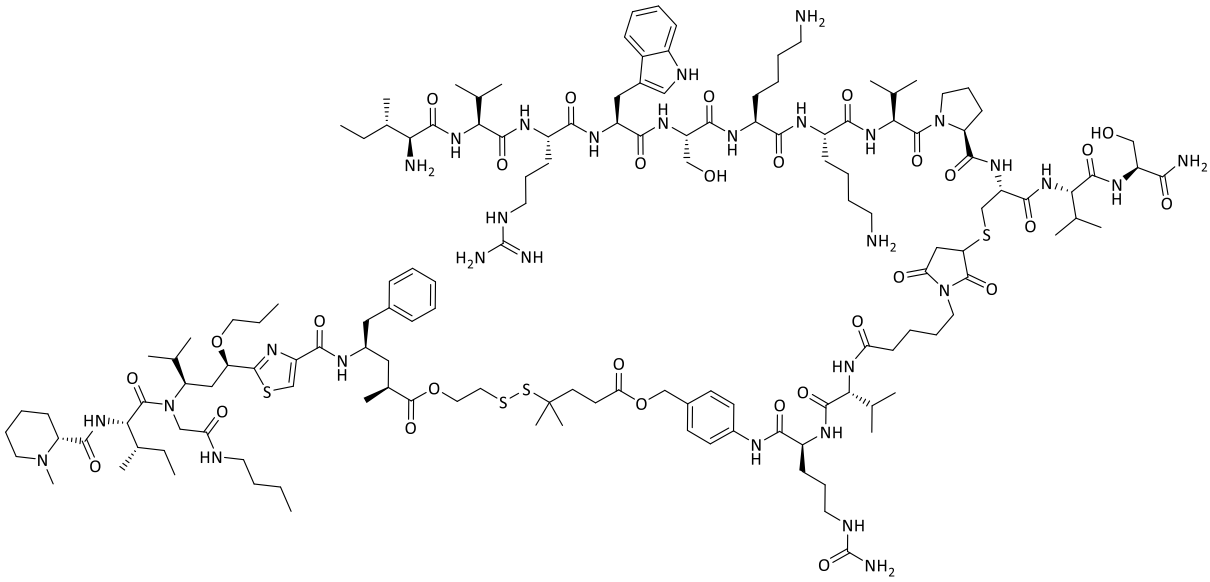

Compound **85** (15.0 mg, 0.01 mmol, 5 mM) was dissolved in dry DMF (0.65 mL). To that solution **37** (6.8 mg, 0.01 mmol) dissolved in dry DMF (0.65 mL) was added. The mixture was left to stir at rt

for 7 d. The crude product was purified by an RP C18 column (water/methanol) to obtain **87** (7 mg, 37 %) as a colorless solid.

t_R = 8.9 min (10 % ACN (2min)>15 min 95 %>5 min 100 %>100 % (5 min))

HRMS calculated for $C_{143}H_{233}N_{31}O_{29}S_4$ $[M+H]^{4+}$: m/z = 744.1650, found: m/z = 744.1645.

4.4.2. Syntheses of fluorophore conjugates

Rhodamine B labeled WSC02 (**88**)

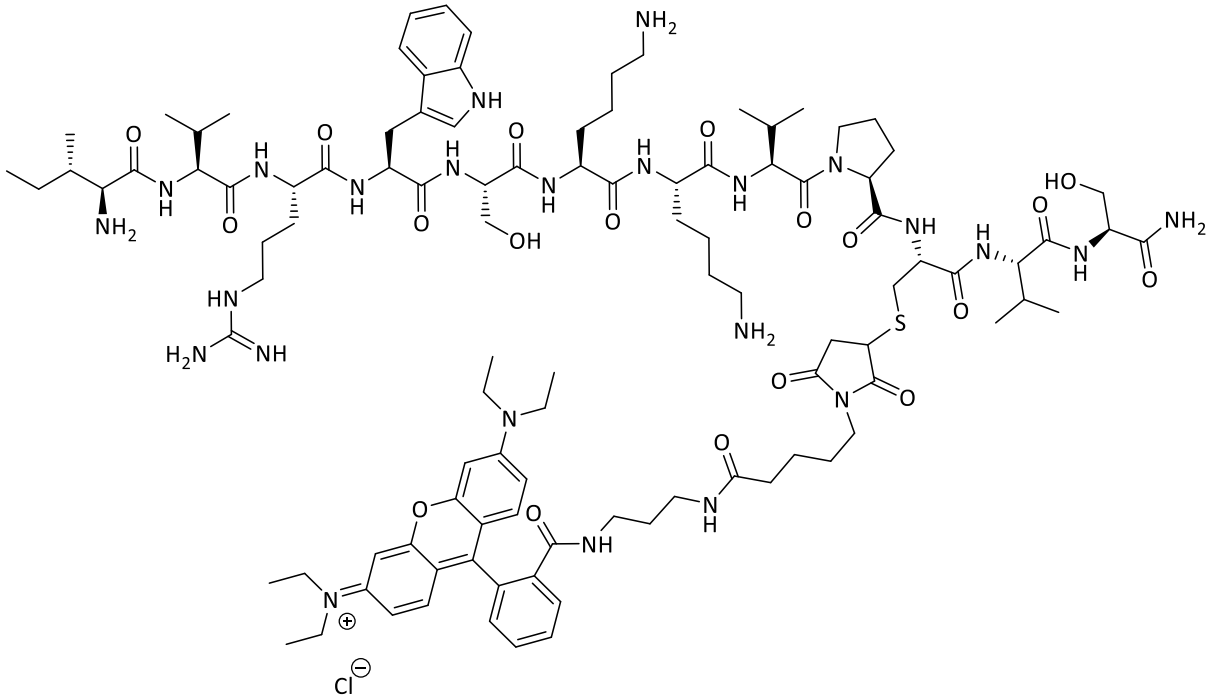

Compound **84** (50.0 mg, 0.03 mmol, 5 mM) was dissolved in dry DMF (3.39 mL). To that solution **82** (40.3 mg, 0.05 mmol) dissolved in dry DMF (3.39 mL) was added dropwise. The mixture was left to stir at rt for 2 d. The crude product was purified by an RP C18 column (water/methanol) to afford **88** (51 mg, 47 %) as a pink solid.

t_R = 10.9 min (10 % ACN (2min)>15 min>95 %>5 min>100 % (10 min))

HRMS calculated for $C_{104}H_{161}N_{24}O_{19}S$ $[M+H]^{3+}$: m/z = 520.5523, found: m/z = 520.5516.

Cleavable and fluorescently labeled WSC02 conjugate (**89**)

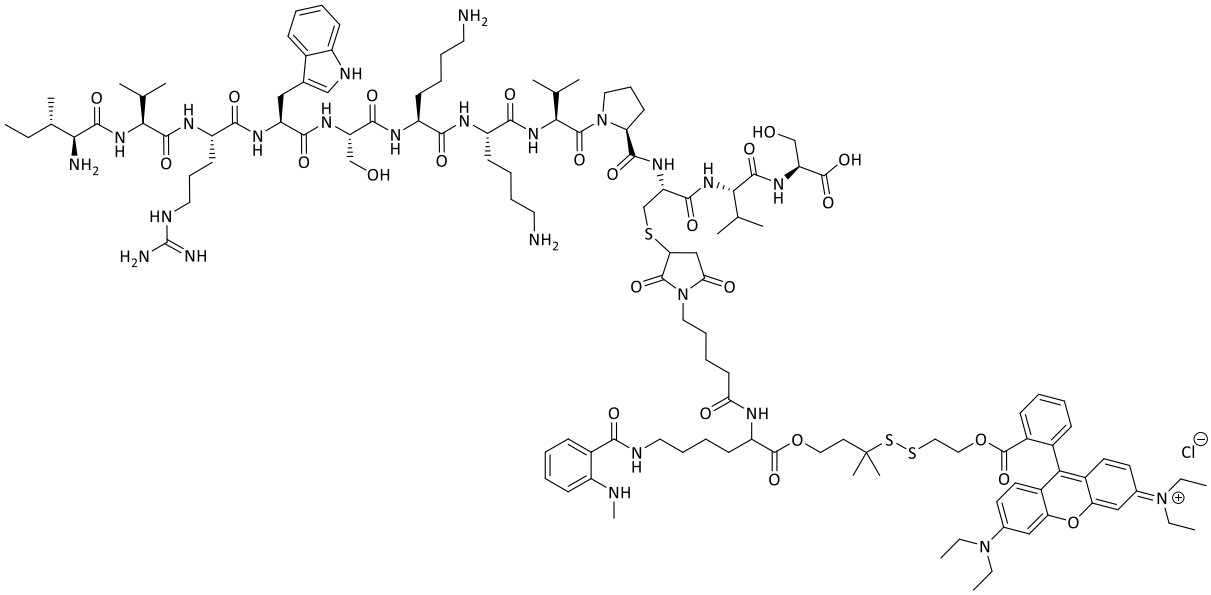

Compound **84** (2.5 mg, 0.002 mmol, 2 mM) was dissolved in dry DMF (0.43 mL). To that solution **80** (3.3 mg, 0.002 mmol) dissolved in dry DMF (0.43 mL) was added. The mixture was left to stir at rt for 3 d. The crude product was purified by an RP C18 column (water/methanol) to obtain **89** (2.8 mg, 74 %) as a pink solid.

t_R = 11.5 min (10 % ACN (2min)>15 min>95 %>5 min>100 % (10 min))

HRMS calculated for $C_{122}H_{185}N_{24}O_{24}S_3$ $[M+H]^{4+}$: m/z = 615.5709, found: m/z = 615.5812.

4.5. Conclusion

The novel WSC02 monomer peptide was presented as targeting peptide towards CXCR4-overexpressing cancer cells. A quick internalization of non-toxic, uncleavable, fluorescently labeled conjugate (**88**) was demonstrated and semi-quantified by fluorescence microscopy and flow cytometry. Though, a selective CXCR4-mediated internalization was not revealed by fluorescence measurements. CXCR4 higher expressing cancer cells (HT-29) and CXCR4 lower expressing cancer cells (SK-N-MC) internalized conjugate **88** in similar dimension after 6 h. This finding might be attributed to the antagonistic property of the WSC02 monomer peptide to CXCR4 hypothesizing that WSC02 selectively targeted the receptor, but did not trigger the internalization. Thus, other unspecific endocytotic mechanisms, for instance rapid receptor recycling like in CXCR4 lower expressing SK-N-MC Ewing's sarcoma cells, might lead to internalization of conjugate **88** and might compensate lower receptor expression. The cleavage of non-toxic, cleavable, fluorescently labeled conjugate **89** inside the cancer cells was supposed to be observed by fluorescence microscopy, but did not succeed due to technical reasons. In future work, the visualization might be rendered possible using a donor fluorophore, exciting an acceptor fluorophore in the same linker system by Förster resonance energy transfer (FRET). The energy transfer might be disrupted by the cleavage inside the cancer cells. Thus, only the donor fluorophore might be detected. The multiple cleavable linker-spacer system shown in chapter 3.2.1 was applied to conjugate the tubugi toxins to the novel

CXCR4-targeting peptide WSC02. The resulting two conjugates (**86**, **87**) were verified to be cleaved within 24 h under reductive conditions mimicking a reductive environment inside cancer cells. Despite of the lacking selectivity shown by flow cytometry, the cell viability assays on WSC02-tubugi conjugates afforded tremendous toxic effects against the tumor cell lines depending on expression level and incubation time. The results of the bioassays indicated a selectivity of the WSC02 conjugate corresponding to the results of the RT-qPCR. The WSC02-tubugi 1 (**86**) conjugate had the strongest activity, since an IC_{50} value about 8.3 ± 2.5 nM was determined. The observations by fluorometric analyses and by cell viability assays were conflicting, but might be explained by considering the properties of fluorescently labeled conjugate **88** and WSC02-tubugi conjugates **86** and **87**. Thus, the internalization of conjugates might be favored by lipophilic tubugi toxins, whereas the internalization of the more hydrophilic rhodamine B conjugate entered more slowly.

4.6. References

1. Zirafi, O.; Kim, K. A.; Standker, L.; Mohr, K. B.; Sauter, D.; Heigele, A.; Kluge, S. F.; Wiercinska, E.; Chudziak, D.; Richter, R.; Moepps, B.; Gierschik, P.; Vas, V.; Geiger, H.; Lamla, M.; Weil, T.; Burster, T.; Zgraja, A.; Daubeuf, F.; Frossard, N.; Hachet-Haas, M.; Heunisch, F.; Reichetzeder, C.; Galzi, J. L.; Perez-Castells, J.; Canales-Mayordomo, A.; Jimenez-Barbero, J.; Gimenez-Gallego, G.; Schneider, M.; Shorter, J.; Telenti, A.; Hocher, B.; Forssmann, W. G.; Bonig, H.; Kirchhoff, F.; Münch, J., Discovery and characterization of an endogenous CXCR4 antagonist. *Cell Rep* **2015,** *11* (5), 737-47.
2. Zirafi, O.; Hermann, P. C.; Münch, J., Proteolytic processing of human serum albumin generates EPI-X4, an endogenous antagonist of CXCR4. *J Leukoc Biol* **2016,** *99* (6), 863-8.
3. Münch, J.; Standker, L.; Forssmann, W. G.; Kirchhoff, F., Discovery of modulators of HIV-1 infection from the human peptidome. *Nat Rev Microbiol* **2014,** *12* (10), 715-22.
4. Buske, C.; Kirchhoff, F.; Münch, J., EPI-X4, a novel endogenous antagonist of CXCR4. *Oncotarget* **2015,** *6* (34), 35137-8.
5. Müller, J. A.; Zirafi, O.; Roan, N. R.; Lee, S. J.; Münch, J., Evaluation of EPI-X4 as a urinary peptide biomarker for diagnosis and prognosis of late acute GvHD. *Bone Marrow Transplant* **2016,** *51* (8), 1137-9.
6. Xu, C.; Zhao, H.; Chen, H.; Yao, Q., CXCR4 in breast cancer: oncogenic role and therapeutic targeting. *Drug Des Devel Ther* **2015,** *9*, 4953-64.
7. Chatterjee, S.; Behnam Azad, B.; Nimmagadda, S., The intricate role of CXCR4 in cancer. *Adv Cancer Res* **2014,** *124*, 31-82.
8. Zhou, Y.; Cao, H. B.; Li, W. J.; Zhao, L., The CXCL12 (SDF-1)/CXCR4 chemokine axis: Oncogenic properties, molecular targeting, and synthetic and natural product CXCR4 inhibitors for cancer therapy. *Chin J Nat Med* **2018,** *16* (11), 801-810.
9. Teicher, B. A.; Fricker, S. P., CXCL12 (SDF-1)/CXCR4 pathway in cancer. *Clin Cancer Res* **2010,** *16* (11), 2927-31.
10. Pozzobon, T.; Goldoni, G.; Viola, A.; Molon, B., CXCR4 signaling in health and disease. *Immunol Lett* **2016,** *177*, 6-15.
11. Xu, C.; Zheng, L.; Li, D.; Chen, G.; Gu, J.; Chen, J.; Yao, Q., CXCR4 overexpression is correlated with poor prognosis in colorectal cancer. *Life Sci* **2018,** *208*, 333-340.
12. Lv, S.; Yang, Y.; Kwon, S.; Han, M.; Zhao, F.; Kang, H.; Dai, C.; Wang, R., The association of CXCR4 expression with prognosis and clinicopathological indicators in colorectal carcinoma patients: a meta-analysis. *Histopathology* **2014,** *64* (5), 701-12.
13. Peng, D.; Cao, B.; Zhou, Y. J.; Long, Y. Q., The chemical diversity and structure-based evolution of non-peptide CXCR4 antagonists with diverse therapeutic potential. *Eur J Med Chem* **2018,** *149*, 148-169.

14. Furusato, B.; Mohamed, A.; Uhlen, M.; Rhim, J. S., CXCR4 and cancer. *Pathol Int* **2010,** *60* (7), 497-505.
15. Van Hout, A.; Klarenbeek, A.; Bobkov, V.; Doijen, J.; Arimont, M.; Zhao, C.; Heukers, R.; Rimkunas, R.; de Graaf, C.; Verrips, T.; van der Woning, B.; de Haard, H.; Rucker, J. B.; Vermeire, K.; Handel, T.; Van Loy, T.; Smit, M. J.; Schols, D., CXCR4-targeting nanobodies differentially inhibit CXCR4 function and HIV entry. *Biochem Pharmacol* **2018,** *158*, 402-412.
16. Romero-Molina, S.; Ruiz-Blanco, Y. B.; Harms, M.; Münch, J.; Sanchez-Garcia, E., PPI-Detect: A support vector machine model for sequence-based prediction of protein-protein interactions. *J Comput Chem* **2019,** *40* (11), 1233-1242.
17. Terai, T.; Nagano, T., Small-molecule fluorophores and fluorescent probes for bioimaging. *Pflugers Arch* **2013,** *465* (3), 347-59.
18. DeAngelis, P. L., Polysaccharide labeling with N-methylisatoic anhydride: generation of ultraviolet chromophores and blue fluorophores. *Anal Biochem* **2000,** *284* (1), 167-9.
19. Chen, X.; Wu, Q.; Henschke, L.; Weber, G.; Weil, T., An efficient and versatile approach for the preparation of a rhodamine B ester bioprobe library. *Dyes Pigm* **2012,** *94*, 296–303.
20. The Broad Institute of MIT & Harvard, Cancer Cell Line Encyclopedia, https://portals.broadinstitute.org/ccle/. (accessed 17.06.2020).
21. Zhou, W.-H.; Wu, X.; Hu, W.-D.; Du, M.-R., Co-expression of CXCR4 and CXCR7 in human endometrial stromal cells is modulated by steroid hormones. *Int J Clin Exp Pathol* **2015,** *8* (3), 2449-2460.
22. Doose, S.; Neuweiler, H.; Sauer, M., A close look at fluorescence quenching of organic dyes by tryptophan. *Chemphyschem* **2005,** *6* (11), 2277-85.
23. Feng, Y. H.; Ding, Y.; Ren, S.; Zhou, L.; Xu, C.; Karnik, S. S., Unconventional homologous internalization of the angiotensin II type-1 receptor induced by G-protein-independent signals. *Hypertension* **2005,** *46* (2), 419-25.
24. Drake, M. T.; Shenoy, S. K.; Lefkowitz, R. J., Trafficking of G protein-coupled receptors. *Circ Res* **2006,** *99* (6), 570-82.
25. Gicquiaux, H.; Lecat, S.; Gaire, M.; Dieterlen, A.; Mely, Y.; Takeda, K.; Bucher, B.; Galzi, J. L., Rapid internalization and recycling of the human neuropeptide Y Y(1) receptor. *J Biol Chem* **2002,** *277* (8), 6645-55.
26. Preusentanz, R.; ad. Wessjohann, L. A. Synthese von Tubulysin-Derivaten, -Chimären und -Konjugaten mit Targeting-Komponenten. Dissertation, Martin Luther University Halle-Wittenberg, 2016

Appendix I: Register of internal IPB codes of compounds

Chapter 2

Compound number	IPB code PAJ
1	477
2	484
3	492
4	432
5	147
6	150
7	172
8	174
9	154a
10	270
11	281
13	470
14	481
15	485
17	386
18	105
19	114
20	115
21	116
22	119
23	155
24	156
25	488
26	173
27	446
28	175
29	416
30	186
31	487
32	208
33	213
34	495
35	299
36	309
37	572
38	458
39	294
40	362
41	210
42	518
43	330
44	515
45	388
46	393
47	610
48	579
49	594
50	595
51	541
52	596
53	597
54	661
55	665
56	668
57	667

Chapter 3

Compound number	IPB code PAJ
58	560
59	561
60	536
61	524
62	100
63	319
64	603 & 605
65	608
66	577 & 585
67	546 & 549
68	547 & 550
69	612
70	613
71	591
72	592
73	593
74	664
75	669
76	442
77	209
78	621
79	526
80	622
81	643
82	646
83	653

Chapter 4

Compound number	IPB code PAJ
84	569
85	601
86	606
87	607
88	666
89	650

Appendix II: NMR spectra

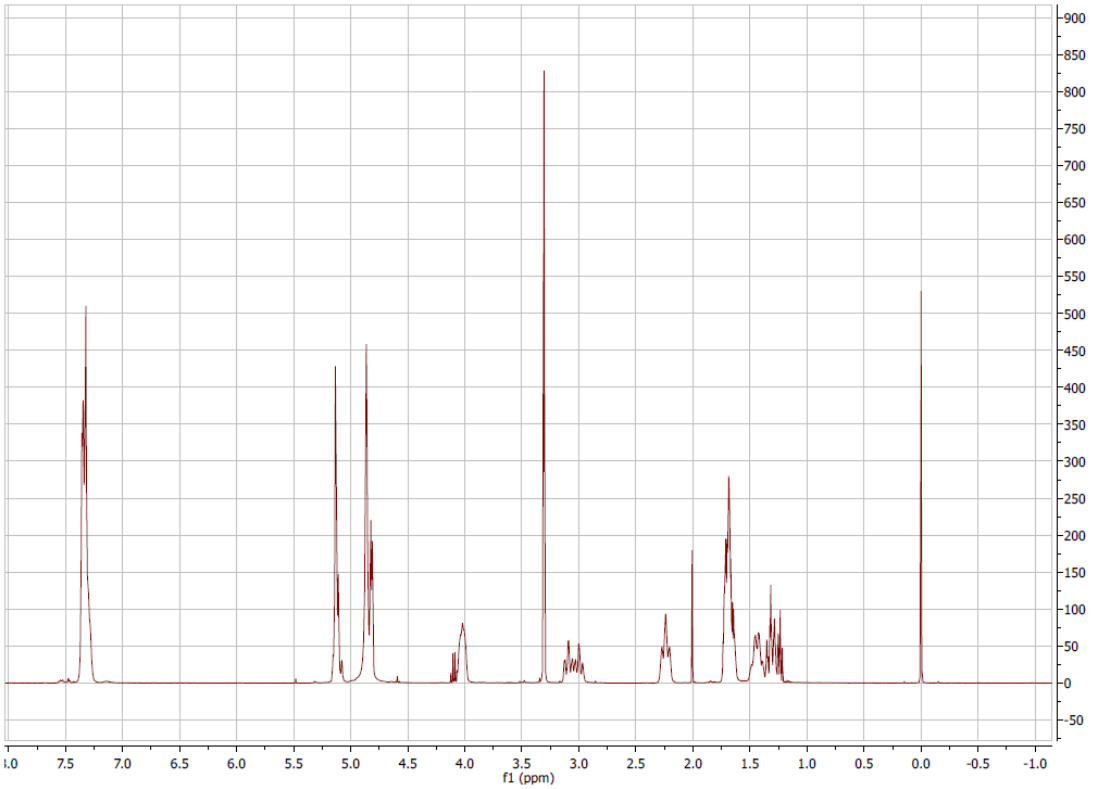

Figure A 1 ^{1}H spectrum (400 MHz, CD_3OD) of compound **1**.

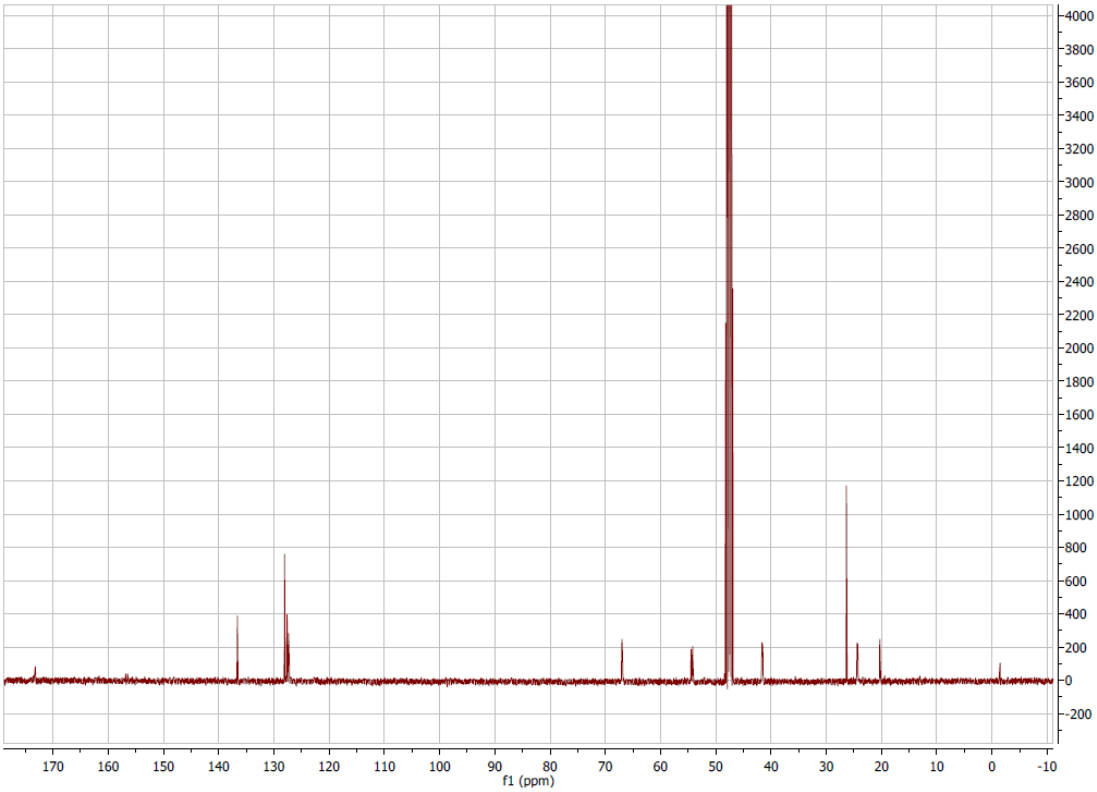

Figure A 2 ^{13}C spectrum (101 MHz, CD_3OD) of compound **1**.

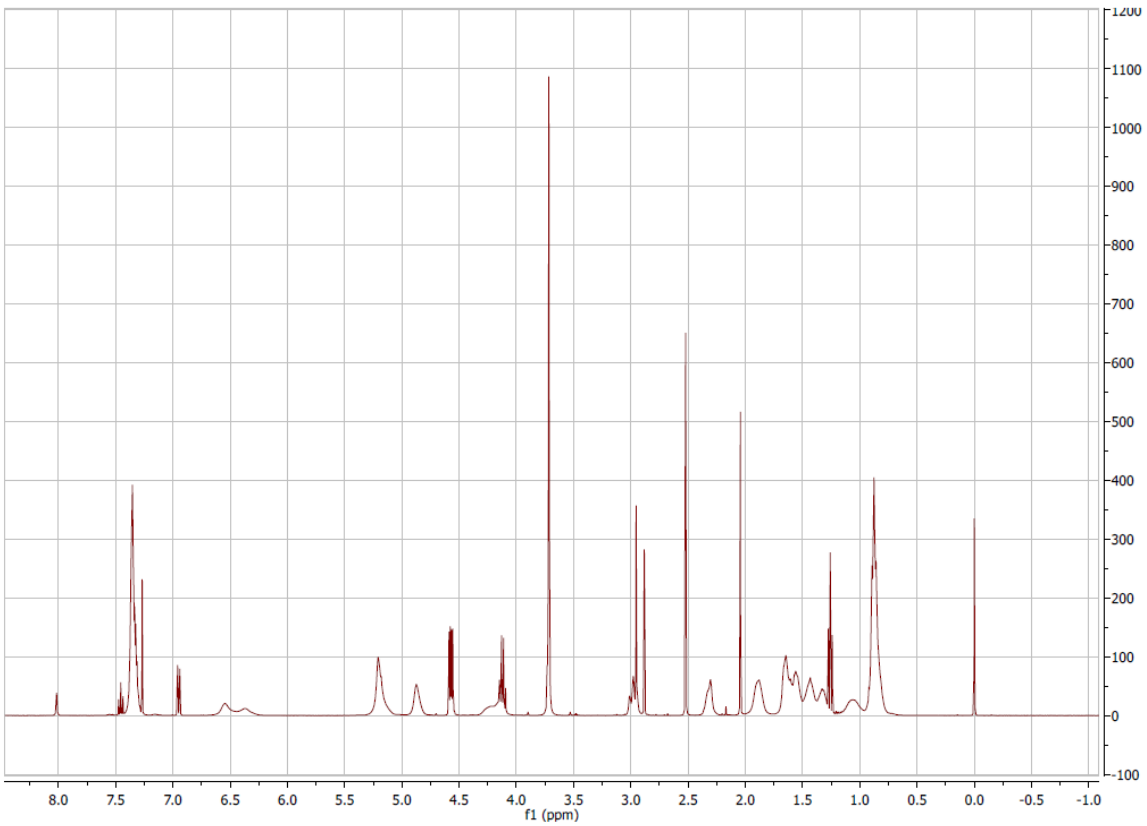

Figure A 3 ^{1}H spectrum (400 MHz, $CDCl_3$) of compound **2**.

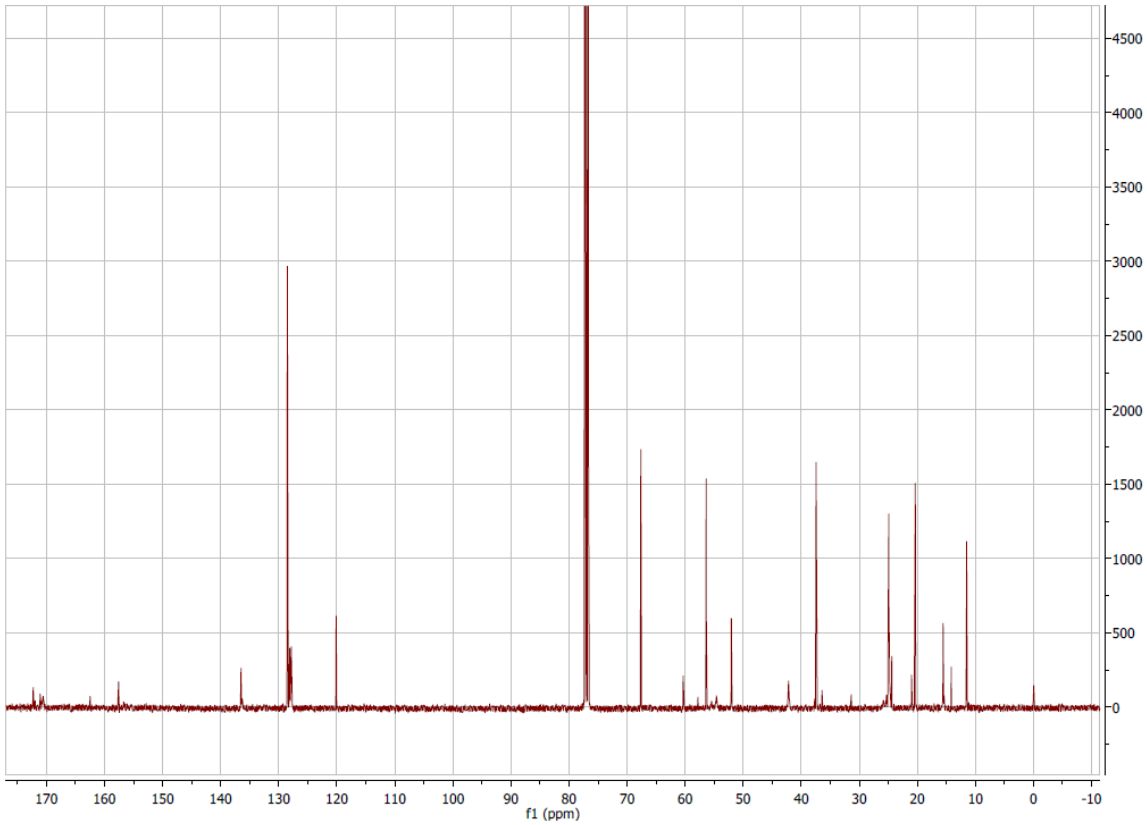

Figure A 4 ^{13}C spectrum (101 MHz, $CDCl_3$) of compound **2**.

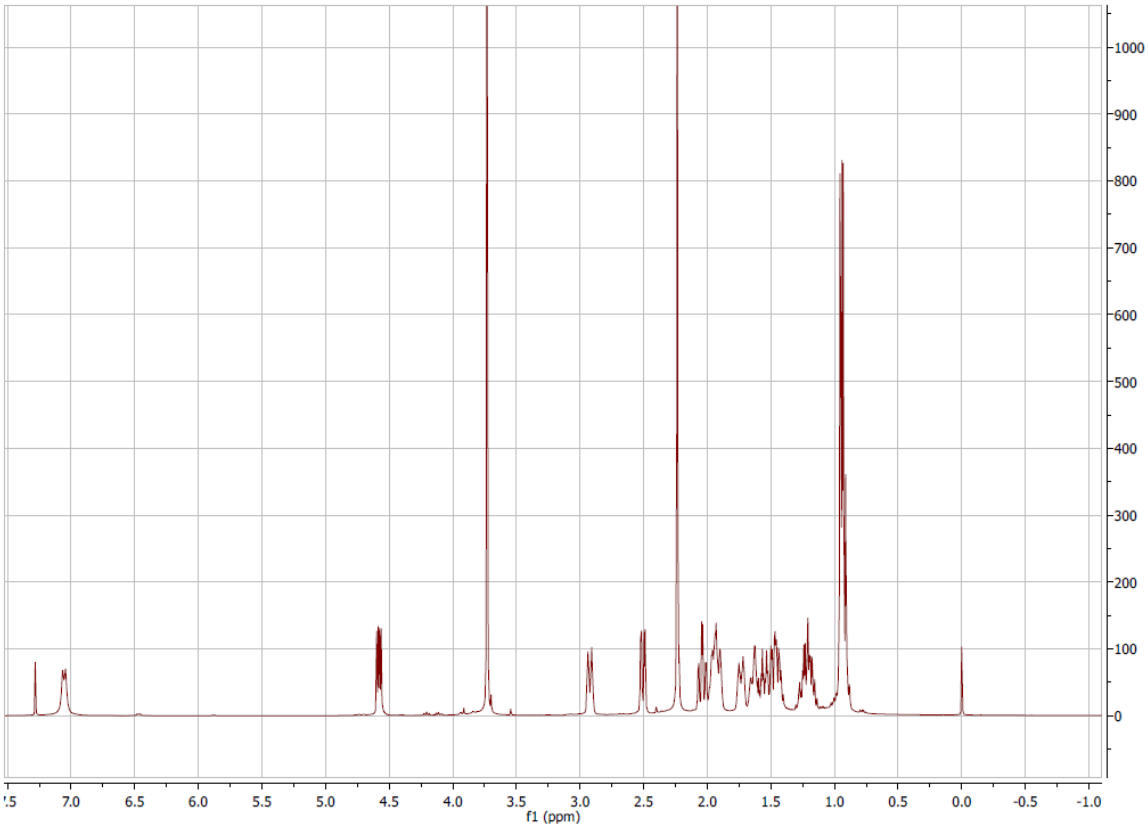

Figure A 5 ^{1}H spectrum (400 MHz, $CDCl_3$) of compound **3**.

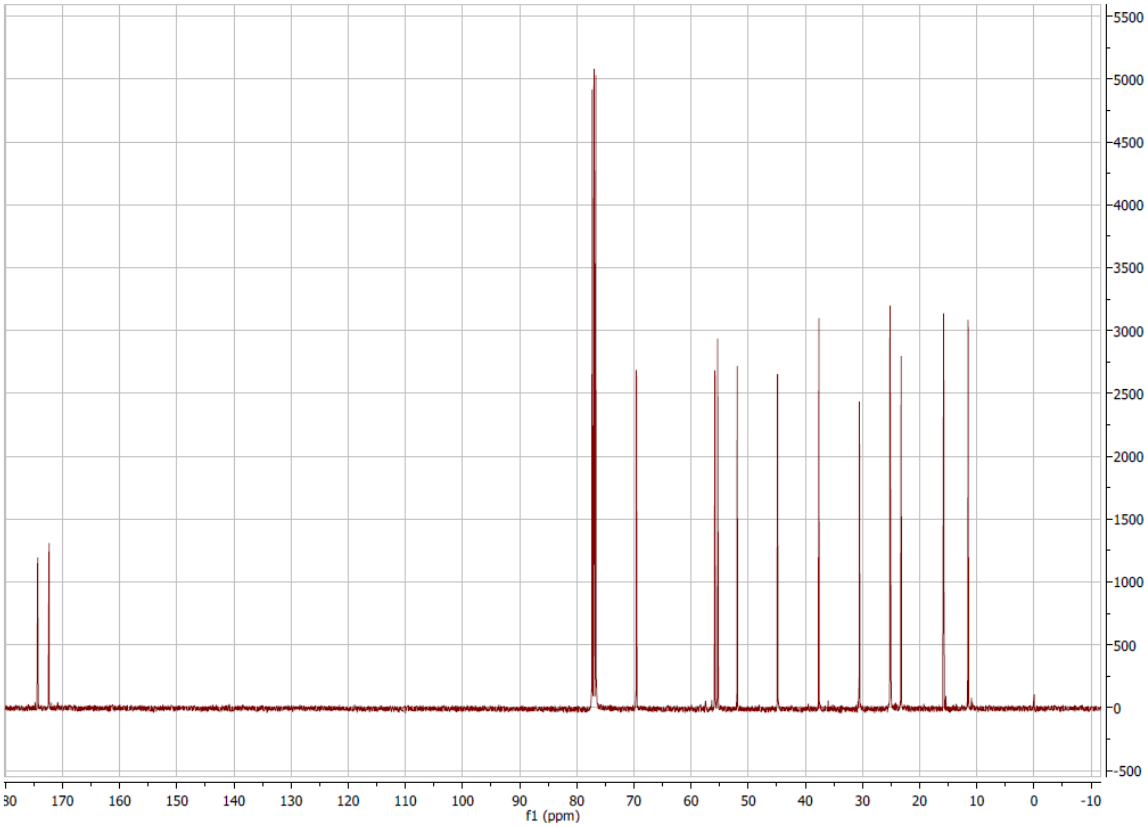

Figure A 6 ^{13}C spectrum (101 MHz, $CDCl_3$) of compound **3**.

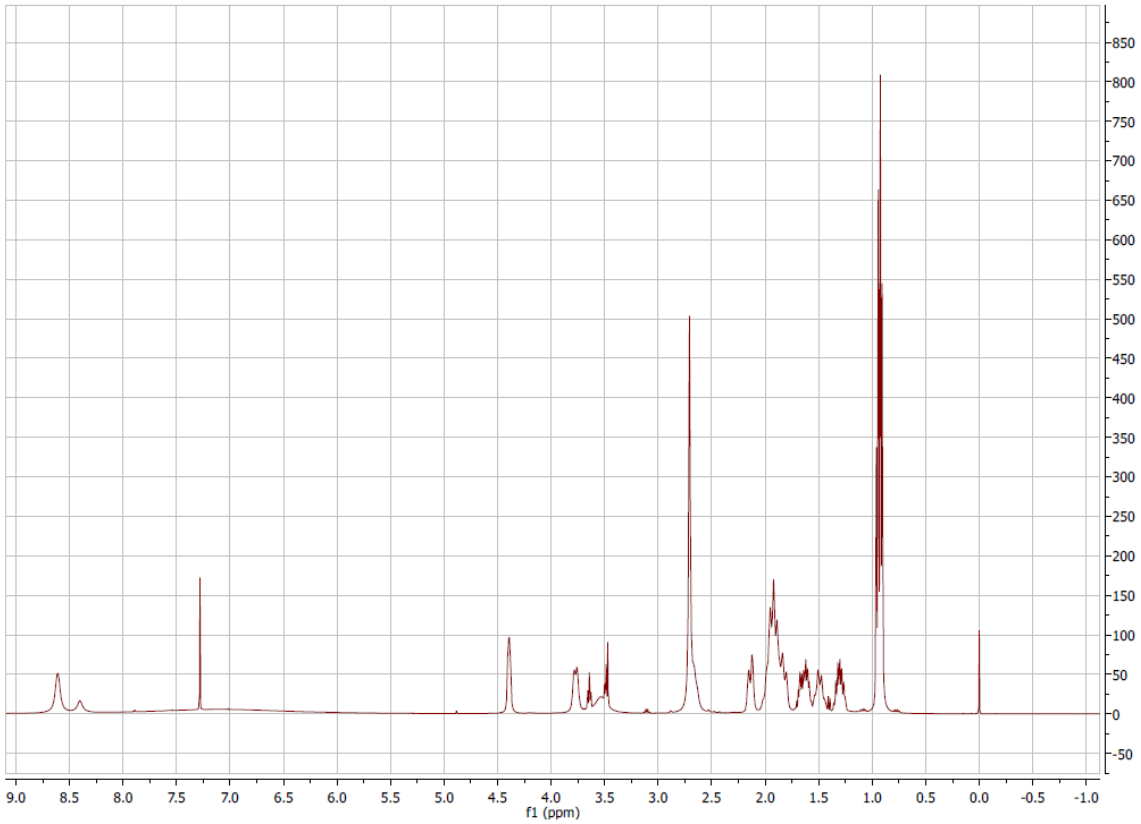

Figure A 7 ^{1}H spectrum (400 MHz, $CDCl_3$) of compound **4**.

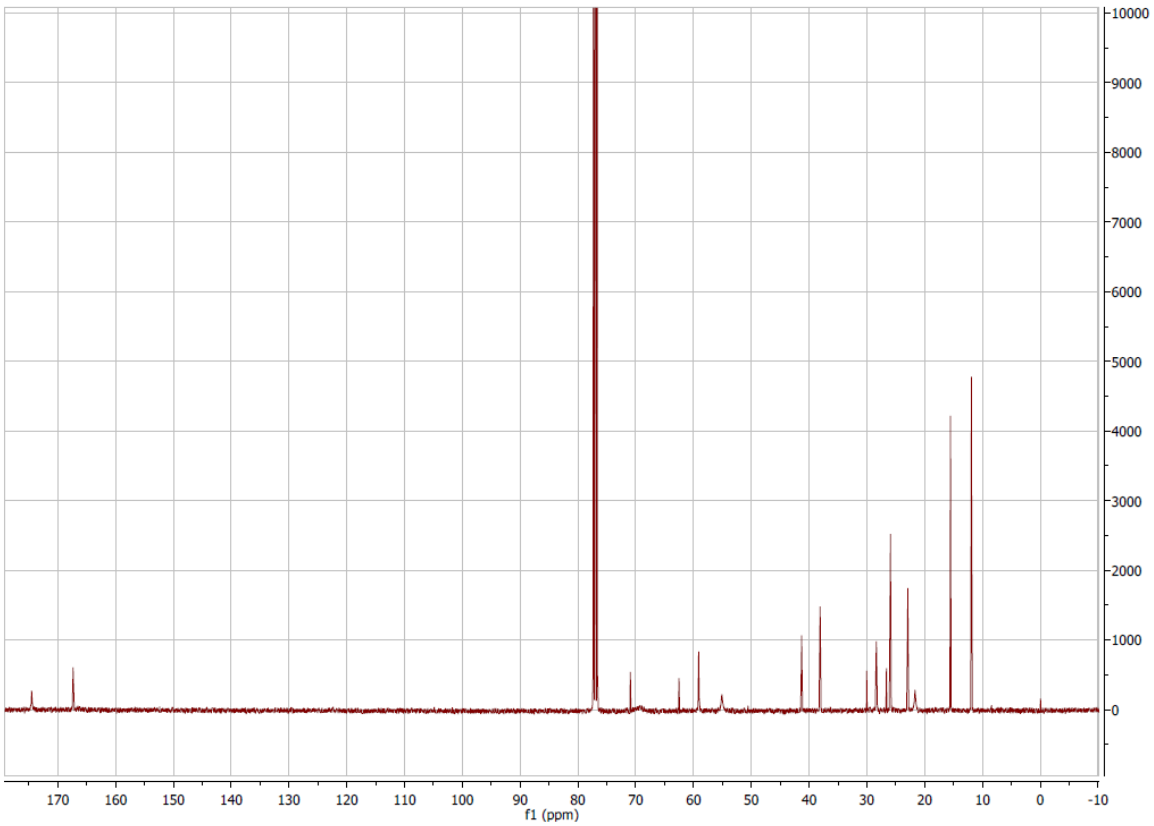

Figure A 8 ^{13}C spectrum (101 MHz, $CDCl_3$) of compound **4**.

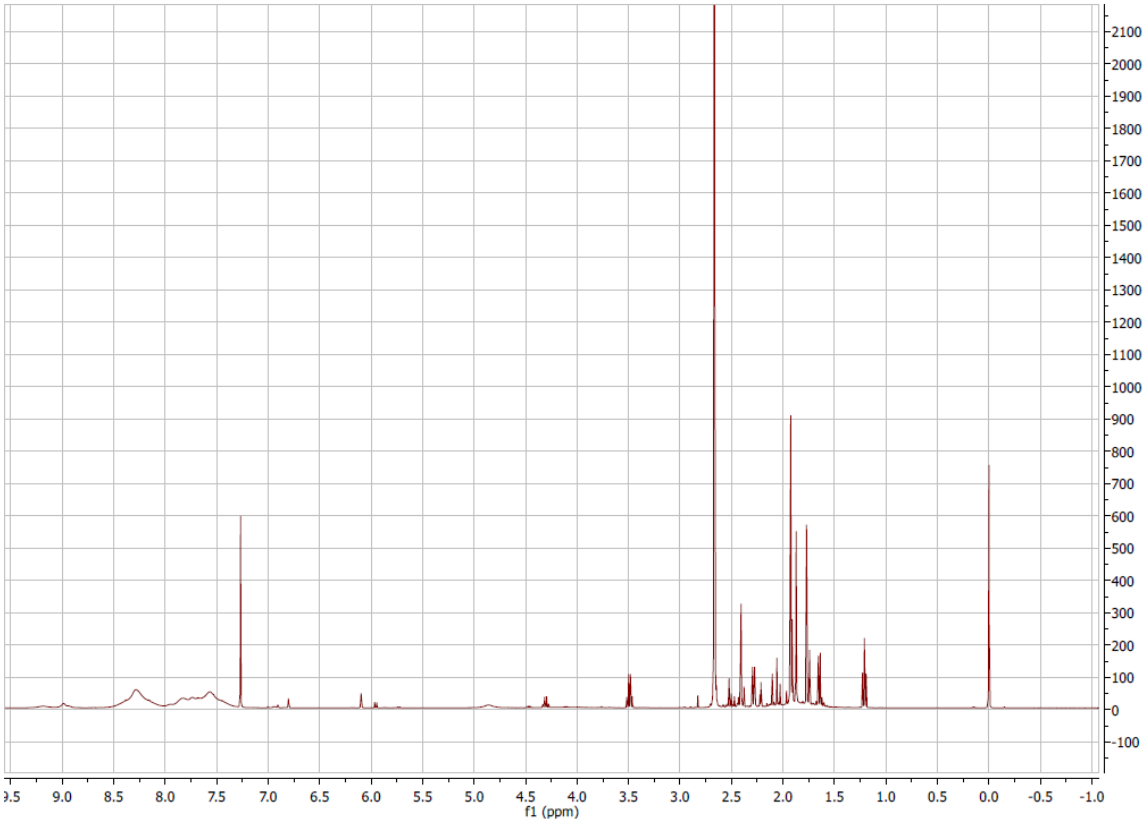

Figure A 9 ^{1}H spectrum (400 MHz, $CDCl_3$) of compound **5**.

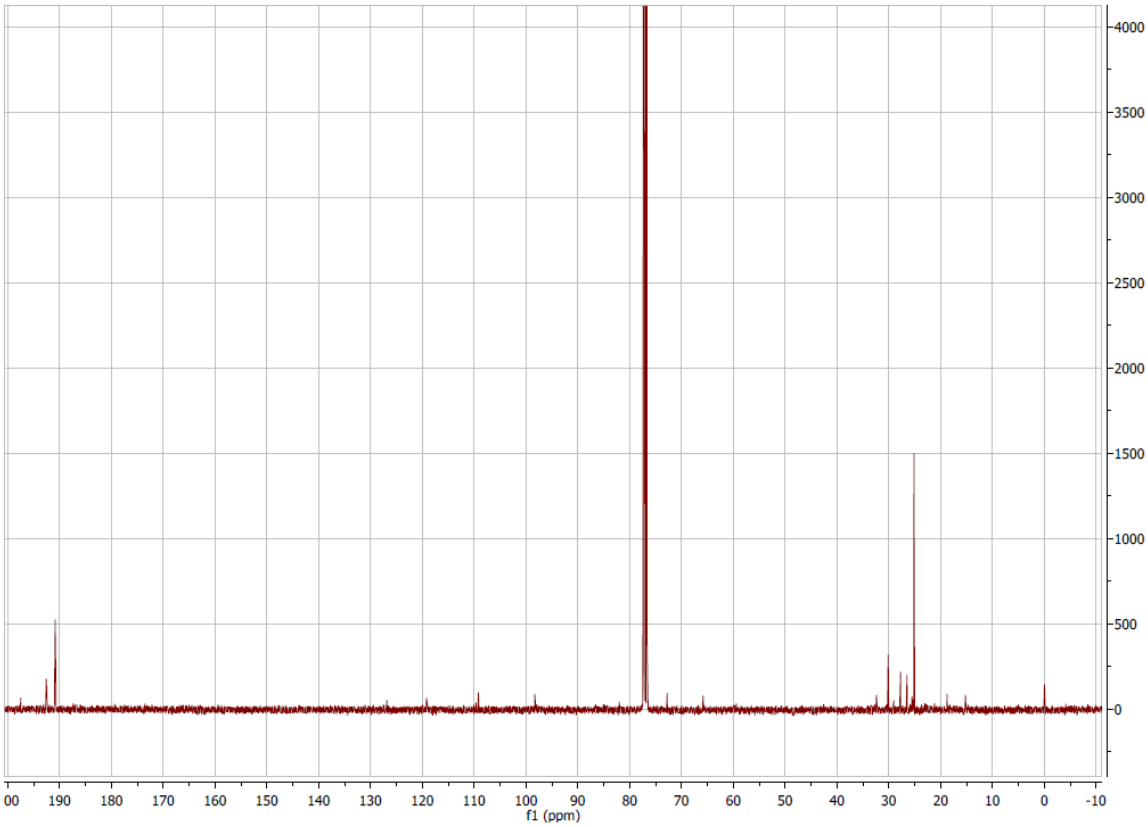

Figure A 10 ^{13}C spectrum (101 MHz, $CDCl_3$) of compound **5**.

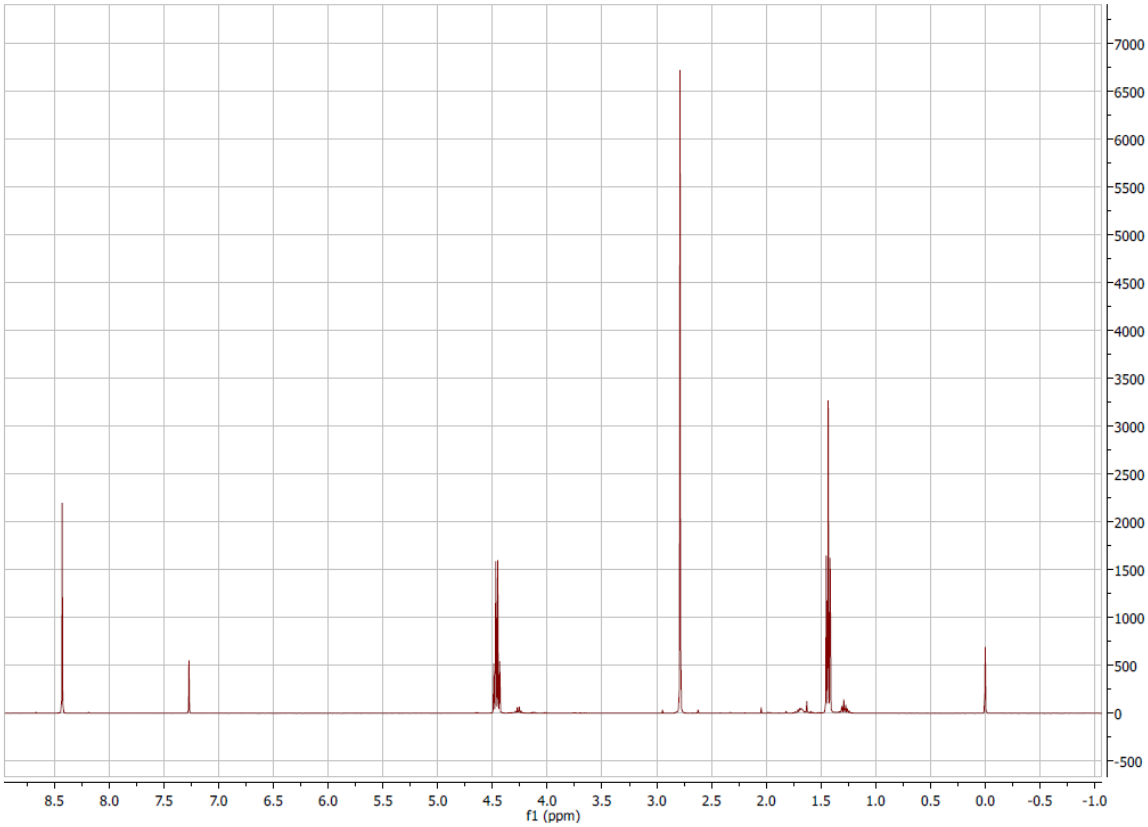

Figure A 11 ^{1}H spectrum (400 MHz, $CDCl_3$) of compound **6**.

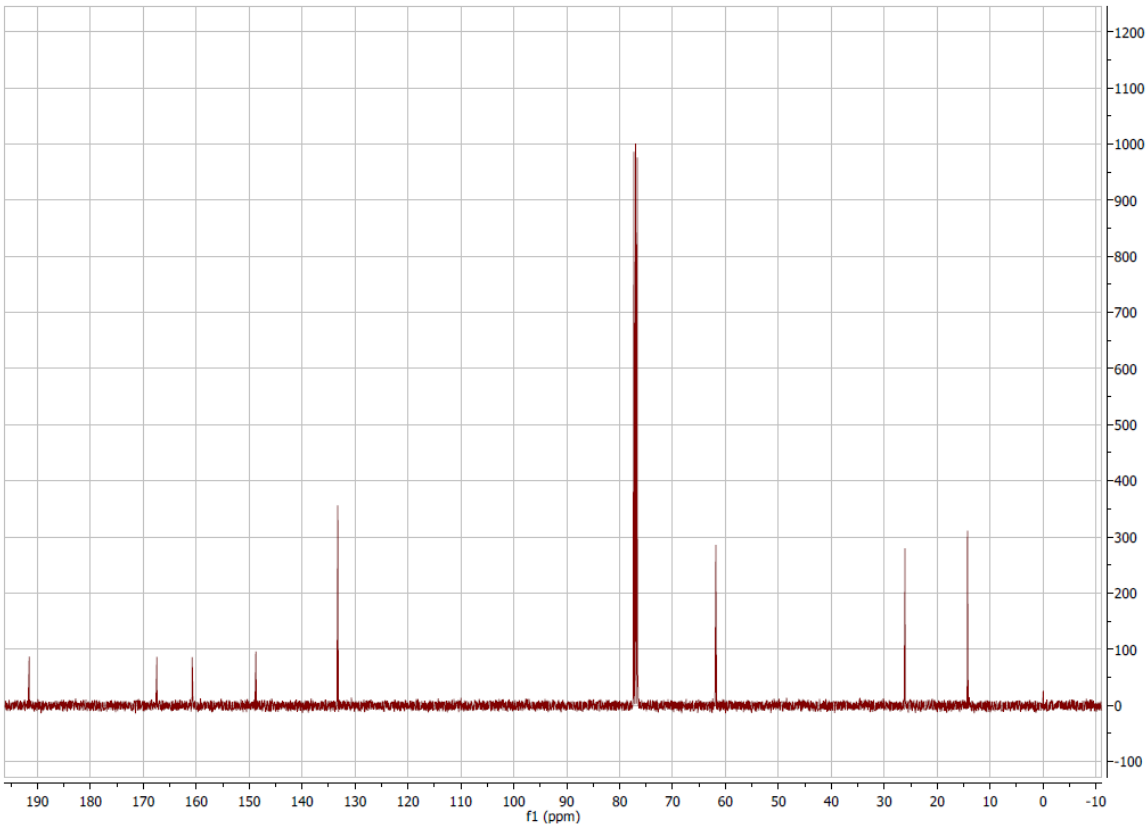

Figure A 12 ^{13}C spectrum (101 MHz, $CDCl_3$) of compound **6**.

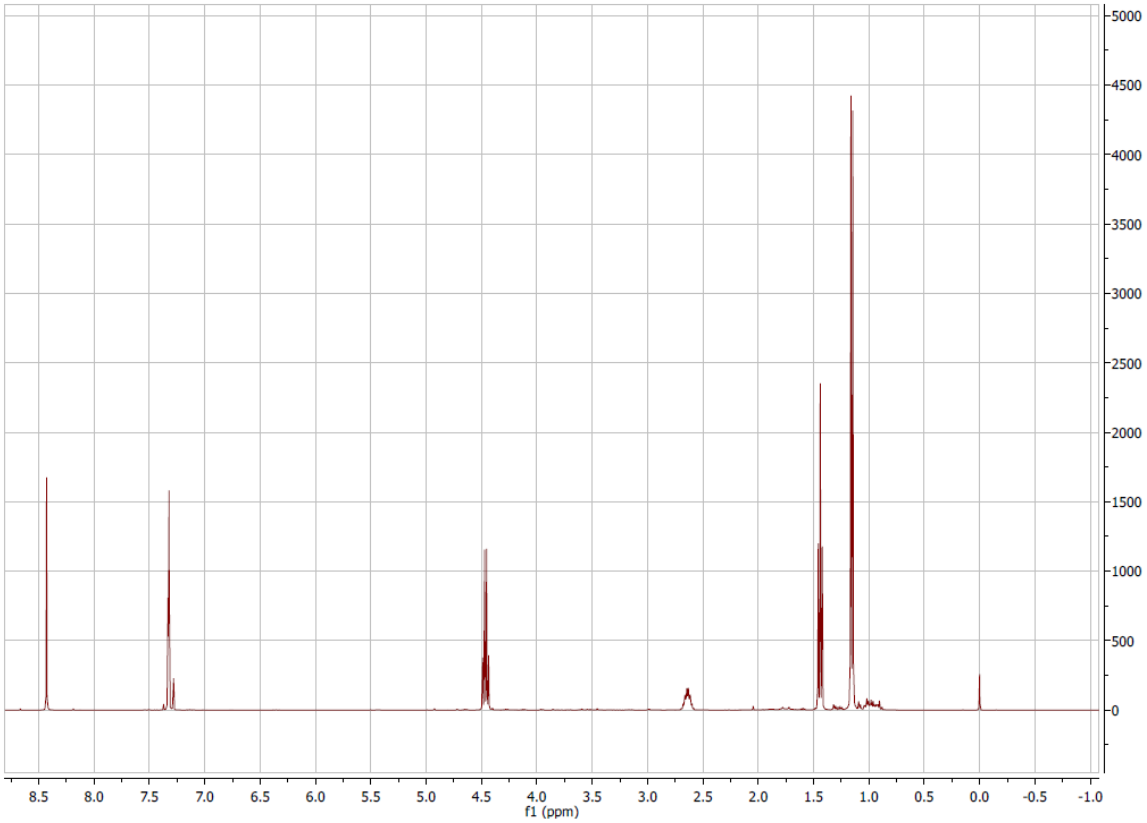

Figure A 13 ^{1}H spectrum (400 MHz, $CDCl_3$) of compound **7**.

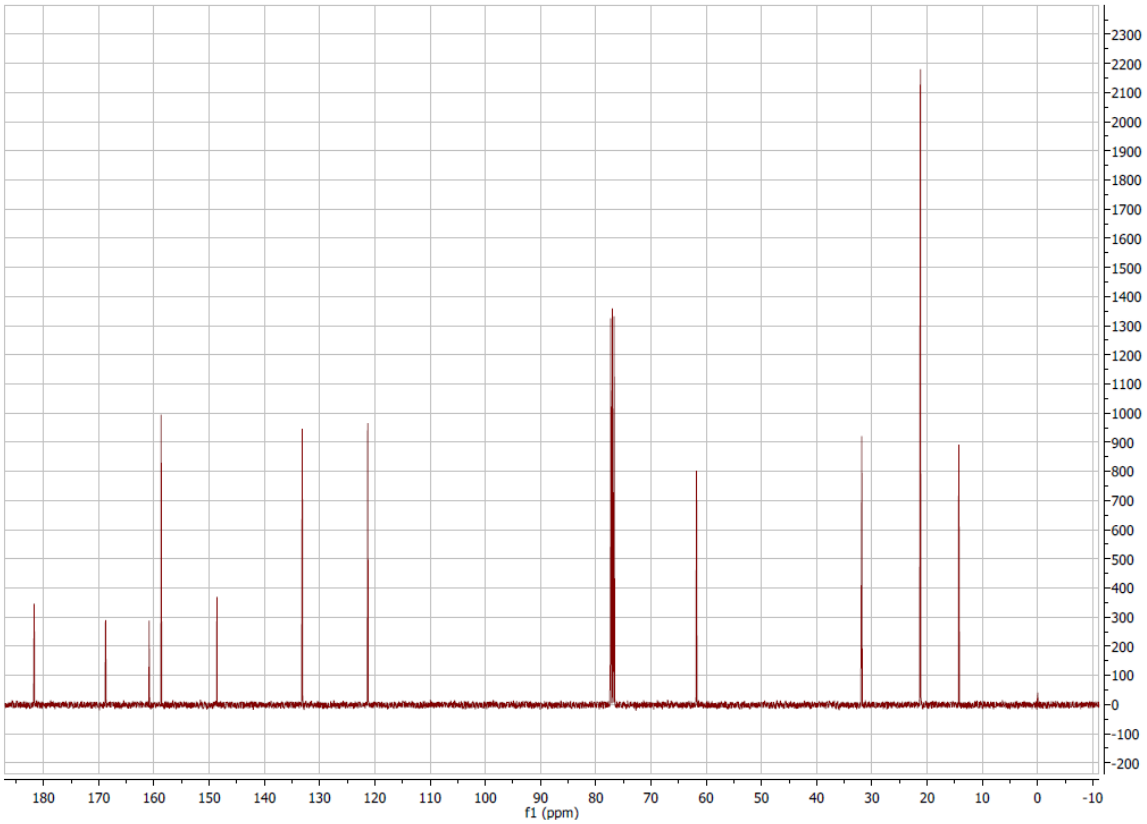

Figure A 14 ^{13}C spectrum (101 MHz, $CDCl_3$) of compound **7**.

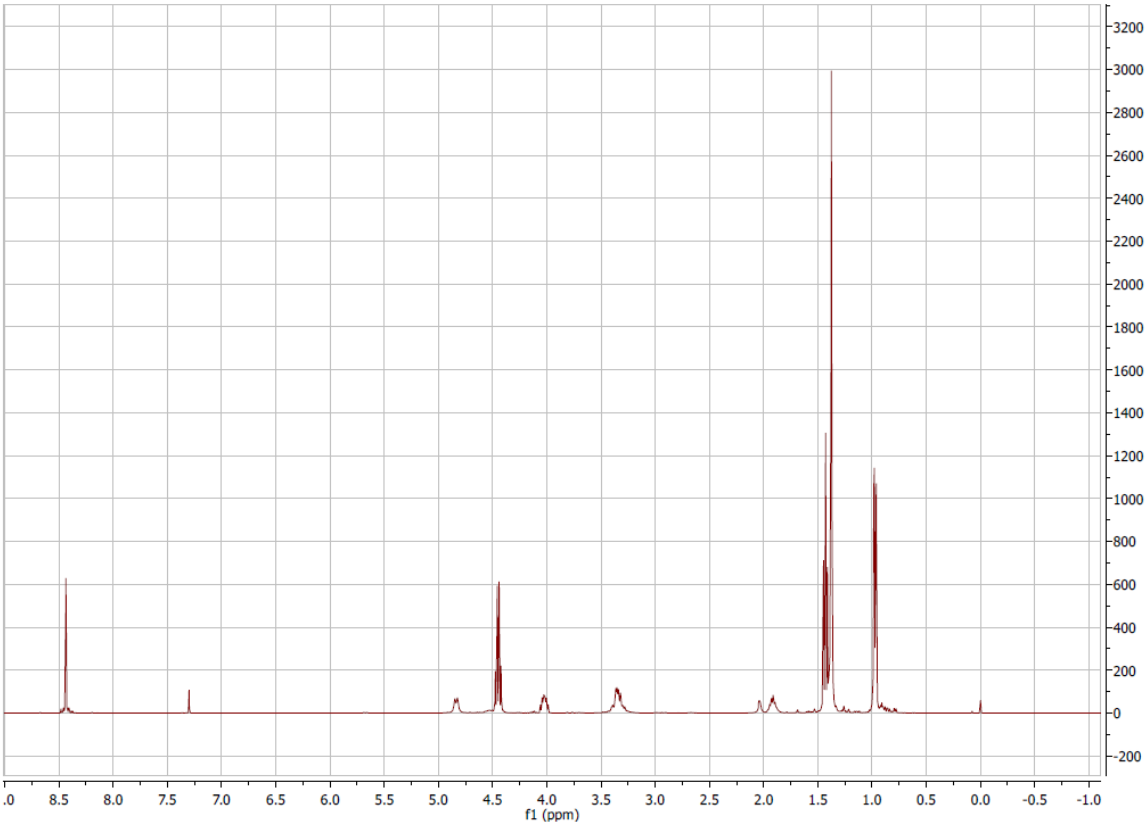

Figure A 15 ^{1}H spectrum (400 MHz, $CDCl_3$) of compound **8**.

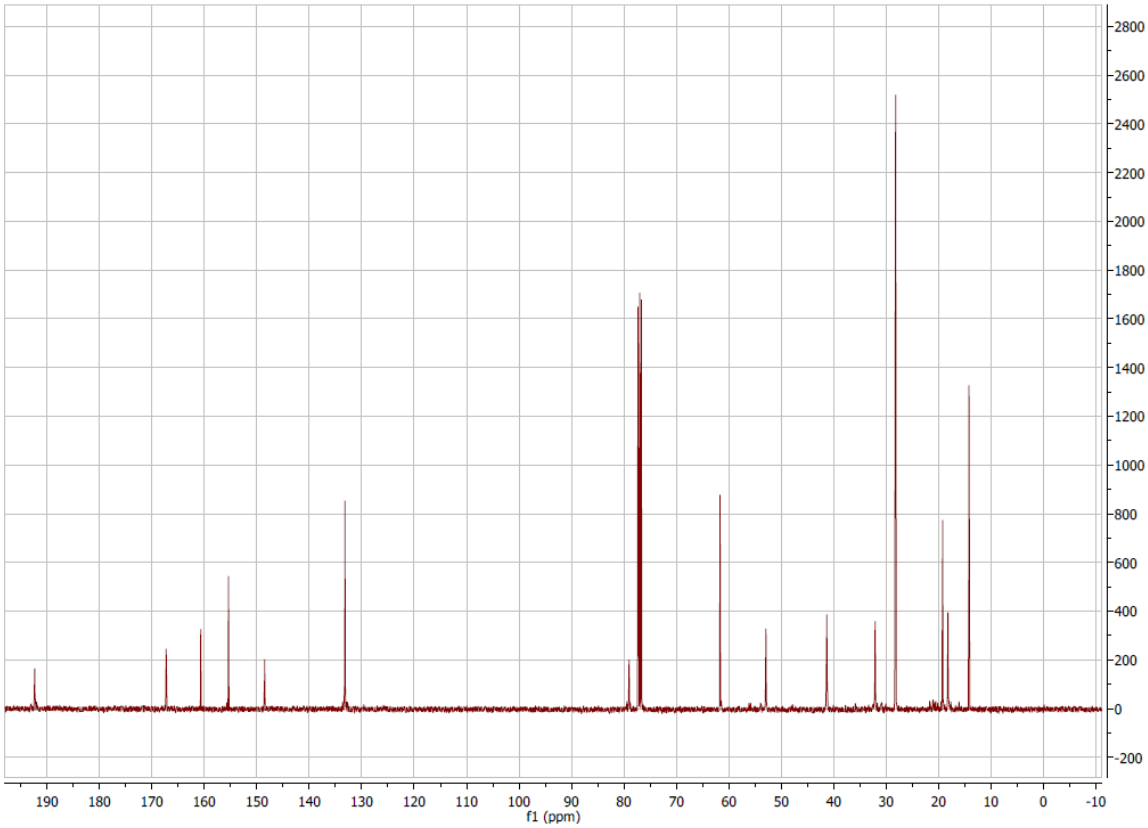

Figure A 16 ^{13}C spectrum (101 MHz, $CDCl_3$) of compound **8**.

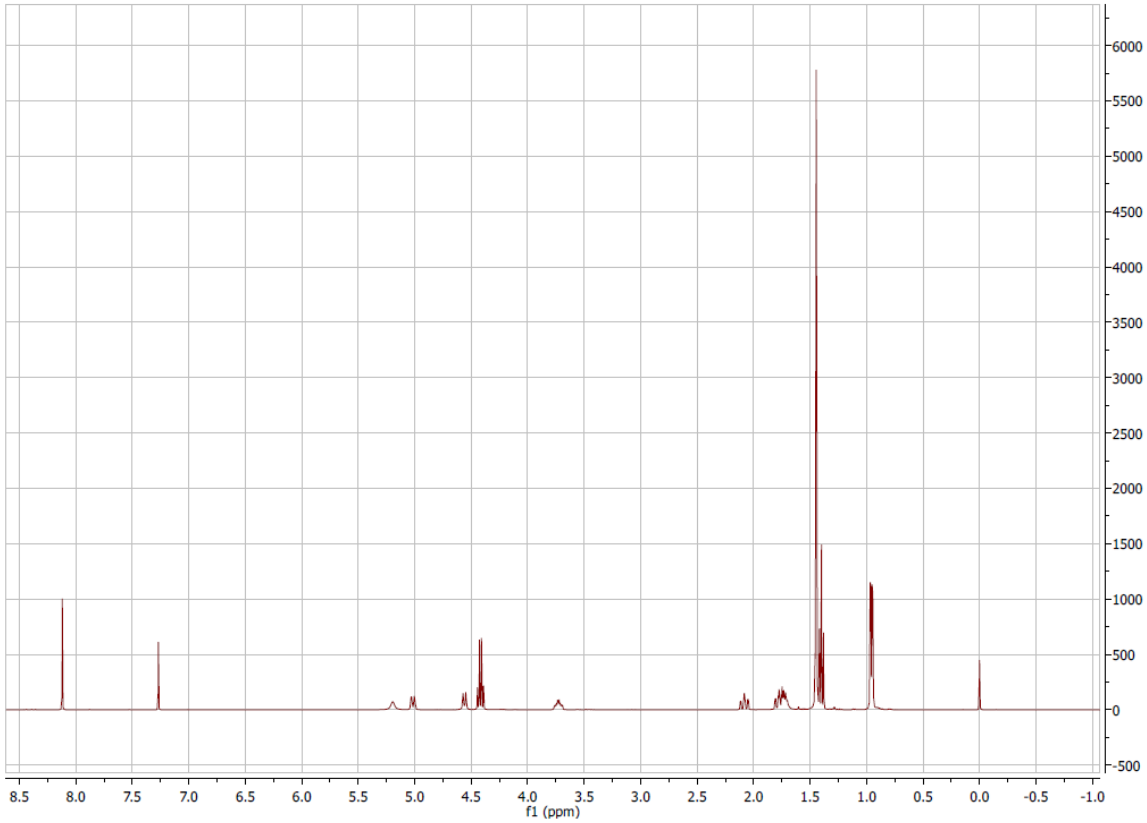

Figure A 17 ^{1}H spectrum (400 MHz, $CDCl_3$) of compound **9**.

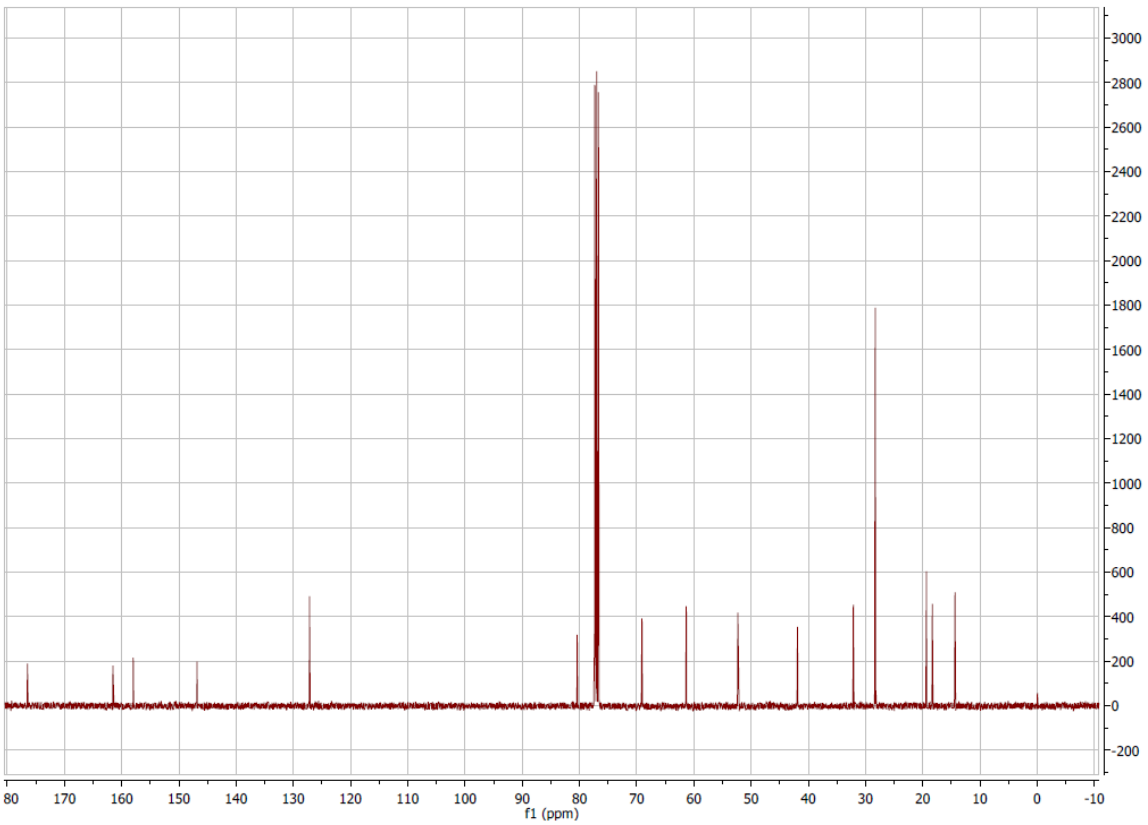

Figure A 18 ^{13}C spectrum (101 MHz, $CDCl_3$) of compound **9**.

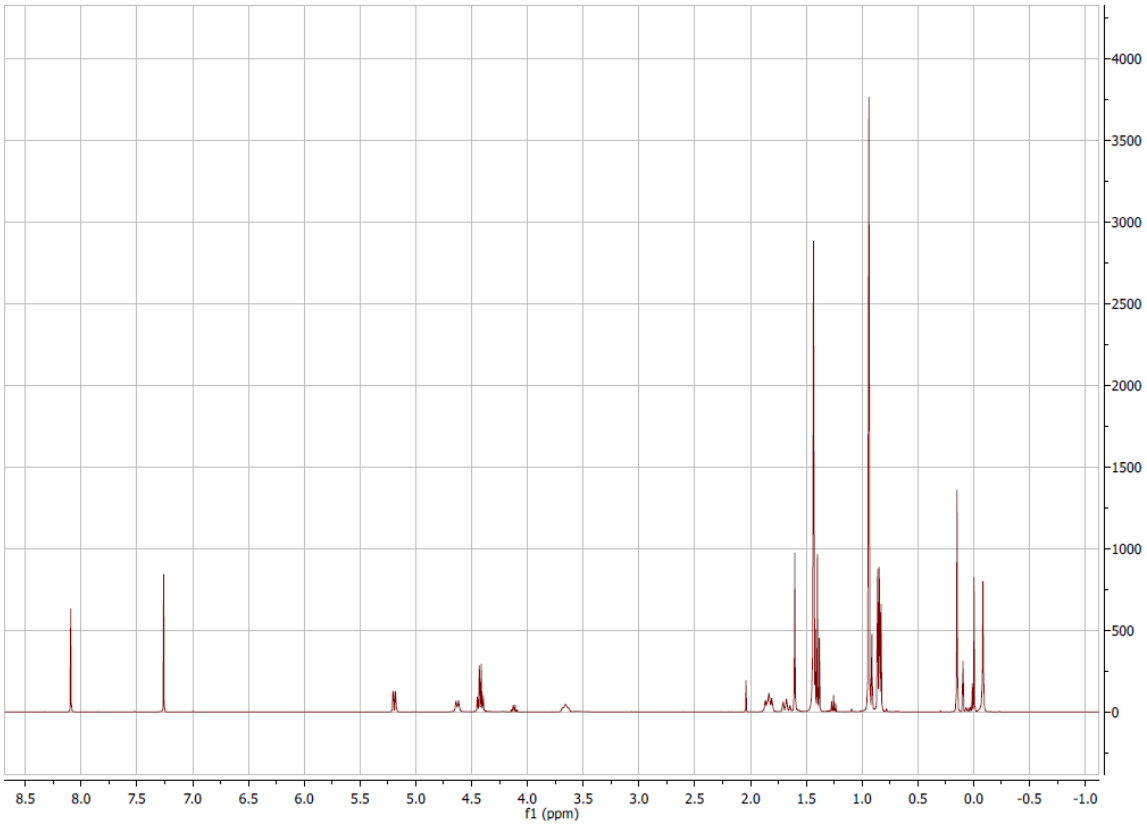

Figure A 19 ^{1}H spectrum (400 MHz, $CDCl_3$) of compound **10**.

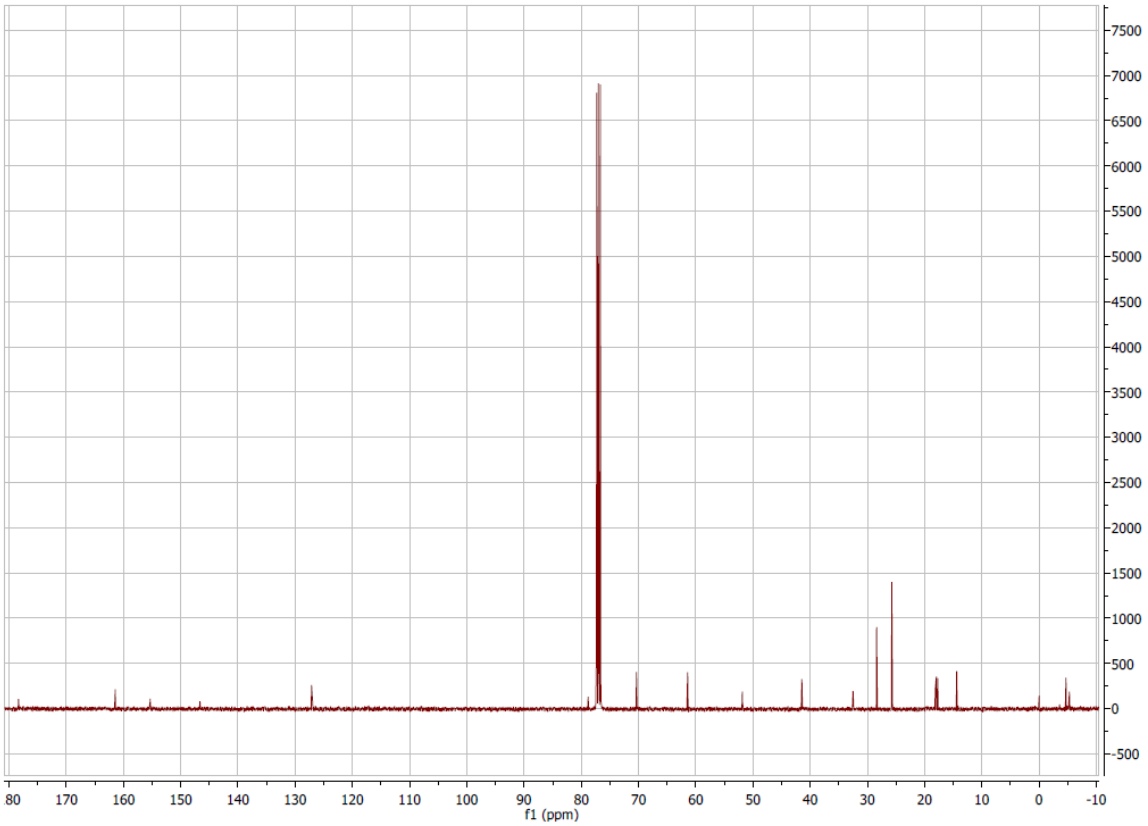

Figure A 20 ^{13}C spectrum (101 MHz, $CDCl_3$) of compound **10**.

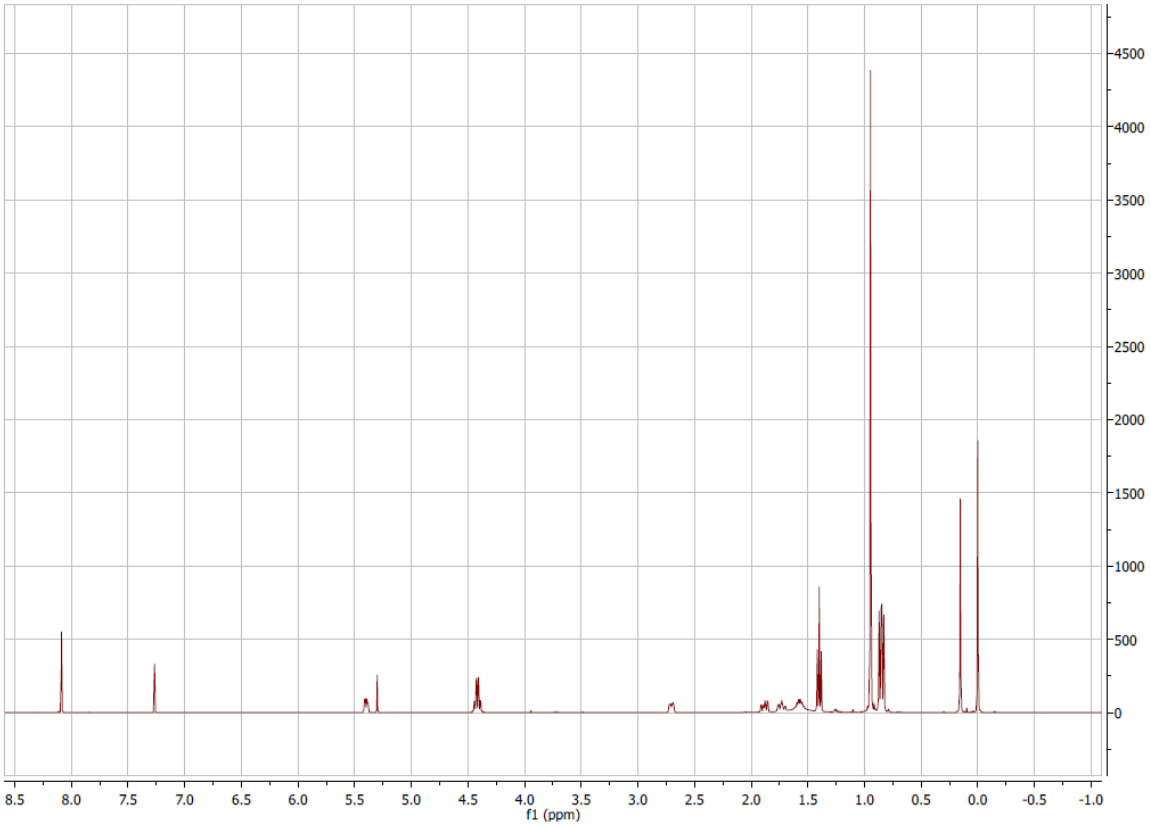

Figure A 21 ^{1}H spectrum (400 MHz, $CDCl_3$) of compound **11**.

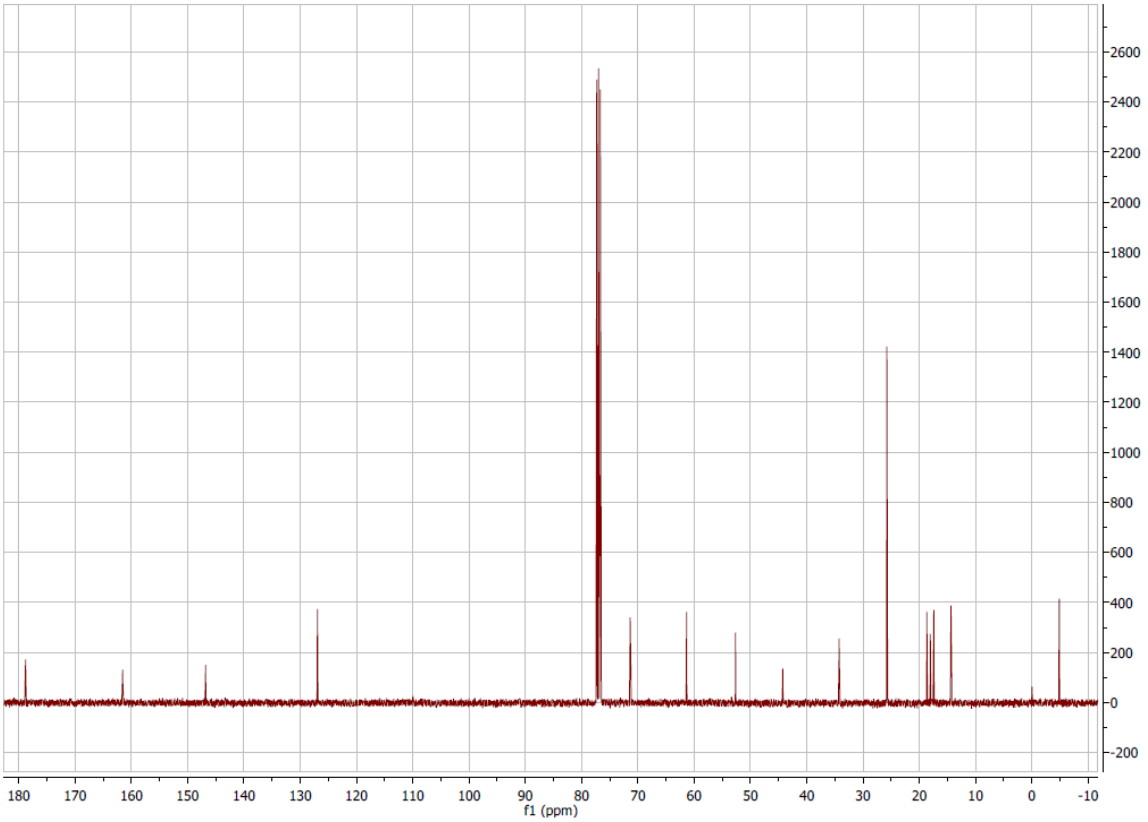

Figure A 22 ^{13}C spectrum (101 MHz, $CDCl_3$) of compound **11**.

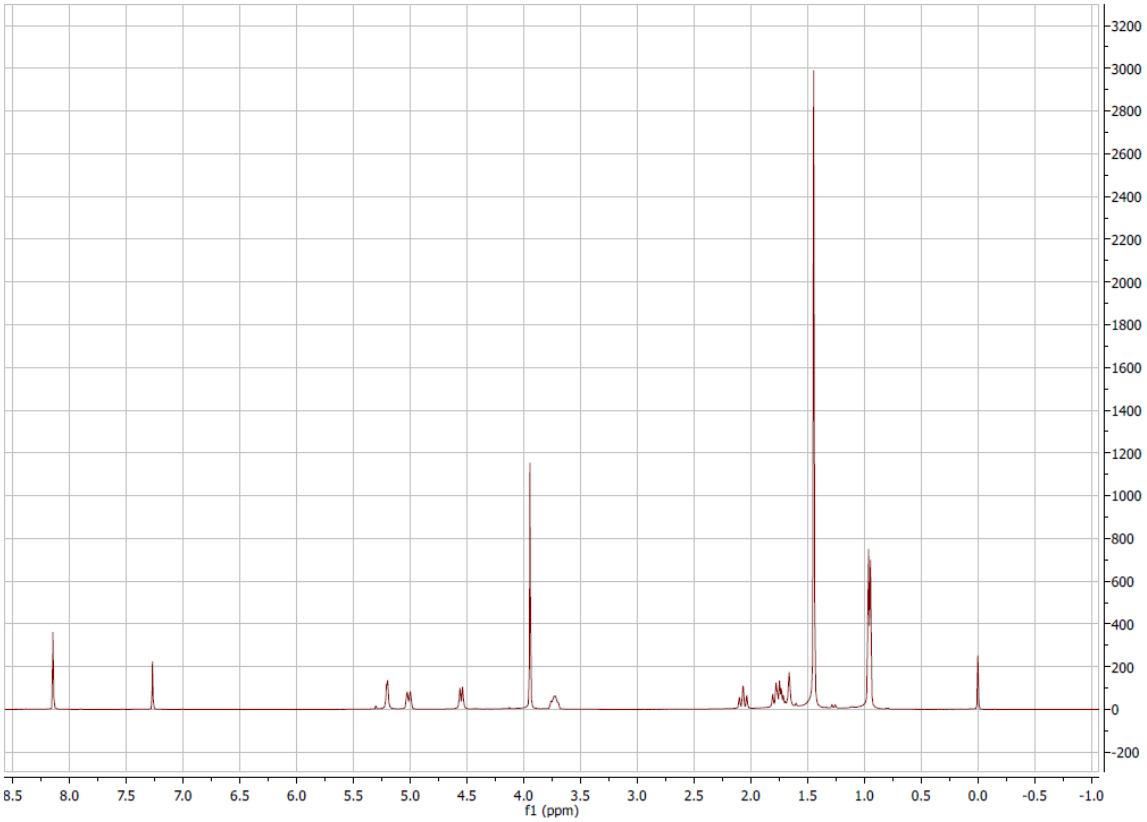

Figure A 23 ^{1}H spectrum (400 MHz, $CDCl_3$) of compound **13**.

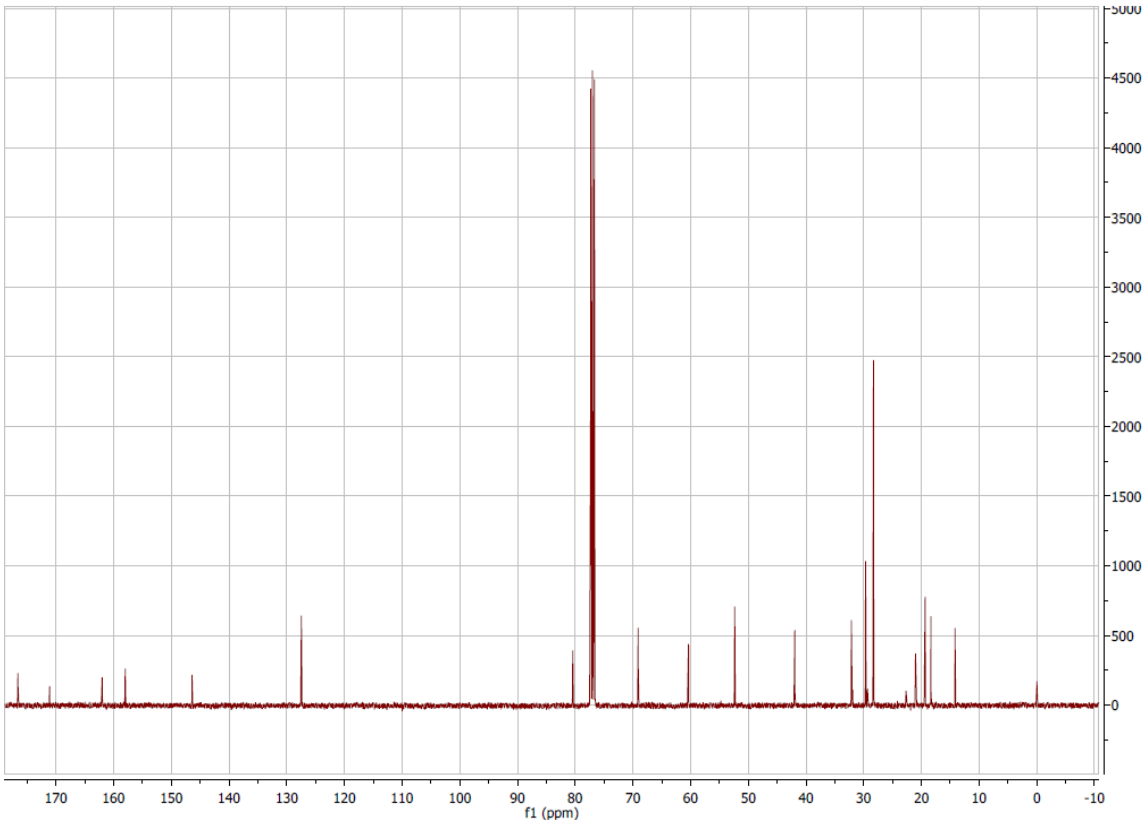

Figure A 24 ^{13}C spectrum (101 MHz, $CDCl_3$) of compound **13**.

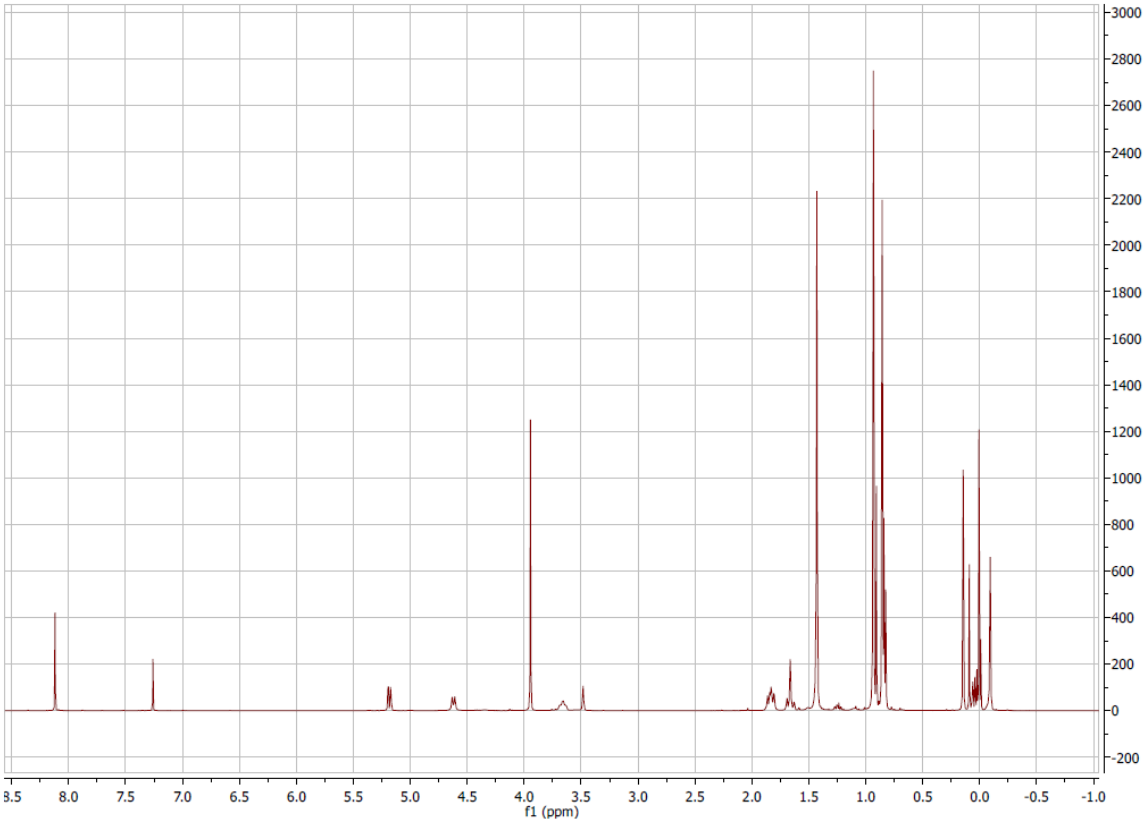

Figure A 25 ^{1}H spectrum (400 MHz, $CDCl_3$) of compound **14**.

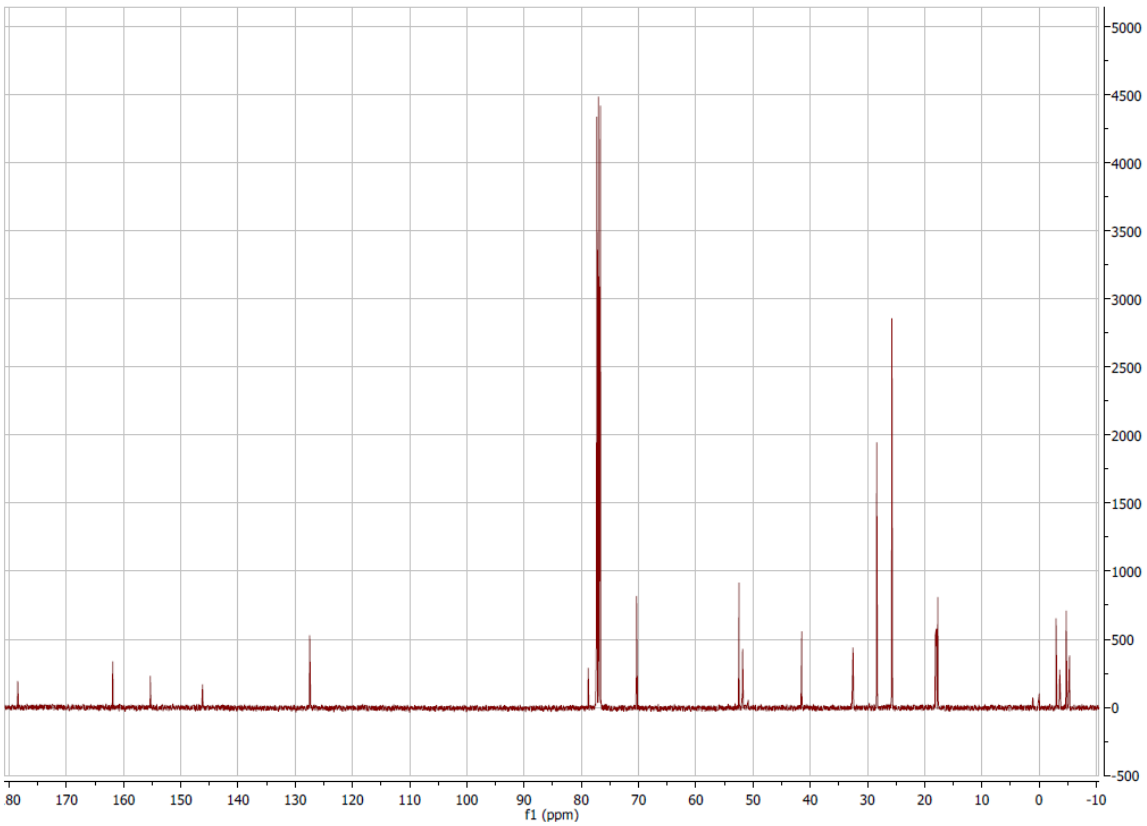

Figure A 26 ^{13}C spectrum (101 MHz, $CDCl_3$) of compound **14**.

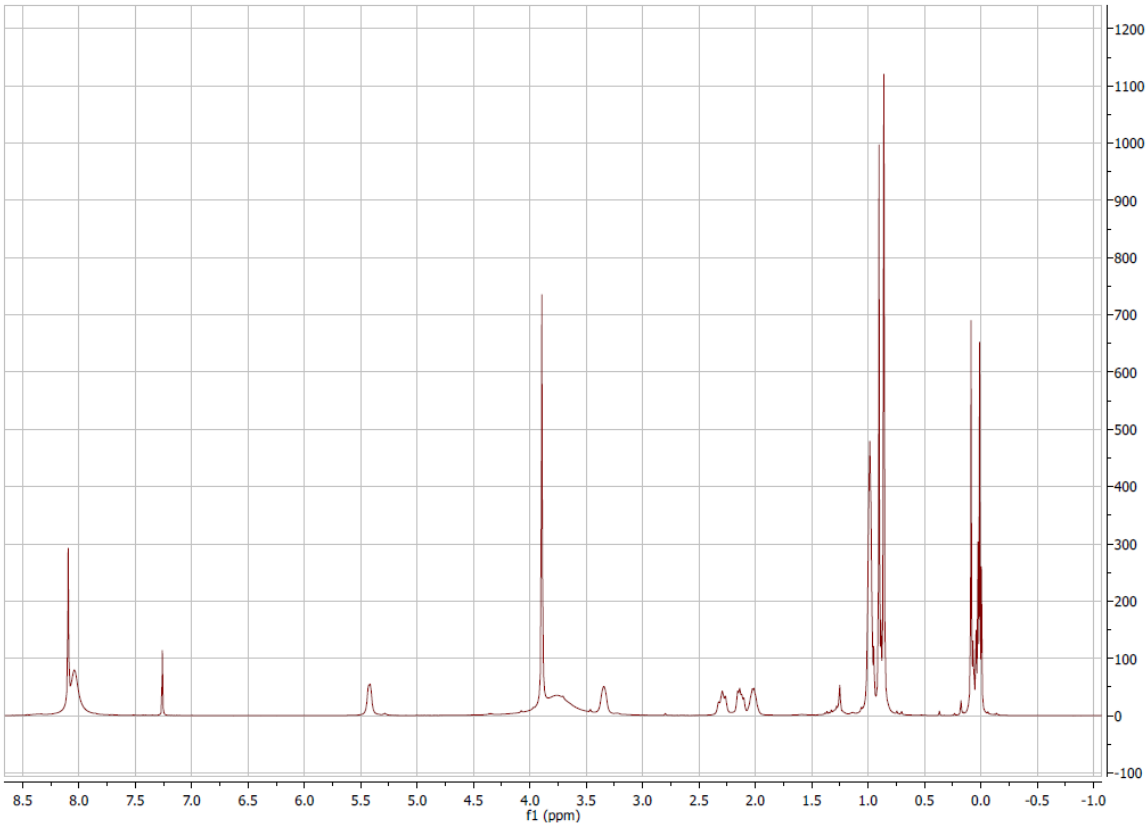

Figure A 27 ^{1}H spectrum (400 MHz, $CDCl_3$) of compound **15**.

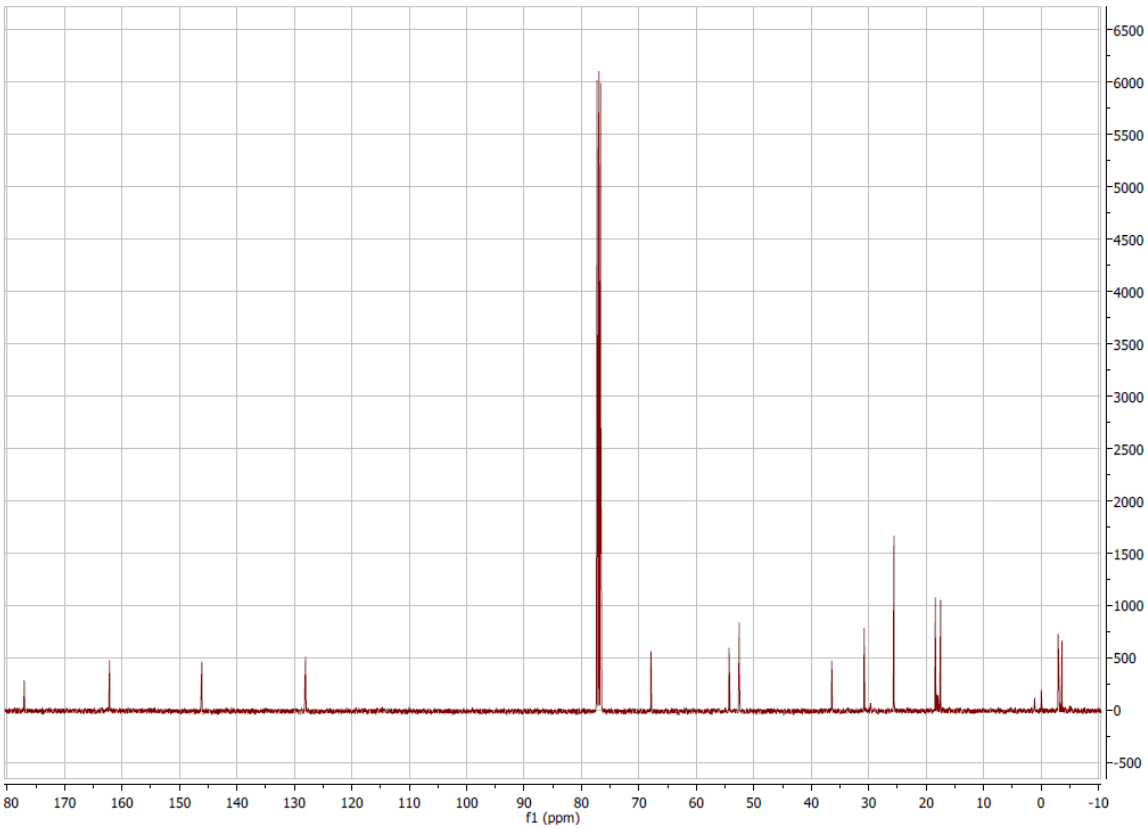

Figure A 28 ^{13}C spectrum (101 MHz, $CDCl_3$) of compound **15**.

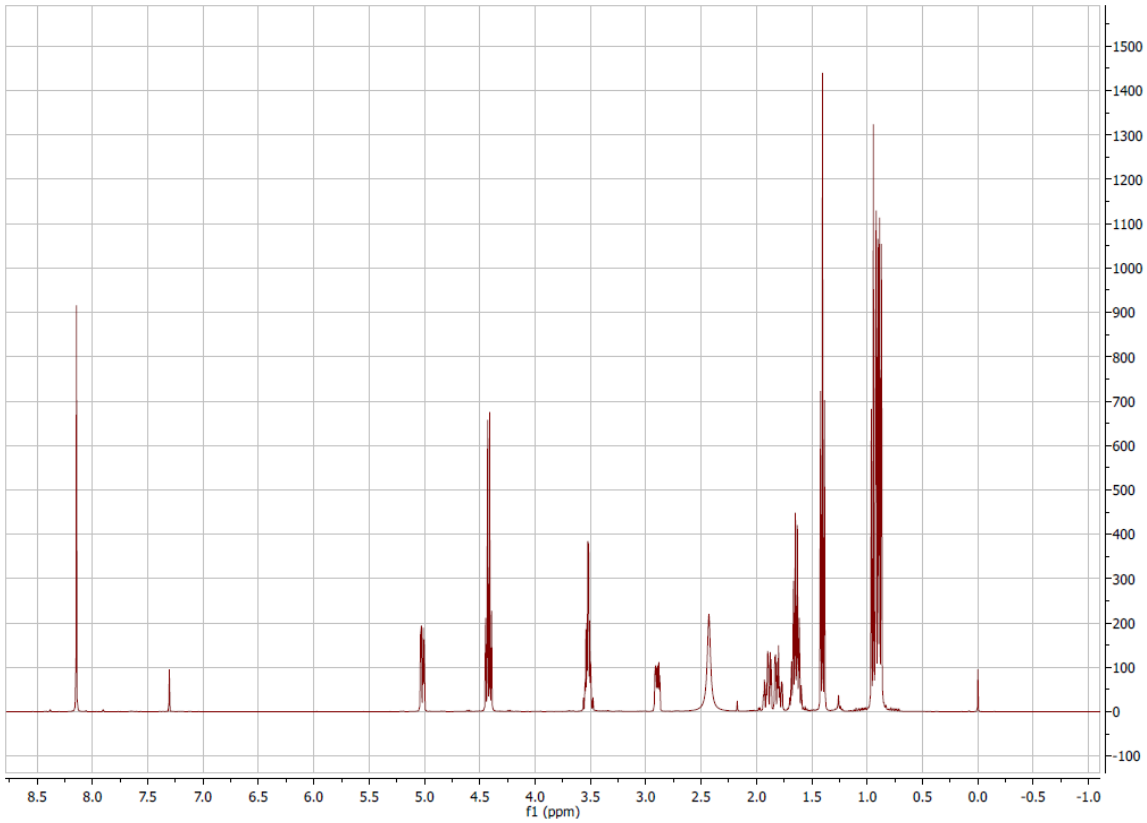

Figure A 29 ^{1}H spectrum (400 MHz, $CDCl_3$) of compound **17**.

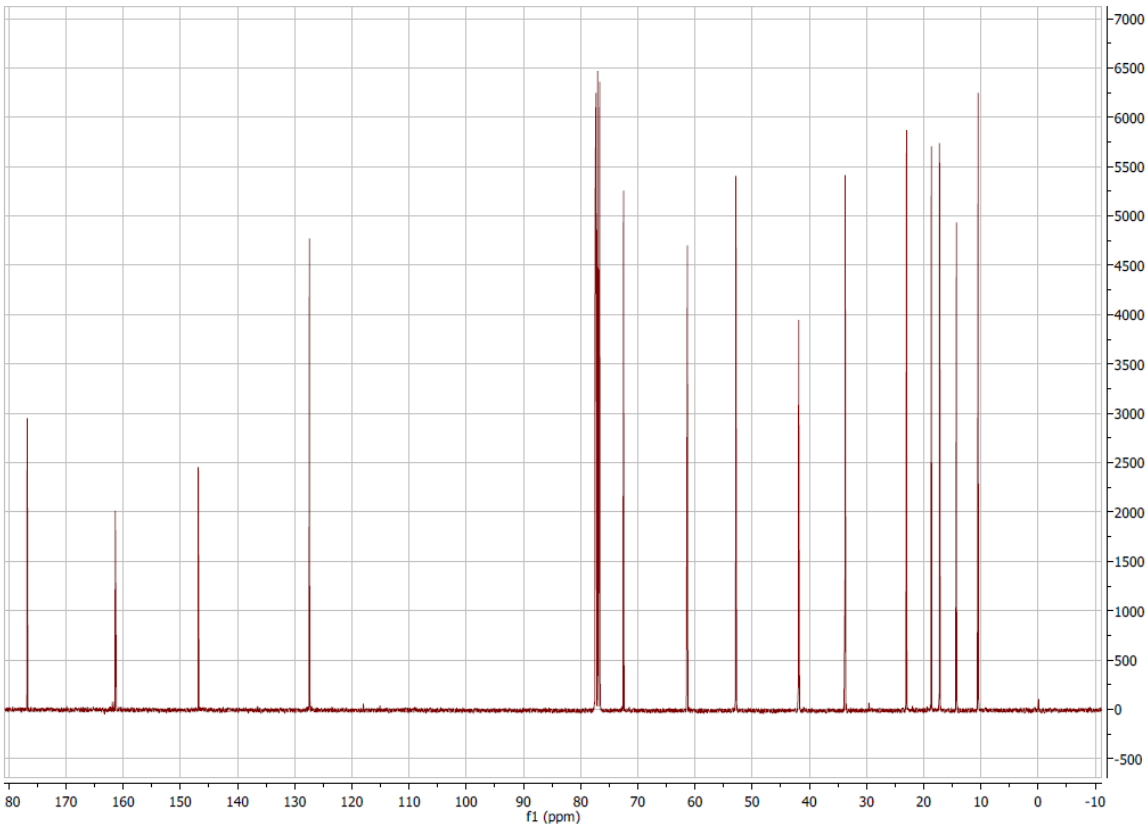

Figure A 30 ^{13}C spectrum (101 MHz, $CDCl_3$) of compound **17**.

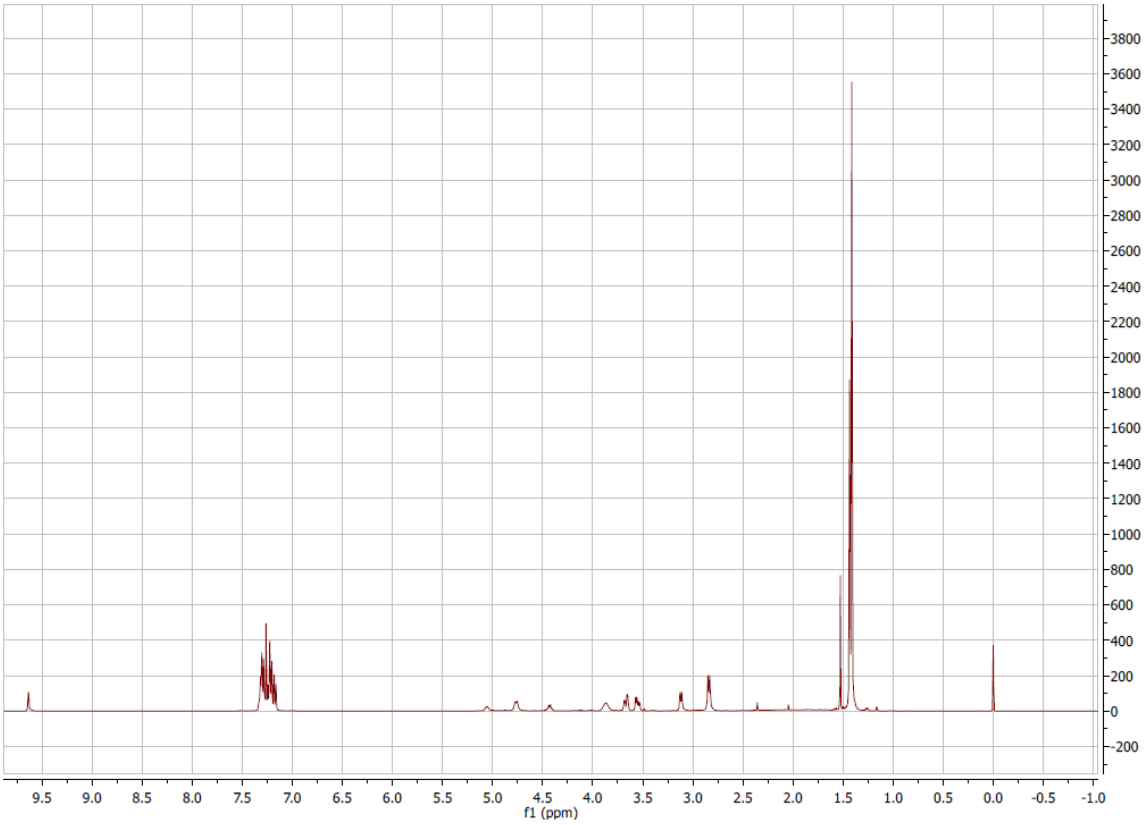

Figure A 31 ^{1}H spectrum (400 MHz, $CDCl_3$) of compound **18**.

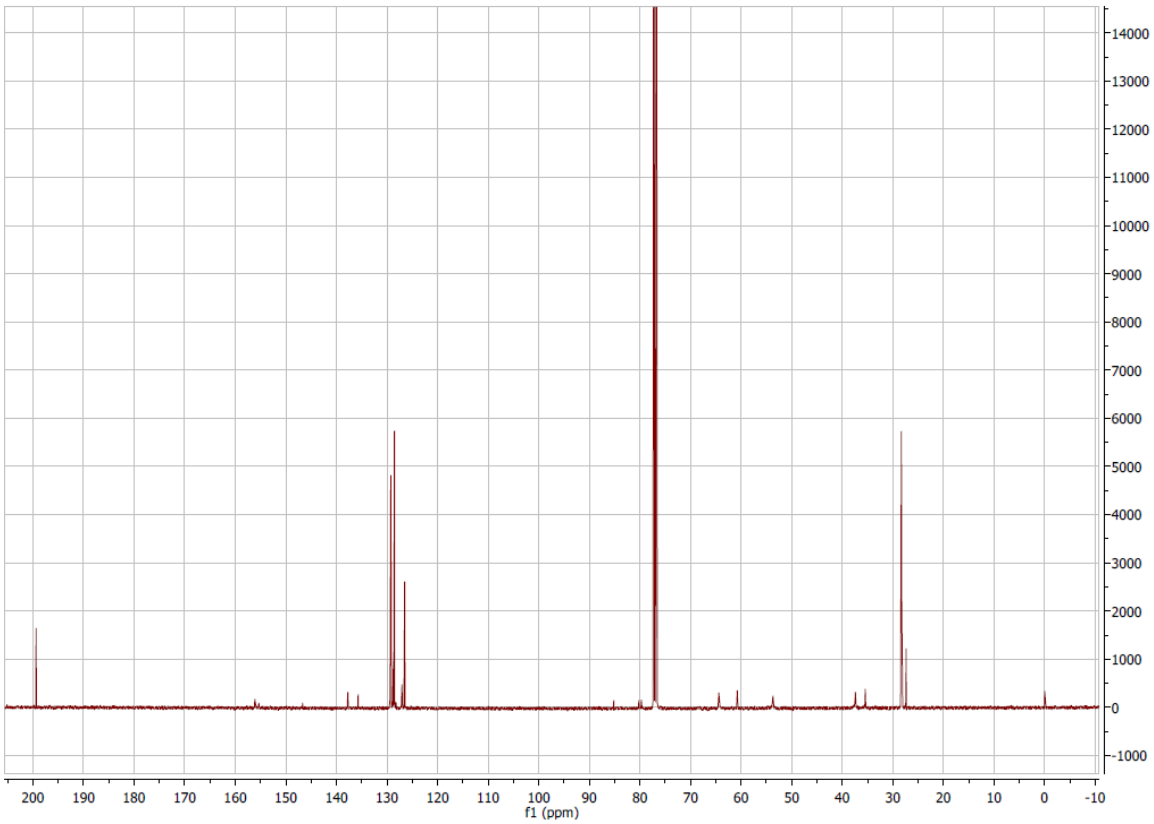

Figure A 32 ^{13}C spectrum (101 MHz, $CDCl_3$) of compound **18**.

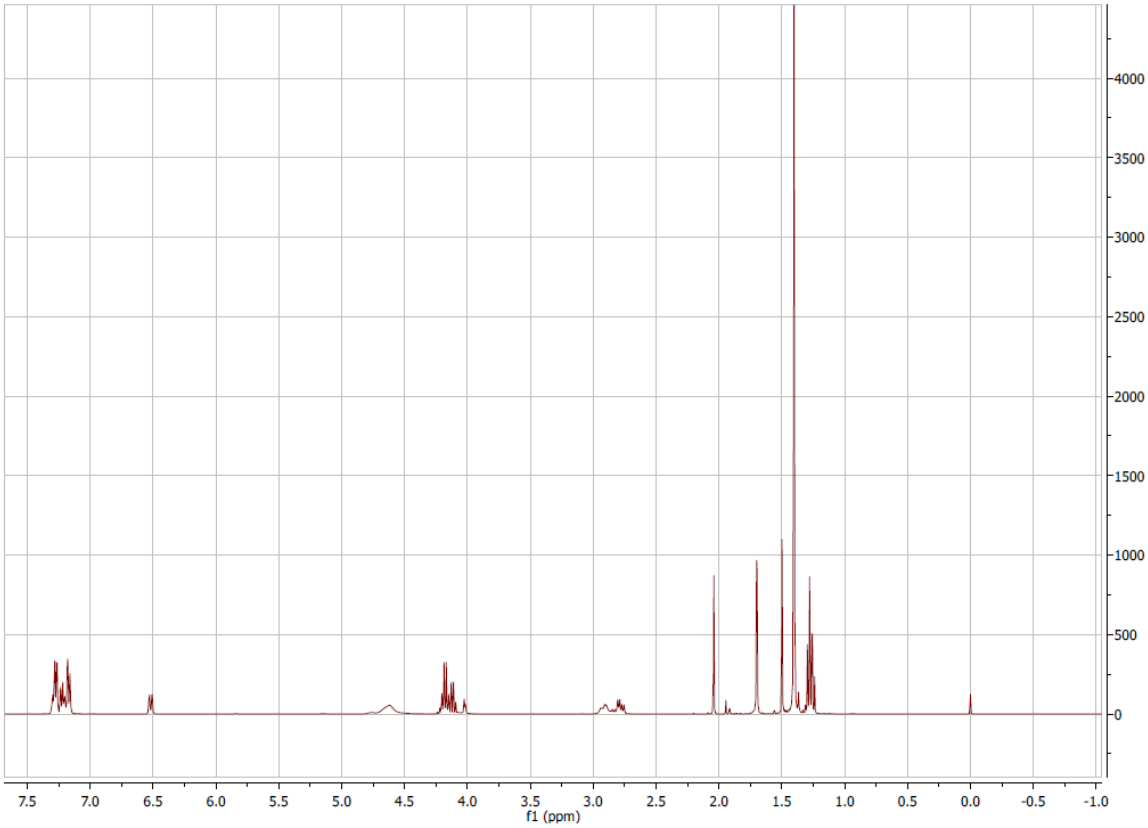

Figure A 33 ^{1}H spectrum (400 MHz, $CDCl_3$) of compound **19**.

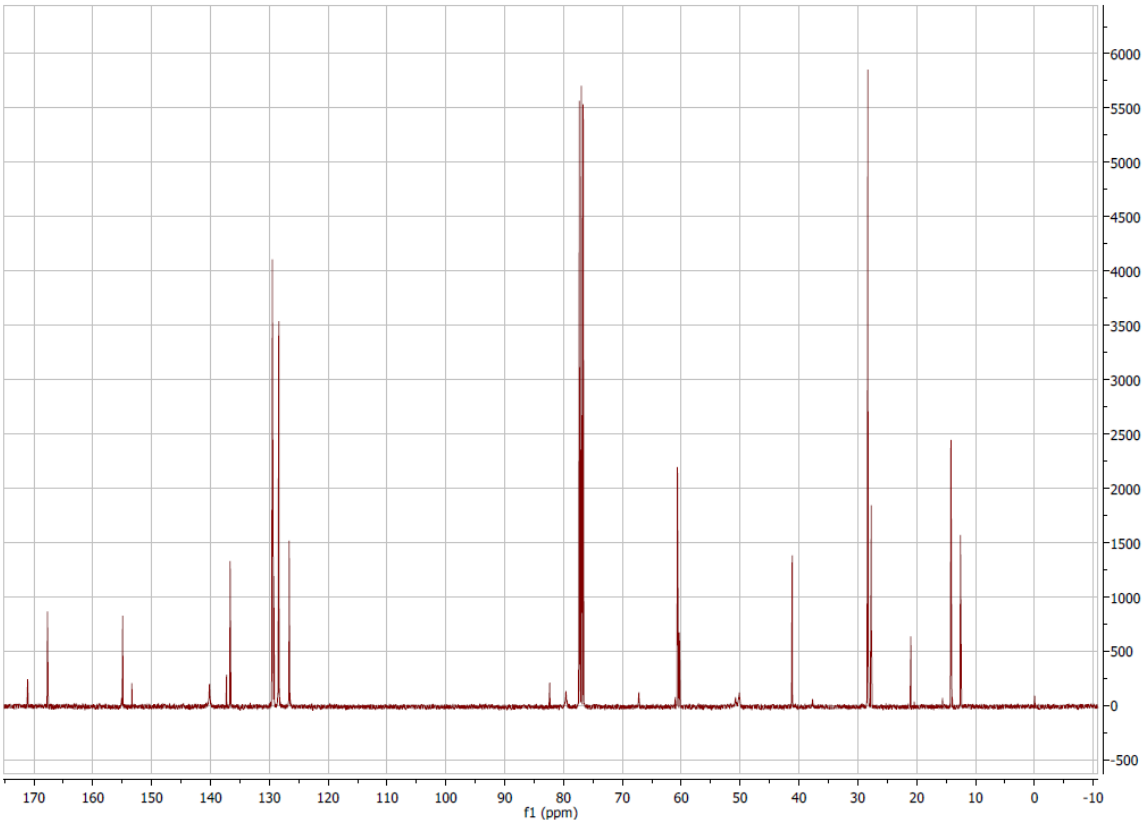

Figure A 34 ^{13}C spectrum (101 MHz, $CDCl_3$) of compound **19**.

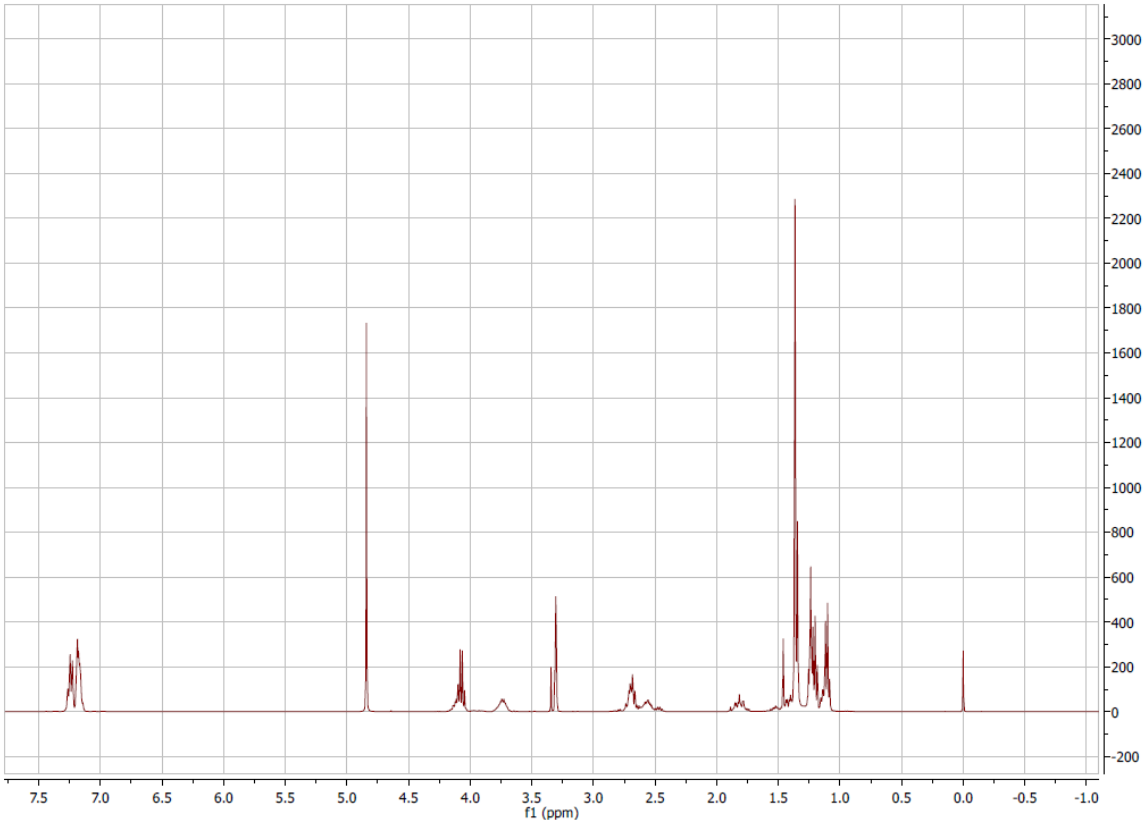

Figure A 35 ^{1}H spectrum (400 MHz, CD_3OD) of compound **20**.

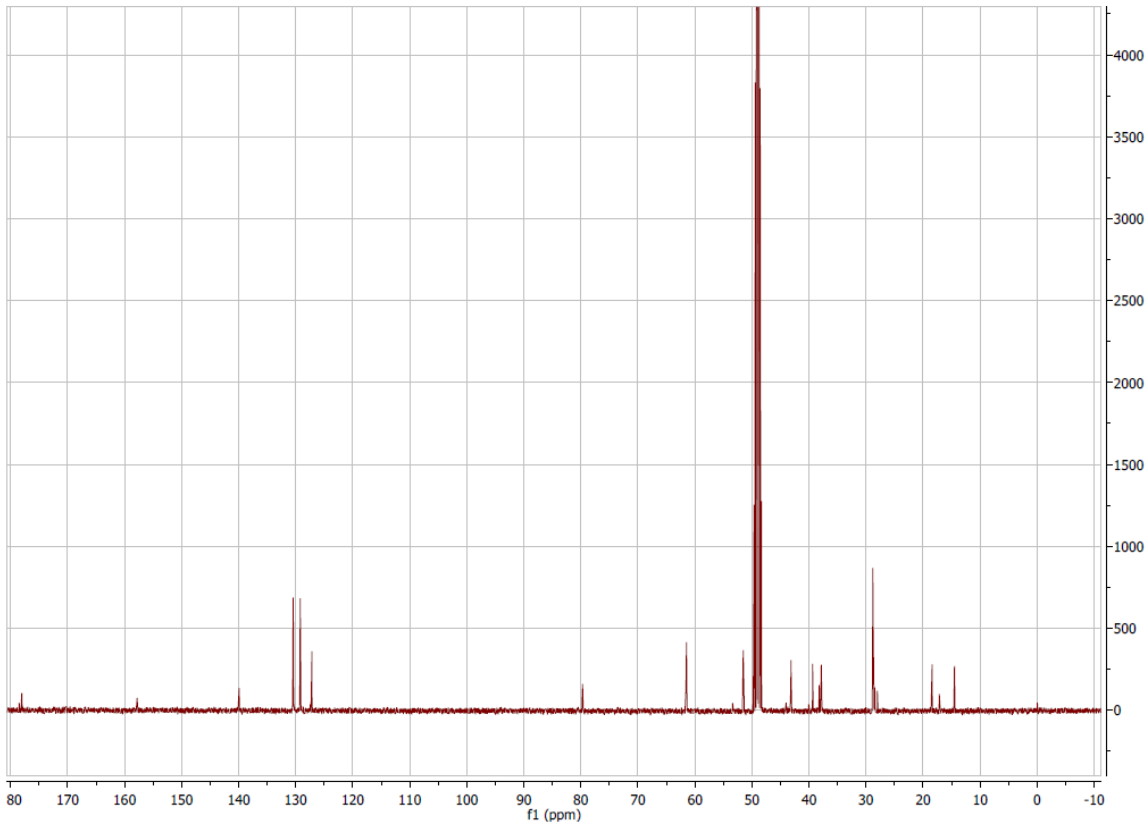

Figure A 36 ^{13}C spectrum (101 MHz, CD_3OD) of compound **20**.

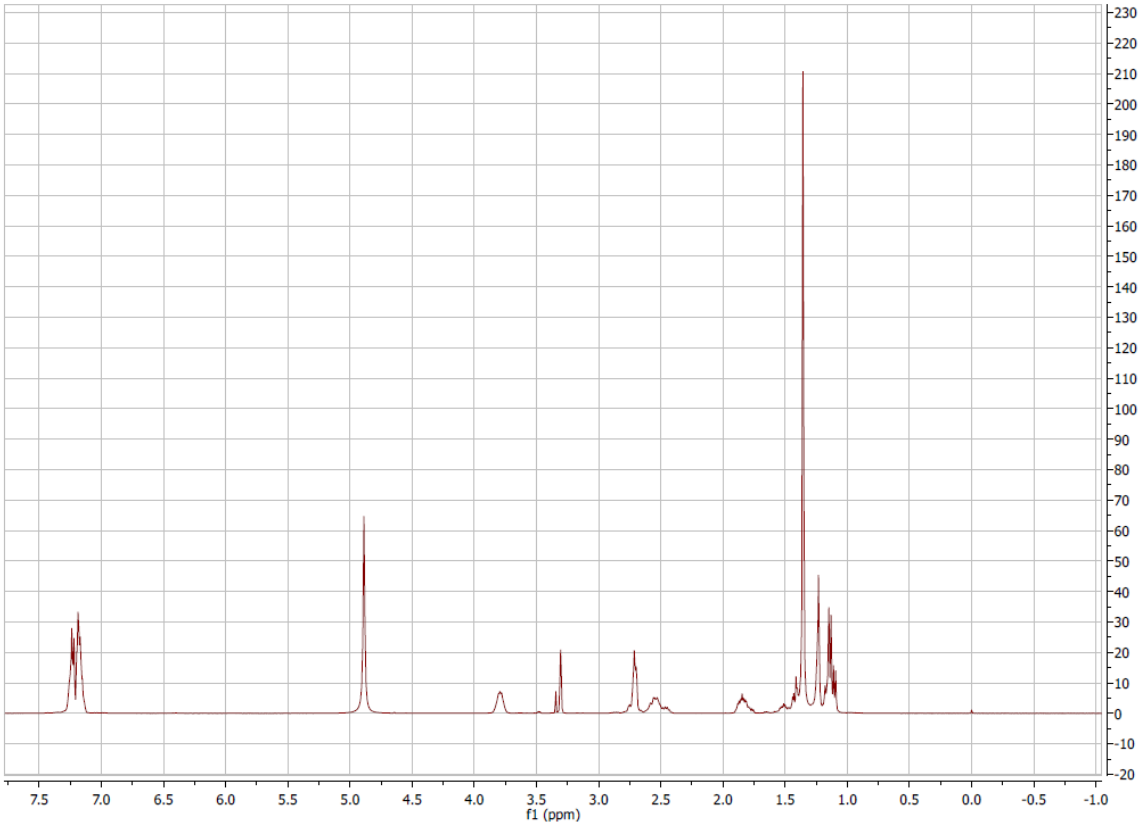

Figure A 37 ^{1}H spectrum (400 MHz, CD_3OD) of compound **21**.

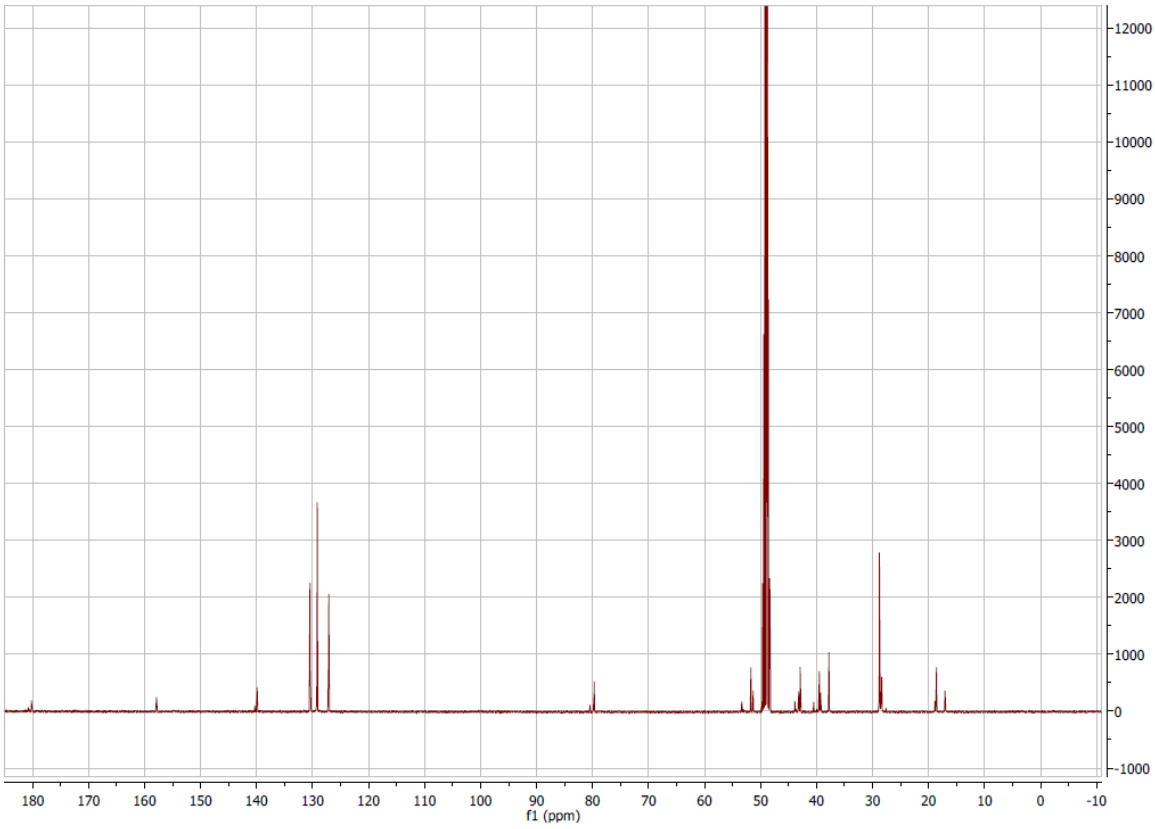

Figure A 38 ^{13}C spectrum (101 MHz, CD_3OD) of compound **21**.

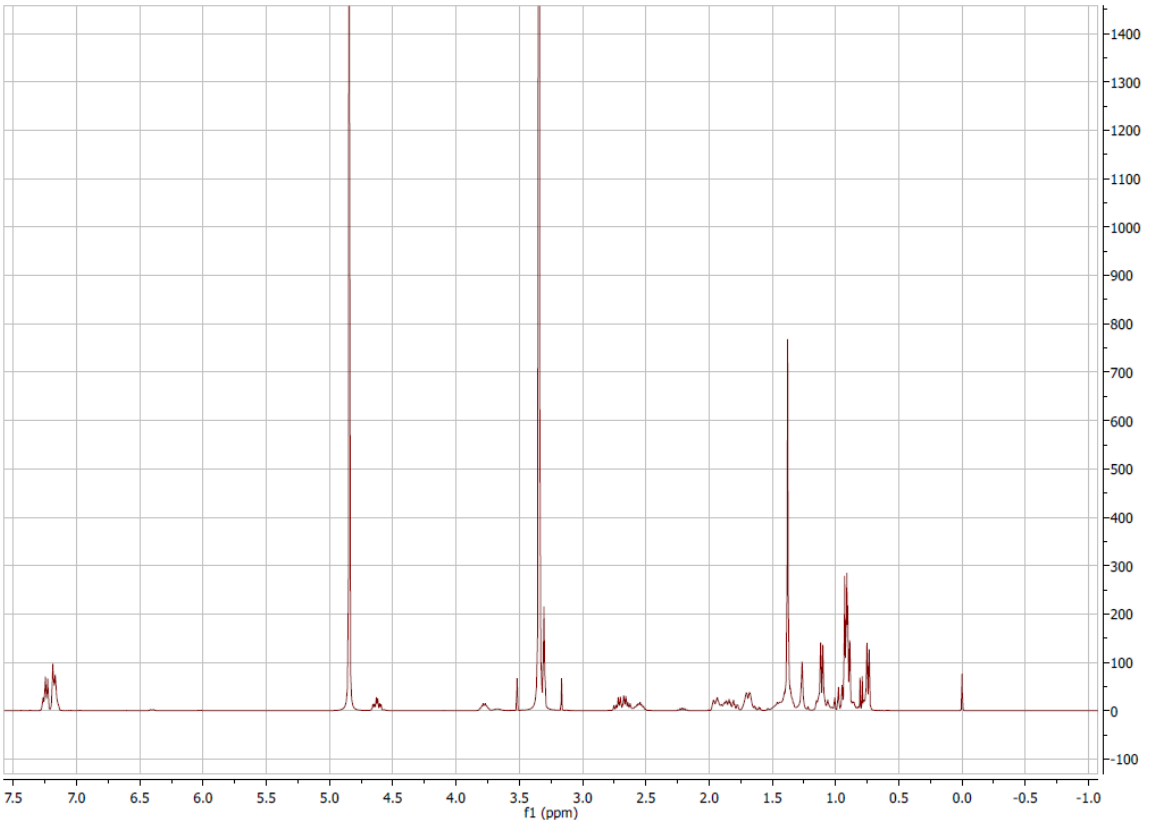

Figure A 39 ^{1}H spectrum (400 MHz, CD_3OD) of compound **22**.

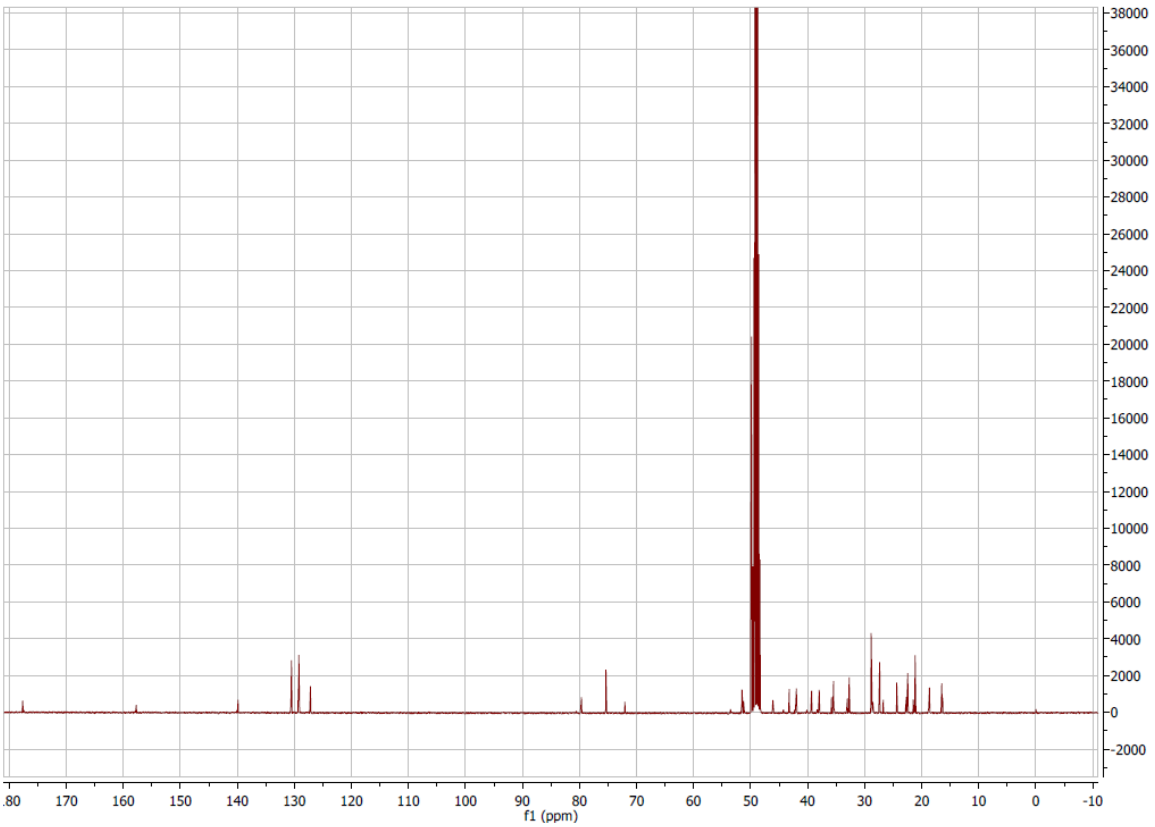

Figure A 40 ^{13}C spectrum (101 MHz, CD_3OD) of compound **22**.

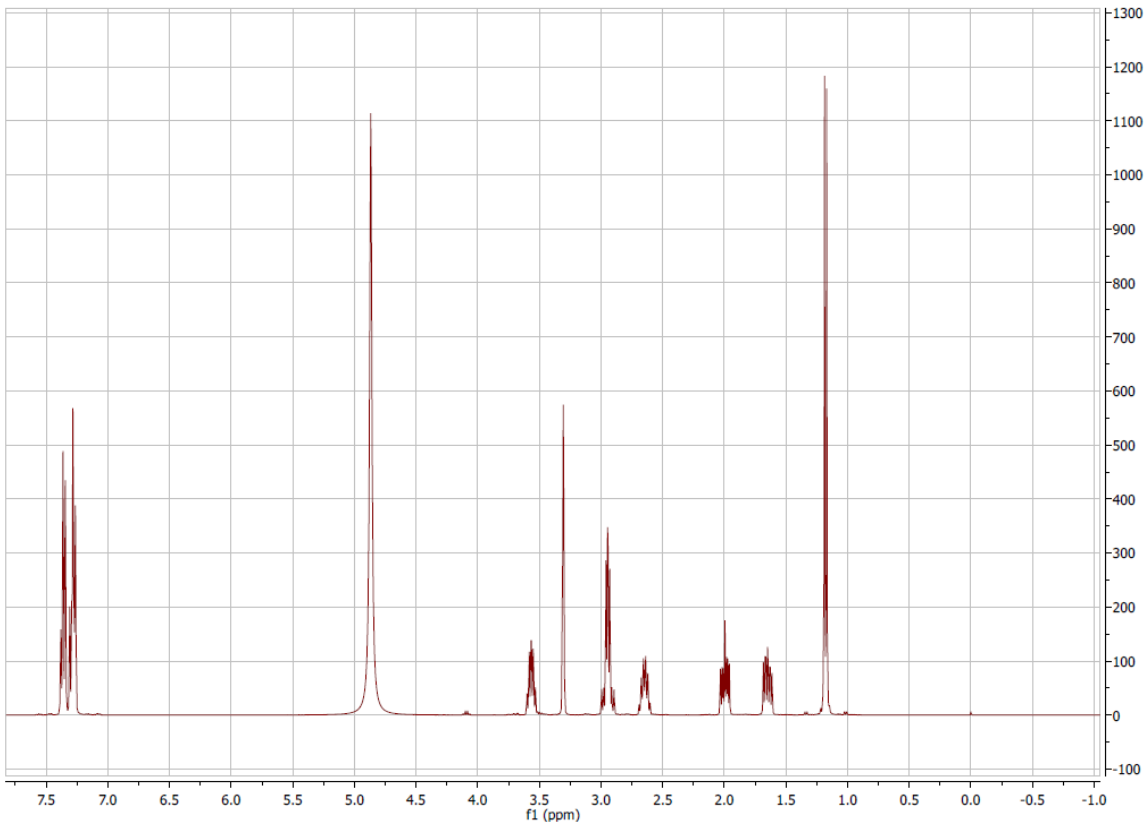

Figure A 41 ^{1}H spectrum (400 MHz, CD_3OD) of compound **23**.

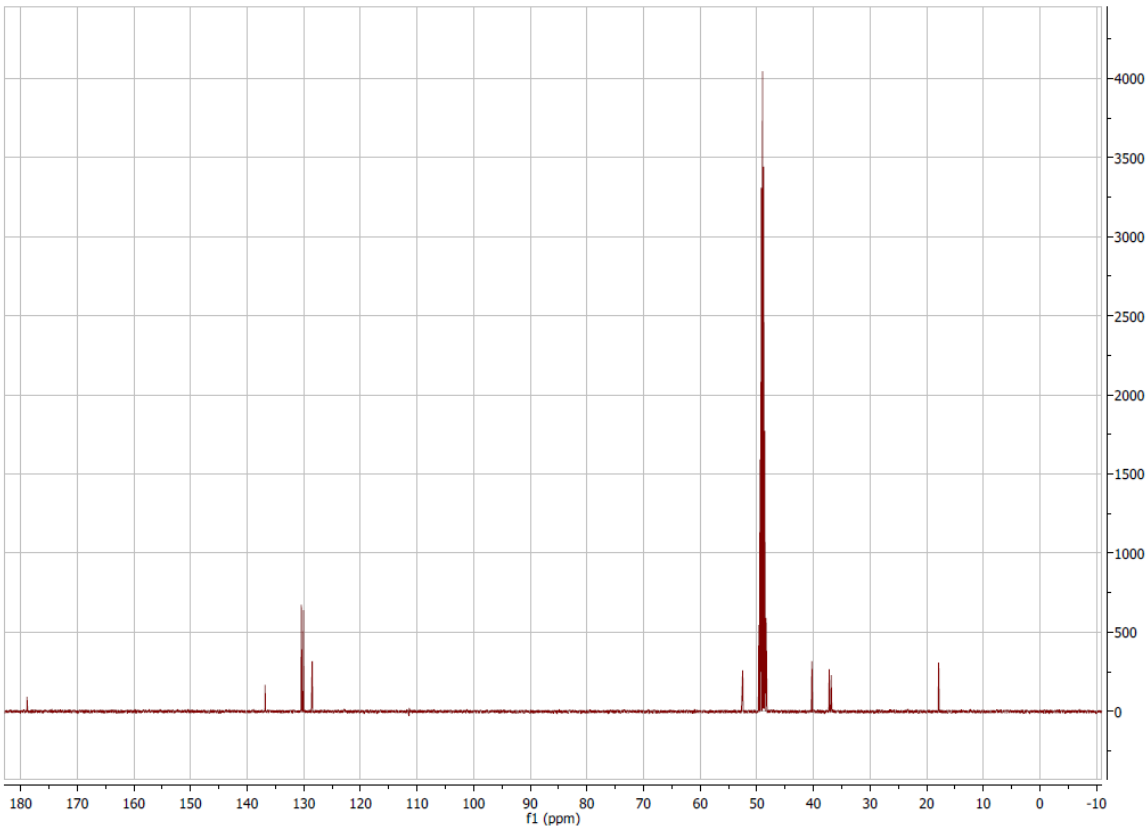

Figure A 42 ^{13}C spectrum (101 MHz, CD_3OD) of compound **23**.

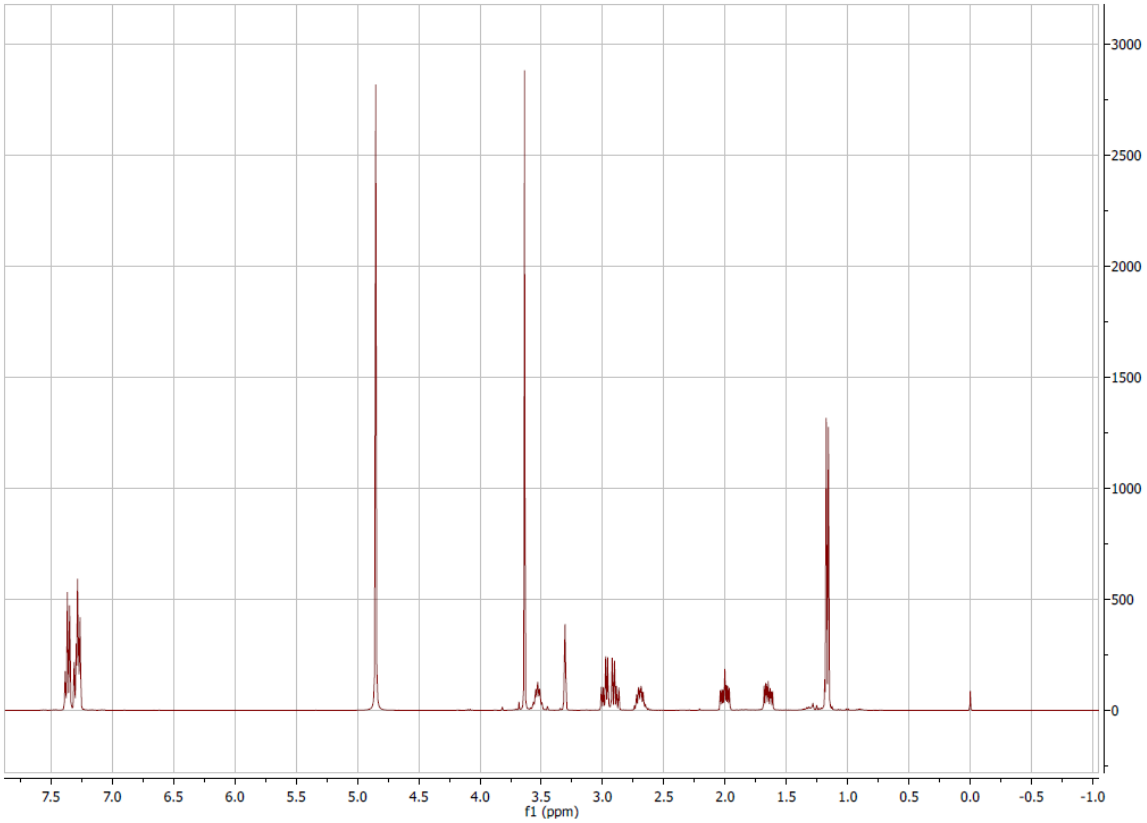

Figure A 43 ^{1}H spectrum (400 MHz, CD_3OD) of compound **24**.

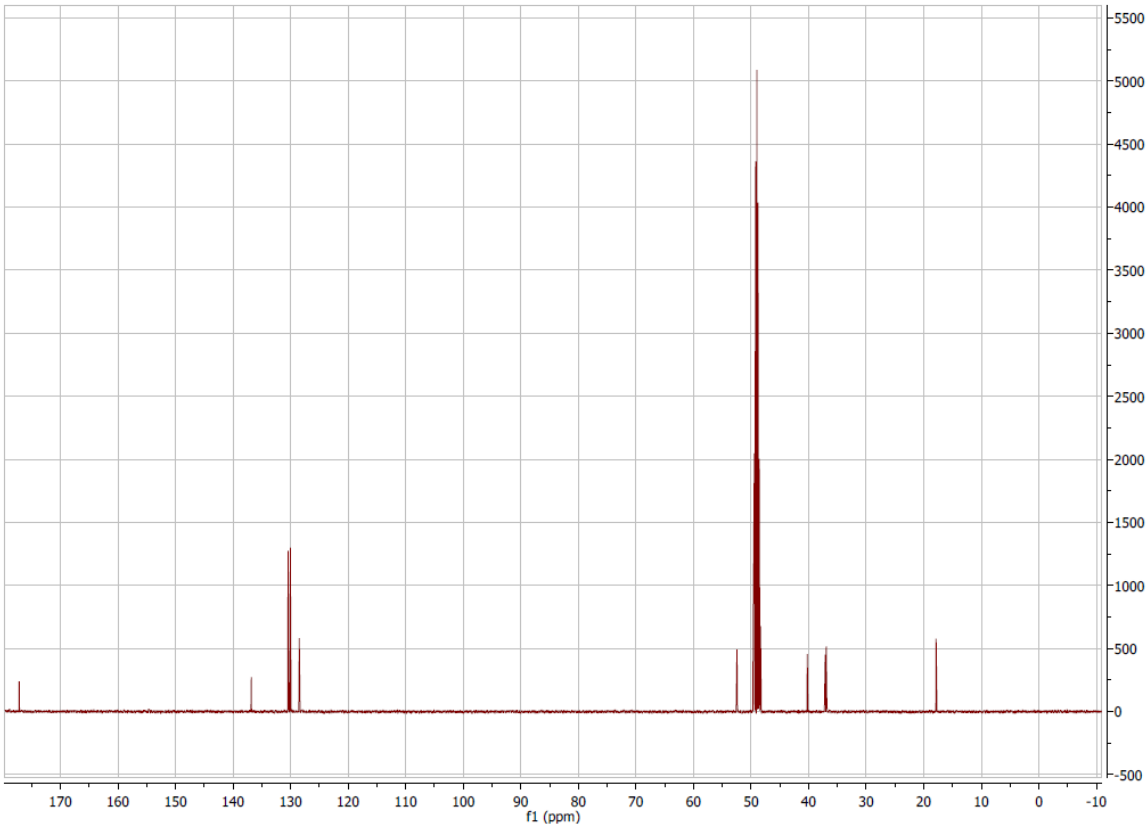

Figure A 44 ^{13}C spectrum (101 MHz, CD_3OD) of compound **24**.

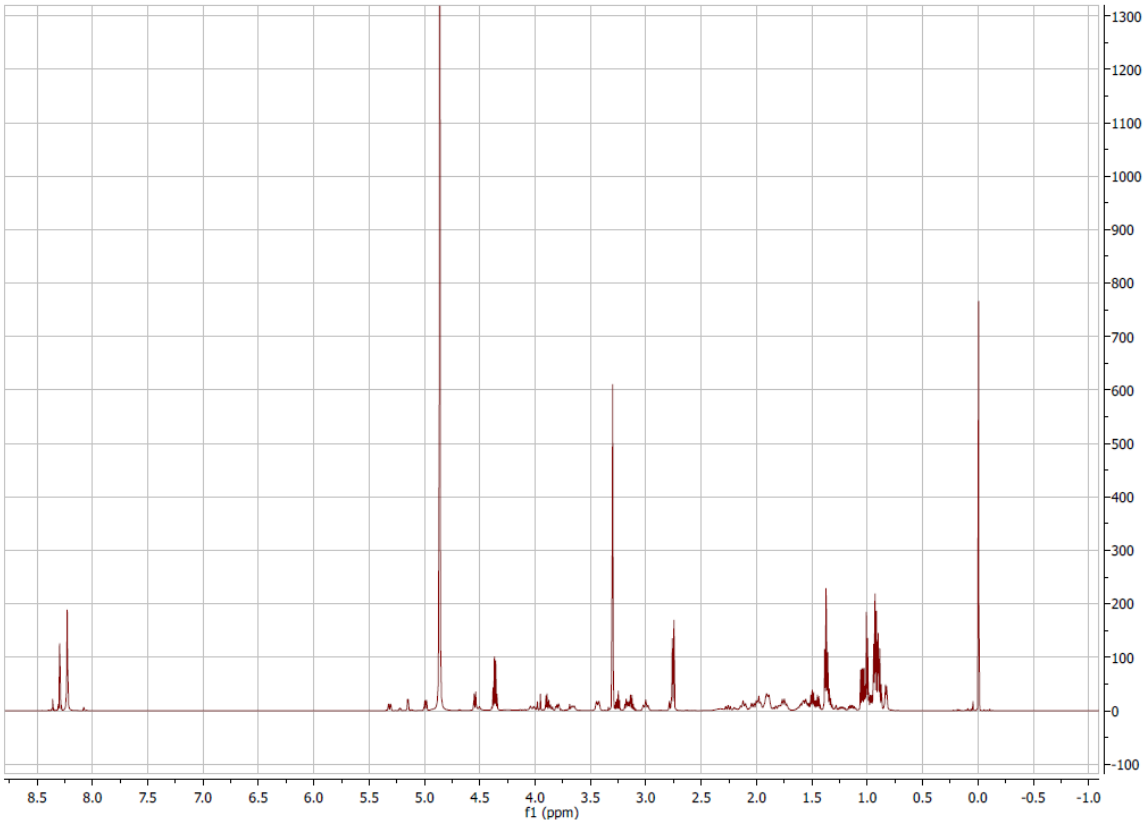

Figure A 45 ^{1}H spectrum (400 MHz, CD_3OD) of compound **25**.

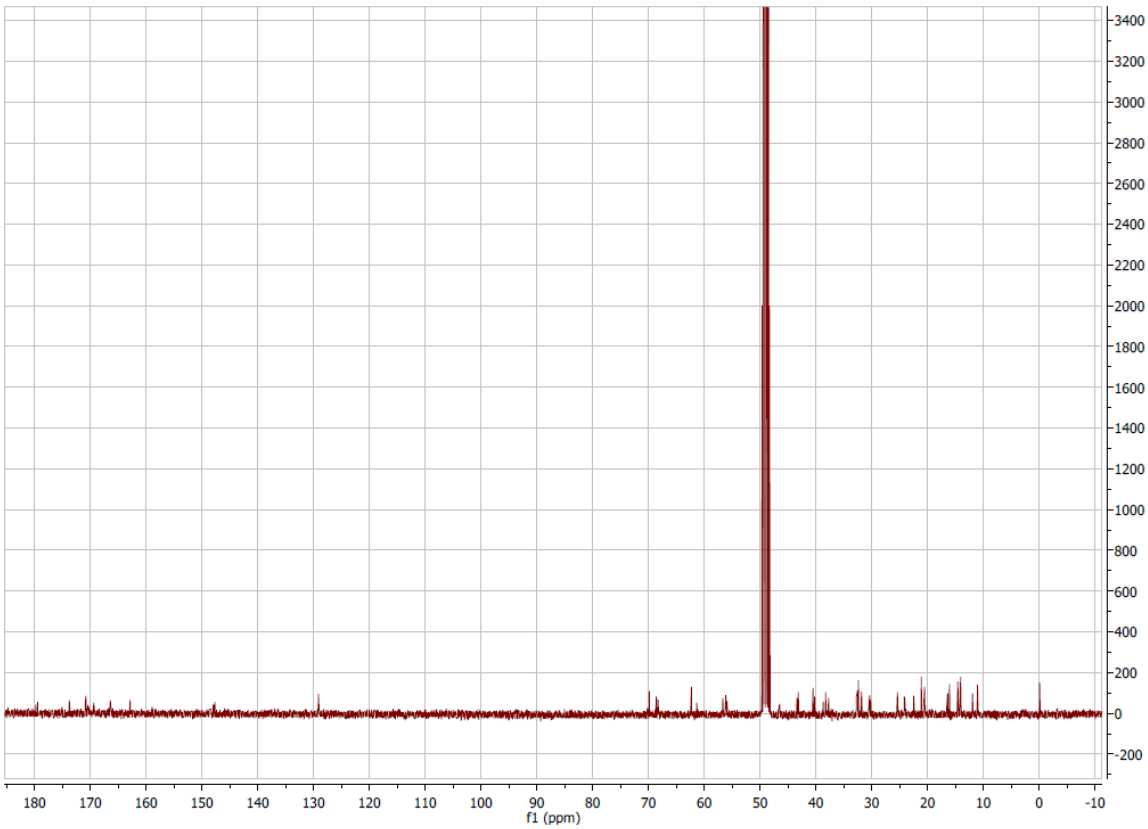

Figure A 46 ^{13}C spectrum (101 MHz, CD_3OD) of compound **25**.

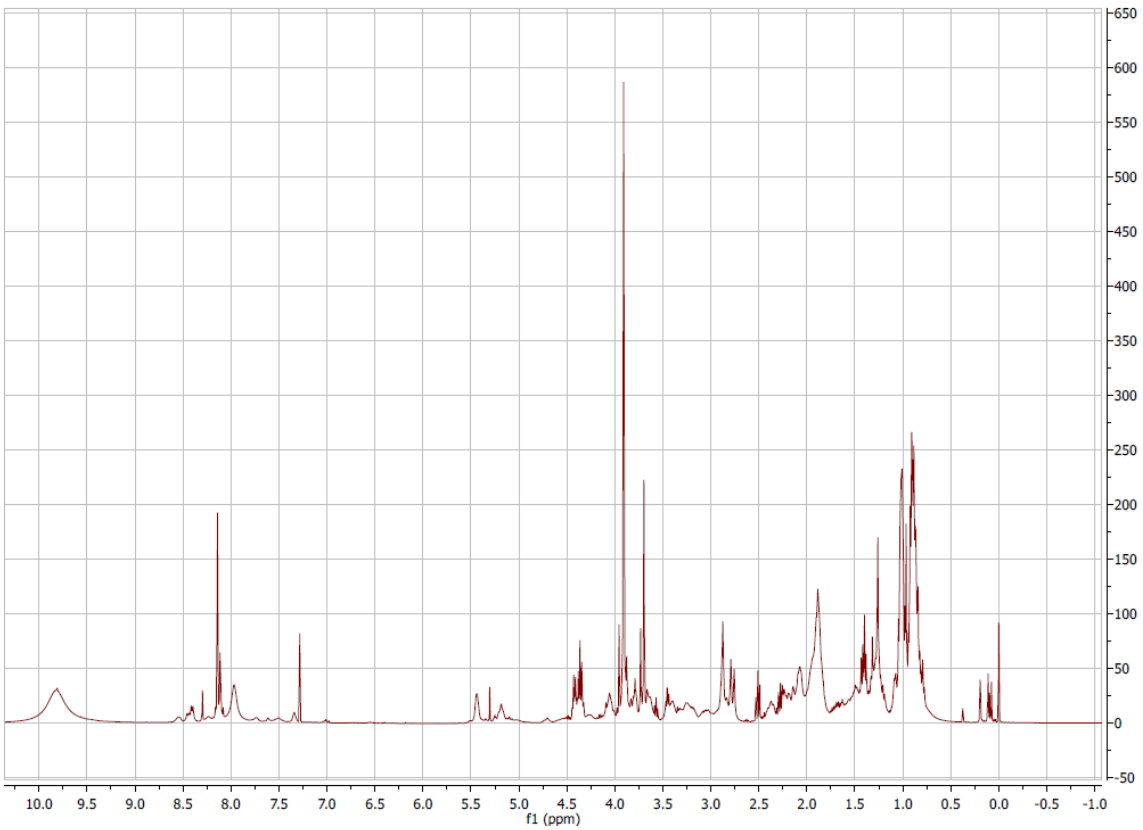

Figure A 47 ^{1}H spectrum (400 MHz, $CDCl_3$) of compound **26**.

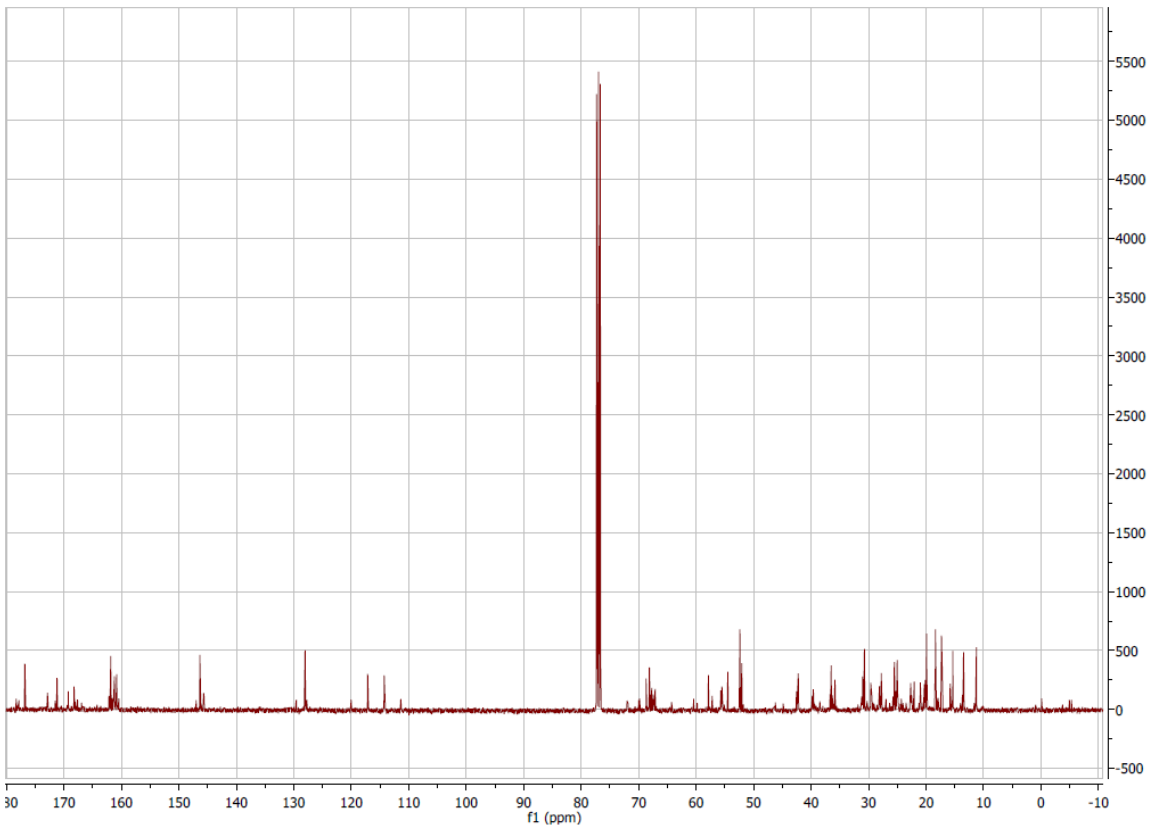

Figure A 48 ^{13}C spectrum (101 MHz, $CDCl_3$) of compound **26**.

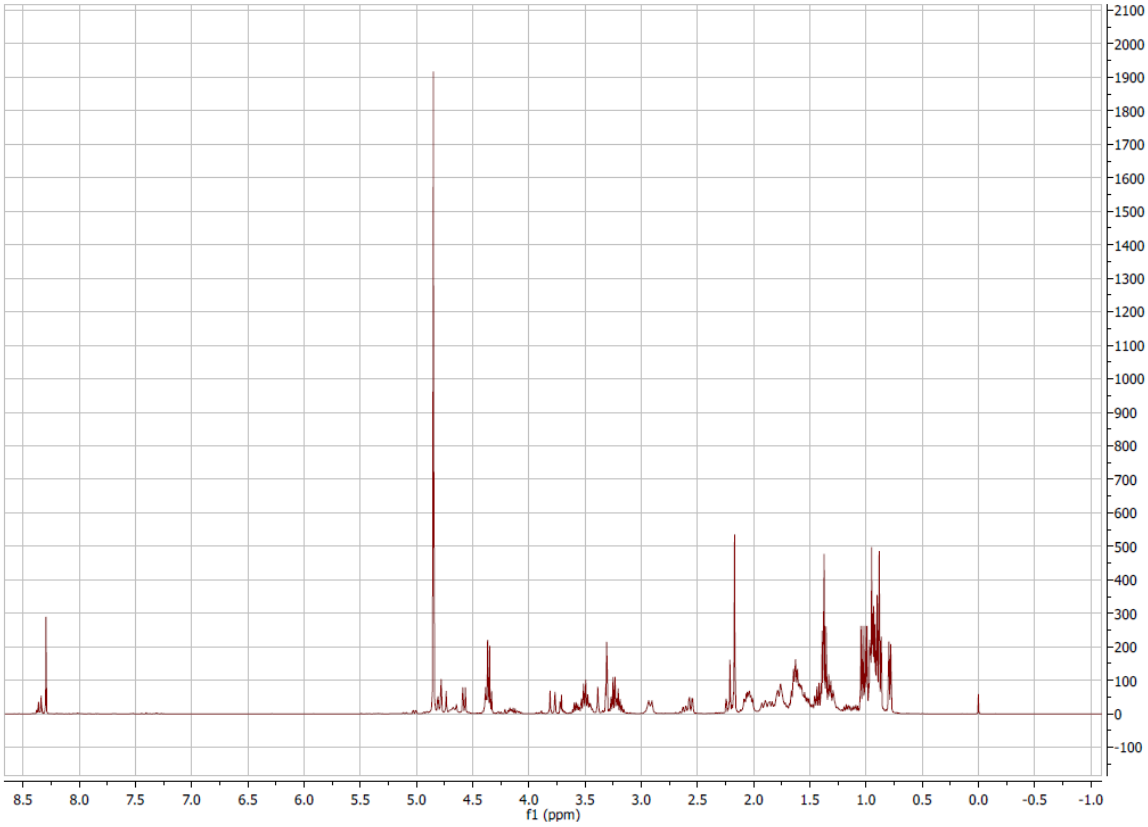

Figure A 49 ^{1}H spectrum (400 MHz, CD_3OD) of compound **27**.

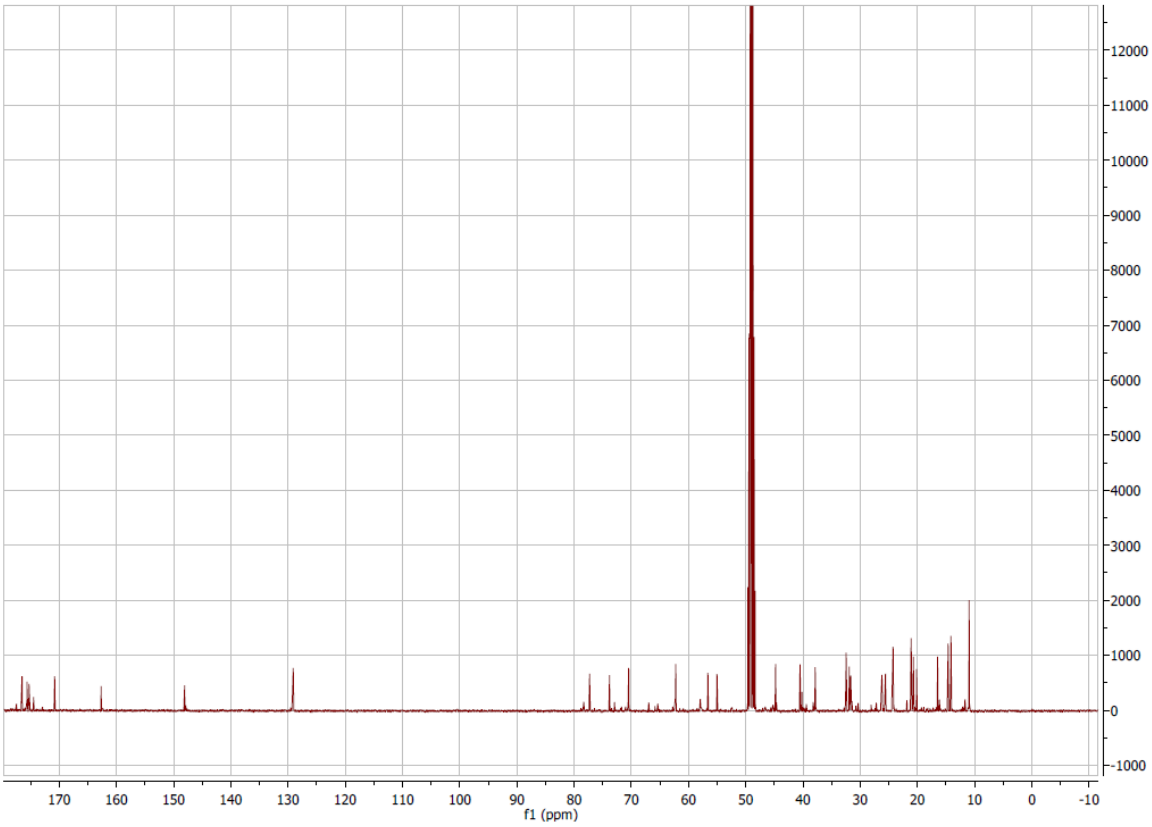

Figure A 50 ^{13}C spectrum (101 MHz, CD_3OD) of compound **27**.

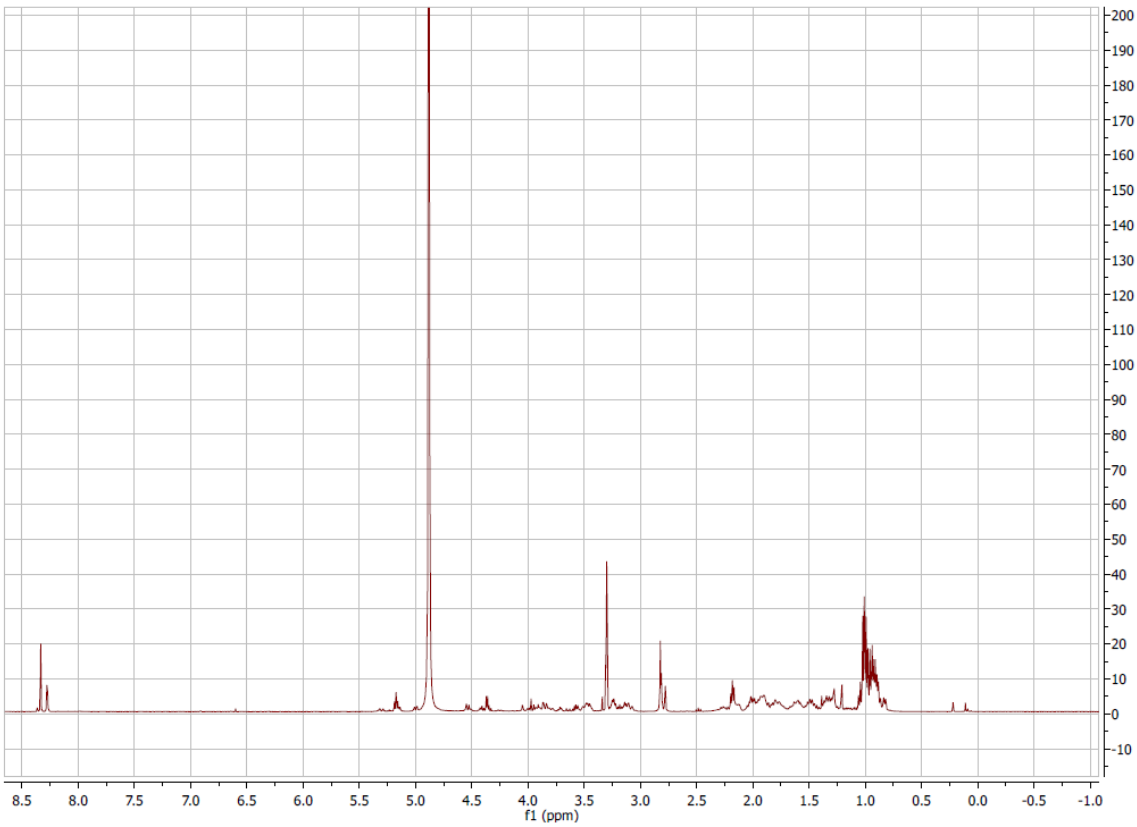

Figure A 51 ^{1}H spectrum (400 MHz, CD_3OD) of compound **28**.

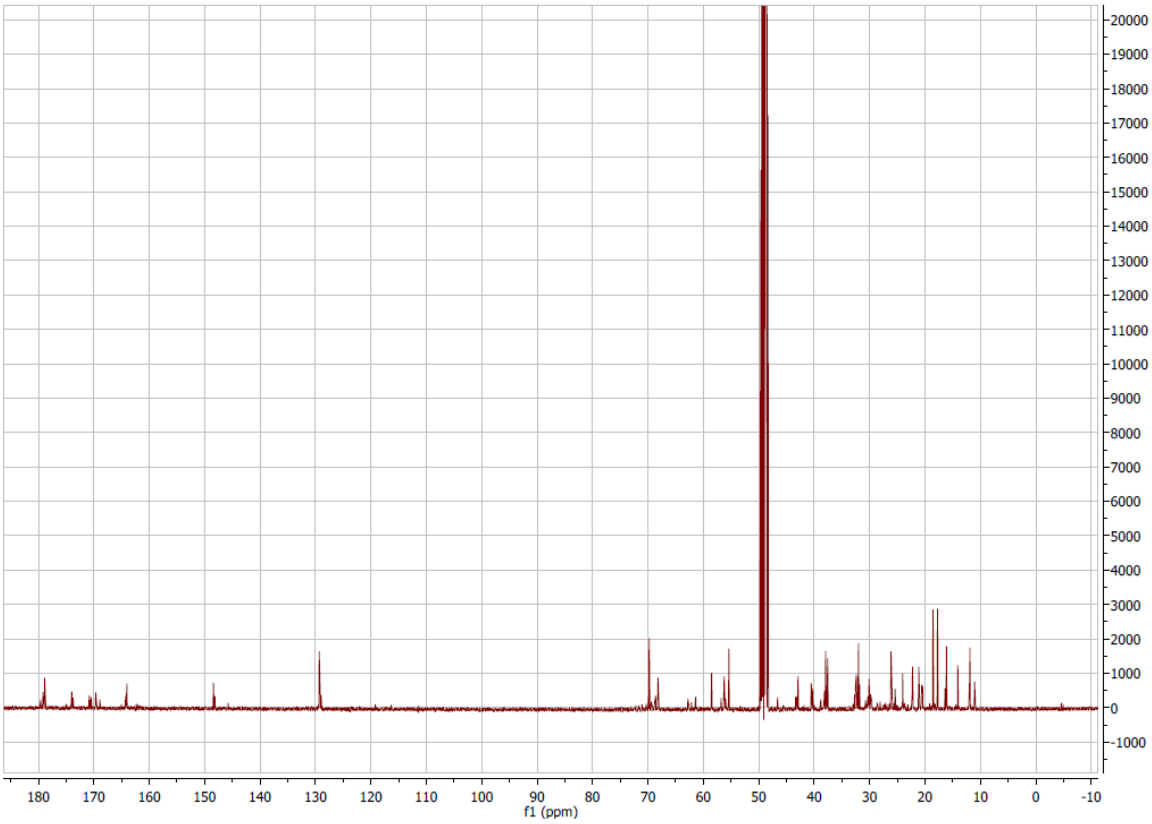

Figure A 52 ^{13}C spectrum (101 MHz, CD_3OD) of compound **28**.

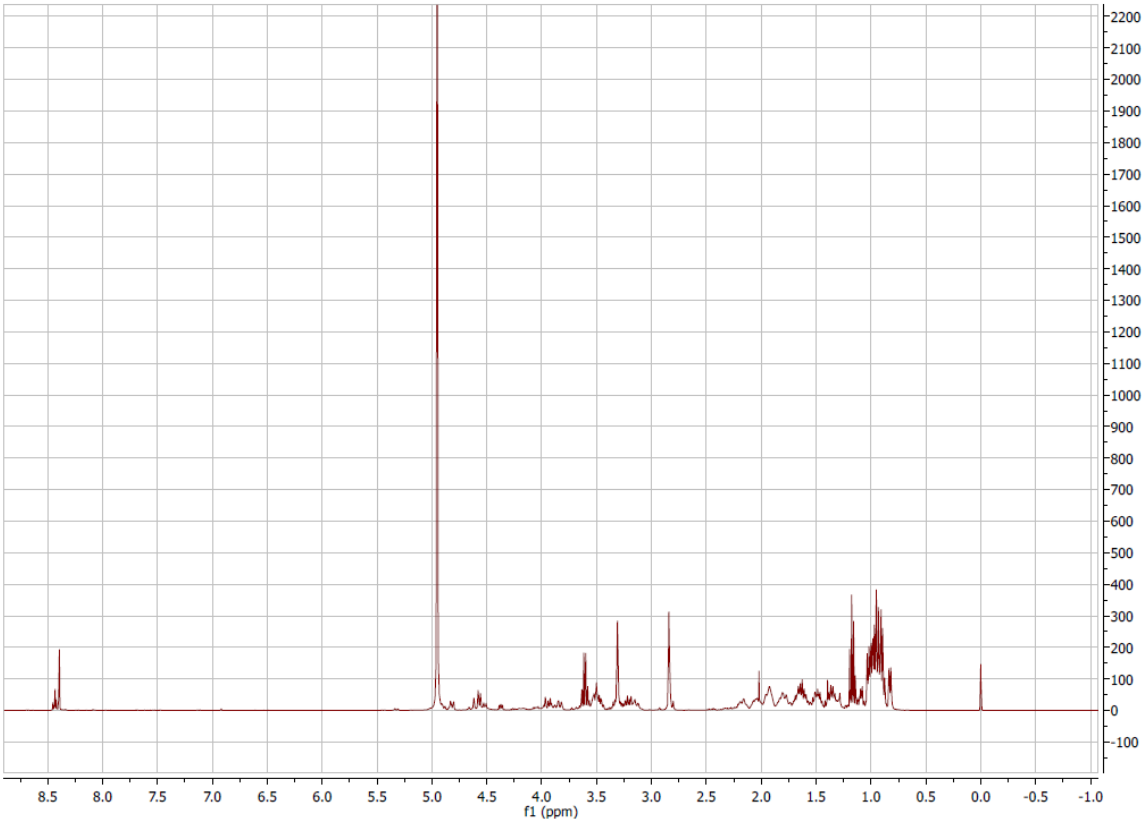

Figure A 53 ^{1}H spectrum (400 MHz, CD_3OD) of compound **29**.

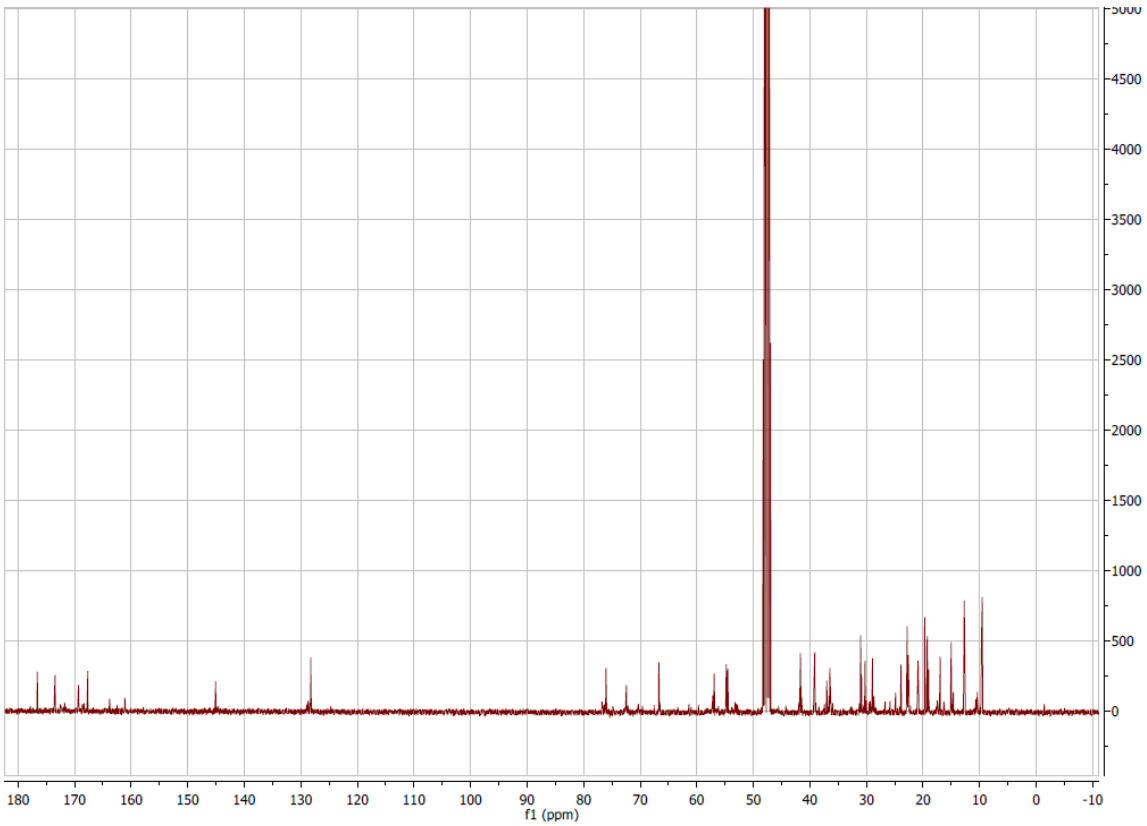

Figure A 54 ^{13}C spectrum (101 MHz, CD_3OD) of compound **29**.

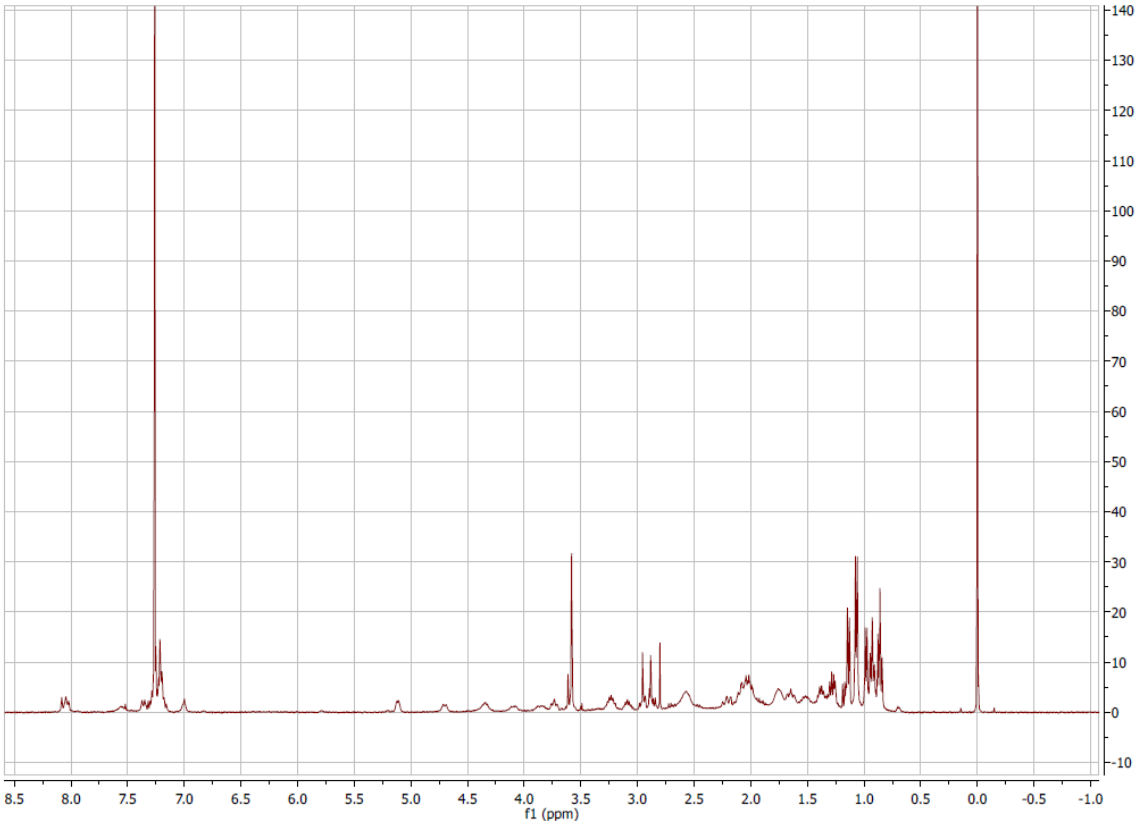

Figure A 55 ^{1}H spectrum (400 MHz, $CDCl_3$) of compound **30**.

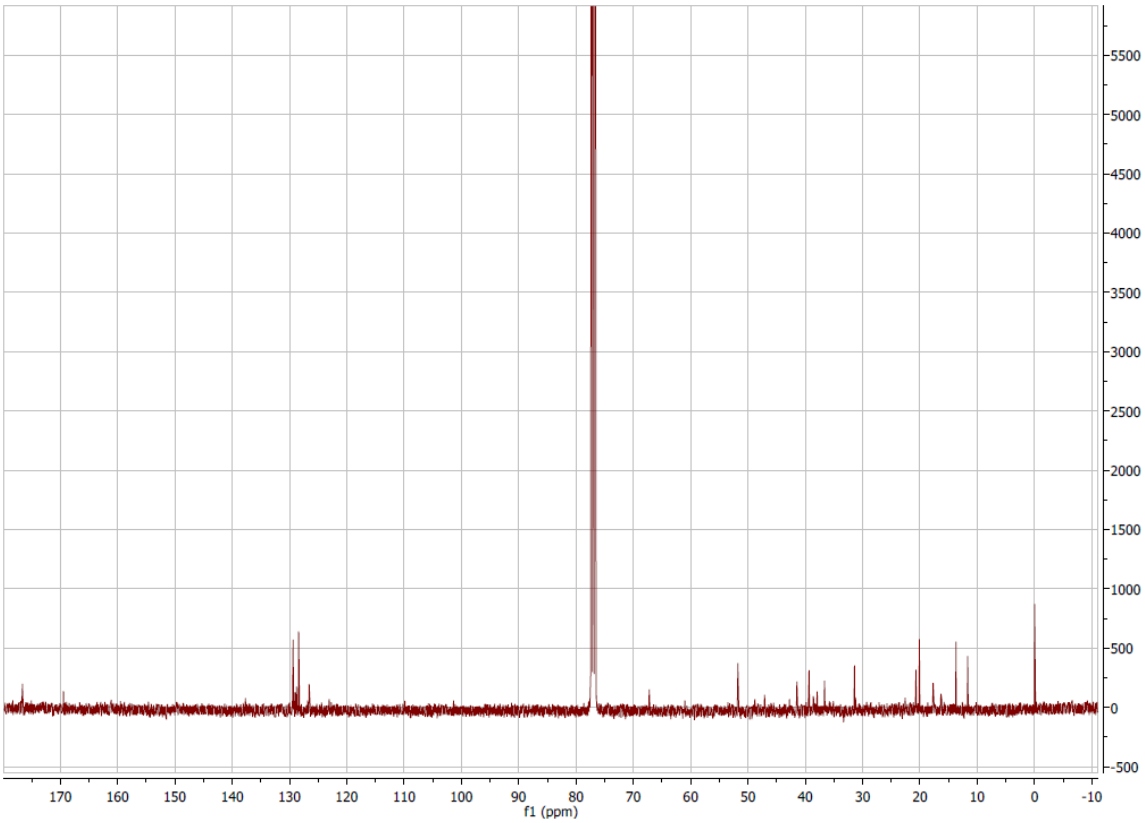

Figure A 56 ^{13}C spectrum (101 MHz, $CDCl_3$) of compound **30**.

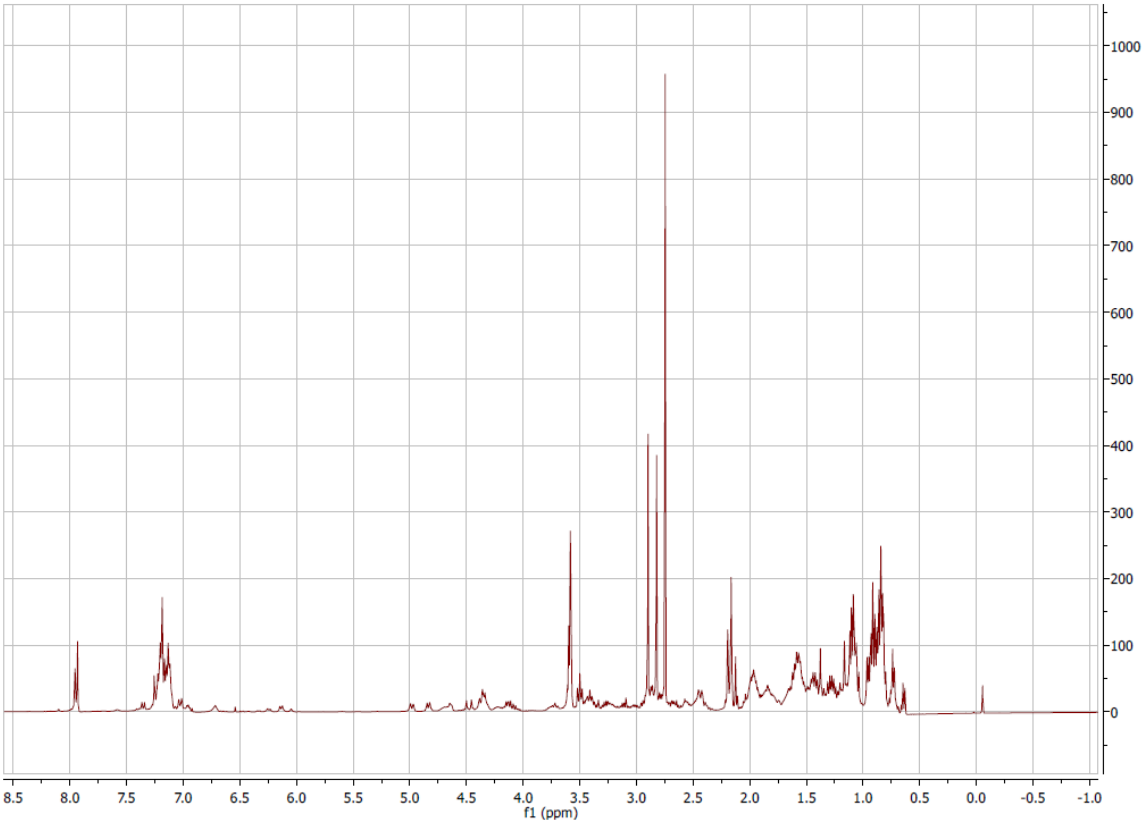

Figure A 57 ^{1}H spectrum (400 MHz, $CDCl_3$) of compound **31**.

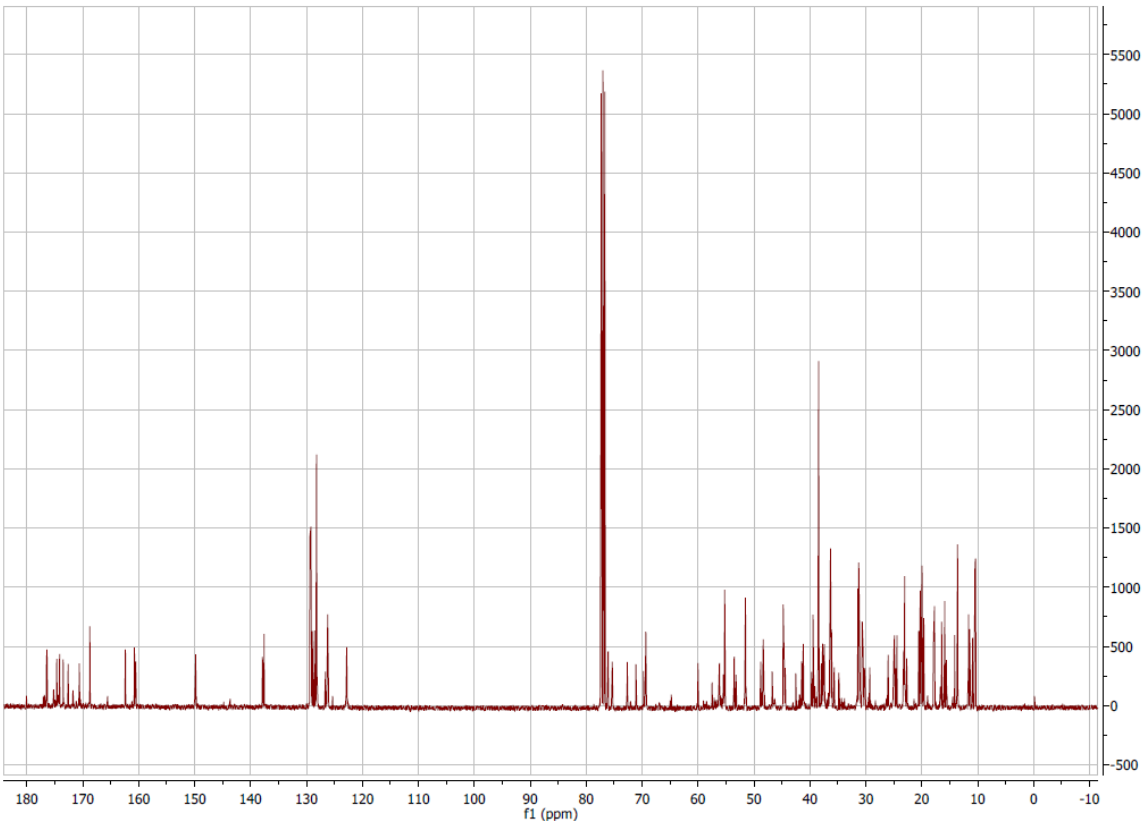

Figure A 58 ^{13}C spectrum (101 MHz, $CDCl_3$) of compound **31**.

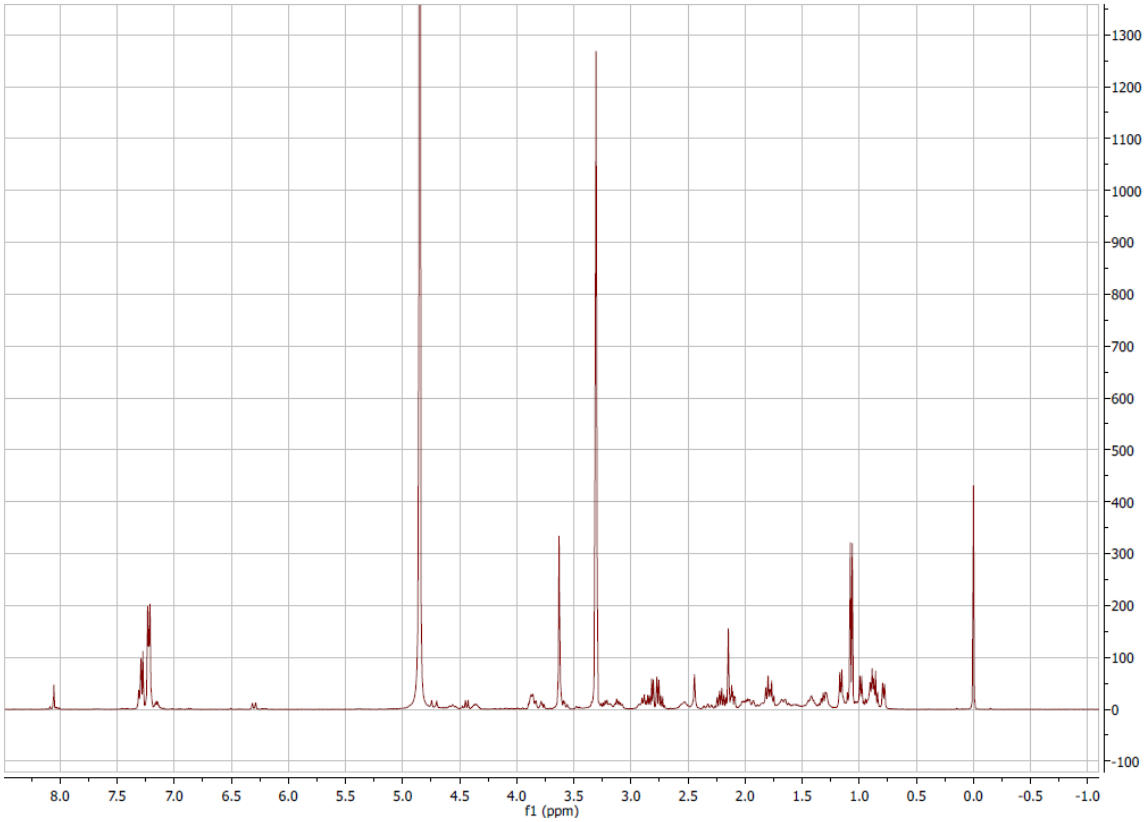

Figure A 59 ^{1}H spectrum (400 MHz, CD_3OD) of compound **33**.

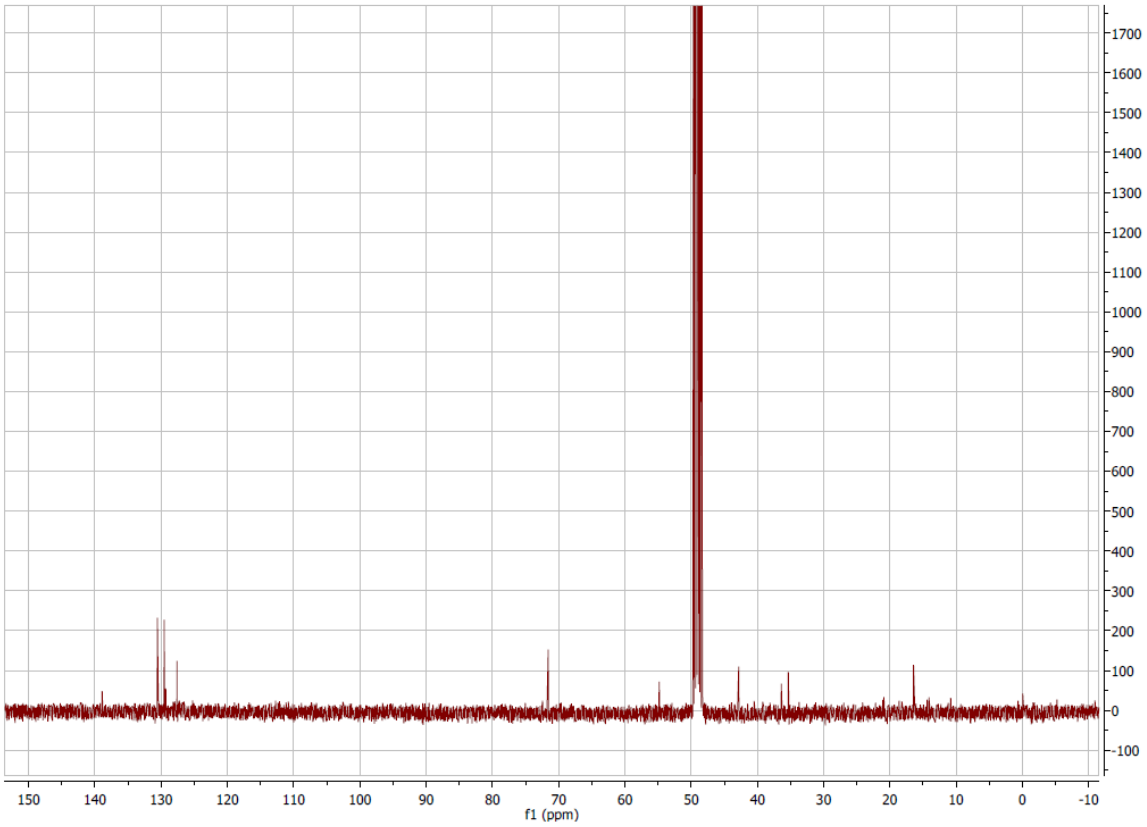

Figure A 60 ^{13}C spectrum (101 MHz, CD_3OD) of compound **33**.

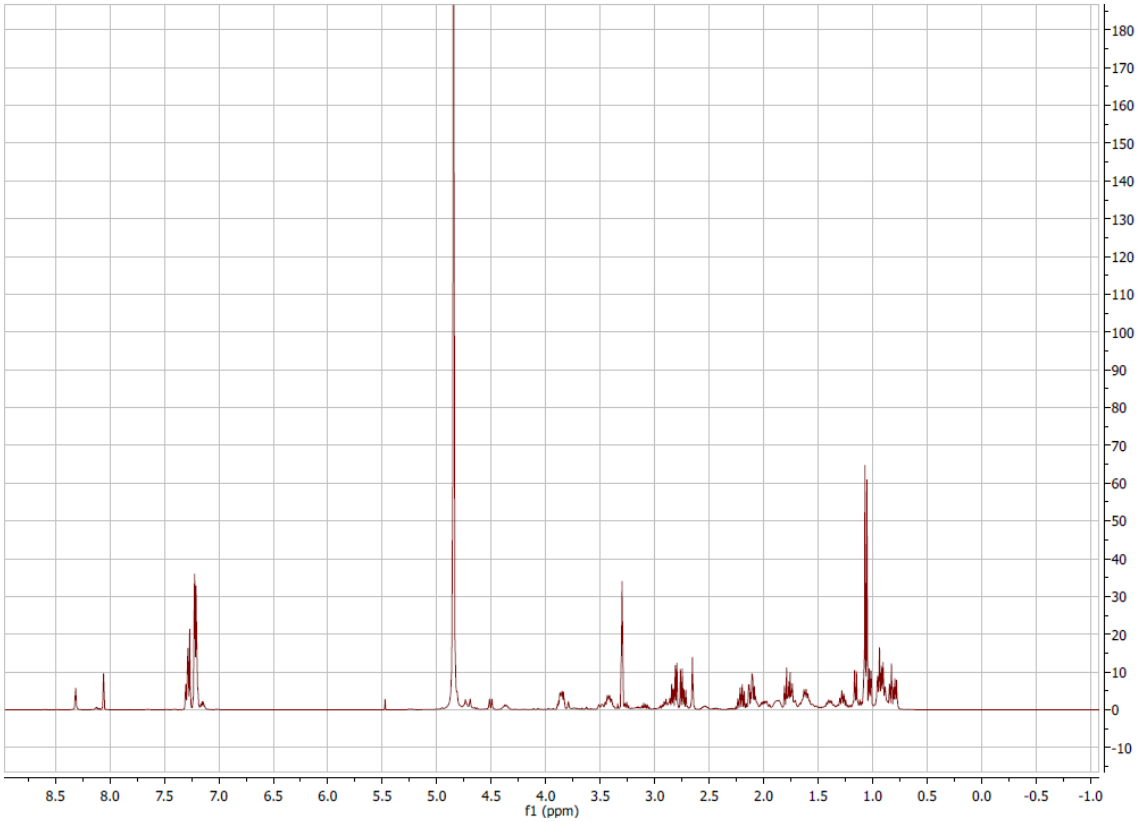

Figure A 61 ^{1}H spectrum (400 MHz, CD_3OD) of compound **34**.

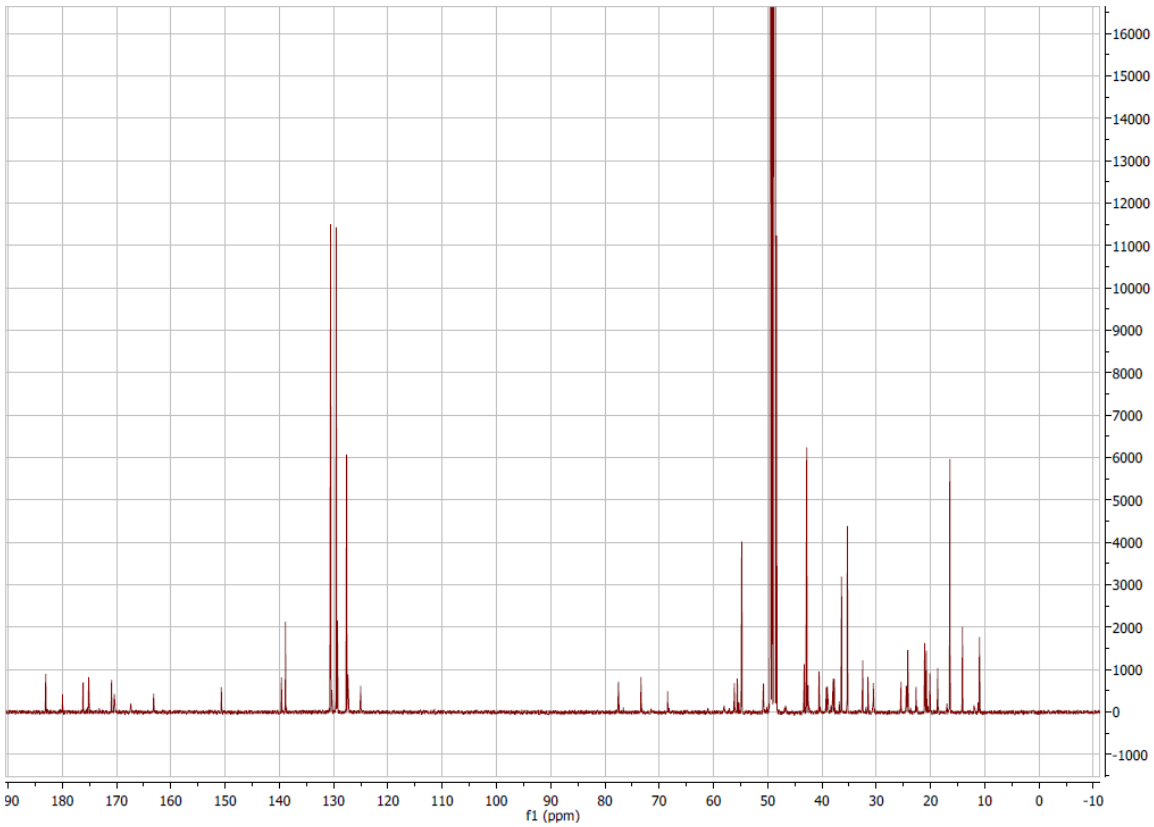

Figure A 62 ^{13}C spectrum (101 MHz, CD_3OD) of compound **34**.

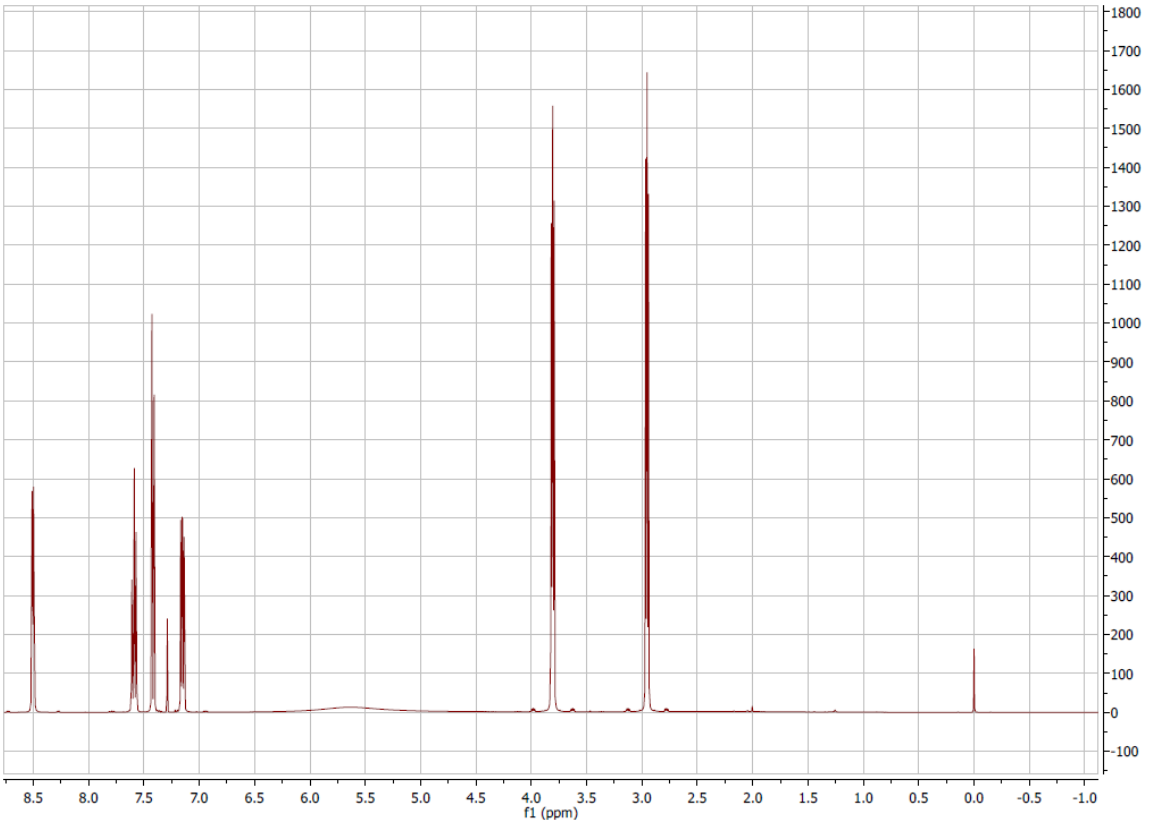

Figure A 63 ^{1}H spectrum (400 MHz, $CDCl_3$) of compound **35**.

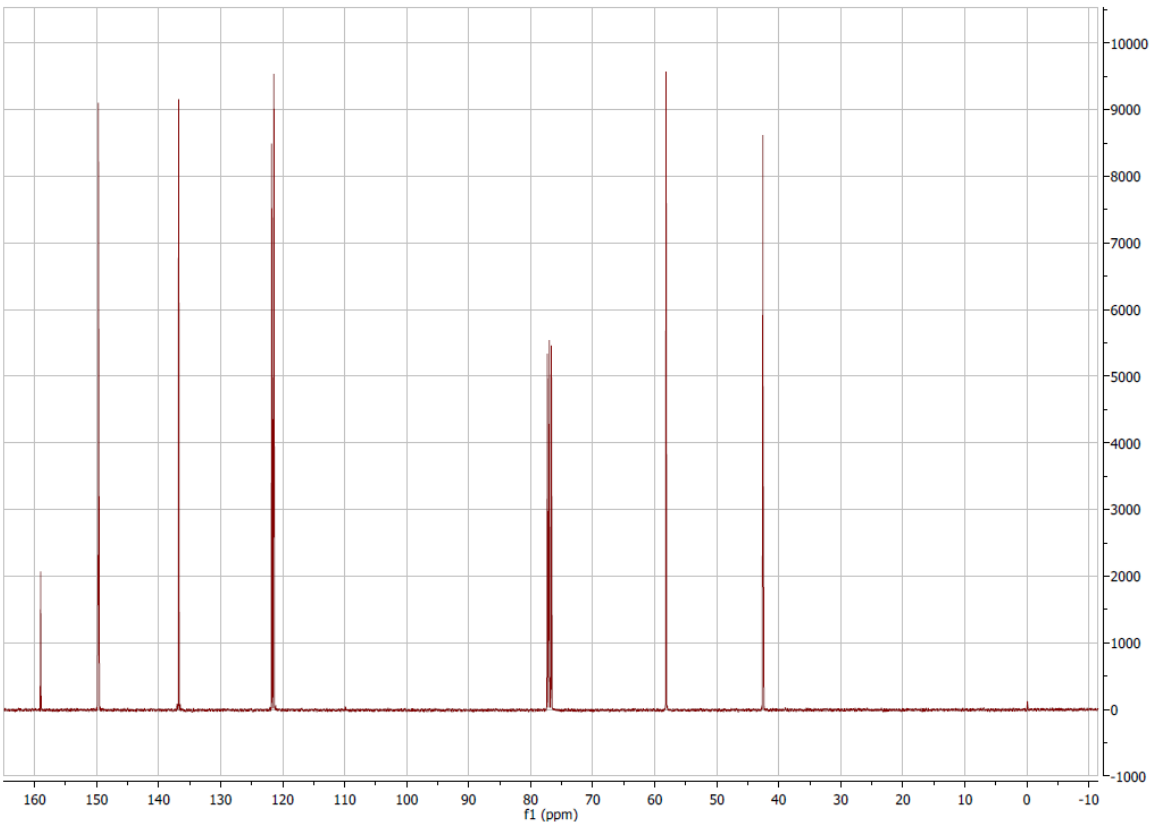

Figure A 64 ^{13}C spectrum (101 MHz, $CDCl_3$) of compound **35**.

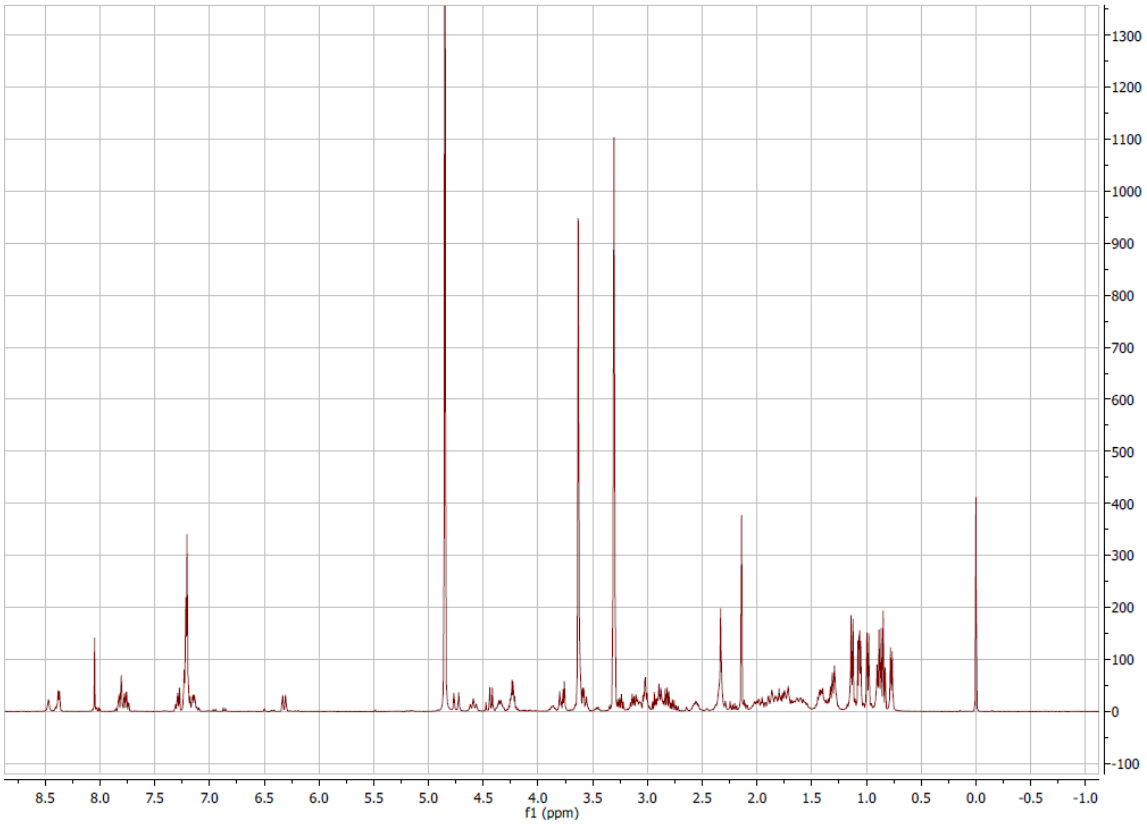

Figure A 65 ^{1}H spectrum (400 MHz, CD_3OD) of compound **36**.

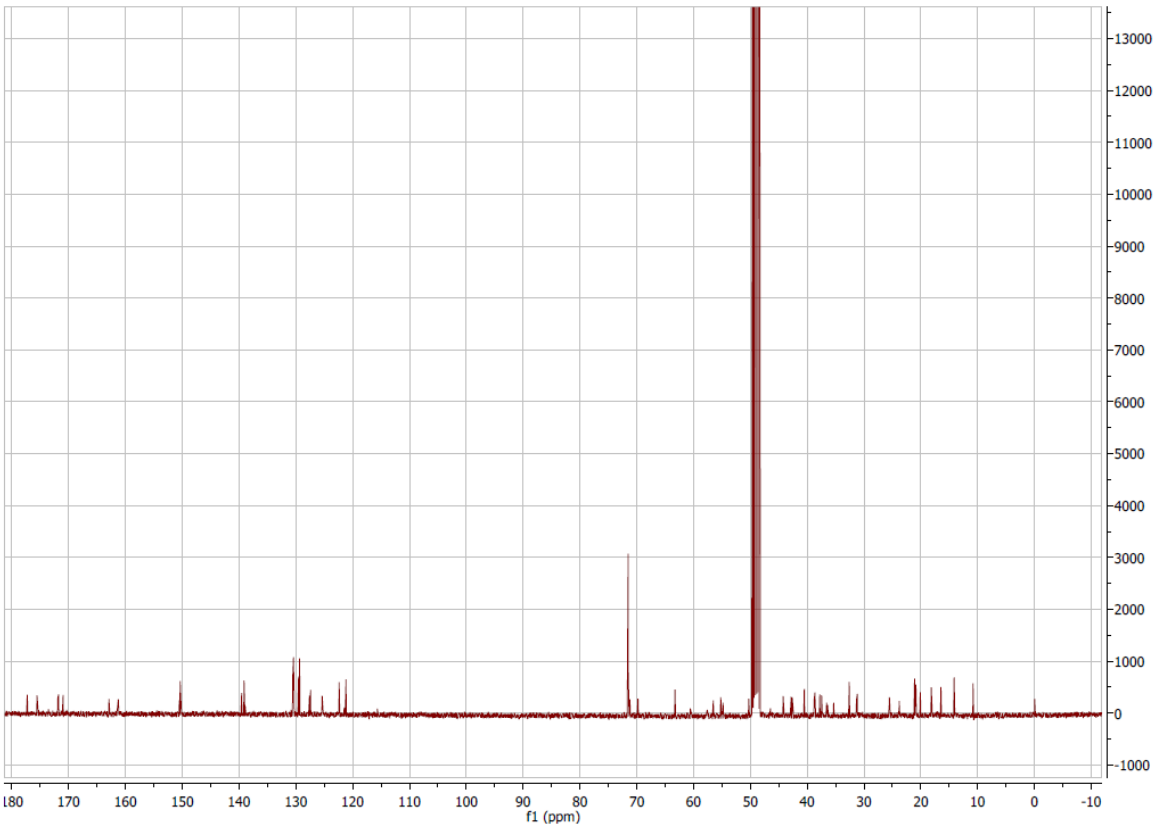

Figure A 66 ^{13}C spectrum (101 MHz, CD_3OD) of compound **36**.

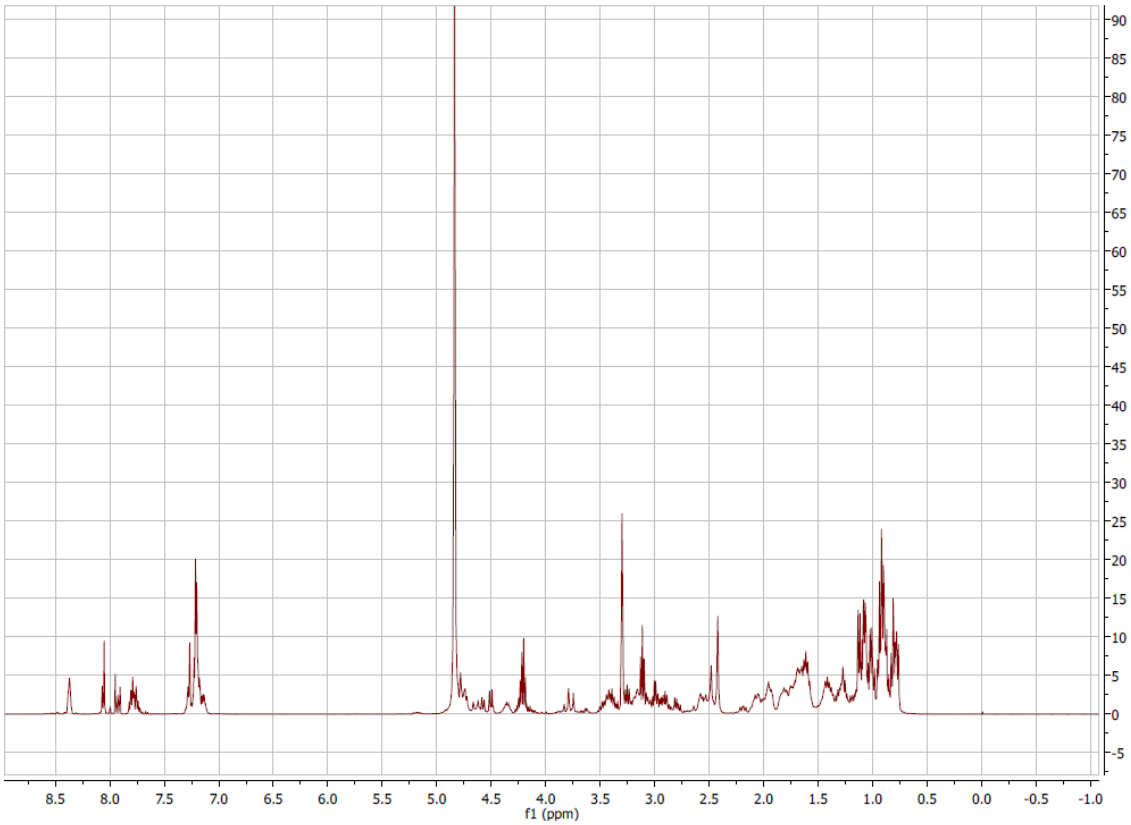

Figure A 67 ^{1}H spectrum (400 MHz, CD_3OD) of compound **37**.

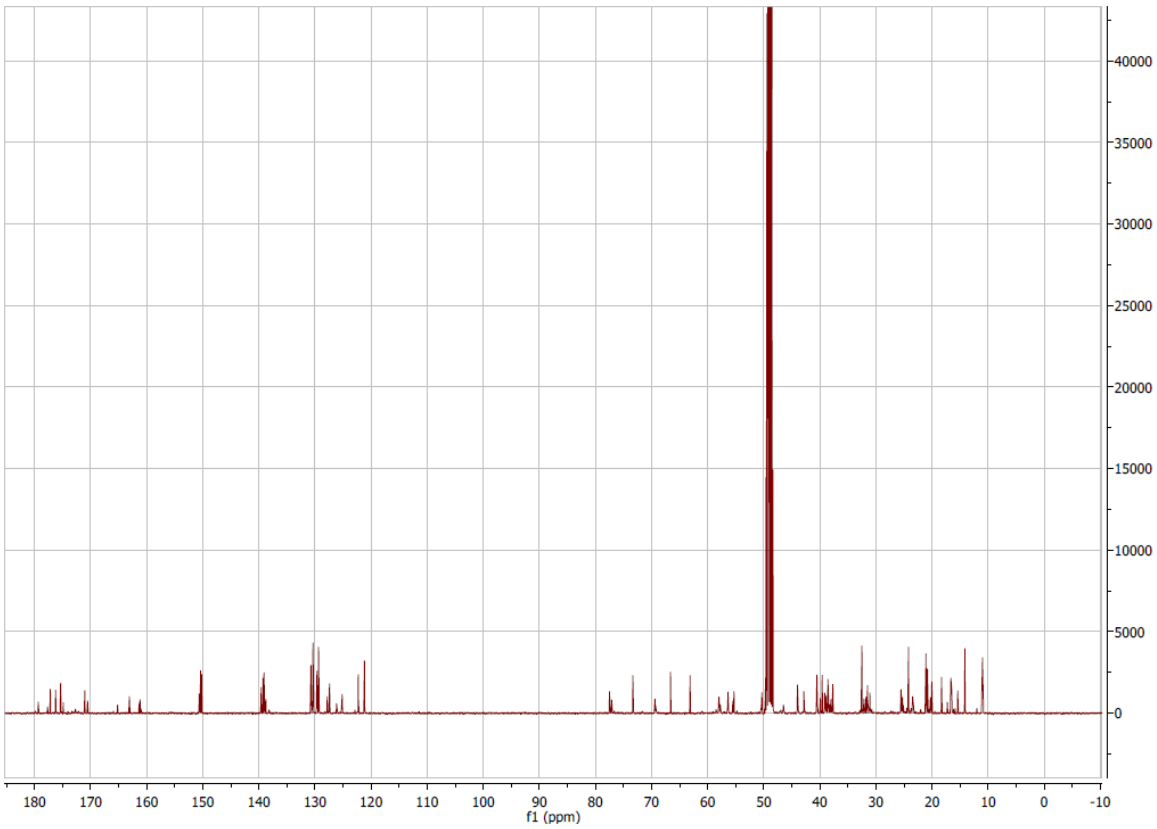

Figure A 68 ^{13}C spectrum (101 MHz, CD_3OD) of compound **37**.

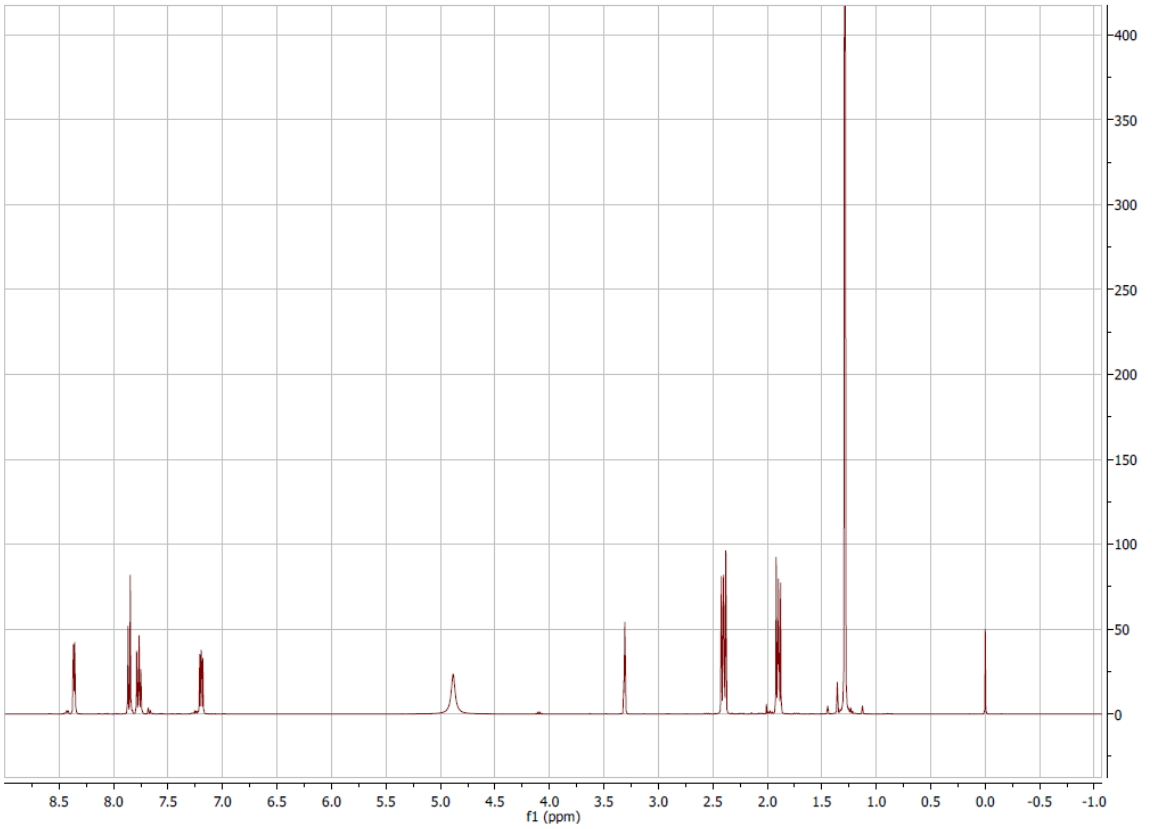

Figure A 69 ^{1}H spectrum (400 MHz, CD_3OD) of compound **38**.

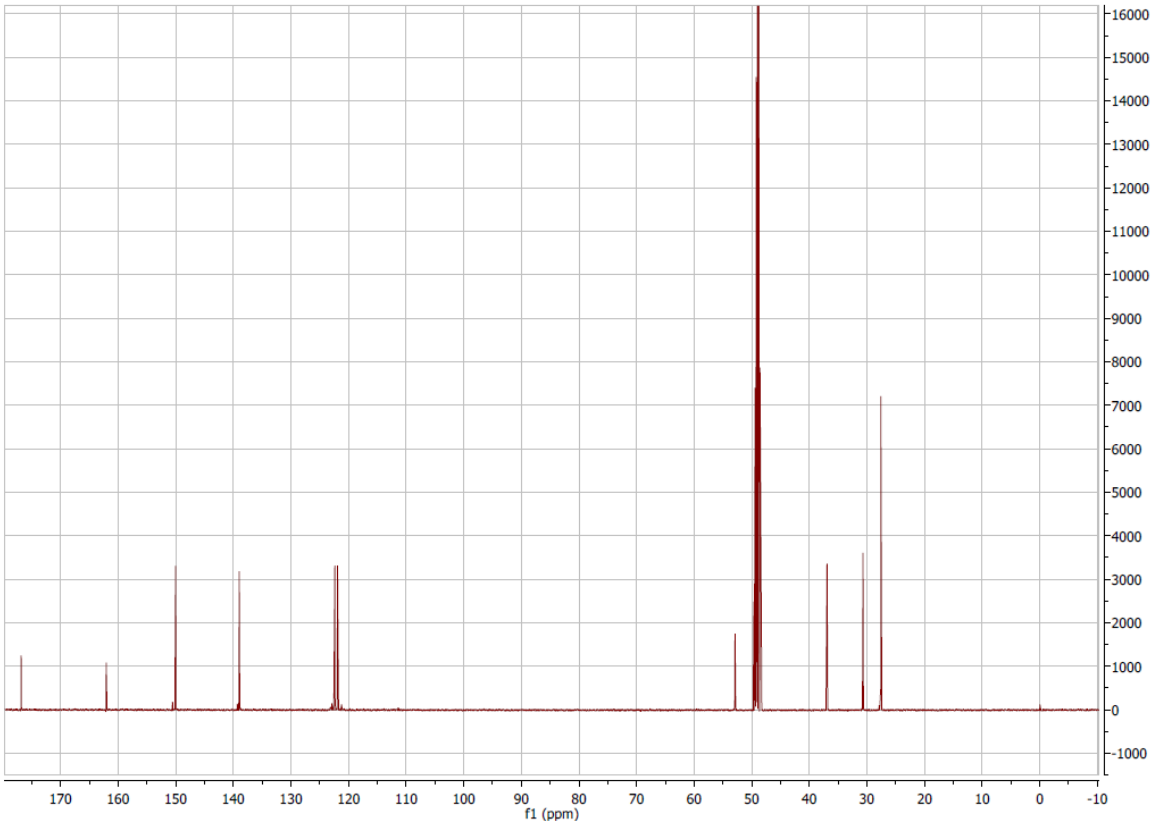

Figure A 70 ^{13}C spectrum (101 MHz, CD_3OD) of compound **38**.

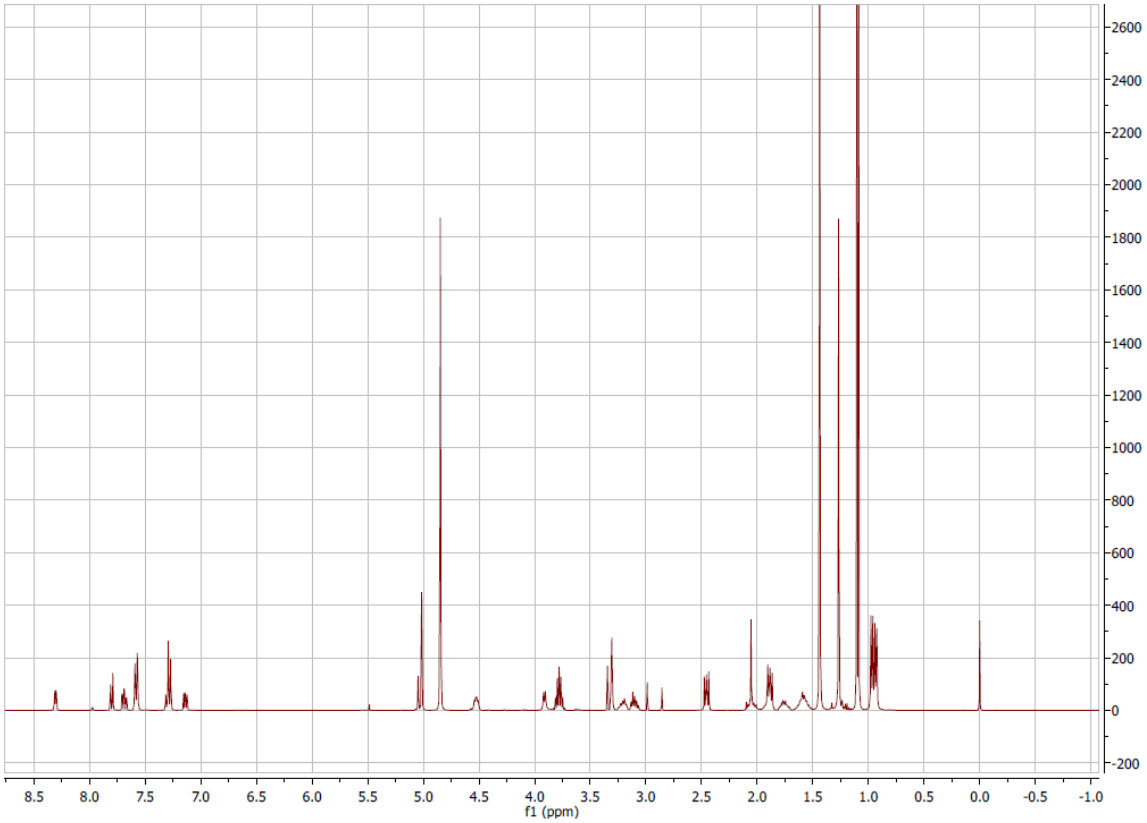

Figure A 71 ^{1}H spectrum (400 MHz, CD_3OD) of compound **39**.

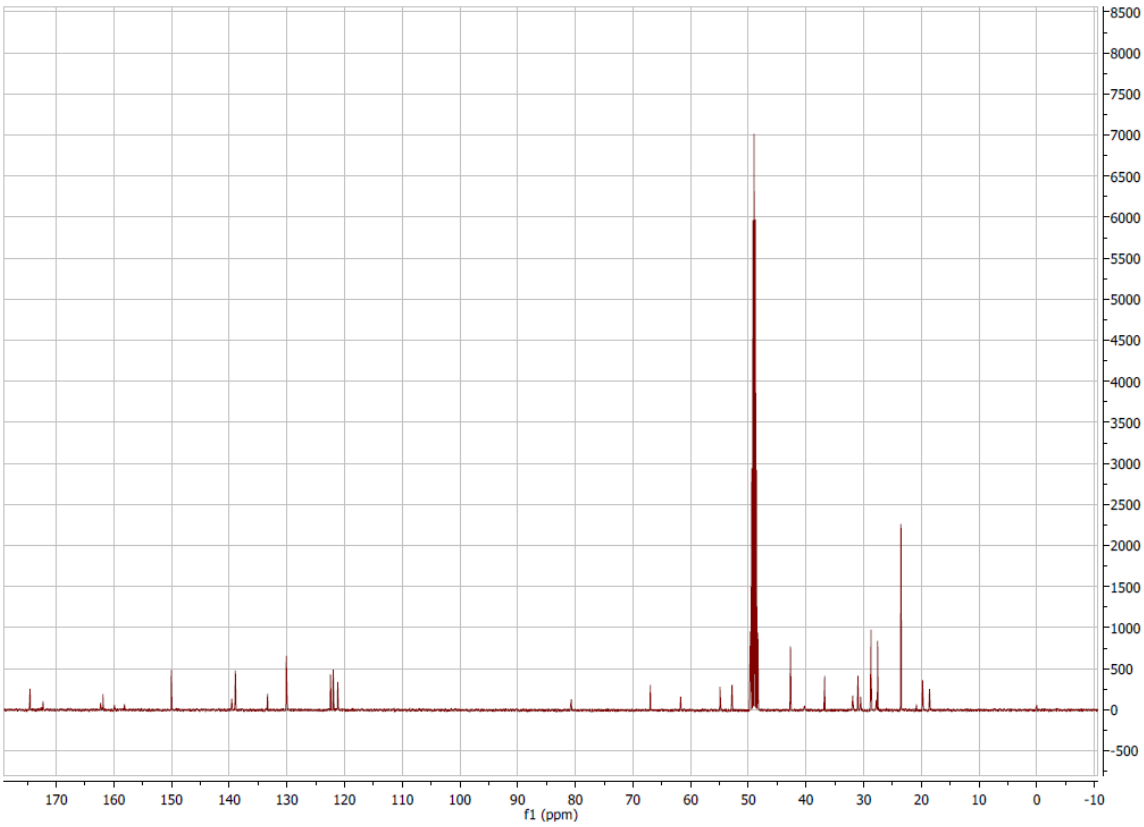

Figure A 72 ^{13}C spectrum (101 MHz, CD_3OD) of compound **39**.

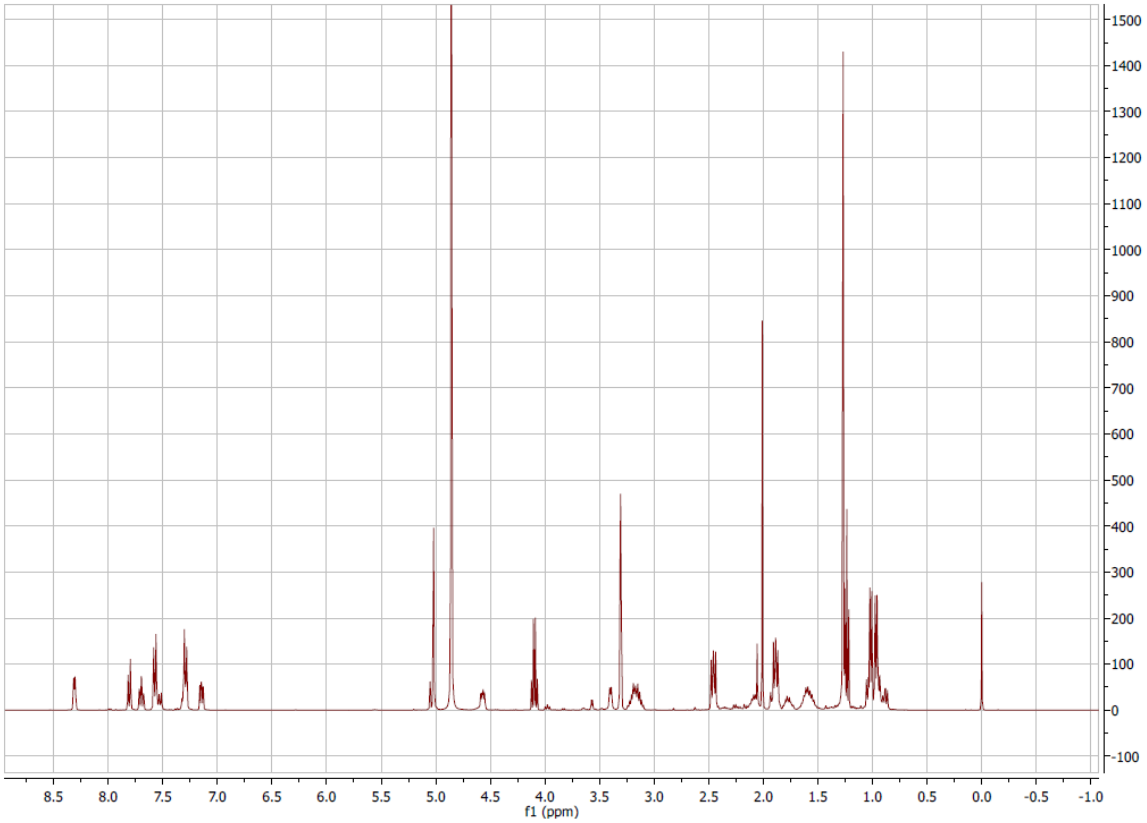

Figure A 73 ^{1}H spectrum (400 MHz, CD_3OD) of compound **40**.

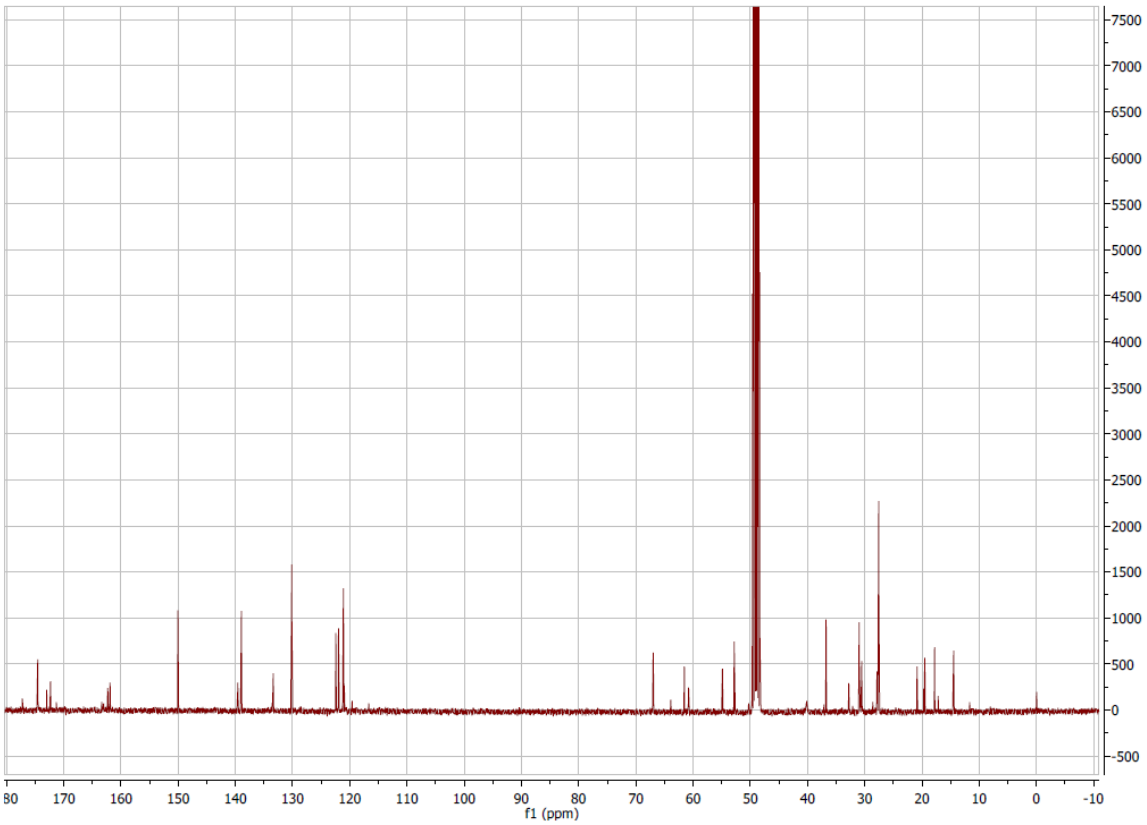

Figure A 74 ^{13}C spectrum (101 MHz, CD_3OD) of compound **40**.

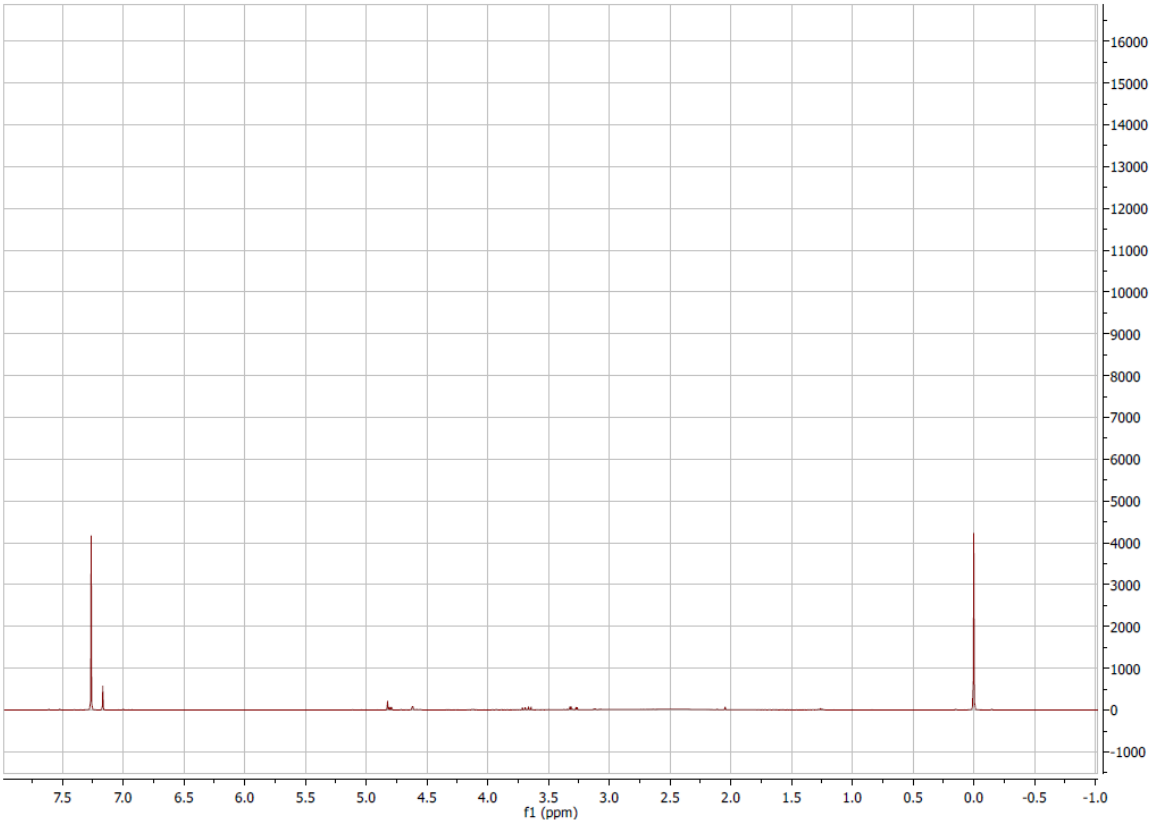

Figure A 75 ^{1}H spectrum (400 MHz, $CDCl_3$) of compound **41**.

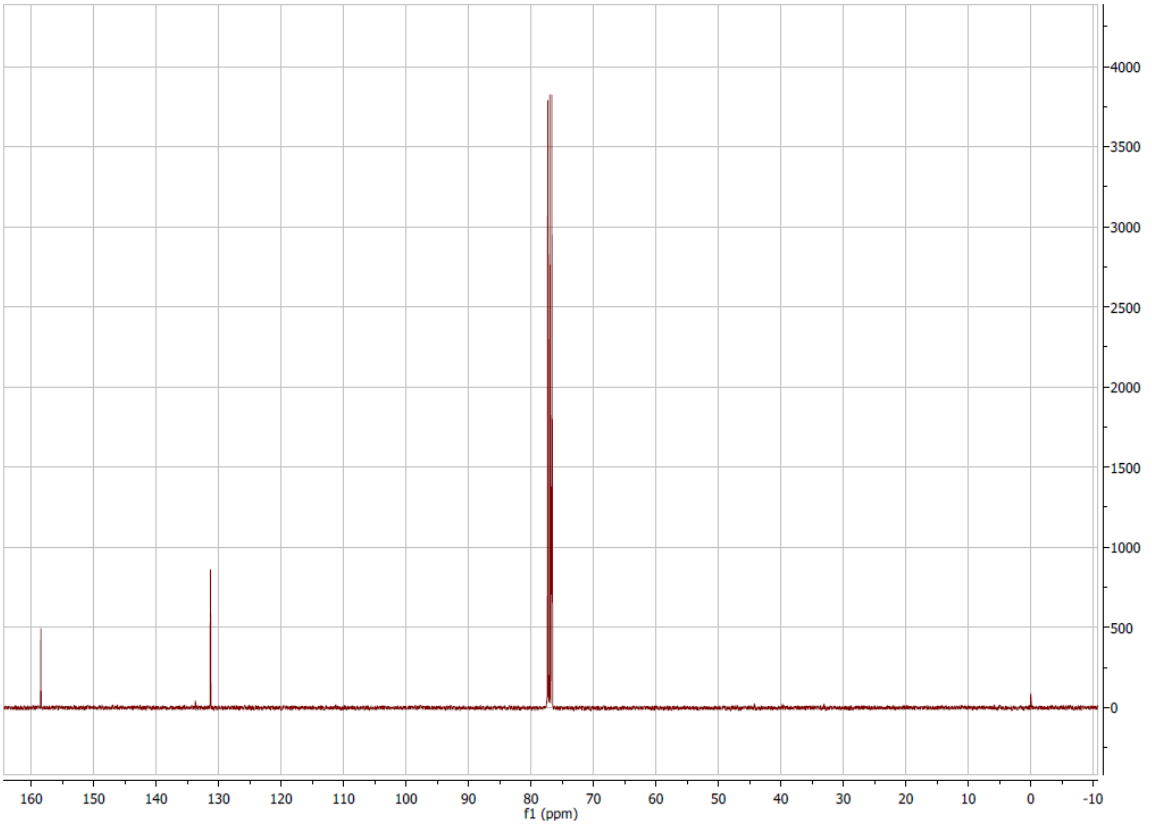

Figure A 76 ^{13}C spectrum (101 MHz, $CDCl_3$) of compound **41**.

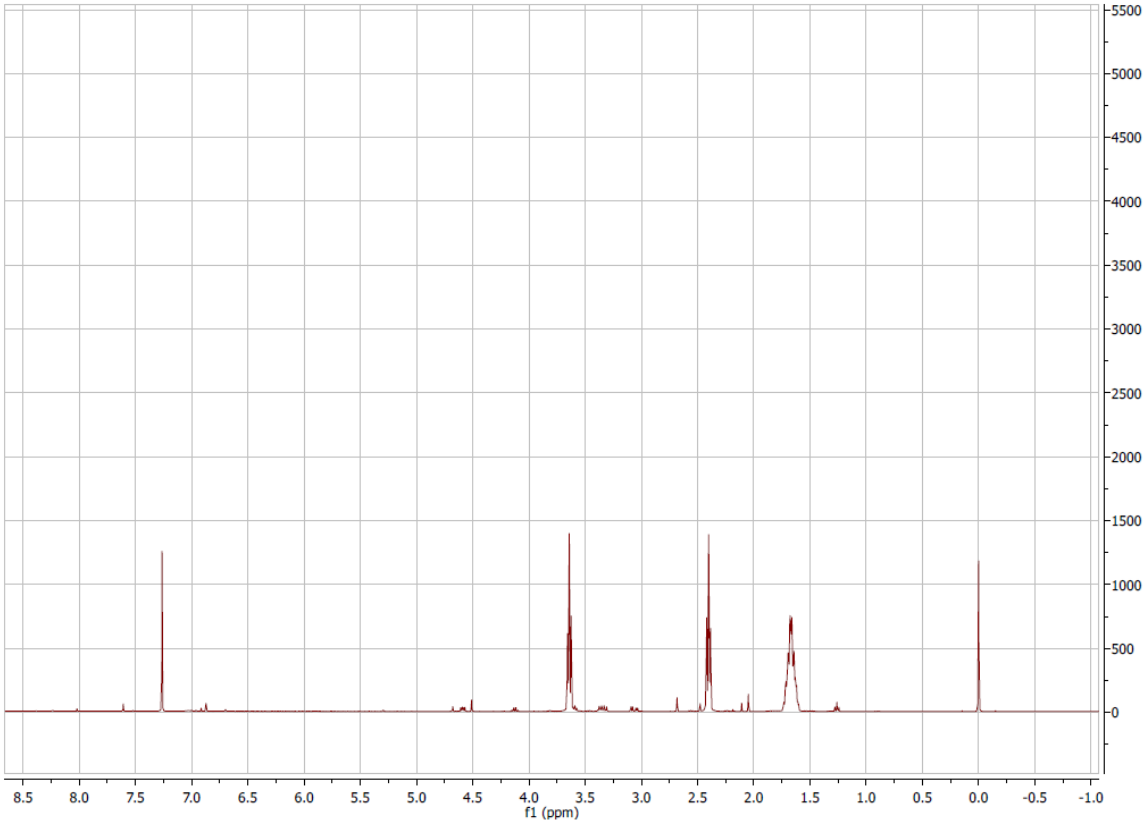

Figure A 77 ^{1}H spectrum (400 MHz, $CDCl_3$) of compound **42**.

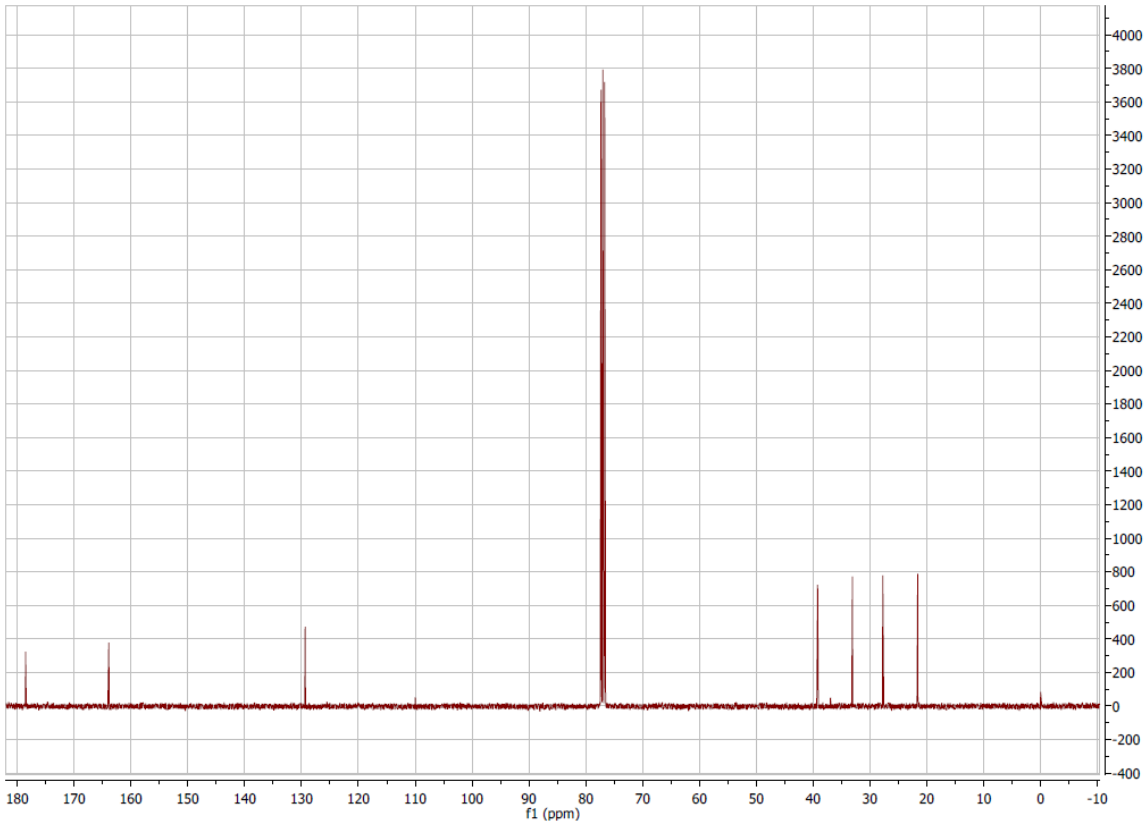

Figure A 78 ^{13}C spectrum (101 MHz, $CDCl_3$) of compound **42**.

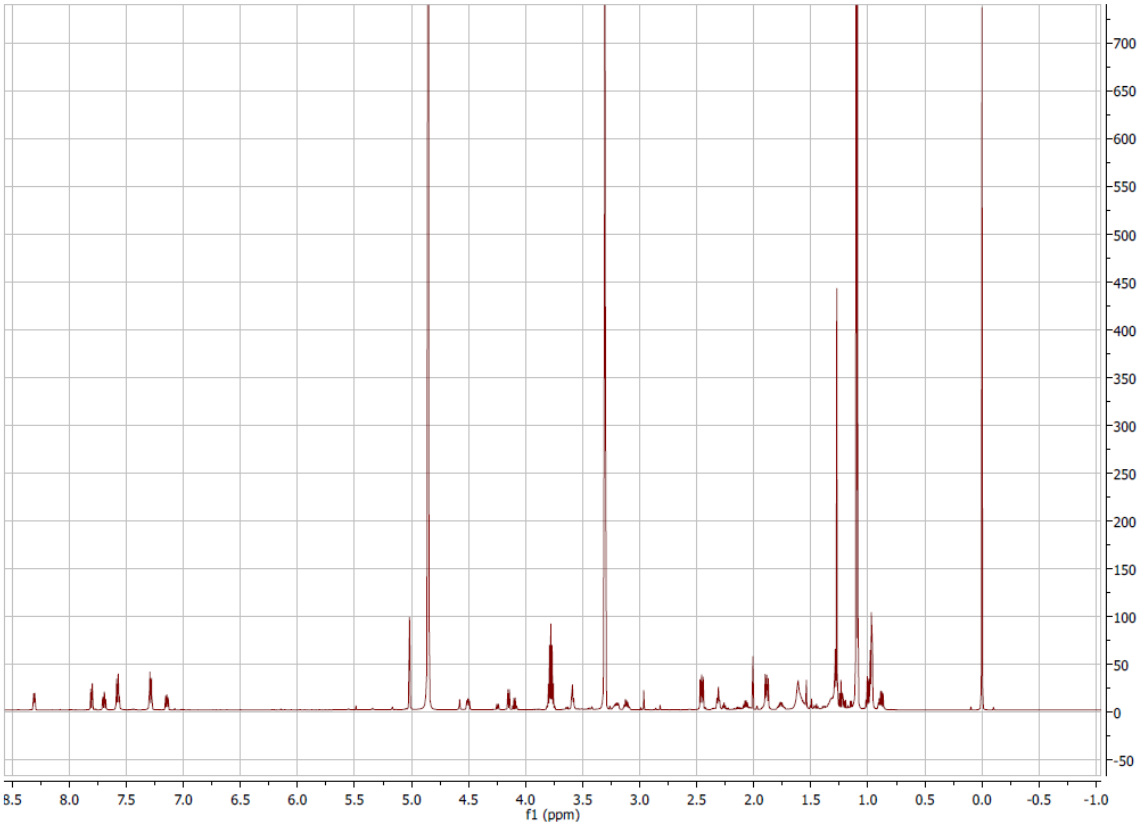

Figure A 79 ^{1}H spectrum (400 MHz, CD_3OD) of compound **43**.

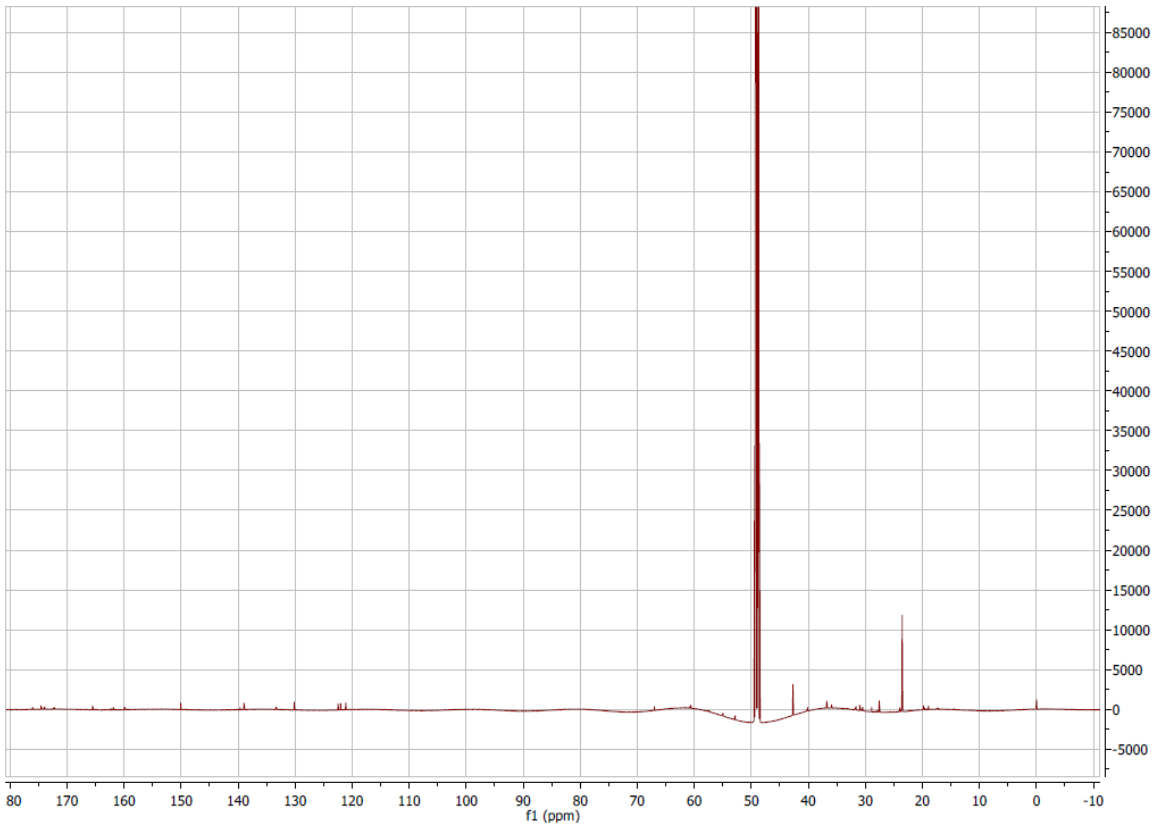

Figure A 80 ^{13}C spectrum (101 MHz, CD_3OD) of compound **43**.

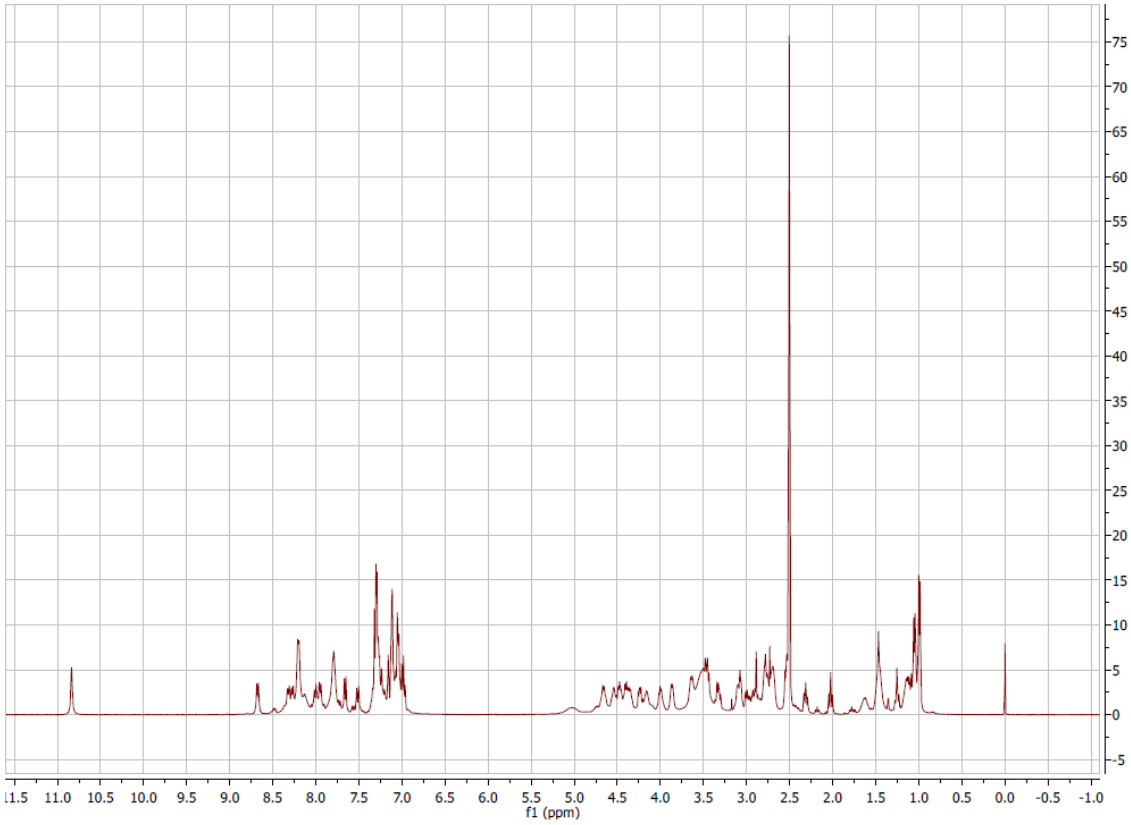

Figure A 81 ^{1}H spectrum (400 MHz, DMSO-d6) of compound **44**.

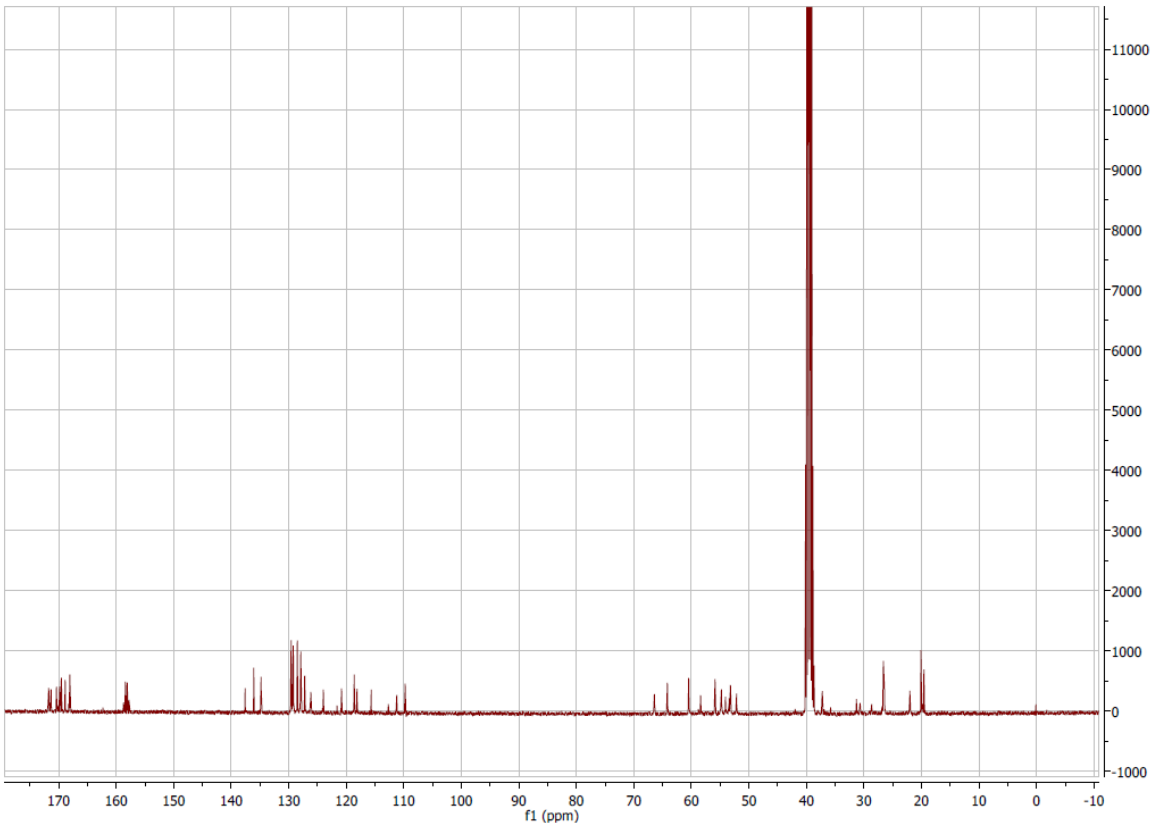

Figure A 82 ^{13}C spectrum (101 MHz, DMSO-d6) of compound **44**.

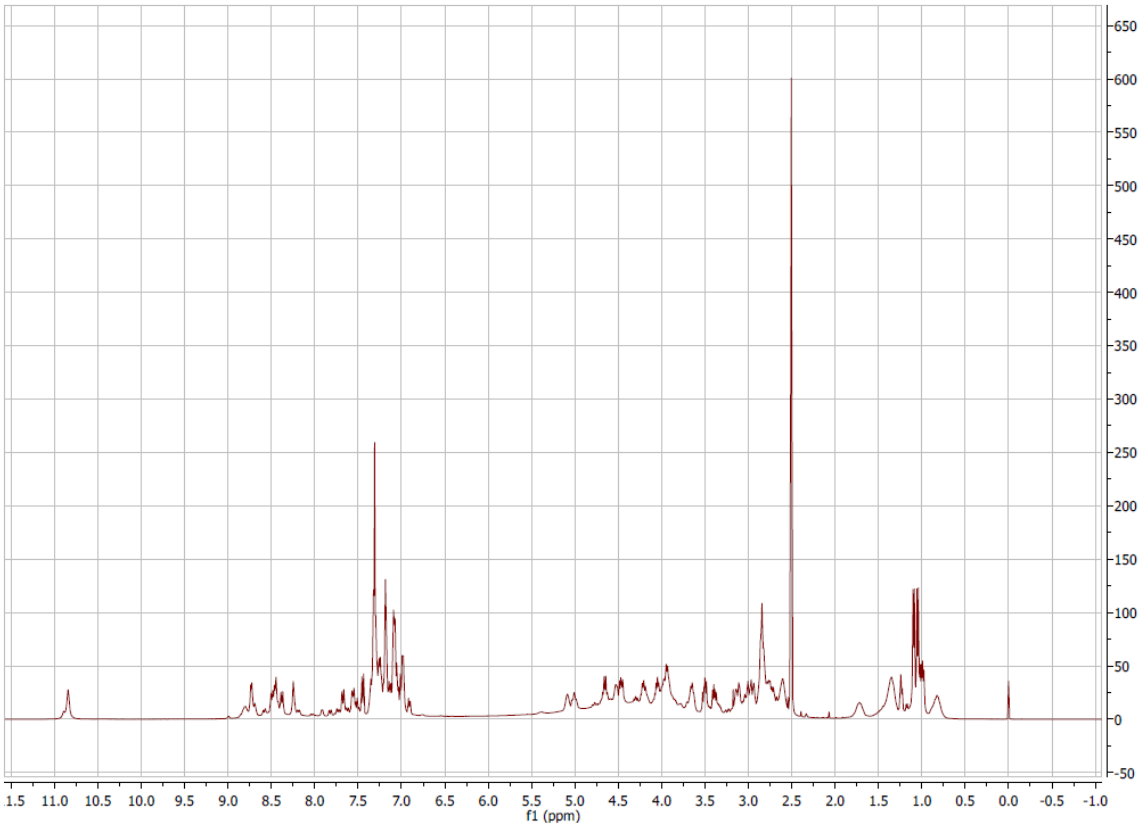

Figure A 83 ^{1}H spectrum (400 MHz, DMSO-d6) of compound **45**.

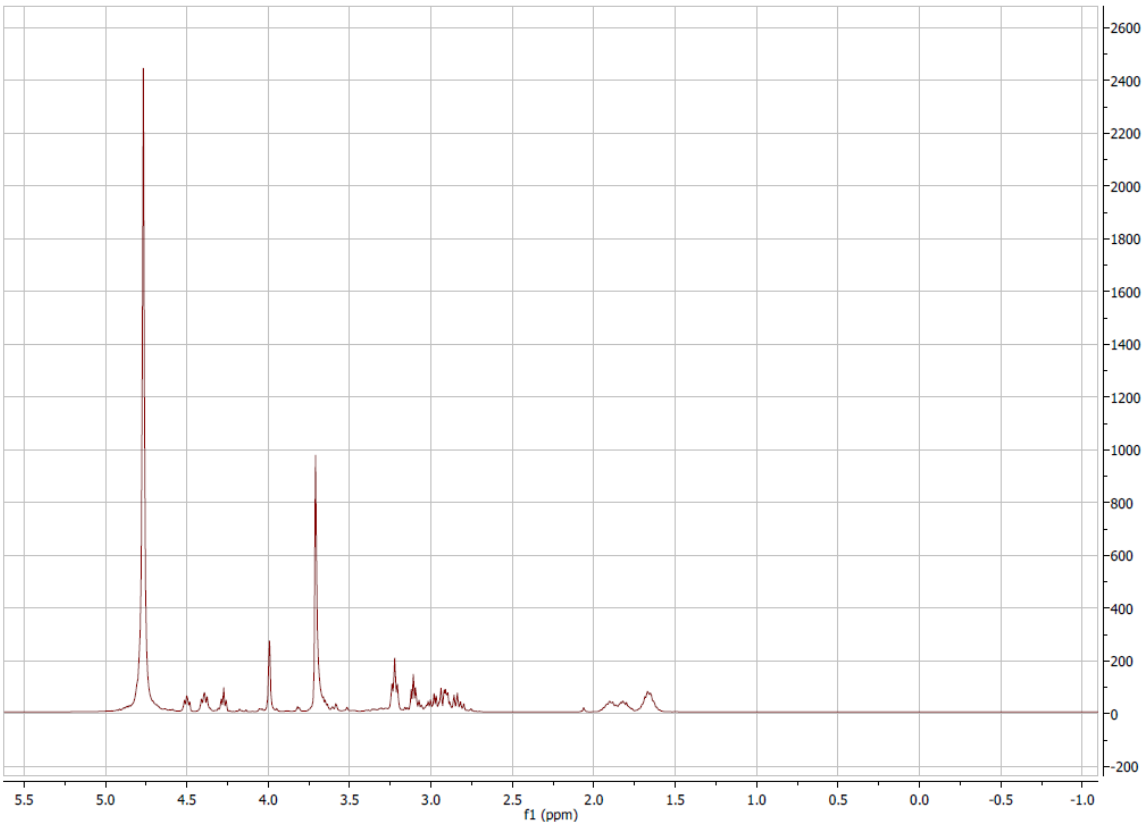

Figure A 84 ^{1}H spectrum (400 MHz, D_2O) of compound **46**.

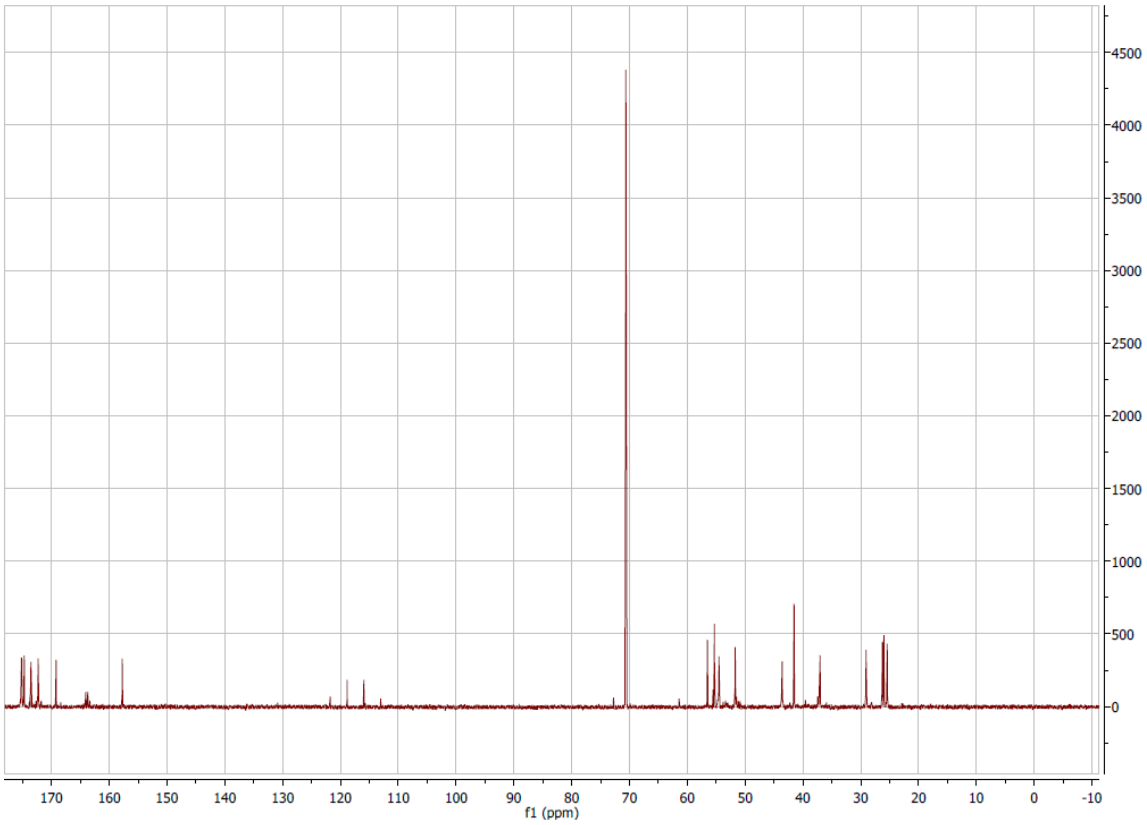

Figure A 85 ^{13}C spectrum (101 MHz, D_2O) of compound **46**.

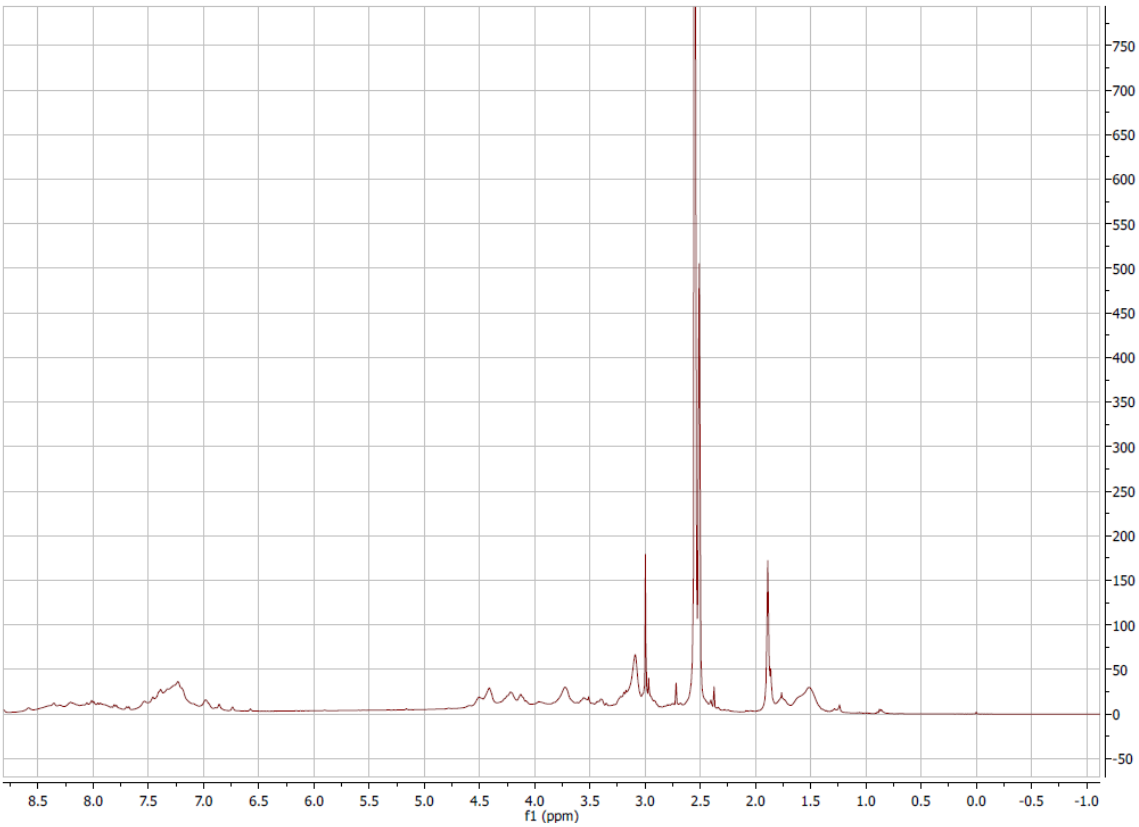

Figure A 86 ^{1}H spectrum (400 MHz, CD_3OD) of compound **47**.

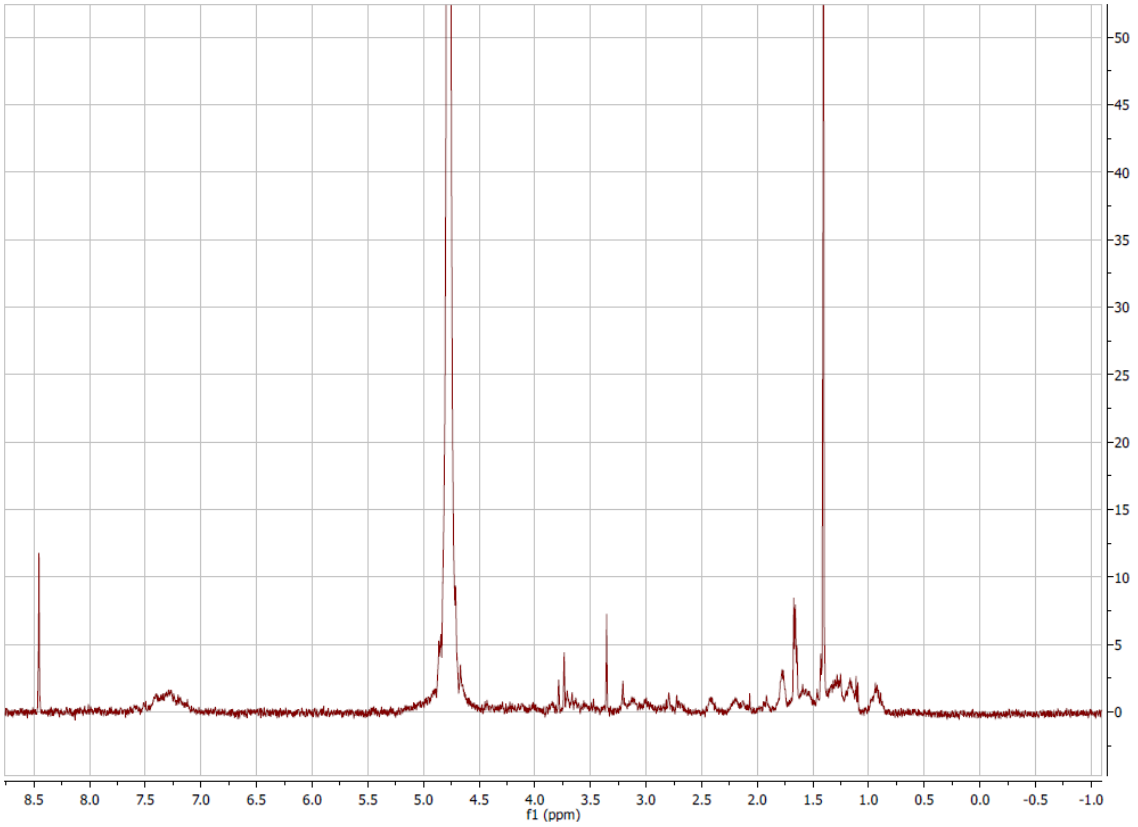

Figure A 87 ^{1}H spectrum (400 MHz, D_2O) of compound **48**.

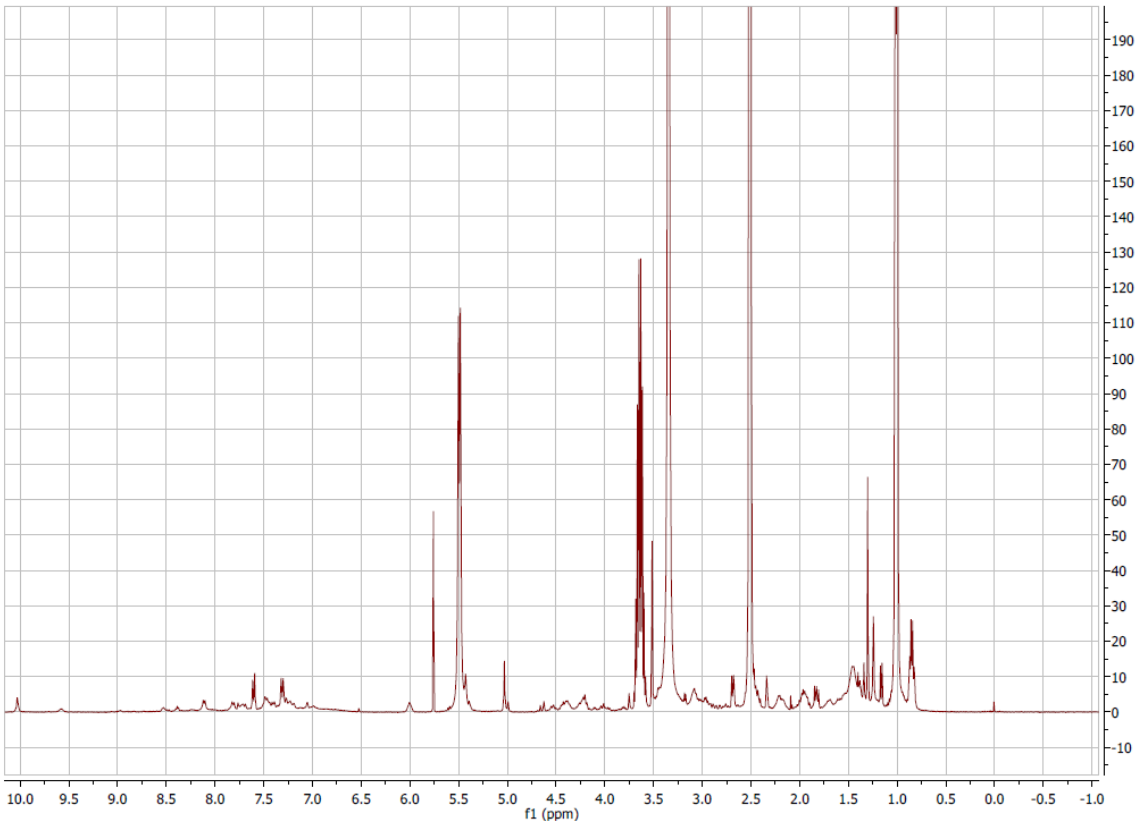

Figure A 88 ^{1}H spectrum (400 MHz, DMSO-d6) of compound **51**.

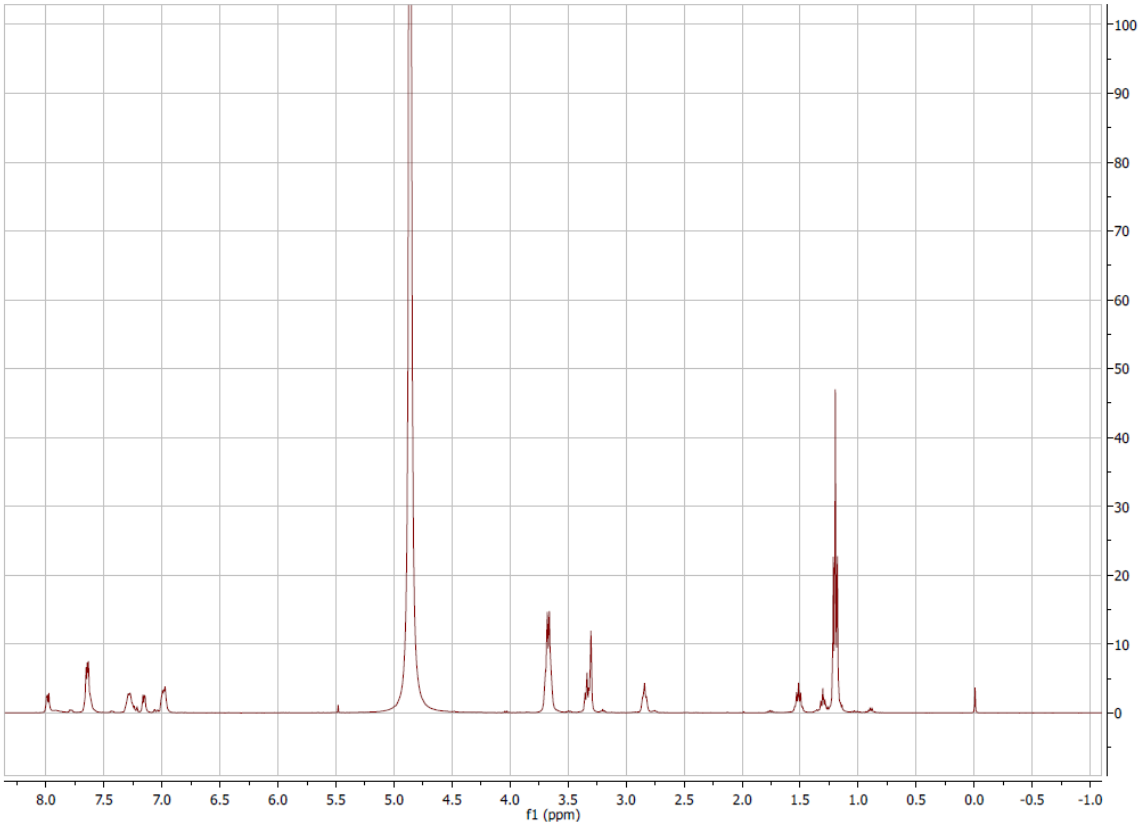

Figure A 89 ^{1}H spectrum (500 MHz, CD_3OD) of compound **54**.

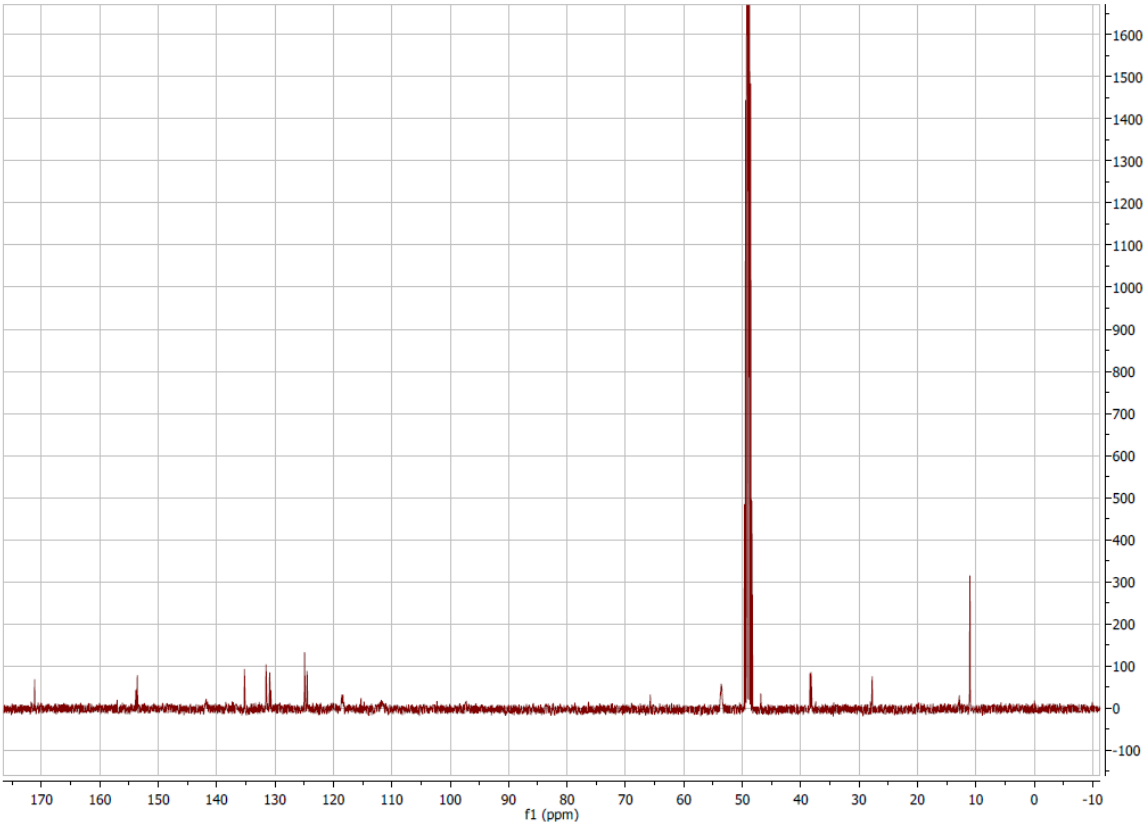

Figure A 90 ^{13}C spectrum (126 MHz, CD_3OD) of compound **54**.

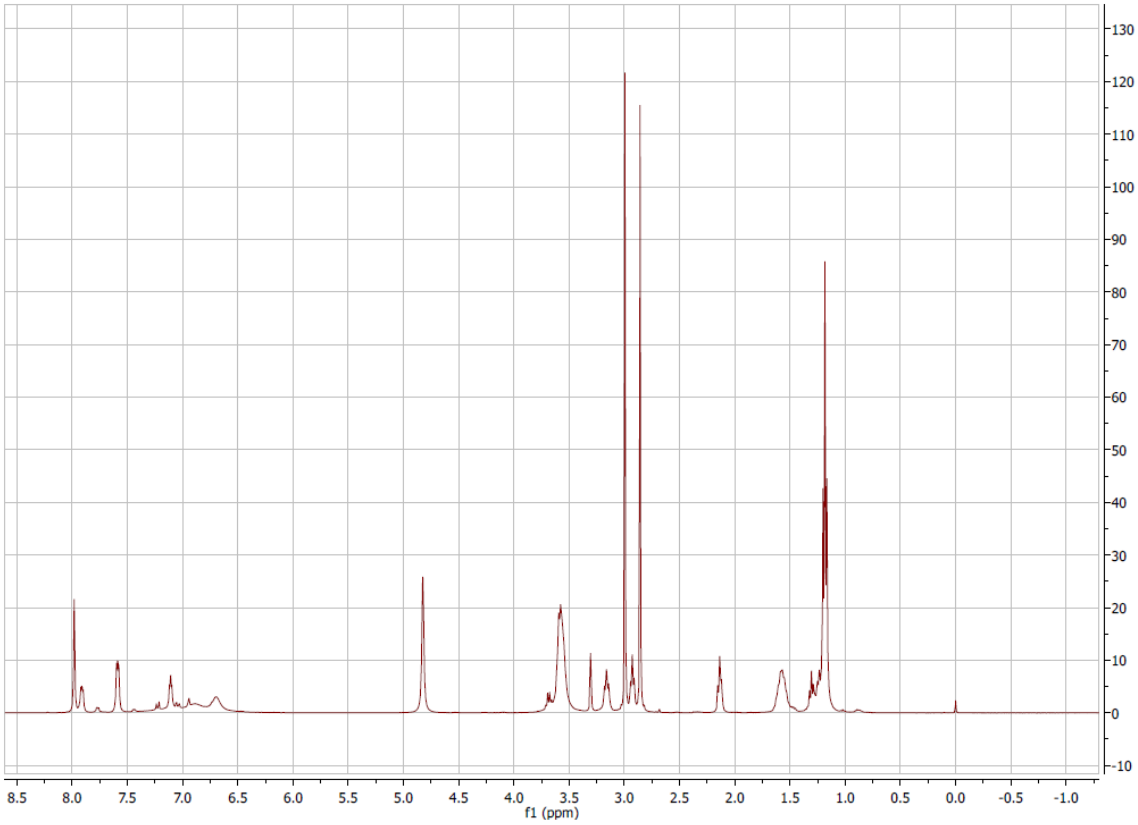

Figure A 91 ^{1}H spectrum (500 MHz, CD_3OD) of compound **55**.

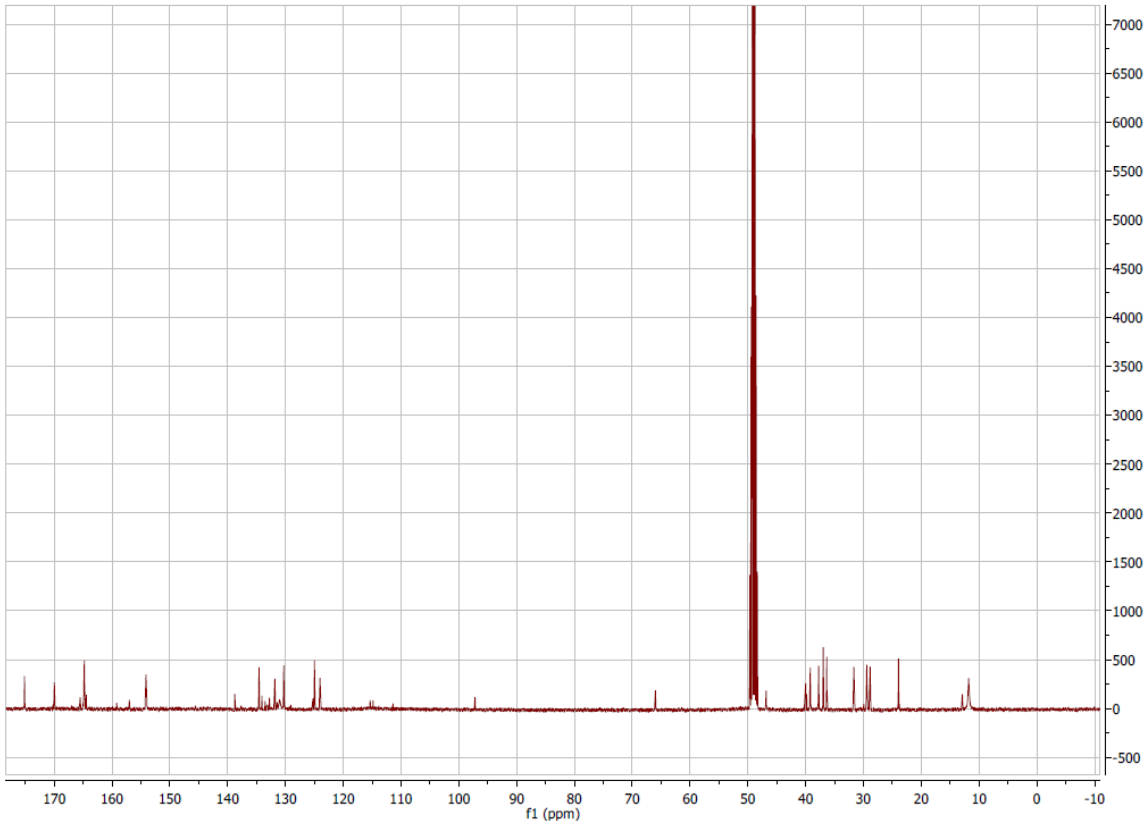

Figure A 92 ^{13}C spectrum (126 MHz, CD_3OD) of compound **55**.

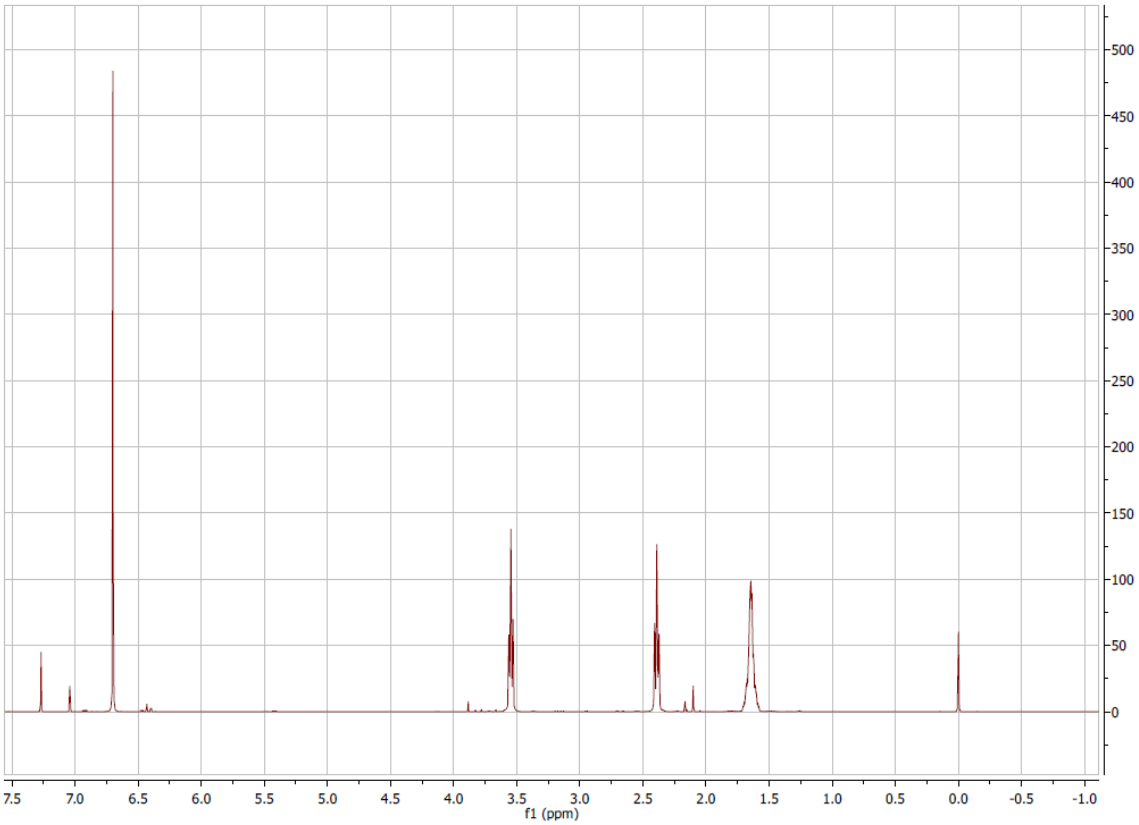

Figure A 93 ^{1}H spectrum (400 MHz, $CDCl_3$) of compound **58**.

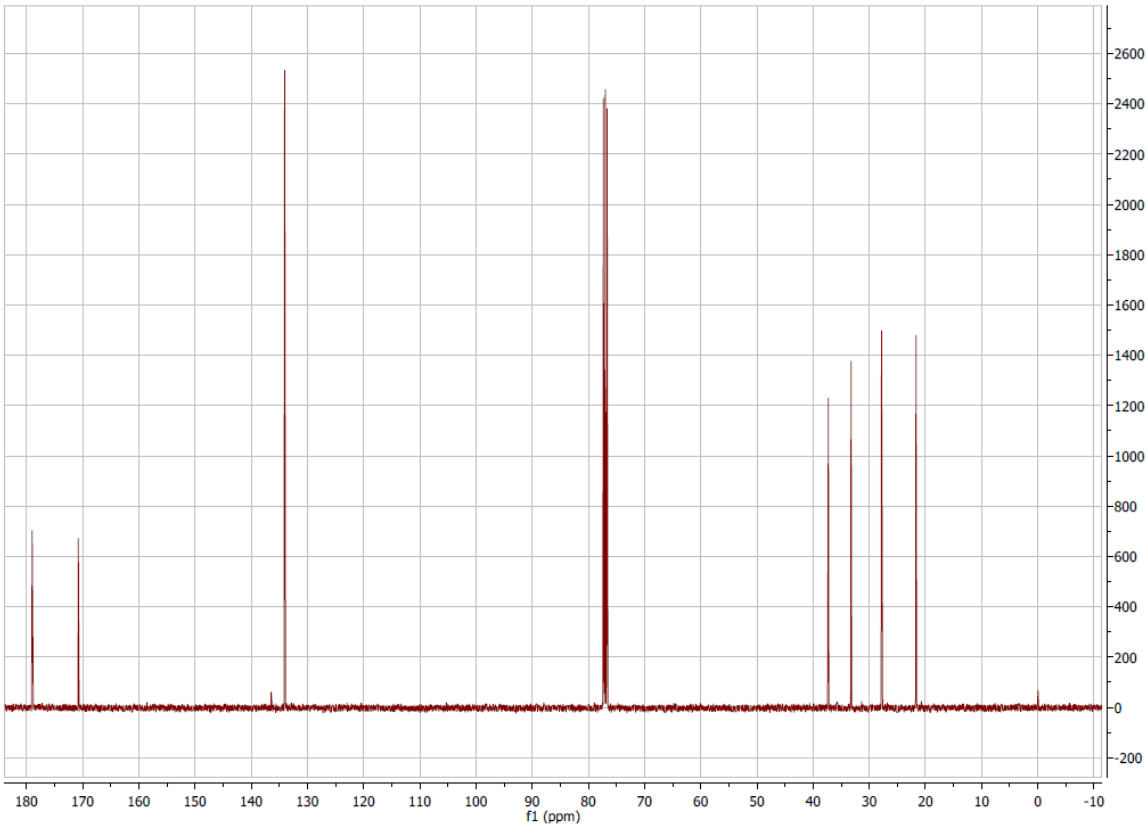

Figure A 94 ^{13}C spectrum (101 MHz, $CDCl_3$) of compound **58**.

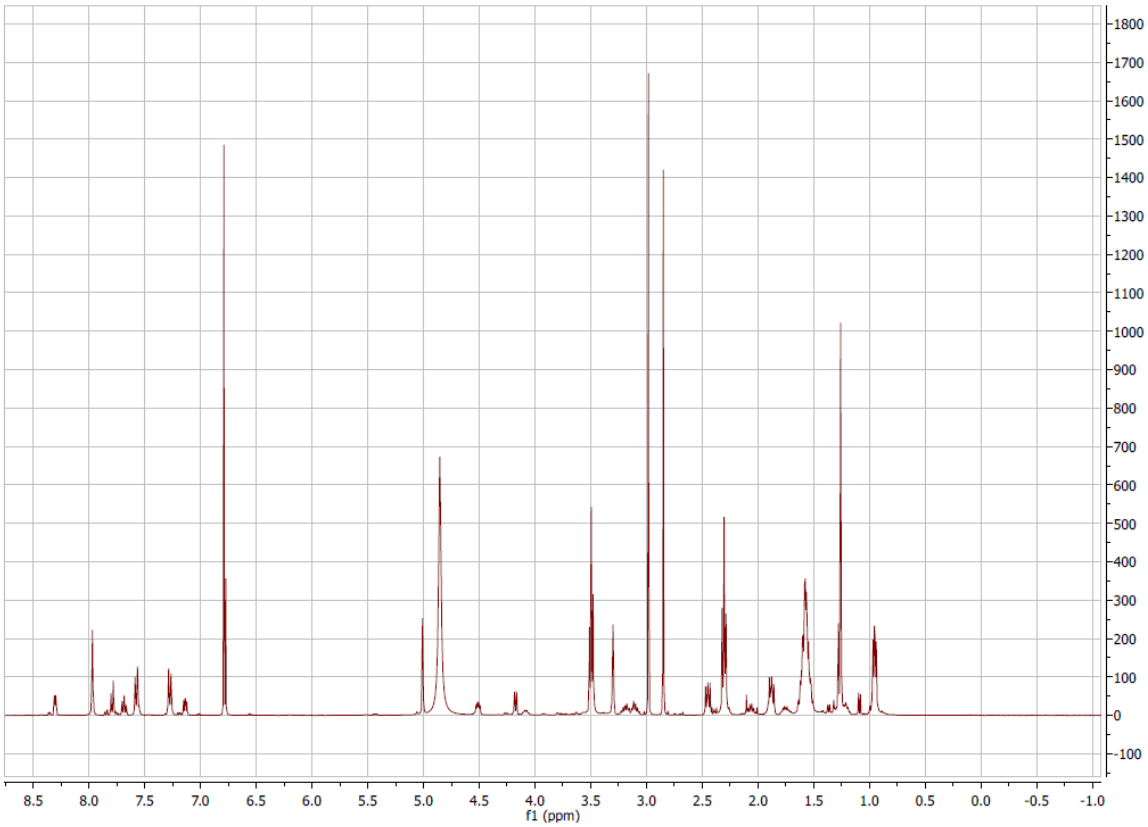

Figure A 95 ^{1}H spectrum (400 MHz, CD_3OD) of compound **59**.

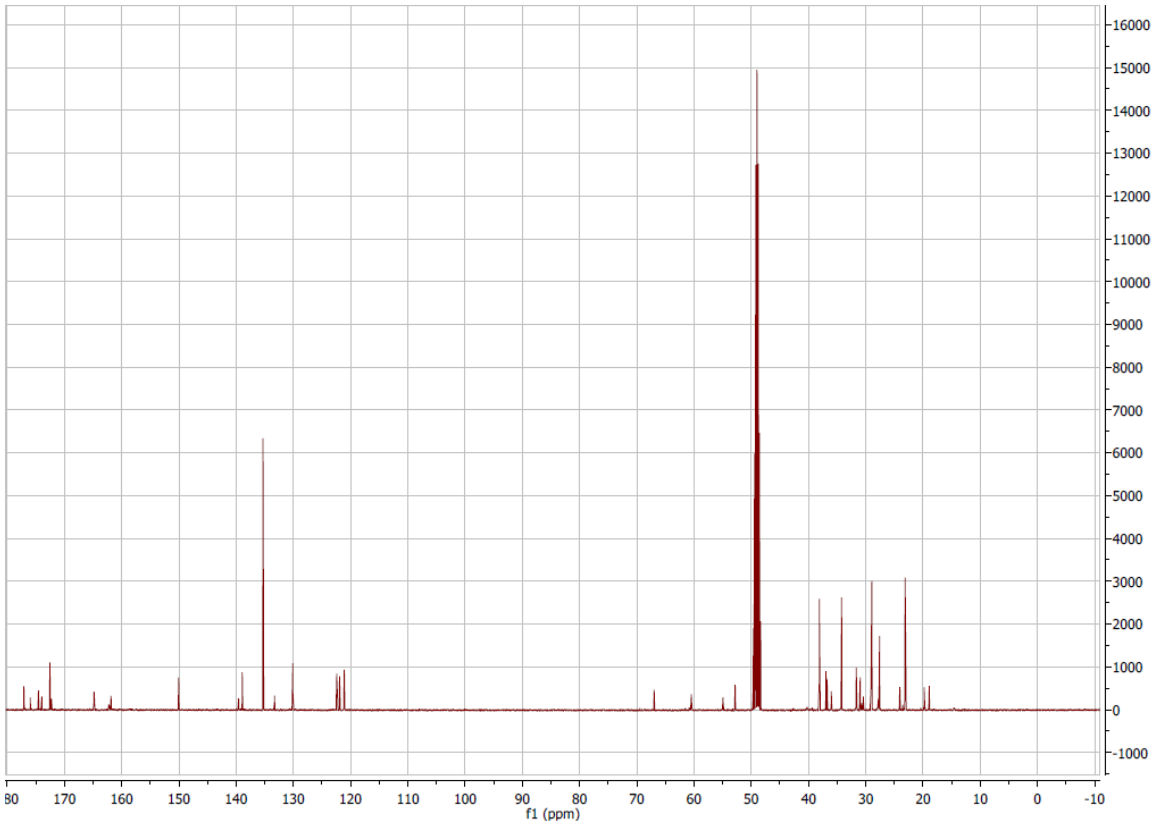

Figure A 96 ^{13}C spectrum (101 MHz, CD_3OD) of compound **59**.

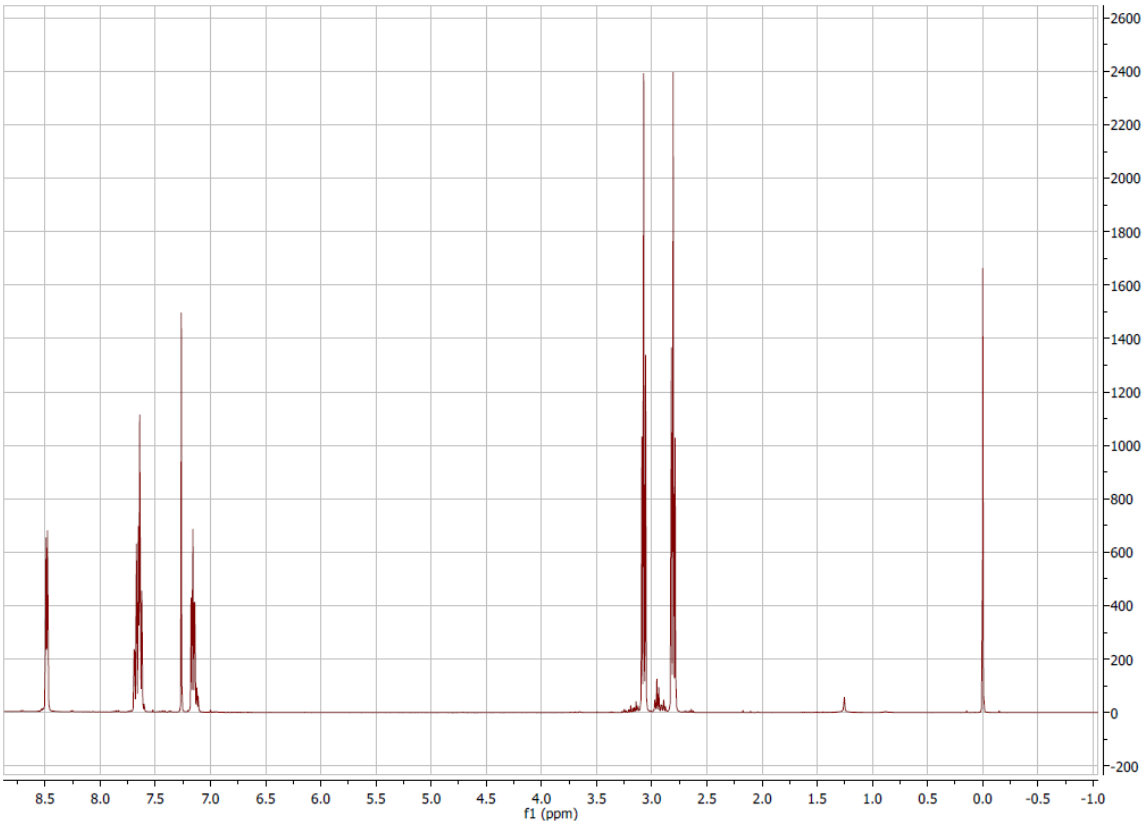

Figure A 97 ^{1}H spectrum (400 MHz, $CDCl_3$) of compound **60**.

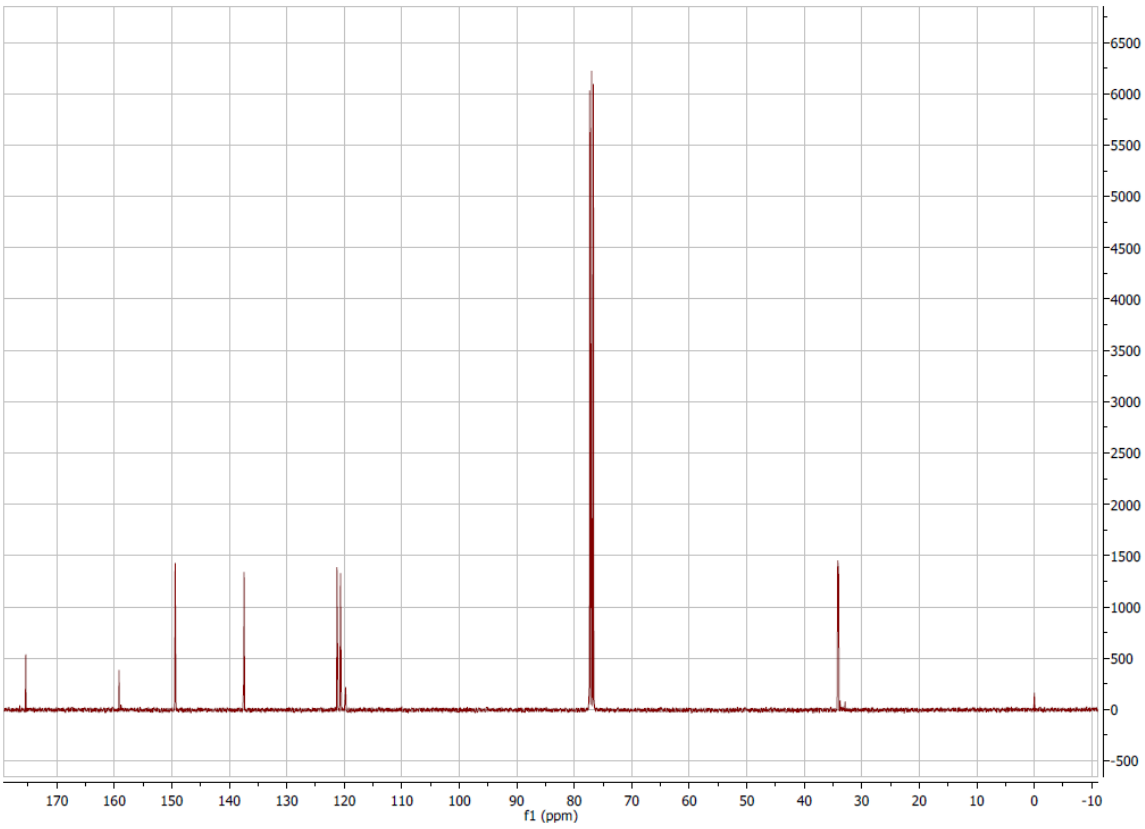

Figure A 98 ^{13}C spectrum (101 MHz, $CDCl_3$) of compound **60**.

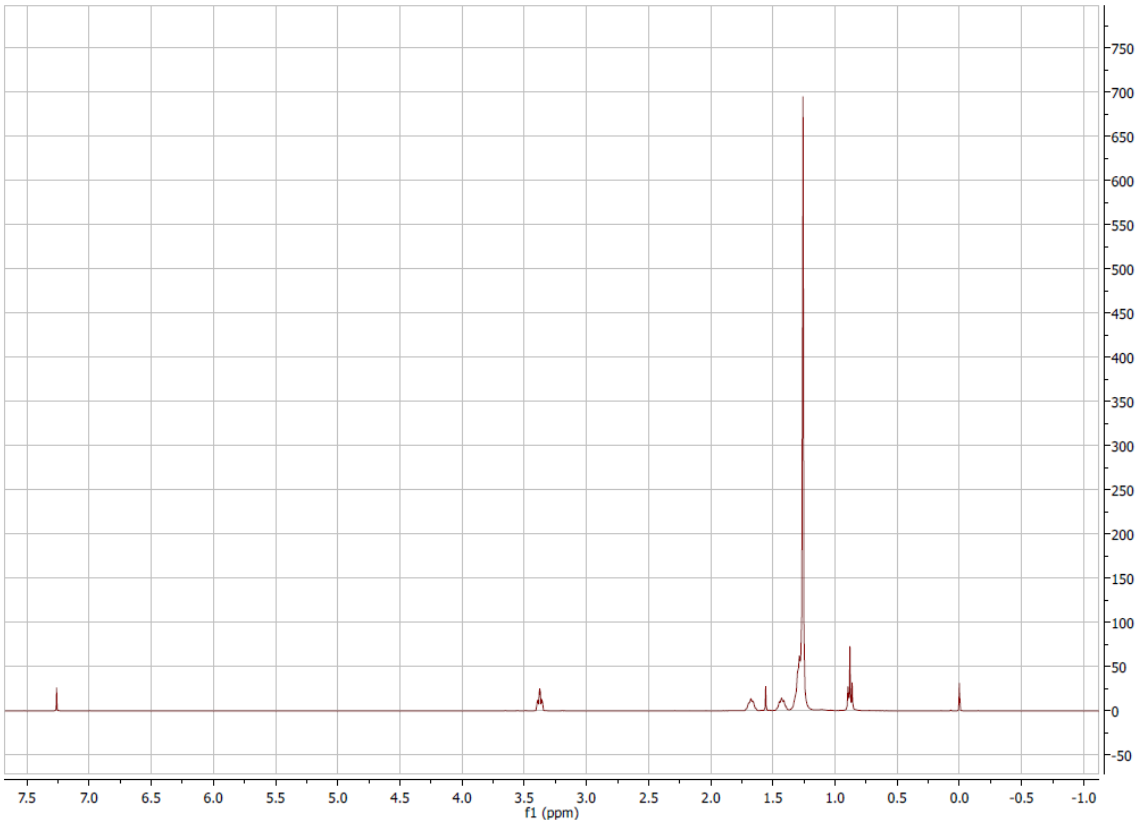

Figure A 99 ^{1}H spectrum (400 MHz, $CDCl_3$) of compound **61**.

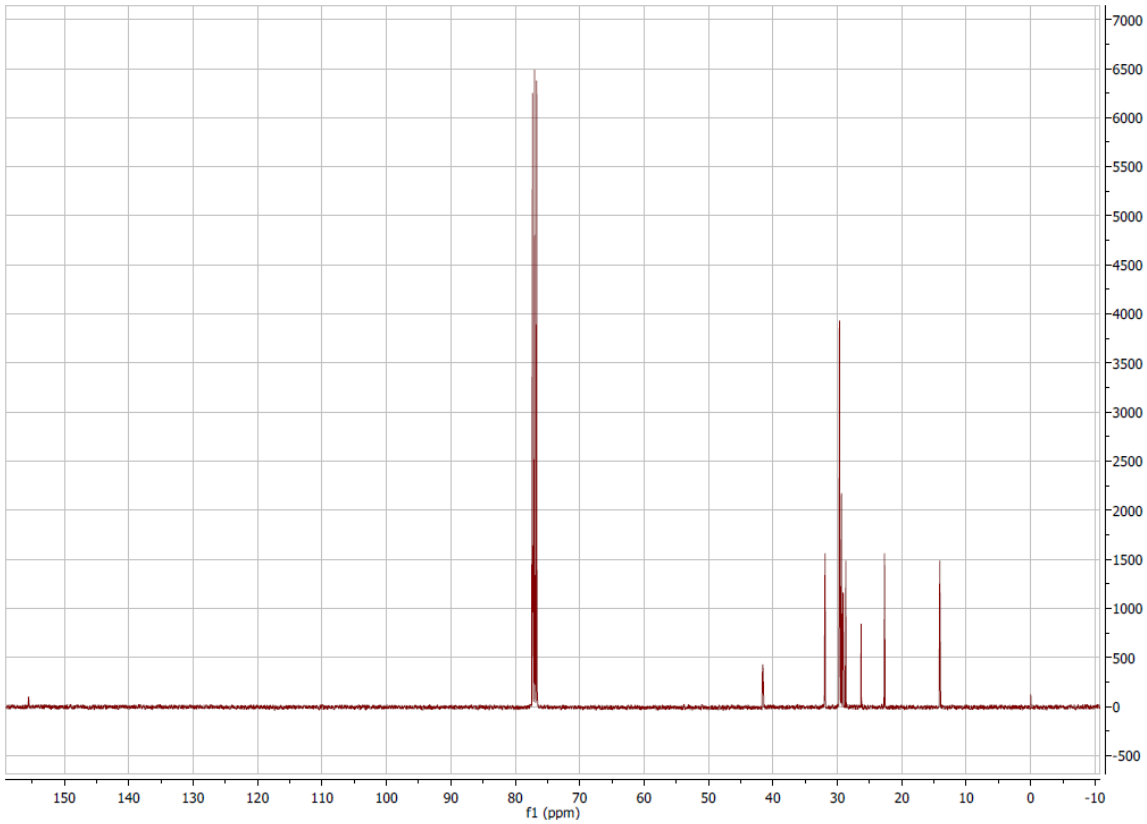

Figure A 100 ^{13}C spectrum (101 MHz, $CDCl_3$) of compound **61**.

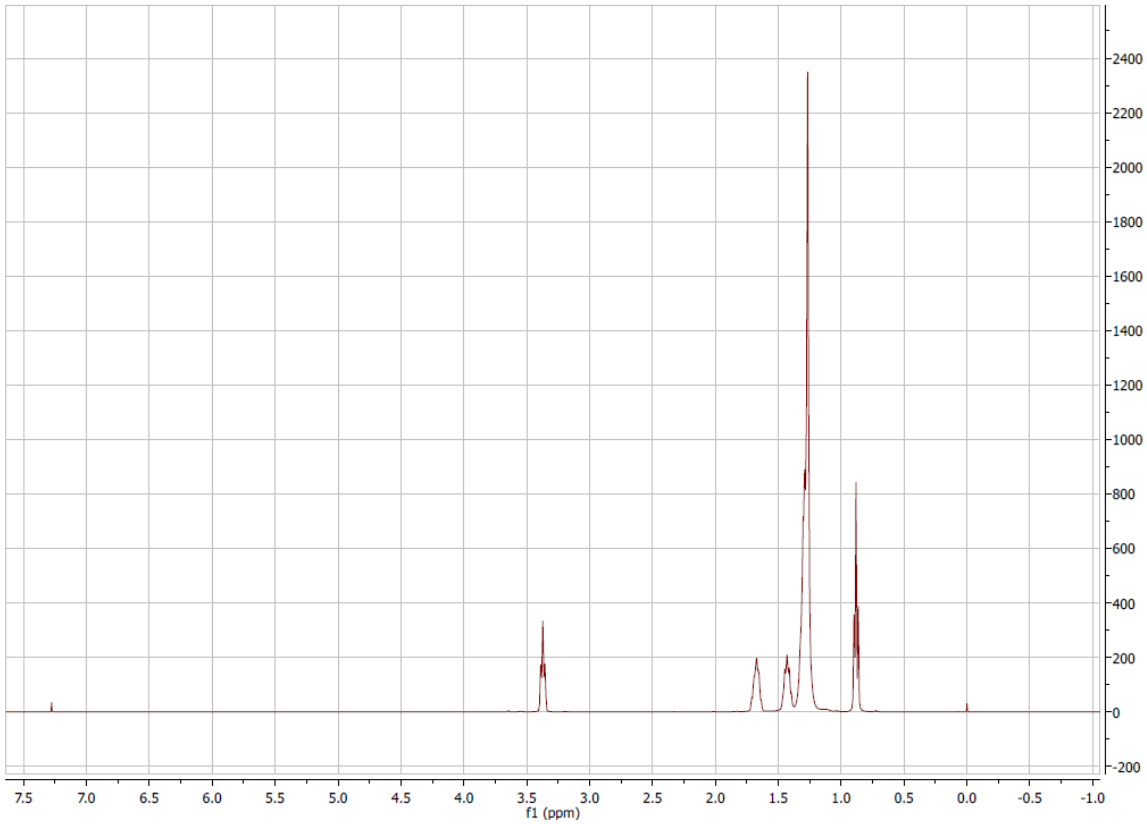

Figure A 101 ^{1}H spectrum (400 MHz, $CDCl_3$) of compound **62**.

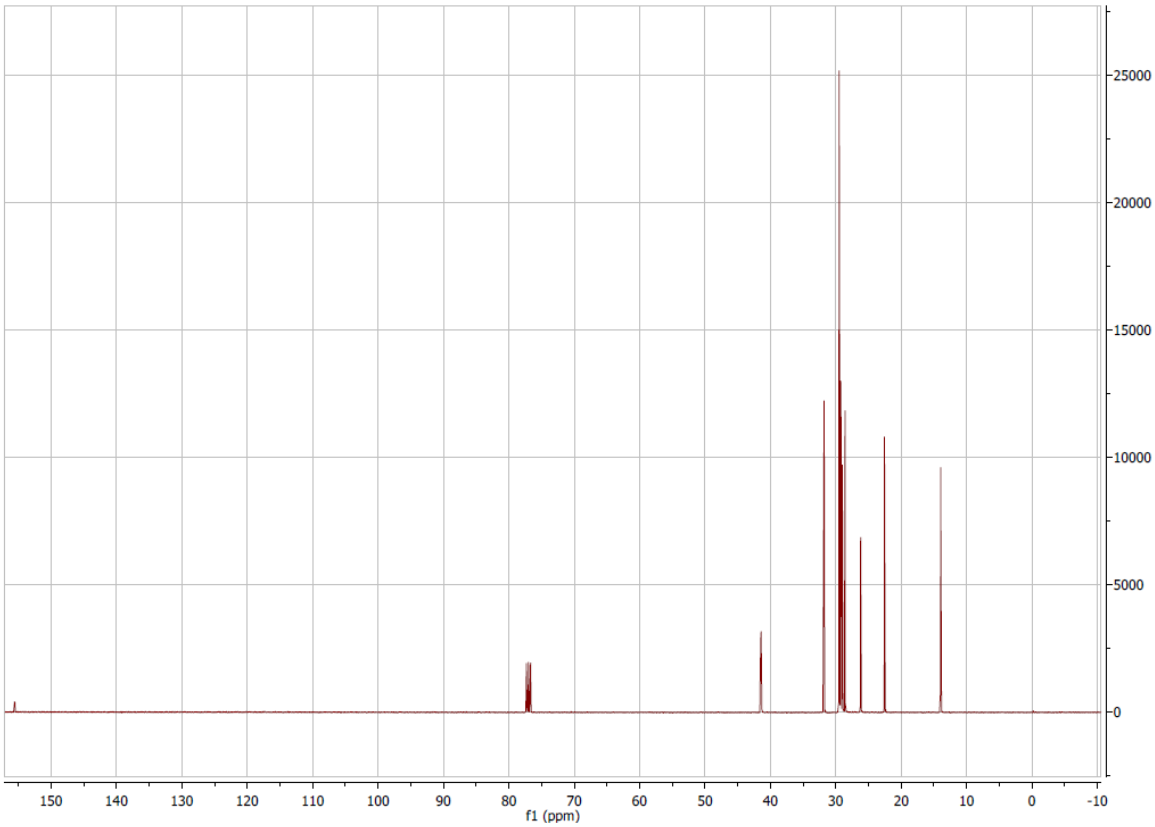

Figure A 102 ^{13}C spectrum (101 MHz, $CDCl_3$) of compound **62**.

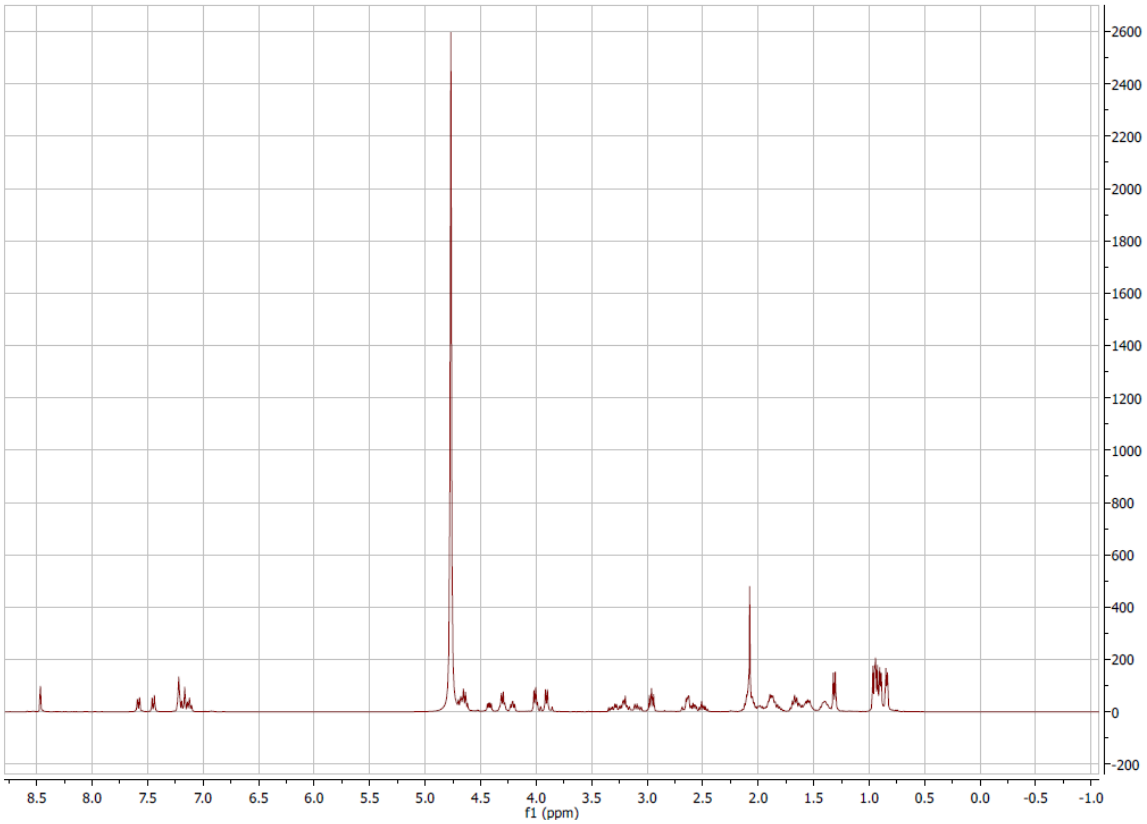

Figure A 103 ^{1}H spectrum (400 MHz, D_2O) of compound **63**.

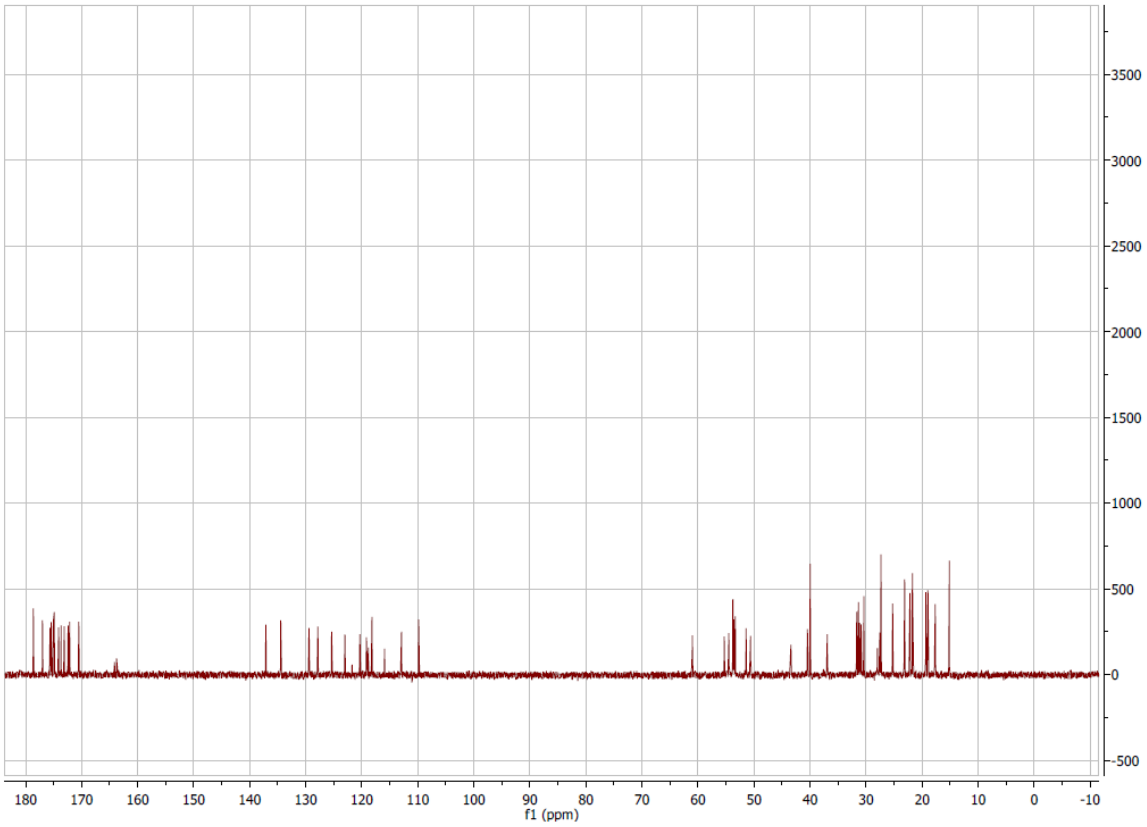

Figure A 104 ^{13}C spectrum (101 MHz, D_2O) of compound **63**.

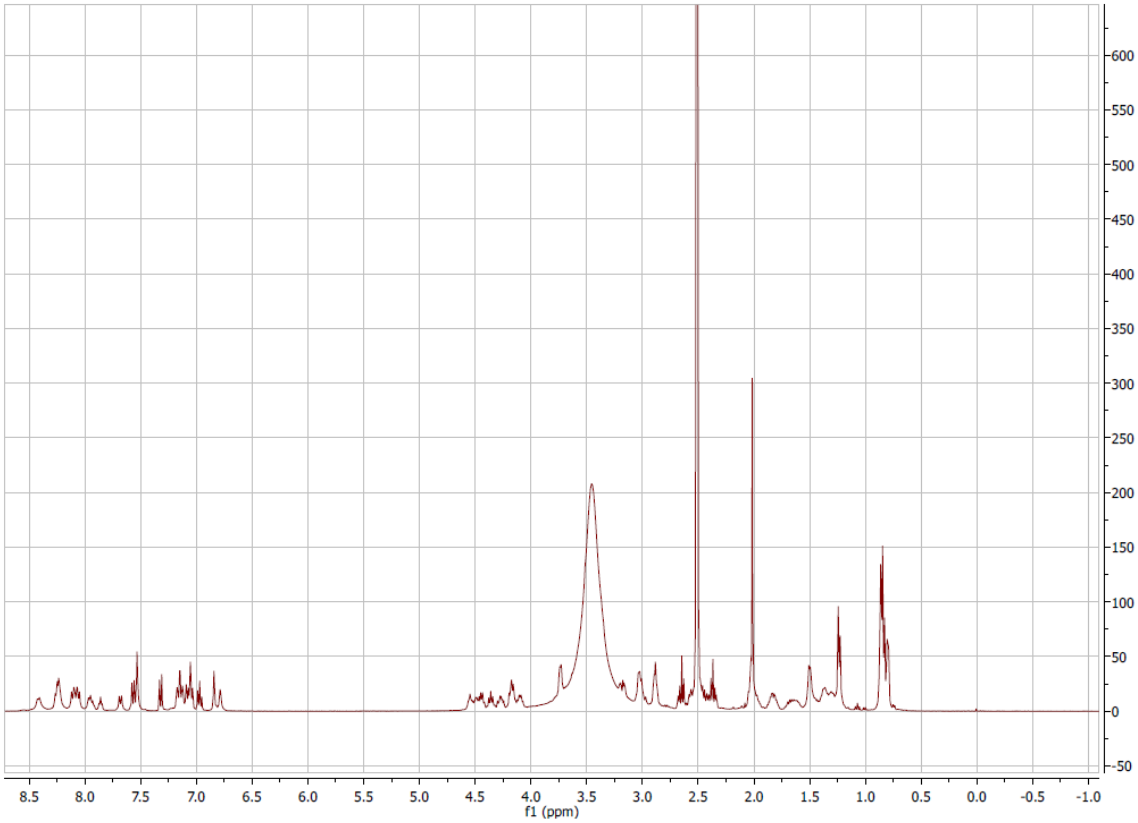

Figure A 105 ^{1}H spectrum (400 MHz, DMSO-d6) of compound **64**.

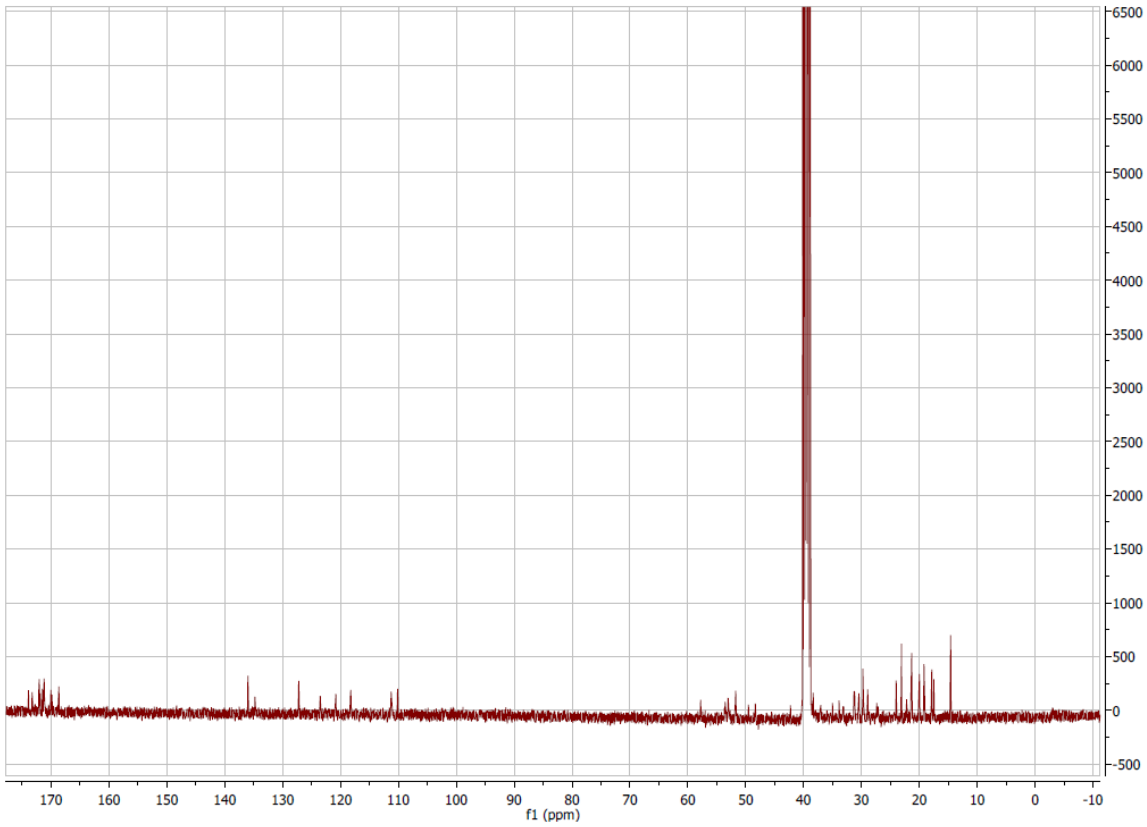

Figure A 106 ^{13}C spectrum (101 MHz, DMSO-d6) of compound **64**.

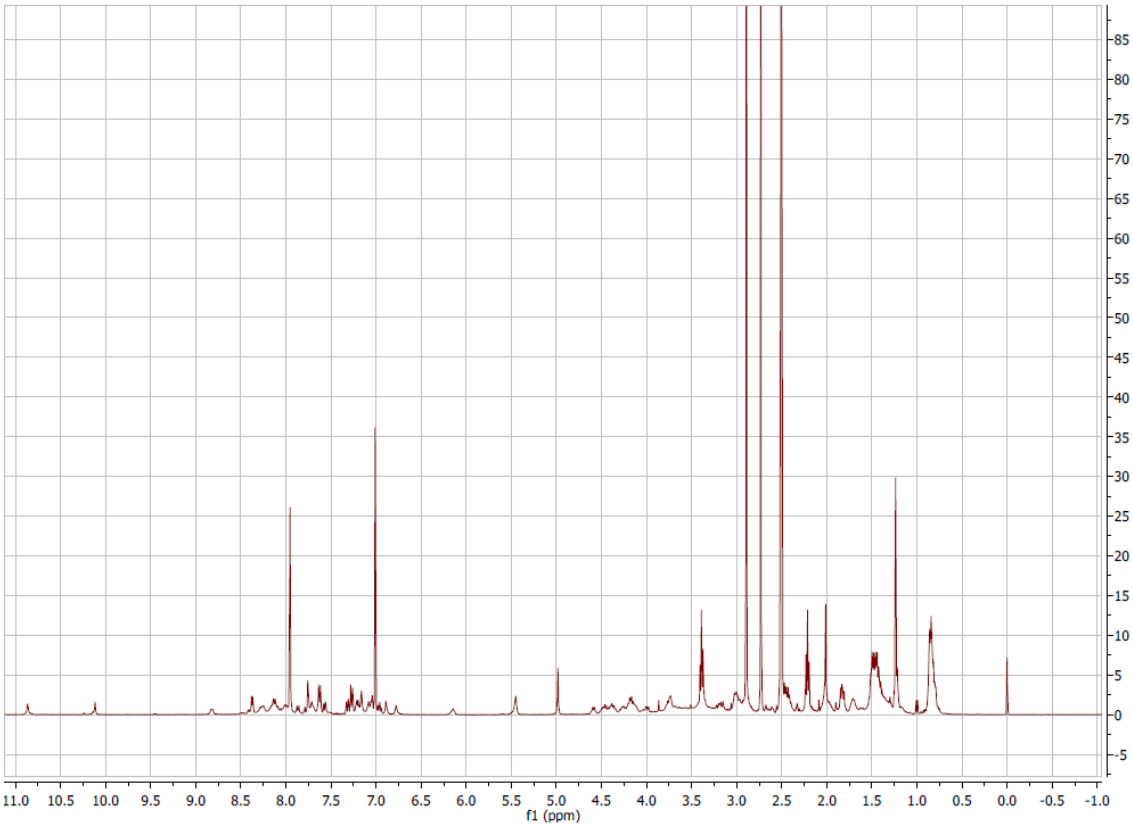

Figure A 107 ^{1}H spectrum (400 MHz, DMSO-d6) of compound **65**.

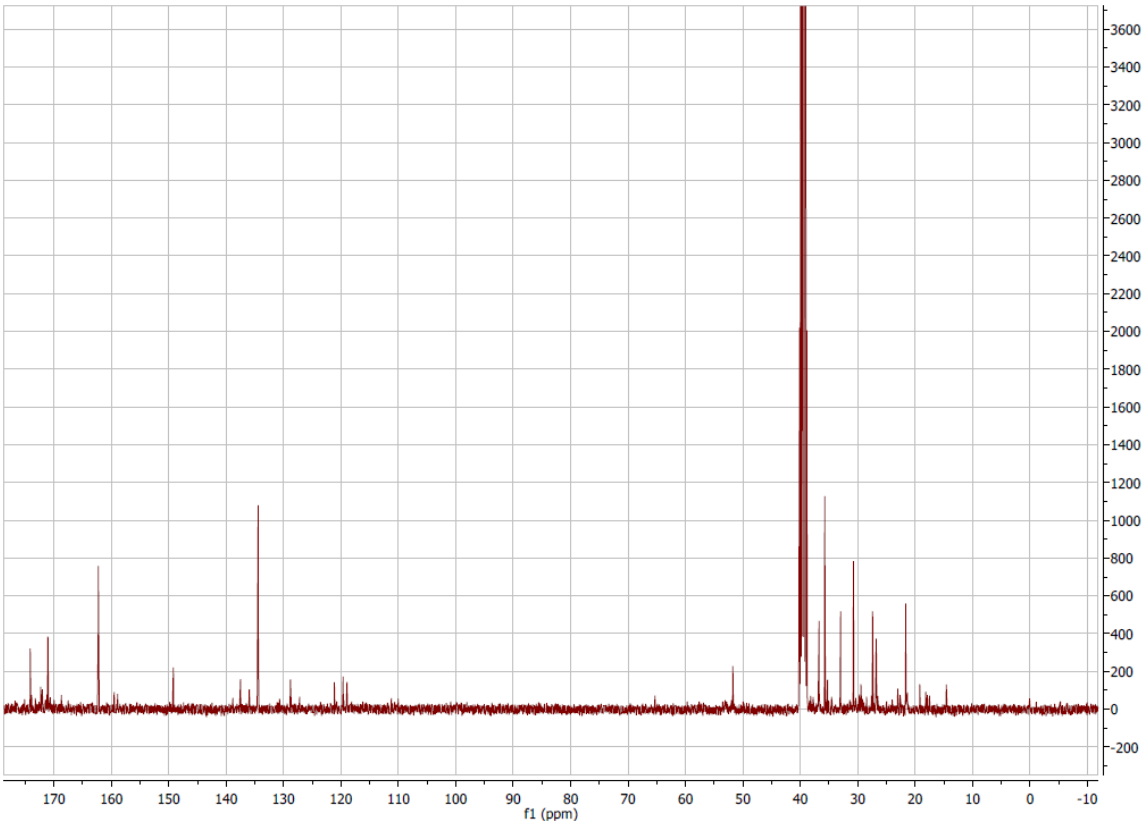

Figure A 108 ^{13}C spectrum (101 MHz, DMSO-d6) of compound **65**.

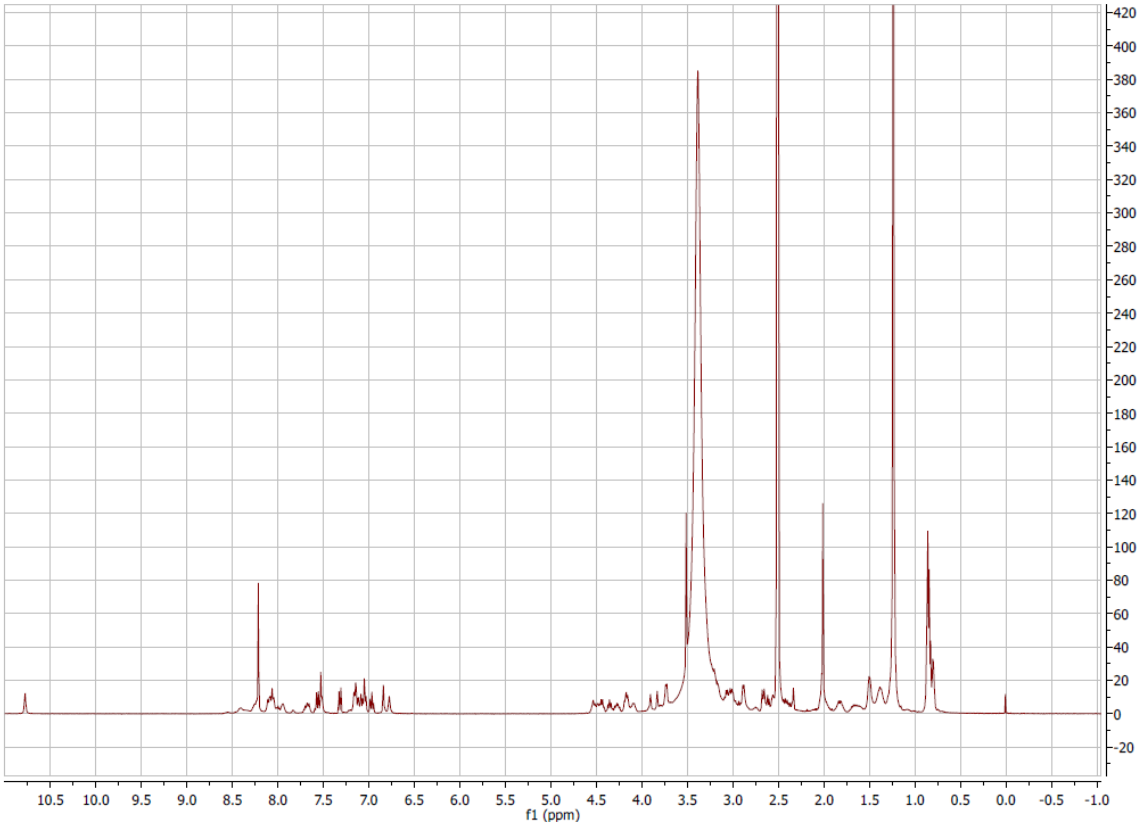

Figure A 109 ^{1}H spectrum (400 MHz, DMSO-d6) of compound **66**.

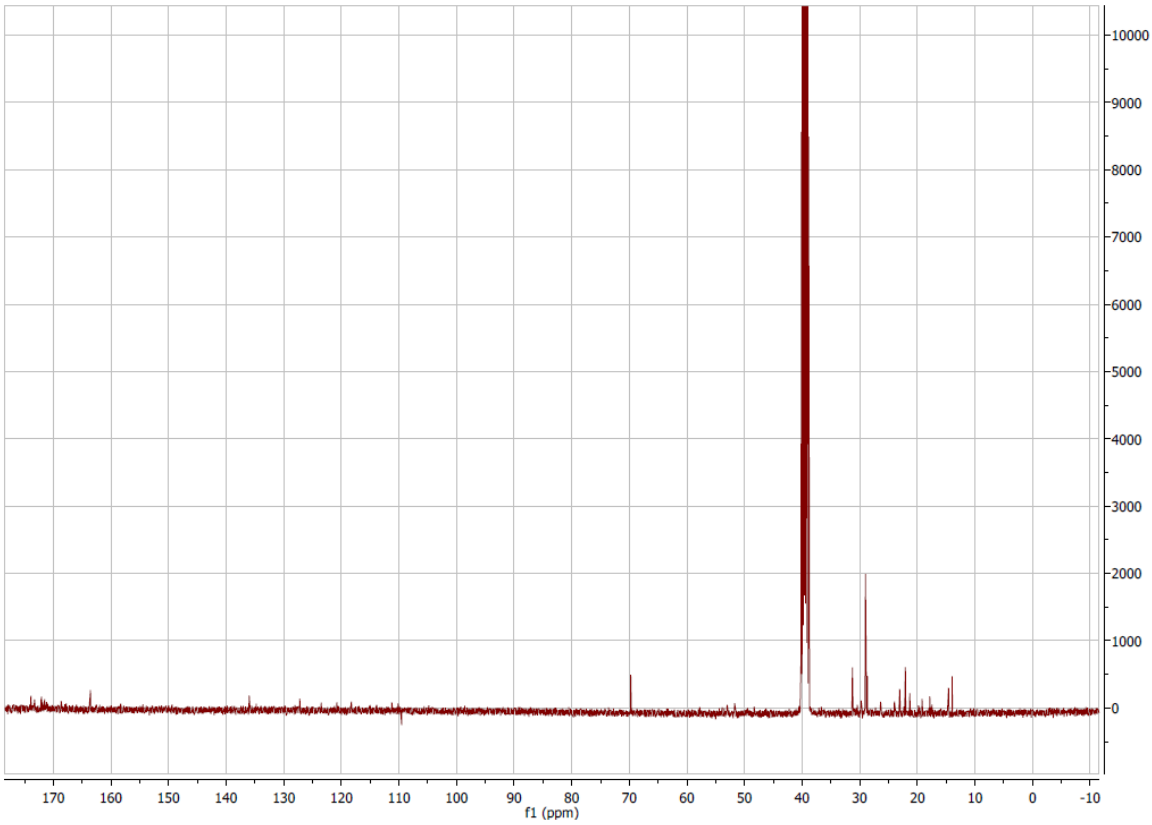

Figure A 110 ^{13}C spectrum (101 MHz, DMSO-d6) of compound **66**.

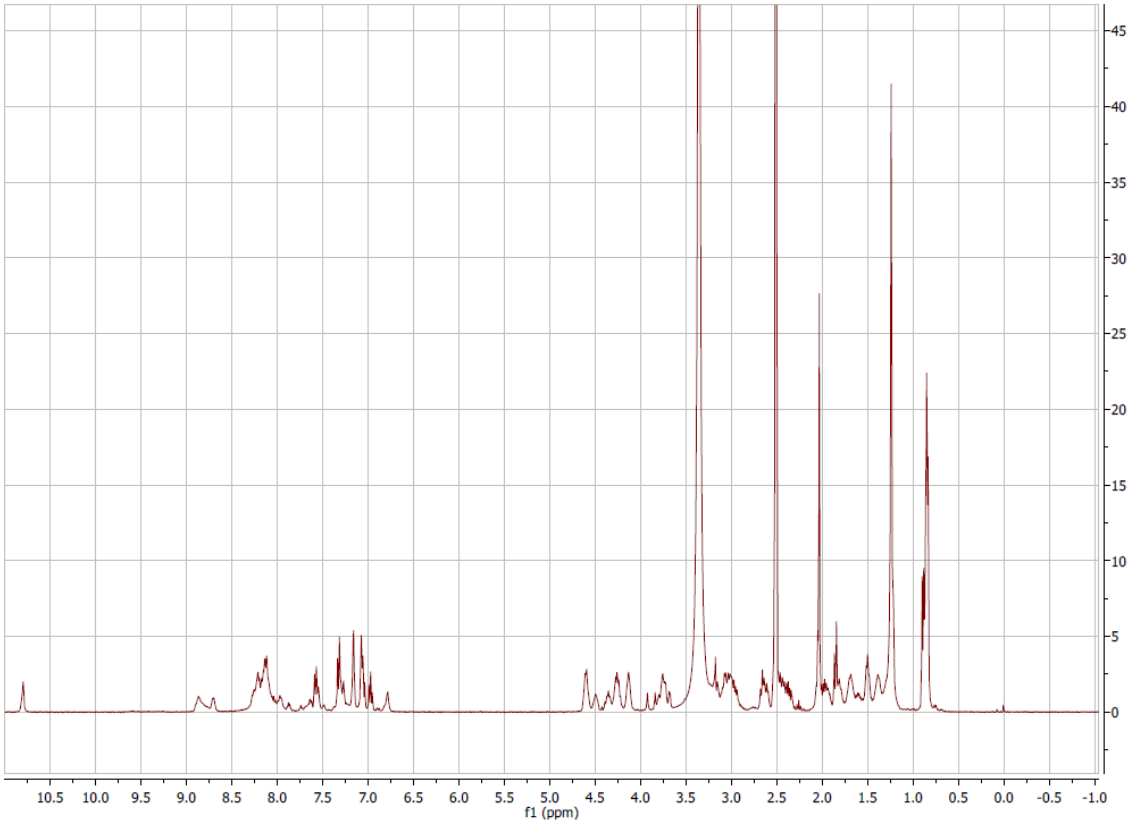

Figure A 111 ^{1}H spectrum (400 MHz, DMSO-d6) of compound **67**.

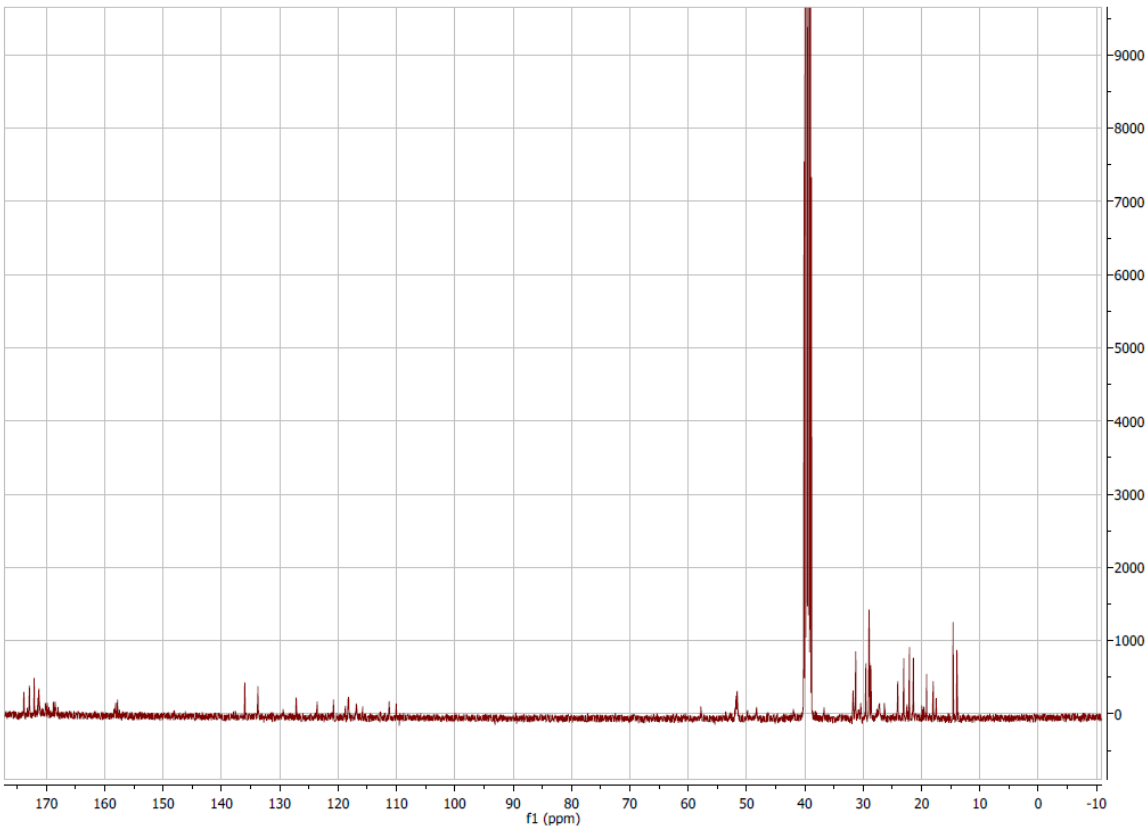

Figure A 112 ^{13}C spectrum (101 MHz, DMSO-d6) of compound **67**.

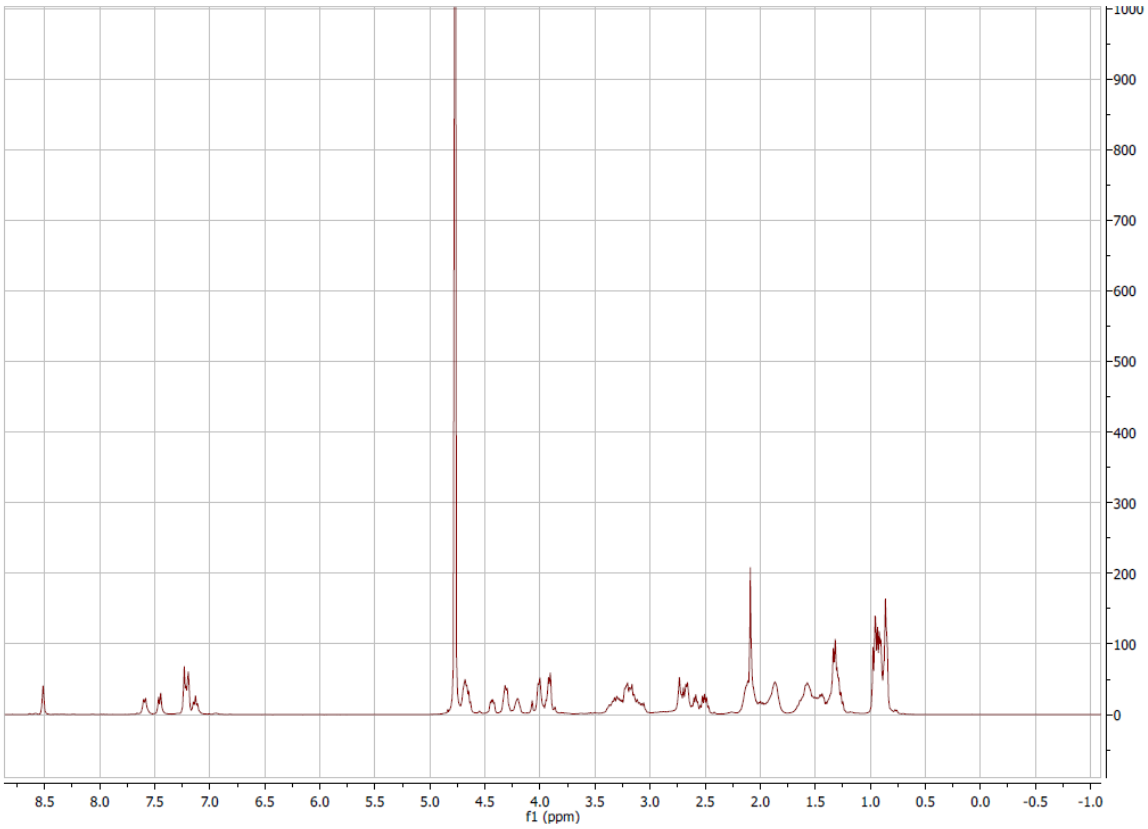

Figure A 113 ^{1}H spectrum (400 MHz, D_2O) of compound **68**.

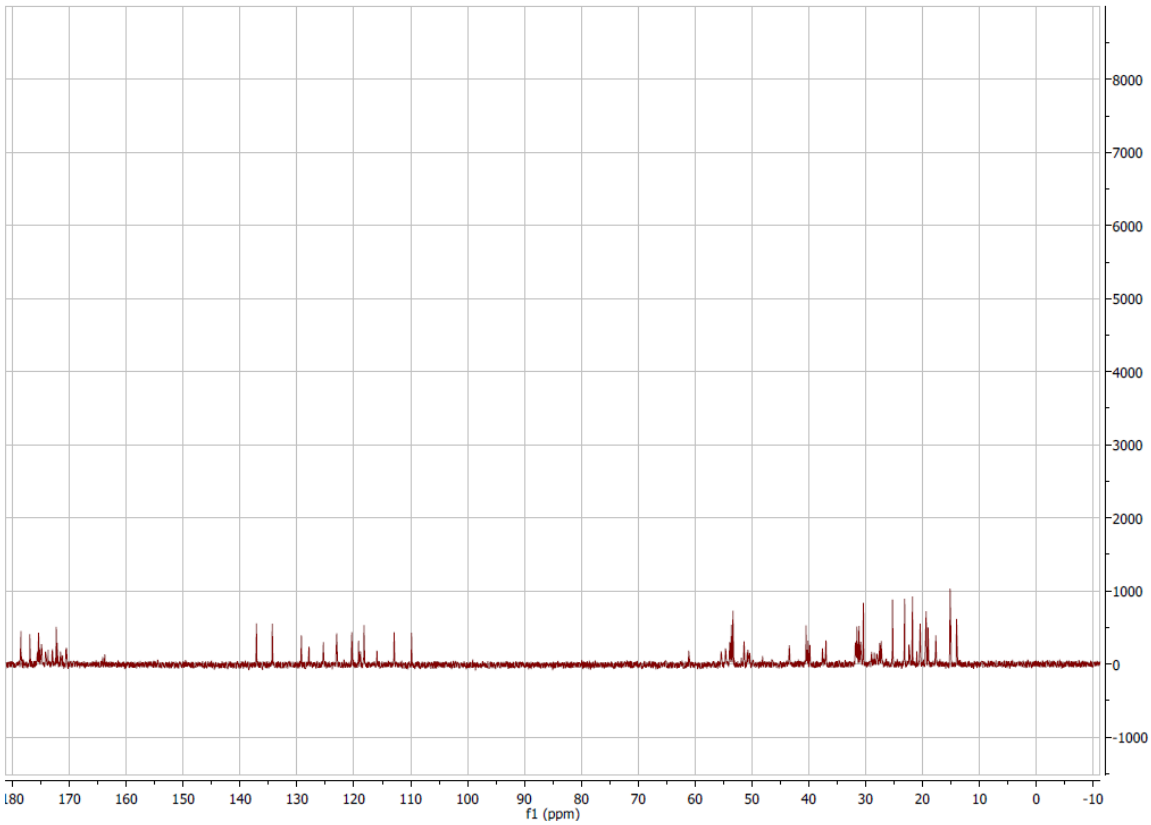

Figure A 114 ^{13}C spectrum (101 MHz, D_2O) of compound **68**.

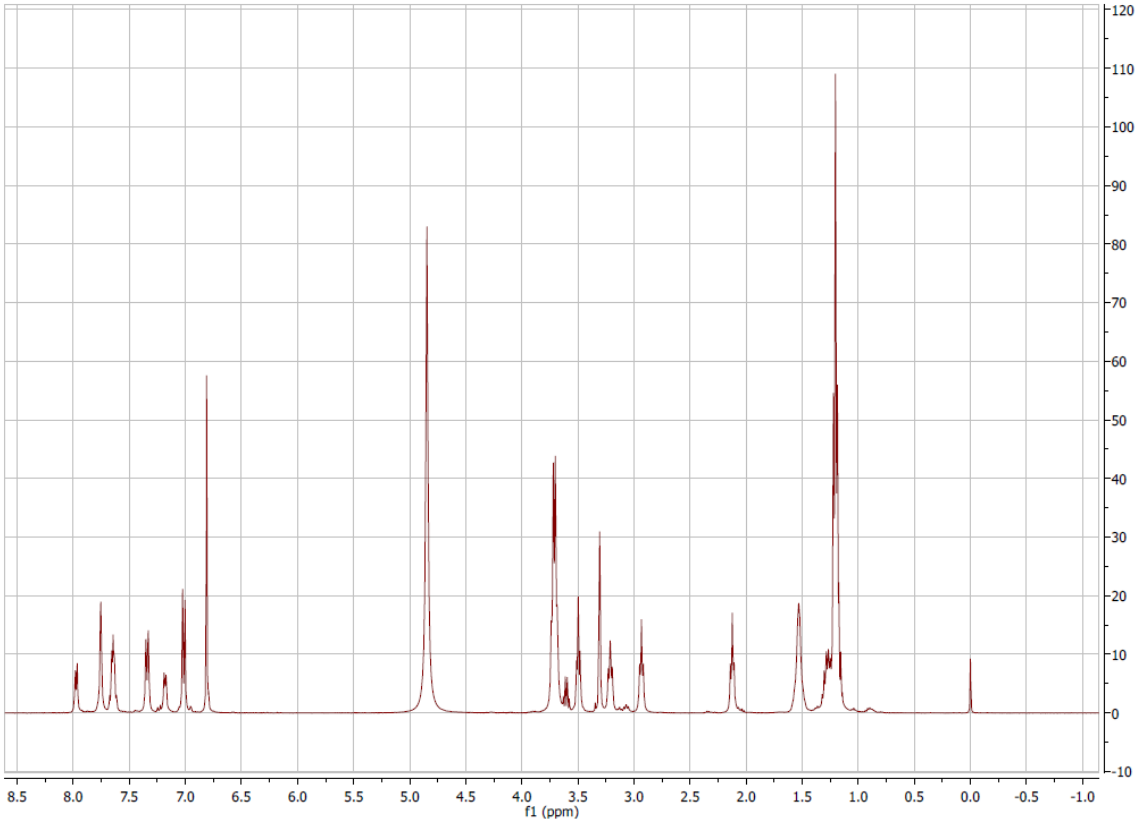

Figure A 115 ^{1}H spectrum (400 MHz, CD_3OD) of compound **74**.

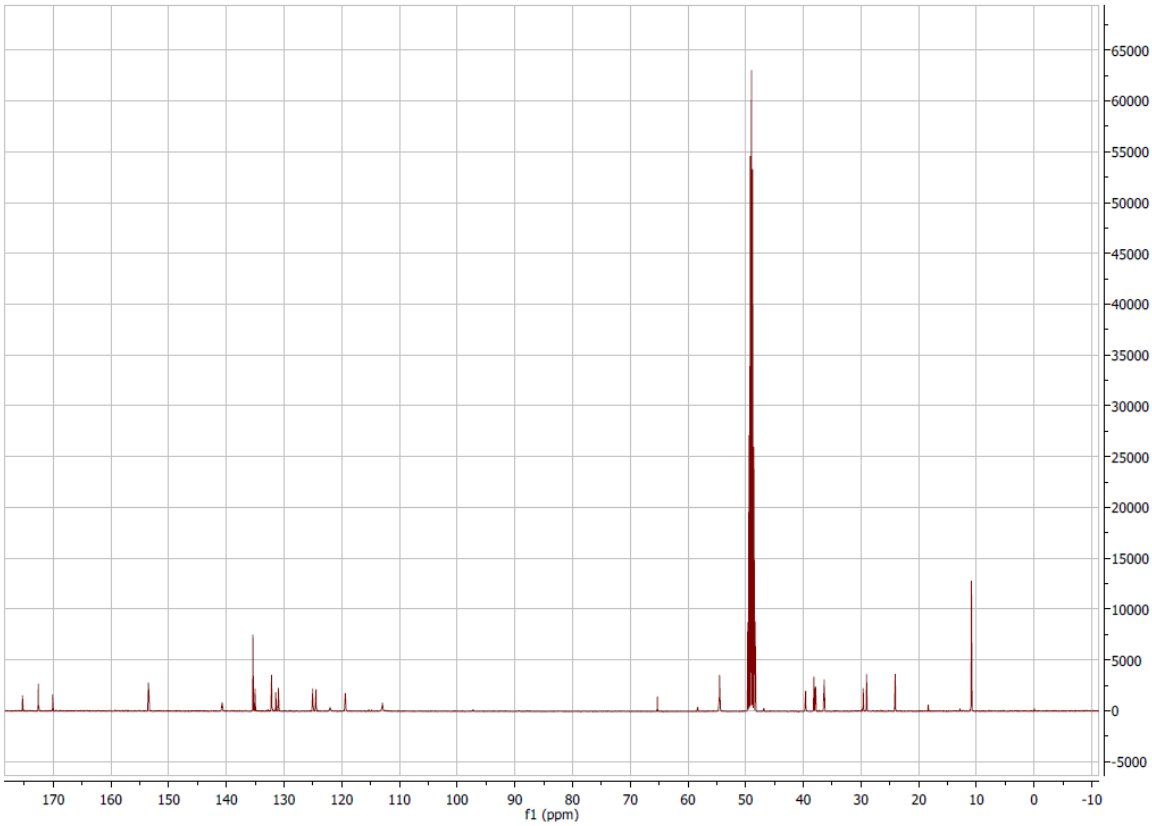

Figure A 116 ^{13}C spectrum (101 MHz, CD_3OD) of compound **74**.

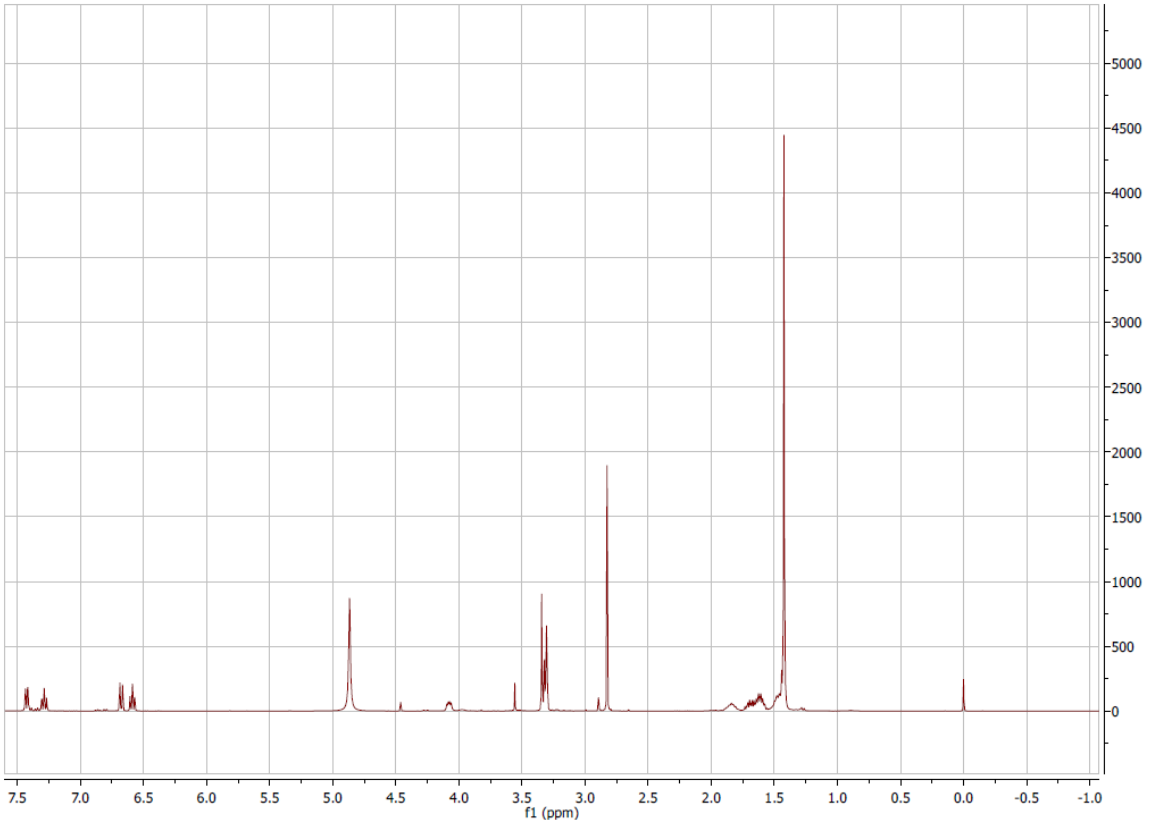

Figure A 117 ^{1}H spectrum (400 MHz, CD_3OD) of compound **76**.

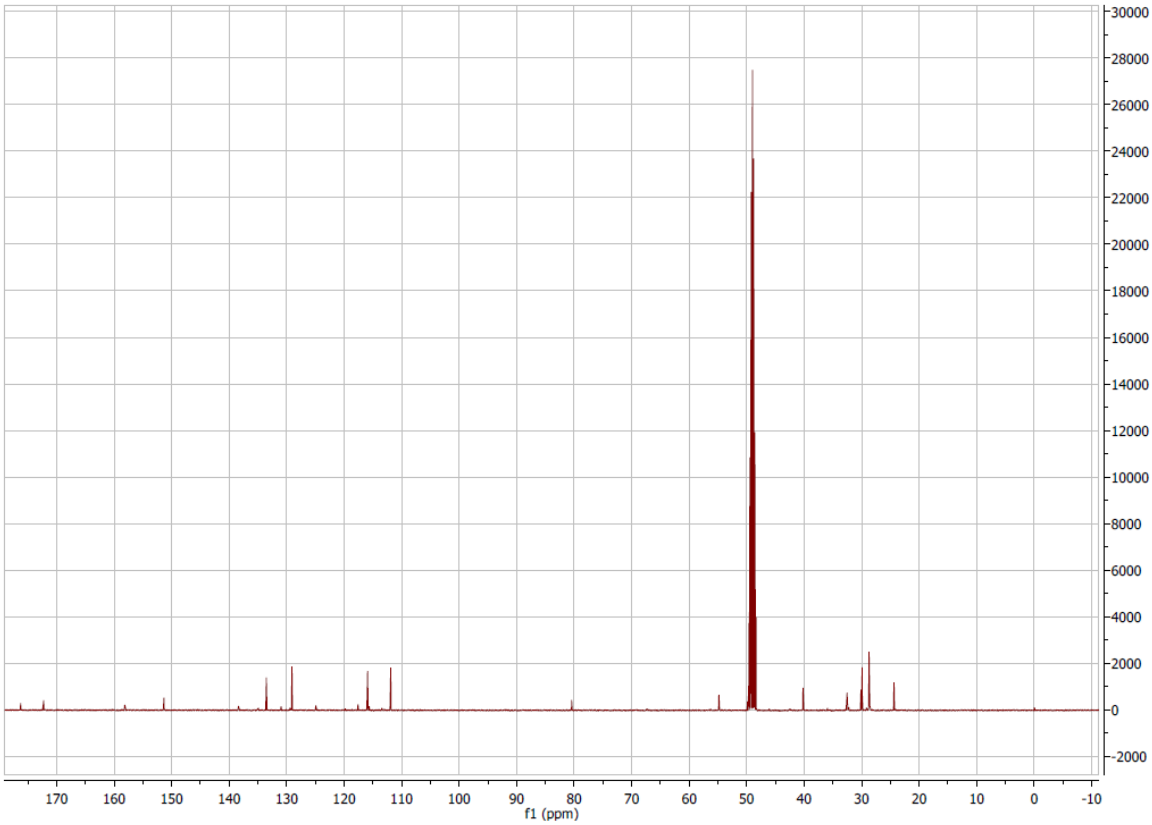

Figure A 118 ^{13}C spectrum (101 MHz, CD_3OD) of compound **76**.

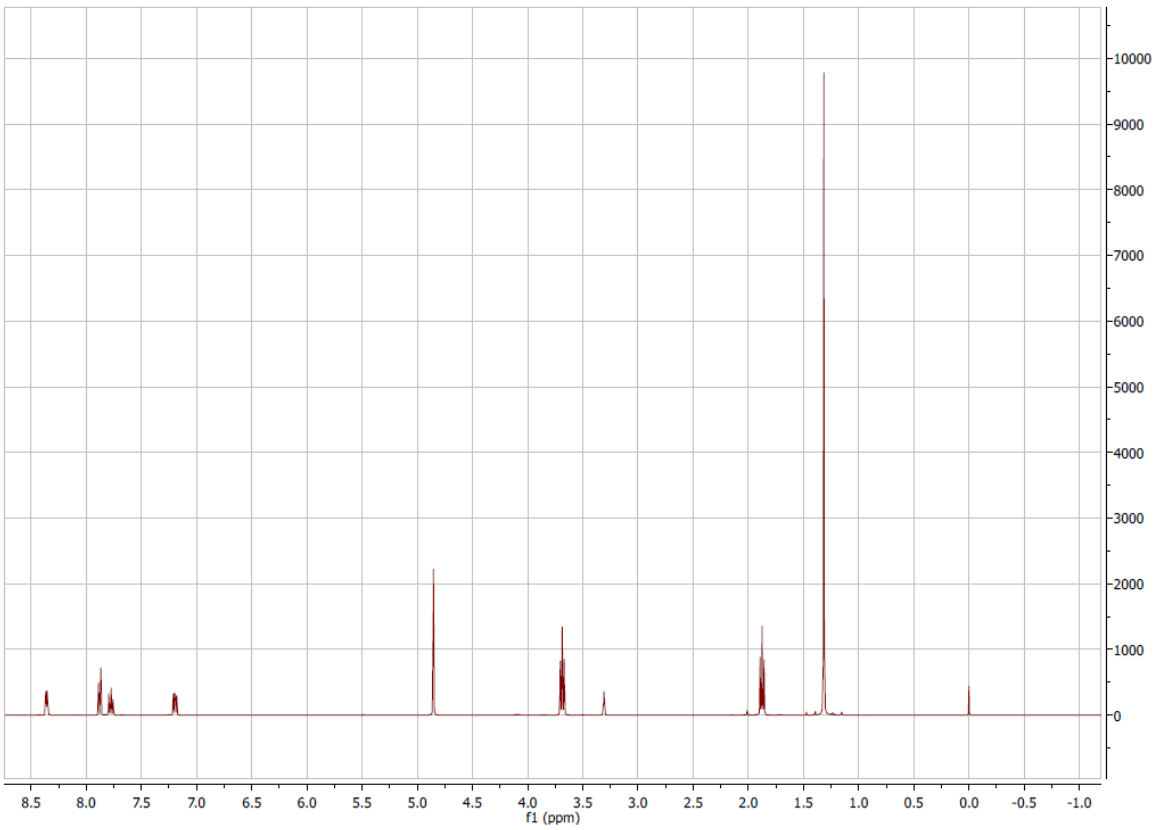

Figure A 119 ^{1}H spectrum (400 MHz, CD_3OD) of compound **77**.

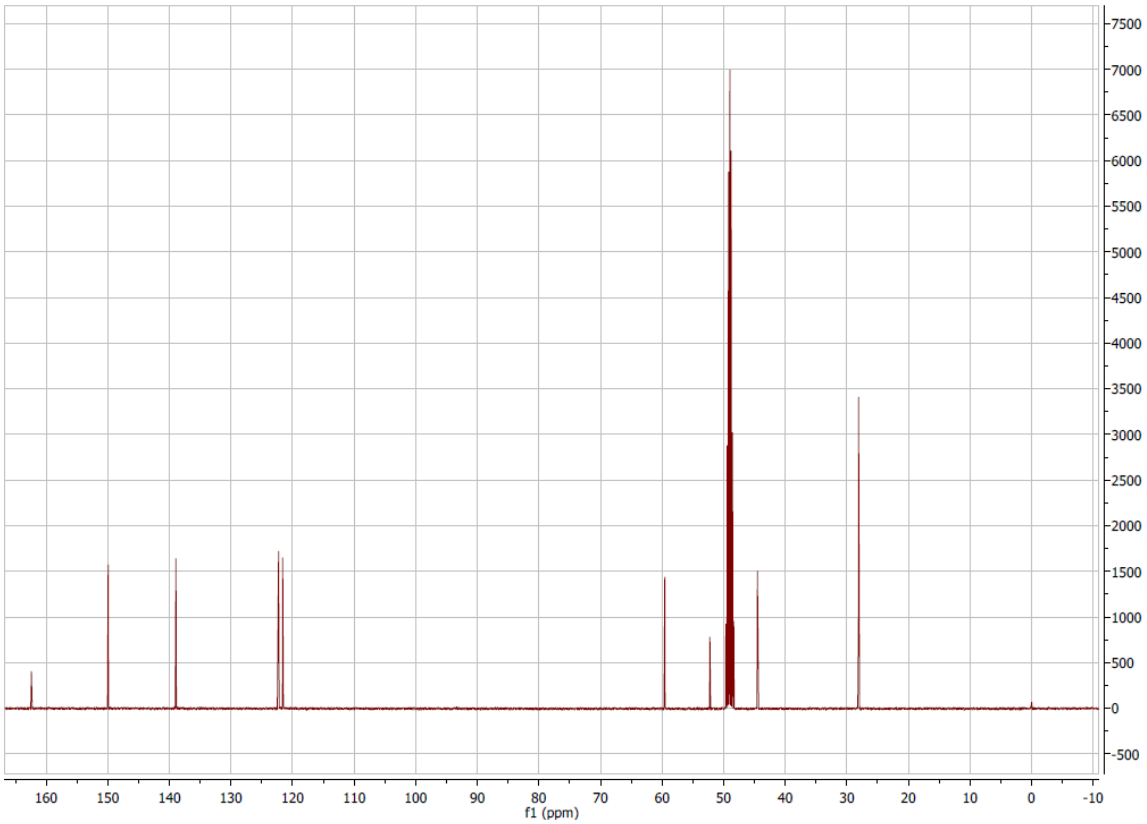

Figure A 120 ^{13}C spectrum (101 MHz, CD_3OD) of compound **77**.

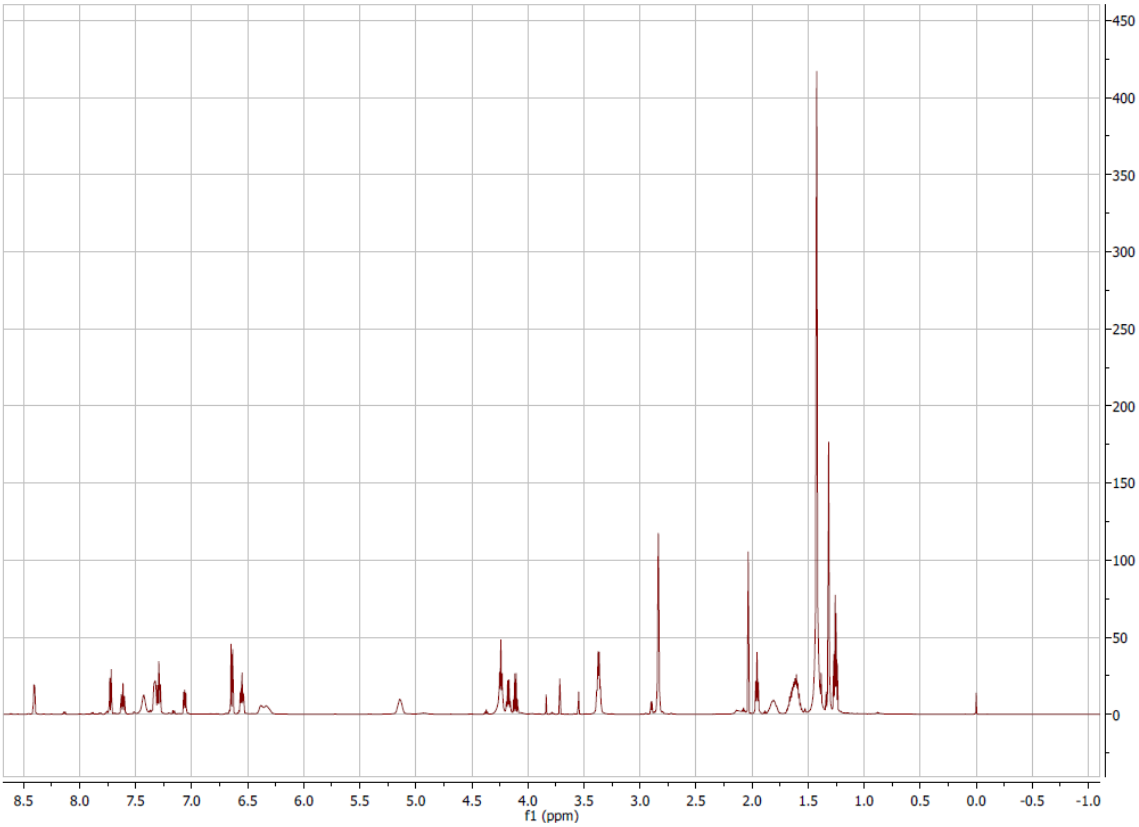

Figure A 121 ^{1}H spectrum (400 MHz, $CDCl_3$) of compound **78**.

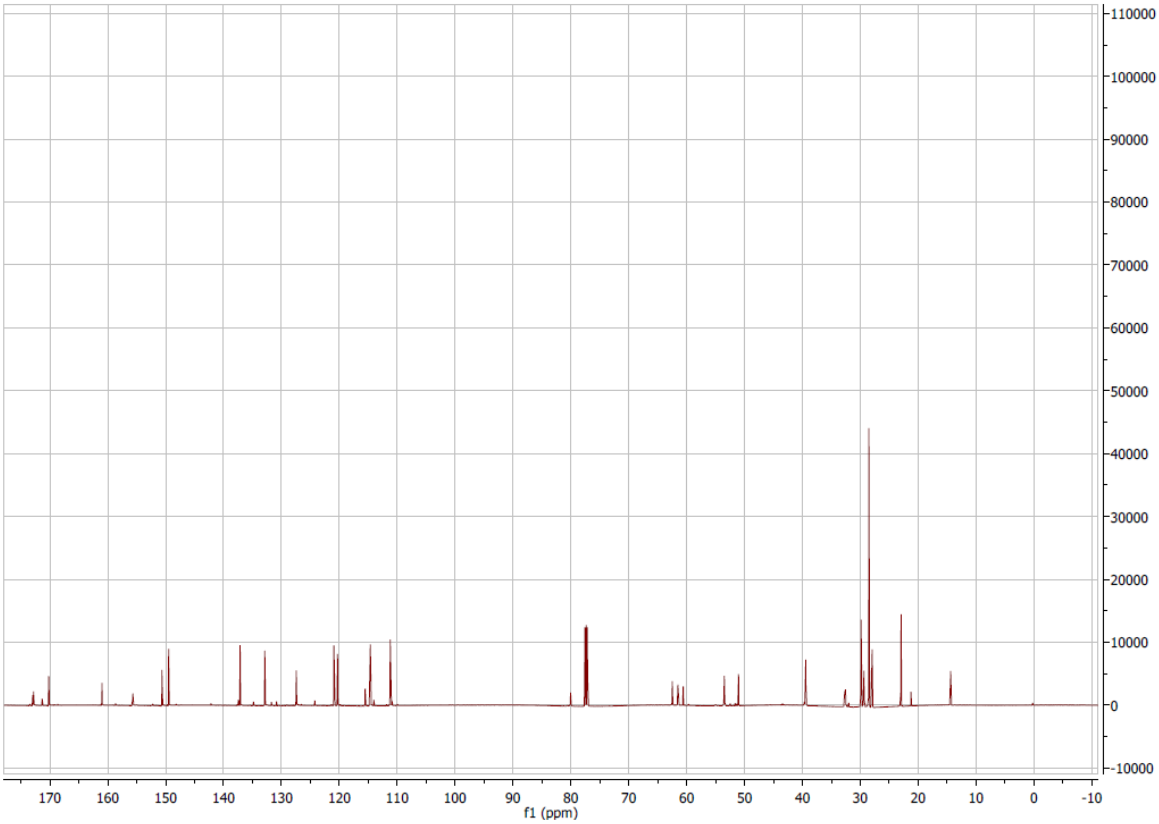

Figure A 122 ^{13}C spectrum (101 MHz, $CDCl_3$) of compound **78**.

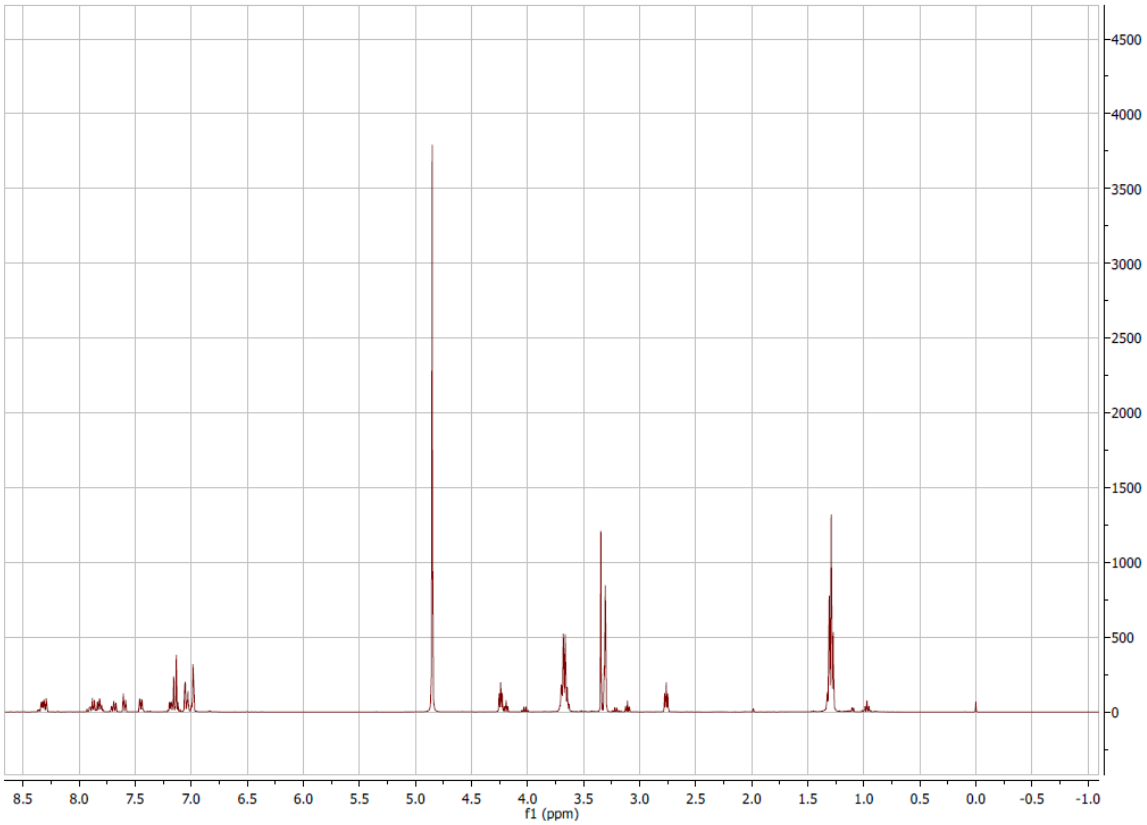

Figure A 123 ^{1}H spectrum (400 MHz, CD_3OD) of compound **79**.

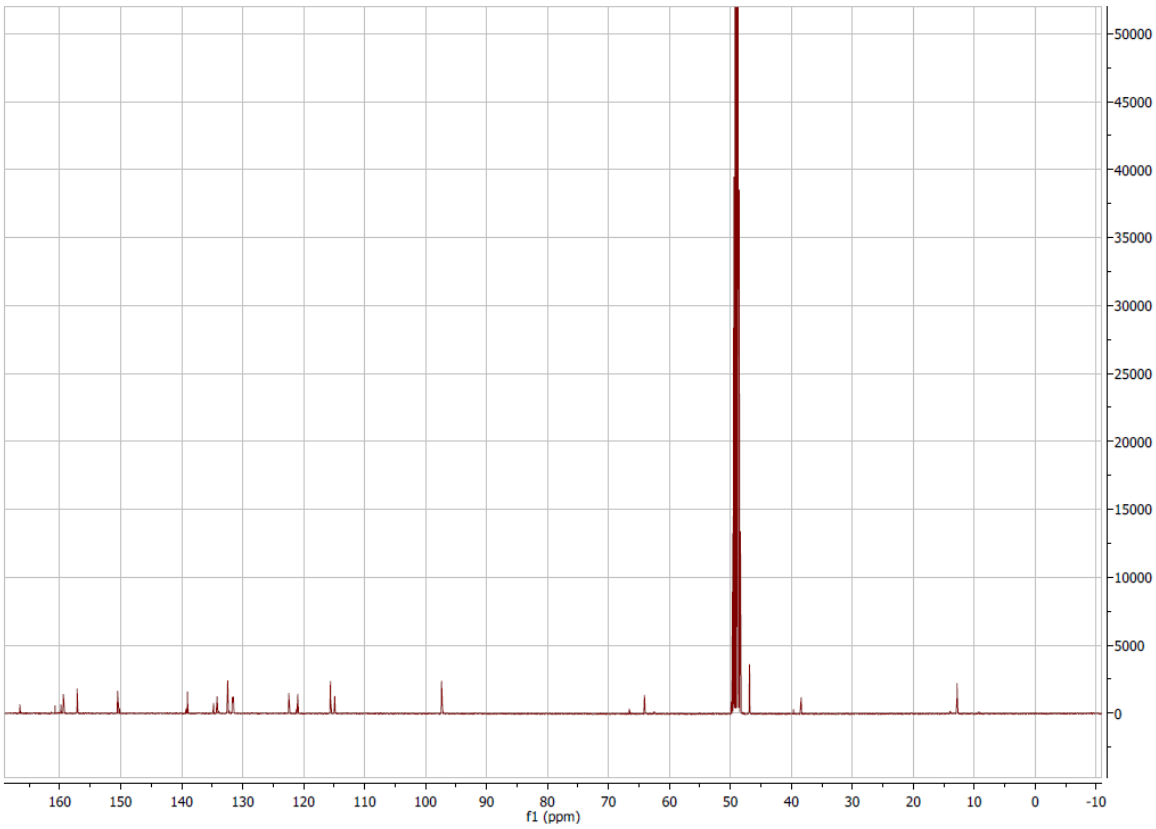

Figure A 124 ^{13}C spectrum (101 MHz, CD_3OD) of compound **79**.

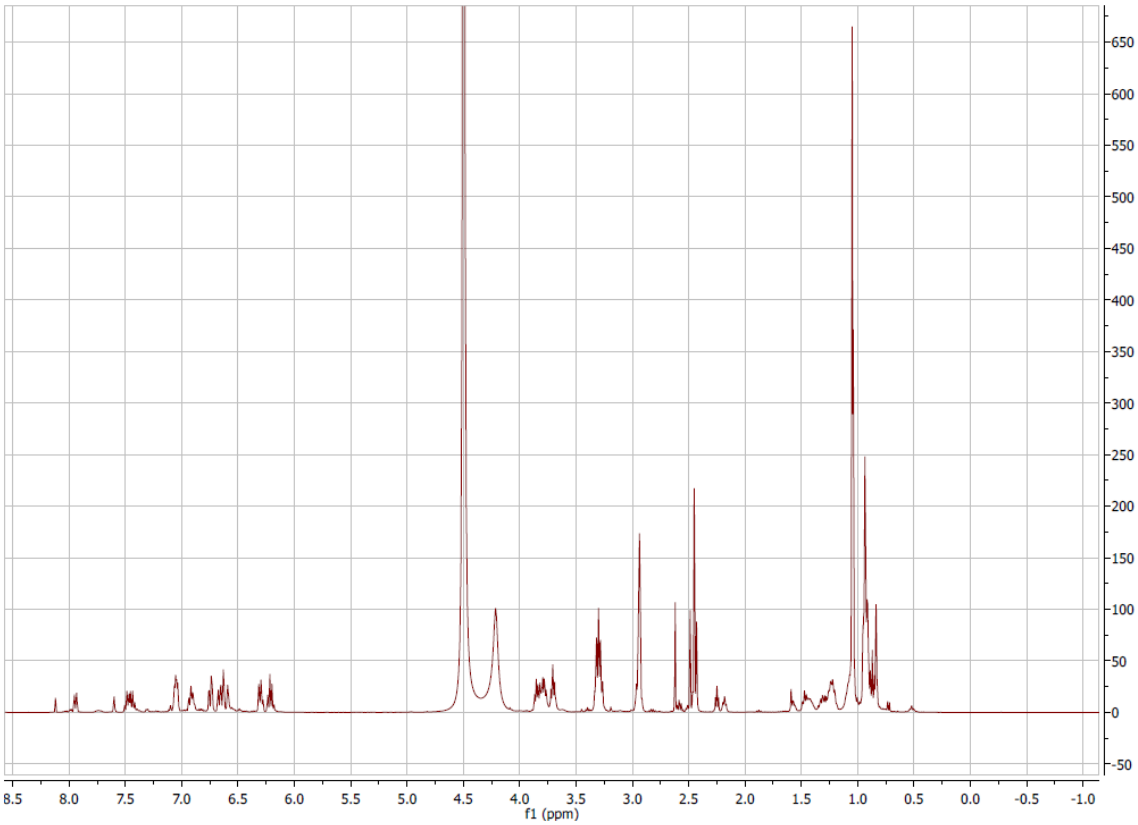

Figure A 125 ^{1}H spectrum (400 MHz, CD_3OD) of compound **80**.

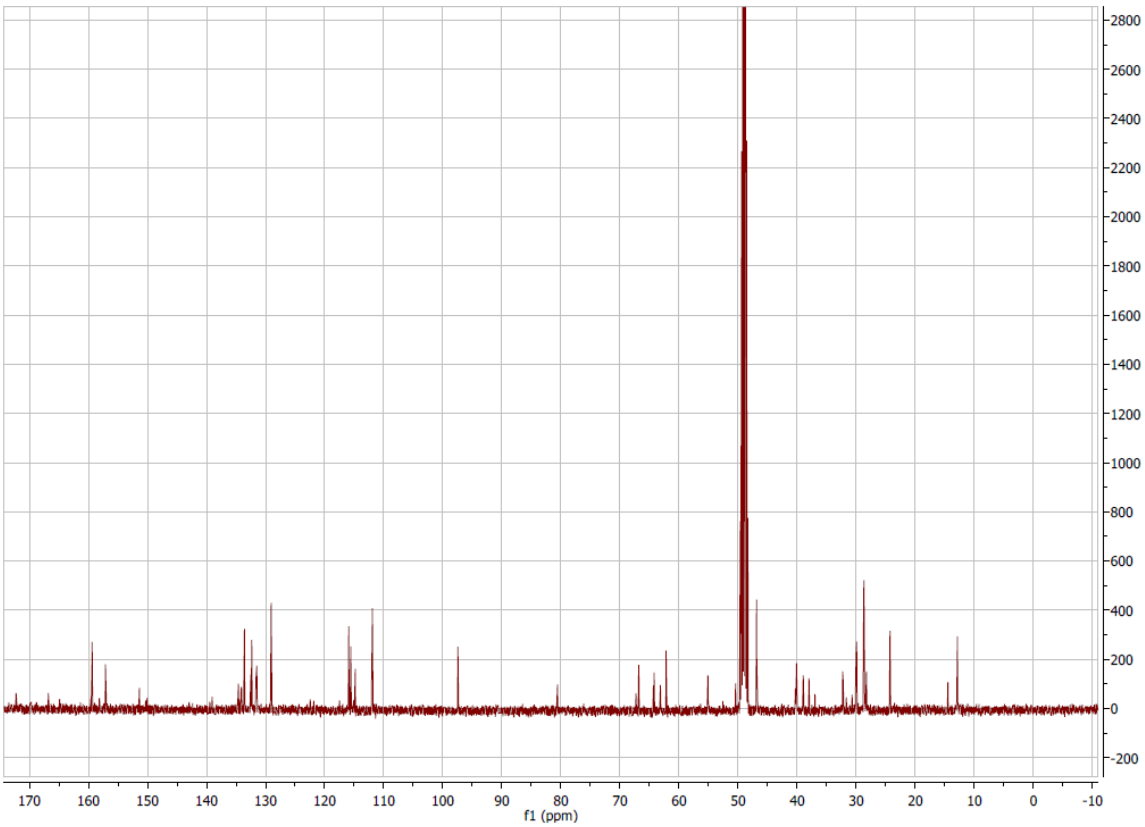

Figure A 126 ^{13}C spectrum (101 MHz, CD_3OD) of compound **80**.

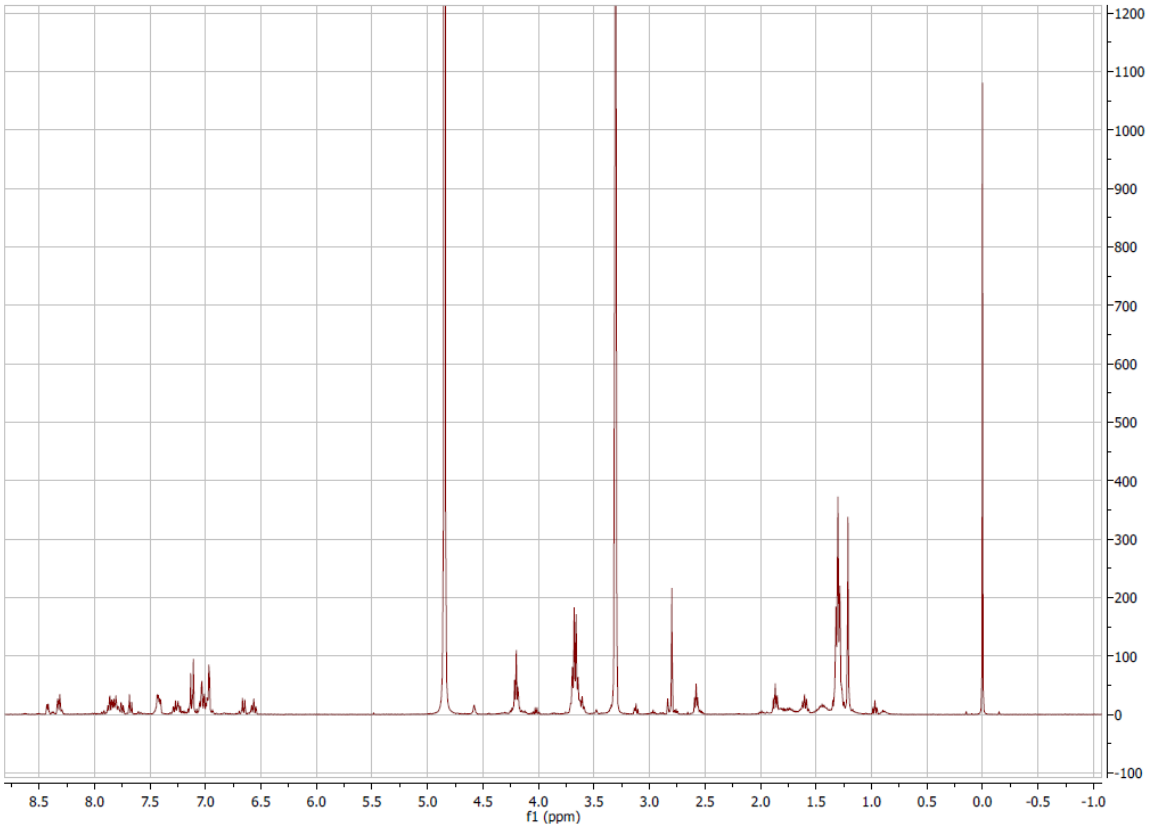

Figure A 127 ^{1}H spectrum (400 MHz, CD_3OD) of compound **81**.

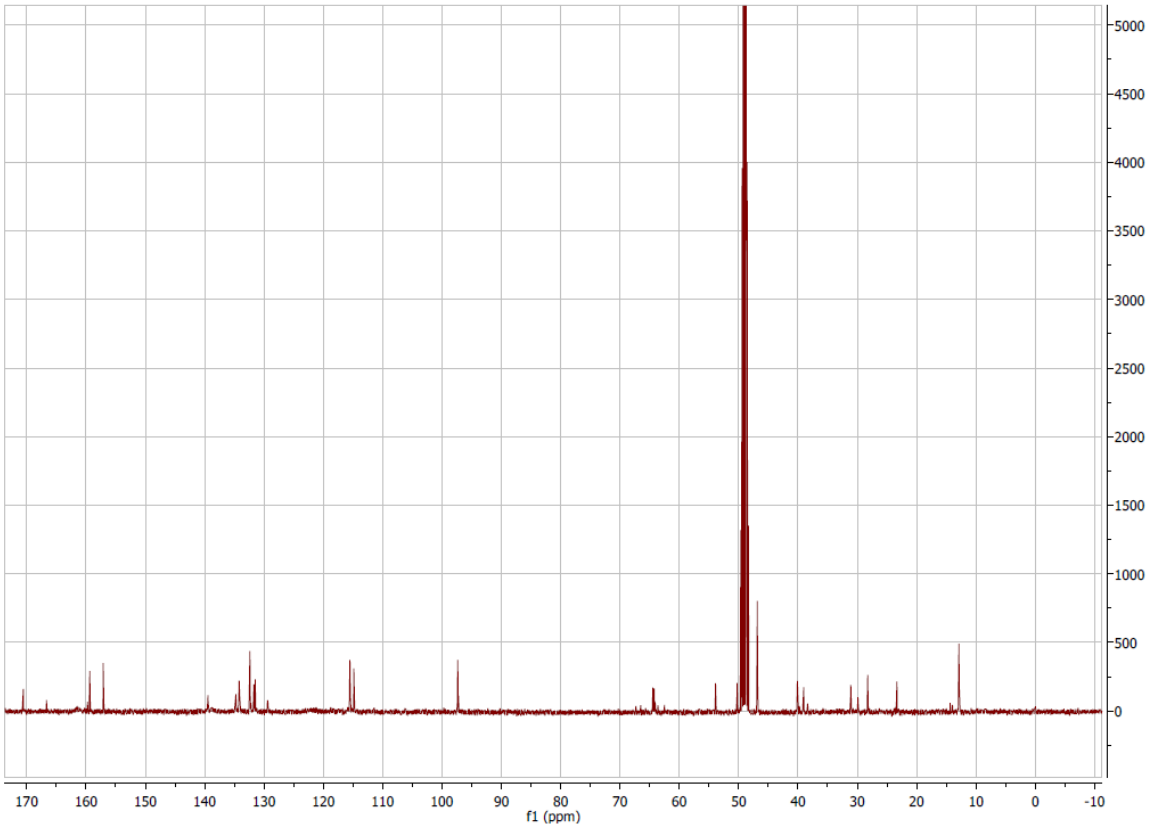

Figure A 128 ^{13}C spectrum (101 MHz, CD_3OD) of compound **81**.

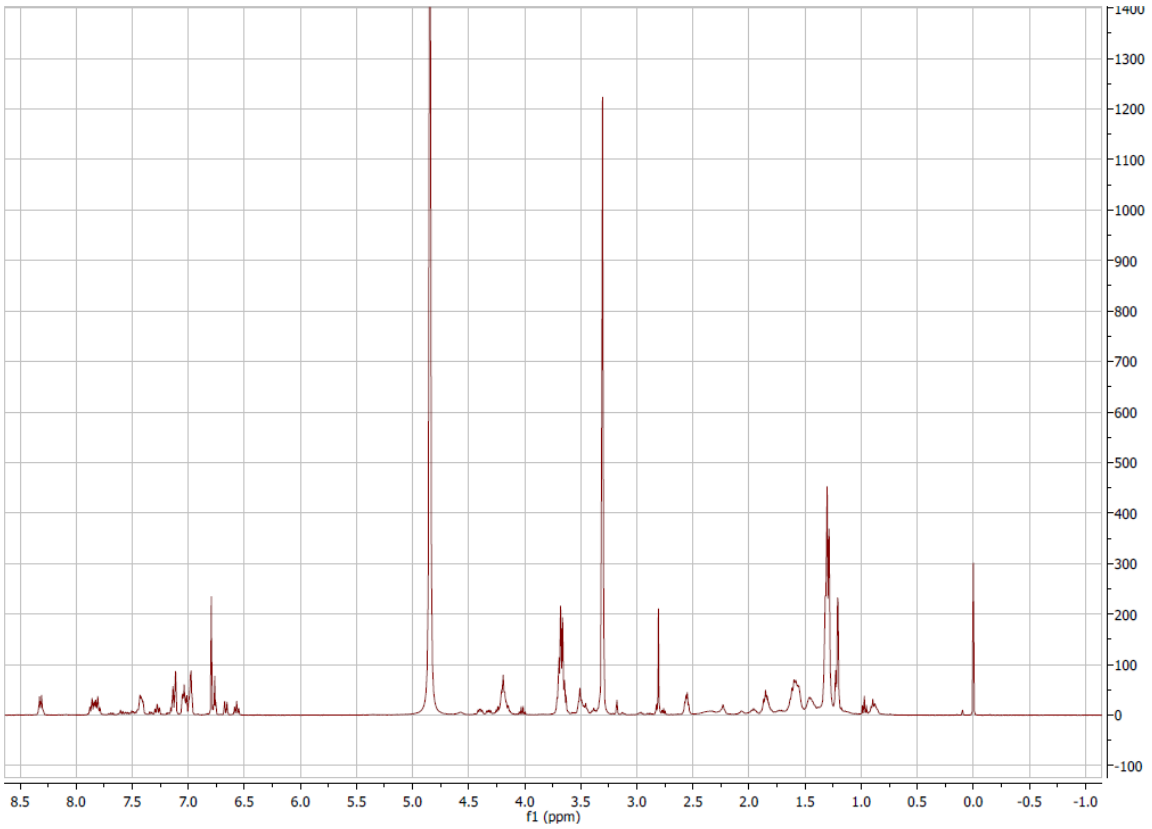

Figure A 129 ^{1}H spectrum (400 MHz, CD_3OD) of compound **82**.

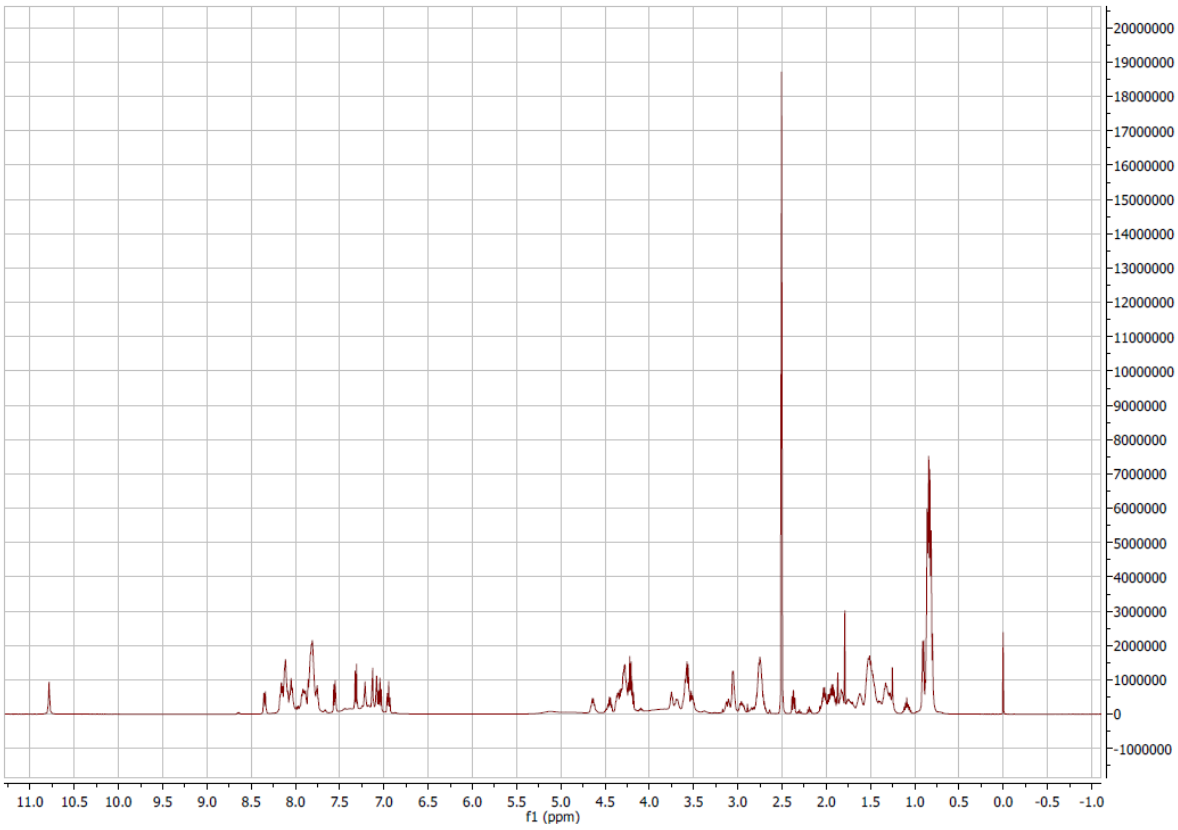

Figure A 130 ^{1}H spectrum (500 MHz, DMSO-d6) of compound **84**.

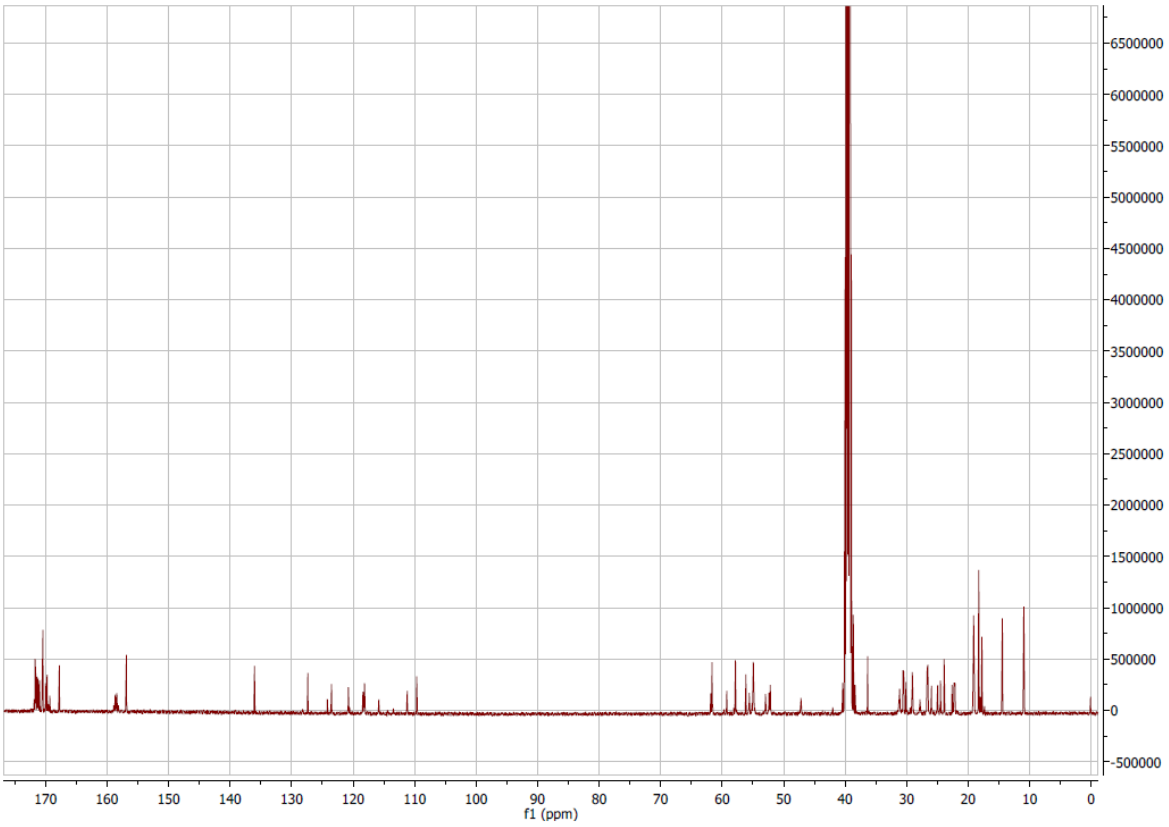

Figure A 131 ^{13}C spectrum (126 MHz, DMSO-d6) of compound **84**.

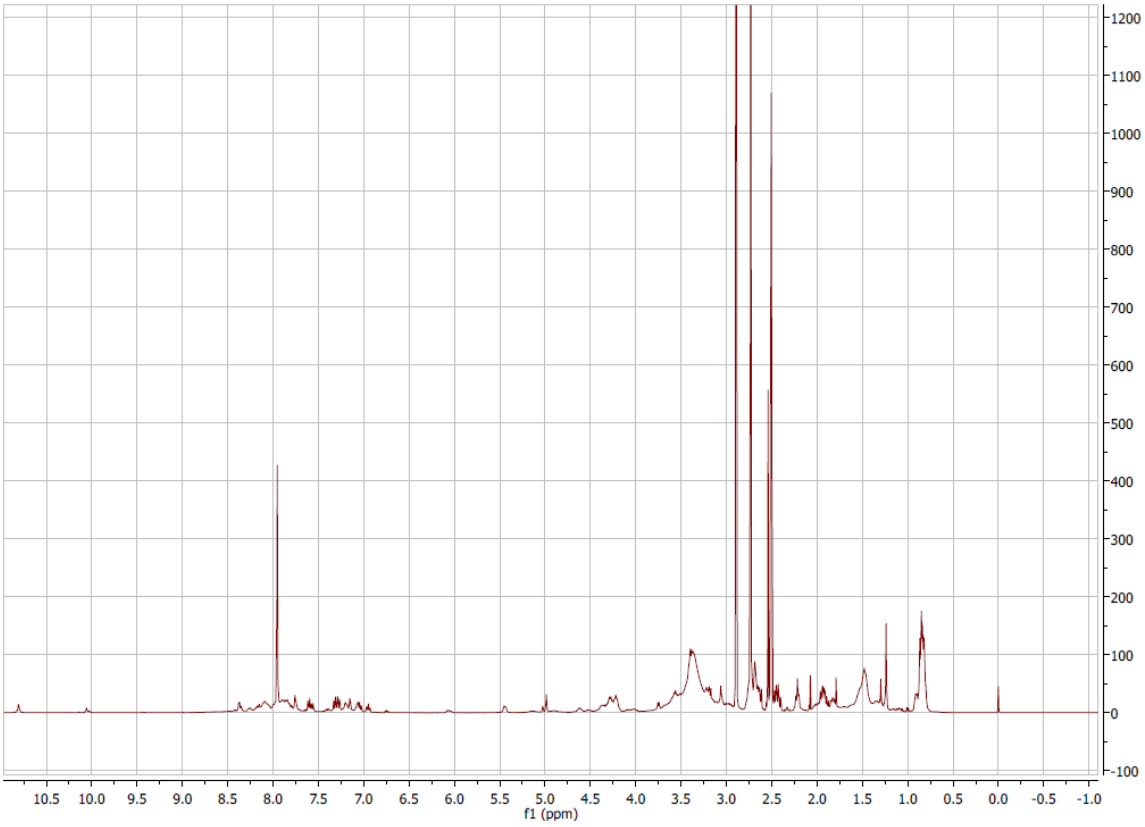

Figure A 132 ^{1}H spectrum (500 MHz, DMSO-d6) of compound **85**.

Appendix III: Fluorescence spectra

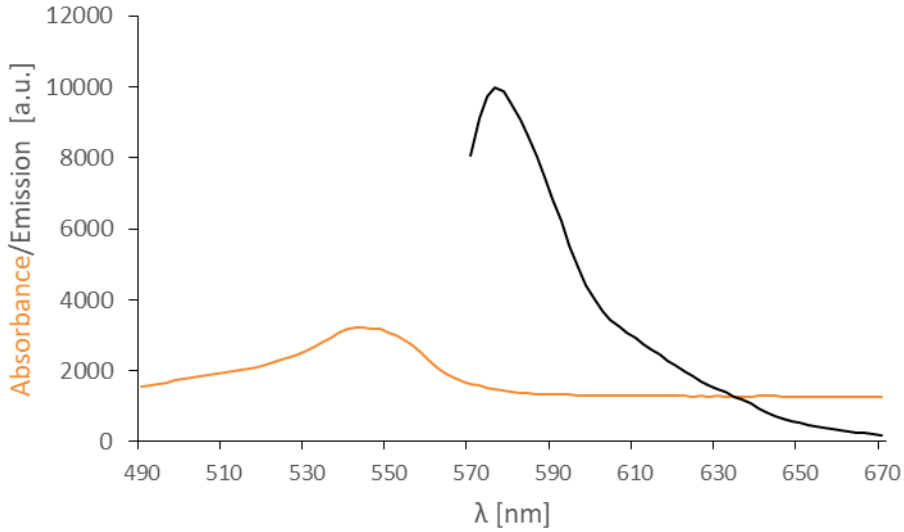

Figure A 133 Fluorescence spectrum of rhodamine B, λ_{ex} = 545 nm, λ_{em} = 576 nm (in MeOH).

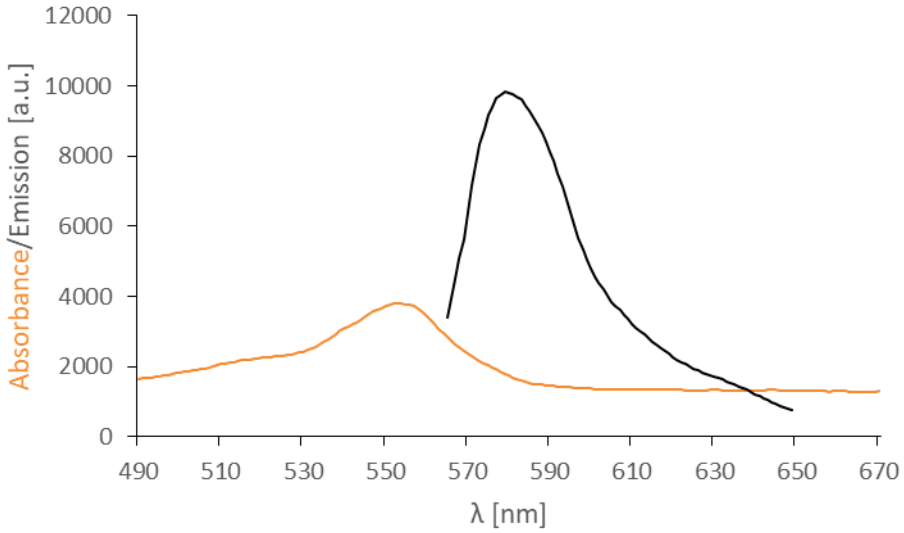

Figure A 134 Fluorescence spectrum of modified rhodamine B **54**, λ_{ex} = 553 nm, λ_{em} = 581 nm (in MeOH).

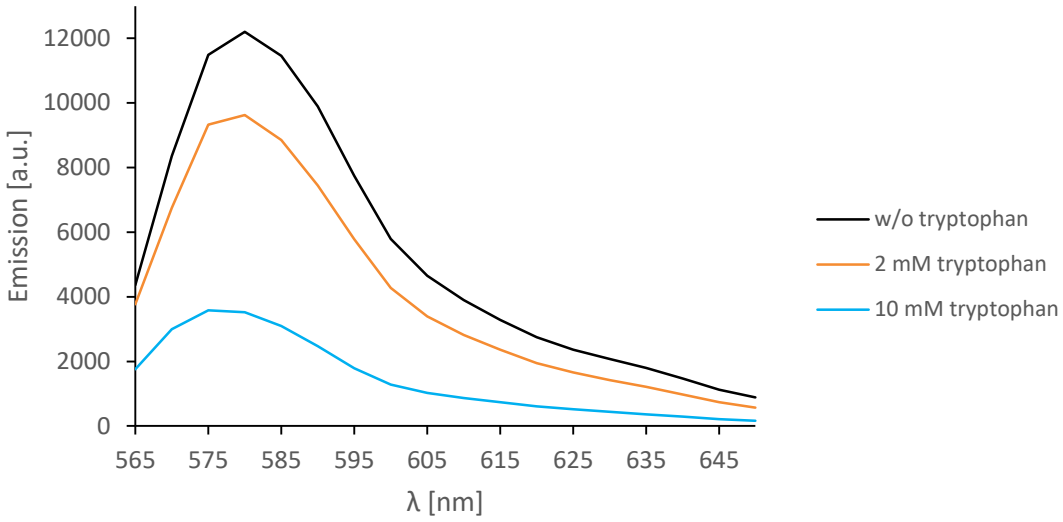

Figure A 135 Quenching of fluorophore **54** by increasing tryptophan concentrations (2 mM, 10mM) (in MeOH).

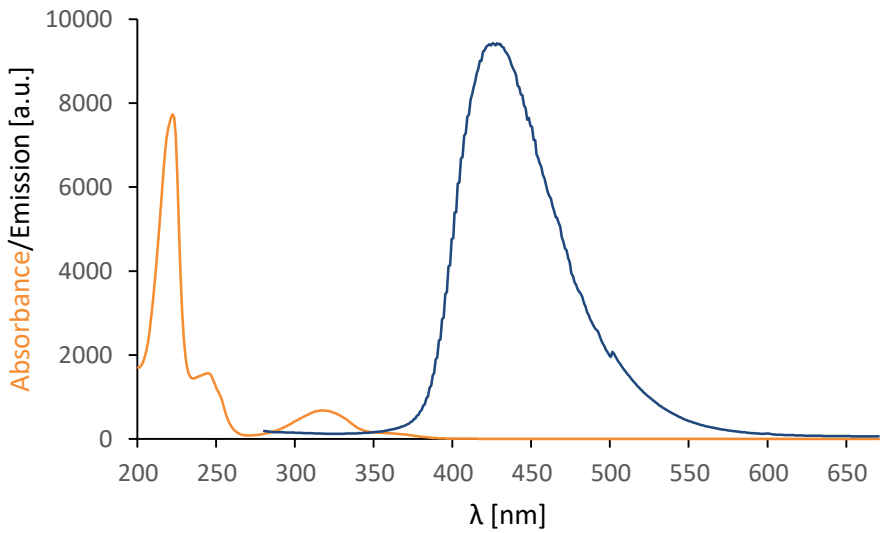

Figure A 136 Fluorescence spectrum of *N*-methyl isatoic anhydride, λ_{ex} = 222 nm, λ_{em} = 428 nm (in MeOH).

Appendix IV: Graphs and tables of IC_{50} values

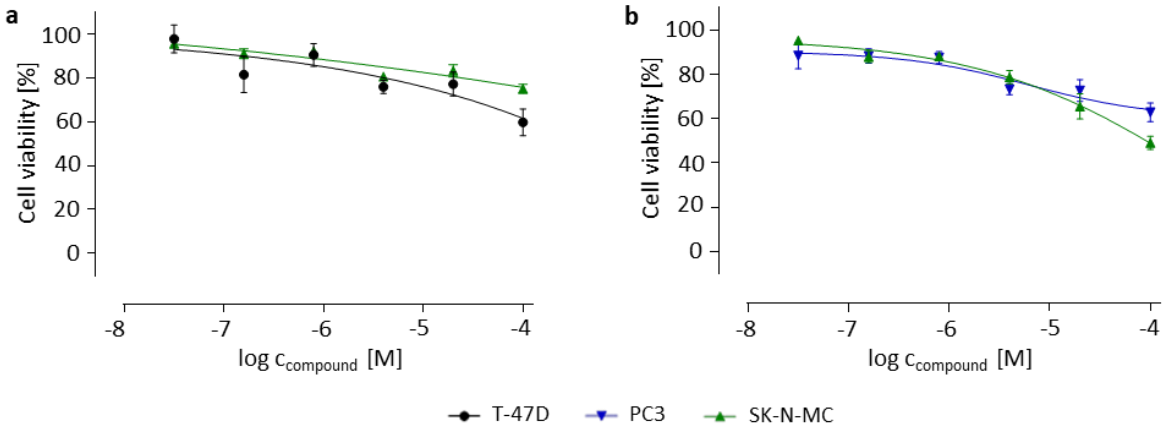

Figure A 137 *In vitro* antitumor activity of fluorescent conjugates a) **56** and b) **57** after 72 h.

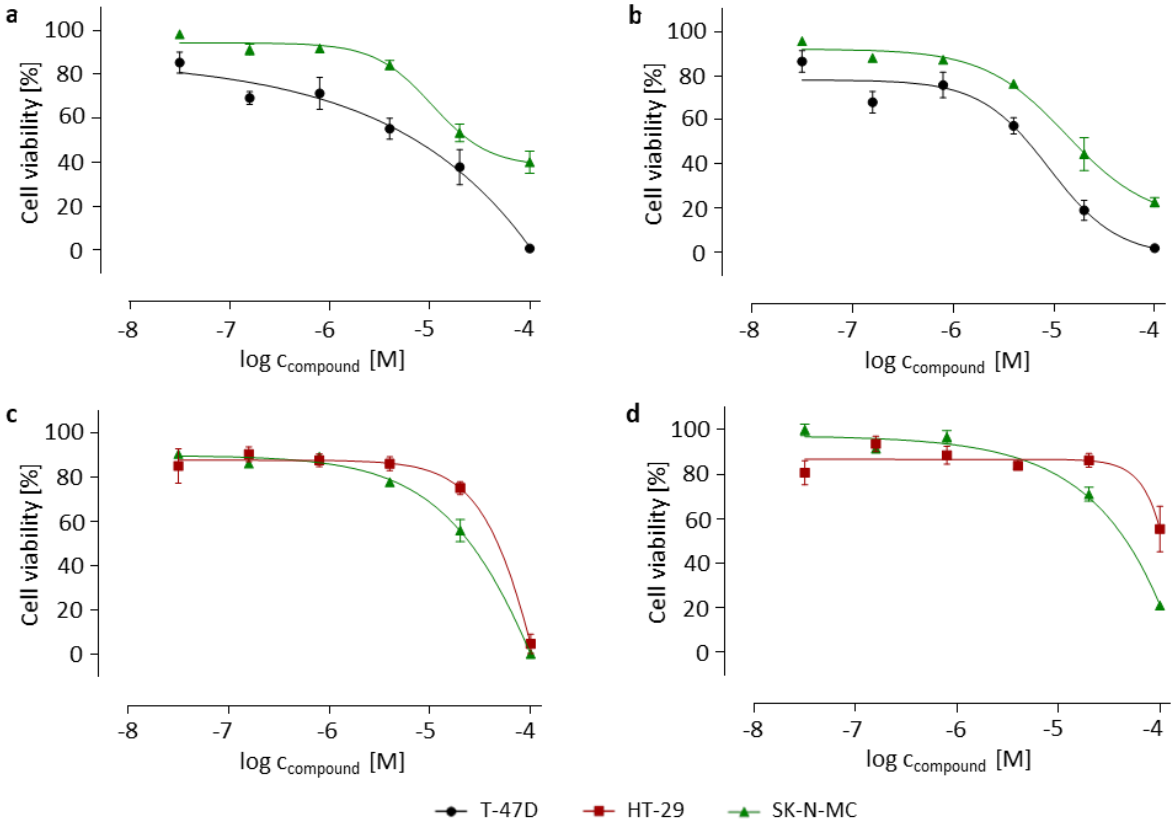

Figure A 138 *In vitro* antitumor activity of fluorescent conjugates a) **75**, b) **83**, c) **88** and d) **89** after 72 h.

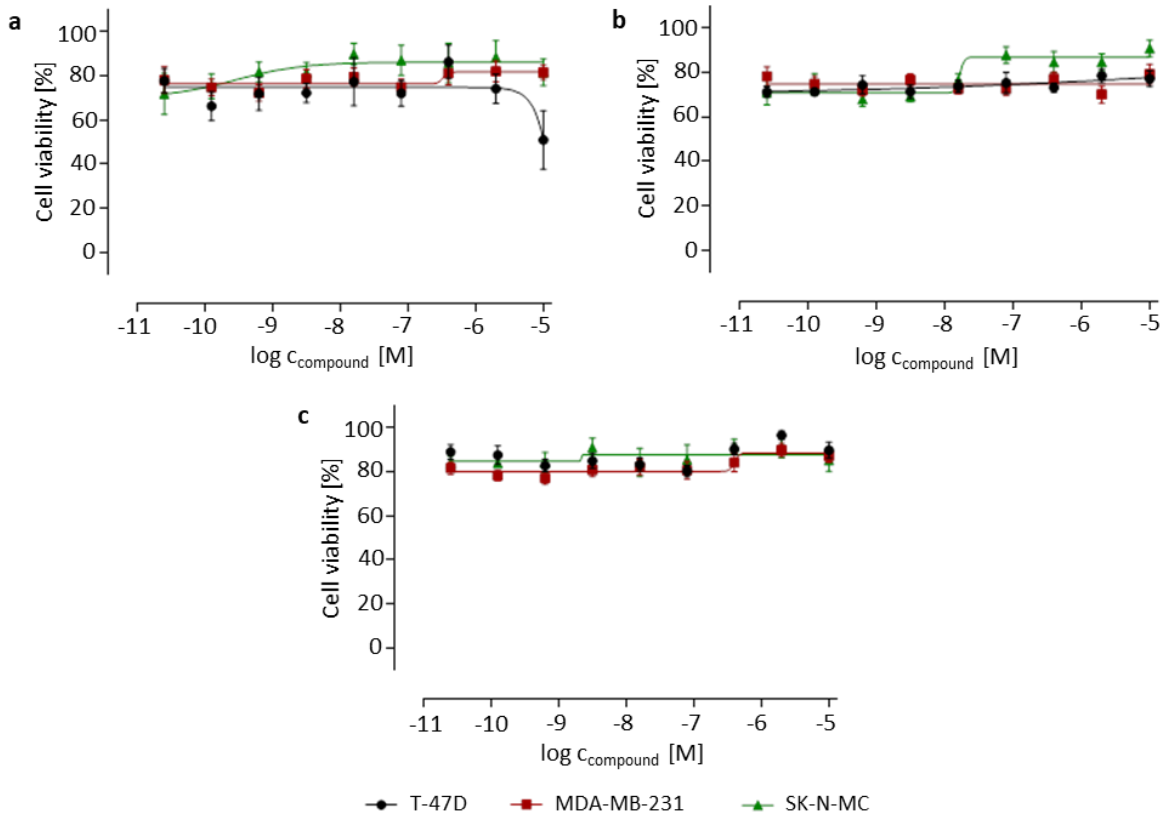

Figure A 139 *In vitro* antitumor activity of peptide **45** after a) 6, b) 24 and c) 72 h.

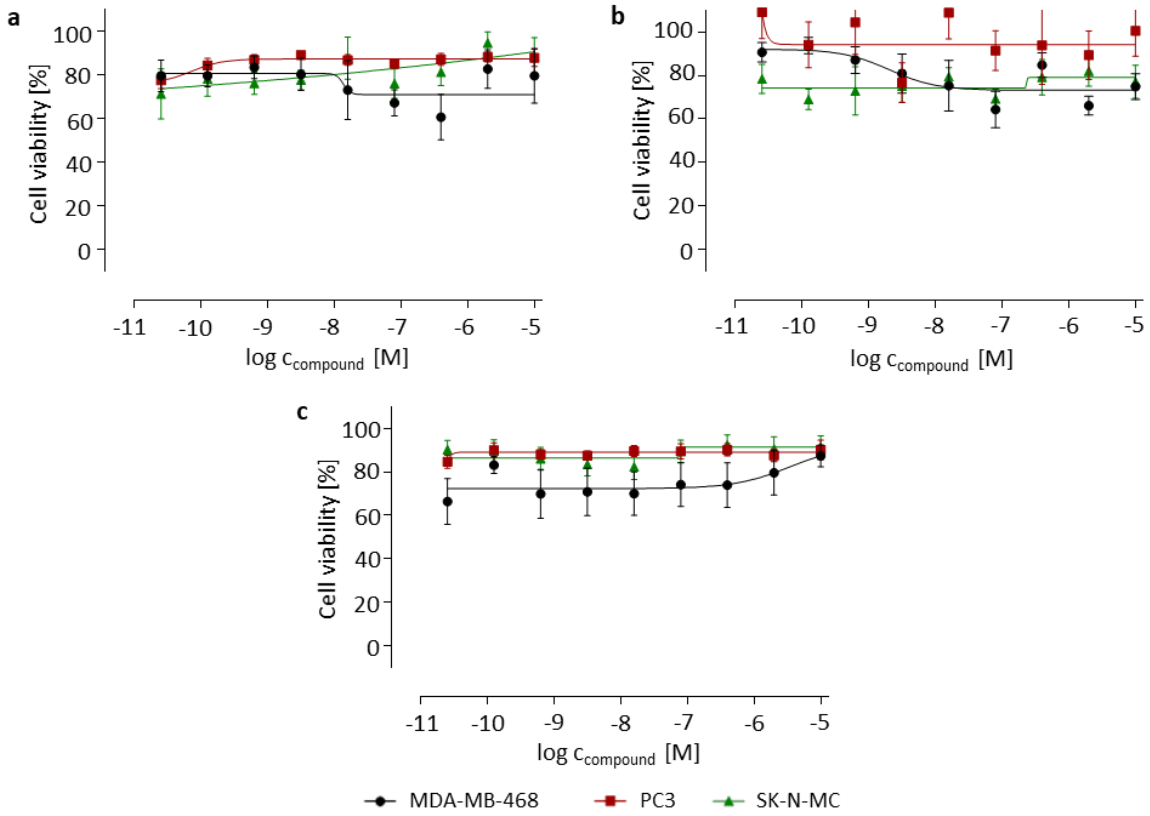

Figure A 140 *In vitro* antitumor activity of peptide **47** after a) 6, b) 24 and c) 72 h.

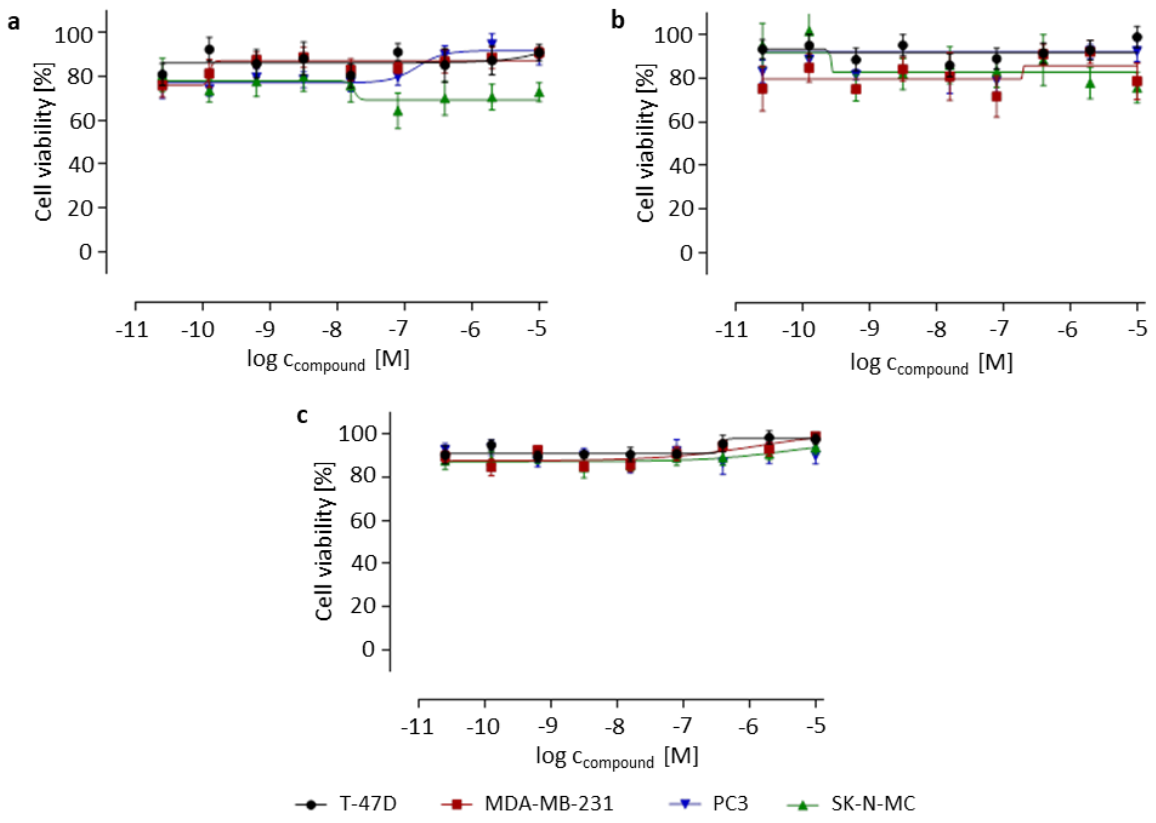

Figure A 141 *In vitro* antitumor activity of peptide **63** after a) 6, b) 24 and c) 72 h.

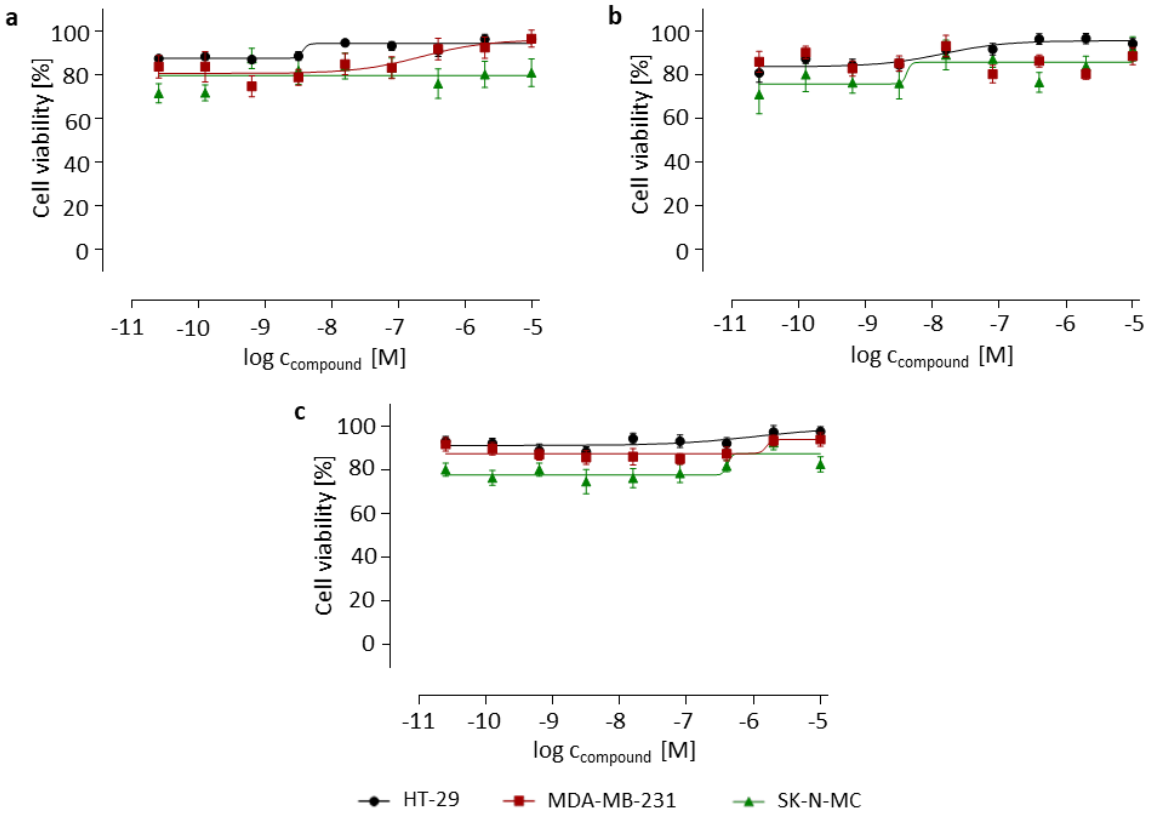

Figure A 142 *In vitro* antitumor activity of peptide **84** after a) 6, b) 24 and c) 72 h.

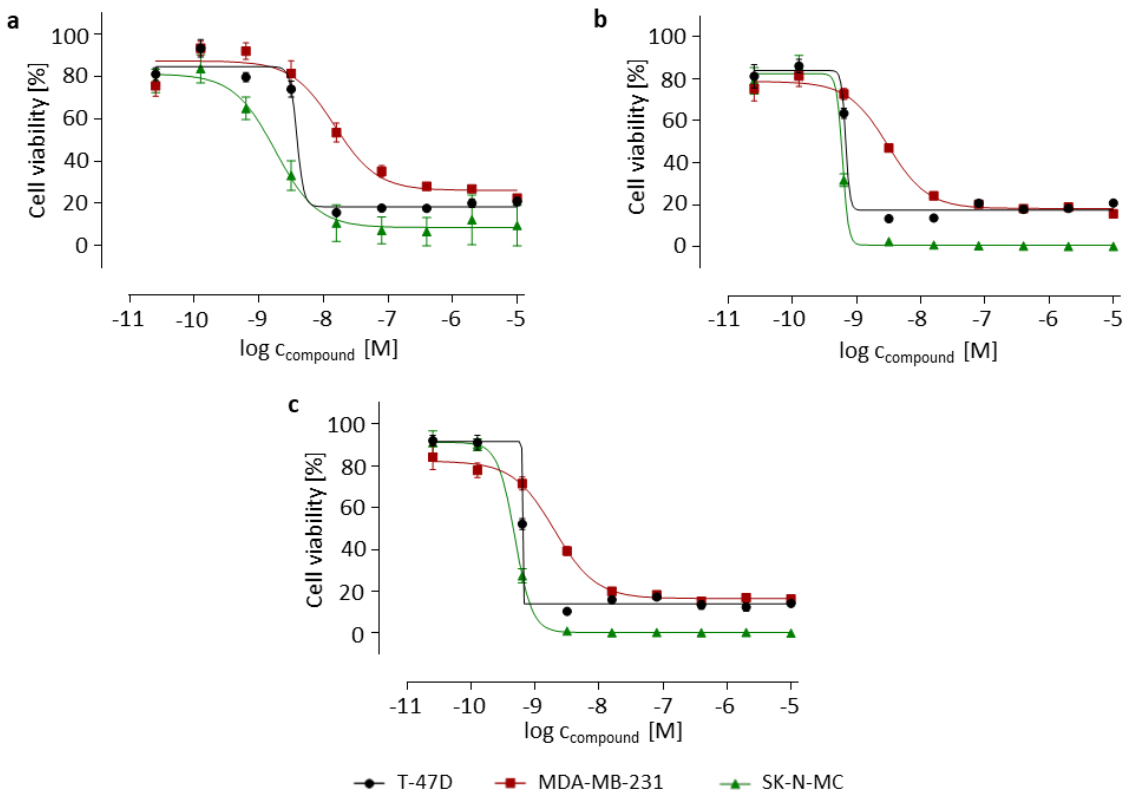

Figure A 143 *In vitro* antitumor activity of toxin **33** after a) 6, b) 24 and c) 72 h to cells expressing high (T-47D), moderate (MDA-MB-231) and low (SK-N-MC) level of SSTR2.

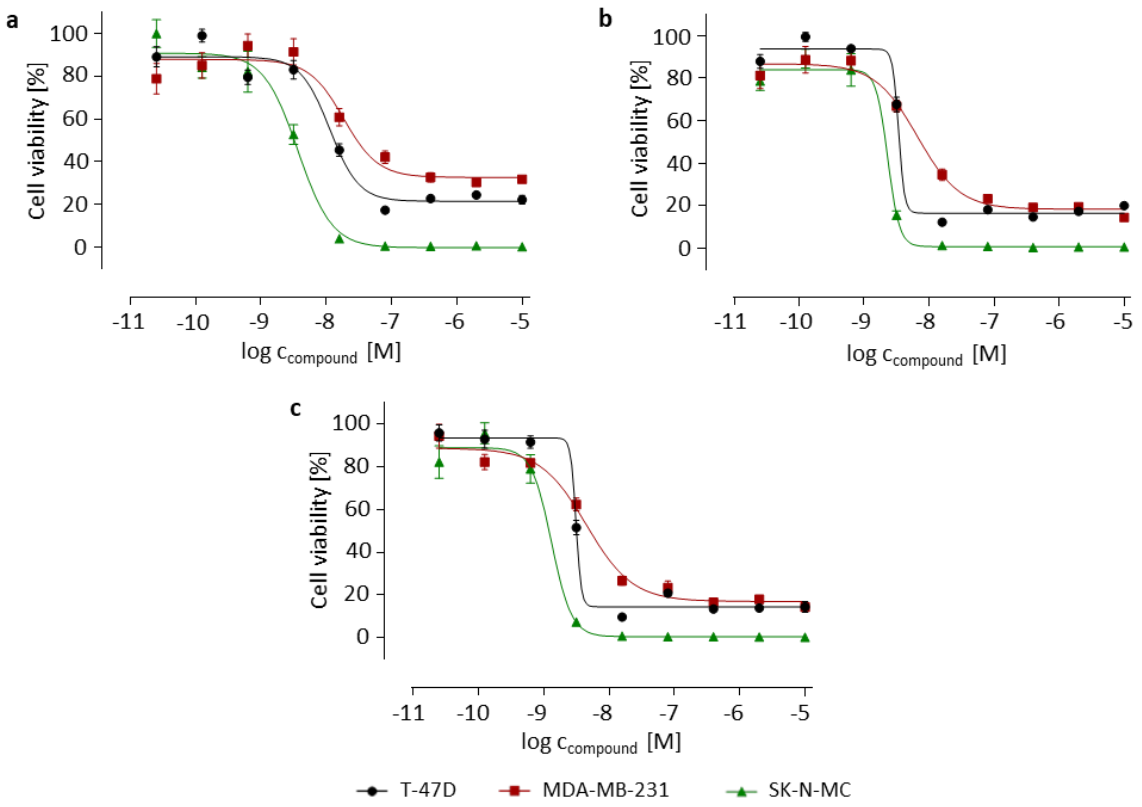

Figure A 144 *In vitro* antitumor activity of toxin **34** after a) 6, b) 24 and c) 72 h to cells expressing high (T-47D), moderate (MDA-MB-231) and low (SK-N-MC) level of SSTR2.

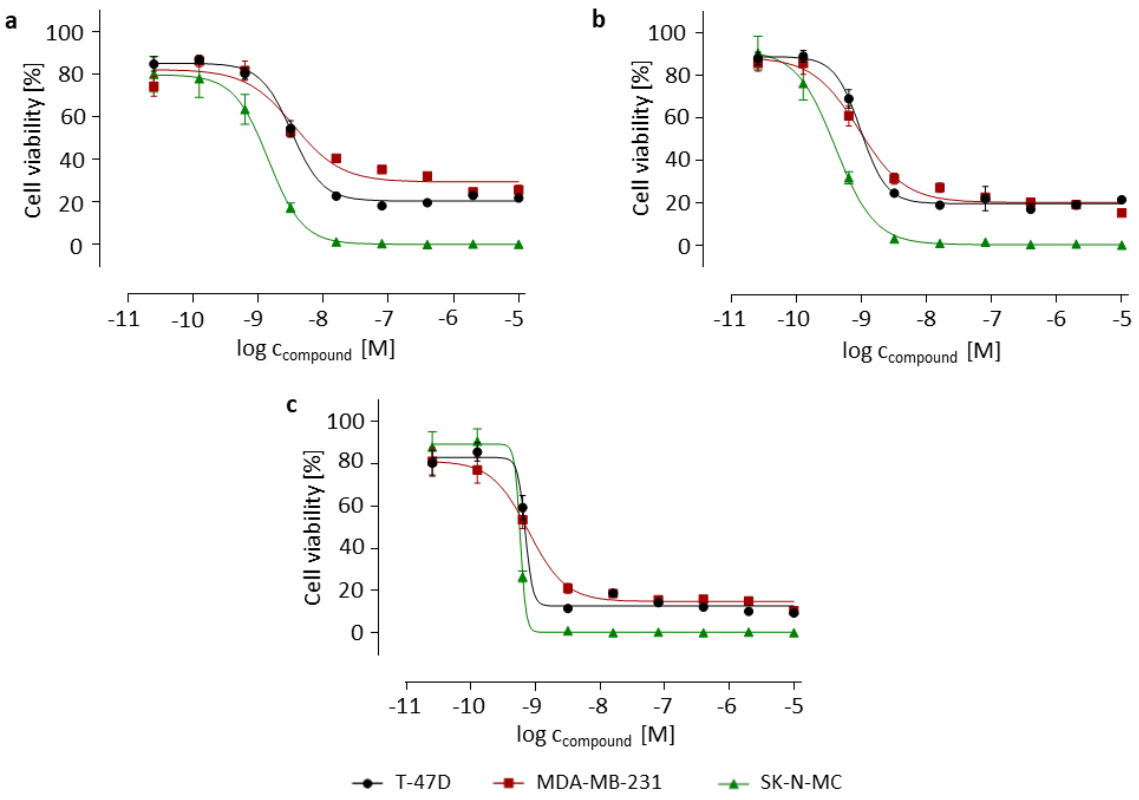

Figure A 145 *In vitro* antitumor activity of toxin **36** after a) 6, b) 24 and c) 72 h to cells expressing high (T-47D), moderate (MDA-MB-231) and low (SK-N-MC) level of SSTR2.

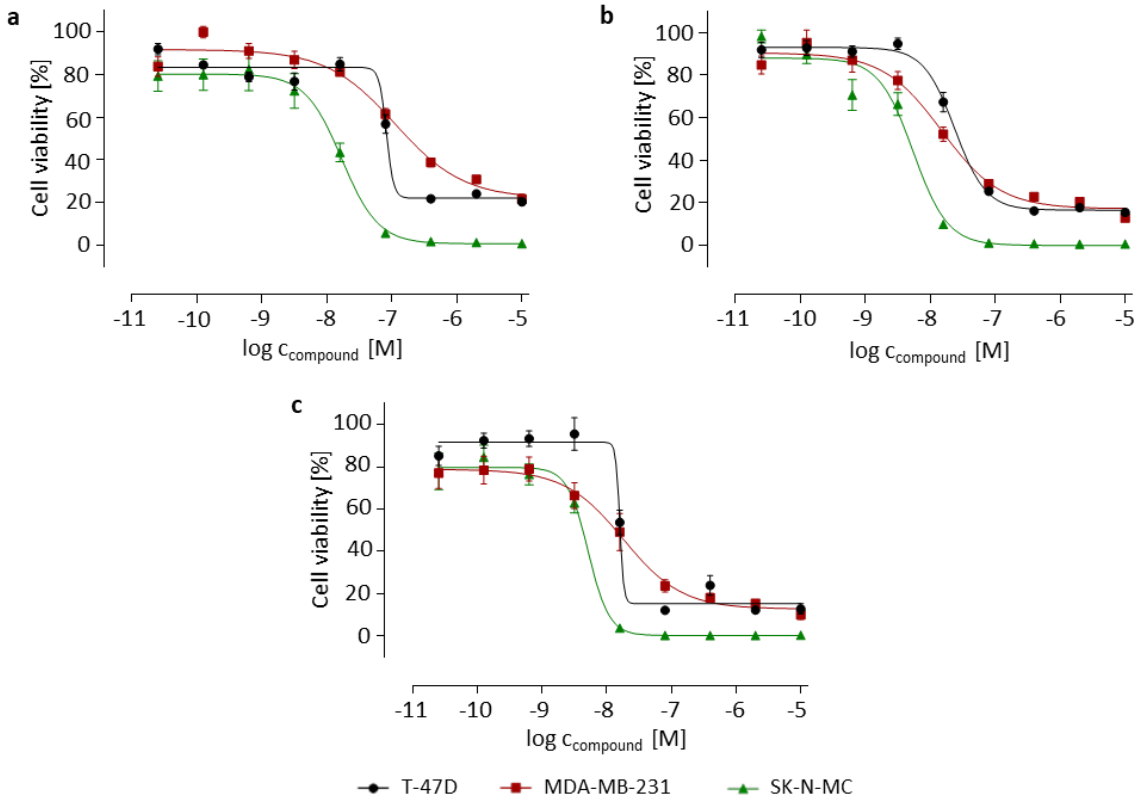

Figure A 146 *In vitro* antitumor activity of toxin **37** after a) 6, b) 24 and c) 72 h to cells expressing high (T-47D), moderate (MDA-MB-231) and low (SK-N-MC) level of SSTR2.

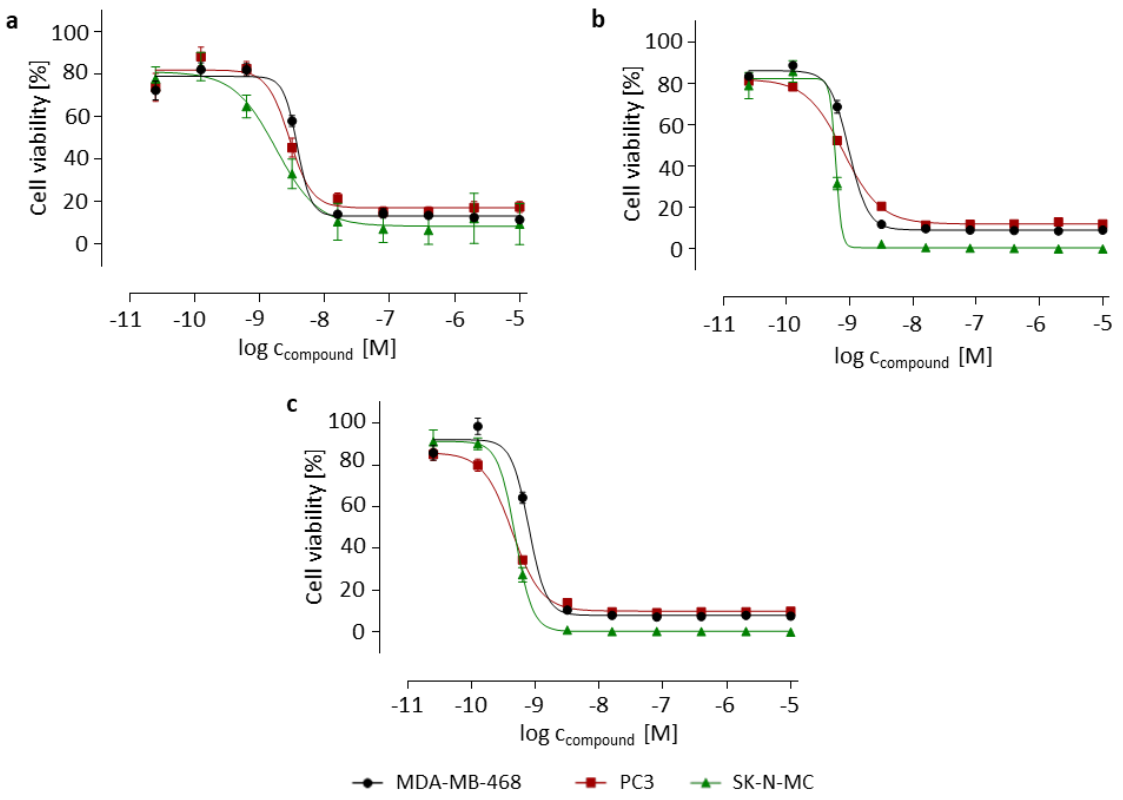

Figure A 147 *In vitro* antitumor activity of toxin **33** after a) 6, b) 24 and c) 72 h to cells expressing high (MDA-MB-468), moderate (PC3) and low (SK-N-MC) level of CD13.

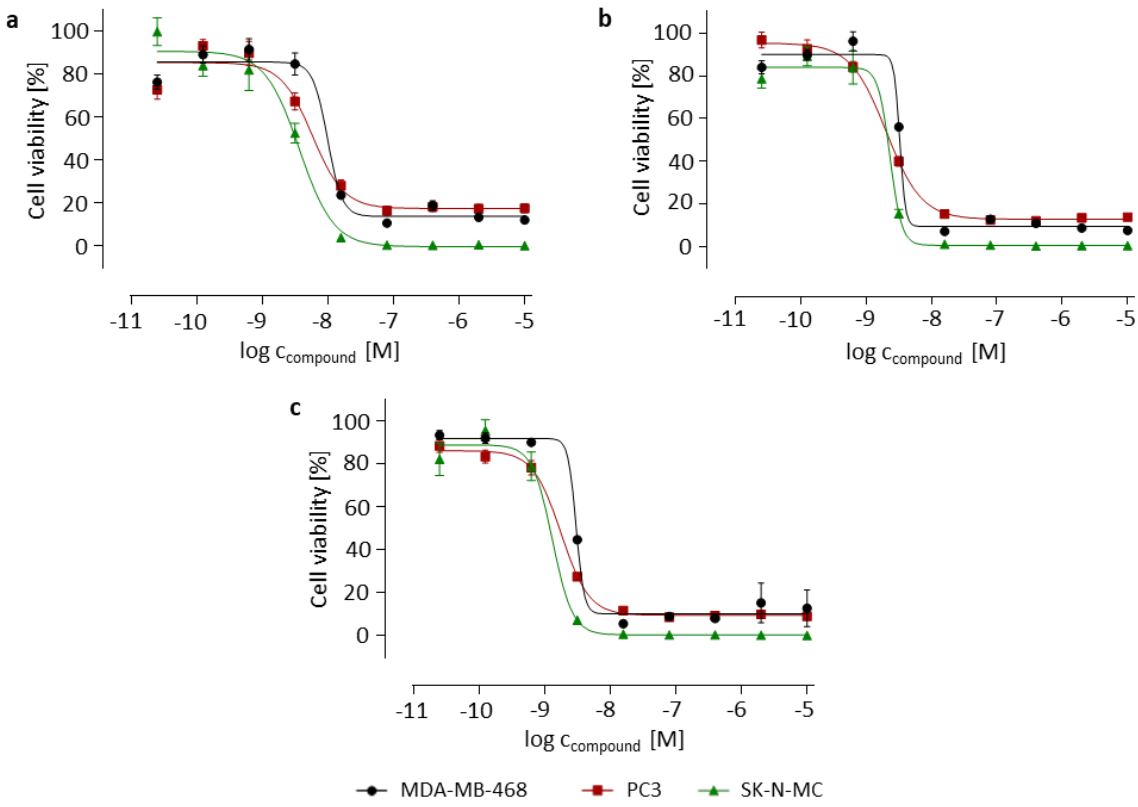

Figure A 148 *In vitro* antitumor activity of toxin **34** after a) 6, b) 24 and c) 72 h to cells expressing high (MDA-MB-468), moderate (PC3) and low (SK-N-MC) level of CD13.

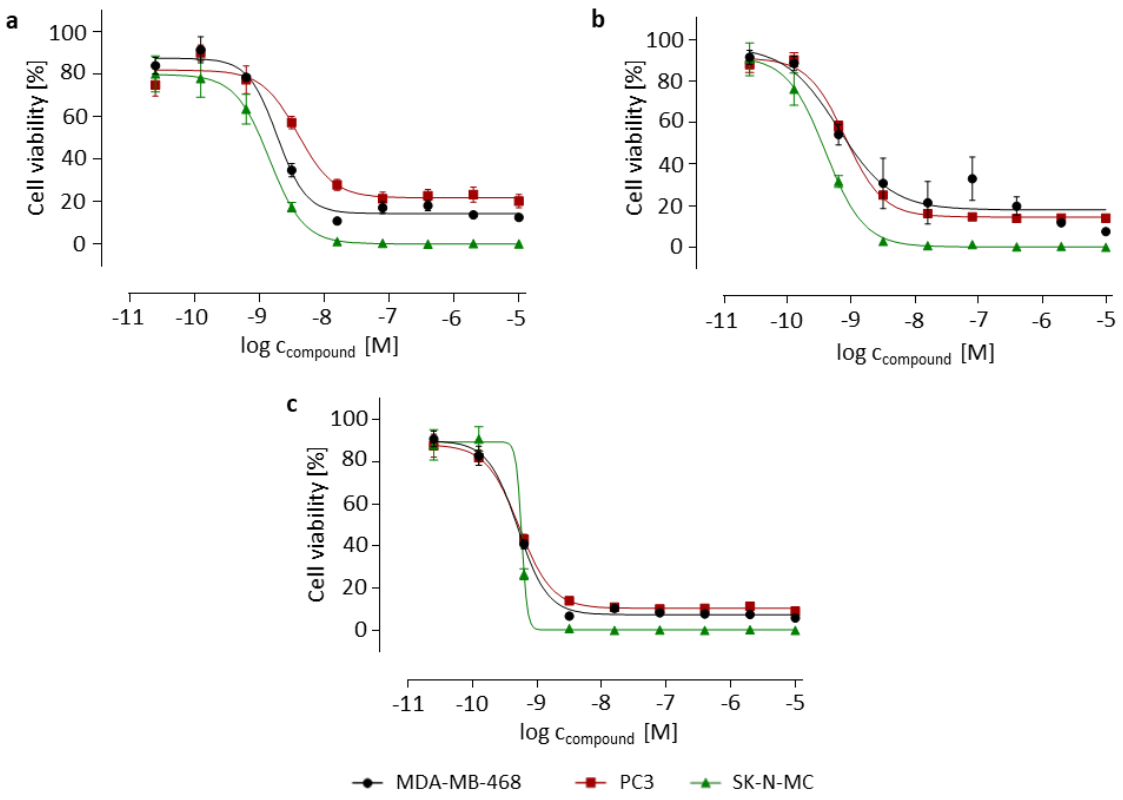

Figure A 149 *In vitro* antitumor activity of toxin **36** after a) 6, b) 24 and c) 72 h to cells expressing high (MDA-MB-468), moderate (PC3) and low (SK-N-MC) level of CD13.

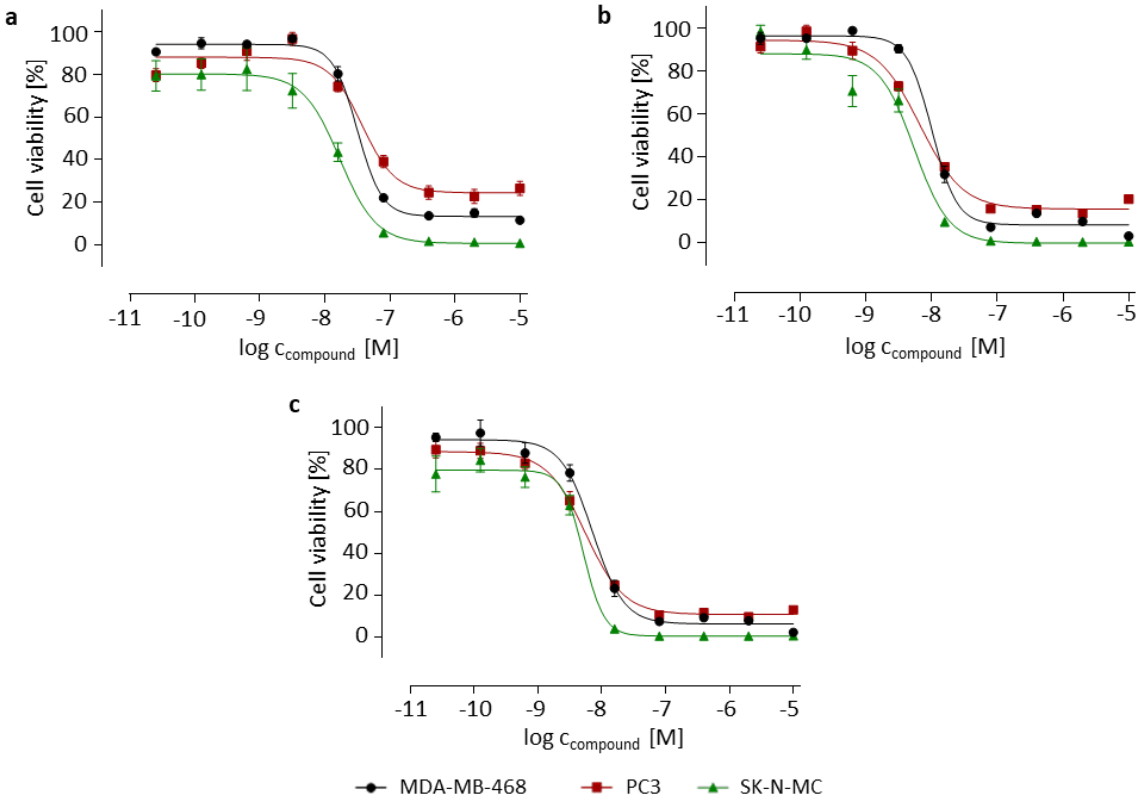

Figure A 150 *In vitro* antitumor activity of toxin **37** after a) 6, b) 24 and c) 72 h to cells expressing high (MDA-MB-468), moderate (PC3) and low (SK-N-MC) level of CD13.

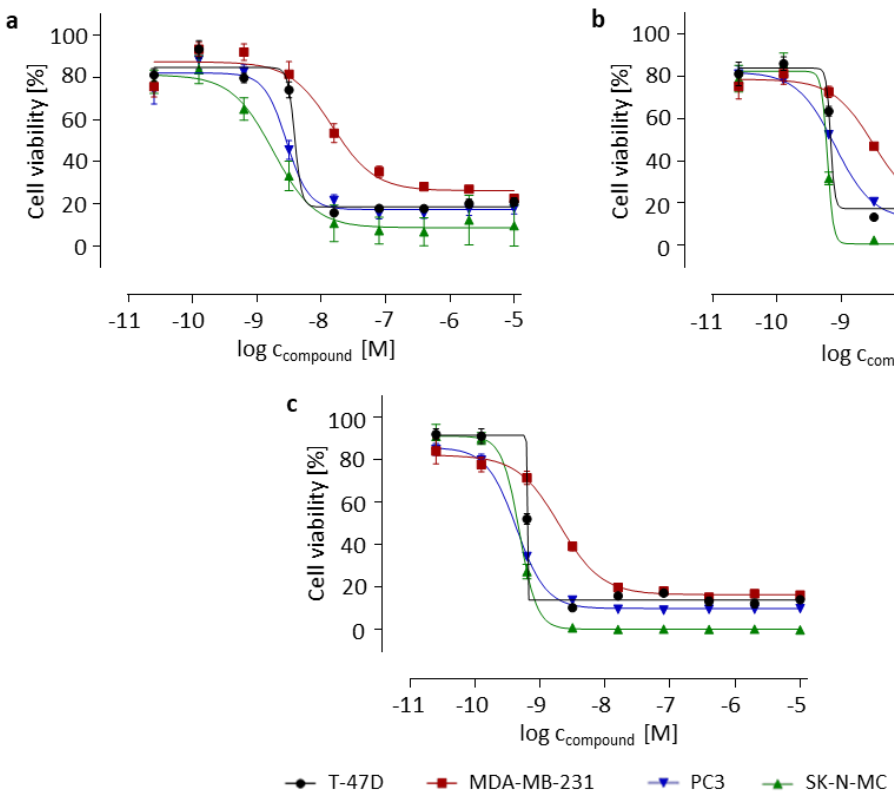

Figure A 151 *In vitro* antitumor activity of toxin **33** after a) 6, b) 24 and c) 72 h to cells expressing high (T-47D), moderate (MDA-MB-231) and low (PC3, SK-N-MC) level of GRPR.

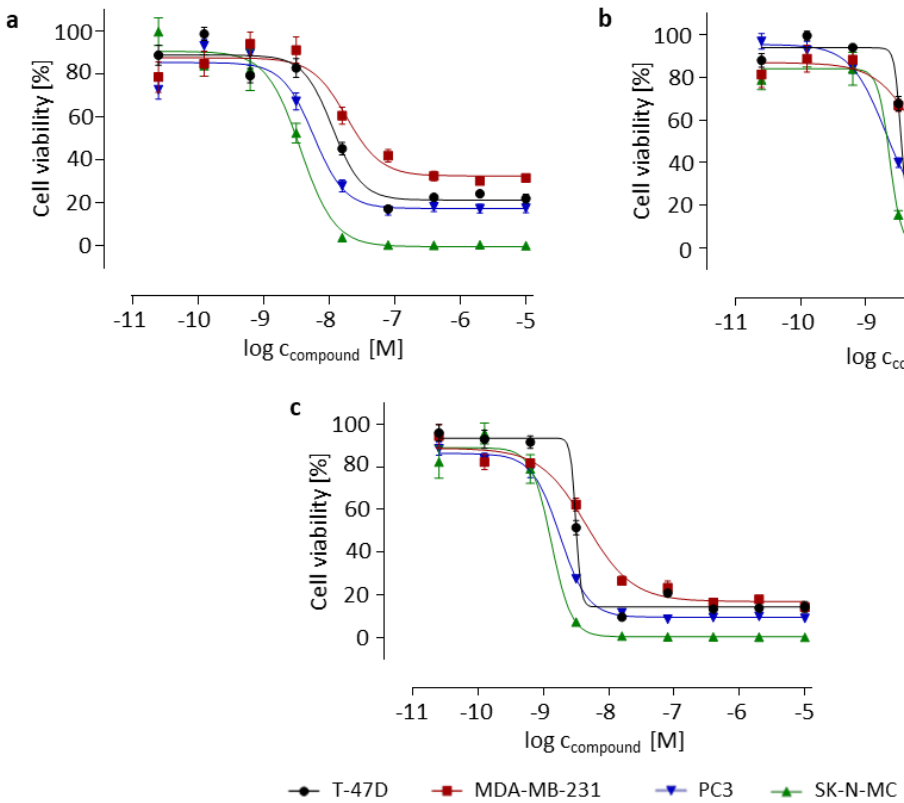

Figure A 152 *In vitro* antitumor activity of toxin **34** after a) 6, b) 24 and c) 72 h to cells expressing high (T-47D), moderate (MDA-MB-231) and low (PC3, SK-N-MC) level of GRPR.

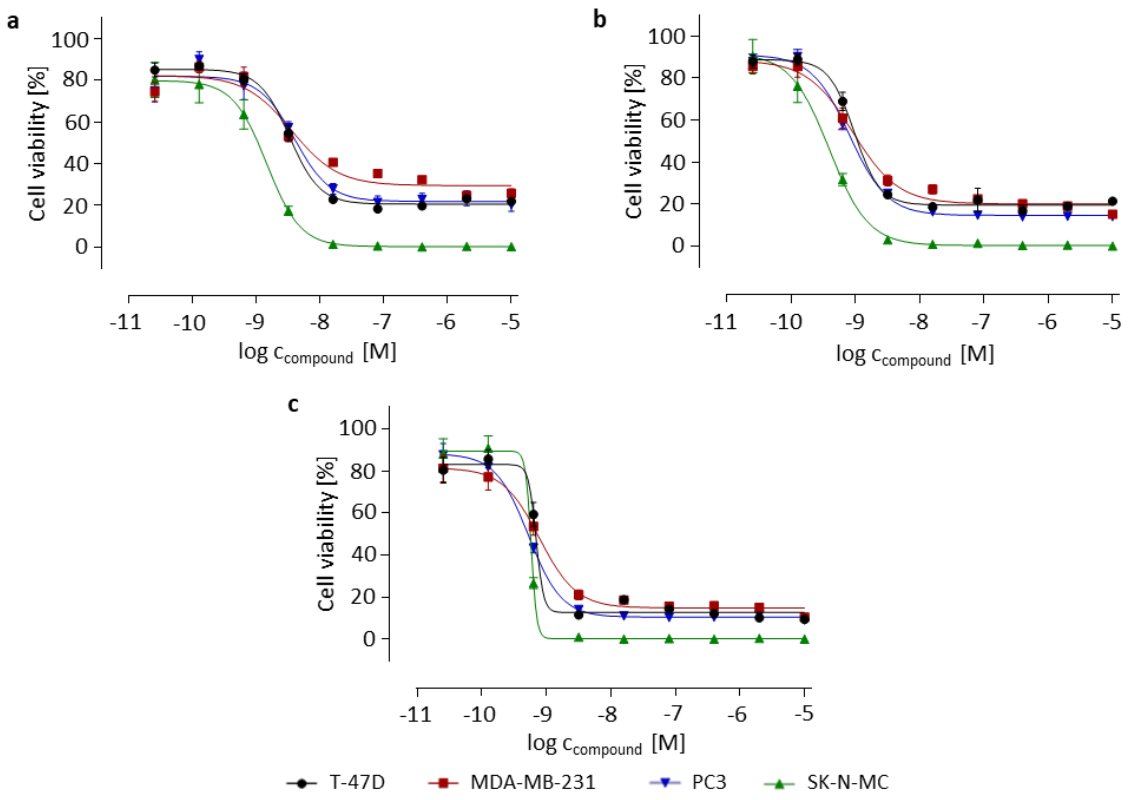

Figure A 153 *In vitro* antitumor activity of toxin **36** after a) 6, b) 24 and c) 72 h to cells expressing high (T-47D), moderate (MDA-MB-231) and low (PC3, SK-N-MC) level of GRPR.

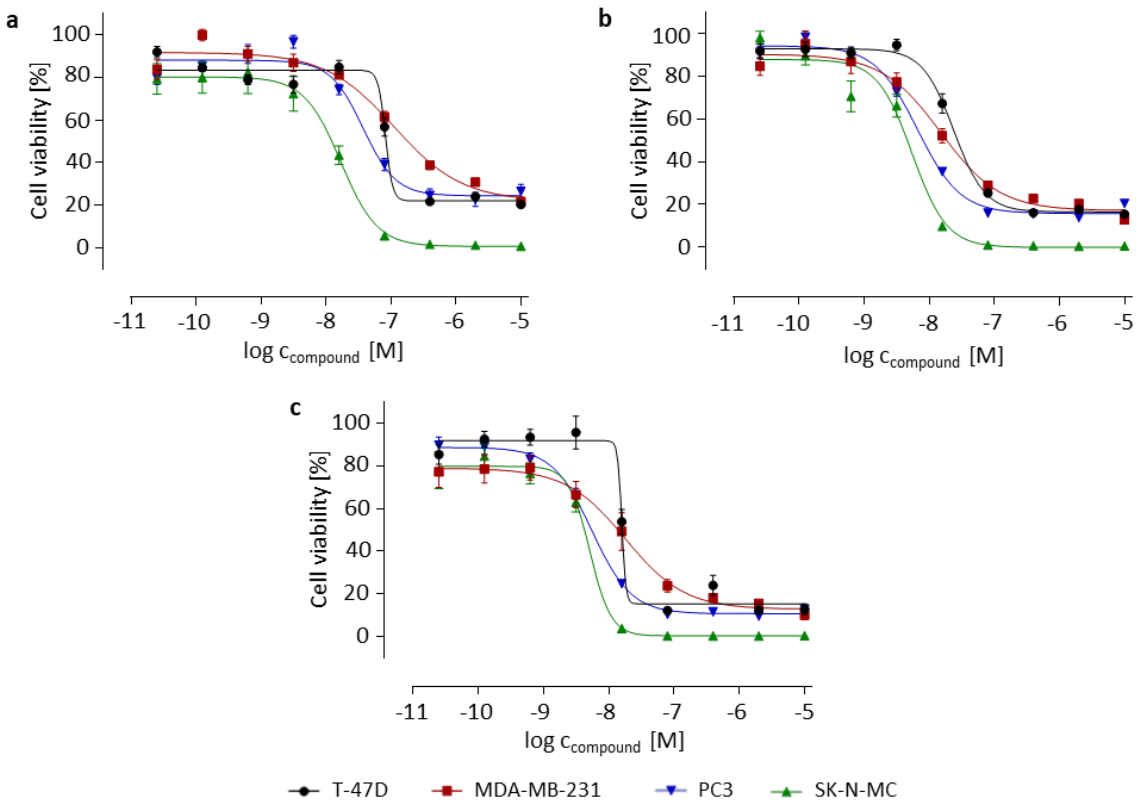

Figure A 154 *In vitro* antitumor activity of toxin **37** after a) 6, b) 24 and c) 72 h to cells expressing high (T-47D), moderate (MDA-MB-231) and low (PC3, SK-N-MC) level of GRPR.

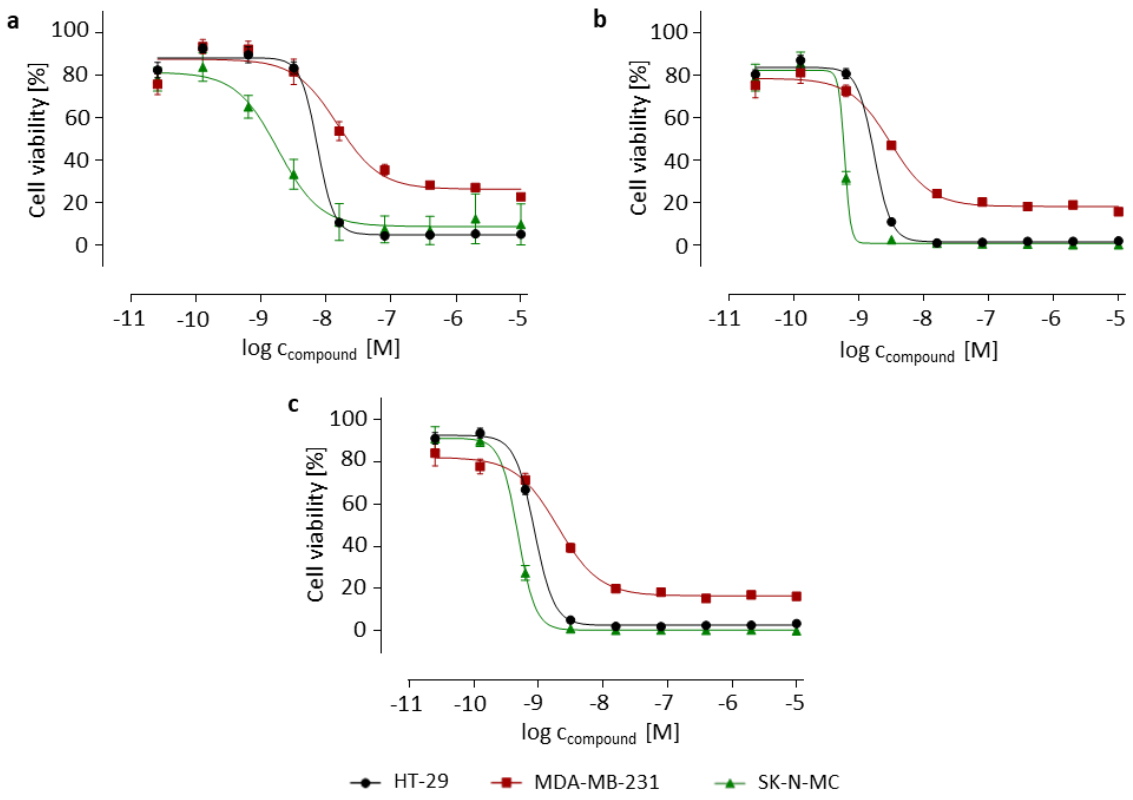

Figure A 155 *In vitro* antitumor activity of toxin **33** after a) 6, b) 24 and c) 72 h to cells expressing high (HT-29), moderate (MDA-MB-231) and low (SK-N-MC) level of CXCR4.

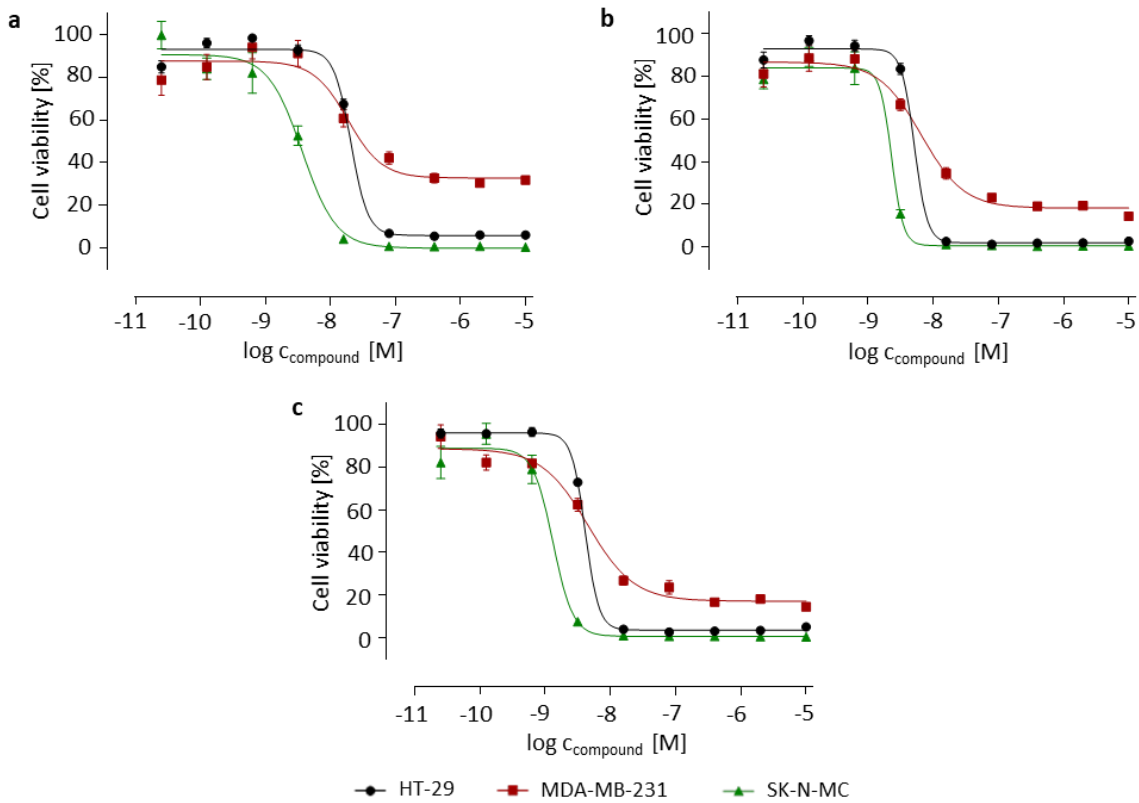

Figure A 156 *In vitro* antitumor activity of toxin **34** after a) 6, b) 24 and c) 72 h to cells expressing high (HT-29), moderate (MDA-MB-231) and low (SK-N-MC) level of CXCR4.

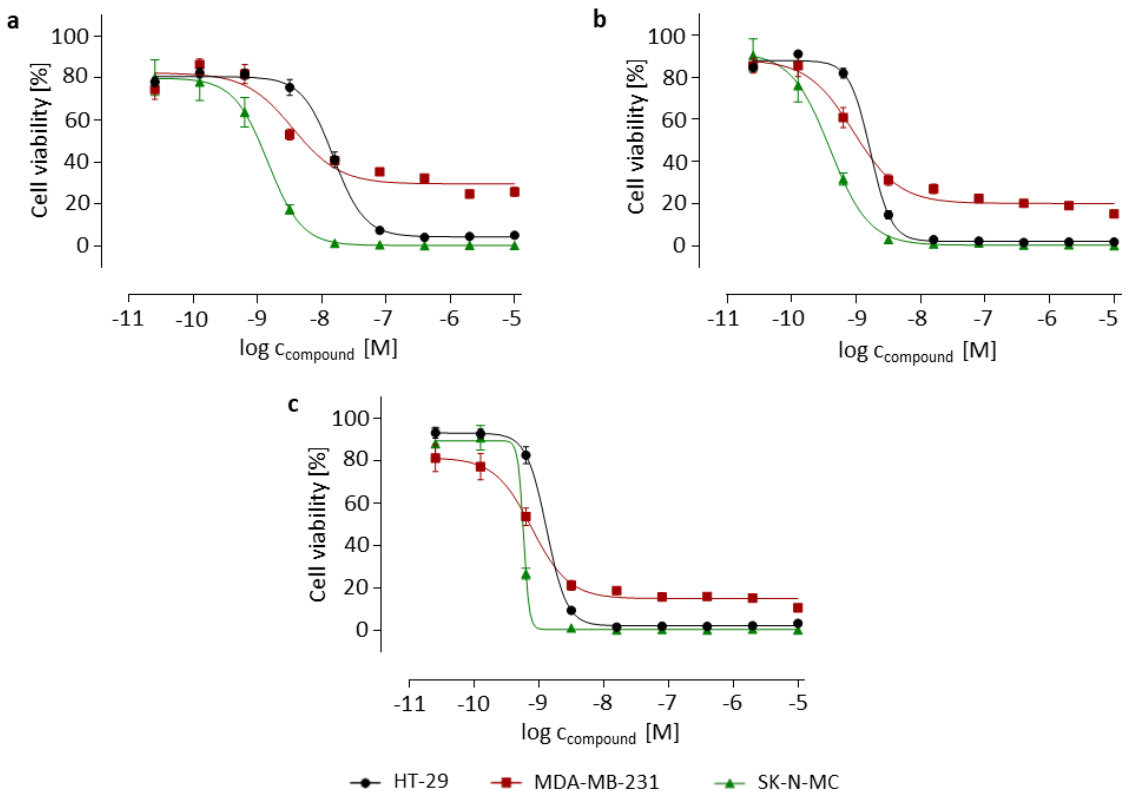

Figure A 157 *In vitro* antitumor activity of toxin **36** after a) 6, b) 24 and c) 72 h to cells expressing high (HT-29), moderate (MDA-MB-231) and low (SK-N-MC) level of CXCR4.

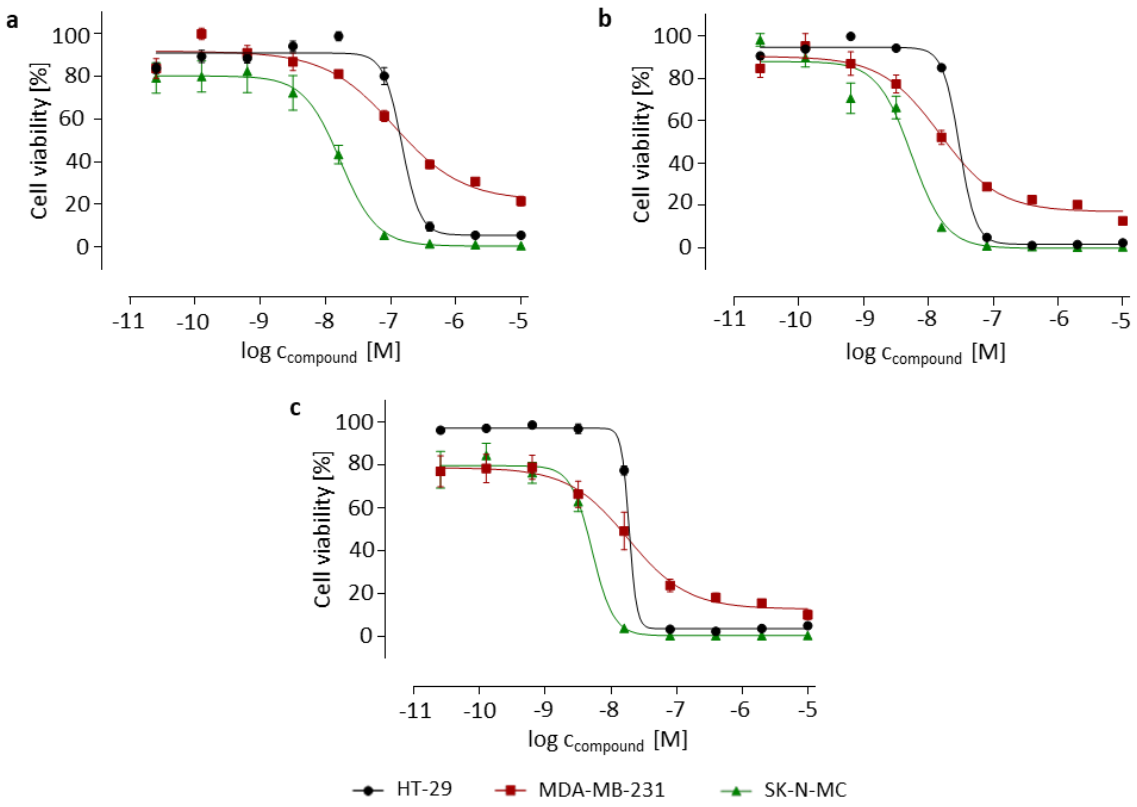

Figure A 158 *In vitro* antitumor activity of toxin **37** after a) 6, b) 24 and c) 72 h to cells expressing high (HT-29), moderate (MDA-MB-231) and low (SK-N-MC) level of CXCR4.

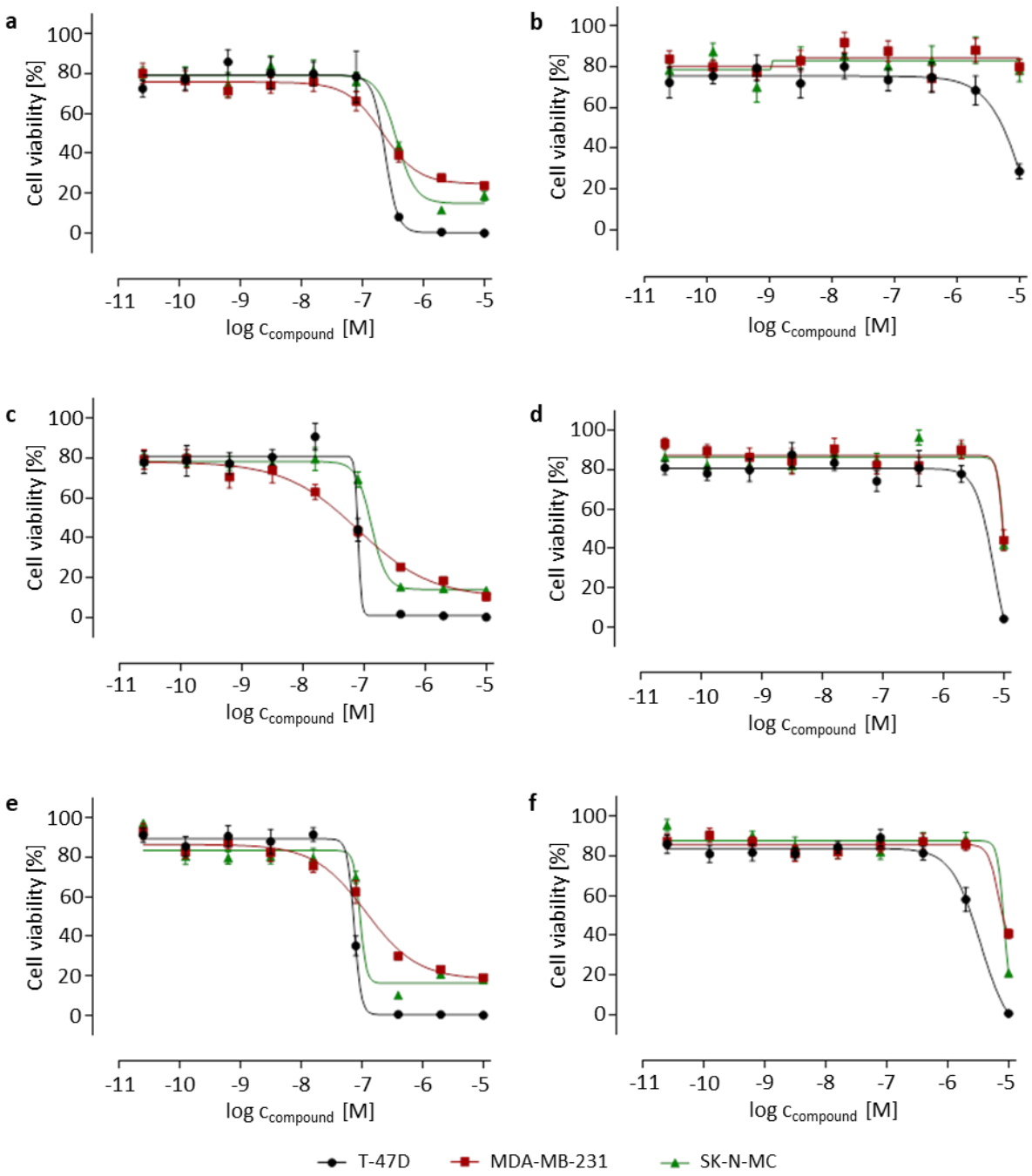

Figure A 159 *In vitro* antitumor activity of **49** after a) 6, c) 24, e) 72 h initial treatment and of **50** after b) 6, d) 24 and f) 72 h initial treatment in T-47D breast cancer cells (high SSTR2), MDA-MB-231 breast cancer cells (medium SSTR2) and SK-N-MC Ewing's sarcoma cells (low SSTR2).

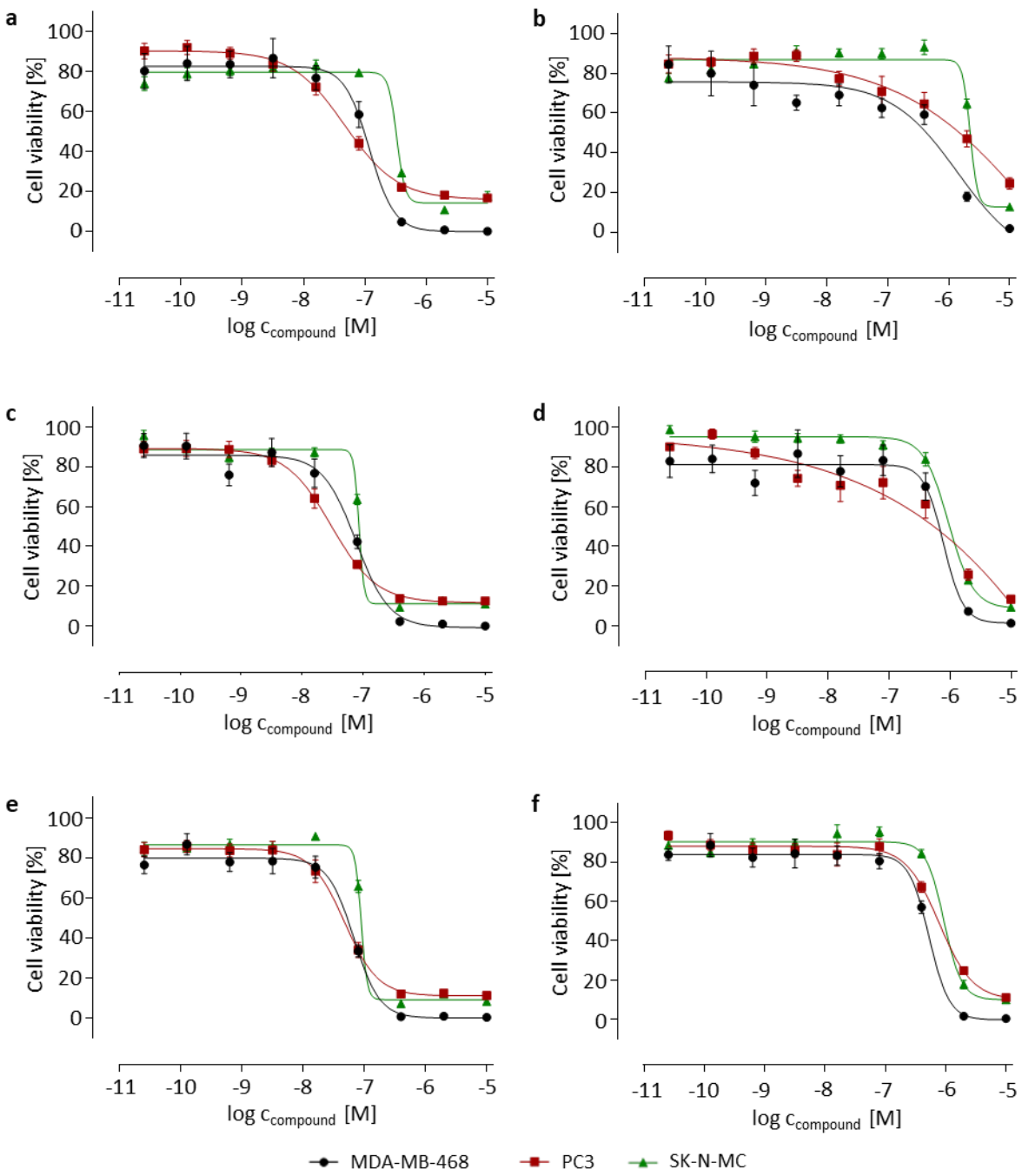

Figure A 160 *In vitro* antitumor activity of **52** after a) 6, c) 24, e) 72 h initial treatment and of **53** after b) 6, d) 24 and f) 72 h initial treatment in MDA-MB-468 breast cancer cells (high CD13), PC3 prostate cancer cells (medium CD13) and SK-N-MC Ewing's sarcoma cells (low CD13).

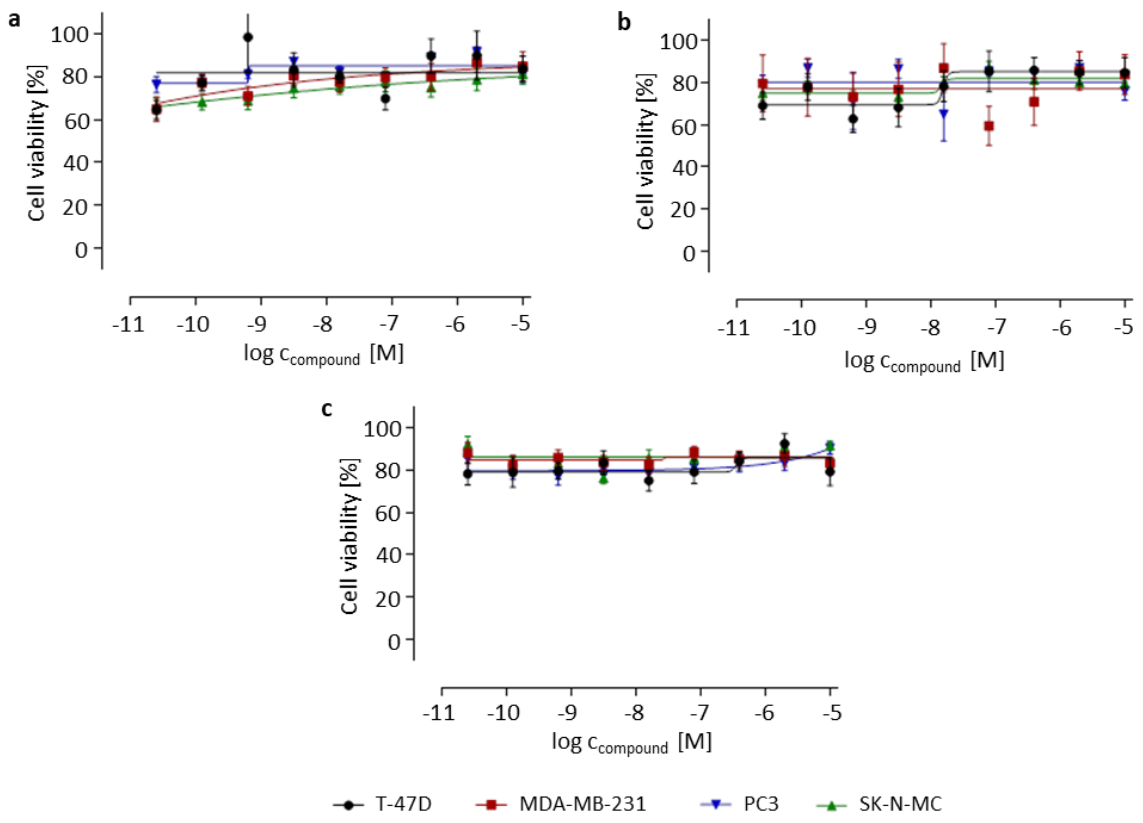

Figure A 161 *In vitro* antitumor activity of PDC **69** after a) 6, b) 24 and c) 72 h to cells expressing high (T-47D), moderate (MDA-MB-231) and low (PC3, SK-N-MC) level of GRPR.

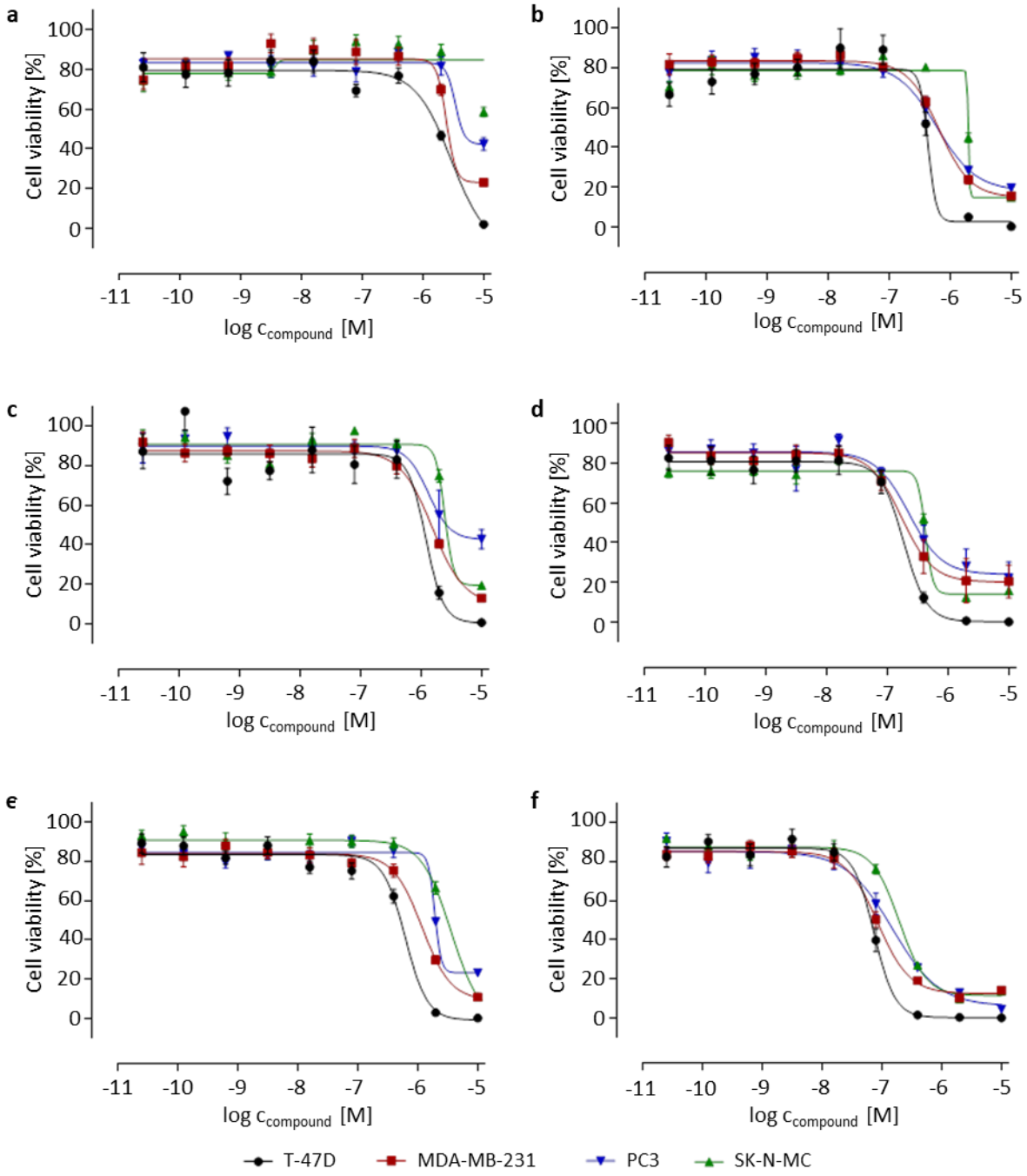

Figure A 162 *In vitro* antitumor activity of **70** after a) 6, c) 24, e) 72 h initial treatment and of **71** after b) 6, d) 24 and f) 72 h initial treatment in T-47D breast cancer cells (high GRPR), MDA-MB-231 breast cancer cells (medium GRPR), PC3 prostate cancer cells and SK-N-MC Ewing's sarcoma cells (low GRPR).

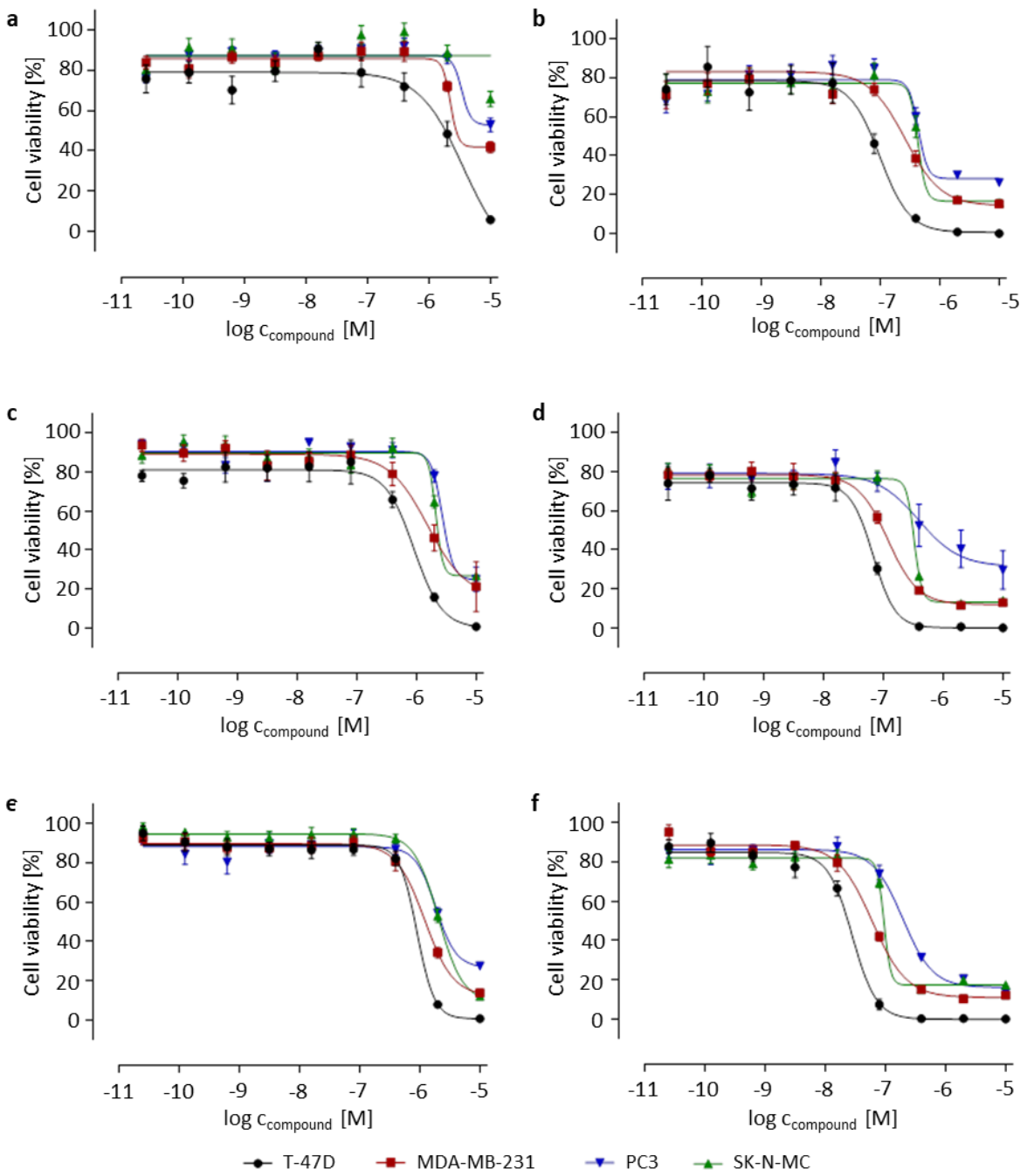

Figure A 163 *In vitro* antitumor activity of **72** after a) 6, c) 24, e) 72 h initial treatment and of **73** after b) 6, d) 24 and f) 72 h initial treatment in T-47D breast cancer cells (high GRPR), MDA-MB-231 breast cancer cells (medium GRPR), PC3 prostate cancer cells and SK-N-MC Ewing's sarcoma cells (low GRPR).

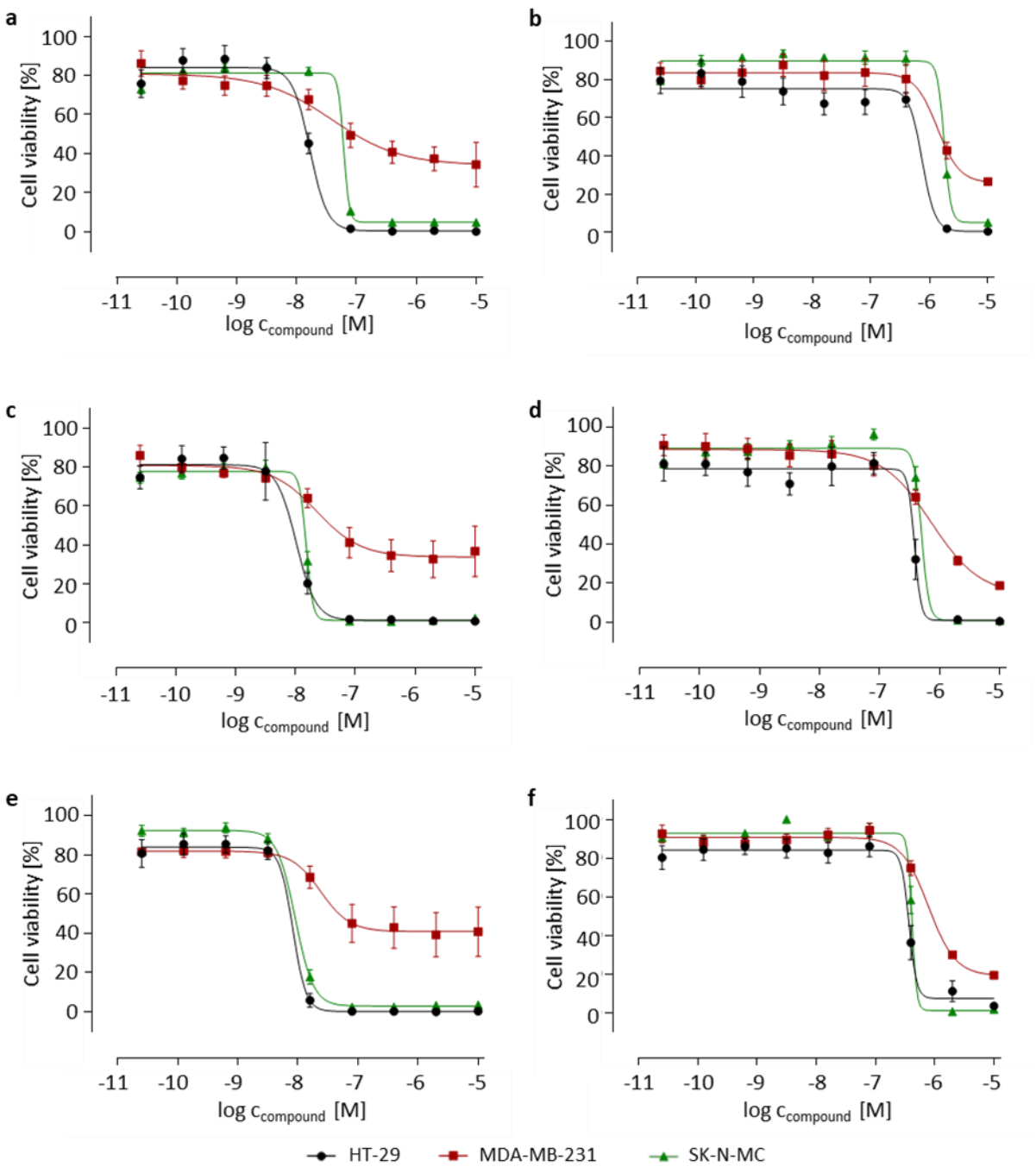

Figure A 164 *In vitro* antitumor activity of **86** after a) 6, c) 24, e) 72 h initial treatment and of **87** after b) 6, d) 24 and f) 72 h initial treatment in HT-29 colon cancer cells (high CXCR4), MDA-MB-231 breast cancer cells (medium CXCR4) and SK-N-MC Ewing's sarcoma cells (low CXCR4).

Table A 1 *In vitro* IC_{50} values of toxin **33** on several cancer cell lines: T-47D (breast), HT-29 (colon), MDA-MB-468 (breast), MDA-MB-231 (breast), SK-N-MC (Ewing's sarcoma) and PC3 (prostate) (resazurin assay).

	IC_{50} [nM]		
	6 h	24 h	72 h
T-47D	3.87 ± 1.4	0.67 ± 0.1	0.63 ± 0.1
HT-29	7.31 ± 1.1	1.71 ± 0.1	0.87 ± 0.1
MDA-MB-468	3.80 ± 1.3	0.97 ± 0.1	0.79 ± 0.2
MDA-MB-231	14.84 ± 2.4	3.03 ± 0.2	1.99 ± 0.2
PC3	2.89 ± 1.8	0.79 ± 0.1	0.43 ± 0.1
SK-N-MC	1.80 ± 0.5	0.60 ± 0.1	0.48 ± 0.1

Table A 2 *In vitro* IC_{50} values of toxin **34** on several cancer cell lines: T-47D (breast), HT-29 (colon), MDA-MB-468 (breast), MDA-MB-231 (breast), SK-N-MC (Ewing's sarcoma) and PC3 (prostate) (resazurin assay).

	IC_{50} [nM]		
	6 h	24 h	72 h
T-47D	3.28 ± 1.4	0.96 ± 0.1	0.69 ± 0.2
HT-29	15.09 ± 1.2	1.65 ± 0.6	1.32 ± 0.1
MDA-MB-468	1.89 ± 1.4	0.62 ± 0.3	0.50 ± 0.1
MDA-MB-231	3.54 ± 1.7	0.91 ± 0.1	0.78 ± 0.1
PC3	3.94 ± 0.5	0.81 ± 0.1	0.53 ± 0.1
SK-N-MC	1.44 ± 0.4	0.39 ± 0.2	0.58 ± 0.1

Table A 3 *In vitro* IC_{50} values of toxin **36** on several cancer cell lines: T-47D (breast), HT-29 (colon), MDA-MB-468 (breast), MDA-MB-231 (breast), SK-N-MC (Ewing's sarcoma) and PC3 (prostate) (resazurin assay).

	IC_{50} [nM]		
	6 h	24 h	72 h
T-47D	11.31 ± 1.8	3.39 ± 1.2	3.13 ± 1.3
HT-29	20.59 ± 1.2	5.18 ± 1.0	4.12 ± 0.6
MDA-MB-468	9.91 ± 1.7	3.26 ± 1.2	3.03 ± 2.0
MDA-MB-231	18.44 ± 2.8	6.62 ± 1.9	4.50 ± 1.6
PC3	5.82 ± 1.9	2.02 ± 1.0	1.78 ± 0.9
SK-N-MC	3.68 ± 2.3	2.31 ± 1.5	1.32 ± 1.7

Table A 4 *In vitro* IC_{50} values of toxin **37** on several cancer cell lines: T-47D (breast), HT-29 (colon), MDA-MB-468 (breast), MDA-MB-231 (breast), SK-N-MC (Ewing's sarcoma) and PC3 (prostate) (resazurin assay).

	IC_{50} [nM]		
	6 h	24 h	72 h
T-47D	82.14 ± 2.0	23.79 ± 1.6	15.87 ± 2.4
HT-29	148.30 ± 1.9	29.95 ± 0.8	18.86 ± 0.8
MDA-MB-468	31.65 ± 1.2	10.16 ± 1.1	7.16 ± 1.8
MDA-MB-231	112.10 ± 3.7	14.99 ± 2.5	18.04 ± 3.7
PC3	37.27 ± 2.1	6.64 ± 1.3	5.54 ± 1.4
SK-N-MC	16.90 ± 3.2	5.46 ± 2.0	5.16 ± 2.0

Table A 5 *In vitro* IC_{50} values of PDC **49** on SSTR2 high (T-47D, breast), medium (MDA-MB-231, breast) and low (SK-N-MC, Ewing's sarcoma) expressing cancer cell lines (resazurin assay).

	IC_{50} [nM]		
	6 h	24 h	72 h
T-47D	237.4 ± 4.2	80.1 ± 3.2	75.0 ± 2.3
MDA-MB-231	215.0 ± 3.3	79.5 ± 4.9	116.2 ± 3.3
SK-N-MC	363.5 ± 3.3	132.2 ± 2.3	93.5 ± 2.5

Table A 6 *In vitro* IC_{50} values of PDC **50** on SSTR2 high (T-47D, breast), medium (MDA-MB-231, breast) and low (SK-N-MC, Ewing's sarcoma) expressing cancer cell lines (resazurin assay).

	IC_{50} [nM]		
	6 h	24 h	72 h
T-47D	> 10000	6889.0 ± 72.7	3431.0 ± 36.3
MDA-MB-231	> 10000	9672.0 ± 35.0	6731.0 ± 15.1
SK-N-MC	> 10000	> 10000	8379.0 ± 90.0

Table A 7 *In vitro* IC_{50} values of PDC **52** on CD13 high (MDA-MB-468, breast), medium (PC3, prostate) and low (SK-N-MC, Ewing's sarcoma) expressing cancer cell lines (resazurin assay).

	IC_{50} [nM]		
	6 h	24 h	72 h
MDA-MB-468	118.3 ± 4.6	76.1 ± 3.5	67.3 ± 2.6
PC3	46.8 ± 2.3	28.8 ± 2.0	47.6 ± 2.0
SK-N-MC	330.0 ± 1.8	85.1 ± 1.5	88.7 ± 1.6

Table A 8 *In vitro* IC_{50} values of PDC **53** on CD13 high (MDA-MB-468, breast), medium (PC3, prostate) and low (SK-N-MC, Ewing's sarcoma) expressing cancer cell lines (resazurin assay).

	IC_{50} [nM]		
	6 h	24 h	72 h
MDA-MB-468	1400.0 ± 27.6	785.1 ± 7.4	531.0 ± 4.3
PC3	6309.6 ± 24.7	891.3 ± 26.7	780.6 ± 4.2
SK-N-MC	2245.0 ± 17.5	943.5 ± 2.4	934.7 ± 2.8

Table A 9 *In vitro* IC_{50} values of PDC **69** on GRPR high (T-47D, breast), medium (MDA-MB-231, breast) and low (PC3, prostate, SK-N-MC, Ewing's sarcoma) expressing cancer cell lines (resazurin assay).

	IC_{50} [nM]		
	6 h	24 h	72 h
T-47D	> 10000	> 10000	> 10000
MDA-MB-231	> 10000	> 10000	> 10000
PC3	> 10000	> 10000	> 10000
SK-N-MC	> 10000	> 10000	> 10000

Table A 10 *In vitro* IC_{50} values of PDC **70** on GRPR high (T-47D, breast), medium (MDA-MB-231, breast) and low (PC3, prostate, SK-N-MC, Ewing's sarcoma) expressing cancer cell lines (resazurin assay).

	IC_{50} [nM]		
	6 h	24 h	72 h
T-47D	2914.0 ± 24.3	1200.0 ± 8.4	620.3 ± 3.9
MDA-MB-231	2434.0 ± 46.5	1540.0 ± 5.3	1177.0 ± 4.5
PC3	3410.0 ± 23.6	1315.0 ± 6.3	1925.0 ± 4.0
SK-N-MC	> 10000	2464.0 ± 44.7	3595.0 ± 33.9

Table A 11 *In vitro* IC_{50} values of PDC **71** on GRPR high (T-47D, breast), medium (MDA-MB-231, breast) and low (PC3, prostate, SK-N-MC, Ewing's sarcoma) expressing cancer cell lines (resazurin assay).

	IC_{50} [nM]		
	6 h	24 h	72 h
T-47D	435.6 ± 5.9	186.0 ± 3.9	74.0 ± 2.6
MDA-MB-231	656.0 ± 3.4	172.0 ± 4.9	85.2 ± 2.2
PC3	601.8 ± 5.0	225.7 ± 5.1	150.6 ± 3.9
SK-N-MC	1990.0 ± 13.4	423.7 ± 2.7	195.9 ± 1.9

Table A 12 *In vitro* IC_{50} values of PDC **72** on GRPR high (T-47D, breast), medium (MDA-MB-231, breast) and low (PC3, prostate, SK-N-MC, Ewing's sarcoma) expressing cancer cell lines (resazurin assay).

	IC_{50} [nM]		
	6 h	24 h	72 h
T-47D	3620.0 ± 46.4	908.4 ± 6.9	901.0 ± 3.6
MDA-MB-231	2235.0 ± 19.1	1548.0 ± 12.4	1208.0 ± 3.9
PC3	3413.0 ± 18.9	2712.0 ± 85.7	1844.0 ± 5.5
SK-N-MC	> 10000	2107.0 ± 10.3	2039.0 ± 4.6

Table A 13 *In vitro* IC_{50} values of PDC **73** on GRPR high (T-47D, breast), medium (MDA-MB-231, breast) and low (PC3, prostate, SK-N-MC, Ewing's sarcoma) expressing cancer cell lines (resazurin assay).

	IC_{50} [nM]		
	6 h	24 h	72 h
T-47D	98.7 ± 5.0	67.7 ± 2.9	28.3 ± 2.0
MDA-MB-231	262.0 ± 11.4	119.4 ± 2.6	60.4 ± 1.8
PC3	438.1 ± 4.5	390.3 ± 8.0	194.3 ± 2.6
SK-N-MC	431.8 ± 4.6	328.9 ± 2.1	94.8 ± 2.0

Table A 14 *In vitro* IC_{50} values of PDC **86** on CXCR4 high (HT-29, colon), medium (MDA-MB-231, breast) and low (SK-N-MC, Ewing's sarcoma) expressing cancer cell lines (resazurin assay).

	IC_{50} [nM]		
	6 h	24 h	72 h
HT-29	16.6 ± 2.6	10.2 ± 2.9	8.3 ± 2.5
MDA-MB-231	38.7 ± 6.2	22.5 ± 4.6	23.9 ± 4.6
SK-N-MC	60.9 ± 1.1	15.1 ± 1.3	9.0 ± 1.0

Table A 15 *In vitro* IC_{50} values of PDC **87** on CXCR4 high (HT-29, colon), medium (MDA-MB-231, breast) and low (SK-N-MC, Ewing's sarcoma) expressing cancer cell lines (resazurin assay).

	IC_{50} [nM]		
	6 h	24 h	72 h
HT-29	751.1 ± 5.8	379.0 ± 5.1	369.7 ± 4.0
MDA-MB-231	1650.0 ± 6.2	721.9 ± 8.8	787.2 ± 3.6
SK-N-MC	1785.0 ± 2.7	498.7 ± 3.3	416.0 ± 2.5

Curriculum vitae

Personal details

Name:	Paul Jänicke
Date of birth:	25.12.1991
Place of birth:	Merseburg
Nationality:	German

Education

07/2016–10/2020	Ph.D. study at Leibniz Institute of Plant Biochemistry in Halle (Saale)
10/2013–05/2016	Masters study in Chemistry (M.Sc.) at Martin Luther University Halle-Wittenberg Majoring in Organic Chemistry Final grade: 1.5 Master thesis with Prof. Dr. Ludger A. Wessjohann: „Mesoporous silica nanoparticles grafted with plant natural products and extracts“, Grade: 1.0
10/2010–09/2013	Bachelors study in Chemistry (B.Sc.) at Martin Luther University Halle-Wittenberg Final grade: 1.8 Bachelor thesis with Prof. Dr. Jörg Kreßler: „Einsatz der dynamischen Lichtstreuung zur Untersuchung anisotroper Nanopartikel“, Grade: 1.0
09/2007–06/2010	Domgymnasium Merseburg, Abitur, Grade: 1.0

Work experiences

10/2019−11/2019	Project in collaboration with Centro Inmunologia Molecular in Havana/Cuba with Tania Carmenate
05/2016−06/2016	Student assistant at the Leibniz Institute of Plant Biochemistry in Halle (Saale) in the department of Bioorganic Chemistry with Prof. Dr. Ludger A. Wessjohann
02/2015–07/2015	Practical internship at Stockholm University in Sweden in the department of Organic Chemistry with Prof. Dr. Göran Widmalm
04/2012–04/2013	Student assistant at Martin Luther University Halle-Wittenberg in the department of Physical Chemistry with Prof. Dr. Jörg Kreßler

Honors

06/2010	GDCh-Preis
04/2012–09/2013	Deutschlandstipendium
01/2014–09/2015	Jacob-Volhard-Stipendium
01/2017−12/2019	Promotionsstipendium der Konrad-Adenauer-Stiftung

Presentations

14. Mitteldeutsches Anorganiker Nachwuchs Symposium MANS-14, P. Jänicke, L. A. Wessjohann, G. N. Kaluđerović,: *Mesoporous silica nanoparticles grafted with emodin*, 15.09.2016, Halle/Saale (oral presentation)

13th Plant Science Student Conference PSSC, P. Jänicke, C. Lennicke, B. Seliger, L. A. Wessjohann, G. N. Kaluđerović: *Silica nanoparticles carrying bioactive natural products and their impact on cancer cells*, 06.06.–09.06.2017, Halle/Saale (poster presentation)

Leibniz Conference on Bioactive Compounds and Biotechnology, P. Jänicke, C. Lennicke, B. Seliger, L. A. Wessjohann, G. N. Kaluđerović: *Silica nanoparticles carrying bioactive natural products and their impact on cancer cells*, 10.04.–11.04.2017, Freising (poster presentation)

Leibniz Conference on Bioactive Compounds and Biotechnology, P. Jänicke, P. Ebersbach, E. Freier, G. N. Kaluđerović: *Traceable nanomaterials for drug delivery*, 23.04.2018, Halle/Saale (poster and oral presentation)

Conference on Interdisciplinarity, P. Jänicke, P. Ebersbach, E. Freier, L. A. Wessjohann, G. N. Kaluđerović: *Traceable nanomaterials for drug delivery*, 21.06.–22.06.2018, Magdeburg (poster presentation)

European Federation for Pharmaceutical Sciences EUFEPS Annual Meeting 2019, R. Kufka, R. Rennert, P. Jänicke, G. N. Kaluđerović, L. Weber, W. Richter, L. A. Wessjohann: *Synthesis of a tubugi-1-toxin conjugate by a modulizable disulfide linker system with a neuropeptide Y analogue showing selectivity for hY1R-overexpressing tumor cells*, 05.03.–08.05.2019, Frankfurt/Main (poster presentation)

Leibniz Conference on Bioactive Compounds and Biotechnology, R. Kufka, R. Rennert, P. Jänicke, G. N. Kaluđerović, L. Weber, W. Richter, L. A. Wessjohann: *Synthesis of a tubugi-1-toxin conjugate by a modulizable disulfide linker system with a neuropeptide Y analogue showing selectivity for hY1R-overexpressing tumor cells*, 01.04.–02.04.2019, Dresden (poster presentation)

Publications and paper manuscripts

P. Jänicke, C. Lennicke, A. Meister, B. Seliger, L. A. Wessjohann, G. N. Kaluđerović, Fluorescent spherical mesoporous silica nanoparticles loaded with emodin: Synthesis, cellular uptake and anticancer activity, *Mater Sci Eng C* **2021**, *119*. doi: 10.1016/j.msec.2020.111619

M. G. Ricardo, D. Llanes, R. Rennert, P. Jänicke, D. G. Rivera, L. A. Wessjohann, Advancing antibody-drug conjugate payloads: Improving synthetic access to super potent tubulysin analogs and their quaternary ammonium-based peptide linkers via an all-on-resin strategy, *in preparation*.

Eidesstattliche Erklärung

Hiermit erkläre ich an Eides statt, dass ich die vorliegende Arbeit selbstständig und nur unter der Verwendung der angegebenen Quellen und Hilfsmittel angefertigt habe. Zitate und andere Anlehnungen hinsichtlich Aussagen und Konzepten sind als solche gekennzeichnet. Die vorliegende Arbeit wurde in gleicher oder ähnlicher Form noch keiner Prüfungsbehörde zur Begutachtung vorgelegt.

Halle (Saale), 15.06.2021

Paul Jänicke